University of Tasmania.

Structure and sedimentology of the Curdimurka Subgroup, northern Adelaide Fold Belt, South Australia.

Wallace Mackay
(BSc Hons, MSc, MBA)

Date: February, 2011.

Submitted in fulfilment of the requirements for the Degree of PhD.

Supervisors:
Dr. D. Selley, University of Tasmania
Dr. S. Bull, University of Tasmania.

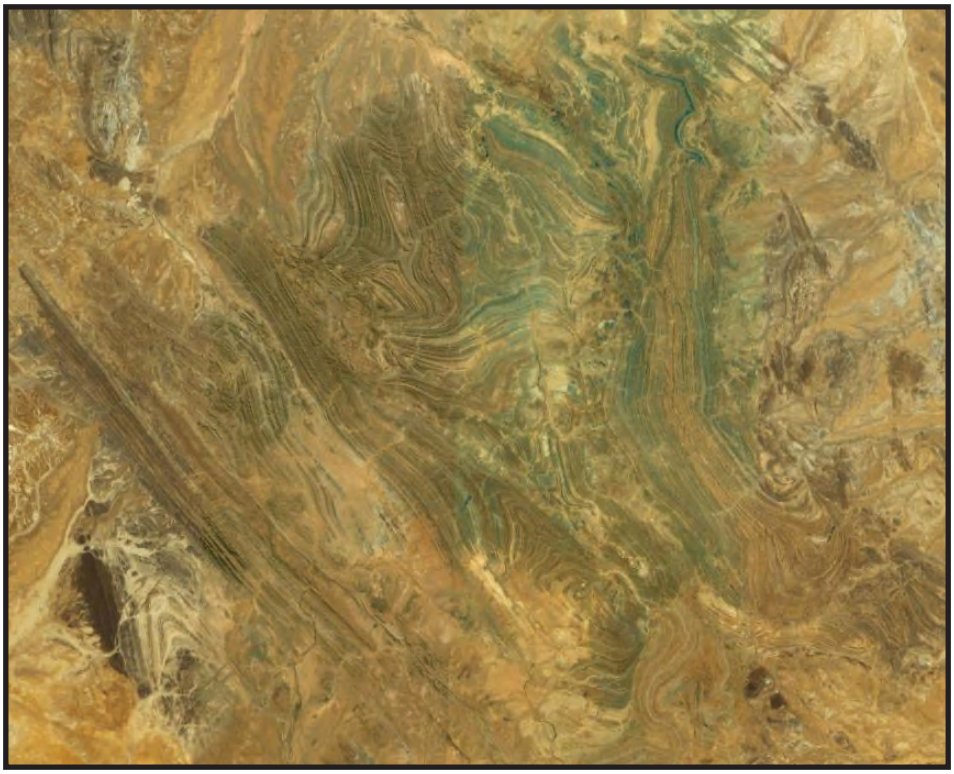

Google Earth image of the Willouran Range.

ABSTRACT

The Curdimurka Subgroup is the upper unit of the Callanna Group, the basal group of a thick Neoproterozoic metasedimentary dominated succession that is preserved as the Adelaide Fold Belt. Throughout the fold belt, the Curdimurka Subgroup typically crops out as megaclasts within breccias, the majority of which formed as salt diapirs or other salt-tectonic related bodies. However, within the Willouran Trough, a depocentre that formed early in the evolution of the northern Adelaide Fold Belt, the package is less fragmentary, albeit bounded by tectonic and brecciated contacts. In this type area of the Curdimurka Subgroup, about 6,000 m of semi-coherent strata are preserved. By examining the stratigraphy and structure of the Curdimurka Subgroup, this study intends to develop an understanding of the early development of the northern Adelaide Fold Belt.

Deposition of the Curdimurka Subgroup was mainly in low energy, shallow water to emergent conditions, with periods of sub-wave base deposition. Evidence from evaporite mineralogy and stable isotope geochemistry suggest that it was deposited in marine conditions, but a lacustrine setting cannot be ruled out. Curdimurka Subgroup depocentres evolved within a rift environment, subsequent to an initial phase of syn-rift, mantle-plume related volcanism. The outcropping part of the succession is lacking in coarse-grained rudaceous facies, a feature interpreted to record sedimentation distal to basin-marginal sediment input points. Detrital zircon age populations demonstrate a clear upsection trend from proximal- to distal-source area contribution, a trend which is consistent with conceptual models of broadening drainage patterns with increasing rift basin maturity.

Field relationships show that the area was subject to three deformation events. D_1 produced a diverse array of macroscopic structures, including listric normal faults, inclined to recumbent folds and low angle reverse faults. Deformation is interpreted to have accommodated bulk extension associated with gravity spreading above a décollement positioned at the base of the Curdimurka Subgroup. Localised compressional structures formed in response to translation above perturbations along both the décollement surface, and additional layer-sub-parallel fault zones positioned higher in the Curdimurka Subgroup succession. Withdrawal and local diapirism of a parent salt layer positioned in older Arkaroola Subgroup strata provided the gravitation instability to drive D_1. The timing of this event is constrained by associated high level accommodation development, involving complex sub-basin growth, during Cryogenian Umberatana Group sedimentation,

D_2 produced upright, northwest – southeast trending folds with a penetrative axial plane cleavage, and northeast dipping reverse faults. D_3 produced open, southwest trending folds, local refolding of F_2, and a spaced cleavage oriented at a high angle to bedding. Both D_2 and D_3 occurred during a Cambrian basin inversion event, the Delamerian Orogeny. Monazite geochronology shows that peak metamorphism occurred during the Delamerian Orogen, at 509 ± 5 Ma. A second thermal event occurred at 429 ± 9 Ma, approximately contemporaneous with the intrusion of the British Empire Granite in the Mt Painter Inlier, 130 km east of the study area.

CONTENTS

APPENDICES

FIGURES

Chapter 1.

Chapter 2.

Chapter 3.

Chapter 4.

Chapter 6.

Chapter 7.

Chapter 10.

TABLES

DECLARATION OF ORIGINALITY

This thesis contains no material which has been accepted for the award of any other degree or diploma in any tertiary institution and, to the best of my knowledge and belief, contains no copy or paraphrase of material previously published or written by another person, except when due reference is made in the text of the thesis.

Wallace Mackay: December 20, 2010.

STATEMENT OF AUTHORITY OF ACCESS.

This thesis may be made available for loan and limited copying in accordance with the Copyright Act of 1968.

Wallace Mackay, December 20, 2010

ACKNOWLEDGEMENTS

This thesis was part of the ARC/AMIRA P544 Proterozoic Sedimentary Copper projects. It was begun with the assistance of an APA(I) research scholarship, reached middle age in penury and now finishes in employment. It's completion owes much to the patience and assistance of my supervisors, Dave Selley and Stu Bull. In particular Dave's cajoling, threats and many corrections saw it reach this stage. All the errors in spelling, grammar, and thinking are purely my own, despite the assistance of Dave and Stu. Peter McGoldrick is thanked for the initiation of the PhD, with Dave and Stu, and for getting me down to Hobart. Thanks also go to Primary Industry and Resources, South Australia, and in particular Wolfgang Preiss and Stuart Robertson, are thank for their assistance with finding data in the PIRSA library and in helping understand the Adelaide Fold Belt. Wolfgang gets a special mention for passing on some of his vast knowledge of the region.

Other participants in P544 are also deserving of gratitude. My fellow students in Hobart, Mawson Croaker and Nicky Pollington for geological discussions in the field and the office.

At the University of Tasmania, Simon Stephens is thanked for doing my too many thin sections and grain mounts and Peter Cornish is thanked for all of his assistance with organising vehicles and logistics for my several field trips. June Pongratz helped with drafting and getting printers, scanners etc to work. Katy McGoldrick helped with general laboratory work. Zircon geochronology was completed with much help from Sebastien Meffre, Leonid Danyushevsky and Sarah Gilbert. The monazite geochronology was almost completed with the help of Ron Berry and Dave Steele. Stable isotopes were completed with the assistance of Garry Davidson.

Thanks go to my fellow students for Friday afternoon beers and other afternoon beers and the usual conversations on geology and the more important things in life such as the football and cricket. My room mates through my too long period on the third floor are deserving of special thanks for tolerating my abilities to create a mess and then my inability to uncreate it, as well as for being easy to get along with in most ways that matter.

On a more personal note, my mother is thanked for helping me through those inevitable financial difficulties, as well as more general support. Silke, a very dear friend who disrupted her routine to be my field assistant in two field trips I also thank. And Yee I thank in particular, for providing all sorts of support over the past few years.

CHAPTER 1.
INTRODUCTION

1.1 The Adelaide Fold Belt

The Adelaide Fold Belt (Figure 1.1) is one of a series of rift basins, recognised worldwide, that record latest Neoproterozoic extension and eventual break-up of Rodinia (Powell et al., 1994). During its evolution, from initiation prior to 827 Ma (Wingate et al., 1998) to final basin inversion during the Cambrian Delamerian Orogeny, it records several of the key phases of the Earth's development including the great Neoproterozoic ice ages (e.g. Howchin, 1924; Mawson, 1940; Preiss, 1987; Hoffman et al., 1998) and the advent of multicellular life forms (Sprigg, 1947; Glaessner, 1958). Its superb exposures make it a natural laboratory for studies of Neoproterozoic stratigraphy (e.g., von der Borch et al., 1980; Preiss and Forbes, 1981; Preiss, 1987; 2000; Powell et al., 1994; Christie Blick et al., 1995; Preiss et al., 1998; Preiss and Cowley, 1999), thrust belt evolution (Flottman et al., 1995; Marshak and Flottmann, 1996; Flottmann and James, 1997) and salt tectonics (e.g., Webb, 1960, 1961; Coats, 1965; Mount, 1975; Lemon, 1985).

From an economic viewpoint, the Adelaide Fold Belt has played an important role in the early development of South Australia and Australia, with the development of the first metallic mine (Pb-Ag) in Australia at Glen Osmond in 1841 and the first copper mine at Kapunda in 1844 (Dickinson, 1944). Since that time, literally hundreds of Cu occurrences have been found in the Adelaide Fold Belt (Wells, 1976; Klaassen, 1990), occurring in all levels of stratigraphy and spread across its outcrop area, although none have been significant producers globally. This is in contrast to the Central African Copperbelt, with which the Adelaide Fold Belt has a number of similarities, and which hosts supergiant stratiform Cu-Co deposists, as well as U, and Zn - Pb mineralization (e.g., Mendelshon, 1961; Unrug, 1988; Selley et al., 2005) . The similarities include sedimentology, stratigraphy and structure, as well as the basins being approximately co-eval. In particular both basins have terrestrial and/or marginal marine depositional environments during early stages which host the majority of mineralization on the Central Afircan Copperbelt (Mendelson, 1961; Annels, 1984; Selley et al., 2005) , and evidence of evaporitic units and salt tectonics which may play an important role in the mineralization process (Selley et al., 2005). It may then be significant that one of the largest Cu deposits in the Adelaide Fold Belt, the Blinman deposit, is hosted by a megaclast within what is interpreted to be breccia of diapiric origin (Dickinson, 1944; Coats, 1964).

The geology of the Adelaide Fold Belt has been subject to a considerable amount of work. Its stratigraphy is well established and there is a sizeable body of work outlining its structural development during the Cambrian Delamerian Orogeny (e.g., Jenkins and Sandiford, 1992; Oliver and Zakowski, 1995; Marshak and Flottmann, 1996; Flottman and James, 1997; Paul et al., 1999). Several studies have traced its development from initiation to inversion (von der Borch, 1980; Preiss, 1987; 2000; Jenkins, 1990; Powell et al., 1994). However there is a poor understanding of the early development of the Adelaide Fold Belt. Part of the

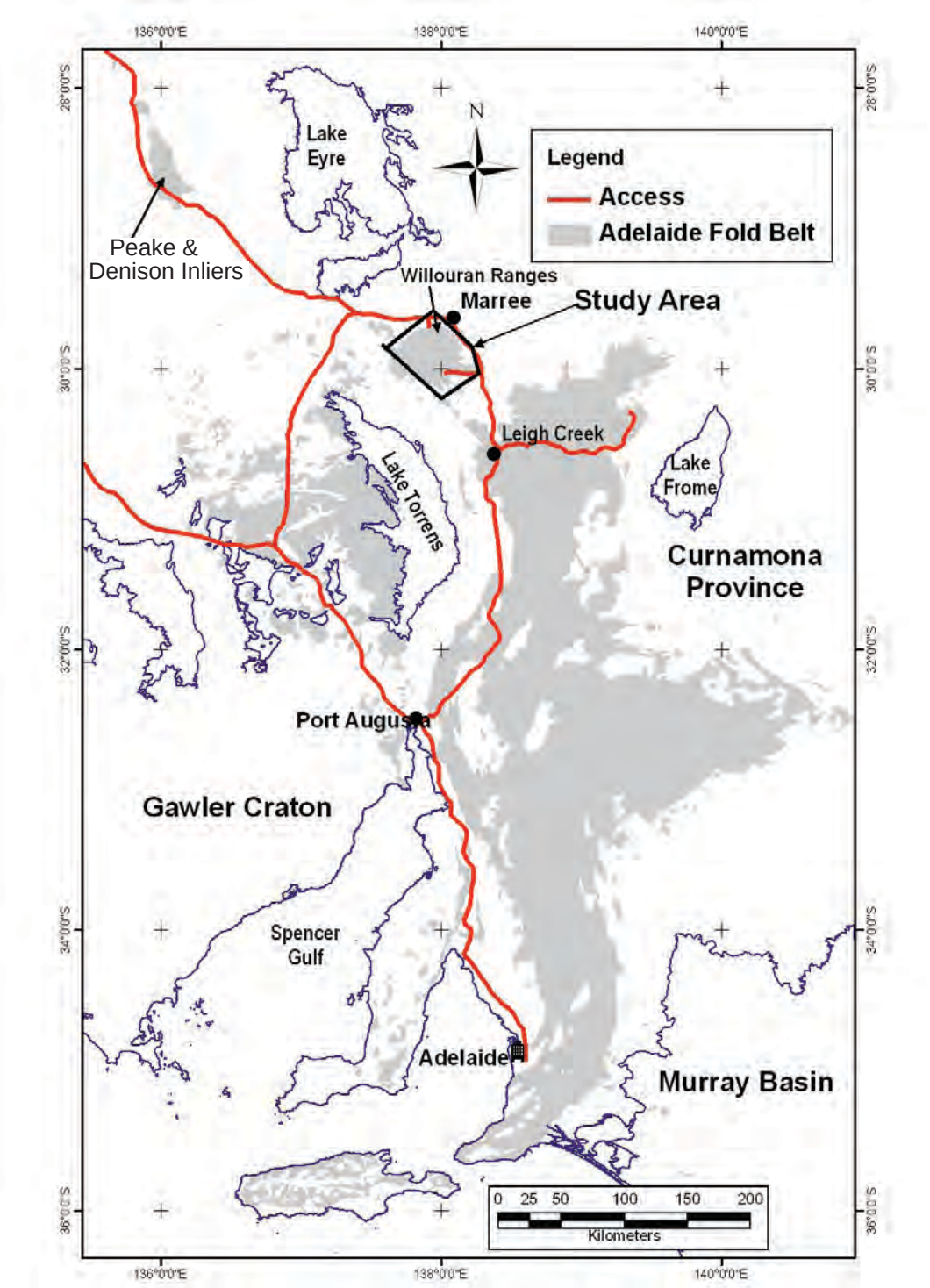

Figure 1.1. Locality map showing the area of outcrop of the Adelaide Fold Belt and the study area.

reason for this is simply because the lowest levels of stratigraphy crop out poorly in widely separated and dismembered occurrences. Another reason is that most of the previous work, and particularly that aimed at understanding the structural history, has concentrated on the central and southern Adelaide Fold Belt, where the effects of the Delamarian Orogeny are spectacularly displayed at the macroscopic scale.

The most continuous and structurally coherent exposures of the lower Adelaidean succession, occur in the northern Adelaide Fold Belt; around the Mt Painter Inlier in the

northeast, the Willouran Range in the northwest, and in the Peake and Denison Inliers northwest of the contiguous outcrop of the Adelaide Fold Belt (Figure 1.1) In the former, the lowest unit of the Callanna Group, the Arkaroola Subgroup crops out around an inlier of Palaeo- to Mesoproterozoic basement (Coats and Blisset, 1971; Preiss, 1987). Within the Willouran Range, the Curdimurka Subgroup, the upper part of the Callanna Group, crops out in a series of elongate fault blocks which preserve much of its stratigraphy intact (Murrell, 1977; Preiss, 1987; Forbes, 1990). The geology of the Peake and Denison Inlier is less well known, but both the Arkaroola Subgroup and the Curdimurka Subgroup are recognized (Ambrose et al., 1981; Preiss, 1987).

1.2 Research Aims

The primary aim of this study is to understand the early evolution of the Adelaide Fold Belt. It will be achieved by examining the development of the Willouran Trough (Figure 1.2). The Willouran Trough is a roughly triangular gravity low in the northern Adelaide Fold Belt, identified by Preiss (1987) as being a major depocentre during the initial stages of the Adelaide Fold Belt development. Its main surface expression is in the Willouran Range and so by studying the geology of this area and in particular the Curdimurka Subgroup it is intended to fulfill the primary aim. Within the primary aim are two secondary aims;

- to understand the early development of the Willouran Trough by examining the sedimentology and detrital zircon geochronology of the Curdimurka Subgroup; and
- by studying the post-depositional history of the Curdimurka Subgroup, in particular its deformational history and relationship to the overlying units; the Burra and Umberatana groups using mapping, aerial photograph interpretation and monazite geochronology.

1.3 Location and Physiography

The field area is at the boundary of the Curdimurka, Andamooka, Copley and Marree 1:250,000 topographic sheets (Figure 1.3). Most of the area is in Zone 53 (Curdimurka and Andamooka maps sheets) of the Australian Map Grid, with a small part on Zone 54 (Copley and Marree map sheets). It is sited on two pastoral properties, mainly the Witchelina Station, with a small area along the southern margin of Callanna Station. About 10 km to the northeast of the northern end of the study area is the small town of Marree. The coal mining town of Leigh Creek lies about 100 km to southeast (Figure 1.3).

Access to the area is from the Adelaide – Marree road, which is sealed to Lyndhurst and is thereafter a graded road (Figure 1.3). The northern end of the area is reached by station track, either from the Adelaide – Marree road, about 14 km south of Marree or via Callanna Station, from the Oodnadatta Track about 12 km west of Marree. The Farina – Mulgaria track, goes through the southern half of the area. Otherwise, movement through the area is by old exploration and station tracks in varying degrees of repair.

The study area is within the Willouran Ranges area which consists of a two northwest – southeast trending ranges separated by an area of low hills and salt flats (Figure 1.4). The

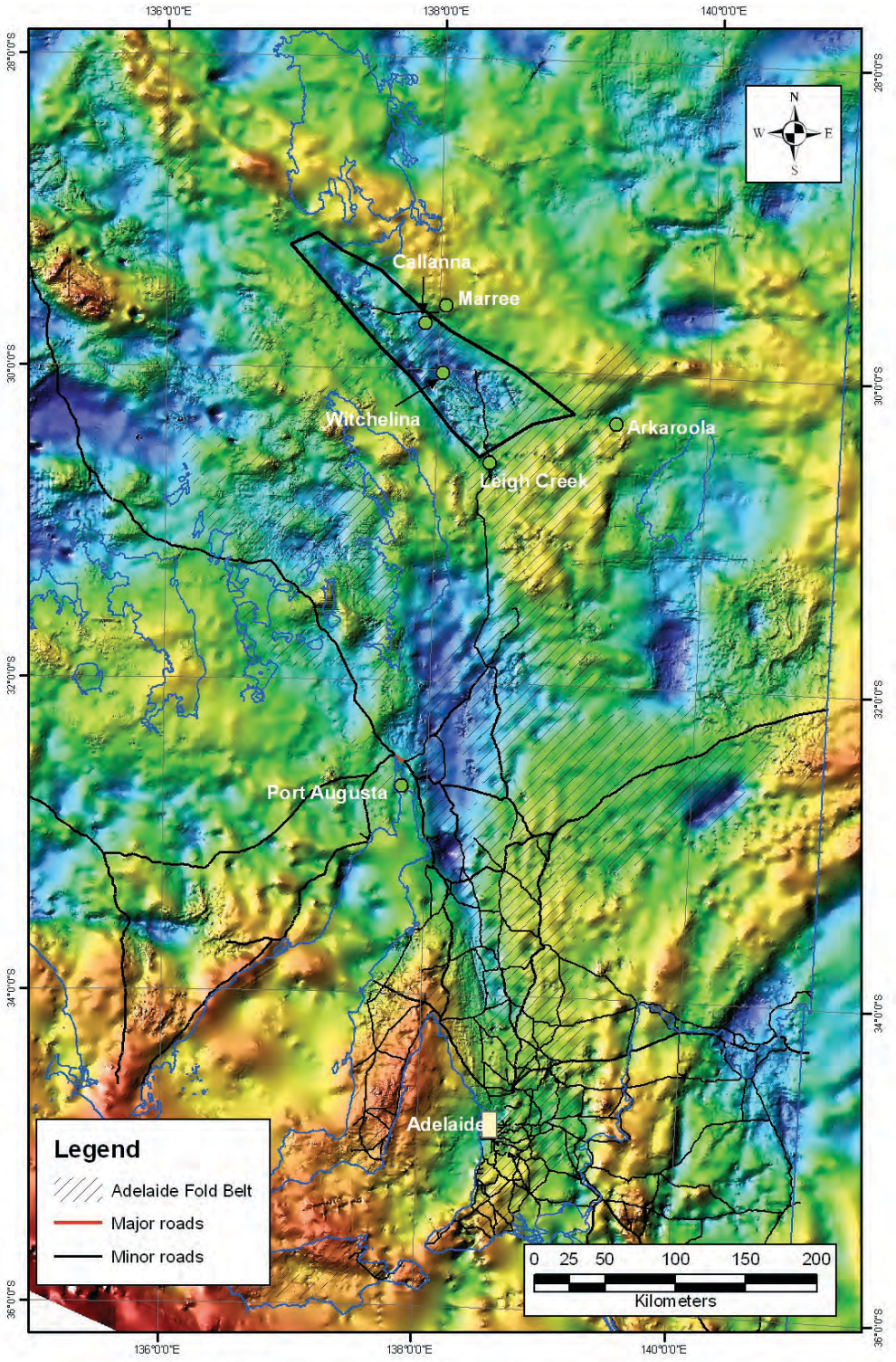

Figure 1.2. Bouger gravity anomaly image of eastern South Australia with the Willouran Trough, a deep gravity low, outlined.

eastern range is the Willouran Range *sensu stricto* with Willouran Hill at 327 m, being the highest point. Mt Norwest is the highest point of the western range at 314 m elevation. The ranges are typically formed from the sandstone units of the Curdimurka Subgroup and the Emeroo Subgroup. Areas of low hills may be formed from Skillogalee Dolomite and the salt flats are formed on siltstone and shale units. A number of intermittent to mainly dry rivers and creeks drain the area. Those in the northern half, Mirra Creek, Screech Owl Creek, Recovery Creek and Boolaroo Creek eventually drain into Lake Eyre. In the

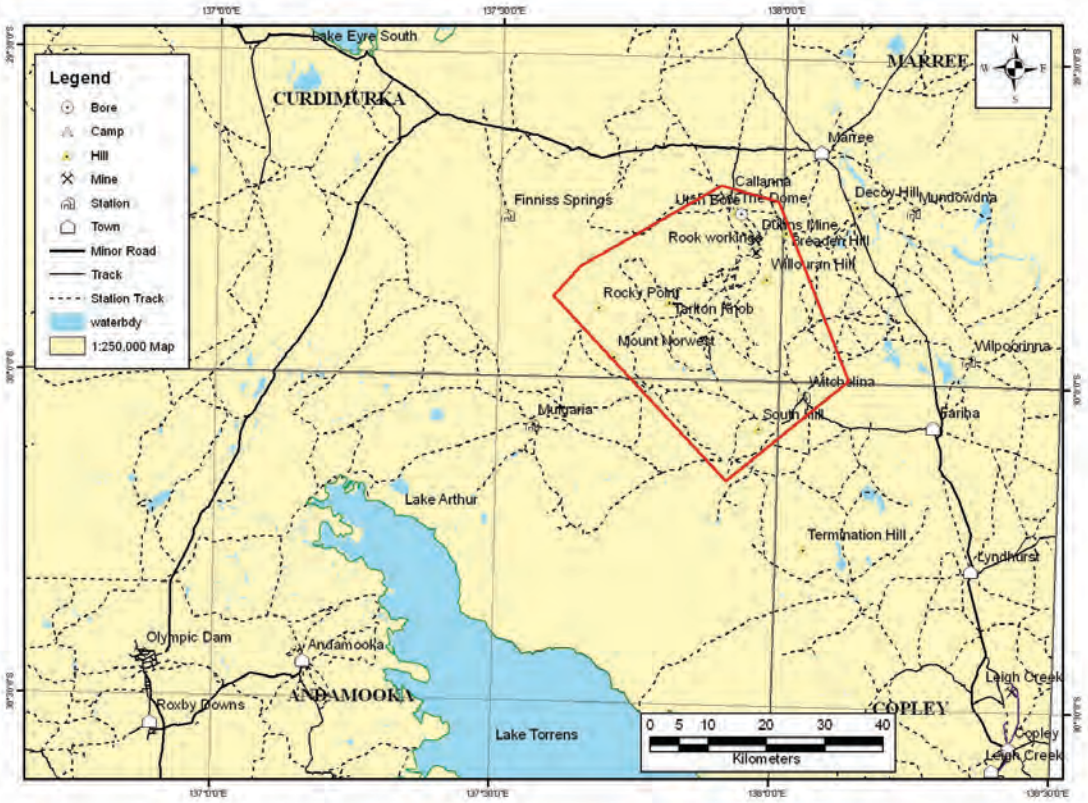

Figure 1.3. The study area with 1:250,000 map sheets, access and surrounding towns and stations.

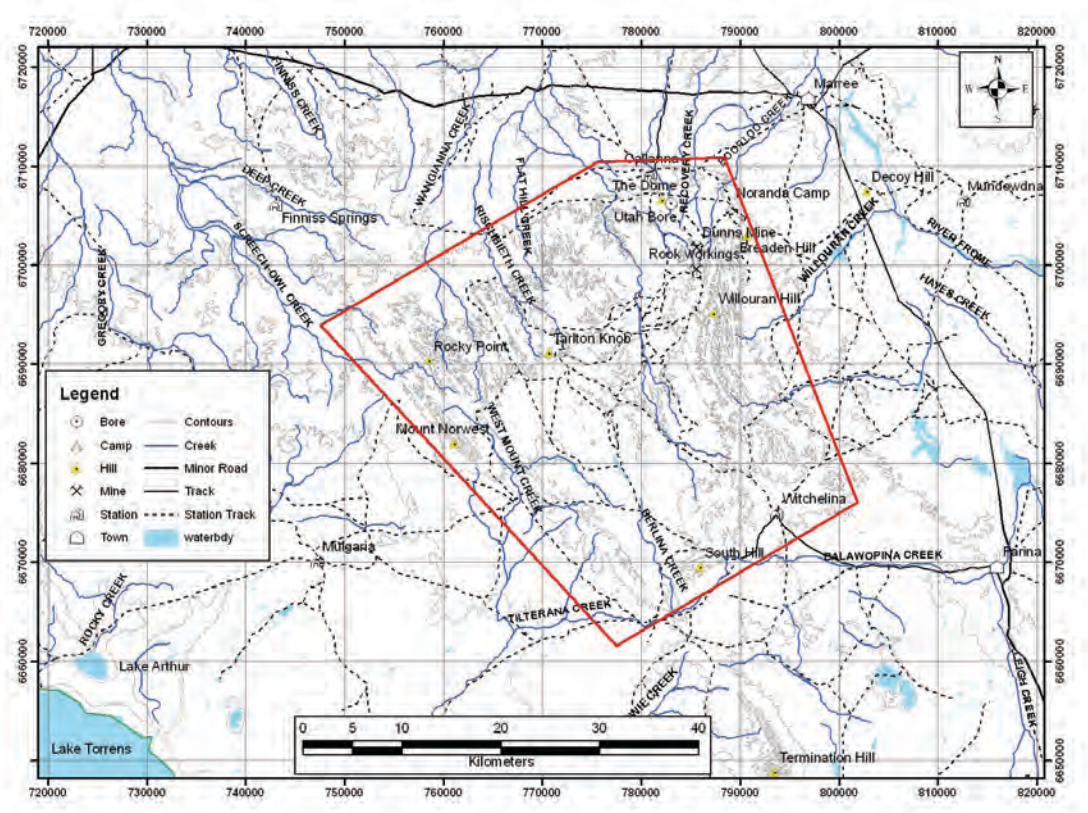

Figure 1.4. The major topographic features of the Willouran Range and surrounding area.

southwest, the creeks drain into Lake Torrens via the Mulgaria Watercourse and in the southeast, the creeks drain into sandy areas (Figure 1.4).

Marree has an average annual rainfall of 162 mm. The January average maximum temperature is 37.7°C with a mean minimum temperature of 21.2°C, and the July average maximum is 19°C with an average minimum temperature of 4.8°C (http://www.bom.gov.au/climate/averages/tables/cw_017031.shtml.).

1.4 Methodology

The basis of the study is provided by geological mapping in the field area. Several types of mapping are used;

- larger-scale reconnaissance mapping using traverses typically two to three kilometres long across outcrop of Curdimurka Subgroup in the Norwest Domain and the South Hill Domain, and across the Bungarider Fault, using either approximately 1:80,000 or 1:40,000 aerial photographs;
- traverses across the entire Curdimurka Subgroup and along structures and key contacts in its type area in the Euchre Pack Domain using colour aerial photographs blown-up to approximately 1:10,000 and 1:20,000;
- small-scale mapping on three selected outcrops to examine the structure in detail;
- and sedimentological mapping of eight key sections for facies analysis at appropriate scales (from 1:10 to 1:100).

Diamond drill hole core logging of eight holes, drilled by the Utah Development Corporation (UDC) as part of an exploration program for copper conducted in the Willouan Ranges in the late 1970's - early 1980's, was also undertaken to assist in understanding the structure, alteration and metamorphism and for facies analysis. Core logging was conducted at differing levels of detail from 1:20 to 1:100. The diamond drill hole core is stored at the Primary Industry and Resources, South Australia (PIRSA) core storage yard in Adelaide.

Gravity modeling of the Willouran Trough was conducted on a subset of the South Australian gravity data set (PIRSA, 2000) specific to the Willouran Range and surrounding area. The data was modeled using the Potent potential field modeling program, and the model used to develop a cross-sections and long-section of the Willouran Trough, through the Willouran Range area.

During mapping and core logging, a number of samples were collected for petrographical, stable isotope and sedimentary zircon provenance studies. Laboratory studies completed are outlined briefly here, with the full methodology reported in the relevant chapters.

Detrital zircon ages from ten sandstone samples were determined using the School of Earth Sciences laser ablation – inductively coupled plasma – mass spectrometer (LA-ICP-MS). Monazite dating to assist in determining the age of the alteration and diagenesis was executed using a chemical method. Electron microprobe analysis of monazites was

conducted using initially the University of Tasmania Central Science Laboratory Cameco SX-50 electron microprobe for two heavy mineral grain mounts and then a Cameco SX-100 electron microprobe for several polished sections. Analyses for stable isotopes ($\delta^{13}C$ and $\delta^{18}O$) were conducted on carbonates including sedimentary limestone and dolomite, veins, diagenetic carbonates and breccia clasts and matrix.

1.5 Thesis Organization.

The thesis comprises ten chapters. Chapter 2 introduces the stratigraphy, geochronology and structure of the Willouran Trough as studied by previous workers. The sedimentology of the Curdimurka Subgroup is examined in Chapter 3, aiming to identify the depositional and tectonic environments at this time. Chapter 4 uses a model of changes in zircon provenance through time to determine the tectonic environment as well as examining possible continents that rifted away from the Adelaide Fold Belt with the break-up of Rodinia. The fifth chapter uses $\delta^{13}C$ and $\delta^{18}O$ variations of the carbonates in the Curdimurka Subgroup to determine whether the depositional environment was lacustrine or marine. Electron microprobe age determinations of monazites are used to examine the post-depositional history of the Curdimurka Subgroup in Chapter 6. Chapters 7 and 8 examine the structural history of the Willouran Trough. In Chapter 7, the examination and discussion is confined to the type-area of Curdimurka Subgroup outcrop, whereas in Chapter 8 the structural study is expanded to cover the entire Willouran Range. Chapter 9 is a brief excursus on the role of salt tectonics in the structural development of the Willouran Trough. Finally, Chapter 10 develops a model for the evolution of the Willouran Trough as seen in the rocks of the Willouran Range, expanding it to the northern Adelaide Fold Belt and beyond where appropriate.

Appendices are included in the accompanying data disk. Appendix 1 contains the analytical and geochronological data used in Chapter 4. Appendix 2 contains the sample information and stable isotope analyses used in Chapter 5. Appendix 3 contains the monazite electron microprobe analyses and geochronological results used in Chapter 6. Appendix 4 includes the gravity models used in Chapter 8.

CHAPTER 2.
GEOLOGICAL SETTING

2.1 Stratigraphic and Structural Framework of the Adelaide Fold Belt

2.1.1. Introduction

The Adelaide Fold Belt crops out extensively in central and eastern South Australia, between 28°S in the Peake and Denison Inliers and 36°S on Kangaroo Island (Figure 2.1). It is a Neoproterozoic intra-cratonic rift that was initiated between about 1,000 Ma and 827 Ma, at the onset of the break-up of Rodinia, the Meso- to Neoprotoerozoic supercontinent. Over a period of about 300 Myr, it progressed from an intra-cratonic rift to a passive margin before deposition within the Adelaide Fold Belt ceased in the earliest Cambrian. It underwent basin inversion in the Cambrian Delamerian Orogeny (Powell et al., 1994, Preiss, 2000).

Basement to the Adelaide Fold Belt is the Archaean to Mesoproterozoic Gawler Craton along its western margin and the Curnamona Province in the northeast (Figure 2.1). The contact between the basement and the overlying Adelaide Fold Belt is best observed on the margins of the Mt Painter Inlier (Figure 2.1). On the southern and western margins of the Mt Painter Inlier, the Arkaroola Subgroup (Figure 2.2) was deposited unconformably on metasediments and granite, but on its northwestern margin, and on the Mt Babbage Inlier, the Umberatana Group (Figure 2.2) unconformably overlies the basement (Coates and Blisset 1971; Preiss, 1987). On the southern margin of the Curnamona Province, the Burra Group unconformably overlies the basement in a series of thrust slices (Berry, 1977; Paul et al., 1999). On its western margin, flat-lying Adelaide Fold Belt rocks unconformably overlie the Gawler Craton on the Stuart Shelf (Preiss, 1987). Further south in the Fleurieu Arc (Figure 2.1), basement and Adelaide Fold Belt rocks are interleaved in thrust blocks, as thick-skinned thrusts have transported thrust sheets of Adelaide Fold Belt rocks and underlying basement westward on to the basement (Flottmann and James, 1997).

Rutland et al. (1981) and Preiss (1987) identified eight structural elements within the Adelaide Fold Belt (Figure 2.1; Table 2.1). They are fundamental to the development of the Adelaide Fold Belt. The Northern Flinders Zone was an area of deep trough development, initially the Willouran Trough (see below) and then later, the Yudnamutana Trough, whereas the Central Flinders Zone may have been emergent during deposition of the Burra Group (Preiss, 1987). Most fundamental is the Torrens Hinge Zone. It was a platform area early in the basin development but began to subside during deposition of the Burra Group, continuing until deposition ceased in the Adelaide Fold Belt. It underwent mild basin inversion during the Delamerian Orogeny (Preiss, 1987).

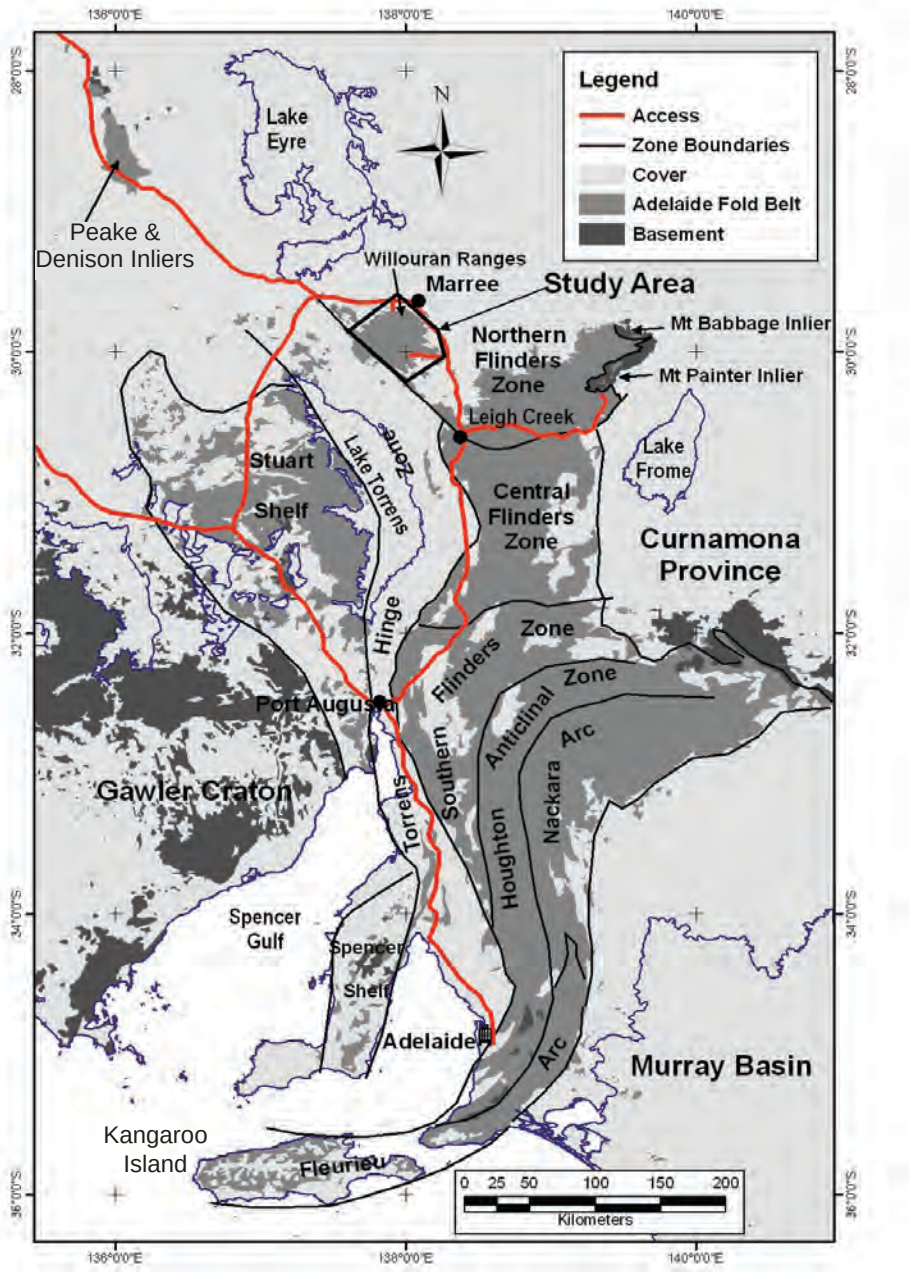

Figure 2.1. Locality map showing the extent of the Adelaide Fold Belt, from Kangaroo Island in the south to the Peake and Denison Inlier in the north, with the eight structural elements of Rutland (1981) and Preiss, (1987: PIRSA Regional GIS data).

2.1.2 Stratigraphy and Geochronology of the Adelaide Fold Belt.

2.1.2.1 Historical Development of the Stratigraphy

Mawson and Sprigg (1950) first developed a three fold stratigraphy of the Adelaide Fold Belt, comprising the Torrensian, Sturtian and Marinoan Series. Sprigg (1952) added the Willouran Series to this initial stratigraphy, placing it below the Torrensian. These series are chronostratigraphic and away from their type sections the boundaries cannot be defined precisely (Preiss, 1987). Therefore Thomson et al. (1964) first defined four new stratigraphic units; the Callanna Beds, and the Burra, Umberatana and Wilpena groups (Figure 2.2) which could be mapped and correlated across the Adelaide Fold Belt. The Callanna Beds was formalized as the Callanna Group by Forbes et al., (1981). Preiss (1987) described

Table 2.1. Elements of the Adelaide Fold Belt with their main stratigraphic, sedimentological and structural features (Rutland et al., 1981; Preiss, 1987).

Element	Stratigraphy/ Sedimentology	Structure
Northern Flinders Zone	Callanna to Wilpena. Deep troughs and thick packages	Arcuate folds, the trends of which swing from NE-SW in the NE to E-W in the south to NW-SE in the NW. Continues to Peak and Denison Inlier. Salt-related breccias
Central Flinders Zone	Callanna to Wilpena. Mainly shallow water.	Broad dome and basin folds. Diapiric breccias
Nackara Arc	Callanna to Wilpena. Sediment wedge thickens to the southeast, deeper water sediments	Arcuate fold and thrust belt which trend N-S in the south, NE-SW in the NW and E-W in the east.
Southern Flinders Zone	Callanna to Wilpena. Shallower water sediments	A zone of arcuate upright folds.
Houghton Anticlinal Zone	Callanna to Wilpena.	Mainly lower Adelaidean rocks exposed
Fleurieu Arc	Burra to Wilpena	Has the most intense deformation and highest grade metamorphism.
Torrens Hinge Zone	Burra to Wilpena. Shallow water and sub-aerial sediments	Flexuring and faulting, marks the transition from undeformed thinner AFB and Cambrian packages to the west from strongly folded packages to the east
Stuart Shelf (+ Spencer Shelf)	Callanna(?), Umbertana & Wilpena	A platform area with flat-lying AFB rock on basement.

the Adelaide Fold Belt stratigraphy in detail, and made subsequent modifications to the Burra and Umberatana groups stratigraphy (Preiss, 1997; Preiss et al., 1998; Preiss and Cowley, 1999). Preiss (1982) suggested that the Precambrian and Cambrian deposits define three major successions, each with its own tectonics and palaeogeography, and separated by major regional unconformities. He proposed that the Callanna and Burra groups be combined in the Warrina Supergroup, the Umberatana and Wilpena groups combine as the Heysen Supergroup and the Cambrian sedimentary rocks that sit above the Adelaide Fold Belt be termed the Moralana Supergroup (Preiss, 1982). The Warrina Supergroup reflects the initial intracontinental rift development of the Adelaide Fold Belt and the Heysen Supergroup reflects the break-up of Rodinia and transition to a passive margin (Figure 2.2: Powell et al., 1994; Preiss, 2000). However some authors (e.g., Veevers, 1997; Direen and Crawford, 2003) suggest that the break-up should be placed much later, during the latest Neoproterozoic). The Moralana Supergroup reflects the change in tectonics to an active continental margin prior to the Delamarian Orogeny (Haines and Flottman, 1998).

The chronostratigraphic subdivision has been retained. It places all of the rocks within the Adelaide Fold Belt in the Adelaidean which Preiss (1987) restricted to the period of deposition of the Adelaide Fold Belt. It has four sub-divisions; the Willouran, Torrensian, Sturtian and Marinoan (Figure 2.2), which reflect the four-fold stratigraphic division, except that the base of the Sturtian is placed at the base of the Belair Subgroup (of the

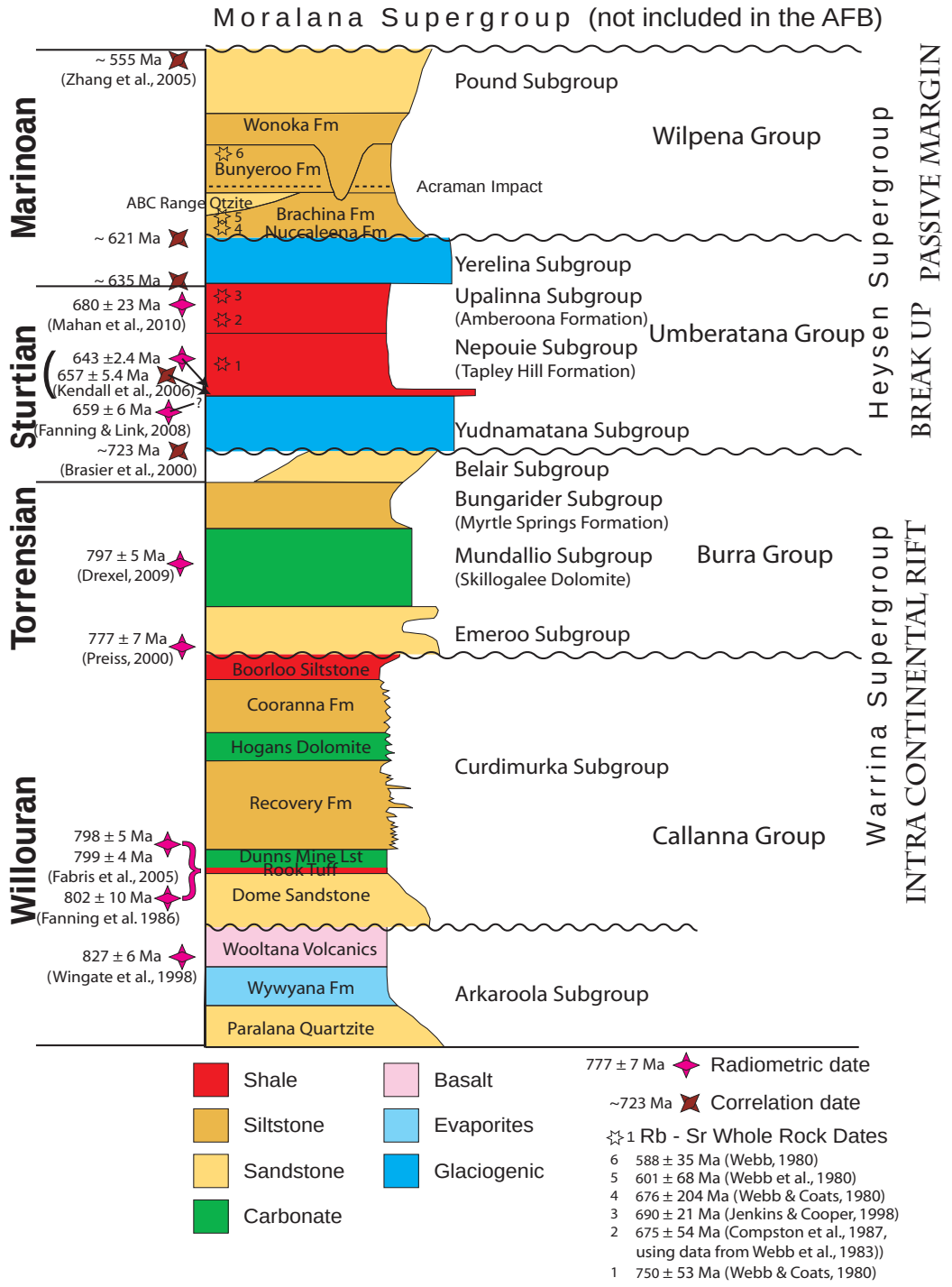

Figure 2.2. Semi-figurative stratigraphic section of the Adelaide Fold Belt, showing the age controls and chronostratigraphy on the left and and tectonic setting on the right.

Formation names for units in the Willouran Range area are shown in brackets under their Subgroup names. Colours represent the main lithology in each unit.

Burra Group) and the base of the Marinoan is placed at the base of the Yerelina Subgroup (Preiss, 1987).

2.1.2.2 The Callanna Group.

The Callanna Group comprises the Arkaroola and Curdimurka subgroups (Figure 2.2). At the type area of the Arkaroola Subgroup, in the Arkaroola area, the Curdimurka Subgroup

does not crop-out, and in the type area of the Curdimurka Subgroup, in the Willouran Range (Figure 2.1), the Arkaroola Group occurs only as megaclasts within breccias. Forbes (1990) quoted a personal communication from Preiss, that the Dome Sandstone overlies the Noranda Volcanics (a correlative to the Wooltana Volcanics in the Willouran Range) in a megaclast in the central Willouran Range, otherwise no contact between the Arkaroola and Curdimurka subgroups has been found.

The Arkaroola Subgroup consists of the basal Paralana Quartzite, which lies unconformably on the Meso- to Palaeoproterozoic Mt Painter Inlier, and the successively overlying Wywyana Formation and Wooltana Volcanics (Figure 2.2). It crops out as an intact succession in the vicinity of the Mt Painter Inlier. Elsewhere it occurs as megaclasts within breccias scattered through the Adelaide Fold Belt (Figure 2.3). Around the Mt Painter Inlier, the Paralana Quartzite and Wooltana Volcanics show rapid variations in thickness, controlled by syn-

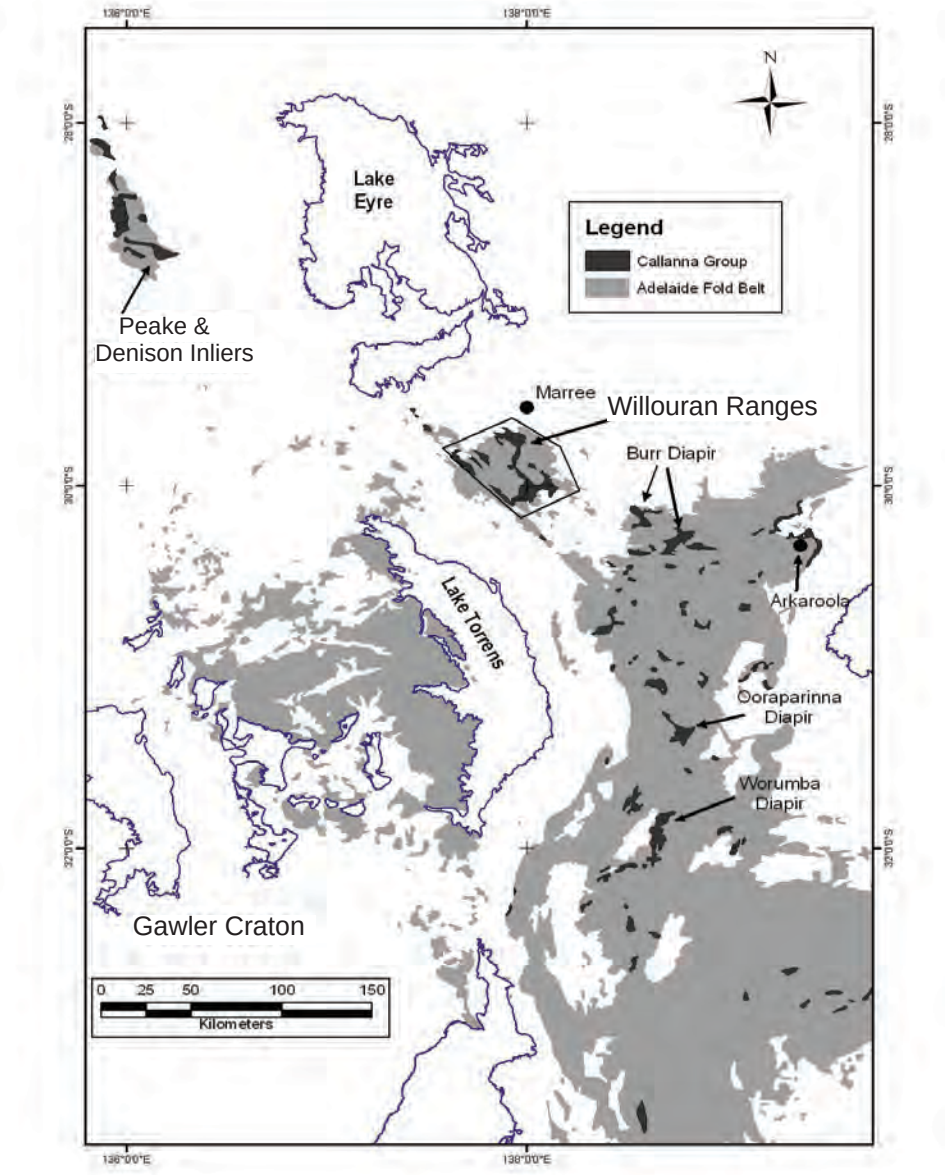

Figure 2.3. Outcrop of the Callanna Group (PIRSA Regional GIS data).
The Callanna Group outcrops in isolated fragments throughout the northern two thirds of the Adelaide Fold Belt, including the Peak and Denison Inliers.

depositional faulting (Coats and Blisset, 1971) and they reach a maximum thickness of about 2,700 m (Priess, 1987).

The Wooltana Volcanics are interpreted to correlate with the Beda Volcanics, which intertongue with sandstone of the Backy Point Beds, the basal unit of the Adelaidean on the Stuart Shelf (Mason et al., 1978). Other probable correlatives include the Cadlareena Volcanics in the Peake and Denison Inlier and the Wilangee Basalt in the Barrier Ranges of western NSW (Preiss, 1987). Hilyard (1990) concluded from geochemical similarities that the Wooltana Volcanics and the Gairdner Dyke swarm, a group of NW – SE trending dolerite dykes that intrude the Gawler Craton, have the same source. Mafic volcanic mega-clasts are also common in diapiric breccias throughout the northern and central Adelaide Fold Belt and the Nackara Arc, (Dalgarno and Johnson, 1968; Preiss, 1987; Hilyard, 1990). Together, all these units have been included within the Willouran Basic Province and were derived from a mantle plume (Crawford and Hilyard, 1990). Baddeleyite from the Gairdner Dyke swarm gave an age of 827 ± 6 Ma (Wingate et al. 1998), which provides the minimum age for the initiation of the Adelaide Fold Belt. In the eastern Curnamona Province, the Little Gabbro, interpreted by Gibson et al. (1996, 1997) to be a magma chamber that fed dykes at a higher level has been dated by Wingate et al., (1998) at 827± 9 Ma. Hilyard (1990) estimated that the Willouran Basic Province covered about 210,000 square kilometres.

Zhao et al (1994) concluded from geochemical data that the Gairdner Dyke swarm and the coeval Amata Suite in the Musgrave Block formed from the decompressional melting of a large-scale mantle plume. In Australia, the diameter of the plume is in excess of 1,000 km, from the Adelaide Fold Belt to the central Australia. They suggested that the plume may have been responsible for large-scale crustal extension and thinning, leading to the formation of the Centralian Superbasin (Zhao et al. 1994). Von der Borch (1980), Zhao et al., (1994) and Williams and Gostin (2000) placed the plume head below a postulated triple point centred in the vicinity of Leigh Creek. Li et al., (1999) suggested that the break-up of Rodinia was initiated by a mantle plume beneath South China, which they placed adjacent to the Adelaide Fold Belt at this time. Mafic and ultramafic intrusives in South China have been dated at 828 ± 7 Ma, and they suggested that the Gairdner Dyke swarm forms part of a radial dyke swarm, the focus of which was to the southeast of the Adelaide Fold Belt (Li et al., 1999).

Coats and Blisset (1971) and Preiss (1987) concluded that deposition of the Paralana Quartzite was fault controlled within an intracontinental rift basin. In a later paper, based on the absence of conglomerates and sedimentary breccias, (Preiss, 2000) suggested that the Paralana Quartzite was deposited on a gradually subsiding peneplained stable craton and not within a rift zone. Where it crops out around the southern half of the Mt Painter Inlier, the thickness is fault-controlled, with Coats and Blisset (1971) showing that the faulting is syn-depositional.

The Curdimurka Subgroup crops out widely but in dismembered packages and as megaclasts in breccia, with the most complete section at its type section in the Willouran Range (Figure

2.3). Its initial depositional area is thought to be reflected in the distribution of its occurrences in breccias (Preiss, 1987) and so it was likely restricted to the Northern and Central Flinders Zones, the Nackara Arc and Houghton Anticlinal Zone. It has been divided into six units (Figure 2.2) and consists mainly of siltstone and shale with minor carbonate and sandstone (Murrell, 1977; Forbes, 1980; Preiss, 1987). Rowlands et al. (1980) interpreted it to have been deposited in a lacustrine environment in an intracontinental rift. There are two dates published for the Curdimurka Subgroup. In the Willouran Range, a SHRIMP U-Pb age of 802 ± 10 Ma from zircons taken from a lenticular porphyritic dacite from within the Rook Tuff has been reported (Fanning et al., 1986). The second is for a volcanic unit, the Oodla Wirra Volcanics, that occur as rafts within the Mt Grainger Diapir in the Nackara Arc. Two two separate samples of felsic volcanic rocks gave zircon U – Pb ages of 798 ± 5 Ma and 799 ± 4 Ma (Fabris et al., 2005); i.e. within error of the Rook Tuff. They are interpreted to have been deposited within evaporitic siltstone of the Callanna Group (Fabris et al., 2005). The Curdimurka Subgroup is described in more detail in section 2.3.5.

2.1.2.3 The Burra Group

The Burra Group is divided into four subgroups; the Emeroo Subgroup, the Mundallio Subgroup, the Bungarider Subgroup and the Belair Subgroup (Figure 2.2: Preiss, 1987; Preiss and Cowley, 1999). All are Torrensian in age except for the Belair Subgroup which is lowest Sturtian. The division of the Burra Group broadly reflects a gradual deepening of the basin; from the clastic Emeroo Subgroup through the carbonate-dominant Mundallio Subgroup, mainly represented by the Skillogalee Dolomite, to the shale and siltstone of the Bungarider Subgroup. The Belair Subgroup has a coarse-grained clastic unit at its base, overlain by a finer-grained clastic unit and records the final shallowing of the basin at this time. All subgroups are widespread except for the Belair Subgroup, which is limited to the southern Adelaide Fold Belt (Preiss, 1987; Preiss and Cowley, 1999). Preiss (1993) suggests that the limited occurrence of the Belair Subgroup may be due to its erosion prior to deposition of the Umberatana Group in the northern Flinders Ranges. The acid to basic Boucaut Volcanics have been dated as 777 ± 7 Ma (quoted as a personal communication from Preiss, 1998, Foden and Barovich, 2000). Fanning and Link (2008) suggested that this date is unreliable but no reason is given as to why. They crop out in two occurrences in the southern part of the Olary Region. Based on structural associations, Forbes (1978) suggested that they are older than the Burra Group but Preiss (1987) placed them near the base of the Emeroo Subgroup. Undated basalt flows interbedded with sandstone of the Emeroo Subgroup have been intersected in drill core in the Port Pirie region (Cowley and Parker, 1987; Parker et al., 1990).

A U-Pb age of 797 ± 5 Ma has been published recently (in a South Australian Geological Survey Report Book) for a porphyry interpreted to intrude the Skillogalee Dolomite at the Burra Copper mine (Drexel, 2009; Reid, 2009). The dated porphyry sample was from one of five pods that were mapped over 30 m, with the maximum thickness being two metres (Drexel, 2009). Previously the pods had been interpreted to have intruded the Skillogalee Dolomite after the Delamerian Orogeny. As this date contradicts much of the earlier dating,

it is addressed here. To do so requires some mention of conclusions from this study, and the chapters from where those conclusions are drawn are given.

As both the intrusion into the Skillogalee Dolomite and the Rook Tuff are based on intrusive rocks, in both cases, presumably shallow intrusives, it may be concluded that both ages are correct, but it does not follow that the Skillogalee Dolomite and the Rook Tuff are the same age; only that they were intruded by felsic volcanics at the same time. This means that the entire Curdimurka Subgroup and Emeroo Subgroup of the Burra group are somewhat older than 800 Ma. If the age correlation of the Wooltana Subgroup with the Gairdner Dyke Swarm is correct, then about 6 - 8,000 m of sediments were deposited in about 27 million years, at a rate of about 1,000 m per 4 – 4.5 million years. Not only that, two periods of extension are required to occur in that time. On the other hand, if the correlation is incorrect, then there is no way of knowing how old the Callanna Group is, except to say that it is older than about 800 Ma.

The second possibility is that they are indeed volcanic, with shallow intrusive intruding into newly deposited sediments. If this is the case, then the Rook Tuff and rocks of the Curdimurka Sub-group correlate with the upper Skillogalee Dolomite and the Myrtle Springs Formation. In the Willouran Range area, one of the distinguishing features of the Skillogalee Dolomite is the abundant magnesite layers (e.g., Belperio, 1990; Franks, 2004). Nowhere is magnesite seen in the Curdimurka Subgroup. The Emeroo Subgroup may then be equivalent to the Dome Sandstone. It is clear from detrital zircon spectra that these rocks have seen different sediment source areas and have received different proportions of material from the source areas (Chapter 4). Field observations show that the contact between the Curdimurka Subgroup and Burra Group are always faulted (Chapters 8 and 9) and so the juxtaposition could be purely structural. In the case of the Boorloo Siltstone this would require about 4,000 m of vertical movement on a reverse fault. Although this could explain the spatial relationship between the Boorloo Dolomite and Emeroo Subgroup, the timing of the movement would be during the deposition of the Umberatana Group. This would require north-directed thrusting, field evidence shows that the main movement in the Willouran Trough at this time was to the southeast, controlled by movement on a decollement at the base of the Dome Sandstone. There is late, north-directed movement on some faults, but overall this movement is of the order of ten’s to hundred of metres at most; not the 4,000 m required. On the southwestern margin of the Euchre Pack Domain, the Skillogalee Dolomite is in contact with the Boorloo Siltstone along what is interpreted to be a reverse fault; the Bungarider Fault. However, if the Boorloo Siltstone is younger than the Skillogalee Dolomite, this makes the Bungarider Fault a normal fault, which does not accord with the regional tectonics or structure.

Or finally, the rocks dated have not been interpreted correctly. The rocks were collected some 30 years ago, during which time the understanding of the Adelaide Fold Belt has increased greatly, particularly with regard to the origins and characteristics of the breccias. The porphyry pods are within about 30 m of the mapped edge of a diapir that contains acid volcanics clasts. Their pod-like geometry, sub-parallel to the diapir (Figure 18 of Drexel,

2009), and the lack of alteration relative to the surrounding rocks (Drexel, 2009) suggests that they may have been emplaced with the diapir, and are equivalents to the Oodla Wirra Volcanics.

Although the absolute dates are not essential to this study, a definite geochronological framework will assist in developing and discussing the evolution of the Willouran Trough. Given the doubts on the material being dated for the new Skillogalee Dolomite age, the field relationships of other similar ages and the Boucaut Volcanics age, this new age has sufficient doubt to ignore it for now. If further work does confirm the field relationships and the date; the absolute timing for deposition of the Curdimurka Subgroup may be affected but based on the field relationships, the story will not differ significantly. Unfortunately for this study, this date came out rather late in the day and so it was not possible to design or amend the study to test some of these implications.

2.1.2.4 The Umberatana Group

The Umberatana Group is divided into four subgroups; the Yudnamutana, Nepouie, Upalinna and Yerelina subgroups (Figure 2.2; Priess et al., 1998). The Yudnamutana Subgroup consists of the Sturt glaciogene sediments and are widespread throughout the Adelaide Fold Belt. It reaches a maximum thickness of 5,000 m in the Yudnamutana Trough but elsewhere it is less than 1,500 m thick (Preiss, 1987).

In the Willouran Range area, the Nepouie Sub-group has a thin conglomerate, the Serle Conglomerate at it's base, overlain by a thick fine-grained unit, the Tapley Hill Formation, with a thin coarser-grained or carbonate unit at the top (Preiss, 1987; Preiss et al., 1998). The Tapley Hill Formation represents the first major transgression across the Stuart Shelf. There is an unconformity between the Nepouie and Upalinna subgroup, and the latter consists of two transgressive-regressive packages (Preiss et al., 1998). It comprises sandstones and siltstones with minor carbonates deposited in both terrestrial and marine environments (Preiss, 1987). In the Willouran Range area, the Amberoona Formation, comprising siltstone and shale, is the main unit of the Upalinna Subgroup. The Yerelina Subgroup comprises the Elatina glacial sedimentary rocks and crops out across the Adelaide Fold Belt and onto the Stuart Shelf (Preiss, 2000).

The geochronology of the Umberatana Group is the subject of much study because of the role it has played in the development of the understanding of the Neoproterozoic (Cryogenian) glaciations. However, the absence of directly dateable volcanic material has led to the reliance on other methodologies which are open to question in terms of what is actually being dated. Much of the early dating used the whole rock Rb-Sr method (e.g., Webb, 1980; Webb and Coates, 1980; Webb et al., 1983; Compston et al., 1987; Jenkins and Cooper, 1998), which produced a series of ages from 750 ± 53 Ma for the Tapley Hill Formation to 588 ± 35 Ma for the upper Bunyeroo Formation of the Wilpena Group (see below). Broadly speaking the results produced matched the stratigraphy (i.e., stratigraphically older rocks have older ages), but with large errors. There were also concerns that the results were affected by detrital mica and feldspar (Preiss, 2000) and that the Rb-Sr ages had been

affected by a basin-wide fluid flow event at about 580 Ma (Foden et al., 2001). Kendall et al. (2006) dated black shale from the Tindelpena Shale Member (basal Tapley Hill Formation) using the whole-rock Re-Os method to give an age of 643 ± 2.4 Ma. Mahan et al. (2010) has reported an *in situ* Th-U-total Pb (electron microprobe) age of 680 ± 23 Ma for the earliest phase of authigenic monazite from the Enorama Shale (Upallina Subgroup: Figure 2.2). This sample was collected from just below the Elatina glacial rocks and so is about two kilometres above the Tindelpina Shale dated by Kendall et al. (2006). There are questions on whether whole rock Re-Os ages are reset by basinal fluid flow (Kendall et al., 2009; Mahan et al., 2010). Interpretation of monazite ages is complex due to: Pb-loss, which will result in young ages; dissolution and reprecipitation of monazite; analyses of overlapping age domains; and episodic monazite growth (e.g., Townsend et al., 2000; Catlos et al., 2002; Kelsey et al., 2003). The date given by Mahan et al. (2010), being older than that of the Tindelpina Shale (and therefore older than the depositional age of the Enorama Shale according the the date of Kendall et al., 2006), may reflect mixing of monazite age domains (e.g., Catlos et al., 2002; Williams et al., 2006) or incomplete re-setting of detrital monazite (e.g., Ayers et al., 1999; Catlos et al., 2002). Fanning and Link (2008) have presented a U-Pb zircon age of 659 ± 6 Ma for a Sturt interglacial volcanoclastic (they do not report where within the Yudnamutana Subgrop the sample was collected), which supports the Re-Os age of Kendall et al (2006) for the Tindelpina Shale.

Outside of the Adelaide Fold Belt but still within Australia, Kendall et al. (2006) reported a whole rock Re-Os age for the Aralka Formation of the Amadeus Basin (correlated with the Tapley Hill Formation) of 657 ± 2 Ma, which supports their Tindelpina Shale age. Kendall et al. (2009) reported a whole rock Re-Os age of 640.7 ± 4.7 Ma from black shales in the upper Black River Dolomite of northwestern Tasmania. This provides a minimum age for the diamictite-bearing unit Julius River Member of the Togari Group, and is within error of the whole-rock Re-Os age from the Tindelpina Shale (Kendall et al., 2006, 2009). Calver et al. (2004) reported an age of 582.1 ± 4.1 Ma for a rhyodacite unit immediately below the Croles Hill Diamictite in northwestern Tasmania. Calver et al. (2004) and Hoffman et al. (2009) suggested that this unit was deposited in a mid-Ediacaran glacial event which includes the Gaskiers glaciation of eastern Canada, which is not recorded in the Adelaide Fold Belt. But they also conceded that it may be of wholly volcanic origin or was deposited from a (volcanic) mountain glacier (Hoffman et al., 2009).

There has been debate on the global correlation of the Neoproterozoic glaciations, and their number (e.g., Hoffman et al., 1998; Kennedy et al., 1998; Lund et al., 2003; Zhou et al., 2004; Fanning and Link, 2008). For the Sturt glaciation, a broad although not wholly accepted concensus appears to have been reached that the glacial events around the world were diachronous and therefore cannot be correlated with confidence. The maximum age reported is from a tuffaceous horizon from the lowest glaciogenic unit in the Huqf Supergroup, Oman was dated at 723 +16/-10 Ma (U – Pb zircon age, Brasier et al. 2000), although from more recent analysis, a slightly younger age of about 712 Ma is suggested by Allen et al., (2002) and Kilner et al., (2005). Fanning and Link (2008) concluded that

the Sturt glacial section of the Pocatello Formation in Idaho has a maximum age (based on dates from felsic volcanic clasts) of 701 ± 4 Ma and a youngest age of 667 ± 5 Ma. Zhou et al. (2004) report a U- Pb zircon age of 663 ± 4 Ma for a tuffaceous unit overlying glaciogenic sediments in South China. Hence, despite the diachronicity of the Sturt glacials, in the absence more precise dating from the Adelaide Fold Belt, the maximum age of the Yudnamutana Subgroup may be as old as 723 Ma and the better constrained youngest age is about 643 Ma.

Hoffmann et al (2004) derived a U – Pb zircon age of 635.5 ± 1.2 Ma for an ash layer that is interbedded with diamictites in the Ghaub Formation (Namibia). They interpreted this age to be a maximum age of the Ghaub glaciations and equivalent world-wide. Condon et al. (2005) reported a date of 635.2 ± 0.4 Ma for the cap dolostone from the Doushantuo Formation in south China, with Zhang et al. (2008) dating the underlying diamictite at 636.3 ± 4.9 Ma. Zhang et al. (2005) reported a U – Pb zircon age of 621 ± 7 Ma from a tuff directly above the cap carbonate from the Doushantuo Formation. They attributed the glaciogenic rock below to be Elatina equivalent in age. In contrast to the Sturt glaciation, the debate on the global correlation of the cap dolomites immediately above the Elatina-equivalent glacials has reached a consensus for their contemporaneous deposition (e.g., Knoll et al., 2006). Hence the age of the cap dolomite to the Yerelina Subgroup, the Nucaleena Formation (see below) is about 635 Ma.

2.1.2.5 The Wilpena Group

The Wilpena Group (Figure 2.2) occurs throughout the Adelaide Fold Belt and unconformably overlies the Curnamona Province and the Stuart Shelf (Preiss, 1987). At the base of the Wilpena Group is the Nucaleena Formation. This thin, micritic dolomite is correlated on chemo- and litho-stratigraphic grounds with Elatina-equivalent glaciogenic cap carbonate units recognized world-wide (e.g., Kennedy, 1996; Kennedy et al., 1998; Hoffman et al., 1998; Knoll, 2000; Kennedy et al., 2001; Halverson et al., 2005). The Brachina Formation, a brown and olive, thinly bedded siltstone deposited in a shallowing upward sequence conformably overlies the Nucaleena Formation. Conformably overlying the Brachina Formation is the ABC Range Quartzite, a flaggy, thinly bedded sandstone deposited in a prograding delta complex (Preiss, 1987, 1993). The Bunyeroo Formation overlies the ABC Range Quartzite. It consists of red siltstone and shale, and contains a gritty layer with fragments of acid volcanics that are ejecta from the Lake Acraman Impact Structure in the Gawler Ranges (Williams, 1986; Gostin et al., 1986; Hill et al., 2004).

The Wonoka Formation overlies the Bunyeroo Formation. Its base cuts down through the Bunyeroo Formation in several deep (to 1.2 km) canyons, but otherwise the boundary is conformable (Preiss, 1993). The Wonoka Formation records an upward shallowing sequence from siltstone through calcareous and sandy turbidites to storm deposited shelf carbonates, with a very shallow water carbonate member at the top (Haines, 1988). Reid and Preiss (1999) included these shallow water carbonates and inter-tonguing sandstones in the overlying Bonney Sandstone which is part of the conformably overlying Pound Subgroup. It comprises clastic sediments which are the major ridge forming sandstones

of the Flinders Ranges (Preiss, 1987). Within the top member of the Pound Subgroup, the Rawnsley Quartzite, the Ediacara Member contains the Ediacaran metazoan assemblage (Sprigg, 1947; Preiss, 2000). A single detrital zircon grain from the lower part of the Rawnsley Quartzite has been dated at 556 ± 24 Ma (Preiss, 2000) provided an estimate for its maximum age. Zhang et al (2005) derived a U – Pb zircon age of 555.2 ± 6.1 Ma for a tuff unit interbedded with biostratigraphically equivalent sedimentary rocks containing Ediacaran fossils in the Doushantou Formation in southern China, giving an approximate age for that level of the stratigraphy. The top of the Rawnsley Quartzite marks the top of the Adelaidean, which is earliest Cambrian.

The rocks of the Adelaide Fold Belt are overlain by a series of rocks deposited in Cambrian basins that formed in response to a change in tectonic processes. These are from the south, the Kanmantoo Group, the Arrowie Group, the Hawker Group and the Mt Frome Group. Haines and Flottman (1998) interpreted these to have formed as foreland basins in front of the Delamerian Orogeny fold and thrust belts.

2.1.2.6 Deformation, metamorphism and intrusives.

The Adelaide Fold Belt underwent basin inversion in the the latest Early Cambrian to the Late Cambrian (about 515 Ma to 490 Ma) Delamerian Orogeny (Thomson, 1969; Preiss, 2000). Marshak and Flottman (1996) and Preiss (2000) observed that in those areas where there is no evidence of the Callanna Group being present, the deformation was thick-skinned whereas in those areas where there are diapirs or other evidence of the Callanna Group, the deformation was thin-skinned, although Paul et al. (1999) showed that this is not so in the Northern Flinders Zone.

The Delamerian Orogeny was initiated when the palaeo-Pacific margin of Australia changed from a passive to a convergent margin, with west-directed subduction and accretion at the continent margin (Flottman et al., 1993). In the southern Adelaide Fold Belt, the collision caused northwest directed thrusting, with the development of a fold-thrust belt in the Nackara Arc. Interaction between the developing fold belt with the southeast corner of the Gawler Craton and the deposition of the Kanmantoo Group caused a regional change in the shortening direction to NNW (Marshak and Flottman, 1996). Coward (1976) considered that the regional pattern of folds in the Nackara Arc was formed as an over-printing of northwest - southeast directed sinstral shear zone on originally northeast southwest trending fold axes. Sandiford et al (1998) attributed the variation in shortening between the elements of the Adelaide Fold Belt to the differing thickness of sedimentation in each element.

In the southern Adelaide Fold Belt, Manktelow (1990) identified four deformations. The major regional deformation is D_1 and Manktelow (1990) considered it to dominate the Adelaide Fold Belt as a whole. In the southern Adelaide Fold Belt, D_1 comprises a major anticline-syncline pair with their axial traces forming a broad arc, striking from north-south east of Adelaide to east-west on Kangaroo Island, defining the Fleurieu Arc. D_1 has an associated cleavage S_1 in the southern Adelaide Fold Belt (Manktelow, 1990). D_2 is seen only within limited areas. It displays a range of morphologies from a weak crenulation of

S_1 to a strong schistosity. Major D_2 folds are rare and are usually found in higher grade metamorphic zones (Manktelow, 1990, Sandiford et al., 1995). D_3 and D_4 are rarely seen and occur as crenulation cleavages. The S_3 crenulation cleavage has a consistent east to northeast trend and dip to the south (Manktelow, 1990). D_4 is only seen in the Harrogate - Kanmantoo area and has an open, kink-like crenulation overprinting S_3, with steeply dipping axial planes striking between north and northwest (Manktelow, 1990).

In the northern Flinders Zone, Paul et al. (1999) concluded that there was only one generation of folding during the Delamerian. North to south directed shortening was a result of left lateral transpression, with deformation being controlled by the inversion of former extensional faults such as the Norwest and Paralana Faults. Deformation was thick-skinned in style and resulted in shortening of 10 - 20% (Paul et al., 1999).

Berry (1978), Paul et al. (1999), Elburg et al (2002) and Dutch et al (2005) showed that the Curnamona Province was also deformed by the Delamerian Orogeny. Paul et al (1999) mapped thick-skinned Delamerian thrusting along its southern edge and Elburg et al (2002) showed that deformation within the Mt Painter Inlier was confined to shear zones and faults. These formed pathways for pegmatitic and A-type granite intrusions dated at 496 ± 2 Ma (Sm-Nd garnet-whole rock isochron), and monazite growth in shear bands formed at 485 ± 2 Ma (Elburg et al., 2002). Dutch et al (2005) concluded that shear zones in the southern Curnamona Craton formed between 517 - 497 Ma.

Deformation in the Delamerian Orogeny was accompanied by high-grade metamorphism and granite intrusion in the Fleurieu Arc. The metamorphic grade reaches granulite facies and is a Buchan-style, low pressure-high temperature metamorphism, with concentric zoning of isograds around a belt of deformed synmetamorphic intrusives (Offler and Fleming, 1968; Manktelow, 1990). Sandiford et al. (1995) showed that peak metamorphism was synchronous with D_2.

In the Arkaroola region, peak metamorphism occurred at about 490 Ma (Elburg et al., 2002). Mildren and Sandiford (1995) attributed metamorphism to an unconformity-related, high temperature-low pressure style where high heat flow basement provided the heat to metamorphose the overlying rocks. Adjacent to the basement, the metamorphic grade reaches the amphibolite facies and decreases away from the basement with isograds being roughly parallel to the basement-cover contact (Mildren and Sandiford, 1995).

In the southern Adelaide Foldbelt, the syn-tectonic Tanunda Creek Gneiss and Rathjen Gneiss were intruded at 513 ± 5 Ma (Heinisch and Foden, 2002) and 514 ± 5 Ma (Foden et al., 1999) respectively. Metamorphism in the southern Fleurieu Arc on Kangaroo Island occurred in the interval 509 Ma – 512 Ma but in the eastern Fleurieu Arc, metamorphism occurred at 498 ± 5 Ma (Webb et al., 2002).

Elburg et al (2002) dated a series of Palaeozoic igneous, metamorphic and hydrothermal events in the basement of the Mt Painter Inlier near Arkaroola. The British Empire Granite intruded at 449 ± 2 Ma (S-type) and 455 ± 4 Ma (I-type). At about the same time, quartz

and diopside-sphene veins were deposited along faults in the basement at 449 ± 4 Ma. The British Empire Granite is thought to have formed from a mix of melts sourced from a range of rock-types in the mid-crust (McLaren et al., 2002a). The Bungalina Monzonite which intrudes the Adelaide Fold Belt metasediment rocks in the Peake and Denison Inlier is considered to be Cambrian in age (Morrison and Foden, 1990).

2.1.2.7 Salt Tectonics and the Adelaide Fold Belt.

Breccias in the central Adelaide Fold Belt were first identified as diapirs in the early 1960's (e.g., Webb, 1960; Coats, 1965; Dalgarno and Johnson 1968) but discussion on their origins has continued. Other suggested origins include carbonatitic intrusions (White, 1983), tectonic brecciation (e.g., Preiss, 1987: Krieg et al., 1991; Mendis, 2002) and olistostromic sedimentation related to graben foundering (Rowlands et al., 1981). Today there is a general consensus that salt tectonics gave rise to the formation of the diapirs and breccias of much of the central and northern Adelaide Fold Belt. Early workers described many of these structures as diapirs but because this term has a specific meaning and implies a specific origin, the broader 'salt tectonic origin' is preferred here.

The first movement of salt within the central Adelaide Fold Belt has been shown to be during deposition of the early- to mid-Umberatana Group (e.g., Coates, 1973; Mount, 1975; Lemon, 1985). It continued into the Cambrian (e.g., Lemon, 1985; Dyson, 1999) with possibly some Quaternary movement (Lemon, 1985). Evidence for the timing is mainly stratigraphic, with Lemon (1985) mapping salt withdrawal basins around the margins of interpreted diapirs and Dyson (1998) mapping 'Christmas tree' diapirs within Umberatana Group rocks. In the northern Adelaide Fold Belt, salt movement has generally been considered to have begun a little earlier at the onset of deposition of the Umberatana Group and continuing into the Cambrian (Coats, 1973). Lemon (1985) suggested that diapirism may have continued into the Triassic, with the Leigh Creek Coal Measures being deposited in a salt withdrawal basin. Dyson (2004) however suggested that diapirism began within the Willouran Range area as early as during deposition of the Curdimurka Subgroup, continuing during deposition of the Burra Group.

2.2 The Willouran Trough.

Within the northern Adelaide Fold Belt is the Willouran Trough, a prominent gravity low extending from the Willouran Range to south of Lake Eyre (Figure 2.4; Preiss, 1987). Preiss (1987) identified the western margin of the Willouran Trough to be the Norwest Fault but did not explicitly identify an eastern or southern margin in his description. However, these can be inferred from Preiss (1987: Figures 95 and 96, page 264) and the eastern margin is the Muloorina Gravity Ridge. The southern margin corresponds broadly with the western trace of the Paralana Fault Zone.

The Willouran Trough records the initial northeast - southwest extension in the Adelaide Fold Belt in which Callanna Group strata were deposited (Preiss 1987). It continued to be the main depocentre in the northern Adelaide Fold Belt during the deposition of the

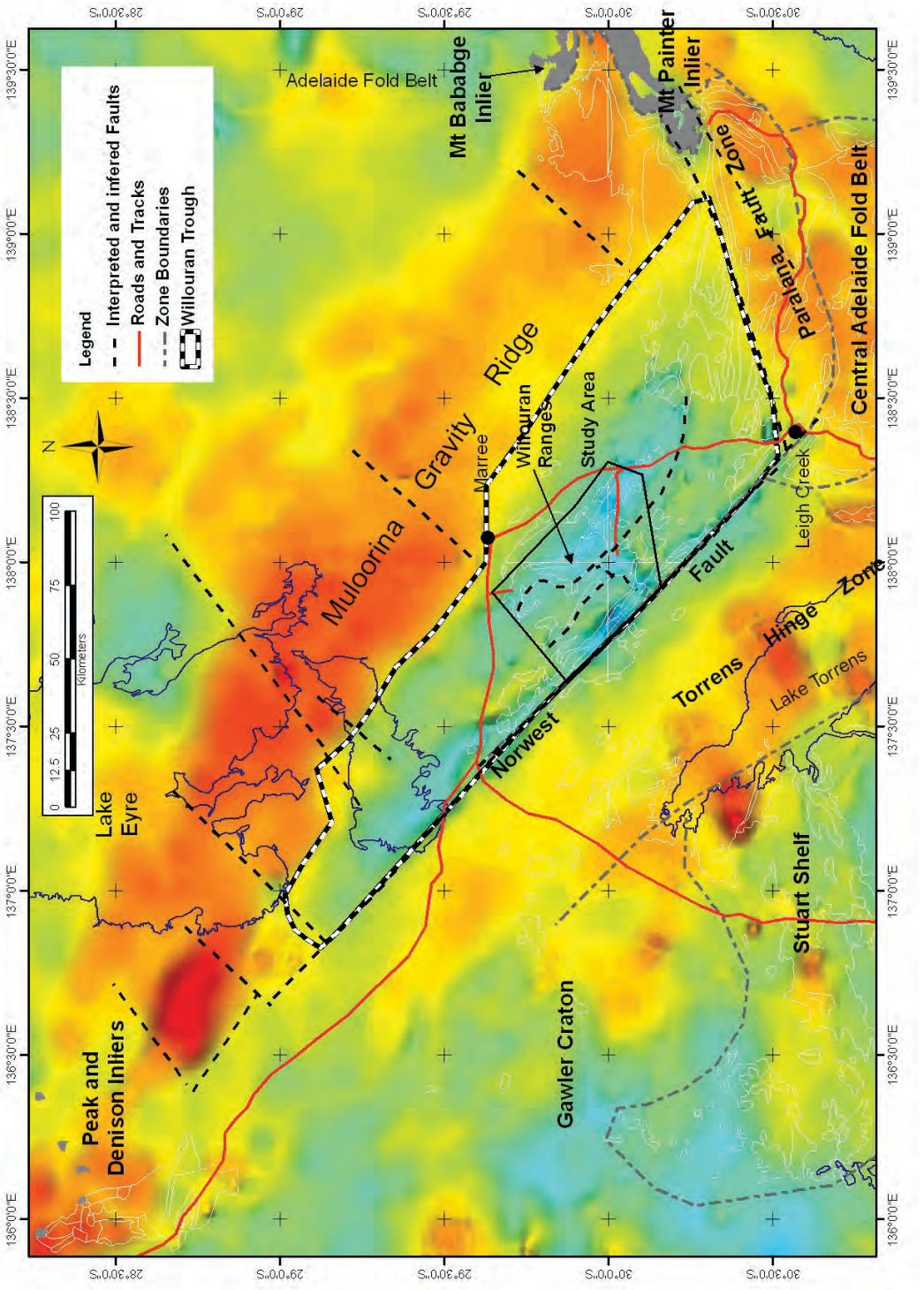

Figure 2.4. The Willouran Trough is a regional gravity low in the northern Adelaide Fold Belt (PIRSA regional gravity data set). Its boundaries are the Muloorina Gravity Ridge, the Norwest Fault and the Paralana Fault Zone. The Willouran Range provides its best outcrop.

overlying Burra Group (Paul et al., 1999). Paul et al. (1999) showed that during this time, the Norwest Fault was the major influence on the trough development but at some time sedimentation stepped beyond the margins of the trough onto the Torrens Hinge Zone. This occurred certainly during deposition of the Burra Group but possibly during deposition of the Curdimurka Subgroup (Krieg, 1992). To the east, the Muloorina Gravity Ridge likely remained a topographically positive feature in the early to mid Sturtian, but by the late Sturtian, it too began to be covered by sedimentation (Preiss, 1987; 1993). It was during deposition of the Umberatana Group that the Willouran Trough ceased to be a major depocentre, when the depocentre of the northern Adelaide Fold Belt moved east into the Yudnamutana Trough, adjacent, but at a high angle to the Paralana Fault Zone (Preiss, 1987; Paul et al., 1999).

The Willouran Trough takes its name from the Willouran Range, an area of about 60 km x 60 km which provides the most complete outcrop of the strata accumulated within the Willouran Trough (Figure 2.4). Within the Willouran Range, the Curdimurka Subgroup crops out in a series of narrow fault-bounded blocks trending northwest-southeast and north – south. The Burra Group crops out in three blocks within the Willouran Range, and west of the Norwest Fault on the Torrens Hinge Zone. The overlying Umberatana Group is thickest north and east of the Willouran Range, with a complete section occurring south and west on the Torrens Hinge Zone, and rare thin intervals within the Willouran Range. The uppermost Adelaide Fold Belt unit, the Wilpena Group does not crop out in the Willouran Range.

2.3 The Geology of the Willouran Range.

2.3.1 Introduction

The earliest geological observations in the area of the Willouran Range are those of Tate (1883), who observed east-dipping clay slates, quartzites and quartzose sandstones on the western flank of the Aroona Range, and Scoular (1886) who noted slate in the vicinity of Farina and west-dipping quartzite at the northern end of the Willouran Range in a traverse from Farina to Mt Margaret. Howchin (1924) visited the area south and southwest of Marree in 1906 noting the occurrence of Sturtian Tillite and a tillite above the Tapley Hill Formation. He also noted the presence of breccias up to six feet in thickness. Mawson (1927) published a brief report of observations made in the area during a visit in 1920.

The first detailed work was that of Sprigg (1949) who used aerial photographs to map the area between Mount Norwest and Boorloo Creek. Sprigg noted the presence of large scale high- and low-angle thrust faulting, which followed zones of weakness and are the loci of intense brecciation.

Johns (1953) published a map of the Farina Military Area, which covered the area from Termination Hill in the south to Mount Norwest in the north and Delusion Hill in the east. The mapping was mainly of a descriptive nature describing the major groups as then understood and the structure of the mapped area.

2.3.2 Modern Studies

The beginning of the modern studies in the Willouran Range is the mapping of the Callanna 1:63,360 map sheet by the South Australian Geological Survey beginning in 1960 (Webb et al., 1963). The 1:250,000 geological maps which cover the area are Marree (Forbes, 1963), Curdimurka (Daily, 1970; Krieg et al., 1991), Copley (Coats, 1973) and Andamooka (Dalgarno, 1982). All of this mapping has been largely descriptive in character, although the 1992 Curdimurka map sheet (Krieg et al., 1991; Kreig and Anthony, 1992) has benefited from more detailed mapping than the other map sheets.

The key text of Willouran Range geology is the PhD thesis of Murrell (1977). He mapped a transect from the Stuart Shelf, across the Torrens Hinge Zone and Willouran Range to Marree, examining not only the Adelaidean rocks but also the Mesozoic and Tertiary rocks. Utah Development Company (UDC) applied a sedimentological model to their exploration for copper mineralisation in the area, and as such much of their mapping had a sedimentological basis. Their reporting was of sufficient detail to provide much information on the sedimentology and their results are presented in unpublished company reports and summarized in Rowlands et al. (1980).

Following the work of UDC (Rowlands et al., 1980), and Murrell (1977), Forbes et al. (1981) defined the stratigraphy of the Curdimurka Subgroup in the Willouran Range. Parker (1983) mapped the Rischbieth Structure and and Forbes (1990) described the structure of the Willouran Range. Belperio (1990) conducted a detailed study of the Skillogalee Dolomite. Dyson (2002, 2004) examined the relationship between the Burra Group and salt tectonics in the Willouran Range.

2.3.3 Structural Domains

To simplify the discussion of the geology of the Willouran Range, the area has been divided into nine structural domains (Figure 2.5). They will be discussed more fully below. Some of these domains have long-recognised names including the Witchelina Diapir (Coates, 1973). A number of areas of Curdimurka Subgroup outcrop have been named structures, the Rischbeith Structure (Parker, 1983), the South Hill Structure and the Stony Range Structure, or sub-basins or depocentres such as the Kingston Depocentre (Belperio, 1990). Because these names have genetic connotations they are avoided here, unless they are used in a historical context. Where an existing geographic name is in general use, that name is used in naming the domain, otherwise new names pertaining to geographical features within the domains are used.

2.3.4 The Arkaroola Subgroup in the Willouran Range.

The presence of the Arkaroola Subgroup is inferred from megaclasts within breccias that occur throughout the Willouran Range (Figure 2.2). Large blocks of limestone, varying in colour from dark-grey to black were mapped by Murrell (1977) and defined by Forbes et al. (1981) as the Black Knob Marble; its type section being at Black Knob in the western Rocky Point Sub-domain. Typically these blocks are coarse-grained, highly deformed and

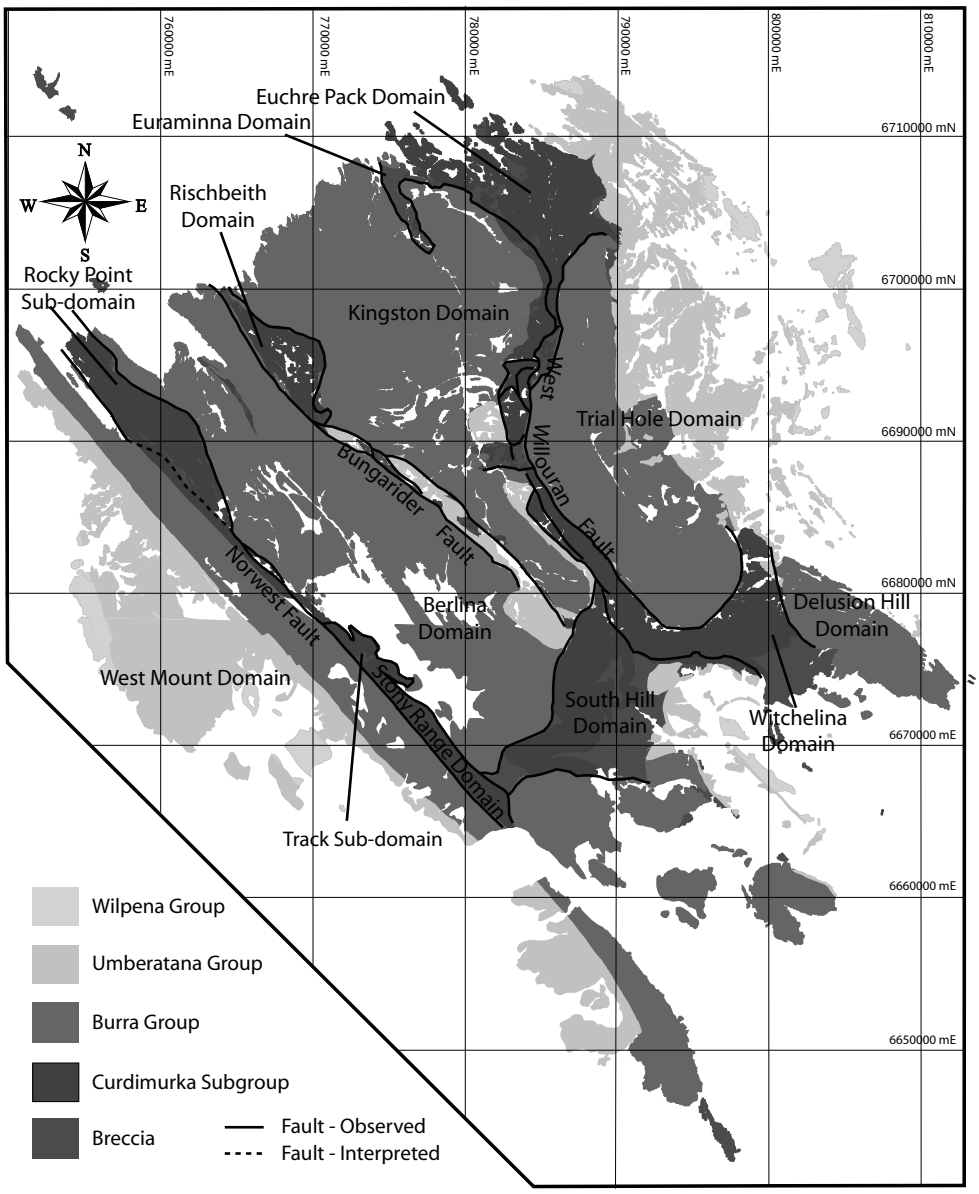

Figure 2.5. Structural domains of the Willouran Range (PIRSA 1:100,000 GIS data). There are 11 domains defined, with the domain boundaries being faults. The Rocky Point and Track sub-domains are part of the Stony Range Domain.

completely recrystallised (Figure 2.6a,b). Quoted stratigraphic thickness ranges from 25 m in the type section to over 100 m (Preiss, 1987). They have been correlated with the Wywyana Formation (Forbes et al., 1981).

Volcanic megaclasts within the breccias are correlated with the Wooltana Volcanics (Forbes et al., 1981). In the Willouran Range they are termed the Noranda Volcanics, after the Noranda Exploration base camp southwest of Marree where a megaclast of volcanics crops out (Figure 2.6c: Forbes et al., 1981). Other clasts of volcanics are mapped in the western Willouran Range and along the Bungarider Fault, where about 80 m of amygdaloidal basalt appears to have a transitional contact with sandstone tentatively attributed to the Dome Sandstone (B.G. Forbes, quoted in Preiss, 1987).

Figure 2.6. The Arkaroola Subgroup in the Willouran Range.
a) Outcrop of the Black Knob Marble in the Breaden Hill Breccia, Euchre Pack Domain. b) Typical green colour and layer-parallel deformation features of the Black Knob Marble. c) Outcrop of the Noranda Volcanics at their type locality. The top of the hill is Yudnamutana Subgroup.

2.3.5 The Curdimurka Subgroup within the Willouran Range

2.3.5.1 Introduction

The Curdimurka Subgroup crops out in a series of fault-bounded blocks within the Willouran Range (Figures 2.2, 2.7). The western-most outcrop is bounded by the Norwest Fault in the Stony Range Domain. There are a series of disjointed outcrops within and east of the Bungarider Fault zone, including the Rischbieth Domain. The largest series of outcrops occurs in the hanging wall of the West Willouran Fault, from the Euchre Pack Domain in the north to the Witchelina Domain in the south. The final major outcrop is in the northeast trending South Hill Domain.

The Euchre Pack Domain is the type area of the Curdimurka Subgroup (Figure 2.8). Here it has been divided into seven members; from the base, the Dome Sandstone, Rook Tuff,

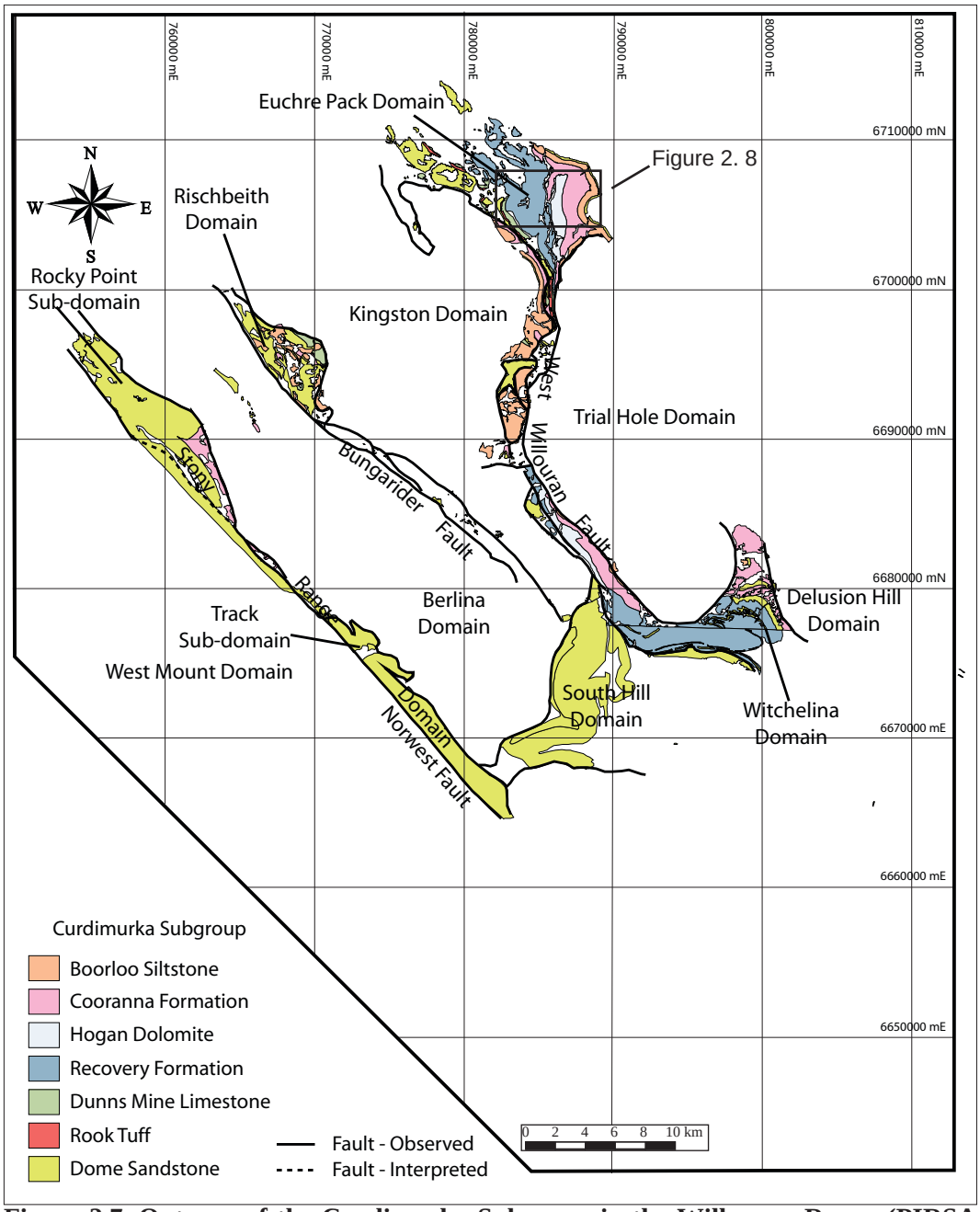

Figure 2.7. Outcrop of the Curdimurka Subgroup in the Willouran Range (PIRSA 1:100,000 GIS data).

Outcrop of the Curdimurka Subgroup is confined to the Euchre Pack, Witchelina, Rischbeith, Stony Range and South Hill domains, within the West Willouran Fault zone, and a narrow, fault-bound outcrop within the Berlina Domain.

Dunns Mine Limestone, Recovery Formation, Hogan Dolomite, Cooranna Formation and the Boorloo Dolomite (Table 2.2; Forbes et al., 1981). These divisions have been applied to outcrops along the West Willouran Fault and in the Witchelina Domain but not consistently elsewhere. In the South Hill and Stony Range domains the Curdimurka Subgroup is mapped solely as Dome Sandstone but in the Rischbeith Domain the stratigraphy is applied although with some units missing (Figure 2.7). Rowlands et al. (1980) identified a similar stratigraphy from the UDC mapping (Table 2.2).

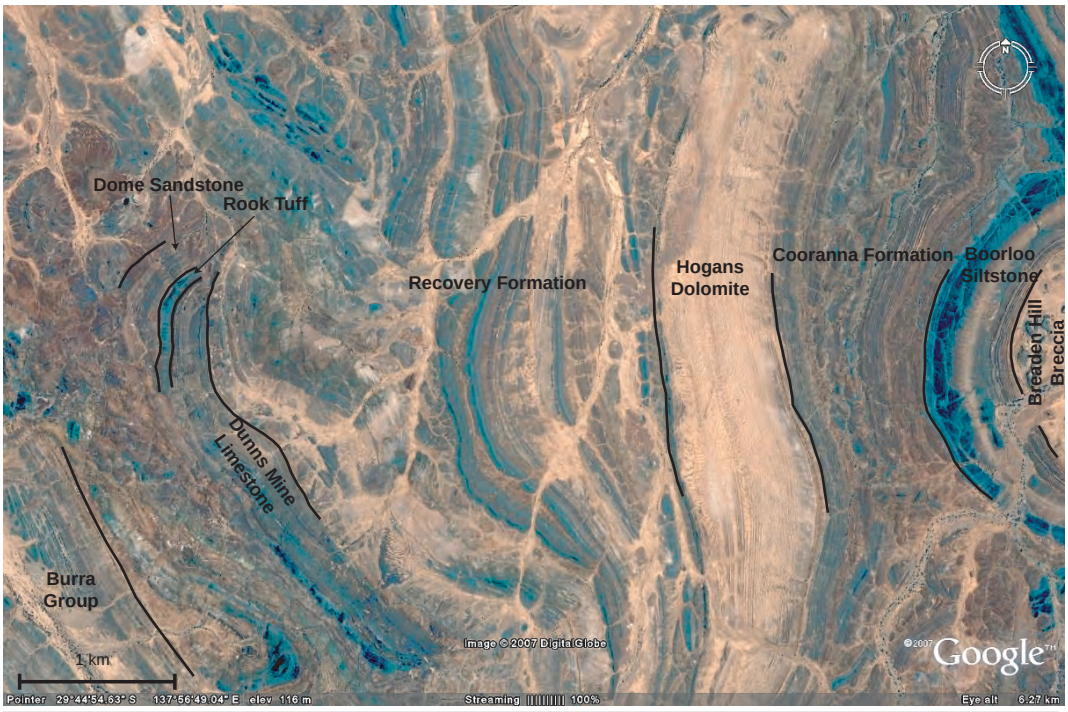

Figure 2.8. Google Earth image of the Curdimurka Subgroup in its type area, the Euchre Pack Domain.

Table 2.2. Stratigraphy of the Curdimurka Subgroup with estimated thickness at the type section. UDC nomenclature and depositional setting from Rowlands et al. (1980) and Preiss (1987).

Unit	Thickness	UDC Stratigraphy	Depositional Setting
Breaden Hill Breccia*		BS6	
Boorloo Siltstone	520 m	BS3 - BS5	Deep water to sabkha
Cooranna Formation	780 m	BS1, BS2	Supra-tidal to shoreface
Recovery Formation	2,217 m	R4	Cyclic intertidal to sub-tidal
Hogan Dolomite	650 m	R5	Intratidal
Recovery Formation	2,217 m	R4	Cyclic intertidal to sub-tidal
Un-named Breccia*		R3.5	
Dunns Mine Limestone	334 m	R3.2 – R3.4	Alkaline playa to deep water
Rook Tuff	42 m	R3.1	Off-shore marine or lacustrine
Dome Sandstone	1,480 m	R2.	Fluvial to shallow marine

Note: * UDC gave stratigraphic names to breccia units, reflecting their interpretation of the breccias as being sedimentary in origin. The acronyms refer to different prospect names used by UDC where the rocks crop out. B refers to the Boorloo area, R to the Rook area.

2.3.5.2 The Dome Sandstone

The Dome Sandstone was defined by Forbes et al., (1981) as being a prominent basal sandstone – siltstone unit of the Curdimurka Subgroup (Figure 2.2). In outcrop it typically forms rounded hills with beds of sandstone interspersed between zones of sandstone and minor silstone float (Figure 2.9a). The type-section is three kilometers southwest of Callanna Station homestead where it is at least 1,480 m thick. Its basal boundary is faulted and the upper boundary is conformable with the Rook Tuff. Murrell (1977) named the equivalent rocks the Dome Formation and Rowlands et al (1980) called the equivalent rocks the R2 unit in the Euchre Pack Domain (Table 2.2). It also occurs in the Stony Point, South Hill, Witchelina and Rischbeith Domains (Figure 2.7).

The Dome Sandstone is interpreted to have been deposited in a fluvial to shallow marine environment, possibly intertidal (Preiss, 1987). Rowlands et al (1980) concluded that the Dome Sandstone was deposited as an inter-tidal littoral-zone sand sheet.

2.3.5.3 The Rook Tuff

The Rook Tuff is described as being dark flaggy fine-grained rocks between the Dome Sandstone and Dunns Mine Limestone (Preiss, 1987). It crops out in the slopes of hills capped by either the Dome Sandstone (Figure 2.9a) or the Dunns Mine Limestone (Figure 2.9b). At its type-section it is 42 m thick but varies in thickness from 15 m to 60 m and has been mapped only in the Euchre Pack Domain (Forbes et al., 1981). The lower contact with the Dome Sandstone is gradational, but the upper contact with the Dunns Mine Limestone is sharp, with a thick massive dolomite bed of the sitting on black shale (Figure 2.9b). Fanning et al., (1986) report a SHRIMP U-Pb age of 802 ± 10 Ma from zircons taken from a lenticular porphyritic dacite from within the Rook Tuff. The depositional environment is interpreted by Preiss (1987) as being an off-shore lacustrine or marine setting (Table 2.2).

2.3.5.4 The Dunns Mine Limestone.

The Dunns Mine Limestone is defined as a prominent ridge-forming sandy carbonate sequence below the sandier Recovery Formation (Figures 2.8, 2.9a: Forbes et al., 1981). In its type-section it is 334 m thick but thins to less than 50 m about 1,500 m southeast of the type section. Its upper contact with the Recovery Formation is conformable near Dunns Mine but northwest of there, a narrow (a few metres) breccia sits along the contact. The interpreted depositional environment of the Dunns Mine Limestone is an alternating alkaline carbonate – sulphate evaporate environment, followed by sub-tidal braided channels and finally a humid phase high-stand environment (Rowlands et al., 1980).

2.3.5.5 Recovery Formation.

The Recovery Formation is defined as a thick silty to sandy sequence between Dunns Mine Limestone and Hogan Dolomite (Forbes et al., 1981: Figure 2.8). In its type section the Recovery Formation is 2,217 m thick. It comprises a range of mainly clastic sediments; quartzite, sandstone and siltstone, with minor carbonates, both dolomite and limestone. The upper contact with the Hogan Dolomite is conformable, but sharp with a thick limestone unit at the base of the overlying unit. Forbes et al. (1981) estimated an overall shale content

of 45% within the Recovery Formation. It is interpreted to have been deposited in cyclic intertidal to subtidal environment (Table 2.2; Rowlands et al., 1980).

2.3.5.6 The Hogan Dolomite.

The Hogan Dolomite is defined as poorly outcropping dolomite beds forming a plain between prominent narrow ridges of the lowermost and uppermost dolomite members (Forbes et al., 1981: Figure 2.9c). Its upper contact with the Cooranna Formation does not crop out well but is gradational and conformable. It is interpreted to have been deposited in an intratidal environment (Table 2.2; Rowlands et al., 1980).

2.3.5.7 The Cooranna Formation.

The Cooranna Formation is a thick sequence of mixed lithologies lying between the more distinctive Hogan Dolomite and Boorloo Siltstone (Forbes et al., 1981: Figure 2.9d). It comprises a series of fine-grained sandstone, siltstone, limestone and dolomite units; typically interbedded but occurring in units where either clastic or carbonate units are dominant. The upper contact with the Boorloo Siltstone is gradational and conformable, and mainly marked by a change in colour. Rowlands et al. (1980) interpreted the depositional environment to have ranged from deeper water to supratidal (Table 2.2).

2.3.5.8 The Boorloo Siltstone.

The Boorloo Siltstone is defined as a distinctively layered dark siltstone and dolomite sequence at the top of the less disturbed beds of the Callanna Group (Forbes et al., 1981). It is up to 520 m thick and comprises light- to dark-grey siltstone with an upper unit to about 150 m thick of interbedded carbonate and grey-green siltstone (Forbes et al., 1981). Within the siltstone unit is a narrow (less than five metres) dolomitic unit towards the base and, fine-grained sandstone unit (less than 10 metres thick) at about the middle of the unit. The upper contact is structural, with a breccia overlying it in the northern half of the Euchre Pack Domain and a faulted contact with the Burra Group in the southern half. It is interpreted to have been deposited in a deep water lagoonal environement, shallowing upward to a high intertidal mudflat fringing a playa or sabkha depocentre to a prograding sabkha (Table 2.2; Rowlands et al., 1980).

2.3.6 The Burra Group.

The Burra Group in the Willouran Range has been discussed in the context of wider studies by Murrell (1977), Parker (1983), Preiss (1987, 1993), Forbes (1990) and Kreig et al. (1991). There has been only the one study, Belperio (1990), that concentrated on the Burra Group and this was focused on the Skillogalee Dolomite (Mundallio Subgroup).

Three subgroups of the Burra Group crop out in the Willouran Range; the Emeroo, Mundallio and Bungarider subgroups (Figures 2.2, 2.10: Priess, 1987; Preiss et al., 1999). The Emeroo Subgroup is primarily a clastic unit, comprising sandstone, siltstone with minor conglomerate limestone and shale. It consists of three formations, the Top Mount Sandstone, the Willawalpa Formation and the Witchelina Quartzite, which are all present in the Trial Hole Domain (Figure 2.11a), or is correlated with the Copley Quartzite in the

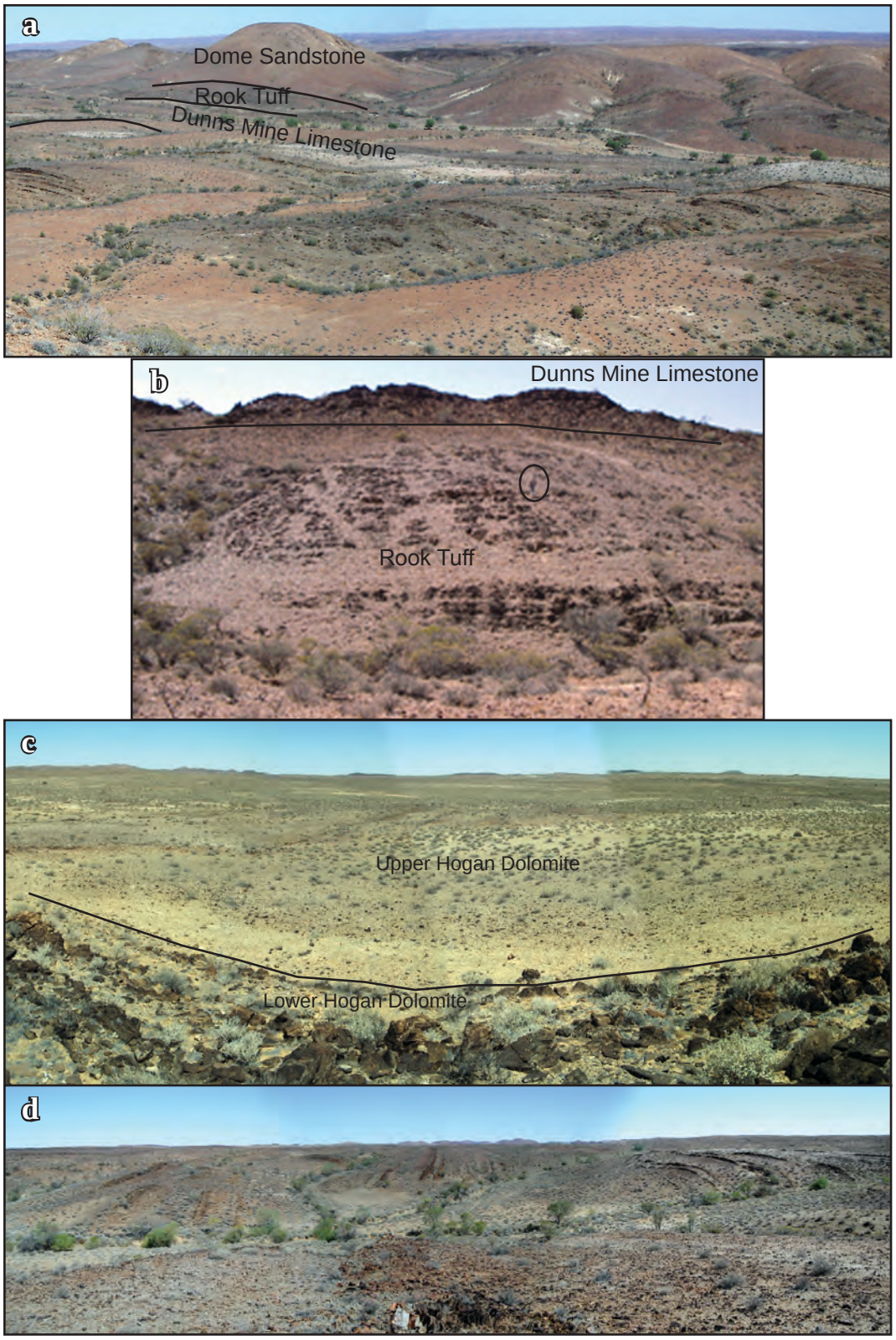

Figure 2.9. Outcrop of the Curdimurka Subgroup, Euchre Pack Domain.
a) Outcrop of the Dome Sandstone. It typically forms rounded strike ridges shown here. b) The Rook Tuff and basal Dunns Mine Limestone outcrop on this hill side (field assistant, circled, for scale). c) A panorama view (the contact between the Upper and Lower Hogan Dolomite is straight) of the Hogan Dolomite at its northern-most outcrop standing on the Lower Hogan Dolomite which crops out prominently, looking across the Upper Hogan Dolomite, which crops out poorly. d) Typical outcrop of the basal Cooranna Formation. The dark narrow ridges are dolomite within siltstone-shale dominated units.

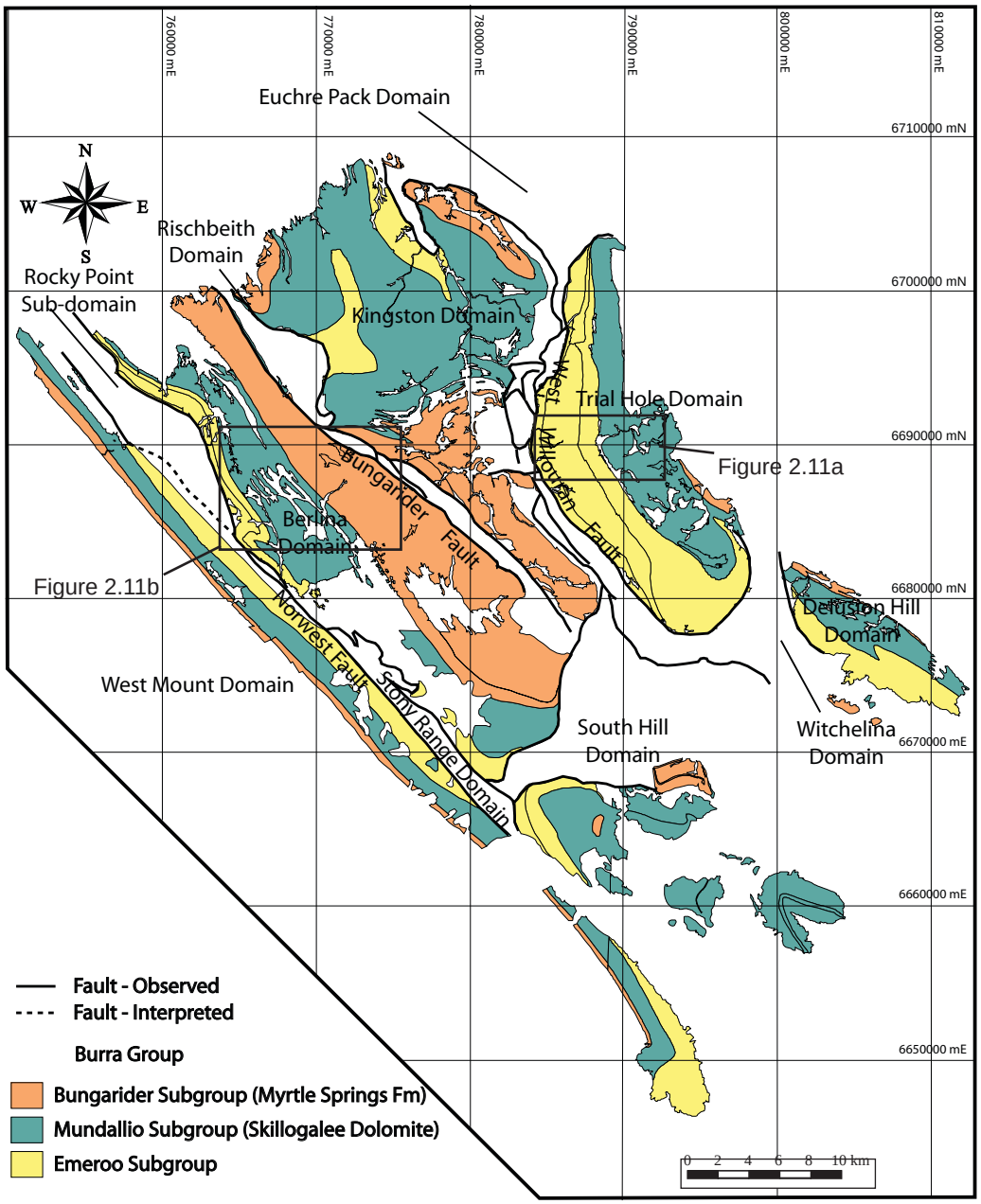

Figure 2.10. Outcrop of the Burra Group in the Willouran Range.

Leigh Creek 1:250,000 geological map sheet or is not sub-divided (Forbes, 1963; Coats, 1973; Dalgarno, 1982; Kreig et al., 1991). The estimated thickness of the Emeroo Subgroup varies from over 4,000 m in the Trial Hole Domain to about 200 m in the West Mount Domain.

The Mundallio Subgroup in the Willouran Range consists only of the Skillogalee Dolomite (Figure 2.11b,c,d). Belperio (1990) showed that it contains varying proportions of dolomite, magnesite, sandstone and siltstone. The proportion of sandstone decreases and carbonate increases from east to west. A distinctive feature is the presence of well-bedded magnesite units in the Kingston and Berlina Domains. It reaches a maximum thickness of about 4,000 m in the Kingston Domain. Franks and Fielding (2003) reported shortite pseudomorphs

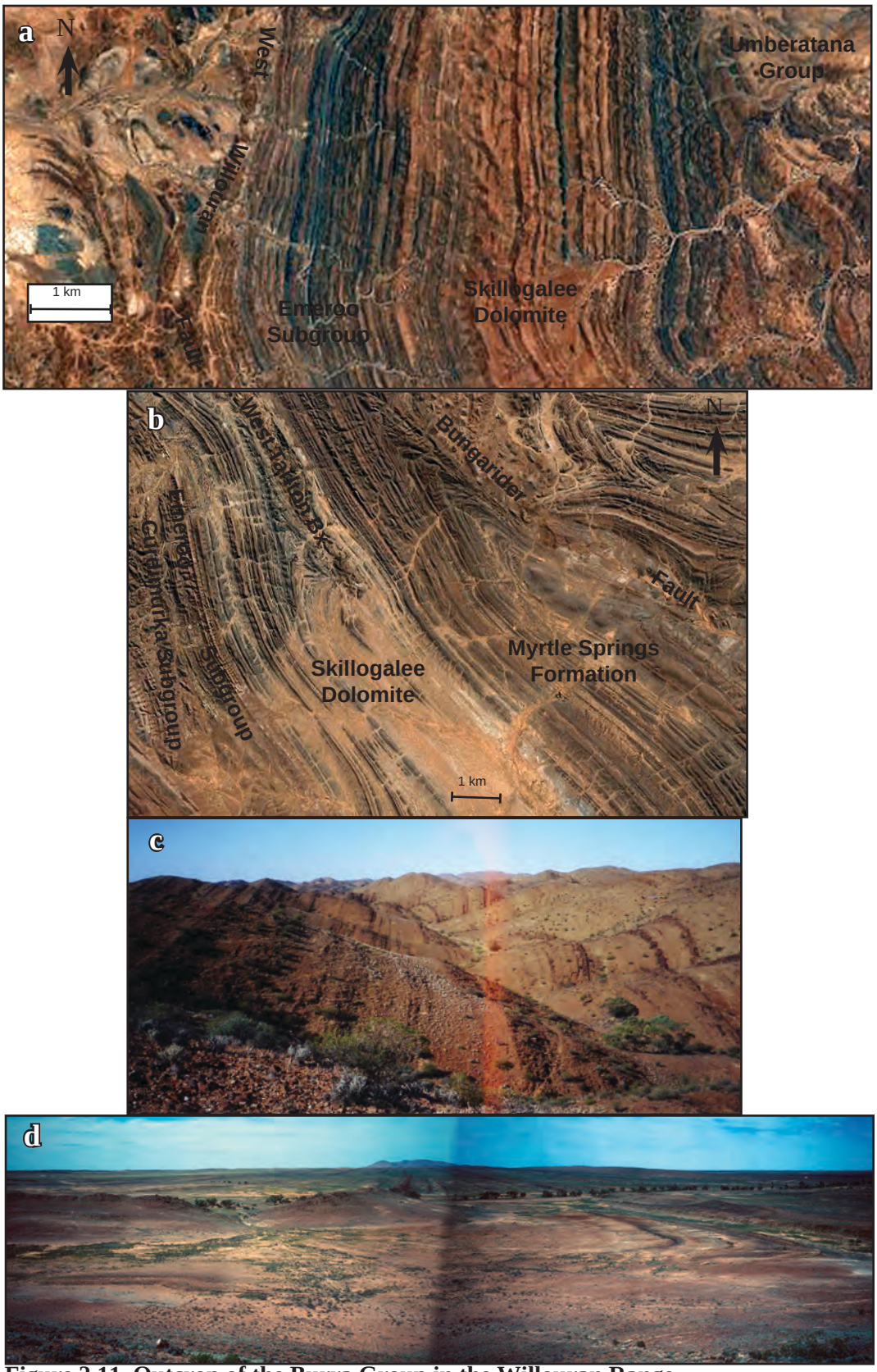

Figure 2.11. Outcrop of the Burra Group in the Willouran Range.
a)The Burra Group in the Trial Hole Domain. b) The Burra Group in the Berlina Domain. c) The Skillogalee Dolomite in the Trial Hole Domain. d) The Skillogalee Dolomite south of the South Hill Domain. The differnces in the outcrop of the Burra Group from the Trial Hole Domain to other domains reflects the greater amount of clastic rocks in the former, including within the Skillogalee Dolomite (Belperio, 1990).

within the Skillogalee Dolomite and suggested that it was deposited in a marine environment with the sea having an alkaline chemistry.

The Bungarider Subgroup in the Willouran Range consists of the Myrtle Springs Formation and an un-named unit (Preiss, 1987; Preiss and Cowley, 1999). It is thickest in the Berlina Domain where it reaches a maximum thickness of 3,000 m and absent from the northern three quarters of the Trial Hole Domain (Figure 2.10).

Belperio (1990) measured sections across the Skillogalee Dolomite, and estimated the true thickness of the Emeroo Subgroup and Myrtle Springs Formation. His figures show that the Emeroo Subgroup is thickest in the Trial Hole Domain, and both the Skillogalee Dolomite and the Myrtle Springs Formation are thickest in the Berlina Domain. Belperio (1990) suggested that the Burra Group was deposited within a series of northwest - southeast trending fault bounded sub-basins, reflected in the present day distribution. Preiss (1987) and Dyson (2002, 2004) concluded that the Burra Group in the Trial Hole Domain was deposited within a salt withdrawal basin.

2.3.7 The Umberatana Group.

The Umberatana Group consists of the Yudnamutana, Nepouie, Upalinna and Yerelina subgroups (Figure 2.2, Preiss et al., 1998). Murrell (1977) conducted the most detailed study of the Umberatana Group in the Willouran Range as part of his PhD and Rayner and Rowlands (1980) discussed it in the northeast of the Willouran Range. Selley and Bull (2002) studied the Umberatana Group in the northeast and the centre of the Willouran Range. It crops out extensively to the west and east of the Willouran Range, and in three smaller areas within the range (Figure 2.12).

The Yudnamutana Subgroup consists of all the Sturtian glacial deposits. In the Willouran Range at any one locality there is only one glacial unit although it is variously named the Bolla Bollanna Tillite (Curdimurka 1;250,000 geological maps, Kreig and Anthony, 1992), the Apilla Tillite (Andamooka geological map sheet) and the Wilyerpa Formation (Marree 1:250,000 geological map sheet) (Preiss, 1987: Krieg et al., 1991; Preiss et al., 1998). It crops out in the Norwest, Trial Hole, Kingston and Berlina Domains. In all of these areas, its thickness is highly variable ranging from 0 m (i.e. removed by erosion during deposition of later Umberatana Group rocks) to 1080 m in the West Mount Domain. Within the Willouran Range, it reaches a maximum thickness of about 200 m in the Kingston Domain and northeast of the Euchre Pack Domain (Murrell, 1977). It comprises diamictite, siltstone and arkose. Adjacent to the Bungarider and the West Willouran Faults, the lower contact is a moderate to high angle unconformity with the Burra Group (Figure 2.13b: Murrell, 1977; Krieg et al, 1991; Selley and Bull, 2002).

The Nepouie Subgroup comprises the Serle Conglomerate and overlying Tapley Hill Formation. The Serle Conglomerate is a pebbly arkosic quartzite and crops out only in the Trial Hole Domain (Preiss, 1987; Krieg et al., 1991). The Tapley Hill Formation consists predominantly of thinly laminated grey and black silty shale (Murrell, 1977; Preiss, 1987),

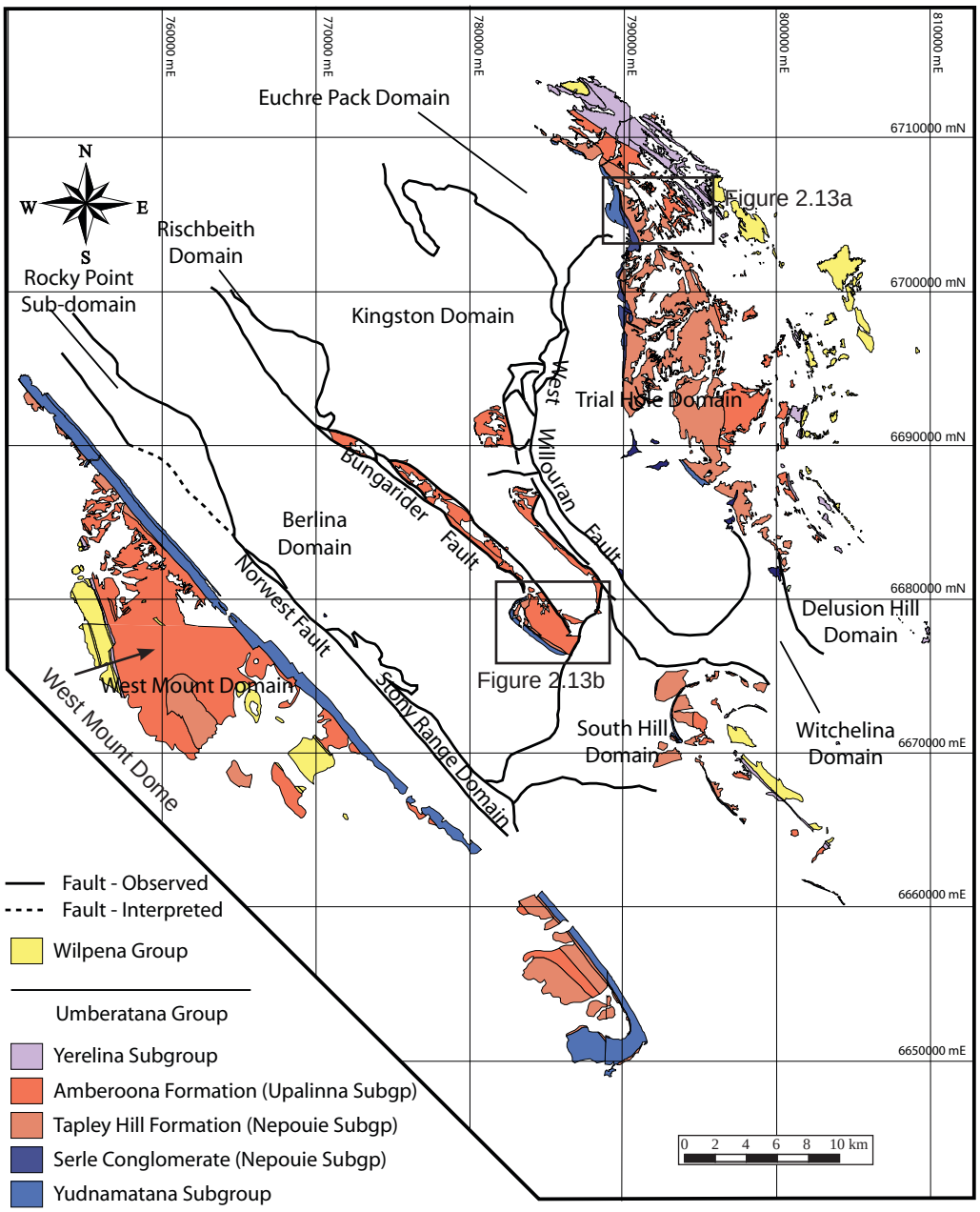

Figure 2.12. Outcrop of the Umberatana and Wilpena Groups in the Willouran Range (PIRSA 1:100,000 GIS data).

although Rayner and Rowlands (1980) and Selley and Bull (2002) mapped a number of conglomerate and sedimentary breccia beds within the unit north of the Euchre Pack Domain. In the West Mount Domain, the Tapley Hill Formation reaches a maximum thickness of 720 m, but has been removed on the eastern limb of West Mount Dome (Figure 2.12). It is thickest north of the Euchre Pack Domain (Figure 2.13a) to the Delusion Hill Domain, reaching an estimated 1,300 m thickness but within the Willouran Range, it is less than 300 m thick (Figure 2.13b; Murrell, 1977).

The Upalinna Subgroup in the Willouran Range area comprises the Amberoona and Etina formations and the Enorama Shale although Preiss et al. (1998) considered the Enorama Shale to be a lateral equivalent of the Amberoona Formation. The Amberoona Formation is mainly grey to green siltstone and shaley siltstone, with sedimentary breccia beds

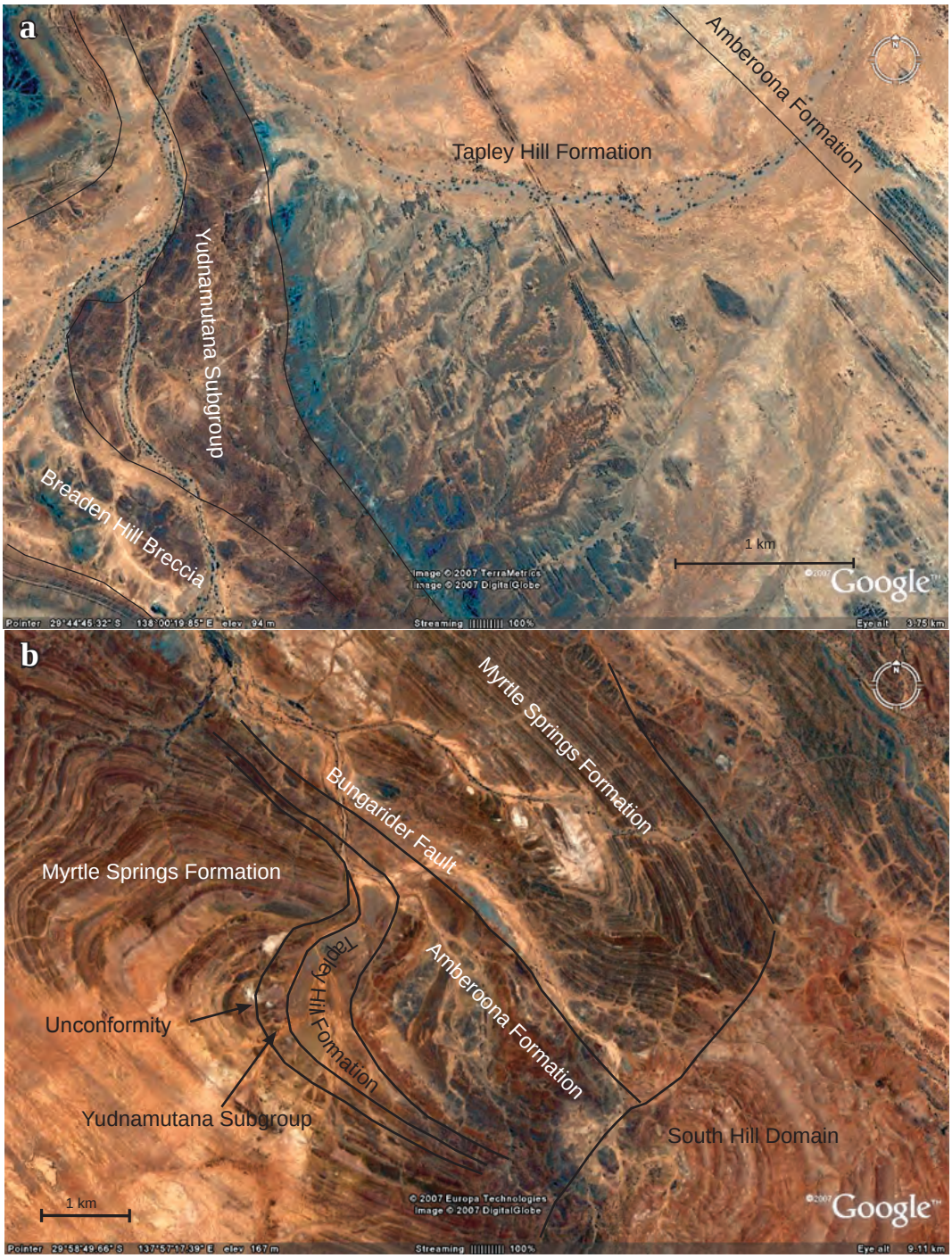

Figure 2.13. Outcrop of the Umberatana Group in the Willouran Range.
a). Outcrop of the Umberatana Group east of the Euchre Pack Domain, from the Yudnamutana Sub-group to the Amberoona Formation. b) Outcrop within the Berlina Domain, showing the thinTapley Hill and Amberoona Formations, and the unconformable contact with the underlying Burra Group.

mapped in the West Mount Domain and in the Kingston Domain (Murrell, 1977; Coats and Dalgarno, 1983; Selley and Bull, 2002). It crops out in the West Mount Domain, where its lower contact cuts down through the Tapley Hill Formation and Yudnamutana Subgroup to the Burra Group (Murrell, 1977). In the Berlina Domain, Murrell (1977) mapped it sitting directly on the Burra Group, having been deposited in large scour channels that have cut down through the Tapley Hill Formation and the Yudnamutana Sub-group (Figure 2.13.

The Yerelina Subgroup crops out to the northeast and west of the Willouran Range (Figure 2.12), but is absent from the study area (Murrell, 1977; Krieg et al., 1991). It comprises the Elatina-equivalent glacial deposits of the Fortress Hill Formation and Mount Curtis Tillite.

2.4 Breccias

Howchin (1926) and Mawson (1927) were the first workers to report on the breccias that crop out in the Willouran Range. There has been much discussion regarding the origins of the breccias but the majority of writers favour a diapiric origin. (e.g., Webb, 1960; Dalgarno and Johnson, 1968; Mount, 1975, 1983; Burns et al., 1977; Lemon, 1985; Dyson, 1998).

Within the Willouran Range, there are numerous breccia bodies that have been identified, the largest being the Witchelina Diapir (here used in the historical sense, Figure 2.14). Clast size ranges up to the kilometre scale, with megaclasts of Callanna Group sediments and volcanics (Parker, 1983; Krieg et al., 1992: Figure 2.15a,b, 2.16). Intrusive igneous rocks are also present within the breccia bodies, most of which pre-date the brecciation (Preiss, 2000). Parker (1983) recognised quartzite, sandy dolomite and slaty shales of the Callanna Group within the Rischbieth Domain, which had also been intruded by albitic monzonite-syenite-diorite plugs. Within the Mirra Breccia (Figure 2.14: Euramina Window of Murrell, 1977), Murrell (1977) mapped a complex of gabbroic rocks that he interpreted to be basement. Other authors suggest that they are intrusive into the breccia body (Preiss, 1987; Forbes, 1990). Sodic alteration of the igneous rocks appears to be common, leading some authors to suggest that the alteration resulted from the dissolution of primary evaporite minerals (e.g., Rowlands et al., 1981). The matrix to the breccias comprises an impure calcareous rock with sand-size and larger fragments, and sometimes containing areas of coarsely recrystallised carbonate (Dewar and Hatch, 1975). Thomas and Dunlop (1968) identified a micaceous, dolomitic and calcitic matrix within the Breaden Hill Breccia.

Three main interpretations of the origin of the breccias have been suggested; decollement structures associated with thrusting (Sprigg, 1949; Murrell, 1977), olithostromes (Rowlands et al., 1980) and diapirs (Coates, 1973: Dewar and Hatcher, 1975; Preiss, 1987; Forbes, 1990; Belperio, 1990; Dyson 2002; 2004). Murrell (1977) concluded that brecciation occurred prior to the deposition of the Burra Group. Dyson (2004) who favoured a salt tectonic origin for the breccias concluded that salt movement (and hence breccia formation) was initiated during deposition of the Curdimurka Subgroup.

2.5 The Structure of the Willouran Range.

The Willouran Trough was initiated as a northwest trending rift zone in response to NE - SW directed extension (Preiss, 1987). However the earliest direct evidence of movment on the Norwest Fault is the deposition of the Burra Group (Murrell, 1977; Belperio, 1990; Paul et al., 1999). Belperio (1990) concluded that within the Willouran Trough, deposition of the Burra Group occurred within three sub-basins controlled by rising diapirs or salt walls

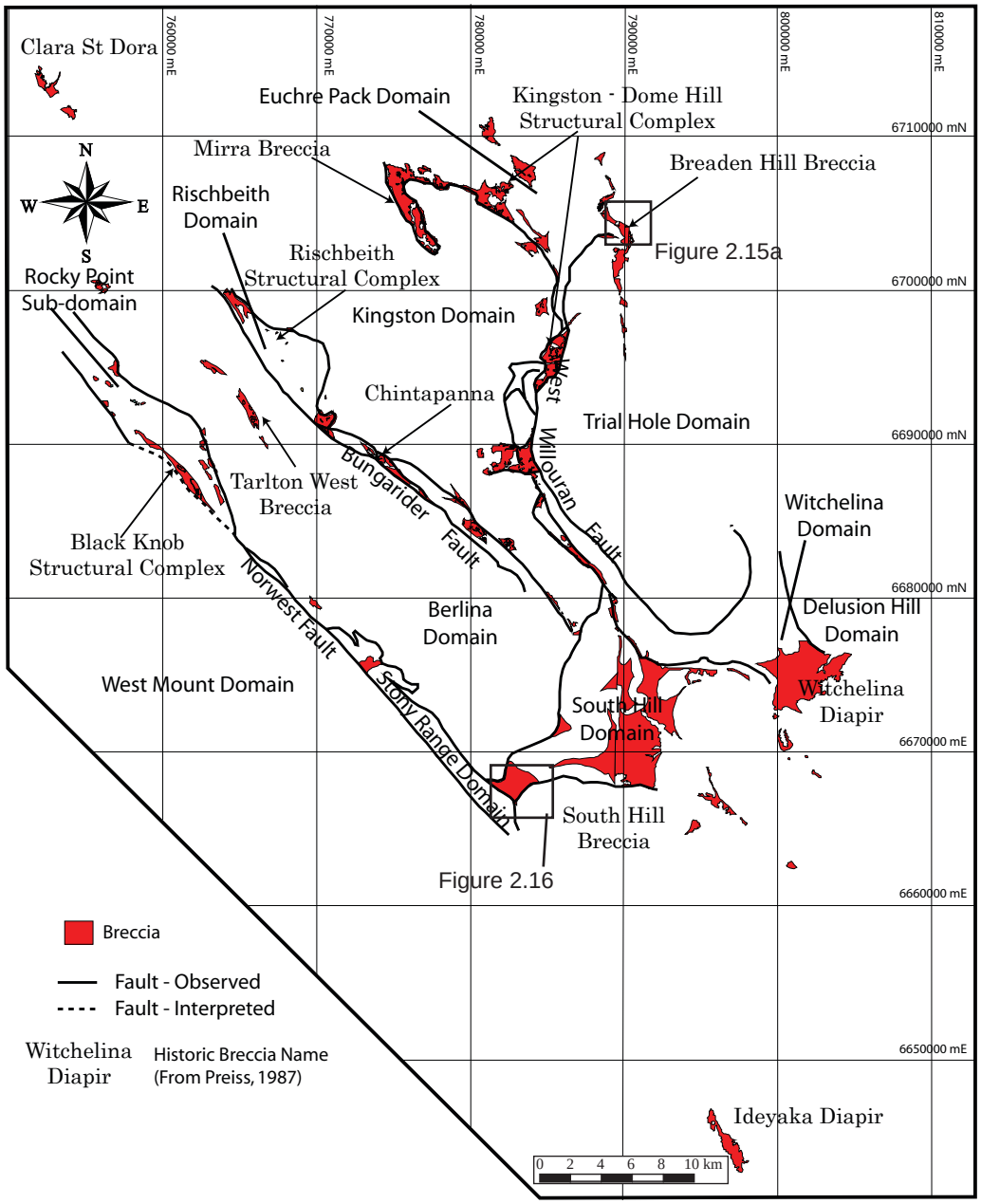

Figure 2.14. Outcrop of the breccias in the Willouran Range, showing historical names (PIRSA 1:100,000 GIS data).

in the position of the Bungarider and West Willouran faults, and that these were initiated at that time. Paul et al. (1999) showed that the Mundy Fault, on the northern side of the Willouran Trough, was active during deposition of the upper Burra Group, giving the basin a graben form at this time. During deposition of the Umberatana Group, the main locus of subsidence moved to the east, to the Yudnamutana Trough (Paul et al., 1999).

Based on differences in deformation styles between the Curdimurka Subgroup and the Burra Group, Murrell (1977) and Parker (1983) concluded that there was a deformation event between the deposition of the Curdimurka Subgroup and the Burra Group, or during the deposition of the lower Emeroo Subgroup. This deformation produced drag folds within the Curdimurka Subgroup in the Stony Range Domain that do not affect the overlying Burra Group. Murrell (1977) and Rowlands and Warrin (1979) interpreted apparent thinning of

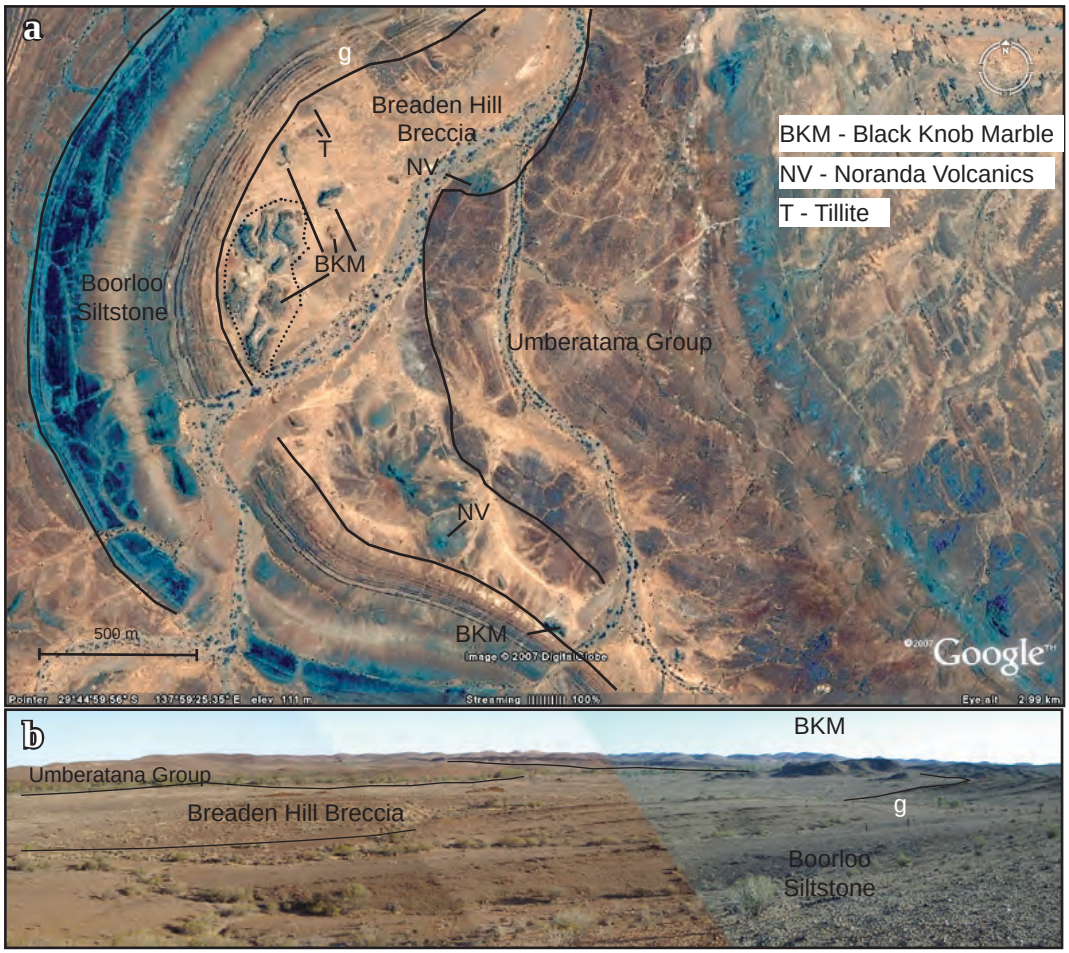

Figure 2.15 The Breaden Hill Breccia.
a) A Google Earth image of the Breaden Hill Breccia showing the Black Knob Marble (BKM), Noranda Volcanics (NV) and tillite (T). b). A panoramic view of the breccia taken from the Boorloo Siltstone, looking southeast. "g" marks the position of the same gully in both images.

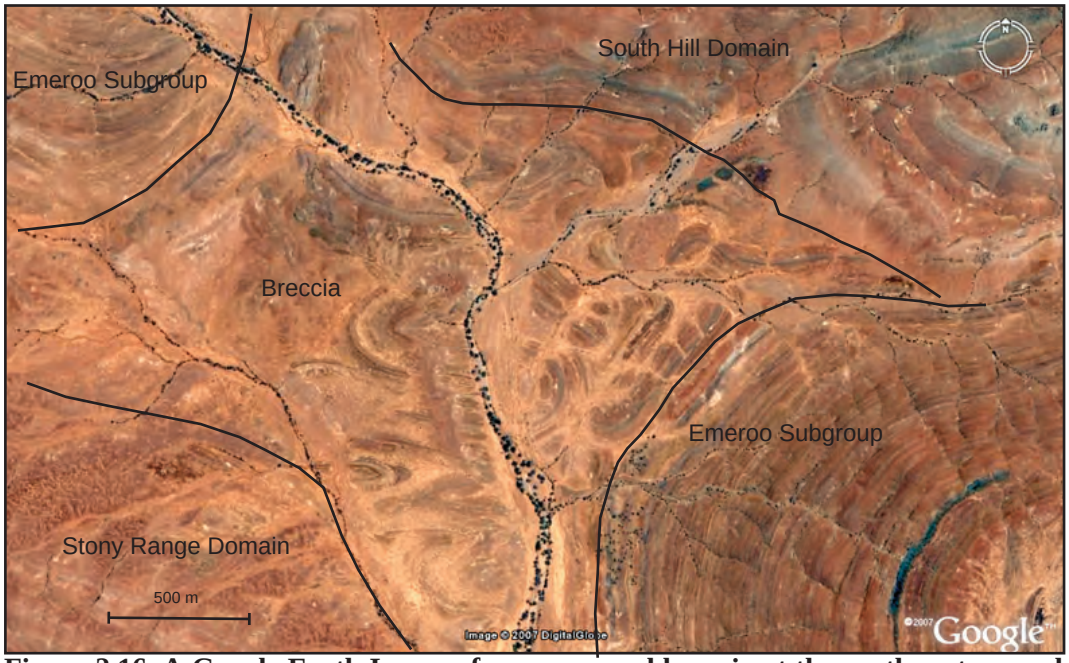

Figure 2.16. A Google Earth Image of an un-named breccia at the southwestern end of the South Hill Domain.
Unlike the Breaden Hill Breccia, this breccia is dominated by folded megaclasts with very little matrix.

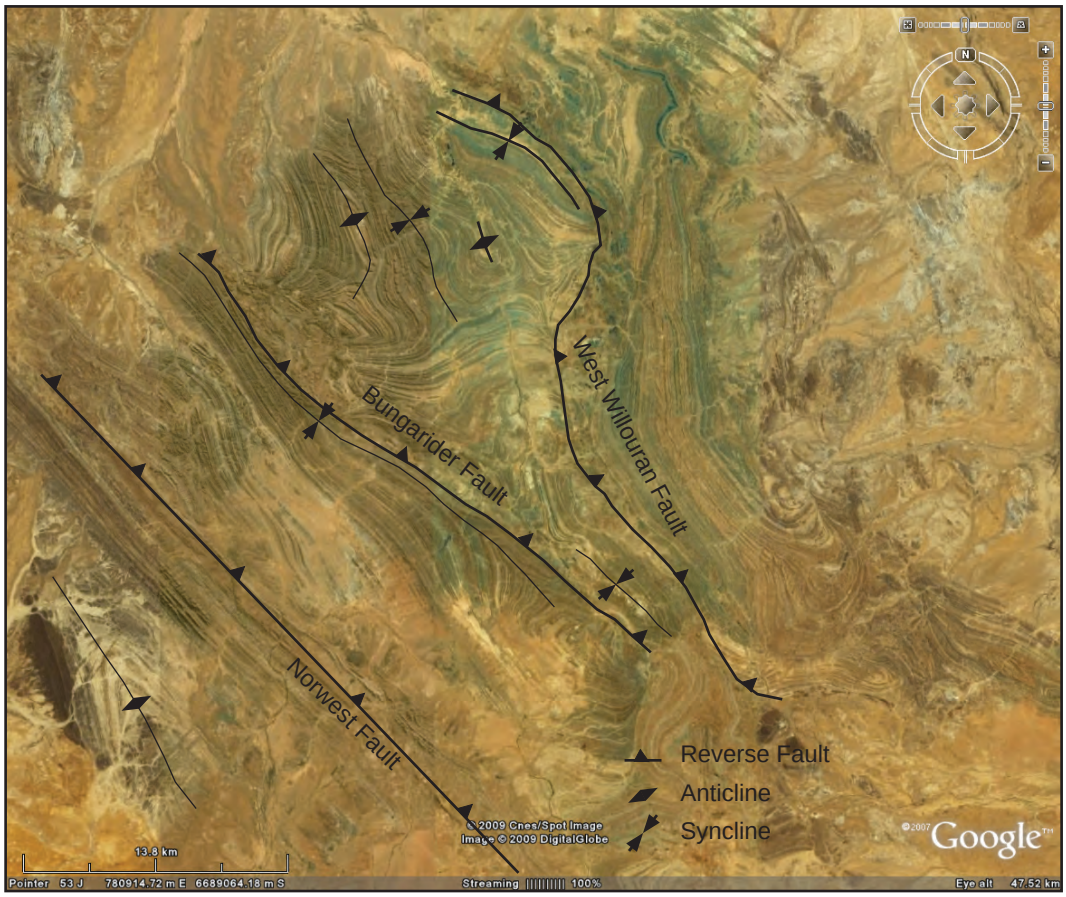

Figure 2.17. GoogleEarth image of the Willouran Range showing the main Delamerian structures.
Delamerian structures are mainly northeast dipping reverse faults and northwest trending folds.

units along the northern margin of the Rischbeith Domain as evidence that it was a horst forming either prior to or during deposition of the Burra Group. Parker (1983) suggested that there was a period of folding and thrusting prior to or during early deposition of the Burra Group, based on Delamerian folds overprinting early formed very tight to isoclinal folds in the Rischbeith Domain. He suggested that the earlier deformation resulted in east-dipping faults, indicating westward movement, with the Burra Group being deposited in front of the thrust complex to the west.

Murrell (1977) interpreted a second pre-Delamerian deformation phase between the deposition of the Burra Group and the basal Umberatana Group. It resulted in formation of a syncline to the west of the Bungarider Fault within the Burra Group, prior to deposition of the Umberatana Group, thereby implying reverse movement along the Bungarider Fault at this time (Murrell, 1977). Murrell (1977) and Selley and Bull (2002) recognized that there is a high-angle unconformity between the Burra Group and the Umberatana Group, in the Chintapanna area. Murrell (1977) inferred this to be due to folding of the Burra Group prior to deposition of the Umberatana Group whereas Selley and Bull (2002) attributed it to low-angle extension and block rotation of the Burra Group during deposition of the lower Umberatana Group.

Forbes (1990) attributed the regional structural grain, comprising northwest trending broadly upright folds, to the Delamerian Orogeny (Figure 2.17) Paul et al. (1999) concluded that the Delamerian Orogeny reactivated extensional sub-basin faults as reverse faults.

2.6 Summary

The Willouran Range is the surface expression of the Willouran Trough, a northwest trending rift that formed at some time between 1,000 Ma and 827 Ma. It records the early evolution of the Adelaide Fold Belt, from deposition of the Callanna Group to the deposition of the Umberatana Group. It underwent major basin inversion in the Delamerian Orogeny, yet has evidence of earlier deformation.

Deposition of the basal unit of the Adelaide Fold Belt, the Arkaroola Subgroup, is recorded by the presence of megaclasts of the Black Knob Marble and the Noranda Volcanics in diapiric breccia but otherwise they do not crop out. The upper part of the Callanna Group, the Curdimurka Subgroup, has its type area in the Willouran Range but outside of this area, its outcrop is fragmentary and dismembered. It is dominantly a fine-grained clastic package with minor carbonate units, deposited in a shallow to deep water environment although it is not clear if it was marine or lacustrine. Geochronological evidence suggests that it was deposited between about 827 Ma and 777 Ma.

The Burra Group overlies the Curdimurka Subgroup but everywhere the contact is structural. It comprises three units, the Emeroo Subgroup, a clastic-dominated package, the Mundallio Subgroup, consisting mainly of carbonates but which also shows some variation in facies across the Willouran Range, and the fine-grained clastic Bungarider Subgroup. Geochronology suggests that depostion of the Burra Group commenced at about 777 Ma, but it's upper age limit is not known precisely. An age of 797 ± 5 Ma from a porphyry interpreted to be a shallow intrusion within the Skillogalee Dolomite (Drexel, 2009; Reid, 2009) is here thought to be spurious, and is thought likely to be from clasts of the Oodla Wirra Volcanics.

The Umberatana Group overlies the Burra Group. Within the Willouran Range, there is a high-angle unconformity between the two units, and the Umberatana Group is considerably thinner than to the east and west. From global correlations of the Sturt glacial rocks at the base of the Umberatana Group, the base may be as old as about 725 Ma, however it may be little older than about 660 Ma, based on a U-Pb zircon age from a tuff within the basal Yudnamutana Subgroup.The upper age of the Umberatana Group is about 635 Ma, based on global correlations of a cap dolomite that sits above the Elatina glacial rocks. The Wilpena Group does not crop out within the Willouran Range.

The area has undergone up to three deformation events. Several workers have identified a deformation event prior to, or during deposition of the lower Burra Group, based on differing deformation styles affecting the Curdimurka Subgroup and Burra Group strata. Deformation prior to or during deposition of the lowest Umberatana Group led to an

angular unconformity between these units within the Willouran Range. Salt tectonics may have played a role in these deformation events. The dominant deformation was the ca. 515 - 490 Ma Delamerian Orogeny which inverted the basin and is responsible for the current outcrop pattern within the Willouran Range.

CHAPTER 3.
SEDIMENTOLOGY OF THE CURDIMURKA SUBGROUP.

3.1 Introduction

It has long been recognised that the Adelaide Fold Belt was initially an intracontinental rift, that evolved into a passive margin, either during deposition of the Umberatana Group (e.g., Powell et al., 1994; Preiss, 2000) or during deposition of the Wilpena Group (e.g., von der Borch, 1980; Veevers, 1997; Foden and Barovich, 2001; Direen and Crawford, 2003). However, initiation and initial development of the rift is poorly understood, due to the fragmented and isolated outcrop of the basal succession, the Callanna Group.

The Callanna Group was deposited within restricted northwest- to north-northwest-trending grabens and half-grabens (von der Borch, 1980; Preiss, 1987; Powell, 1994; Preiss, 2000). Preiss (2000) considered that the basal Arkaroola Subgroup was deposited on a gradually subsiding peneplained stable craton with the overlying Curdimurka Subgroup being the main rift succession. Rowlands et al. (1980) considered that the Curdimurka Subgroup was deposited in two phases of rifting, with breccias interpreted to be olistostrome units that were produced by reactivated grabens. However, most other authors interpret these breccias to be related to salt bodies (e.g., Preiss, 1987; Dyson, 2002; 2005) and so reject this interpretation but not the rift setting.

Previous work has compared the Curdimurka Subgroup with the African Rift Valley on the basis of the presence of alkaline evaporitic facies and alkaline volcanics (e.g., von der Borch, 1980; Rowlands et al., 1981; Preiss, 1987). However, nowhere does the Curdimurka Subgroup crop out adjacent to the basement or the underlying Arkaroola Subgroup, with unequivocal evidence of it being a rift phase. Instead it crops out in fault slices and breccias where all contacts are structural and disturbed by later deformation (Preiss, 1987). In contrast, the underlying Arkaroola Subgroup has contacts with the basement around the Mt Painter Inlier with evidence for syn-sedimentary faulting (Coats and Blisset, 1971; Preiss, 1987). The Wooltana Volcanics, which predate the Curdimurka Subgroup are interpreted to be intracontinental flood volcanics (Preiss, 1987; Hilyard, 1990; Crawford and Hilyard, 1990) and so the Arkaroola Subgroup likely represents an active rift phase of basin development. If this is the case, it is possible that the Curdimurka Subgroup was not deposited as a main rift phase, but in a quiescent period prior to renewed rifting and deposition of the overlying Burra Group.

To test whether the Curdimurka Subgroup was deposited during an active rift or a passive thermal subsidence phase of basin development a two-pronged approach will be adopted. In this chapter, sedimentary facies of the Curdimurka Subgroup will be analysed and compared with facies models of rift sedimentation developed by Leeder and Gawthorpe (1987) and Gawthorpe and Leeder (2000). The second approach is to determine the provenance of sandstone units within the Curdimurka Subgroup using zircon geochronology and this will be discussed in the next chapter.

3.2 Facies Analysis of the Curdimurka Subgroup.

3.2.1 Introduction

With the aim of better determining the depositional environment of the Curdimurka Subgroup, graphic logging and sedimentary facies analysis of key intervals was undertaken in the type area. Figure 3.1 shows the locality of the sections. Previous authors have documented elements of the sedimentology and sedimentary facies of the Curdimurka Subgroup (e.g., Murrell, 1977; Rowlands et al.,1981; Preiss, 1987) but these have been general discussions without detailed sedimentological analysis.

In the initial phase of mapping conducted in the type area, a total of nine Facies were identified:

- Sandstone-Conglomerate Facies,
- Cross-bedded Sandstone Facies,
- Parallel Laminated Sandstone Facies,
- Siltstone-Sandstone Facies,
- Black Shale Facies,
- Interbedded Carbonate-Clastic Facies,
- Interbedded Carbonate-Siltstone Facies,
- Microbial Carbonate Facies,
- Chert-bearing Nodular Carbonate Facies.

Examples of these facies were mapped at appropriate scales, ranging from 1:100 to 1:10, noting lithologies, sedimentary features, evaporite pseudomorphs and the nature of transitions with adjoining facies where possible. Facies were mapped in the field but some crop out poorly and were graphically logged from diamond drill core intersections.

The interpretation of sedimentary bedforms will be based mainly on Allen (1983) and the diagram relating bedform to mean flow velocity and mean sediment size of Harms et al., (1975, 1982; Figure 3.2). Table 3.1 provides a summary of the facies identified and their interpretation.

3.2.2 Sandstone-Conglomerate Facies (SCF)

3.2.2.1 Description.

The Sandstone-Conglomerate Facies (SCF) occurs only toward the base of the Dome Sandstone. It comprises interbedded conglomerates and fine- to very coarse-grained sandstones, with very minor siltstone occurring as millimetre-scale interbeds (Figure 3.3). Intact SCF was only indentified in one outcrop, although clasts of a similar conglomerate were noted in breccia clasts two kilometres along strike to the southeast. In the measured section, it is 2.9 m thick with a lateral extent of tens of metres. At the location of the section

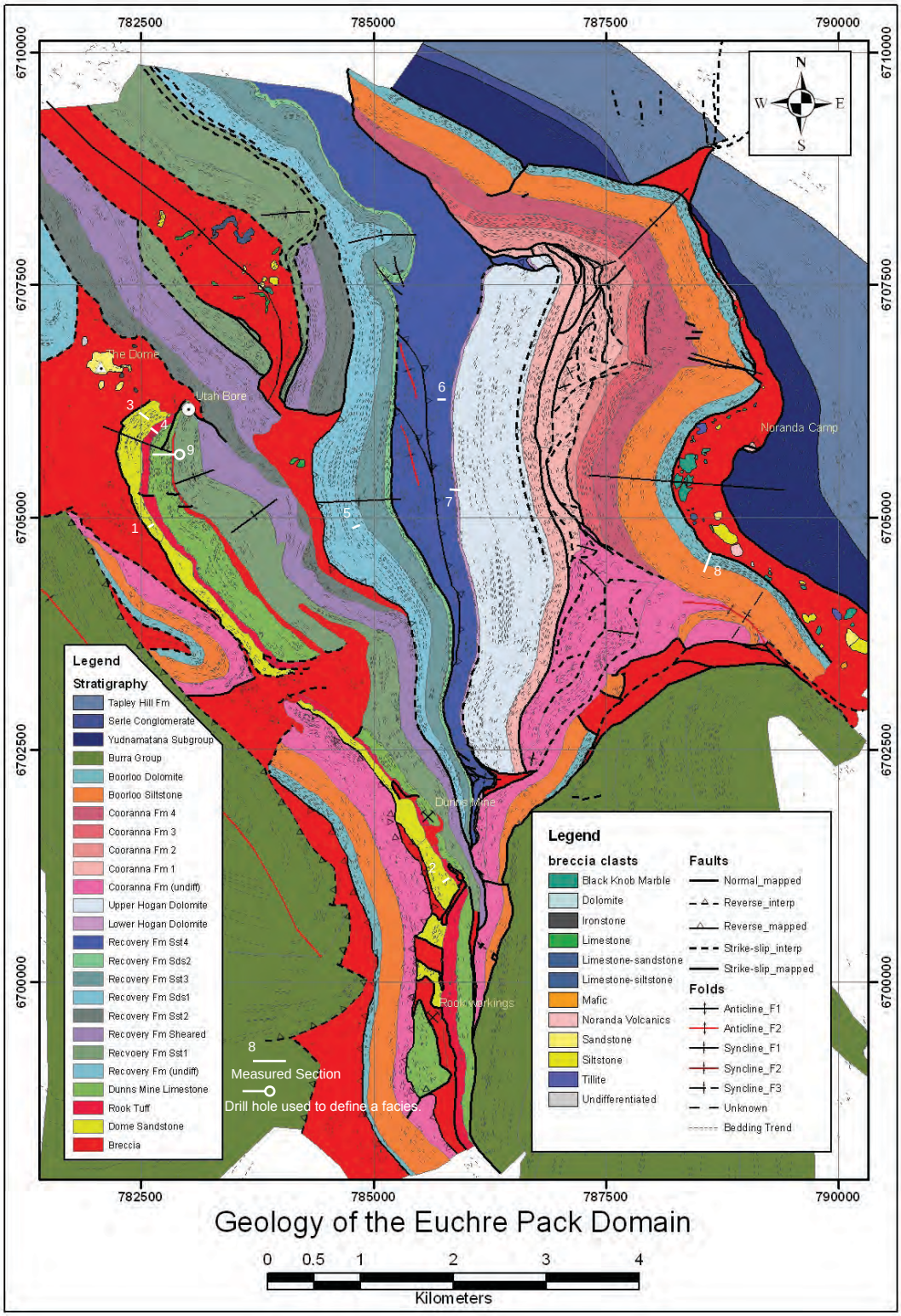

Figure 3.1. Geology of the Euchre Pack Domain showing the localities of the measured sections and diamond core drill holes used to define the facies.

1 Dome Sandstone SC Facies; 2 Dome Sandstone, CBS Facies; 3 Dome Sandstone PLS, SS Facies; 4 Rook Tuff, BS Facies; 5 Recovery Formation, SS Facies; 6 Recovery Formation SS Facies; 7 Hogan Dolomite MC, CC Facies; 8 Boorloo Siltstone, ICC, MC, CC Facies; 9 Dunns Mine Limestone, CC, ICSlt Facies,

Table 3.1. Summary of Facies from the type area of the Curdimurka Subgroup.

Lithofacies	Characteristics	Interpretation	Association	Formation
Sandstone-Conglomerate Facies	Poorly sorted conglomerate Trough cross-beds Low-angle cross-beds Parallel Laminations	Braided Stream	Fluvial	Dome Sandstone
Cross-bedded Sandstone Facies	Medium to coarse-grained Low-angle cross-beds Trough cross-beds Parallel Laminations Ripple cross-beds	Braided Stream	Fluvial	Dome Sandstone
Planar-bedded Sandstone Facies	Fine to medium grained Low-angle cross-beds Parallel Laminations Siltstone interbeds	Braided Stream	Fluvial	Dome Sandstone Recovery Formation Boorloo Siltstone
Sandstone-Dominated Siltstone-Sandstone Sub-Facies	Interbedded sandstone-siltstone Dessication cracks Ripple cross-beds Wave and current ripples Occasional evaporite casts	Sand Flat	Shallow-water to emergent	Dome Sandstone Recovery Formation Cooranna Formation
Siltstone-Dominated Siltstone-Sandstone Sub-Facies	Thinly interbedded to interlaminated Sandstone very fine- to fine-grained Dessication cracks Ripple cross-beds Wave and current ripples Evaporite casts (absent to abundant)	Mudflat	Shallow-water to emergent	Recovery Formation Cooranna Formation
Black Shale Facies	Massive to laminated Black to dark-grey Siltstone interlaminations Pyritic Minor calcite nodules	Sub-wave base, reducing to anoxic	Sub-wave base	Rook Tuff Recovery Formation Cooranna Formation Boorloo Siltstone

Lithofacies	Characteristics	Interpretation	Association	Formation
Interbedded Carbonate-Clastic Lithofacies	Thinly interbedded to interlaminated siltstone, finge-grained sandstone and carbonate Ripple cross-beds	Intertidal	Shallow-water to emergent	Dome Sandstone Boorloo Siltstone
Interbedded Carbonate-Siltstone Facies	Thinly interbedded Carbonate fine to medium grained Siltstone calcitic Graded bedding Authigenic K-feldspar	Sub-wave base reducing	Sub-wave base	Dunns Mine Limestone
Microbial Mat carbonate Facies	Wavy laminations Grain-size silt to clay Intraclast breccia microbial mat fragments Small columnar stromatolites	Supratidal to sub-tidal	Shallow-water to emergent	Recovery Formation Hogan Dolomite Cooranna Formation Boorloo Siltstone
Chert-bearing Nodular Carbonate Facies	Thin Chert layers and nodules Enterolithic Folding of chert layers Microcline pseudomorphs Grain-size silt to fine-grained Massive chert	Sabkha/Playa	Shallow-water to emergent	Dunns Mine Limestone Recovery Formation Hogan Dolomite Cooranna Formation Boorloo Siltstone

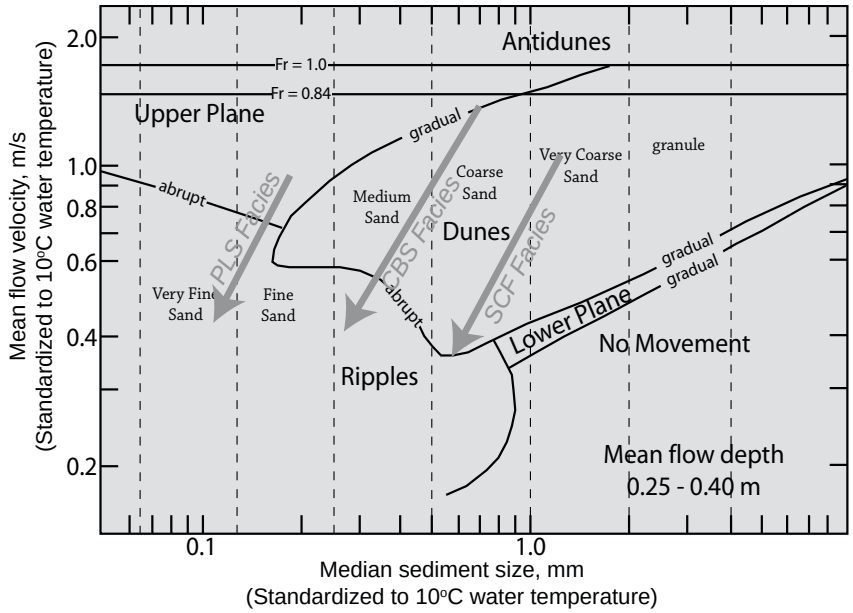

Figure 3.2. Stability fields of bedforms in sand and silt, in a flow-depth of 25 to 40 cm (From Harmes et al., 1975, 1982).

Arrows refer to the interpreted flow conditions for the Parallel Laminated Sandstone, Cross-bedded Sandstone and Sandstone-Conglomerate Facies.

shown, SCF has an abrupt lower contact with the Sandstone Dominant Sandstone-Siltstone Facies and an abrupt upper contact with the Cross-bedded Sandstone Facies (Figure 3.4a). Above the Cross-bedded Sandstone Facies the Sandstone Dominant Sandstone-Siltstone Facies returns and the SCF – Cross-bedded Sandstone Facies combination form a shallow channel in an interbedded sandstone-siltstone package (the Sandstone Dominant Sandstone-Siltstone Facies).

The conglomerates are massive (Figure 3.4b) or have crudely defined planar cross-beds (Figures 3.4c,d). Bed thickness is always less than one metre. Contacts between beds may be sharp or gradational. Two beds coarsen upward from medium- or coarse-grained sandstone to conglomerate, one of which is likely a crude reverse-grading, the second going from low-angle cross-bedded sandstone to massive conglomerate. Planar lamination (Figure 3.4e) and ripple-cross-beds (Figure 3.4f) occur in medium- and coarse-grained beds.

The conglomerates are poorly sorted, with clasts up to 20 mm in diameter, in a coarse-grained matrix that comprises about 60% of the rock. Clasts are angular to sub-angular, and of variable shape. Clasts include chert, quartzite, schist, silicified siltstone and vein quartz, and there are spaces up to 10 mm long where clasts (shale?) have weathered out. Sandstone units are typically coarse-grained but vary from fine- to very coarse-grained. One sandstone bed has a lag of clasts up to 8 mm in diameter, and several others have clasts up to 16 mm in diameter scattered through, in amounts up to 10% of the rock mass (Figure 3.4b).

3.2.2.2 Interpretation.

The presence of cross-bedding and reverse grading indicates that the conglomerates were deposited from unidirectional flows under a high flow regime. The bedforms of the sandstones indicate that they were deposited from unidirectional tractional currents. Planar lamination may result from either a high flow regime or a low flow regime, the former occurring in very fine to coarse grain sizes and the lower flow regime planar laminations occurring in coarse

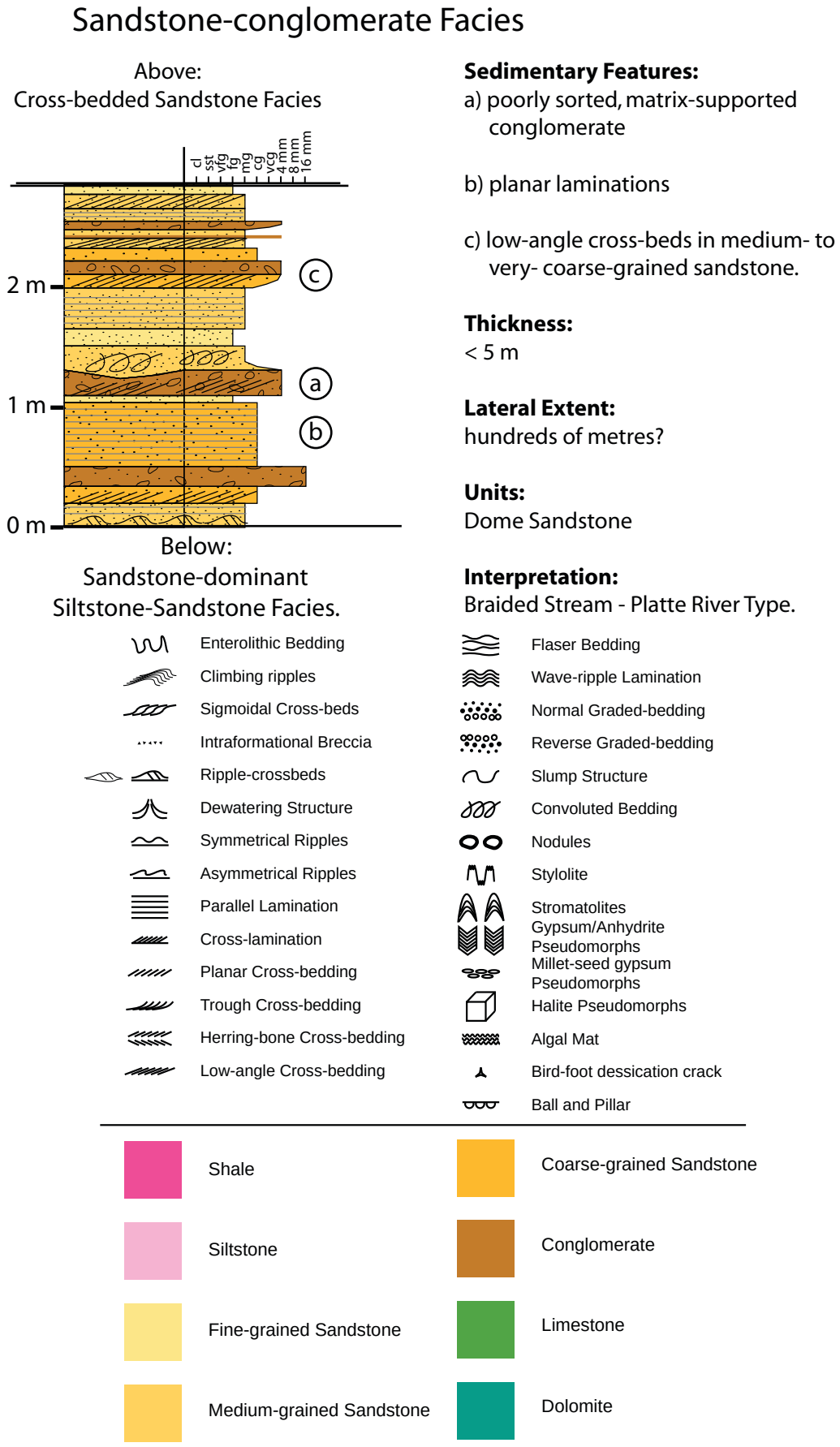

Figure 3.3. The Sandstone - Conglomerate Facies: Section 1 Dome Sandstone (Figure 3.2).
The legend is used for all measured sections shown in this chapter.

Figure 3.4. Sandstone - Conglomerate Facies.
a) View of outcrop, person for scale. Above and below is interbedded sandstone-siltstone facies. b) Massive poorly sorted pebbly conglomerate with isolated clasts of white vein quartz. c) Low-angle cross-beds in coarse-grained sandstone. d) Cross-bedded coarse-grained sandstone cutting down into underlying unit. e) Planar-laminated coarse-grained sandstone. f) Ripple-cross-beds at the top of a fine-grained sandstone.

to very coarse grain sizes (Harms et al., 1975, 1982). The planar laminated sandstones in the SCF occur in coarse and medium-grained sandstone beds above a conglomerate unit in one case and below a conglomerate unit in the other, suggesting high energy conditions. Overall, the SCF is similar to the Platte River type facies of braided streams (Miall, 1977: see section 3.3.2).

3.2.3 Cross-bedded Sandstone (CBS) Facies.

3.2.3.1 Description

The cross-bedded sandstone facies (CBS Facies) is a medium- to coarse-grained sandstone-dominant facies with minor siltstone (Figures 3.5, 3.6). A few beds have a silty matrix but most are moderately- to well-sorted. Colour is usually pale grey to white in outcrop, in some cases weathering to red. Its main feature is the predominance of cross-bedded and

massive beds. The section selected to display the features of the CBS Facies occurs as a block within brecciated Dome Sandstone (Figure 3.6a). It shows two repeating cycles, both about four metres thick. The CBS Facies occurs elsewhere within the Dome Sandstone but the outcrop is typically fractured and blocky. In the type area, the lateral extent is in the order of tens to hundreds of metres, and the thickness is less than ten metres. The Sandstone-Siltstone Facies occurs above and below the CBS Facies, with a gradational contact above and a sharp contact below.

The defining characteristic of the CBS Facies is cross-bedding with trough cross-bedding (Figure 3.6b) toward the bottom of the facies intervals and low-angle cross-bedding more dominant toward the top (Figure 3.6c). Narrow cross-laminated beds occur in sets with parallel-laminated beds (Figure 3.6d). Rippled surfaces, both symmetrical and current ripples (Figures 3.6e,f), and ripple cross-beds (Figure 3.6g) are also more common toward the top of the section. One bed of intraformational conglomerate was noted in the type section but they may be more common as thin beds with flat voids occur in float. Climbing ripples occur in several beds. Bed thickness is variable; the thickest is 40 cm thick, with most being about 20 cm thick. A typical depositional unit would include planar lamination at the base, overlain by either trough cross-beds or low-angle cross-beds and ripples at the top of the unit. Grain-size decreases up section. Basal contacts are usually sharp and some trough cross-beds have erosional contacts with the bed below. There may be a thin (mm to cm scale) siltstone interbed before the next depositional unit begins but this is not typical. Rare halite pseudomorphs occur in siltstone interbeds and occasionally within sandstone beds (Figures 3.6f,h), and rhombic voids also occur within sandstone beds but these may be due to removal of diagenetic dolomite.

The CBS facies sandstones are typically quartz-rich, although they contain voids and kaolin after feldspar. In thin sections from diamond core samples, the feldspars have been converted to muscovite. At some localities, heavy-mineral bands may define laminations and cross-beds but this is atypical.

3.2.3.2 Interpretation.

Cross-bedding indicates deposition from tractional currents. Trough cross-bedding is the internal bedform of three dimensional dunes which form in the high or low flow regime, depending on grainsize (Figure 3.2; Harms et al., 1975, 1982). In this section they are formed in coarse-grained sand. The low-angle cross-beds are similar in form to the concave-upward to sigmoidal cross-strata described by Røe (1987), interpreted to have formed in high-stage, swift and heavily suspension-laded currents in the dune to upper-stage plane-bed transition. Ripples form in the lower flow regime in grain-sizes up to coarse-sand, and the scarcity of ripples reflects the coarse-grained to very-coarse grained sand present.

Sets of beds from planar laminations to low-angle cross-bedding or trough cross-bedding, topped by ripples and ripple cross-bedding suggest a pattern of decreasing flow from the upper flow regime to the lower flow regime (Figure 3.2; Harms et al., 1975, 1982). Thin siltstone interbeds may be deposited either in the waning flow or from suspension

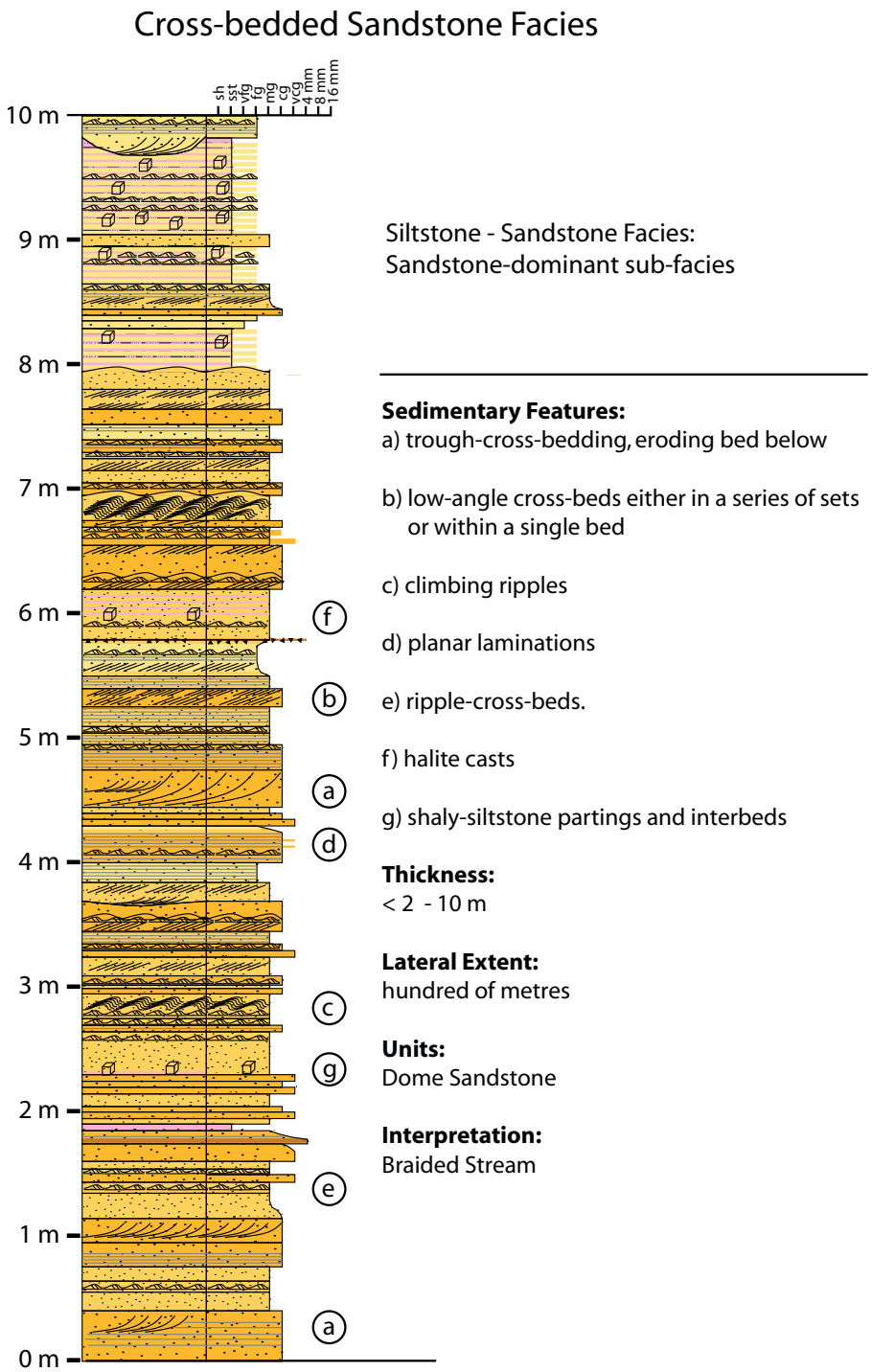

Figure 3.5. The Cross-bedded Sandstone Facies.
Here the cross-bedded sandstone facies extends from 0 m to about 7.9 m, and is overlain by the sandstone-dominant sub-facies of the Siltstone-Sandstone Facies.

in a standing body of water. The rare halite casts and rhombic casts were likely deposited interstitially from brine formed by the evaporation of standing water bodies.

The section as a whole represents a decrease in energy and shallowing of the water depth toward the top (Figure 3.2). Like the Sandstone-Conglomerate Facies, it was probably deposited in a braided stream of the Platte River type (Miall, 1977: see section 3.3.2). The standing bodies of water from which the halite was deposited may be due to overbank

Figure 3.6. Cross-bedded Sandstone Facies.
a) Outcrop of the sandstone facies, Dome Sandstone. b) Trough cross-beds cutting into parallel-laminated sandstone bed below. c) Parallel-laminated sandstone between low-angle cross-bedded sandstone. d) Cross-lamination with ripple-cross-beds on the top of the bed. Parallel-laminated sandstone above that. e) Symmetrical ripples on a medium-grained sandstone bed. f) Current ripples with rhombic casts. g) Ripple cross-beds in medium-grained sandstone. h) Halite casts on a siltstone interbed.

deposits or shallow pools subject to occasional flooding followed by evaporation and depostion of halite in an arid environment.

3.2.4 Parallel Laminated Sandstone (PLS) Facies

3.2.4.1 Description

The Parallel Laminated Sandstone (PLS) Facies is defined by planar laminations being the dominant bedform and an absence of trough cross-beds (Figure 3.7). It typically crops out poorly, with biscuity and broken sandstone fragments on the surface (Figure 3.8a). Planar laminae are typically identified by darker and lighter beds (Figure 3.8b,c). Low-angle cross-beds, ripples and rippled surfaces also occur. Fine-grained sandstone is dominant with minor medium- to coarse-grained sandstone and the colour is typically pale to medium grey. At the outcrop at which the section was logged, the PLS Facies is interbedded with the Sandstone-Siltstone Facies. The lower contact of the PLS Facies is gradational with the Sandstone-Siltstone Facies; the amount of sandstone gradually decreasing whereas the upper contact is abrupt. The section shown is about 18 m thick, which is greater than the typical thickness of less than 10 metres. Laterally the PLS Facies extends for hundreds of metres, and may form broad shallow channels within the Sandstone-Siltstone Facies.

Bed thickness is variable; the planar laminated beds being up to eight centimetres thick and massive beds to ten centimetres thick. Thin beds on the scale of centimetres with ripple cross-beds, low angle cross-beds and sigmoidal cross-beds are more common toward the base of the section (Figure 3.8d), however there is an overall reduction of bed thickness up-section. Planar laminated beds are fine-grained whereas other bedforms occur in medium- to coarse-grained sandstones. Very minor siltstone beds from millimetre-scale to a few centimetres are also present. Ripples are common on bedding surfaces.

The sandstones are quartz-rich and typically silicified in outcrop but samples from drill core are less silicified and contain muscovite after feldspar. Poorly sorted grey-brown sandstones have a clay matrix with feldspars preserved, micas and fragments of mudstone.

3.2.4.2 Interpretation

The PLS Facies is interpreted in a similar manner to the Cross-bedded Sandstone Facies, given that there are many features in common. The bedforms present indicate deposition from tractional currents with the bedforms reflecting the grainsize of the available sediment and the current flow. It likely represents a similar energy regime to the Cross-bedded Sandstone Facies; the factor determining the dominant major bedform being the finer grainsize of the constituent sediment (Figure 2.2). The transition from planar-laminations to ripples within single beds reflects the change to finer grainsize. Medium- to coarse-grained beds have low-angle cross-beds and sigmoidal cross-beds that form at the transition between upper plane-bed and dunes at medium to coarse-grain size (Røe, 1987). The PLS Facies is interpreted to have been deposited in a braided stream of the Bijou Creek type (Miall, 1977: see section 3.3.2).

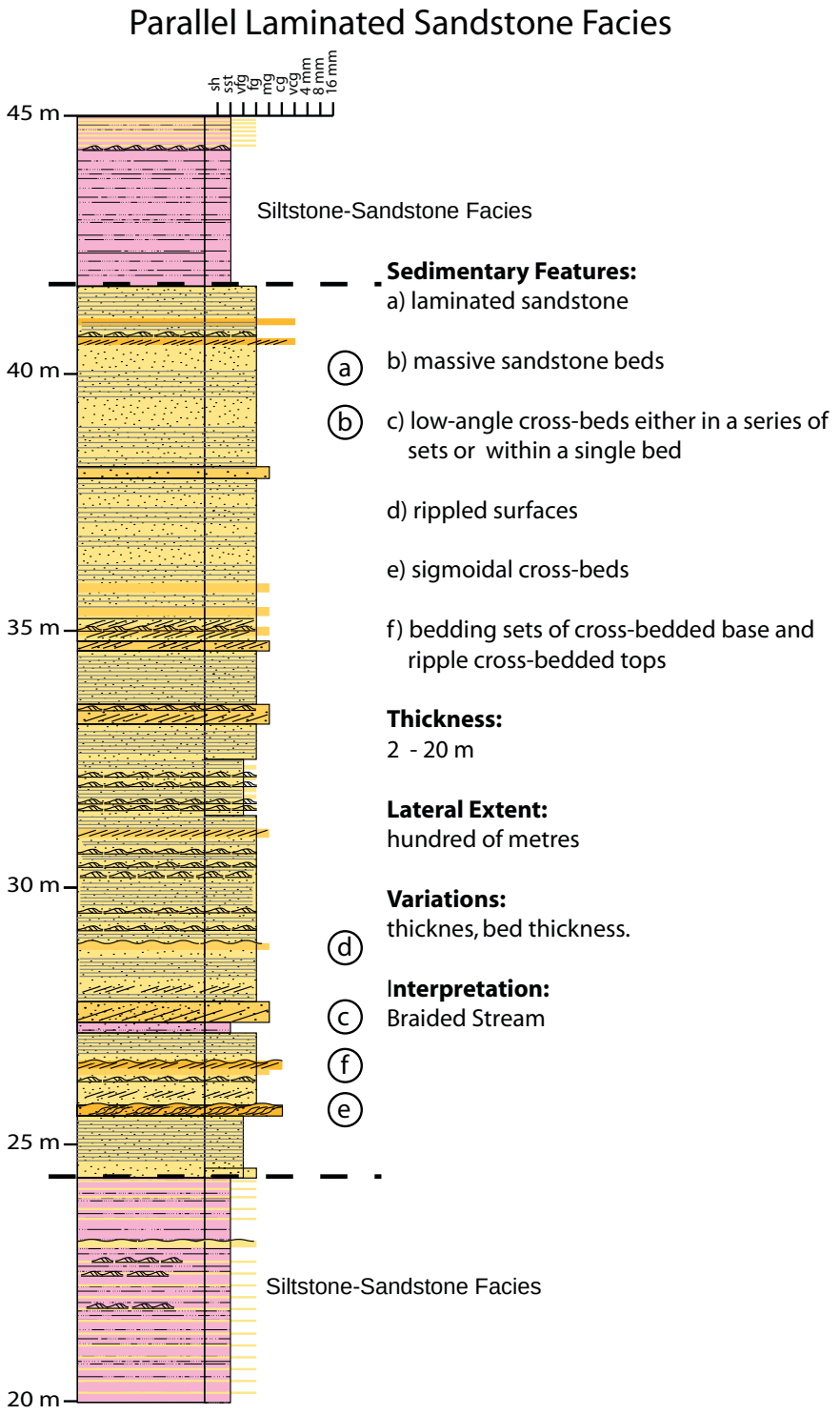

Figure 3.7. Main features of the Parallel Laminated Sandstone Facies.

3.2.5 Siltstone-Sandstone (SS) Facies.

3.2.5.1 Description

The Siltstone-Sandstone (SS) Facies is the dominant facies within the Curdimurka Subgroup. It comprises two end-members, one is sandstone-dominant (Figure 3.9a,b) and the other siltstone-dominant (Figure 3.9c). They have many features in common, including lithologies and sedimentary structures and any attempt to differentiate between them would be based on arbitrary distinctions.

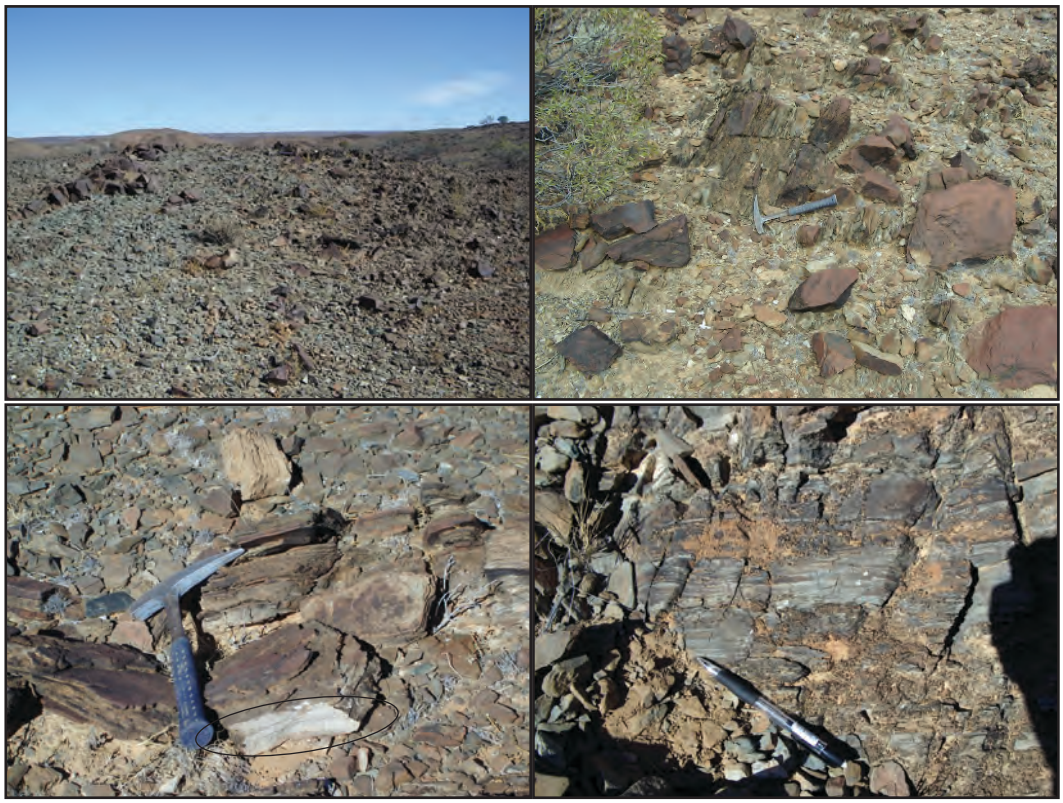

Figure 3.8. Textures of the Parallel Laminated Sandstone Facies.
a) Typical outcrop of the PLS facies, showing narrow fine-grained beds. b) Interbedded to interlaminated fine-grained sandstone. c) Detail of the laminated fine-grained sandstone showing laminae defined by darker bands. d) Centimetre-scale cross-beds in fine-grained sandstone of the PLS.

The SS facies comprises interbedded sandstone and siltstone, with minor mudstone and carbonate. In the sandstone-dominant SS Sub-Facies, sandstone beds are on average thicker than siltstone beds and in the siltstone-dominant SS Sub-Facies, siltstone beds are on average thicker than sandstone beds. The outcrop of the sandstone-dominant SS Sub-facies is reasonably well preserved, cropping out on low hills (Figure 3.10a,b) or with the sandstone-based facies. The siltstone-dominant SS Sub-facies typically only crops out as low, rounded rises with biscuity sandstone and ferruginous siltstone float or is covered by soil and alluvium (Figure 3.10c).

The sandstone beds are pale- to medium-grey and siltstone is medium- to dark-grey except near the top of the Cooranna Formation, where the siltstone is red. Upper and lower contacts with other facies may be gradual or sharp. Thin (< 1 m) sandstone units belonging to the Planar Laminated Sandstone Facies or the Cross-bedded Sandstone Facies may occur in sections otherwise dominated by the SS Facies. Its thickness is highly variable, from less than one metre to tens of metres, and its lateral extent is kilometres.

Individual beds range in thickness from millimetres to tens of centimetres (Figure 3.10d). Sandstone is typically quartz-rich and fine- to very fine-grained but thin beds of coarse-grained sandstone do occur. Bed forms include planar laminations, isolated sandstone ripples in siltstone, (Figure 3.10e), ripple cross-beds (Figure 3.10f) and flaser and lenticular bedding (Figure 3.10g). Rippled surfaces are common (Figures 3.10h,i,j). The ripples may be either wave- or current-ripples but the former are most common. Current ripples range from having straight to catenary shaped crests, with amplitudes of less than two centimetres

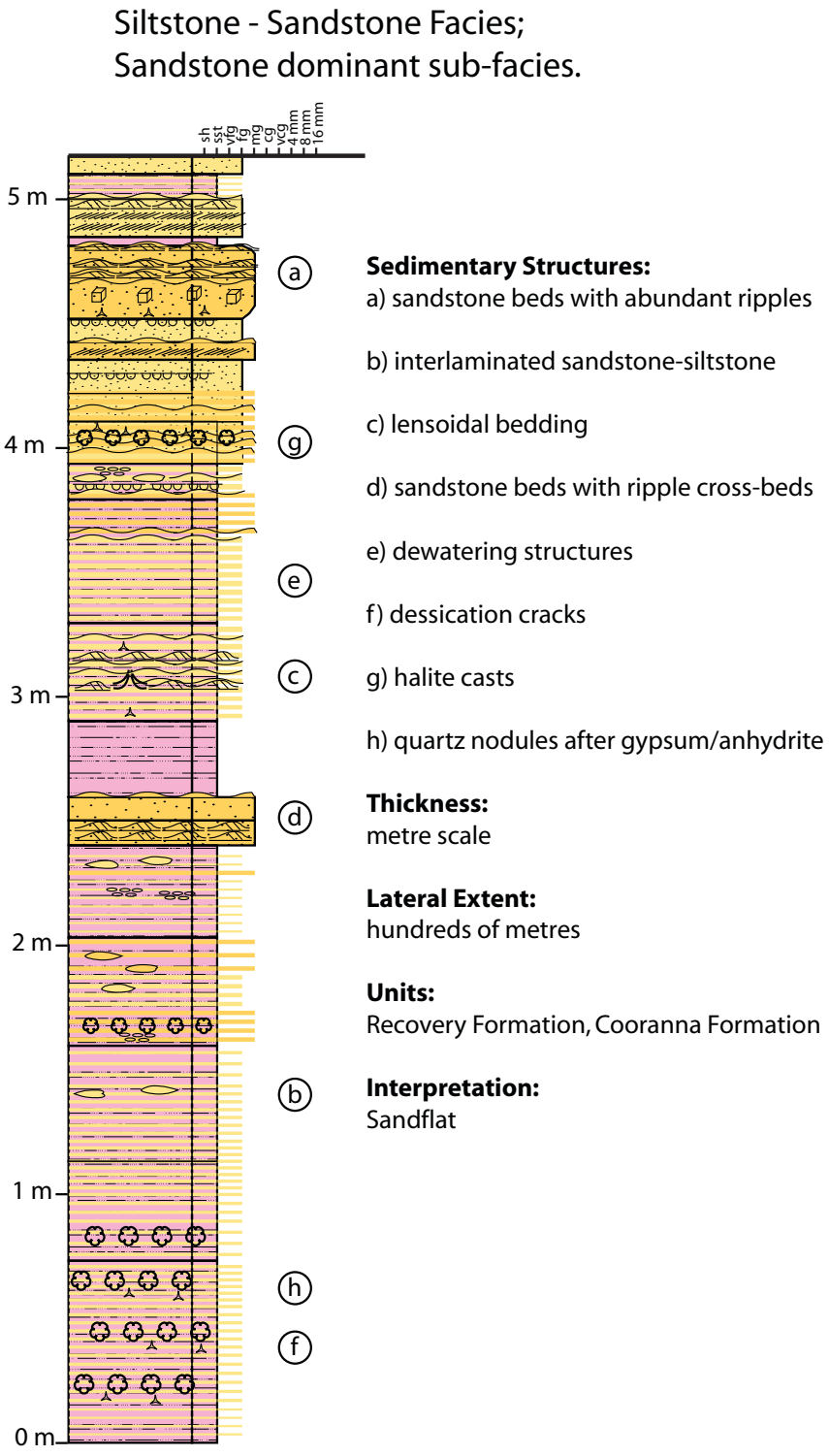

Figure 3.9a. The Siltstone - Sandstone Facies; Sandstone dominant sub-facies.

and wavelengths less than 10 cm. Desiccation cracks are common (Figure 3.10i), quartz nodules (typically less than 5 mm in diameter) after anhydrite and halite and gypsum casts range in occurrence from rare to abundant (Figure 3.10j,k). Sand wedges in mudstone, ball and pillar, pseudo-nodules and load casts are moderately common (Figure 3.10l,m). Water-escape structures occur in interlaminated sandstone and siltstone (Figure 3.10n). Lower contacts of sandstone beds are typically sharp with upper contacts being either sharp or transitional. Siltstone beds are either laminated or massive, and carbonate beds are usually calcilutites. Carbonate beds are silty and grey. Black to dark-grey carbonaceous mudstone occurs rarely.

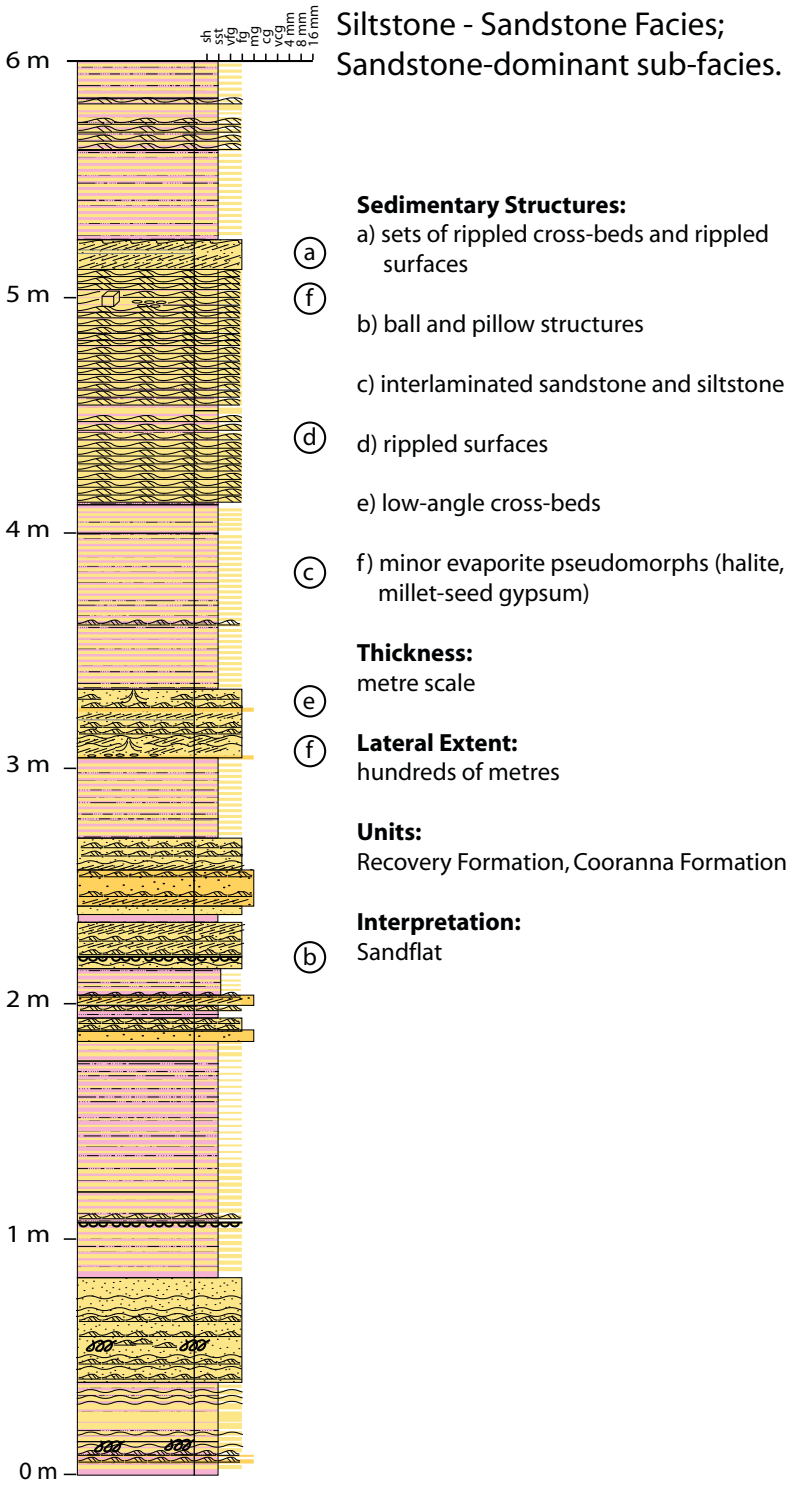

Figure 3.9b. The Siltstone - Sandstone Facies; Sandstone dominant sub-facies.
This example is dominated by thin rippled fine-grained sandstone beds in contrast to Figure 3.9a, which has thicker sandstone beds but fewer rippled surfaces.

Sandstone beds in outcrop appear to be quartz-rich with some silicification occurring locally. On fresh surfaces however, the sandstones are kaolinitic, with patches of kaolin after feldspar, and a kaolin cement. They comprise between 85% and 70% quartz; 10% to 20% feldspars (now kaolin) and 5% to 10% porosity (estimated from hand specimen) and are subarkosic to arkosic. Lithic fragments usually consist of claystone. Mud drapes also consist of white clay. Sandstone units within the SS Facies are locally calcitic.

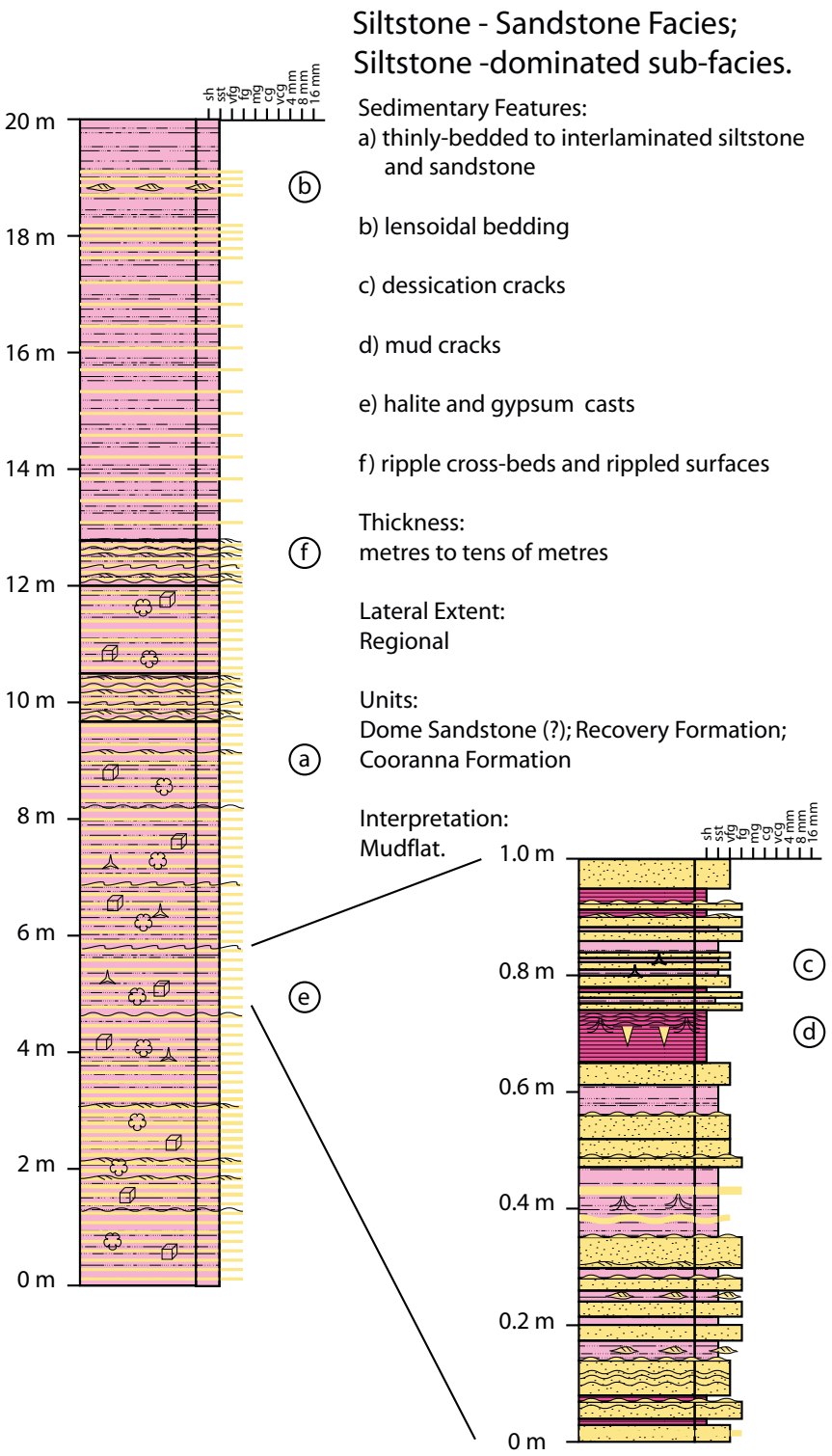

Figure 3.9c. The Siltstone - Sandstone Facies; Siltstone dominant sub-facies.

3.2.5.2 Interpretation.

The medium- to thinly-bedded sandstones have sedimentary structures indicative of deposition from low-flow regime tractional currents; that is low-angle cross-beds, ripple cross-beds and rippled surfaces (Figure 3.2). Flaser bedding, wavy bedding and lenticular bedding represent periods of deposition from currents with the intervening mud being deposited during slack water. Typically, they are associated with the upper zones of tidal flats, and from subtidal depths in channels and just off-shore (Allen, 1984). The current ripples observed have straight or catenary crest lines, indicating that they are not

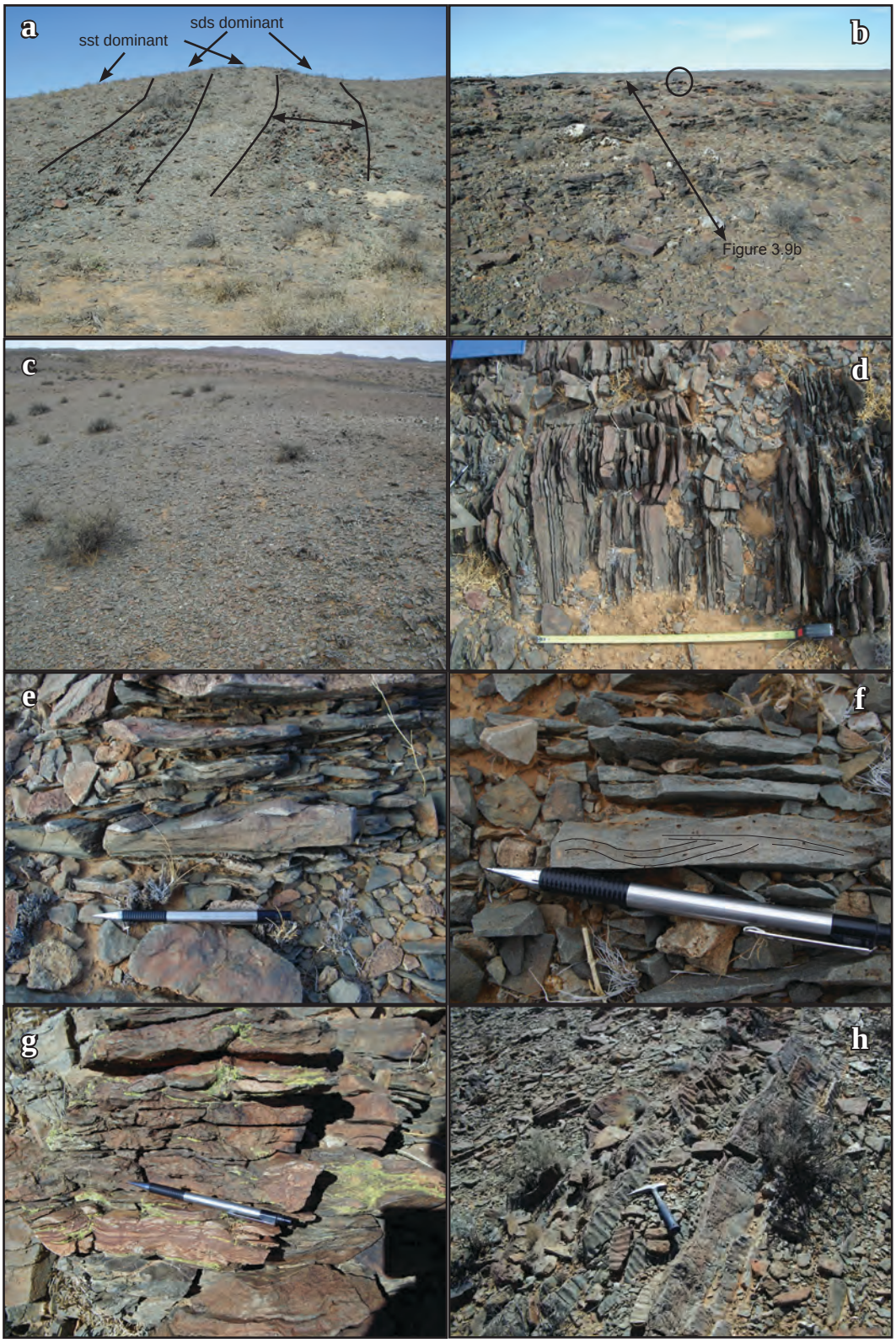

Figure 3.10. The Siltstone-sandstone facies.
a) Repeating cycles of sandstone-dominant and siltstone-dominant Siltstone-Sandstone Facies. b) The outcrop at which the section in Figure 3.9b was measured. Circled is a geological hammer for scale. c) Typical outcrop of the siltstone-dominant sub-facies of the SS Facies. d) Laminated sandstone in sandstone-dominant SS facies. e) Isolated wave ripples in siltstone. f) Ripple cross-beds in medium-grained sandstone g) Isolated fine-grained sandstone ripples interbedded with siltstone. h) Repeating rippled surfaces in sandstone-dominated SS facies. i) Dessication cracks on a rippled surface. j) Quartz nodules after gypsum on a rippled surface in medium-grained sandstone. k) Hal-

ite casts on fine-grained sandstone. l) Ball and pillar structures in fine-grained sandstone m) Load casts on the underside of sandstone bed. n) Water-escape structure in interlaminated sandstone and siltstone.

equilibrium bedforms and so are not the product of a long-lasting current (Baas, 1999). Short wavelengths and amplitudes suggest the ripples were deposited in shallow water. Sand may have been introduced from either; deeper water by tidal action or storms or from landward by small distributary channels or sheet floods, or possibly both.

Siltstone may have been deposited in the waning stages of the tractional flows or possibly from suspension. Desiccation cracks indicate periodic subaerial exposure. The halite pseudomorph shapes include cubes, hopper crystals and rare pagoda shapes. These forms are typical of displacive halite, which grows from saturated brines beneath the sediment-water interface (Smith, 1971; Gornitz and Schreiber, 1981). Two mechanisms are thought to be possible for their growth; downward diffusion of brines formed in shallow water by evaporation, or upward diffusion if the sediment is subaerial and intermittently inundated (Gornitz and Schreiber, 1981). The association of halite casts with desiccation cracks suggests an emergent environment, such as a sandflat or mudflat (Allen, 1984), is the most

likely depositional setting. However, where emergent sedimentary features are absent, sub-tidal and off-shore environments (Allen, 1984) cannot be ruled out for the siltstone-dominant SS Sub-facies. On the basis of Lithofacies Associations (between the Black Shale Facies and the emergent carbonate Facies, see below), a sub-tidal setting may be inferred in this case.

The interpreted depositional environment is a sand flat (sandstone-dominated SS Facies) transitional to a mudflat (Siltstone-dominated SS Facies), but it is likely that a sub-tidal siltstone-sandstone facies also exists.

3.2.6 Black Shale (BS) Facies.

3.2.6.1 Description

Blocky to laminated dark-grey to black shale, with variable amounts of interbedded to interlaminated siltstone and very minor fine-grained sandstone define the Black Shale (BS) Facies (Figure 3.11). The thickest unit of the BS Facies is about 150 m thick, in the Boorloo Siltstone, and elsewhere, the thickness ranges from metres to tens of metres. Thicker units crop out as low dark hills that are prominent in aerial photographs and have lateral continuities measured over kilometres. Units less than ten metres thick have lateral continuity measured in hundreds of metres but outcrop is typically poor and this may reflect that. Upper contacts of the thicker units can be gradational (the Boorloo Siltstone) or abrupt (Rook Tuff - Dunns Mine Limestone contact). Lower contacts are gradational with the Siltstone-Dominant Siltstone-Sandstone Facies. In the Cooranna Formation, thin units of the BS Facies are interbedded with the Sandstone-Siltstone Facies and Siltstone-Dominant Siltstone-Sandstone Sub-Facies.

In outcrop, the BS Facies appears to be massive across almost its entire thickness and lacking internal structure (Figure 3.12a). However diamond drill core shows that it comprises beds of massive black shale and packages of thinly interbedded to interlaminated grey and black shale and siltstone (Figure 3.12b,c). Small scale post-depositional folds and faults restricted to narrow zones are occasionally present (Figure 3.12d,e).

Grain size is too small to determine the mineralogy of the black shale but the siltstone typically contains muscovite with angular grains of feldspar and quartz. Pyrite is common, both bedded and in veins and black calcite nodules occur in the Boorloo Siltstone. Diagenetic siderite is moderately common (Figure 3.12f). The BS Facies can be weakly calcitic, over a few metres of stratigraphic thickness, due to thin very fine-grained calcitic sandstone. There may also be a few thin carbonate beds, especially close to contacts with carbonate facies (see below). The BS Facies has patches up to one metre thick that contain a few percent of sand grains up to one millimetre in diameter scattered through what is otherwise massive black shale.

3.3.6.2 Interpretation

The clay to silt grain size of the BS Facies suggests deposition primarily by the settling of material from suspension. Thin siltstone to fine-grained sandstone and carbonate beds likely result from turbidity currents. Isolated sand grains within the black shale may have been

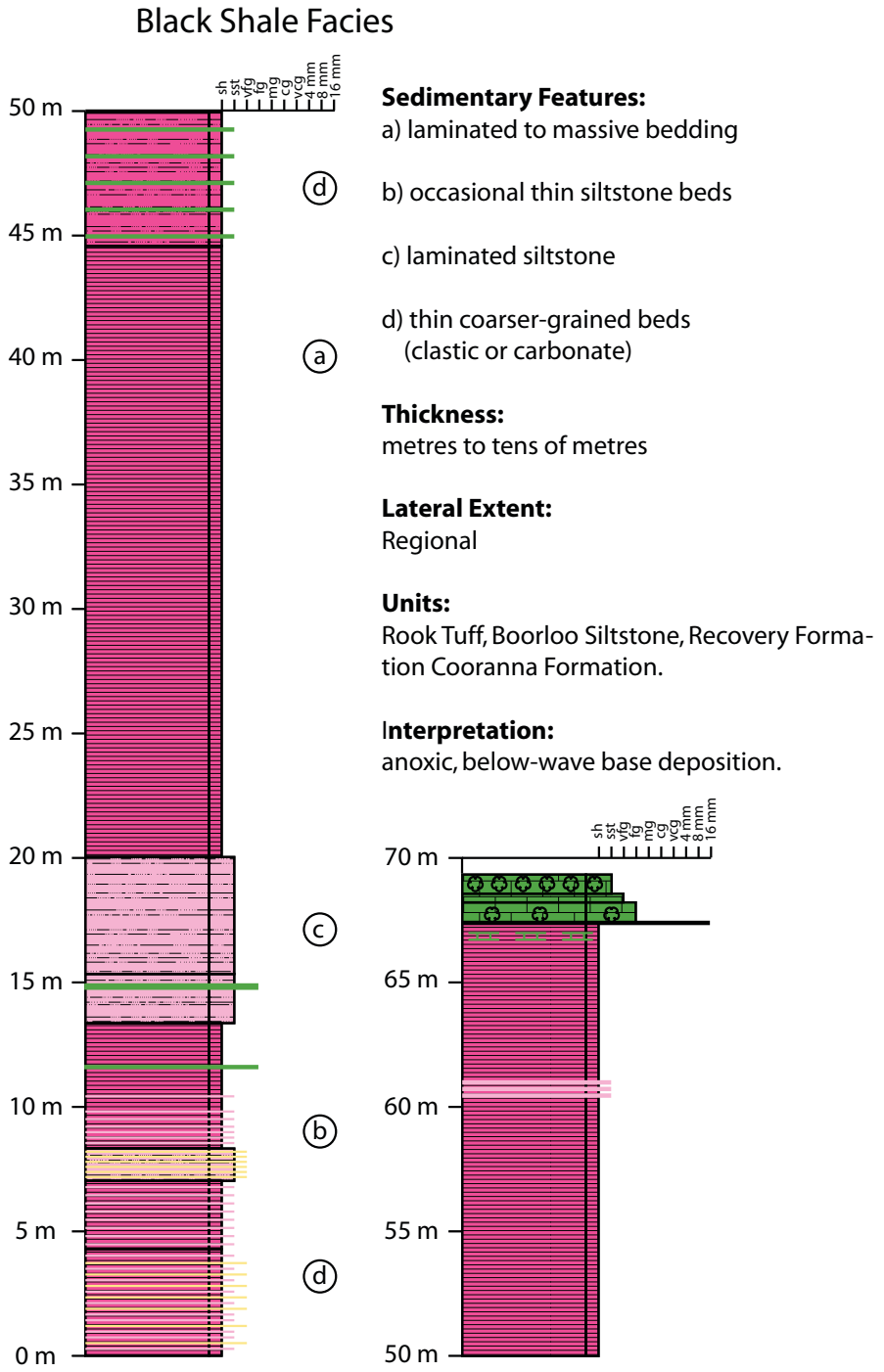

Figure 3.11. Main features of the Black Shale Facies.

deposited as wind-blown sand. The organic-rich nature of the facies indicates deposition in a reduced environment. A lack of sediment re-working textures (wave-ripples, hummocky cross-stratification etc.) indicates that deposition occurred below wave-base. Therefore, the BS Facies is interpreted to have been deposited in a sub wave-base environment.

3.2.7 Interbedded Carbonate-Clastic (ICC) Facies.

3.2.7.1 Description

The Interbedded Carbonate-Clastic (ICC) Facies comprises muddy to fine-grained, detrital carbonates interbedded with siltstone to fine-grained sandstone (Figure 3.13). When associated with a siltstone-dominant package, this facies stands a metre or two above the

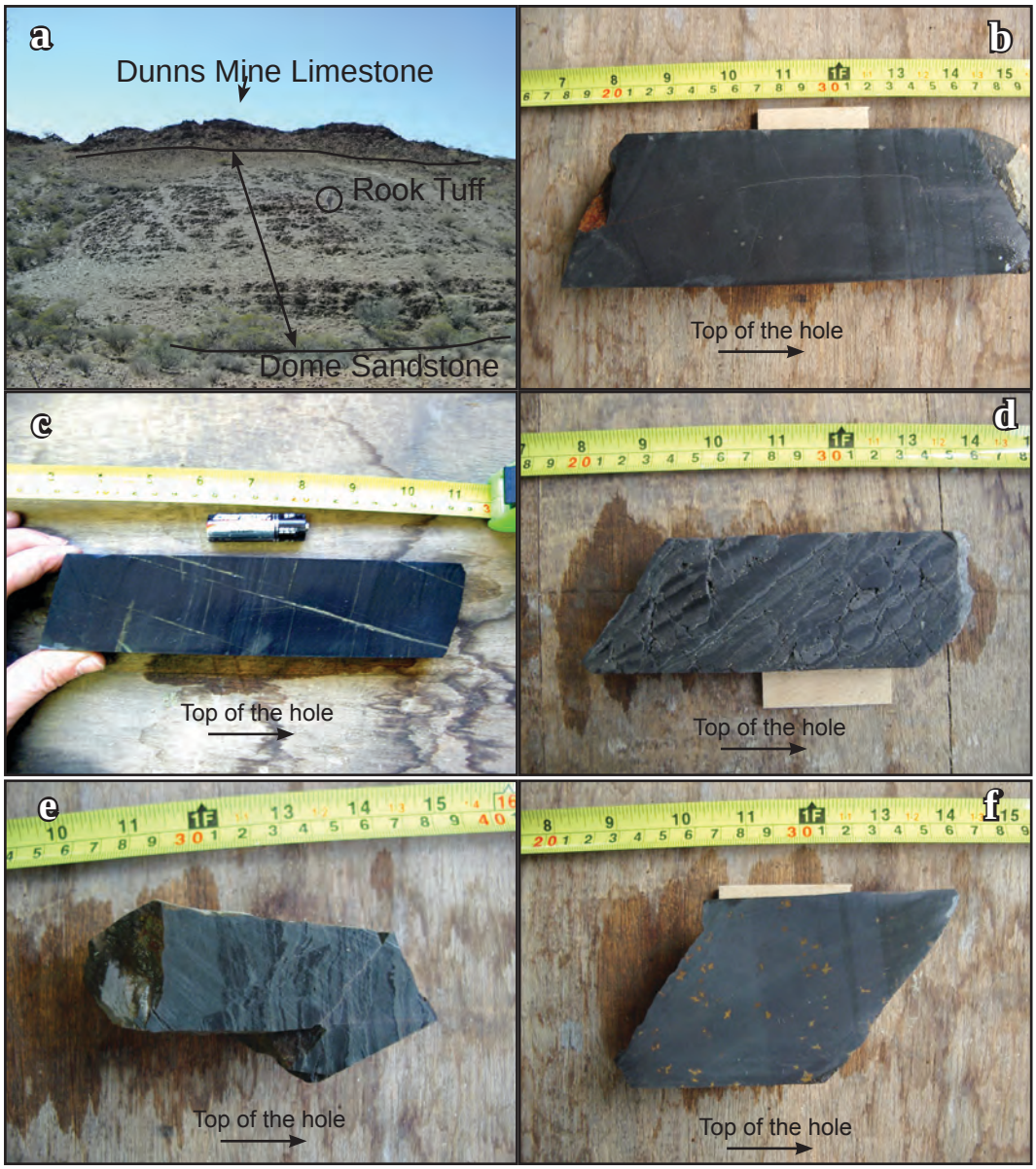

Figure 3.12. The Black Shale Facies in outcrop and diamond drill core.
a) Outcrop of the Rook Tuff, Black Shale Facies. At the top of the ridge is the Chert-Carbonate Facies of the basal Dunns Mine Limestone. Field assistant for scale (circled). b) Massive black Shale, Rook Tuff. c) Laminated black shale, Boorloo Siltstone. d) Interlaminated black and grey shale cut by low-angle normal faults, Rook Tuff. e) Interlaminated grey and black shale cut by normal faults, Rook Tuff. f) Massive black shale with diagenetic siderite, Rook Tuff.

surrounding surface (Figure 3.14a) but amongst other carbonate-dominated facies, the ICC Facies may be difficult to distinguish. Typically this facies is two to three metres thick, with a lateral extent of kilometres. Outcrop is yellow-brown to green-brown on weathered surfaces but on a fresh surface, the carbonate is green to grey-green.

Typically the carbonate is dolomite but limestone is not uncommon. The clastic component occurs in thin interbeds and lenses (Figure 3.14b,c), with planar laminations, lensoidal bedding, ripple cross-beds and graded bedding the primary sedimentary features (Figure 3.14b,d). De-watering structures and possible synaresis cracks occur within this facies in the Boorloo Siltstone (Figure 3.14e,f). Grain-size in the carbonates is silt to fine-grained whereas the grain-size of the clastic beds is very fine- to medium-grained.

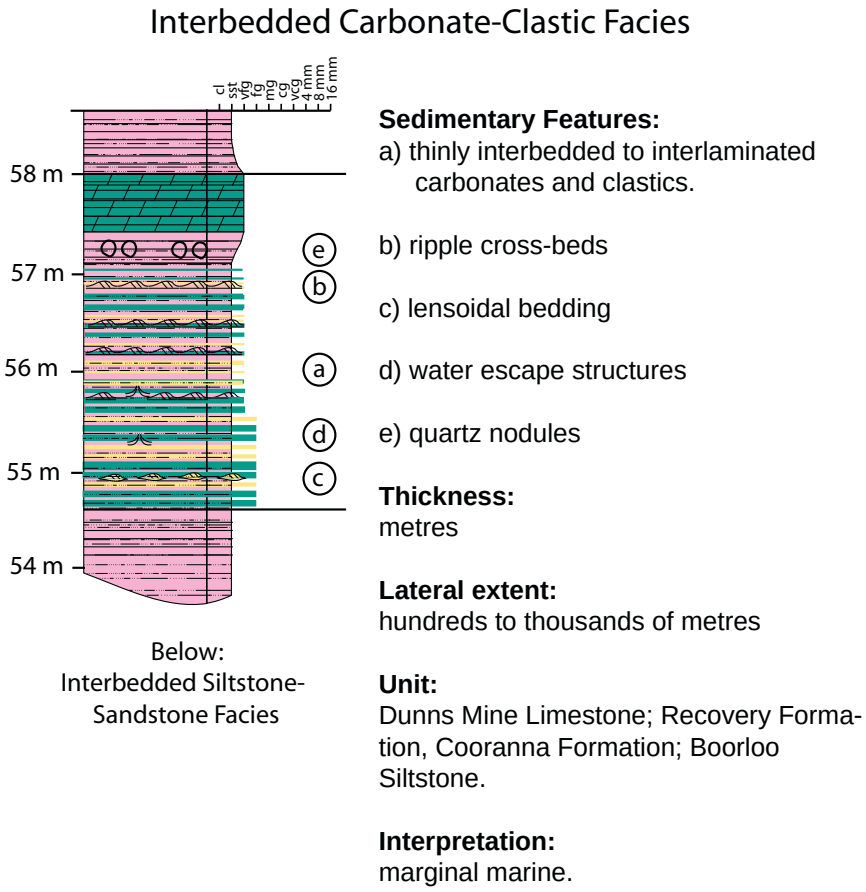

Figure 3.13. Interbedded Carbonate-Clastic Facies.

In hand specimen carbonate layers may be defined by blue-grey and yellow-grey laminations. Clastic-rich beds tend to stand a few millimetres above the carbonate beds (Figure 3.14b) and have a carbonate cement. Carbonate units may be recrystallised with a tight fabric, or granular and porous.

3.2.7.2 Interpretation.

The small ripples and ripple cross-beds indicate deposition from tractional currents, and their small size as well as the fine-grain size of the constituent sediment indicates these were low energy. The laminations may indicate deposition from a unidirectional traction flow in the upper flow regime, or settling out of the water column but the fine-grain size suggests the latter. Abrupt contacts between the clastic units and the carbonates suggests a separate source for each and the preferred interpretation is that the clastic component represents influx of material via current activity whereas the carbonates represent in situ sedimentation, most likely from chemical precipitation from the water body. Coarser-grained carbonates were likely introduced mechanically.

Two depositional settings are likely for the ICC Facies. The first is inferred from it position in the Boorloo Siltstone where it is transitional from the Black Shale Facies to the Microbial Carbonate Facies and the Carbonate-Chert Facies. In this situation it appears to be shallow water and offshore from a carbonate producing environment. The carbonates are either introduced down-slope from the shallower water or directly precipitated from seawater (e.g., Kinsman and Holland, 1969; Eugster and Hardie, 1978; Shinn et al., 1989). In the

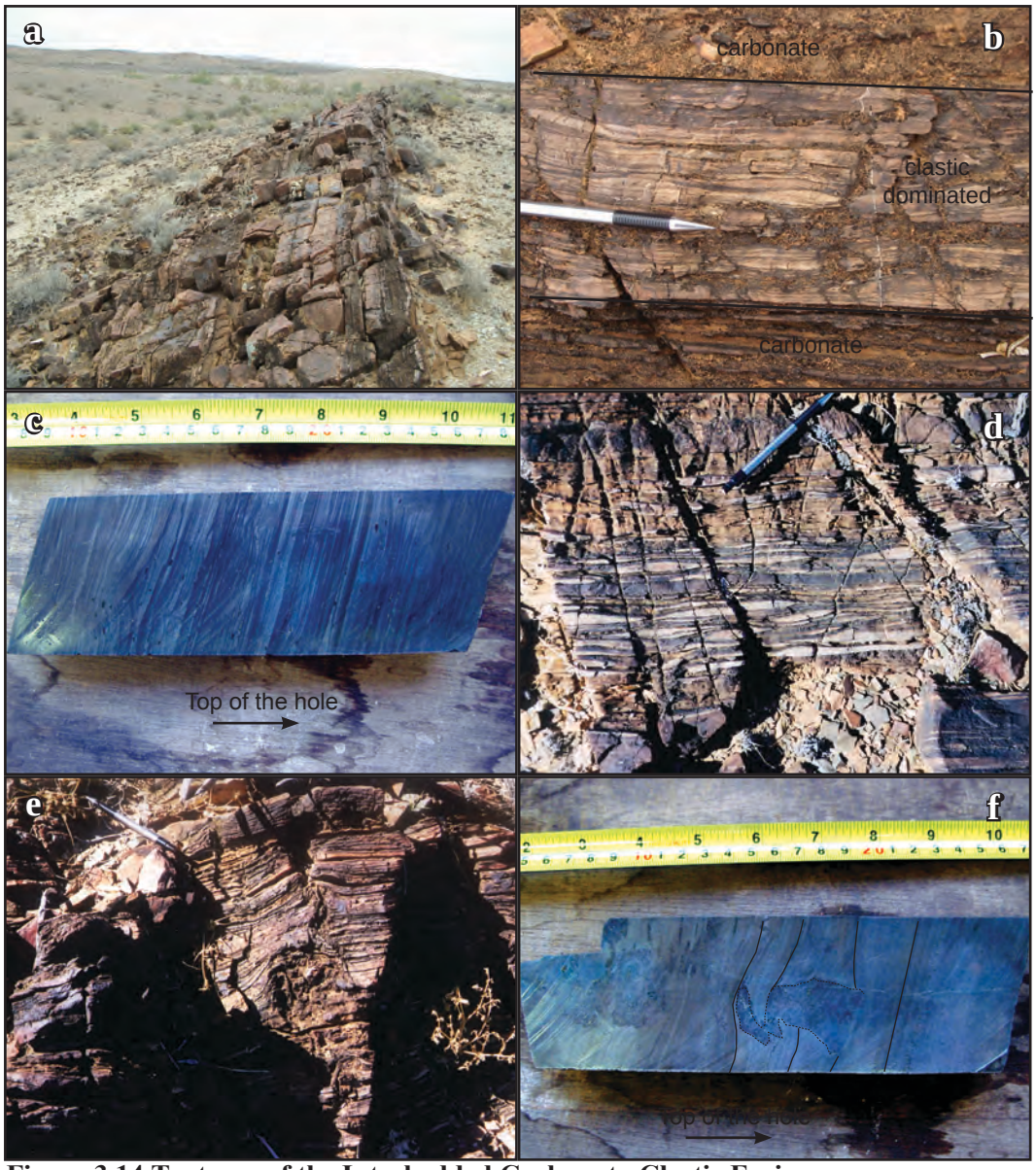

Figure 3.14 Textures of the Interbedded Carbonate-Clastic Facies.
a). Outcrop of the ICC Facies, BDol. b). Thinly interbedded to interlaminated very fine-grained sandstone standing above fine-grained carbonate, BDol. c) Interlaminated carbonate and clastic in diamond drill core, BDol. d) Lensoidal bedding in sandstone-siltstone within the ICC Facies, Cooranna Formation. e) dewatering structure in the ICC Facies, BDol. f) A dewatering structure or a synaresis structure in the ICC Facies, BDol.

other setting, inferred from the association with the Sandstone-Siltstone Facies and the Siltstone-dominant Siltstone-Sandstone Subfacies, the ICC Facies is a carbonate analogy of these facies and may be supratidal. In both cases, the presence of the ICC Facies indicates a carbonate factory in shallow water, but in the former instance, carbonate moves downslope into the basin and in the other, carbonate is moved shoreward perhaps by storms or tides or short-term transgressions.

3.2.8 Interbedded Carbonate-Siltstone (ICSlt) Facies.

3.2.8.1 Description

The Interbedded Carbonate-Siltstone (ICSlt) Facies (Figure 3.15) is restricted to the Dunns Mine Limestone. At the northern end of its outcrop it forms the eastern slopes of a ridge,

with the Carbonate-Chert Facies along the top of the ridge. At the southern end of its outcrop it forms a low rounded rise protruding a few metres above the surrounding area. Siltstone interbeds are poorly preserved in outcrop and the illustrated section is from diamond drill core hole WD005 (Figure 3.15). Its outcrop is rubbly (Figure 3.16a), and is dominated by green-weathering carbonates with feldspar needles and rods up to one centimetre long on weathered surfaces (Figure 3.16b). In the upper part of the facies, the carbonate mineralogy is limestone whereas the lower part is dolomite (Figure 3.15). The facies is laterally extensive and the thickness is variable, from tens to hundreds of metres. It overlies the Carbonate-Chert Facies, but the contact is typically brecciated and underlies the Siltstone-dominant Siltstone-Sandstone Sub-facies with a gradual transition locally.

The defining feature of the ICSlt Facies is thinly interbedded, cycles of siltstone - mudstone and carbonate (Figure 3.16c,d,e,f). Beds are typically about one centimetre thick in the section shown (Figure 3.16c,d), but in other drill holes, the carbonate beds may be up to three centimetres thick, with little variation in the siltstone bed thickness (Figure 3.16e). There are rare beds of calcitic sandstone which increase in frequency and thickness toward the top of the facies (Figue 3.16g). Bed contacts are usually abrupt and sedimentary structures are minimal with only normal grading (Figure 3.16c) and lenticular bedding of carbonates (Figure 3.16d) within siltstone. Drill-hole WD016, which intersects the same section, contains a higher proportion of carbonate to siltstone and this represents the main textural variation of this facies (Figure 3.16e,f). Carthew (1975) noted flute- and drag-casts, and slump structures within the Dunns Mine Limestone, which would also be included within this facies.

The carbonate is fine- to medium-grained but has been recrystallised and the original grainsize is not preserved. Limestone beds contain four and eight-sided needles and rods of K-feldspar, that make-up between 10% and 40% of the rock mass and have associated Mg-chlorite. Siltstone beds are grey to black and may be carbonaceous. In the upper part of the section shown, siltstone is calcitic but down the section, the amount of carbonate in the siltstone decreases to zero. Where the ICSlt Facies is dolomitic, both the carbonate and the siltstone are a cream colour. In thin-section, K-feldspar occurs as anhedral masses within the carbonate beds and within the siltstone beds. Both the siltstone and the carbonate layers are pyritic and chalcopyrite is present, albeit rare.

3.2.8.2 Interpretation

The probable destruction of sedimentary features by the recrystallisation of the carbonate beds in the ICSlt Facies places some doubt over its interpretation. There are similarities between the ICSlt Facies and the Siltstone-dominant Siltstone-Sandstone Facies in the thinly bedded fine-grained and silty to muddy fractions, which suggests a similar environment of deposition. The K-feldspar and chlorite pseudomorphs may be after evaporitic minerals which would add greater weight to such an interpretation.

If the lack of sedimentary structures is a primary feature and not due to recrystallisation of the carbonates, then this is the key difference between the ICSlt Facies and the Siltstone-dominant Siltstone-Sandstone Facies. A lack of sedimentary structures is evidence of there

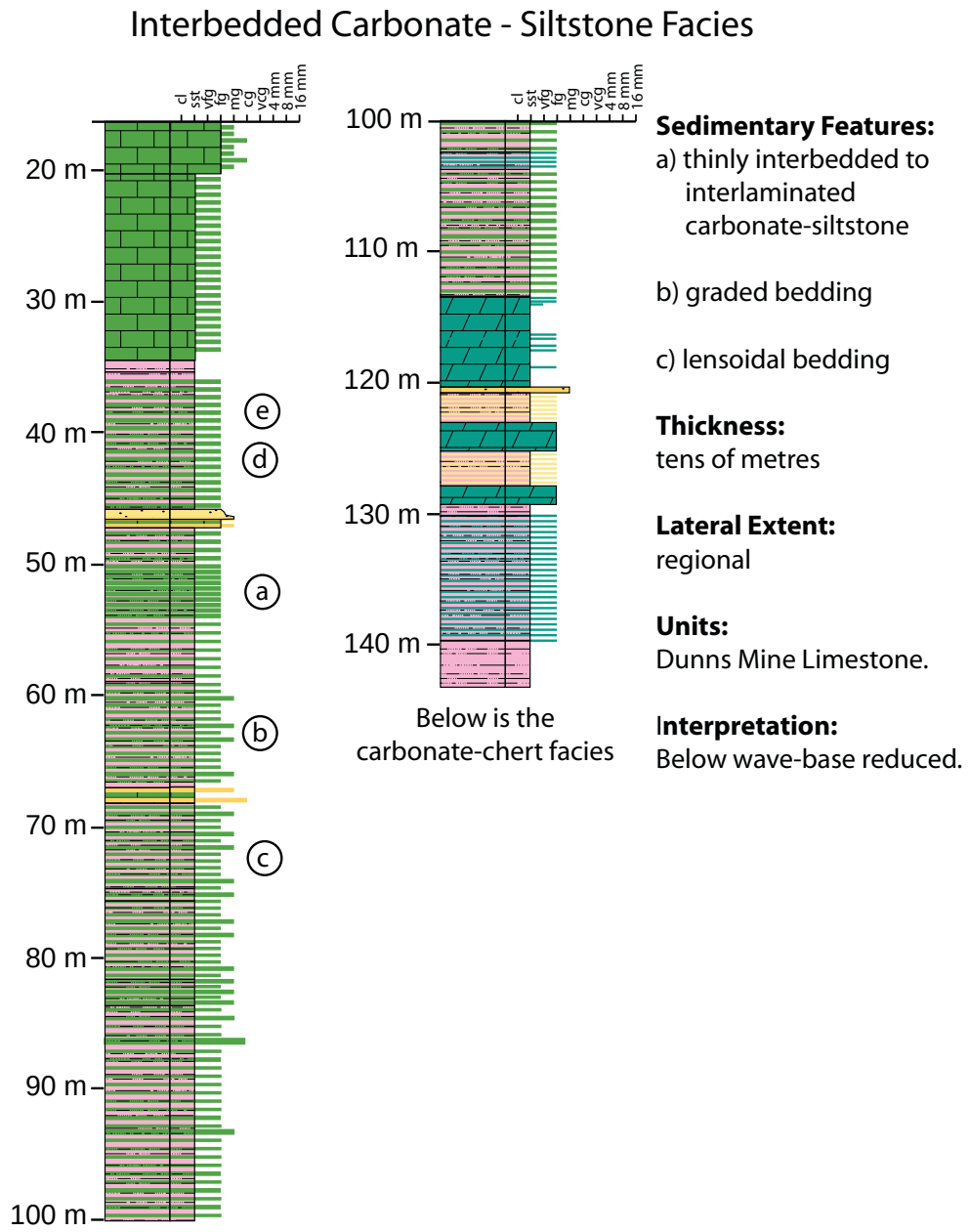

Figure 3.15. Main features of the Interbedded Carbonate-Siltstone Facies.

having been no reworking of the sediments after deposition. In this, the ICSlt Facies has more in common with the Black Shale Facies. Flute- and drag-casts (scour and tool marks) and graded bedding are features of turbidites (Walker, 1992) and suggest deeper water deposition. Another feature of the ICSlt Facies is the dolomitisation of the basal section, which may represent a transition from the influence of continental waters to marine waters (Knoll and Swett 1990; Sun, 1994; Hill et al., 2000).

The thin laminations, the graded bedding in siltstone units, and the lack of sediment reworking suggest that the ICSlt Facies was deposited below wave-base. An evaporitic origin for the K-feldspar and chlorite pseudomorphs is rejected for reasons which are discussed below, hence a shallow water to emergent environment is also rejected. The carbonate was transported from a shallow-water carbonate factory down slope into the sub-wave base environment by turbidity currents with the siltstone and mudstone being

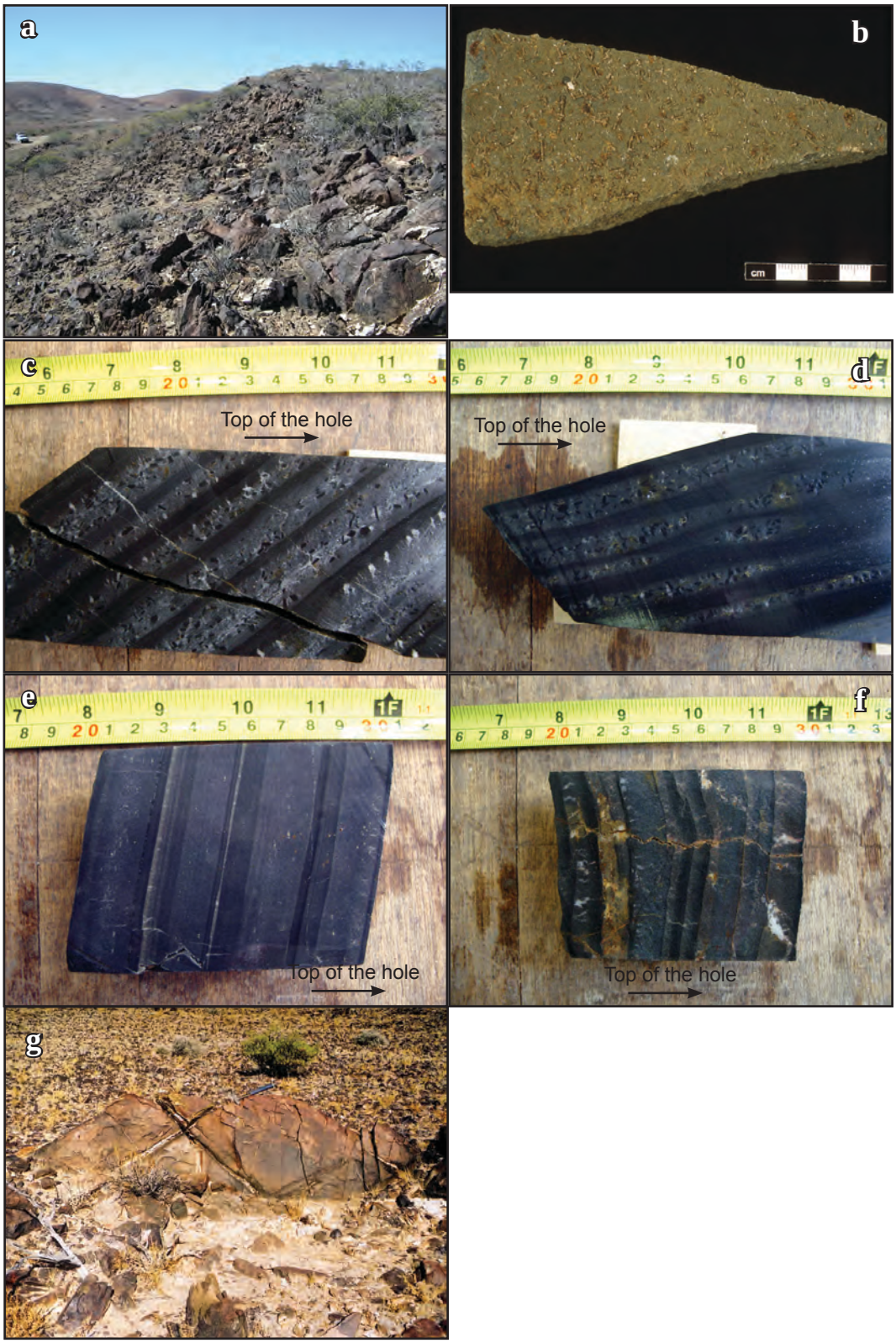

Figure 3.16. Textures of the Interbedded Carbonate-Siltstone Facies.
a) Typical outcrop of the interbedded carbonate-siltstone Facies, near the Dunns Mine. Along the crest of the hill is a coarser-grained sandy unit and on the slope is the interbedded carbonate and siltstone. b) Typical green calcite float containing needles and rods of K-feldspar and muscovite. c) Interbedded limestone-siltstone with cm-scale beds of silstone-shale and limestone, and graded bedding; WD005. d) Lensiodal bedding, with lenses of limestone within siltstone-shale; WD005. e) A variant with fine-grained limestone and thinner siltstone beds; WD016. f) The coarser-grained variant, with graded bedding in clastic beds; WD016 g) A boudin of calcitic sandstone within this facies, near Dunns Mine.

deposited from suspension. The absence of coarser-grained siliciclastic material suggests that the area is distal to a siliciclastic source.

3.2.9 Microbial Carbonate (MC) Facies

3.2.9.1 Description

The Microbial Carbonate (MC) Facies occurs in the Recovery Formation, the Hogan Dolomite, the Cooranna Formation and the Boorloo Siltstone, where the section shown was logged (Figure 3.17). Microbial mats are the most common sedimentary feature and stromatolites occur at the base of the Hogan Dolomite. On weathered surfaces, the carbonate is typically yellowish (Figure 3.18a) whereas on fresh surfaces it is typically green. It occurs in units one to two metres thick with a lateral extent in the order of kilometres. The MC Facies typically overlies the Siltstone-dominant Siltstone-Sandstone sub-facies or the Black Shale Facies with an abrupt contact, and underlies the Siltstone-dominant Siltstone-Sandstone sub-facies or the Black Shale Facies with abrupt contacts, or the Carbonate-Chert Facies with a gradational contact. The abrupt contacts with the Siltstone-dominant Siltstone-Sandstone sub-facies or the Black Shale Facies may be related to the nature of the outcrop, in which the MCF stands above the surrounding surface whereas siltstone-dominant facies are recessive.

The defining feature of the MC Facies is the presence of wavy laminations of alternating green-grey carbonate and darker laminations (Figure 3.18b). Grain size is silt to mud. At the top of this section is a zone where fragments of this material have random orientation within a muddy dolomite matrix. Molar-tooth structure is tentatively identified at one locality within the basal Hogan Dolomite. In other outcrops of the MC Facies, chert nodules up to 1 cm in diameter and white rod-like pseudomorphs, up to 15 millimetres long and four millimetres across occur. The rod-like pseudomorphs have four or eight sides and are typically rectangular in cross-section. They do not usually have associated micas, unlike those that occur in the Dunns Mine Limestone. Linked columnar stromatolites are 30 cm tall and 10 to 15 cm across (Figure 3.18c) and many have been replaced by chert (Figure 3.18d). Most, but not all, occurrences of the MC Facies are dolomite.

3.3.9.2 Interpretation

The laminations in the MC Facies are attributed to the collection of material from suspension by microbial mats and also carbonate precipitation. Microbial mats by themselves are not indicative of a particular environment. In Recent sediments they occur in a range of environments from sub-tidal to supratidal (Tucker, 1990) but their preservation is limited due to the grazing of animals and destruction in high-energy environments (Browne et al., 2000). However, in the Neoproterozoic, the preservation potential of microbial mats was higher due the absence of grazing animals. In the absence of wave or current generated structures, they are probably sub-tidal in this case. The juxtaposition of the MC Facies with the Black Shale Facies (Section 3.3.4) indicates a gradual shallowing in the section shown, where the MC Facies is succeeded by the evaporative Carbonate-Chert Facies. Where it is succeeded by the Black Shale Facies, a transgression is indicated.

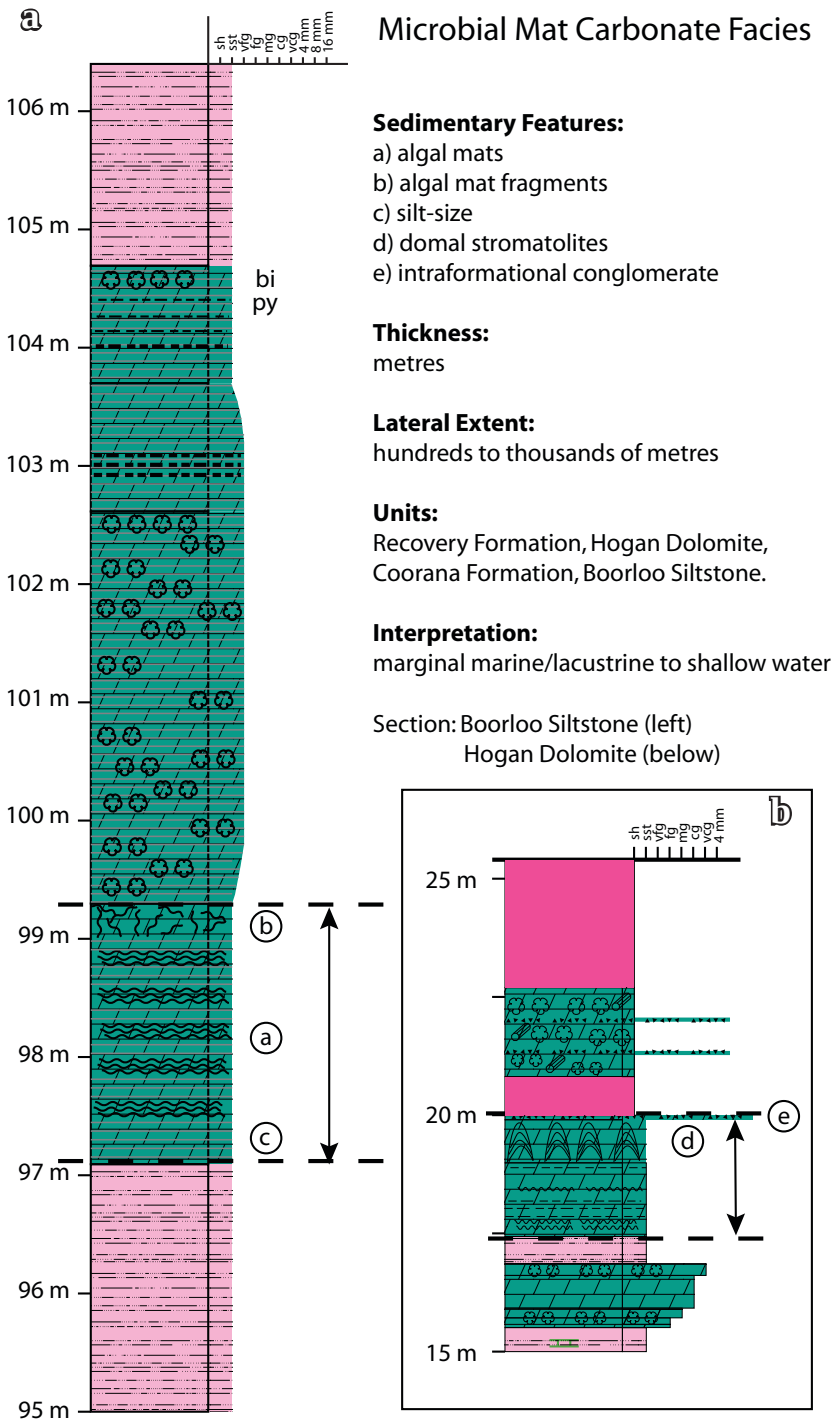

Figure 3.17. Main features of the Microbial Mat Carbonate Facies.
a) (left) the Microbial Mat Carbonate Facies in the Boorloo Dolomite b) (right) the Microbial Mat Carbonate Facies in the Lower Hogan Dolomite.

Stromatolites can exist in a range of environments from inter-tidal to sub-tidal settings (Tucker and Wright, 1990). Columnar stromatolites in the Neoproterozic Dal Formation of northern Canada are interpreted by Turner et al., (2000) to have formed in high energy environments. In the absence of either thicker stromatolitic units or a wider variation of stromatolite forms, it is difficult to be more precise on the depositional environment of this unit. The local presence in the MC Facies of chert or quartz nodules after anhydrite suggests an emergent depositional environment similar to the Carbonate-Chert Facies (see below).

Figure 3.18. Textures of the Microbial Carbonate Facies.
a) Outcrop of stromatolitic dolomote, base of the the Hogan Dolomite. b). Folded laminated microbial dolomite, Recovery Formation. c) Outcrop of stromatolitc dolomite, Lower Hogan Dolomite. d) Chert replacing columnar stromatolites, Lower Hogan Dolomite.

3.2.10 Carbonate – Chert (CC) Facies

3.2.10.1 Description

The Carbonate - Chert (CC) Facies (Figure 3.19) is a yellow-brown weathering unit carbonate unit one to five metres thich that contains varing proportions of chert, either as layers or nodules (Figure 3.20a,b). It occurs in the Boorloo Siltstone, the Cooranna Formation, Hogan Dolomite and the Recovery Formation. Typically the CC Facies is dolomite only but limestone can occur locally. The CC Facies can occur with the Microbial Carbonate Facies, in which case the contact is gradational, or the Black Shale Facies, where the contact is gradational or abrupt. Thin siltstone beds sometimes occur in this facies as a minor component.

The key feature of the CC Facies is the presence of chert in thin layers and nodules typically a few millimetres in diameter (Figure 3.20c,d,e). These smaller nodules tend to be quartz rather than chert but true chert nodules are present and tend to be larger, up to a four centimetres in diameter. A few larger nodules are sub-spherical and may have tails (Figure 3.20e). Nodules consist of quartz and sulphides, with or without dolomite. Most chert layers are less than 1 cm thick but at the base of the Dunns Mine Limestone, a chert layer 20 cm thick replaces dolomite (Figure 3.20f,g). Enterolithic folding of the thin chert layers is common (Figure 3.20b). Microcline pseudomorphs after gypsum are confined to very fine- to medium-grained carbonate units. Rod-like pseudomorphs of microcline after scapolite occur in the CC Facies within the Hogan Dolomite (Figure 3.20h). Unoriented

muscovite or biotite flakes and crystals up to 5mm long and 2 mm across make up to 5% of the rock mass.

Sedimentary structures are rare in the CC Facies. Dolomite varies from silt-size to dominantly fine-grained. It is thinly-bedded to laminated with variable amounts of siltstone occurring as thin beds and laminations. Individual beds have sharp boundaries. Wavy and

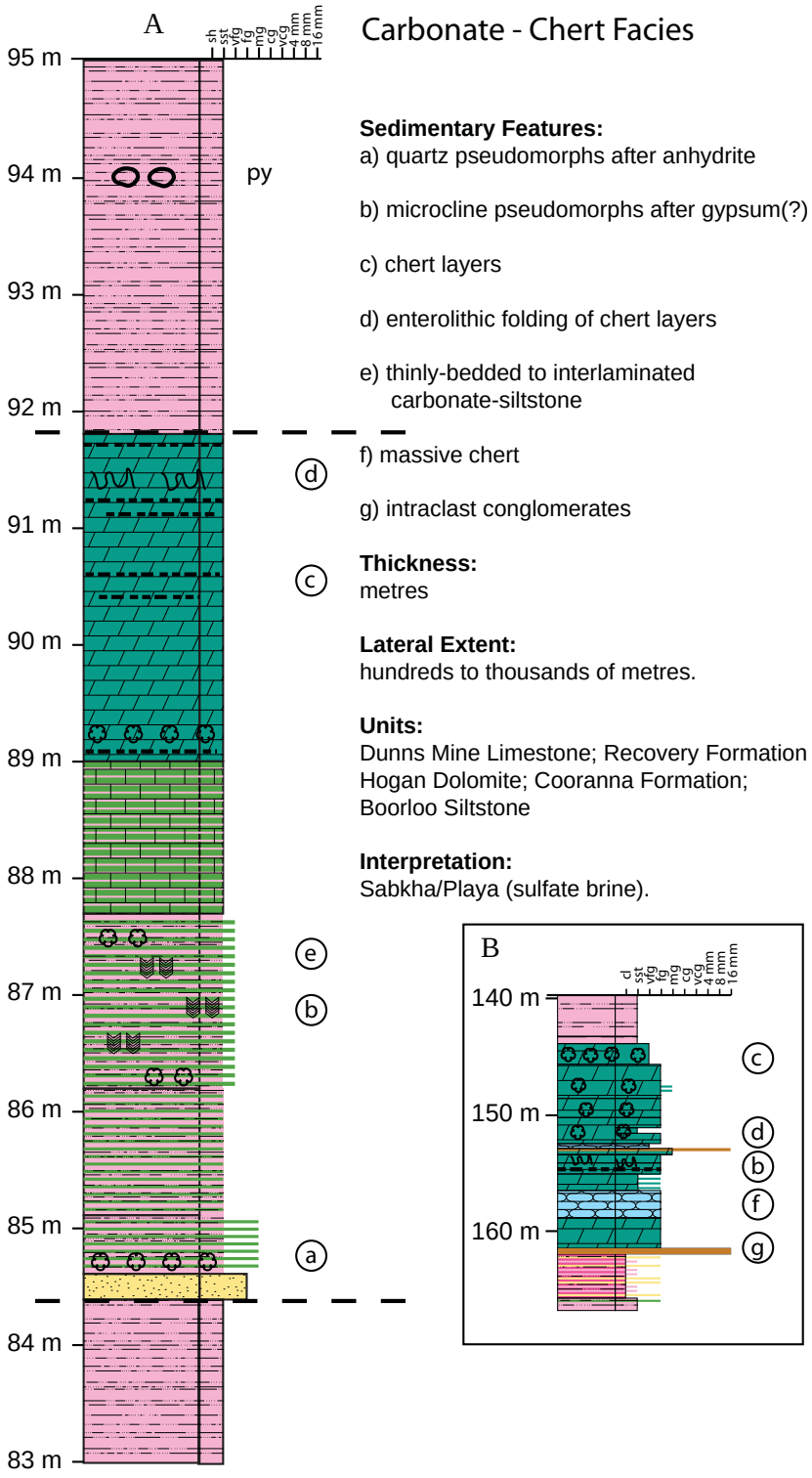

Figure 3.19. Main features of the Carbonate - Chert Facies.
Column A is from surface outcrop of the Boorloo Dolomite and Column B is from diamond drill core in the Dunns Mine Limestone; WD016.

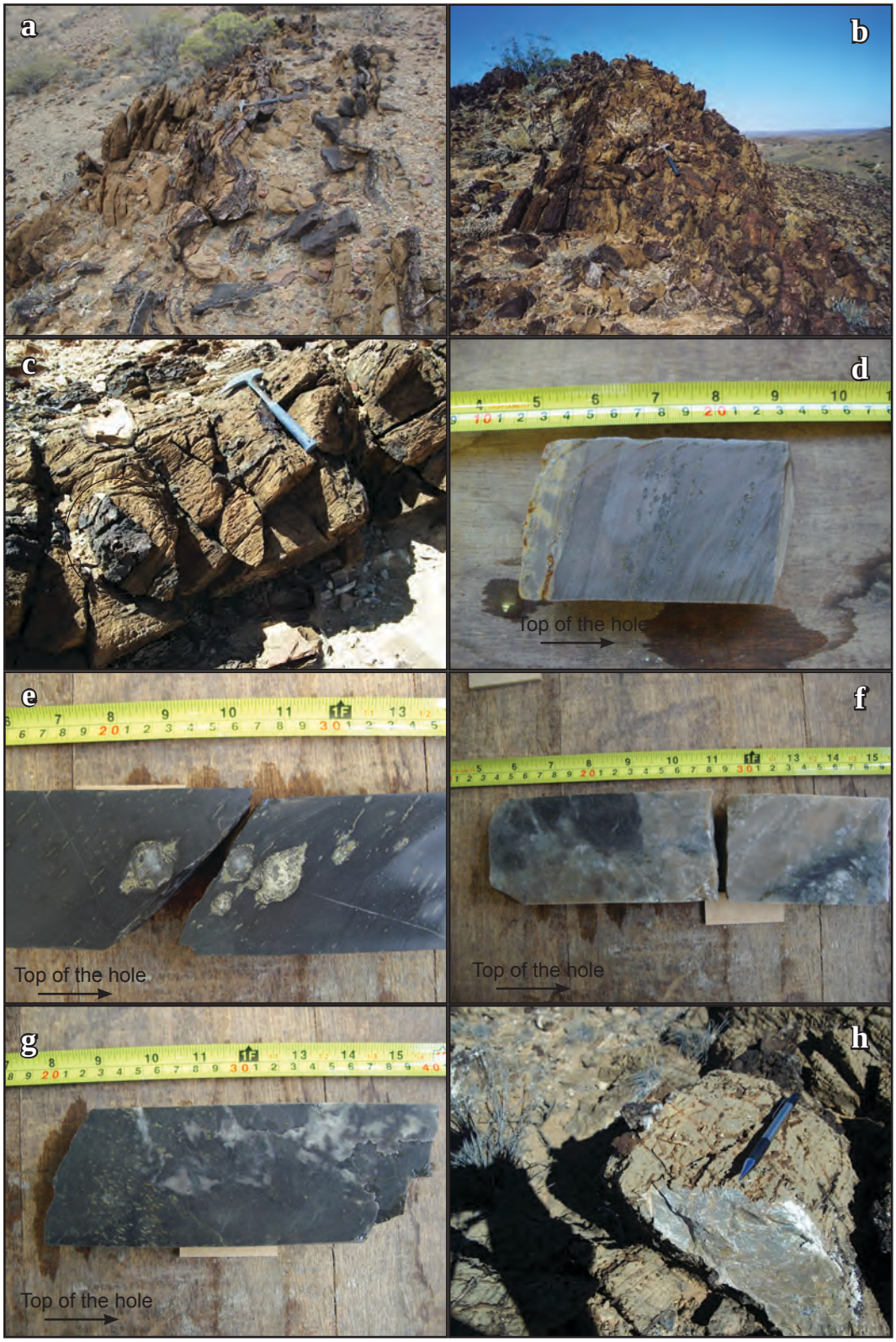

Figure 3.20. Textures of the Carbonate-Chert Facies.
a) Outcrop of chert-dolomite facies in the Boorloo Siltstone. b). The CC Facies at the base of the Dunns Mine Limestone, showing enterolithic folded chert beds. c) Chert nodules (one example circled) in dolomite from the base of the Dunns Mine Limestone d) Small chert nodules (darker bedded features) in the CC Facies, Boorloo Siltstone. e) Chert nodules from the base of the Dunns Mine Limestone. Nodules comprise quartz, dolomite and sulfides. f) Massive chert, base of the Dunns Mine Limestone. g) Chert replacing dolomite, base of the Dunns Mine Limestone. h) The CC Facies from the Lower Hogan Dolomite showing rod-like microcline pseudomorphs.

lensoidal bedding of coarse-grained dolomite occur and intraformational conglomerates, a few centimetres thick are rare.

3.3.10.2 Interpretation.

The interpretation of the CC Facies intervals is that the characteristic structures represent pseudomorphed evaporitic features. Chert layers and nodules are interpreted to have replaced gypsum/anhydrite and the microcline pseudomorphs have the form of gypsum, with swallow-tail twins and flat, lensoidal crystals. If the gypsum was deposited subaqueously, it would have been bottom nucleated, forming a layers of massive and laminated crystals aligned perpendicular to the bedding (Warren, 1999). In sabkha/playa deposits, gypsum occurs as nodules and enterolithically folded layers, formed within supratidal sediments as displacement and/or replacement textures (Warren and Kendall, 1985). A sabkha/playa is the likely depositional environment for the Carbonate-Chert Facies.

3.3 Lithofacies Associations

3.3.1 Introduction

Having described the facies of the Curdimurka Subgroup and providing an interpretation of the processes involved in their formation, this section will identify the key lithofacies associations. In the above descriptions, some of the lithofacies associations have already been touched upon, in particular the similarities between the sandstone facies. In fact there is likely a continuum from the Sandstone-Conglomerate Facies through to the Siltstone-Sandstone Facies and the boundaries between these facies are in many regards arbitrary, depending upon the presence or absence of conglomerates, an estimation of the sandstone:siltstone ratio and the thickness of sandstone beds. Three lithofacies associations are recognised; a fluvial association; shallow-water to emergent association and a sub-wavebase association.

3.3.2 Fluvial Lithofacies Association.

The Fluvial Lithofacies Association comprises the Sandstone-Conglomerate Facies, the Cross-bedded Sandstone Facies, the Planar Laminated Sandstone Facies and the Sandstone-dominated Siltstone-Sandstone Sub-facies. They share several features in common, and from the combination of grain-size and bed forms, there is a decrease in stream flow energy from the Sandstone-Conglomerate Facies to the Cross-bedded Sandstone Facies to the Parallel-Lamination Sandstone Facies (Figure 2.2; Harms, 1975, 1982). Considered together, the fluvial lithofacies association can be interpreted to record a braided stream environment. The Sandstone-Conglomerate Facies and the Cross-bedded Sandstone Facies correspond to the Platte Creek model (Miall, 1977). Characteristics of this model include lingoid, transverse or other types of sand bar that are the dominant depositional feature and it is interpreted to represent very shallow rivers (Miall, 1977). The Parallel-Lamination Sandstone Facies corresponds to the Bijou Creek model of Miall (1977), which is interpreted to result from flash floods in arid environments. The thin beds show that

the channel systems were shallow and the presence of halite casts in siltstone beds are interpreted to represent flood deposits forming shallow water bodies that were prone to drying-up, indicating an arid environment. Alternatively, the siltstone beds with halite casts may indicate the setting was a across an arid marginal marine zone (coastal plain), with occasional storms flooding across the plain, or wind-blown material transporting salt from the coast into shallow ephemeral lakes fed by river flood water. Therefore the change from the Sandstone-Conglomerate facies and the Cross-bedded Sandstone Facies to the Planar Laminated Sandstone Facies may be the result of increasing aridity.

3.3.3 Shallow-water to Emergent Lithofacies Association.

The term shallow water to emergent lithofacies association is preferred because it does not infer either marine or lacustrine environments. In a marine setting, it would be a peritidal zone (Folk, 1973) or a sabkha, and in a lacustrine setting, it would a playa.

Tidal flats comprise sub-tidal, inter-tidal and supra-tidal zones (Shinn 1983; Weimer et al., 1981; Pratt et al., 1992). Tidal channels and sand flats occur in the sub-tidal zone, sand flats, and mixed flats and mud flats in the intertidal zone. The sandstone-dominant siltstone-sandstone sub-facies is interpreted to record the sub-tidal zone to lower intra-tidal zone and the siltstone-dominant siltstone-sandstone sub-facies the upper inter-tidal zone to the supra-tidal zone. Evaporite minerals may be deposited in the supra-tidal zone, either subaerially, in brine-filled depressions or more commonly as displacement crystals within the sediment (Warren, 1999).

The abundance of halite and gypsum/anhydrite pseudomorphs, and the Carbonate-Chert, Microbial Mat Carbonate and Interbedded Carbonate - Clastic Facies indicate an arid zone variation of the Shallow-water to Emergent Lithofacies Association, which can be described using the sabkha model (e.g., Pratt et al., 1992; Warren, 1999). In the sabkha model, the interbedded carbonate-siltstone facies represents the sub-tidal to intertidal zone and the chert-bearing carbonate facies represents the supra-tidal zone. The microbial mats may occur in the sub-tidal to supra-tidal zones and so the carbonate mat facies is not specific to a particular zone (e.g., Tucker and Wright, 1990; Seong-Joo et al., 2000).

Several features typical of tidal zones are lacking or minor in the Curdimurka Subgroup. Herring bone cross-stratification which is indicative of flood and ebb currents (Dalrymple, 1992) is not present, and there is an absence of tidal channels and other high-energy sand bodies (e.g., Wiemer et al., 1982; Dalrymple, 1992). The absence of herring bone cross-stratification may result from one current being dominant (Dalrymple, 1992), and the absence of high energy sand bodies may be the result of a protected embayment or inlet setting (Weimar et al., 1982).

In a lacustrine model, the positions of the facies relative to the water body are reversed. Sand flats occur next to alluvial fans, with the lake (either ephemeral or perennial) at the topographic low (Eugster and Hardie, 1978; Kendall, 1992; Rosen, 1994). The sand flats trap the incoming sediment, so that little or no sand reaches the depocentre. Dry and then saline mudflats occur toward the basin centre, which is the site of an ephemeral salt pan (Kendall,

1992). Dry mudflats typically display cracking but little or no displacive evaporites whereas wet mudflats contain displacive evaporite casts (Benison and Goldstein, 2001). Hence, in this lithofacies association, the sandstone-dominant siltstone-sandstone sub-facies is adjacent to the alluvial fan, the siltstone-dominant siltstone-sandstone sub-facies forming the dry mudflat and the saline mudflat. Although not definititve, playa models often include aeolian sand dunes on the sand flats but these are absent from the Curdimurka Subgroup.

In an evaporitic setting, carbonates are the first mineral to be deposited from solution (Eugster and Hardie, 1978). Hence, directly precipitated carbonate units will overlie deeper water sediments and if evaporation continues, they will be overlain by shoreward facies. Once deposited it is also available for transport either into the deeper basin, or shoreward by storms. Hence, in the absence of evaporite minerals, the Interbedded carbonate - clastic facies could be deposited basinward of the area of carbonate precipitation. At its most extreme, it would belong to the Sub-wave Base Lithofacies Association (see below). If evaporite minerals are present carbonate facies would be either shallow water, with evaporite minerals being displacive, having precipitated from interstitial brines or they could be emergent and evaporite minerals could be displacive or deposited direct from solution, typically in shallow pools (Warren, 1999). In the lacustrine setting this would be the saline mudflats. As chert replaces gypsum and/or anhydrite, the Carbonate-Chert Facies represents the saline mudflat facies in the lacustrine environment. As in the sabkha model, the Microbial Mat Carbonate Facies is not confined to a specific zone.

3.3.4 Sub-wave Base Lithofacies Association

The Sub-wave base Lithofacies Association comprises the Black Shale Facies and the Interbedded Carbonate-Siltstone Facies. It may also include some of the siltstone-dominant siltstone-sandstone sub-facies and the interbedded carbonate-clastic facies, which may be transitional between the Black Shale Facies and obviously shallow water facies. In this case they do not contain evidence of subaerial exposure or evaporites as is typical of the shallow water to emergent lithofacies association. The Sub-wave base lithofacies can occur in either marine or lacustrine settings. Newton (1994) concluded that in Mono Lake (California) finely laminated organic-rich clayey-silts were deposited below the pycnocline in a meromictic lake at depths greater than 12 to 16 m during lake highstands. In Lake Bogoria (Kenya Rift Valley) laminated and massive black muds were deposited in the centre of the basin, below the chemocline (Renaut and Tierclin, 1994). However, in both of these cases, the black shales are only a few metres thick at the most. Organic-rich shales are common in many ancient lacustrine settings including the Congo Basin (Harris, 2000; Harris et al., 2004), the Erlian Basin in northeast China (Changsong et al., 2001), and the Green River Formation (Bradley and Eugster, 1969). In all of these examples, the lacustrine black shales may be tens to hundreds of metres thick, and so the modern examples of saline lakes may not apply to the Curdimurka Subgroup as a whole but may be more relevant to those units that have thin black shale units such as the Cooranna Formation and the basal Hogan Dolomite.

3.4 Facies Architecture

3.4.1 Introduction

Having elucidated further the depositional environments of the Curdimurka Subgroup, this section will integrate the sedimentary facies with the formal stratigraphy. This has been slightly modified (informally) as a result of the mapping conducted as part of this study, and is shown in Table 3.2 and Figure 3.21 with the facies present and depositional cycles. It will discussed in terms of these cycles.

3.4.2 Cycle 1: Dome Sandstone to Rook Tuff

The base of Cycle 1 is faulted out but within the Dome Sandstone it comprises repeating cycles of Parallel Laminated Sandstone and Sandstone-Siltstone Facies. Both the Cross-bedded Sandstone and Sandstone - Conglomerate Facies are minor. Only one outcrop of the latter was noted near the base of the Dome Sandstone and the former decreases in thickness and frequency up-section. There is a increase in the proportion of Sandstone-Siltstone Facies moving up-section and a gradual change to the Black Shale Facies in the Rook Tuff.

The tuff bed which gives the Rook Tuff its name occurs over a strike length of about 2,000 m, from just north of the Dunns Mine, to south of the Rook workings (Figure 3.1). Above the tuff unit and below the Black Shale Facies, there occurs the Parallel Laminated Sandstone Facies and Sandstone-Siltstone Facies. In the absence of the tuff bed, it is not possible to say where the Dome Sandstone ends and the Rook Tuff begins, until the Black Shale Facies is reached.

The transition between Cycle 1 and Cycle 2 occurs at the boundary between the Rook Tuff and the overlying Dunns Mine Limestone, and is abrupt. There is an increase in the proportion of carbonate within the Black Shale Facies near the top of the cycle at the measured section. At Dunns Mine, there is also a higher proportion of sandy beds as the contact is approached, relative to the measured section. At both localities, these form only a small proportion of the rock relative to the amount of black shale and siltstone.

Cycle 1 represents a gradual transition from continental sedimentation in braided streams, possibly across sandflats to a below-wave base depositional environment.

3.4.3 Cycle 2: Dunns Mine Limestone

Cycle 2 is wholly contained within the Dunns Mine Limestone. At its base is the Carbonate-Chert Facies which is overlain by Interbedded Carbonate-Clastic Facies. Dolomite is the main carbonate phase in the basal Carbonate-Chert Facies and up to about 30 m above the base of the Dunns Mine Limestone, in the Interbedded Carbonate-Clastic Facies. A 20 m thick zone then occurs where limestone is the dominant carbonate and thereafter, the only carbonate is limestone. From the three drill hole intersections of the Dunns Mine Limestone (Figure 3.1), there is a decrease in grainsize and a reduction in thickness of coarser-grained beds from northwest to southeast. These suggest increasing water depth

Table 3.2. Summary of the depositional cycles and sub-cycles of the Curdimurka Subgroup.

Cycle	Sub-Cycle	Environment of Deposition	Facies	Formation
	21	Gradual regression, short-lived cycles of flooding and dessication with eventual deposition of carbonates in an evaporitic environment	Slts	BDol
C4	20	Transgression and deposition of silt and mud in an anoxic environment.	BS CC PLS	BShl
	19	Regression. Deposition on a sand flat	Slts	CSlt4
	18	Transgression. Deposition on a mud flat	Slts	CSlt3
	17	Four sub-cycles of regression and transgression with siltstone-sandstone in evaporitic conditions and black shale deposition	Slts	CSlt2
	16	Shallow-water to evaporitic environment,	Slts	CSlt1
	15	Regression with shallow water to evaporitic (?)		Upper-most HD
	14	No outcrop	?	HD
	13	Regression and deposition in an evaporitic environment	Slts ICC MMC CC	base of the HD upper-most RSst4
C3	12	Continuing transgresson and deposition in a sub-wavebase anoxic environment	BS	RSst4
	11	Transgression and deposition on a mud flat, to shallow water	Slts	RSst4
	10	Regression and deposition of a sandsheet from a braided stream	PLS SS	RSds2
	9	Transgression and deposition on a mud-flat	Slts	RSst3
	8	A more prolonged regression and deposition on a sand flat (several fining-upward cyles)	SS Slts	RSds1
	7	A series of transgressions and regression with variation between sand flats and mud flats	Slts SS	SSst2 RSh
	6	Continued regression and deposition of a thin sandstone unit in braided stream	PLS	RSst1
	5	Gradual regression and deposition in sand and mud flats, possibly intertidal	Slts SS	RSst1
C2	4	Gradual transgression with interbedded carbonates and muds/silt in a below wave-base environment	ICS	Dunns Mine Limestone
	3	Rapid (?) regression, with the deposition of evaporites (gypsum) in a dessicated environment	CC	Dunns Mine Limestone
C1	2	Gradual transgression with deposition of muds and silts in an anoxic, below wave-base environment	BS	Rook Tuff
	1	Deposition of sandstone and siltstone in a braided stream environment, possibly through sand flats in an arid environment, overall fining upward.	SC CBS PLS	Dome Sandstone

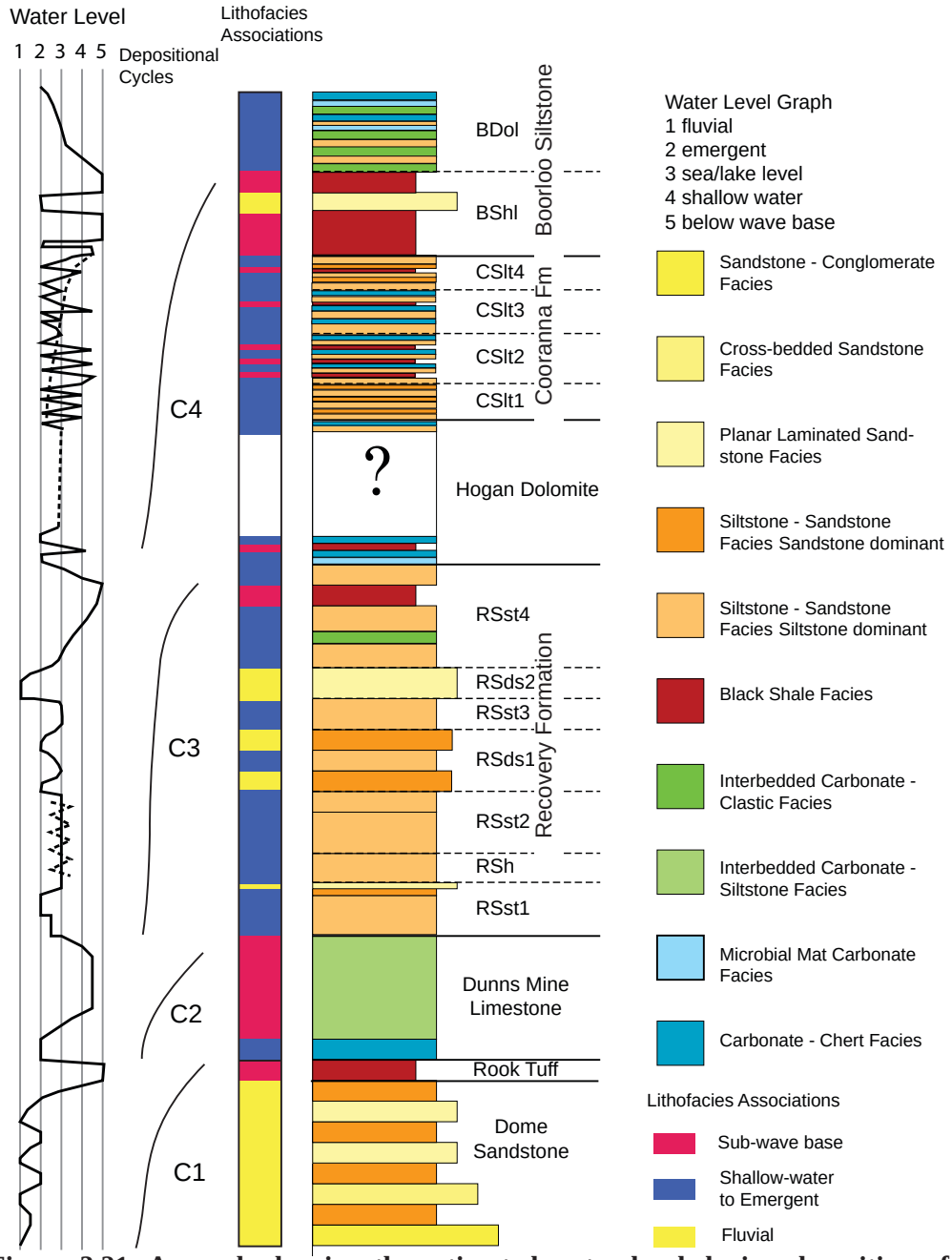

Figure 3.21. A graph showing the estimated water level during deposition of the Curdimurka Subgroup, with depositional cylces, lithofacies associations and a stratigraphic column with lithofacies.

The diagram is partly diagrammatic, particularly in areas of rapid facies changes such as the Recovery and Cooranna Formations. Within the Recovery and Cooranna Formations, beds of Interbedded carbonate - clastic, Microbial mat carbonate and Carbonate - chert facies occur interbedded with the siltstone-sandstone facies, but they constitute only a small percentage of the units and are typically too thin to show at this scale. The Depositional Cycles column shows the four major transgressive cycles during deposition of the Curdimurka Subgroup. The lithofacies associations column emphasises the point that for much of the time, the Willouran Trough was at about the same level relative to the water level.

from north to south. A thin breccia occurs between the Dunns Mine Limestone and the overlying Recovery Formation, in the the northern half of the Euchre Pack Domain (Figure 3.1). However, northwest of Dunns Mine, the contact is abrupt.

The base of Cycle 2 represents a rapid shallowing from the sub-wave base conditions of the Rook Tuff to sub-aerial conditions and deposition of evaporites. This was followed by

a transgression resulting in deposition of the Interbedded Carbonate-Clastic Facies. Based on empirical evidence from Proterozoic carbonates elsewhere (Knoll and Swett, 1990; Sun, 1994; and Hill et al. 2000), the transition from dolomite to limestone suggests an increase in water depth.

3.4.4 Cycle 3: Recovery Formation

Cycle 3 is wholly within the Recovery Formation, which can be divided into six members (Figure 3.21); a lower silty unit RSst1, a sheared siltstone unit with minor carbonate (RSh), a silty unit (RSst2), a lower sandy unit (RSds1), a silty unit (RSst3), an upper sandy unit (RSds2), and an upper siltstone and black shale unit (RSst4: Figure 3.21). RSlt1, RSlt2 and RSlt3 crop out poorly but are likely the Siltstone Dominant Sandstone-Siltstone Sub-facies. Carbonate beds containing chert nodules, occasional rod-like pseudomorphs and microbial laminations occur within these units and are combinations of the Carbonate - Chert, Microbial Carbonate and Interbedded Carbonate-Clastic Facies. Either the Black Shale Facies or Siltstone-dominant Siltstone-Sandstone Facies occur between the carbonate units. The sheared siltstone unit (RSh) comprises siltstone with rare boudinaged carbonate beds up to 20 cm thick. The contact between the Lower Sandy Unit and the Sheared Siltstone is marked by a two metre thick unit of the Parallel Laminated Sandstone Facies.

RSds1 comprises Sandstone Dominant Sandstone-Siltstone Facies and Siltstone Dominant Sandstone-Siltstone Sub-facies in a series of upward-fining cycles (Figure 3.21). RSds2 comprises Parallel Laminated Sandstone Facies and Sandstone-Siltstone Facies in an upward-fining package. RSlt4 provides the best outcrop of the Siltstone-dominant Sandstone-Siltstone Facies. It contains a carbonate couplet in its lower third that has been folded and faulted and in the upper half comprises Black Shale Facies that has a gradual transition to Siltstone-dominant Siltstone-Sandstone Facies.

The along-strike variation within the Recovery Formation is complicated by low-angle normal faults that remove stratigraphy, considerably thinning it from its thickest point in the middle of the Euchre Pack Domain, to the Rook workings where it is faulted out (Figure 3.1). RSds1 thins to the south from a maximum thickness in the centre of the domain to east of Dunns Mine where it is faulted out. The sandstone:siltstone ratio decreases and the thicker sandstone beds (greater than 5 cm) are absent adjacent to Dunns Mine so that it becomes the Siltstone Dominant Sandstone-Siltstone Sub-facies. RSds2 thins to the south from a maximum in the centre to about ten metres northeast of Dunns Mine. The upper surface of RSds2 is a fault zone. Variations in intensity of the deformation are the major cause of thickness variations in the carbonate units. Similarly, the thickness of the RSh unit is a factor of deformation and any thickness variations due to sedimentological reasons cannot be identified. The Black Shale Unit at the top of the Recovery Formation also thins from the centre of the area to the south but this may be due to deformation as in the vicinity of Dunns Mine, it has a layer parallel foliation. The contact between the Recovery Formation and the Hogan Dolomite is gradational, from the Siltstone Dominant Sandstone-Siltstone Sub-facies to Carbonate-Chert Facies.

Cycle 3 is a period of slow changes in water depth; initially from a sub-wave base depositional environment at the top of Cycle 2 to an emergent environment in RSlt1 (Figure 3.21). Thereafter, the depositional environment varies between shallow water to emergent in a series of short sub-cycles, until it reaches a minima in RSds2. Above RSds2, there is a gradual transgression to the Black Shale Facies near the top of RSlt4.

3.4.5 Cycle 4: Upper-most Recovery Formation to the Boorloo Siltstone.

Cycle 4 begins with a rapid transition from the Black Shale Facies at the top of Cycle 3 to emergent in the Lower Hogan Dolomite (Figure 3.21). The lower 30 metres of the Hogan Dolomite comprises from its base, the Microbial Carbonate Facies, Carbonate-Chert Facies and the Black Shale Facies, and then back to the Carbonate-Chert Facies before the poorly outcropping siltstone above (Figure 3.21). Both to the north and south, it is affected by deformation but there is little change along the length of its outcrop until is it faulted out entirely. Most of the Upper Hogan Dolomite does not crop out except for narrow beds of dolomite protruding a few centimetres above the surface.

The upper few metres of the Hogan Dolomite comprises the Siltstone-dominant Siltstone-Sandstone Sub-facies with abundant well formed halite casts in siltstone. Above this is a two metre thick unit of dolomitic Carbonate-Chert Facies, with quartz and chert nodules forming up to 20% of the rock mass. It also contains thin beds and lenses of fine-grained sandstone up to 2 cm thick within the dolomitic unit.

The Cooranna Formation represents a series of short sub-cycles. It was divided by Murrell (1977) into four members; a basal sandstone-siltstone unit (CSlt1), two middle members that are mainly siltstone with minor sandstone (CSlt2 and CSlt3) and an upper siltstone and sandstone unit (CSlt4: Figure 3.21). Carbonate beds occur in all four of these units, although less so in the upper unit. Deformation has altered the thickness of the Cooranna Formation along its outcrop length, with repetitions due to thrusting in the north and middle of the area and removal of stratigraphy at the southern end due to low-angle normal faults (Figure 3.1). Because the Cooranna Formation is mainly siltstone and the faults are low-angle, juxtaposing one thinly-bedded siltstone block against another thinly-bedded siltstone block, it is difficult to analyse any thickness changes due to depositional factors.

In CSlt1 the main lithologies are siltstone and sandstone with a few thin carbonate beds. Halite casts are moderately common. The facies present are the Sandstone Dominant Sandstone-Siltstone Facies and Siltstone-dominant Siltstone-Sandstone Sub-Facies (Figure 3.21, Table 3.2).

The basal section of the CSlt2 comprises repeating units of black shale, carbonates and siltstone. The carbonate beds are up to one metre thick and commonly contain rod-like pseudomorphs of K-feldspar. They are most common in the bottom third of the unit, decreasing in abundance up section. Three or four black shale beds are present, the thickest being about 20 m thick. The upper part of the unit comprises thinly interbedded siltstone and sandstone. The facies present are the Siltstone-dominant Siltstone-Sandstone Sub-Facies, the Black Shale Facies and the Carbonate-Chert Facies (Figure 3.21, Table 3.2).

CSlt3 comprises laminated siltstone with minor sandstone beds, thin carbonate beds and a one metre thick black shale bed. Carbonate beds contain chert after anhydrite. The Siltstone-dominant Siltstone-Sandstone Sub-Facies is dominant, with thin units of the Black Shale Facies and the Carbonate-Chert Facies (Figure 3.21, Table 3.2).

CSlt4 comprises interbedded siltstone and sandstone. It is more sandy toward the base and more silty toward the top. Sedimentary structures include ripple cross-beds, wavy bedding and lenses of sandstone. Desiccation cracks are common. There is a three metre thick black shale near the middle of the member. Hence, the facies present are Sandstone Dominant Sandstone-Siltstone Facies, Siltstone-dominant Siltstone-Sandstone Sub-Facies and the Black Shale Facies (Figure 3.21, Table 3.2).

As a whole, the Cooranna Formation can be interpreted as a time of fairly stable deposition at or about the same water level (Figure 3.21). In detail, it comprises a series of transgressive and regressive cycles, finishing with the beginning of a transgressive cycle.

The Boorloo Siltstone represents a time of maximum transgression followed by a final regression. It comprises two units, a black shale and siltstone dominated lower unit, here termed the Boorloo shale (BShl) and an upper unit comprising interbedded siltstone and dolomite here termed the Boorloo dolomite (BDol). The Boorloo shale is about 250 m thick and the Boorloo dolomite about 120 m thick in the centre and north of the Euchre Pack Domain (Figure 3.21). However, south of 6702500 mN (Figure 3.1), the BShl is about 150 m thick and the BDol is about 20 m thick. The thinning of the BDol is partly due to thinner clastic units between the carbonate beds and partly due to a fault having removed the top of the BDol. About 20 m above the base of BShl is a thin carbonate unit, up to 10 m wide and there is an eight metre thick sandstone unit about 50 m below the base of the BDol, which south of about 6702500 mN (Figure 3.1) has thinned to less than one metre.

BShl comprises mainly the Black Shale Facies (Figure 3.21, Table 3.2). The carbonate unit near the base is the Interbedded Carbonate-Clastic Facies but is too thin to show in Figure 3.21). From the middle to northern end of the area, it is intensely deformed, with folding and shearing destroying primary structures. South of 6702500 mN it is less deformed and contains rod-like pseudomorphs. The sandstone unit belongs to the Parallel Laminated Sandstone Facies, being fine to medium grained and laminated with one bed of planar cross-beds (Figure 3.21). Approaching the BDol, three thin carbonate units (less than 30 cm) occur, over about 30 m true thickness. They are black and very fine-grained and may be due to transport of carbonate down-slope but are too thin to show in Figure 3.21.

The BDol comprises up to 12 carbonate units, separated by clastic siltstone/sandstone intervals. From the base to the top, there is a gradual change in the dominant facies, from Interbedded Carbonate-Clastic Facies, to the Microbial Carbonate Facies with the Carbonate and Chert Facies at the top (Figure 3.21. Table 3.2). The carbonate is mainly dolomite although limestone occurs in one unit likely due to alteration of dolomite and in the upper-most carbonate unit. The clastic units are the Siltstone-dominated Siltstone-Sandstone Facies.

The base of the Boorloo Siltstone is a continuation of a transgressive phase, that commenced at the top of the Cooranna Formation (Figure 3.21). There is a brief regression leading to the deposition of the thin dolomitic unit close to the base, followed by transgression. Again, there is a short regression, with deposition of the sandstone unit, with another transgression, until the final transgression of the BDol (Figure 3.21, Table 3.2).

3.5 The Stony Range and the South Hill Domains.

3.5.1 Introduction

Reconnaissance mapping was conducted in the Stony Range Domain and at the southern end of the South Hill Domain to compare the Curdimurka Subgroup in these areas to the Euchre Pack Domain. The mapping was done as a series of traverses across the ridges that form the outcrop of the Curdimurka Subgroup (Figure 3.22).

3.5.2 Sedimentology

Along the Norwest Fault, a long strike ridge is mapped as the Dome Sandstone (Figures 3.22, 3.23a: Murrell, 1977; Krieg et al., 1992). The ridge comprises a spine of northeast-facing white siliceous sandstone, with interbedded sandstone-siltstone on the margins. Typically there is only one ridge but in the Rocky Point Sub-domain it is repeated due to faulting (Figure 3.22). In the South Hill Domain, there are two to four strike ridges with no structural repetition and the entire package thickens to the north (Figure 3.22).

Along the top of the ridge and down its flanks, the sediments belong to the Cross-bedded Sandstone Facies, the Planar Laminated Sandstone Facies and the Siltstone-Sandstone Facies (Figure 3.23b,c,d). They comprise fine- to very coarse grained, white to grey sandstones. Bed forms are planar laminations, low-angle cross-beds, and rare tabular and sinusoidal cross-beds. Ripples surfaces and ripple cross-beds are common on the northeastern side of the ridge, with both symmetrical and asymmetrical ripples. The thickest sandstone unit is about 50 m, with no siltstone beds. Individual beds are typically less than 2 m thick. The sandstone beds have been strongly silicified, likely as silcrete and are kaolinitic with no feldspar. Rhombic to pyramidal voids up to 5 cm across occur in some sandstone units (Figure 3.23e), as do square voids up to 5 mm across. Both are thought to be due to dissolution of diagenetic minerals and are not after evaporite minerals.

On the northeastern side of the ridge, thinly interbedded siltstone and sandstone are the main lithologies with minor grey shale and carbonate. They show both symmetrical and asymmetrical rippled surfaces, ripple cross-beds and thicker sandstone beds with low-angle cross-beds. Rare halite casts and elongate casts (after gypsum?) are also present.

Moving up-section from the central ridge, the Siltstone-Sandstone Facies is dominant, mainly as the Sandstone Dominant Sub-facies but with some Siltstone-dominant Sub-facies also. Within the siltstone-dominant Siltstone-Sandstone Facies are red and yellow calcitic siltstones with deformed patches of dolomite after anhydrite (Figure 3.23d), not

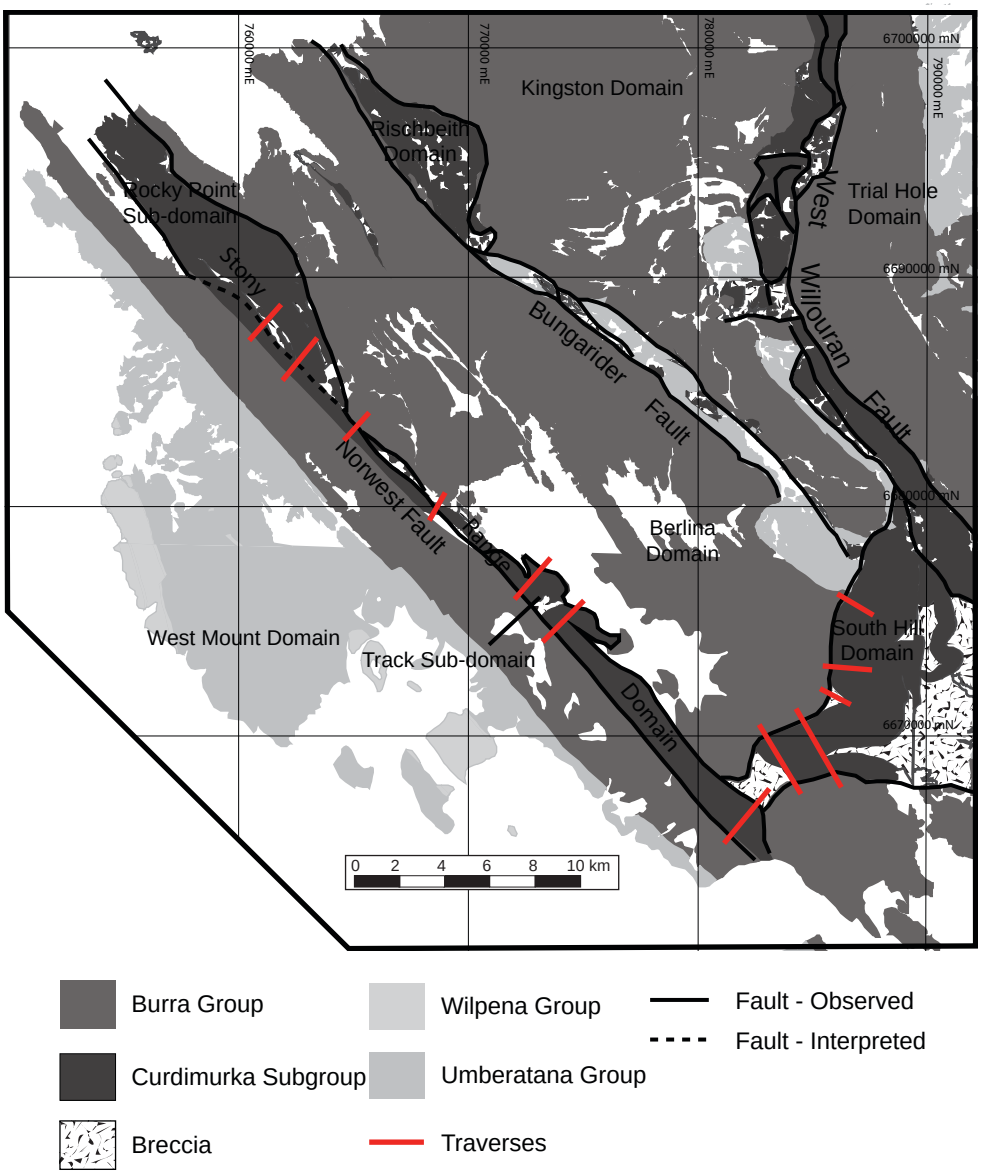

Figure 3.22. Geological map of the Willouran Range showing the localities of traverses across the Stony Range and South Hill Domains (PIRSA 1:100,000 GIS data).
The sedimentology of the Dome Sandstone was examined briefly along these traverses.

seen within the Euchre Pack Domain. Minor carbonate units up to 90 cm thick, belonging to the Microbial Carbonate Facies and the Carbonate-Clastic Facies are interbedded with the sandstone-siltstone facies (Figure 3.23f). The Microbial Carbonate Facies may be stromatolitic although wavy-laminated microbial mats are more common and they may have rippled surfaces, desiccation cracks and elongage casts after gypsum indicating emergent conditions (Figure 3.23g).

3.6 Evaporite Mineralogy

3.6.1 Introduction

In the preceding description and interpretation of the various facies of the Curdimurka Subgroup, it is clear that evaporitic processes have played an important role in the deposition of the Curdimurka Subgroup. The identification of the evaporite mineral assemblage may

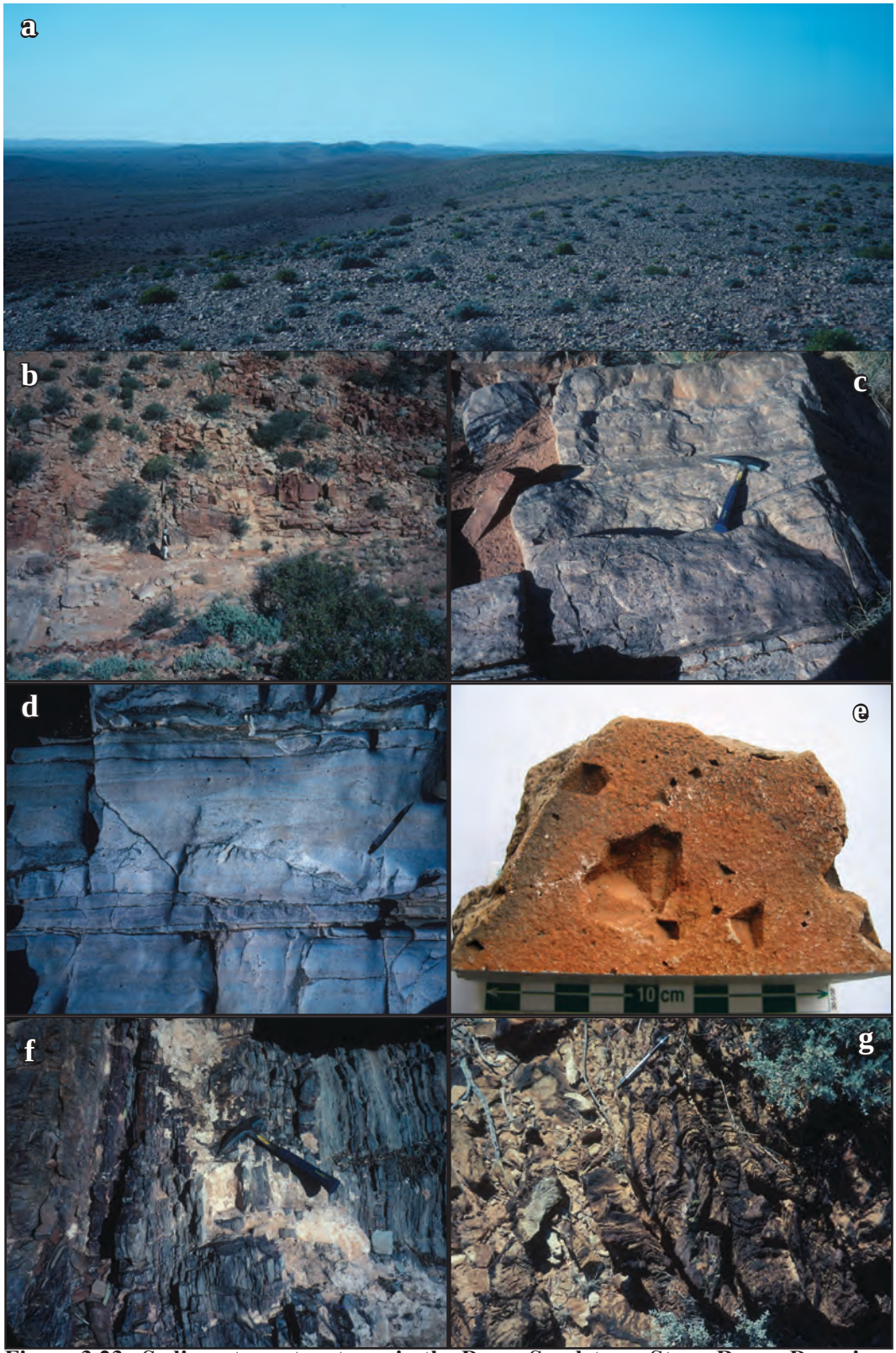

Figure 3.23. Sedimentary structures in the Dome Sandstone, Stony Range Domain. a) view along the strike ridge, looking southeast, shows outcrop of Dome Sandstone. b) Dome Sandstone in a gully, showing much thicker sandstone units than seen in the Euchre Pack Domain, c) Planar cross-bedding and planar laminations from the sandstone units in Figure 3.34c, d) Planar lamination and low-angle cross-beds, Dome Sandstone. e). Sandstone from the Dome Sandstone, Stony Range Domain showing large pyramidal cavities, interpreted to be after a diagenetic mineral. f) Stratigraphically below the sandstone, interbedded sandstone-siltstone, shows lensoidal and wavy bedding. g) A thin unit of microbial carbonate facies above the sandstone-dominated facies along the Norwest Fault.

provide conclusive evidence of a lacustrine – playa setting if it could be shown to be incompatible with deposition from marine waters. Rowlands et al. (1980) described a number of evaporite pseudomorphs and gave conclusions as to what the original evaporite minerals may have been. Pseudomorph morphologies described and named by Rowlands et al. (1980) are given in Table 3.3, with their interpretation. In particular, Rowlands et al (1980) stressed the presence of shortite and gaylussite, both being sodium carbonate minerals and on this basis, when combined with their sedimentological interpretation favour an alkaline playa setting for the deposition of the Curdimurka Subgroup.

There are reasons to question the interpretation of Rowlands et al., (1980). In the first instance, it is not clear why they have interpreted the original minerals from the pseudomorphs as they have, particularly in the case of shortite, gaylussite and scapolite. Rowlands et al., (1980) used the presence of shortite and gaylussite as evidence for an alkaline brine and compare the Curdimurka Subgroup with the Green River Formation, a continental evaporitic unit in the western United States (Bradley, 1962; Bradley and Eugster, 1969). The presence of chert was also used to interpret an alkaline setting, similar to Lake Magadi in Kenya, on the assumption that it is after magadiite (Rowlands et al., 1980). As a counter-point, Frank and Fielding (2003) used the presence of shortite pseudomorphs (with other sedimentological evidence), in the Skillogalee Dolomite to suggest that it was deposited in a marine setting. Frank and Fielding, (2003) based their interpretation on Grotzinger et al. (1989) who suggested that the Neoproterozoic ocean was saturated with respect to carbonate and hence favoured the deposition of alkaline carbonates in evaporitic settings. Hence alkaline carbonates may not be an appropriate depositional indicator in the Proterozoic.

The identification of shortite and gaylussite may also be questioned on geochemical grounds. Based on the geochemical evolution of brines modelled by Eugster and Hardie (1978), gypsum and sodium carbonates should not form from the same brine (Figure 3.24) and Bradley and Eugster (1969) listed gaylussite but not gypsum in their list of evaporitic minerals from the Green River Formation. Finally, Bradley (1962) considered shortite to be a primary mineral in the Green River Formation, but Bradley and Eugster, (1969) suggested that it formed by the dehydration of pirssonite in the presence of calcite at temperatures of about 90^{o}C.

3.6.2 Identification of the Pseudomorphs

The this study, the original evaporite mineralogy was interpreted based on the type and form of the many pseudomorphs recognized in hand-specimens and thin-sections. In the case of halite, forms found were cubes, hoppers, pagoda crystals and skeletal crystals (Figure 3.25a,b). Gypsum and anhydrite were less easy to identify because in most cases, original crystal form is not retained as gypsum is converted to anhydrite and then replaced by K-feldspar, quartz, chert or dolomite (Figure 3.25c,d,e,f). Chicken wire texture was also found at one locality, with the anhydrite replaced by dolomite and quartz (Figure 3.25d). The matchstick texture pseudomorphs and rods (Figure 3.25g,h,i,j) are interpreted to be either scapolite, or microcline or chlorite replacing scapolite. Interfacial angles of the rods are about 90^{o}, indicating a tetragonal crystal form suggesting scapolite as the precursor.

Table 3.3. Evaporite textures described by Rowlands et al., (1980) and their interpretations.

Texture Name	Pseudomorph	Interpretation
Matchstick texture	chert and muscovite	displacive diagenetic shortite ($Na_2CO_3.2CaCO_3$)
Stumpy eight sided crystals	chlorite and K-feldspar	possible scapolite
Chocolate flake texture	microcline	either authigenic microcline or after platy shortite
Displacive shortite moulds	none	shortite
Arrow-head crystal moulds	none	possibly gaylussite ($CaCO_3.Na_2CO_3.5H_2O$)
Discoidal gypsum	microcline	gypsum
Displacive sulfate rosettes (goat droppings)	chert	barite, gypsum or anhydrite
Cauliflower chert	chert and dolospar	gypsum

Scapolite was identified petrographically in a thin section from the Interbedded Carbonate and Siltstone Facies of the Dunns Mine Limestone. In this example it has an octagonal cross-section but otherwise resembles the rod-like pseudomorphs (Figure 3.25i,j). Many of the rod-like pseudomorphs show several generations of microcline growth, with clear margins around inclusion-rich cores (Figure 3.25k,l) and so their external shape is not necessarily the original form. Neither of the two forms of shortite from the Green River Formation have a rod-like appearance, rather they form stubby crystals (Figure 3.26; Bradley, 1962) and on this basis, their identification as shortite is rejected.

Rowlands et al. (1980) identified an arrow-head pseudomorph as gaylussite ($CaCO_3.Na_2CO_3.5H_2O$: Figure 3.27). The published crystal forms of gaylussite do not incorporate an arrow-head shape (Klein et al. 1993; Warren, 1999), and the example shown in Rowlands et al. (1980) resemble skeletal halite (Figure 3.27).

3.7 Discussion

3.7.1 Sedimentary Setting

The lithofacies and facies associations identified here provide the principle basis for determining the depositional environment. It has been shown that the first depositional cycle was in a gradually deepening basin, incorporating fluvial braided stream to sub-wave base environments. Thereafter, deposition mainly occurred in emergent to sub-wave-base conditions, with periods of evaporite deposition. Hence if the depositional setting was marine, it would be a sabkha environment and if non-marine it would be a playa - lacustrine setting, or it could be a combination of both.

Table 3.4 summarizes the evidence for marine and lacustrine environments. The lithofacies could be interpreted as either. More detailed mapping in the Euchre Pack Domain may recognize along-strike variations and associations that could prove definitive but layer-parallel deformation makes correlations over hundreds of metres difficult. Otherwise, the evidence for one or the other is largely negative, refering to what is not seen; an absence of

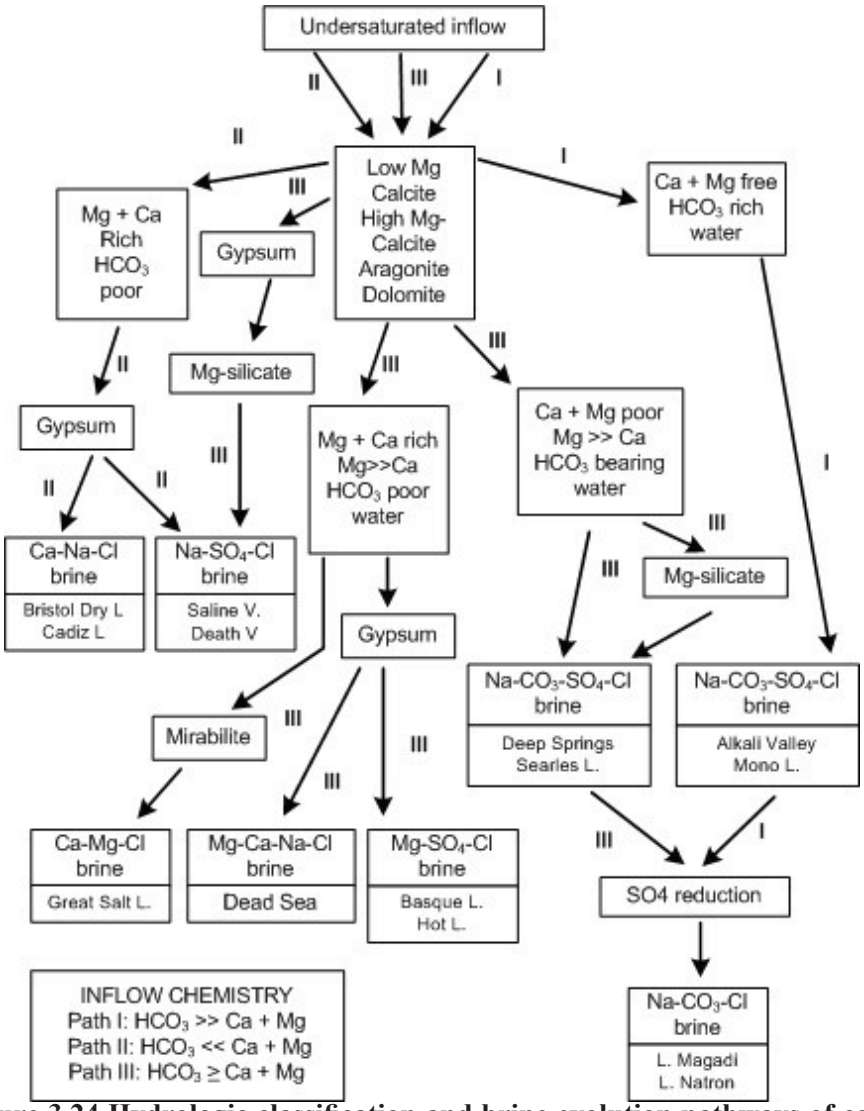

Figure 3.24 Hydrologic classification and brine evolution pathways of concentrating non-marine waters (after Eugster and Hardie, 1978).

Using this diagram, it can be seen that a brine which precipitates gypsum cannot subsequently precipitate alkali carbonates. Initially, the brine will precipitate calcite, aragonite, dolomite or magnesite, which uses Ca and HCO_3. If the HCO_3 is removed, with excess Ca, the brine will go on to precipitate gypsum, whereas if HCO_3 is in excess of Ca, the Ca is consumed precipitating calcite, aragonite or dolomite and so gypsum cannot form. Instead, the brine may precipitate Mg-silicates, Na-carbonates (e.g., natron, thermonatrite) Na-bicarbonates (e.g., trona, nahcolite) and Na-sulfates (e.g., mirabilite, thenardite). In the Curdimurka Subgroup, the abundant gypsum and anhydrite pseudomorphs indicate that the brine from which they were precipitated could not also have precipitated alkali carbonate minerals.

herring bone cross-bedding and high energy sandy units arguing against a peritidal and hence marine setting, and the absence of cyclicity arguing against a lacustrine setting. However, the stability of the sedimentation over hundreds of metres of sedimentary thickness does suggest that small-scale variations in the water levels that would be expected in a lacustrine environment, particularly in an arid setting, are absent, favouring a marine environment.

The evidence from the evaporite mineralogy is also inconclusive. It has been shown that Rowlands et al. (1980) wrongly identified gaylussite and shortite. Gypsum/anhydrite and halite are typical marine evaporite minerals but they may also form in lacustrine-playa environments (e.g., Bristol Dry Lake; Rosen and Warren, 1990). Therefore it is not possible

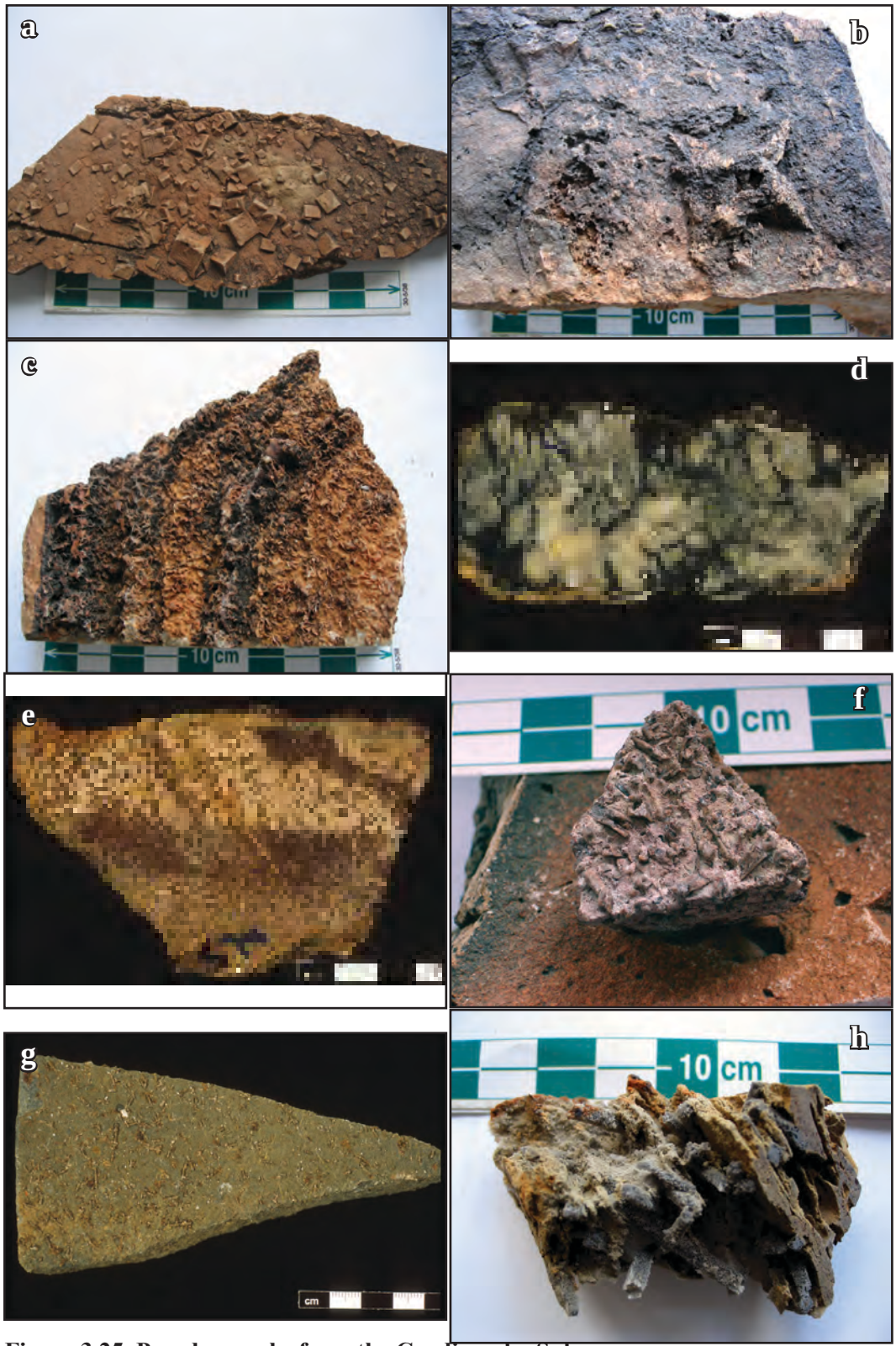

Figure 3.25. Pseudomorphs from the Curdimurka Subgroup.
a) and b) Halite casts in very fine-grained sandstone. (a) shows hopper crystals and cubes; b) is a large pagoda pseudomorph. c) Gypsum pseudomorphs replaced by chert. d) Chicken wire texture in mudstone. The anhydrite is replaced by dolomite (lighter colour) and chert. e) Microcline replacing anhydrite. f) The same sample as (e) but with the limestone dissolved by acid to show the pesudomorphs shape. g) Small needle-like pseudomorphs from Dunns Mine Limestone in a calcitic bed (see also Ch. 6). h) A similar sample to g) although with larger pseudomorphs, treated with acid to remove the limestone. Note the square pseudomorph in the lower centre. These are randomly oriented and are now replaced by K-Feldspar. i) and j) scapolite in limestone, j) shows the eight-sided form of scapolite. k) Mg-chlorite replacing scapolite.l) Microcline in the Dunns Mine Limestone,

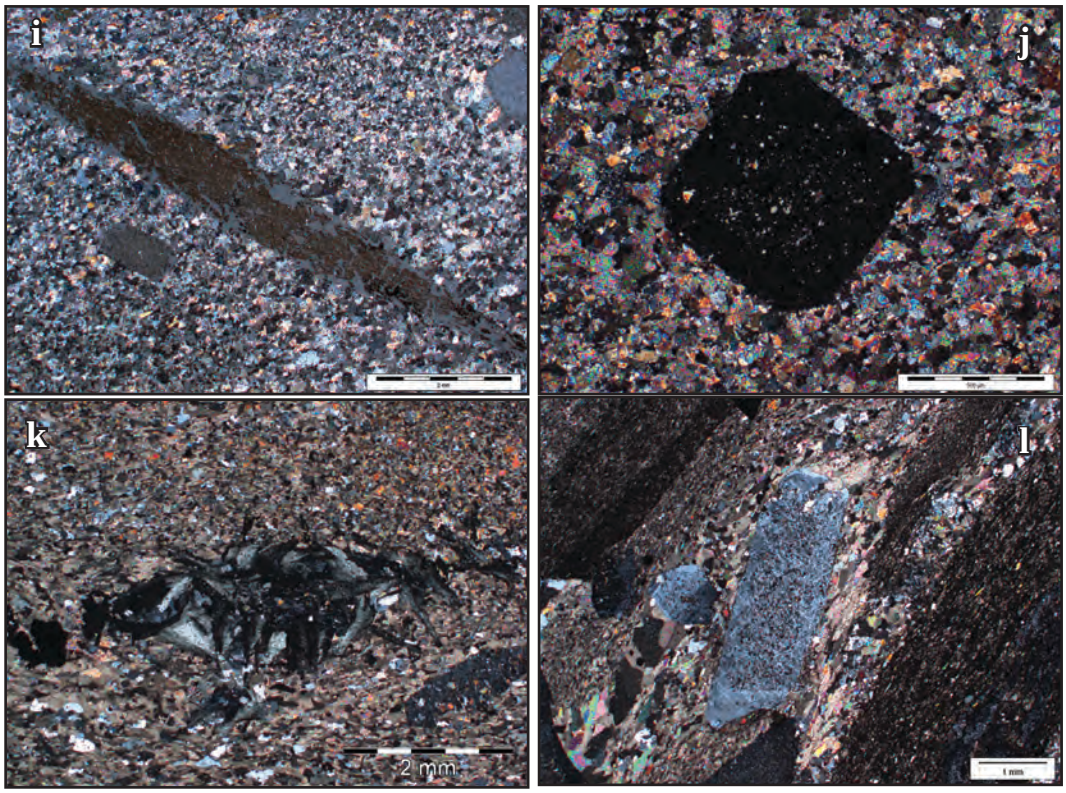

showing an inclusion-rich core and an inclusion-free margin.

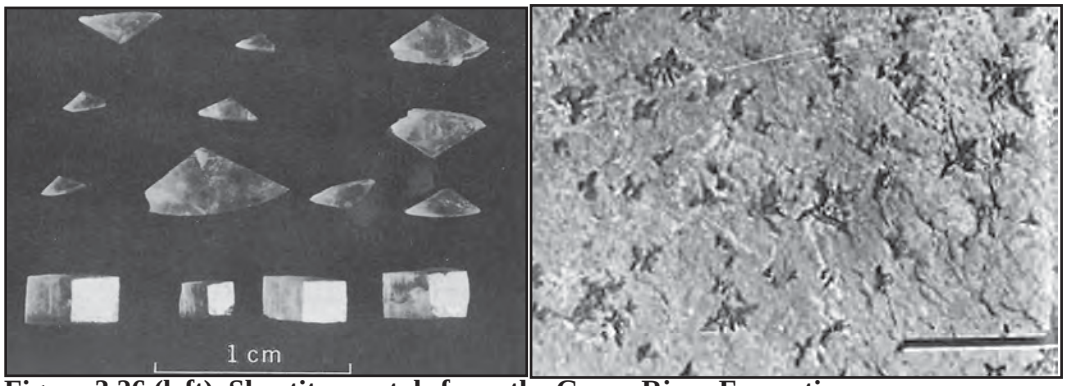

Figure 3.26 (left). Shortite crystals from the Green River Formation.
Note that they do not have a rod-like form. Reproduced from Bradley, 1962.

Figure 3.27 (right). The arrow-head pseudomorphs of Rowlands et al. (1980).
Rowlands et al. (1980) interpreted these to be gaylussite . The best examples look similar to 3.25b, and are interpreted here to be pagoda halite casts. (Reproduced from Rowlands et al. 1980). Scale bar is one centimetre.

to say with certainty whether the Curdimurka Subgroup above the level of the Dome Sandstone was deposited within a marine or lacustrine environment.

3.7.2 Basin Evolution and Tectonic Environment.

Deposition of the Curdimurka Subgroup in the Euchre Pack Domain occurred during four major transgressions (Figure 3.21, Table 3.2). The first began with the deposition of the Dome Sandstone in a continental, braided stream environment changing to sub-wavebase with the deposition of the Rook Tuff. There was then a rapid regression leading to evaporite deposition at the base of the Dunns Mine Limestone, followed by a second transgression and deposition of the Interbedded Carbonate - Siltstone Facies in the Dunns Mine Limestone.

The second regression occurred at the base of the Recovery Formation, reaching a maximum with the deposition of the Planar Laminated Sandstone Facies in RSds2.

The third transgression occurred with a gradual deepening through interbedded siltstone-sandstone facies to the Black Shale Facies in RSst4. There was then a third regression which lead to deposition of the basal Hogan Dolomite to the CSlt4 at or about sea/lake level, with a series of short-term transgressions and regression until the final major transgression leading to the deposition of the Black Shale Facies in the Boorloo Shale. The final regression resulted in a shallowing upward package through the Boorloo Dolomite resulting in deposition of the Carbonate - Chert Facies in a sabkha or playa environment.

There are two points to note about the basin evolution as outlined above. The first is that except for the first regression (Sub-cycle 2, Table 3.2), the changes are gradual, and the second follows on from this; there are extended periods of stability with only minor changes in water level, particularly during deposition of the Recovery and Cooranna Formations. The rapid change of the first regression may indicate that other processes were operating and it is possible that the regression marks a period of basin isolation and evaporation of a standing body of water rather than a rapid change in subsidence or sediment supply. The following regression (Sub-cycle 4) was also rapid with a return to deep water conditions, although with the addition of carbonate-dominated density flows. Decreasing grainsize and bed thickness from northwest to southeast suggests that the source of the carbonate may have been emergent conditions to the northwest. There was no increase in clastic sediments at this time, suggesting either limited topography and sediment was being trapped before entering the deeper part of the basin.

Comparisons with depositional models developed for rift basins (e.g., Leeder and Gawthorpe, 1987; Prosser et al., 1993; Landon, 1994; Lambiase and Bosworth, 1996; Gawthorpe and Leeder, 2000) and the examples outlined does not provide unambiguous support for deposition of the Curdimurka Subgroup in a rift environment (von der Borch 1980; Rowlands et al., 1980; Preiss, 1987, 1993, 2000).

Initial rift sedimentation is dominated by coarse-grained clastic sediments (conglomerates and sandstone) deposited in alluvial fans on the immediate footwall to the bounding fault (Schultz, 1994; Landon, 1994; Smith, 1995; Gawthorpe and Leeder, 2000; Changsong et al., 2001; McLeod, 2002; Mack, 2005). Basinward, the coarse-grained units grade into finer-grained clastic units and evaporitic units as in the Gulf of Suez (Schultz, 1994),

Table 3.4. Evidence for the depositional environment of the Curdimurka Group being either Marine or Lacustrine.

Marine	Lacustrine
evaporite mineralogy (not conclusive)	lithofacies associations
thick black shale facies (not conclusive)	dry and wet mud flat facies
aeolian sand flats absent	absence of herring bone cross-bedding
lack of cyclicity	absence of high energy sandy units
stability of depositional setting	

Reconcavo Basin (Figueiredo et al., 1994), Erlian Basin (Changsong, 2001) or the Mangas Basin (Mack, 2005). The only conglomerates in the Curdimurka Subgroup occur near the base of the Dome Sandstone, and these are matrix-supported pebble conglomerates less than one metre thick, and so alluvial fans are absent. Because the margins of the basin are not exposed, it is possible that the basin margin facies are present but do not crop out. In the Reconcavo Basin, the conglomeratic alluvial fan complex occupies a 10 km wide strip adjacent the basin bounding normal faults (Figueiredo et al., 1994), which could be hidden at depth adjacent to the Mulroona Gravity Ridge, northeast of the Euchre Pack Domain. Then, the observed portion of the Curdimurka Subgroup corresponds to the basin centre fine-grained clastic and evaporitic units.

An alternative model is that of Lambiase and Bosworth (1995) who developed a four stage rift evolution model; initial faulting, half-graben development, filling of half graben, and regional subsidence. They concluded that early rift sedimentation, in the initial faulting stage, is dominated by fluvial sands, followed by paludral and shallow lacustrine sediments in the half-graben development stage (Lambiase and Bosworth, 1995). Harris (2000) suggested that initial sediments in the Congo Basin follow this pattern. The basal Curdimurka Subgroup has similarities with the model of Lambiase and Bosworth (1995) to the level of the top of the Dunns Mine Limestone (allowing for either lacustrine or marine conditions). In the Lambiase and Bosworth (1995) model, the lacustrine sediments are succeeded by fluvial sediments in the third stage of rift development whereas in the

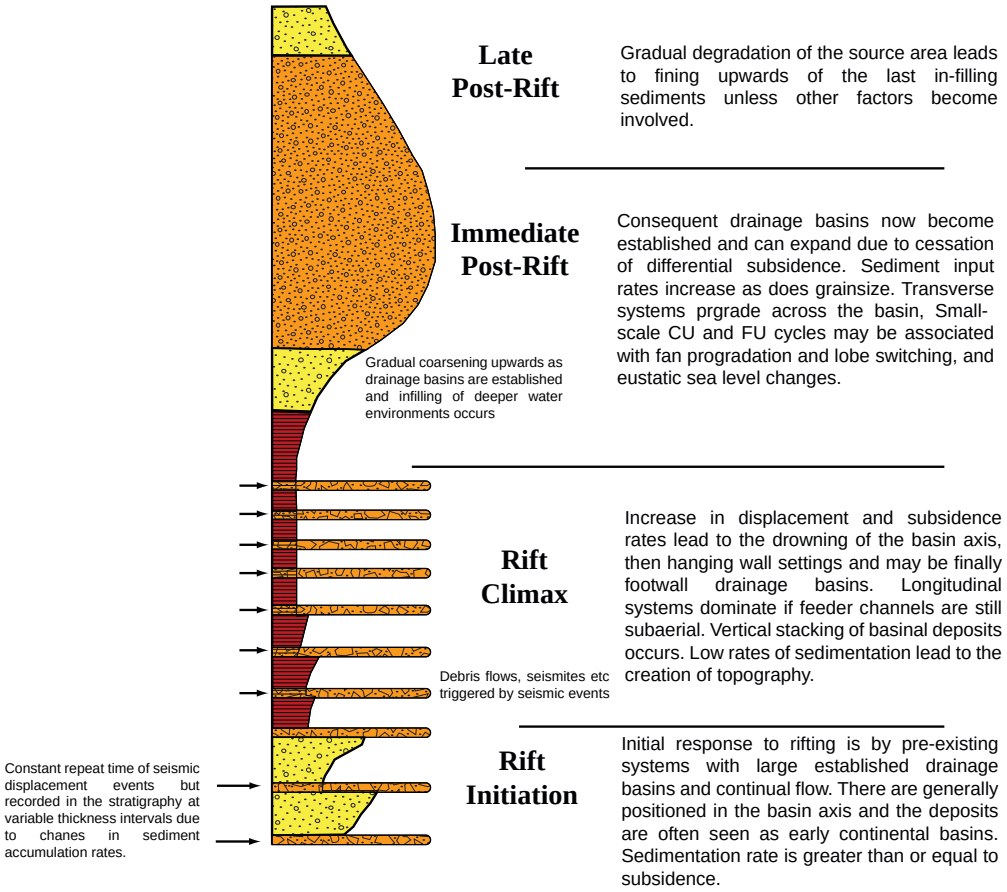

Figure 3.28. An idealized section of the vertical stratigraphy through the basin centre for sedimentation within a half-graben (from Prosser, 1993).

Curdimurka Subgroup, the deeper water sediments are succeeded by shallow water to emergent conditions.

At the scale of the basin, the one-dimensional half-graben model of Prosser et al. (1993) emphasises the relationship between sedimentation and movement on the bounding faults. Periodic uplift of the footwall results in the influx of conglomerates and sedimentary breccias into the hanging wall basin (Figure 3.28). There is no evidence for the deposition of conglomerates but there are several sandstone bodies which may be distal to conglomerates; at the top of RSst1, RSds2 and in the Boorloo Shale. These may be periods of fault movement on the basin margins but otherwise accommodation space is created smoothly and filled smoothly, with no evidence of there being a series of rapid fault movements.

Rift basin sedimentation models and examples also show evidence of significant topographic relief that eventually becomes subdued in the post-rift stage. Harris (2000) interpreted the shallow water lacustrine Toca carbonates as being deposited on the the crests of fault blocks that are surrounded by grabens in which marl is deposited. A similar configuration is noted on the Devonian Lennard Shelf, in a marine environment (Playfair, 1984). In sub-aerial settings, crests of fault-blocks are eroded but basal units typically vary in thickness along strike, perhaps by hundreds of metres (Schultz, 1994). During deposition of the Dome Sandstone, particularly in the Stony Range and South Hill Domains where there is extensive along-strike outcrop with little or no variation of thickness, there is no evidence of significant basement topography in two dimensions. At the scale of the Euchre Pack Domain, the only evidence for topography is inferred from some clastic units thinning to the southeast, and from the Dunns Mine Limestone discussed above.

3.7.3. Relationship between the Curdimurka Subgroup and the Burra Group.

One of the possible consequences of the depositional age of the Skillogalee Dolomite being about 797 Ma (Drexel, 2009; Reid, 2009) is that, based on the 802 ± 10 Ma of the Rook Tuff (Fanning et al., 1986), the Curdimurka Subgroup would be a correlative of the Burra Group. The field work for this study was completed sometime before the 797 Ma age of Drexel (2009) and Reid (2009) was published and so no specific work to examine the possible correlation was undertaken. However, one of the characteristic features of the Skillogalee Dolomite throughout the Willouran Range is the occurrence of abundant magnesite beds throughout (Belperio, 1990). Nowhere in the mapping undertaken as part of this study was magnesite noted in the Curdimurka Subgroup. Not in the Euchre Pack Domain, nor the Stony Range, Witchelina of the South Hill Domains. There is also not the same amount of carbonates as mapped by Belperio (1990). Based on these observations, there is no support to the contention that the Curdimurka Subgroup is a correlative of the Burra Group.

3.8 Conclusions

In this chapter, the sedimentary facies within the type-area of the Curdimurka Subgroup have been described and interpreted, and the facies architecture developed. Ten sedimentary facies have been described, and from these, three lithofacies associations identified; Fluvial,

Shallow Water to Emergent and Below-wave Base. In the Euchre Pack Domain they record four depositional cycles although the changes are gradual with extended periods of stability. Siliciclastic facies are dominant in terms of thickness but from the Dome Sandstone to the Boorloo Siltstone, carbonate facies recur, typically as thin units within a siltstone-dominant package. At the scale of the wider Willouran Range, the facies that occur in the Dome Sandstone in the Euchre Pack Domain are repeated in the Dome Sandstone in the Stony Range and South Hill Domains, showing that the depositional environment was consistent at the base of the Curdimurka Subgroup across a wide area.

Deposition of evaporites occurred throughout the Curdimurka Subgroup. Previously, several of the pseudomorph morphologies have been identified as alkaline carbonates, typical of deposition in lacustrine environments. However, this study has shown that the pseudomorphs were mis-identified and as a whole, inconsistent with theoretical and empirical evidence of brine evolution. The only evaporite minerals deposited were gypsum/anhydrite and halite which are not diagnostic of either marine or lacustrine conditions.

Based on the facies analysis and evaporite mineralogy, it is not possible to state conclusively whether or not the Curdimurka Subgroup was deposited in a marine or continental/lacustrine environment or a combination of the two. Much of the evidence is ambiguous or based on the absence of features that may provide certainty such as evidence of deposition under tidal conditions or small-scale depositional cycles. However, despite there being no one line of evidence favouring either a marine or lacustrine setting, taken together, a marine setting is favoured because of the evaporite mineralogy and the apparent long-term stability seen in the depositional setting relative to the water level, and absence of cyclicty.

The tectonic environment could not be defined with certainty. Features typical of rift environments do not occur, particularly alluvial fans adjacent to bounding normal faults or evidence of variable basement topography. However, because the relationship between the Curdimurka Subgroup and the underlying rocks is not seen it is possible that alluvial facies are present at depth, and outcrop today is from the centre of the rift rather than the margins, and so alluvial fan facies will not be seen.

Because of the ambiguous nature of the evidence for both the depositional and tectonic environment under which the Curdimurka Subgroup was deposited, other evidence must be sought to assist in interpreting the early evolution of the Willouran Trough. In the next chapter, zircon provenance will be combined with the structural and depositional model of Gawthorpe and Leeder (2000) to examine further the tectonic environment. Chapter 5 will use stable isotope analyses of the carbonates from the Curdimurka Subgroup to provide supporting evidence for the sedimentary environment.

Finally, there is no evidence to support the contention that the Curdimurka Subgroup is a correlative of the Burra Group. The two features typical of the Skillogalee Dolomite, abundant dolomite beds and magnesite are not found in the Curdimurka Subgroup.

CHAPTER 4.
PROVENANCE OF THE CALLANNA GROUP

4.1 Introduction

4.1.1 The tectonic setting of the Willouran Trough

The previous chapter has shown that there are several discrepancies between the expected sedimentary facies that typify intracontinental rift environments and those seen within the Curdimurka Subgroup. In particular, there is an absence of the coarse-grained facies associations typical of rift environments such as alluvial fans and cones. As such, additional evidence for the development of the Willouran Trough during deposition of the Curdimurka Subgroup must be sought.

Sediment provenance may be used as a test of tectonic setting and history (e.g. Dickinson, 1988). One method is to correlate the tectonic setting of the source terrane with the framework compositional modes of sandstone (e.g., Dickinson and Suzeck, 1979; Ingersoll et al., 1984) but in rocks that have undergone significant alteration detrital petrofacies cannot be reliably defined. The rocks of the Willouran Trough have undergone diagenetic alteration and been metamorphosed to mid-greeschist (biotite-stable) facies and so detrital petrofacies may not be reliable here.

Another approach to provenance analysis is U-Pb dating of single grains of detrital zircons. A number of studies have compared the variations within zircon age spectra from samples within a basin with the expected source area to gain an insight into the development of an entire basin through several depositional phases (e.g., Ireland et al., 1998; Berry et al., 2001; Speigel et al., 2004; Goodge et al., 2004; Kositcin and Krapex, 2004). Ireland et al., (1998) analysed detrital zircons collected from arenaceous strata located at various levels in the Adelaidean stratigraphy in an attempt to reveal discrete stages of basin evolution by systematic changes in sediment dispersal patterns. They were concerned with the overall change from the initiation of deposition in the Adelaide Fold Belt, through the transition to a passive margin to the cessation of deformation in the Delamerian Orogen.

It is the intention of this study to use zircon provenance to help understand the tectonic development of the Willouran Trough using two methods; comparisons between different stratigraphic levels and between the same stratigraphic level at different sites. To address these factors, a theoretical model has been developed to understand how zircon provenance will change with the development of a rift basin and vary across the basin. The theoretical model is based on studies showing proximal sources dominate the zircon age spectra in areas of active uplift (Cawood et al., 2003; Mapes et al., 2004), and the study of Rainbird et al., (1992) who demonstrated that detrital zircons may be transported several thousand kilometres from their source. These studies, when combined with the rift evolution and sedimentation model of Gawthorpe and Leeder (2000) and the rift evolution model of McKenzie (1978), provide the basis for modelling the expected changes in detrital zircon age spectra as a rift basin evolves from rift initiation to cessation of deposition.

In the rift initiation stage, there are a number of small, isolated depocentres, which may trap pre-existing drainage but will also have localized transverse drainage. Zircons will be sourced from distal areas by the pre-existing drainage and proximal sources by the developing transverse drainage (Figure 4.1a). From Cawood et al. (2003), proximal zircons will dominate the zircon age spectra but distal zircons will be present. As the rift evolves, initially discrete depocentres amalgamate, or link, and broaden (Figure 4.1b). The margins of the rift rise and the external drainage is reversed, taking material away from the rift zone. Within the rift zone, transverse sediment input is dominant but axial drainage has been established, moving sediment along the rift. Proximal zircons will again dominate the zircon age spectra but with some input of distal zircons. At this stage, there is greater mixing of sediment and the zircon spectra from the same stratigraphic level at different localities will be similar As active rifting diminishes, accommodation is developed and driven by thermal subsidence (McKenzie, 1978). At this time the rift shoulders become buried and so the local basement is no longer susceptible to erosion (Figure 4.1c). The catchment-size will be maximised, sampling the widest range of rocks and ages. There may also be some reworking of sediments. The resulting zircon age spectra will be complex and the proximal ages may be minimal. Hence, by collecting a series of samples at different stratigraphic levels in the Curdimurka Subgroup, and comparing their detrital zircon age spectra, it may be possible to determine whether it was deposited in the rift phase. And, by comparing zircons from the same stratigraphic level at different locations, it may be possible to distinguish between the rift initiation and the linked fault stages.

Related to understanding the development of the Willouran Trough is the relationship between the Willouran Trough and the Arkaroola area (Figure 4.2). The Curdimurka Subgroup is not recorded in the Arkaroola area where the Emeroo Subgroup disconformably overlies the Wooltana Volcanics of the Arkaroola Subgroup (Coats and Blisset, 1971; Preiss, 1987), indicating that accommodation developed in the Willouran Trough and Arkaroola area occurred independently. At Arkaroola, the Emeroo Subgroup comprises five units, the Humanity Seat Formation, which is in part overlain by, but also varies laterally with the Woodnamooka Phyllite, the Blue Mine Conglomerate, the Opaminda Formation and the Wortupa Quartzite. By comparing the detrital zircon age spectra of samples from the Willouran Range and the Arkaroola area, particularly from the base of the Emeroo Subgroup in both areas, it is intended to determine whether the interpreted regional lithostratigraphic correlations are correct, and the Curdimurka Subgroup is truly absent from the Arkaroola area.

4.1.2 Detrital zircon ages and the break-up of Rodinia.

Detrital zircon age spectra have been used by numerous authors in the debate on the nature and timing of the assembly and break-up of Rodinia (e.g., Ross et al., 1992; Ireland et al., 1998; Berry et al., 2001; Stewart et al., 2001). Typically detrital zircon age spectra are used to test or support and proposed configuration, by one or both of two methods;

- identifying possible exotic source terranes suggested by a particular configuration for zircon age populations that do not have a source area within current plate

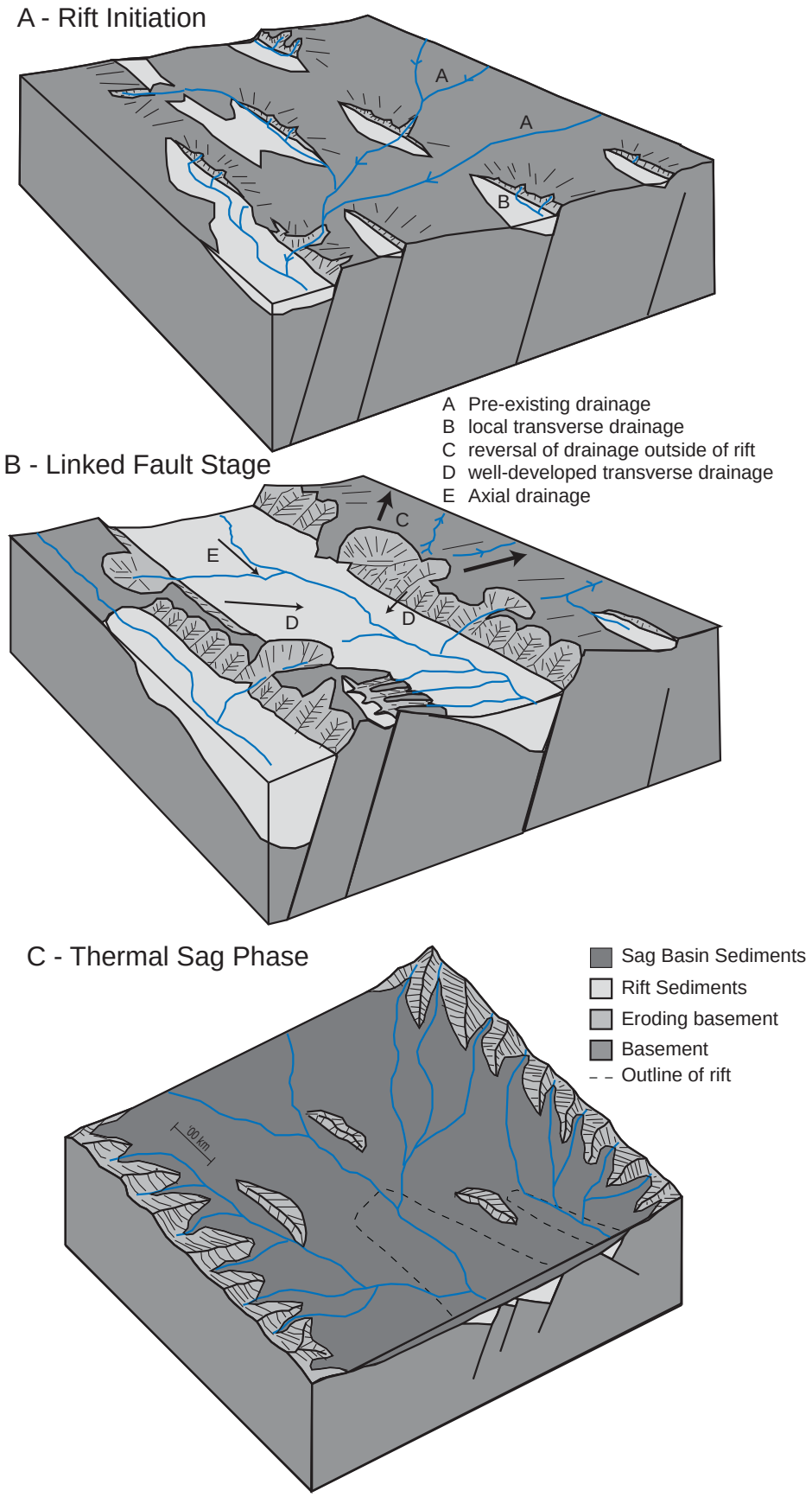

Figure 4.1. Conceptual model of source changes for detrital zircons in an evolving rift to sag basin.

a) Rift initiation stage with small, discrete basins. b) Linked fault stage with transverse drainage dominant but axial drainage is established. c) Thermal sag phase with the rift shoulders buried and distal sediment sources dominating. a) and b) modified from Gawthorpe and Leeder (2000).

boundaries (or well understood relationships such as Australia and Antarctica; (Berry et al., 2001) or;

- by comparing detrital zircon spectra from different continents (Stewart et al., 2002).

Detrital zircon age populations without an identified source have been used to propose plate configurations (Green et al., 1992) or suggest the presence of terranes that no longer crop out (Wysoczanski and Allibone, 2004).

The Adelaide Fold Belt is ideal to test possible configurations of Rodinia prior to break-up; it is on a margin of the continent, and its sedimentary record begins with the initial intracontinental rift development and continues through continent break-up to basin inversion. The Callanna Group in particular is well-placed for identifying the adjacent terrane as when it was deposited, that terrane was still in contact with the Adelaide Fold Belt. Hence, the detrital zircon age spectra calculated here may also provide information

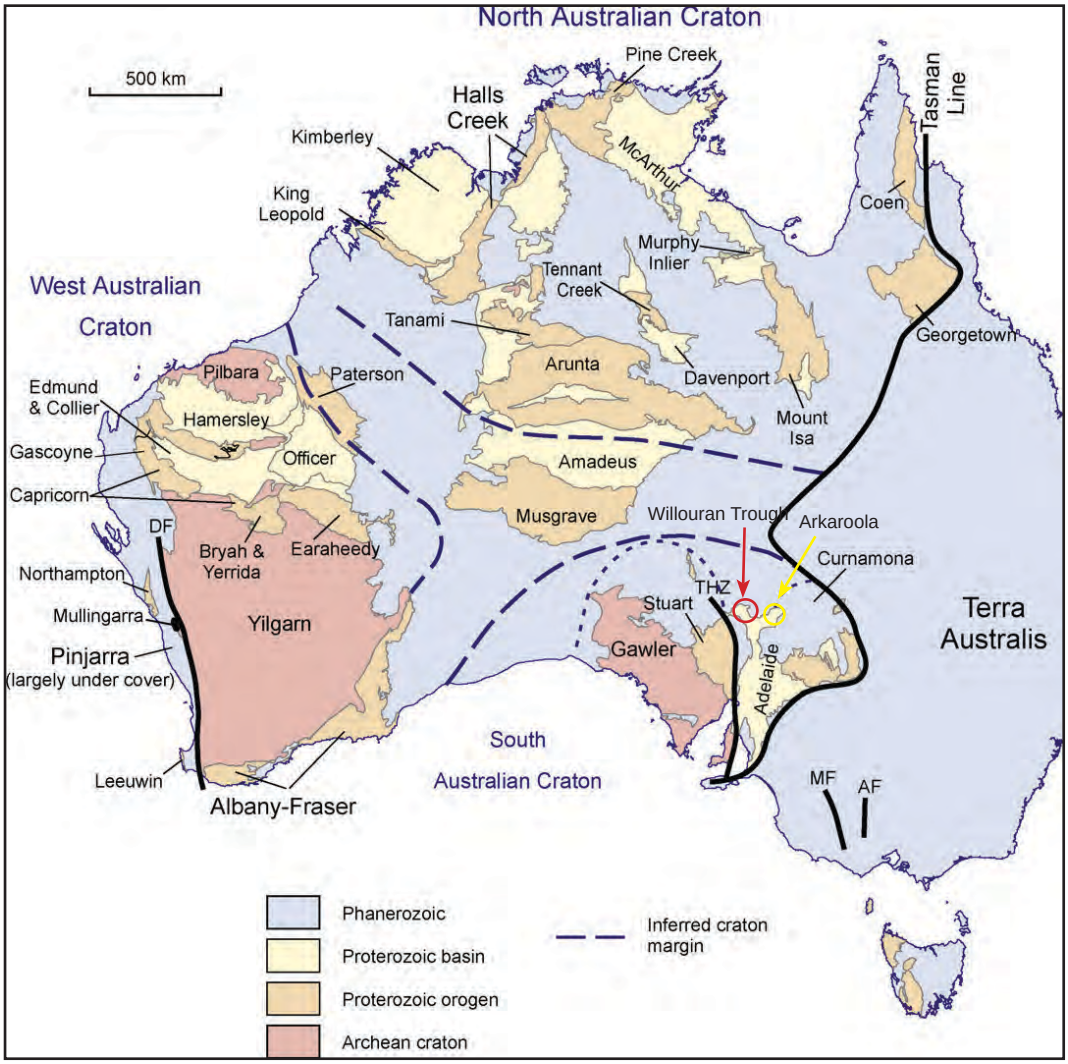

Figure 4.2 Simplified tectonic map of Australia (from Cawood and Korsch, 2008). The Gawler Craton and Curnamona Province are proximal sources of detrital zircons to the Willouran Trough (red circle); the Curnamona Province is proximal to the Arkaroola area (yellow circle) and the Musgrave Block is distal to both. The Albany-Fraser Belt and the Paterson Province are likely to have been continuous with the Musgrave Block.

for identifying the continental land mass that lay to the east of the Adelaide Fold Belt prior to the break-up of Rodinia.

4.2 Geochronology of likely detrital sources to the Willouran Trough

4.2.1 Introduction

The Willouran Trough is well suited for detrital zircon provenance analysis as potential source terranes, both proximal and distal, are well constrained geochronologically (Figures 4.2 and 4.3). It is situated between the Gawler Craton to the west and the Curnamona Province to the east, the latter including rocks of the Mt Painter Inlier (Figure 4.2). Rocks of both crustal blocks record similar magmatic, tectonic and metamorphic histories (from 1700 Ma at least), leading some workers to interpret that they were contiguous prior to the formation of the Adelaide Fold Belt (Glen et al., 1977; Rutland et al., 1981). Distal to the Willouran Trough is the Musgrave Inlier, which trends east-west, joining with the Albany-Fraser Belt to the southwest and the Paterson Province to the northwest (Figure 4.2).

4.2.2 The Gawler Craton.

The Gawler Craton has a complex history of sedimentation, deformation and igneous activity from the Archaean to the Mesoproterozoic. It consists of a Late Archaean to Early Palaeoproterozic basement surrounded by Palaeoproterozoic to Mesoproterozic mobile belts (Figure 4.4: Drexel, 1993; Daly et al., 1998; Fanning et al., 2007). Flat-lying rocks of the Adelaide Fold Belt, from the Umberatana and Wilpena groups, unconformably overlie the Gawler Craton on the Stuart Shelf (Figure 4.4; Preiss, 1987).

The oldest Gawler Craton rocks are the Sleaford Complex in the south and the Mulgathing Complex in the north (Figure 4.4). Granites from the Dutton Suite of the Sleaford Complex (an Archaean to Early Proterozoic granite and gneiss complex), have been dated to between ca. 2520 - 2460 Ma, with high-grade metamorphism between about 2460- 2420 Ma in the Sleafordian Orogeny (Fanning et al., 2007). The Mulgathing Complex comprises mafic to ultramafic volcanics and intrusives, banded iron formation, gneiss and acid intrusives (Swain et al., 2005), and may have been continuous with the Sleaford Complex. A granite vein and rhyodacite have been dated at about ca. 2510 Ma, with metamorphic ages of about 2450 Ma (Fanning et al., 2007). Granitic gneiss from the Miltalie Gneiss in the southern Gawler Craton (Figure 4.4) has been dated at about 2000 Ma (Fanning et al., 2007).

The next phase of magmatism is recorded in the Donington Suite, a granite batholith which crops out from the southern to central Gawler Cration (Figure 4.4). It has been dated at ca. 1850 Ma (Fanning et al., 2007). Following this are a series of volcano-sedimentary packages dated at about 1790 Ma (Myola, and Tidnamurkuna Volcanics), 1760 Ma (the Wallaroo Group) and 1745 Ma (the McGregor Volcanics) (Fanning et al., 2007).

Between about 2000 and 1690 Ma, the Gawler Craton is dominated by a period of rifting that was terminated by the Kimban Orogeny between about 1730 and 1690 Ma. During

Abbreviations (names of orogenic events are italicized): ADS – Amata Dyke Swarm; *AIe* – Argilke Igneous Event; AS –Adelaide Supergroup (containing Supersequences 1–4 (Ss1–4); BAG – Black Angel Gneiss; BbC – Billabong Complex; BC – Birksgate Complex; BDS – Boyagin Dyke Swarm; Bi&LiG – Birrindudu and Limbunya groups and equivalents; BlB – Blair Basin succession; *BO* – Barramundi Orogeny; ByB – Bryah Basin succession; CB – Cariewerloo Basin;CBB – Carr Boyd Basin and equivalent successions; CrB +OB – Crowhurst and Osmand basins and equivalent successions; CG – Cardup Group and correlatives; CoG – Collier Basin succession; *CoO* – Cornian Orogeny; *CpO* – Capricorn Orogeny; CS – Calvert Superbasin succession; CuB – Cullen Batholith; *CwE* – Chewings Event; DdV – Ding Dong Downs Volcanics; *DeO* – Delamerian Orogeny; DG – Dalyup Gneiss; DS – Donington Suite granitic rocks; DSs – Dalgaringa Supersuite; DvS – Devils Suite granite; EaB – Earaheedy Basin succession; EdG – Edmund Basin succession; *EdO* – Edmund Orogeny; ES&ERG – El Sherana and Edith River groups; FC – Fraser Complex; FS – Forrest Home Supersuite; FsG – Fortescue Group; *GbO* – Glenburgh Orogeny; GC – Giles Complex; GDS – Gairdner Dyke Swarm; GFDS – Gnowangenup Fraser Dyke Swarm; GHS – Gawler Range Volcanics and Hiltaba Suite; grn – granite; HcG – Halls Creek Group; *HcO* – Hall Creek Orogeny; HG – Hutchinson Group; HmG – Hamersley Group; HwGn– Halfway Gneiss; IC – Iwupataka Metamorphic Complex; *IO* – Isan Orogeny; IS – Isan Superbasin succession; *JO* – Janan Orogeny; *KaO* – Kararan Orogeny; KbG – Kimberley Group; KIms – King Island metasandstone; *KiO* – Kimban Orogeny; KL – Kalkadoon Granite-Leichhardt Volcanics; *KLO* – King Leopold Orogeny; Ksz – Kalinjala ShearZone; Ld&OnP – Lander and Ongeva metasedimentary packages; *LE* – Liebig Event; LG – Lamil Group; LrWG – lower Wyloo Group; LrYB – lower Yerrida Basin succession; LS – Leichhardt Superbasin succession; MbF – Marboo Formation and equivalents; MBG – Mount Barren Group; metaseds – metasedimentary rock; ME – Miltalie Event;MG – Moora Group; MiG – Miltalie Gneiss; *MgO* – Mangaroon Orogeny; *MiO* – Miles Orogeny; MlG – Malcolm Gneiss; MNG – Mount Neill Granite; MR – Mount Ragged metasedimentary rocks; MrSs – Moorarie Supersuite and related bodies; MuG – Munglinup Gneiss; MWDS – Mundine Well Dyke Swarm; *MWO* – Mount West Orogeny; *MuO* – Musgravian Orogeny; NG - Napperby Gneiss and related units; *Nie* – Nimbuwah Event; NmG – Namooma and Mount Partridge groups; NS – Ninnerie Suite; ogneiss – orthogneiss; *Ole* – Ooldean Event; *OlO* – Olarian Orogeny; Oo&HCG – Ooradidgee and Hatches Creek groups; *OtO* – Ophthalmian Orogeny; Paleo – Paleozoic; *PaO* –Paterson Orogeny; PaS – Pargee Sandstone; PbB – Padbury Basin; *PeO* – Petermann Orogeny; PCG – Pothole Creek Gneiss; gneiss – paragneiss; PS – Pitjantjatjara Supersuite; RG – Recherche Granite; RjC – Rum Jungle Complex; RRG – Reynolds Range Group; RS – Roper Superbasin; *SI* – Stage I of the Albany–Fraser Orogeny; *SII* – Stage II of theAlbany–Fraser Orogeny; SA&FnG – South Alligator and Finniss River groups; SbF – Stubbins Formation; *Soe* – Shoobridge Event; *Sfe* – Stafford Event; S&MC – Sleaford and Mulgathing complexes; *SlO* – Sleafordian Orogeny; SPS – St. Peter Suite; SRF – Stirling Range Formation; SS – Spilsby Suite; Ss1 – Supersequence 1 (Centralian Superbasin);Ss2 – Supersequence 2 (Centralian Superbasin); Ss3 – Supersequence 3 (Centralian Superbasin); Ss3 + 4 – Supersequence 3 + 4 (Centralian Superbasin); *SwE* – Strangways Event; *TaE* – Tanami Event; *TeE* – Tennant Event; TG – Tarcunyah and Throssell Range groups; TnG – Tanami Group; TCS – Tennant Creek Supersuite; TDS – Tournefort Dyke Swarm; TG – Tollu Group; TS – Tunkillia Suite granitic rocks; TuG – Turee Creek Group; uss – unnamed sandstone unit (Arunta region); UpWG – upper Wyloo Group; UpYB – upper Yerrida Basin succession;WaS –Wankanki Supersuite; WDS – Wig Dyke Swarm; WLIP –Warakuna Large Igneous Province;WM–Wirku Metamorphics;WrG –Ware Group;WrF –Warramunga Formation;WS –Willyama Supergroup; *Wu* –Wickham unconformity (King Island); *YaE* – Yambah Event; *YpO* – Yampi Orogeny; YG – Yandanooka Group; *YpO* – Yapungku Orogeny.

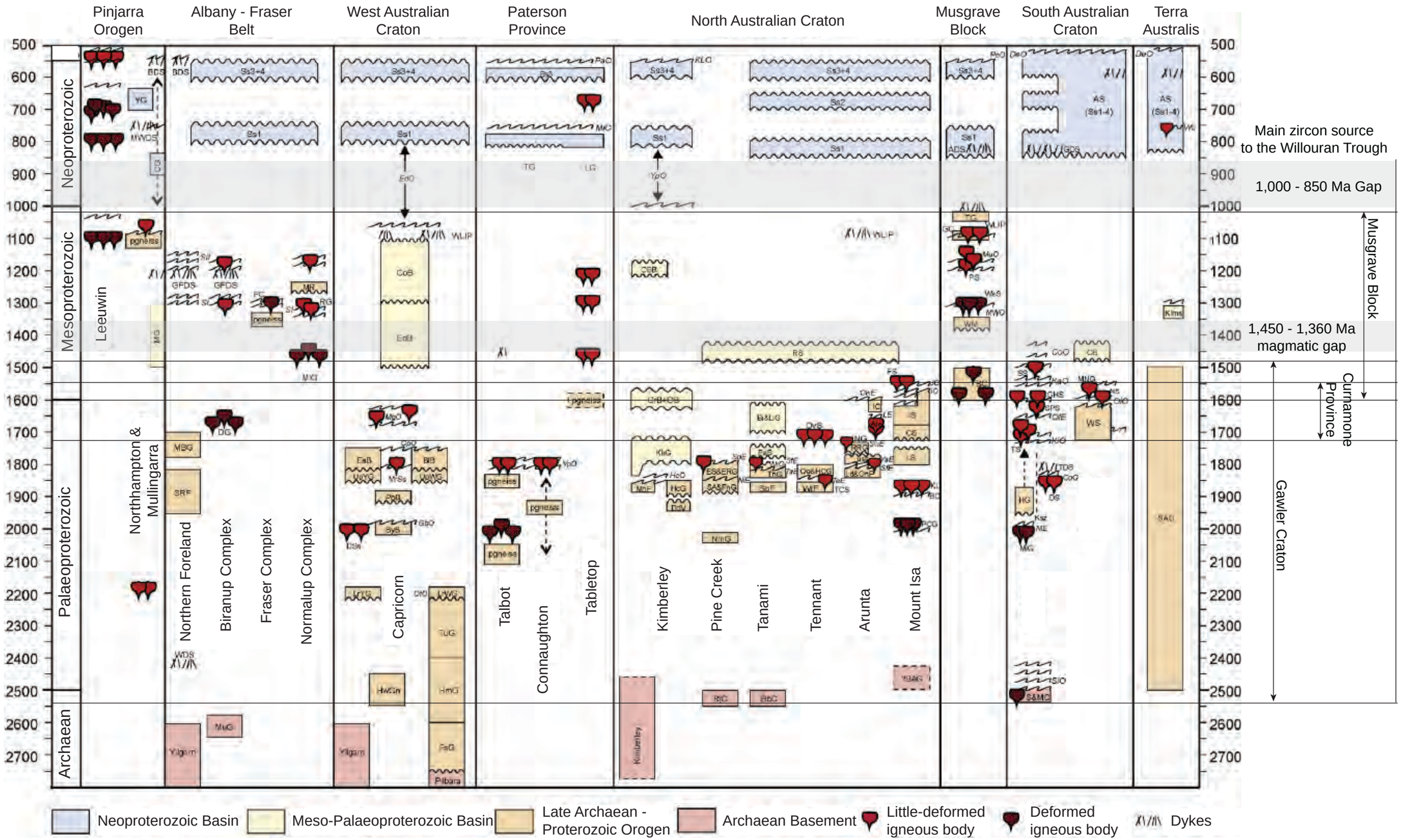

Figure 4.3. A time-space diagram for the Australian Proterozoic, with the age ranges for the cratonic areas adjacent the Willouran Trough. Also shown in pale grey are two age gaps, for which zircon sources are not known in Australia (modified from Cawood and Korsch, 2008).

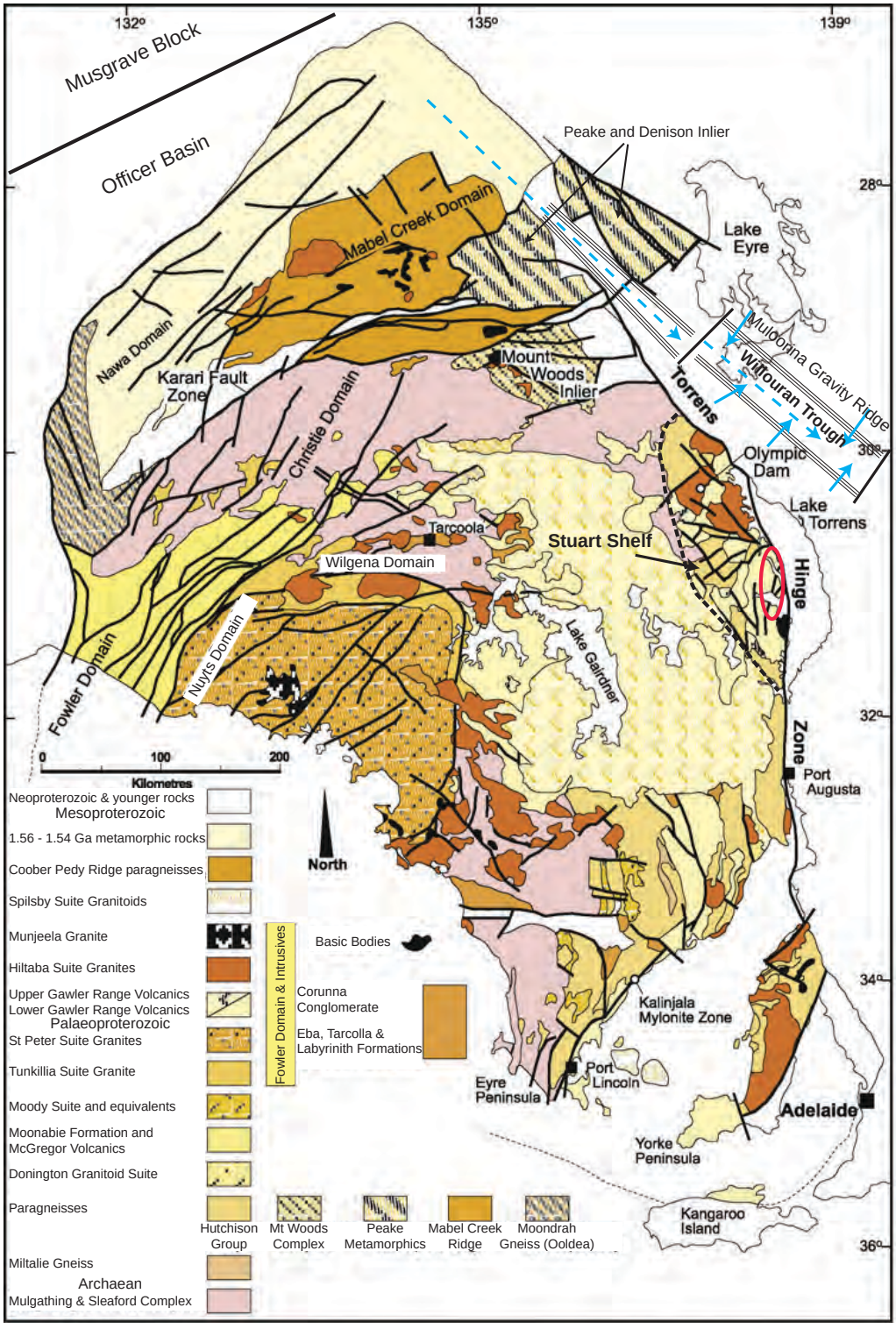

Figure 4.4. Map of the Gawler Craton, with the Willouran Trough (modified after Daly et al., 1998).

The map shows the Willouran Trough relative to the Gawler Craton, with the solid blue arrows being transverse drainage and the dashed blue lines being axial drainage into the trough. In early phases of rifting, transverse drainage will dominate and proximal sources from the Stuart Shelf area and Muloorina Gravity ridge will provide the majority of the detrital zircons. When axial drainage becomes established distal sources will increase, from the Mt Woods Inlier, Mabel Creek, Peake Metamorphics and Nawa Domains, and the Musgrave Block, to the Northwest. The Pandurra Formation crops out in the area of the red ellipse and is a likely source of re-worked zircons from primary distal sources.

this period the Hutchison Group was deposited in the eastern Gawler Craton. It comprises quartzite and massive dolomite overlain by the Middleback Subgroup which includes the iron formations that host the iron ore deposits in the Middle Back Ranges (Daly et al., 1998). The age of the Hutchison Group is constrained by it overlying the ca. 2000 Ma Miltalie Gneiss and the volcano-clastic Bosanquet Formation in the upper Hutchison Group which has been dated at ca. 1860 Ma (Fanning, 1997).

The Kimban Orogeny is the next major event, which involved syn-orogenic magmatism occurred between about 1730 Ma and 1700 Ma (Fanning et al., 2007). Granites and granite gneiss have been dated at 1740 - 1720 Ma (Middle Creek Granite) with post-orogenic granite of the Moody Suite in the southern Gawler Cration and an un-named granite in the central Gawler Cration dated at ca. 1710 Ma (Fanning et al., 2007). Rhyolite from a volcano-sedimentary package in the northern Gawler Craton has a similar age (Fanning et al., 2007).

The Tunkillia Suite comprises I-type felsic and co-magmatic intermediate to mafic intrusives emplaced between about 1690 and 1670 Ma in the central Gawler Cration (Ferris and Schwartz, 2003). Similar aged rocks (refered to as Tunkillia Suite equivalents also crop out and have been intersected in drill holes in the western and northern Gawler Craton (Teasdale, 1997; Ferris and Schwartz, 2004; Fanning et al., 2007). These rocks are interpreted to be syn-orogenic intrusives during the early stages of the Kararan Orogeny, which was responsible for granulite facies metamorphism and magmatic activity (Daly et al., 1998). A second granitic suite, the St Peters Suite and the associated Nuyt Volcanics crop out in the central and southern Gawler Craton, and have also been affected by the Kararan Orogeny (Daly et al., 1998; Ferris, 2001). The St Peter Suite granites have been dated at 1620 Ma, although the Nuyt Volcanics are slightly older (Flint et al., 1990; Ferris, 2001; Fanning et al., 2007).

Cropping out widely in the Gawler Craton are the Gawler Range Volcanics (Figure 4.4). These are bimodal volcanics with a lower assemblage ranging in composition from basalt and andesite to dacite, rhyodacite and rhyolite. The upper assemblage comprises massive porphyritic dacite and rhyodacite (Blisset et al., 1993; Allen et al., 2003). They have intrusive ages of ca. 1590 - 1580 Ma (Fanning et al., 2007). Associated with the Gawler Range Volcanics are the Hiltaba Suite Granites that consist of A-type granites although more mafic lithologies also occur (Creaser, 1996). They have ages ranging between 1590 and 1575 Ma (Fanning et al., 2007). Most Hiltaba Suite granites are undeformed but some have been strongly deformed in the latter stages of the Kararan Orogeny, and high-grade metamorphism on the Coober Pedy Ridge (Figure 4.4) is interpreted to synchronous with the emplacement of the Hiltaba Suite Granites and Gawler Range Volcanics (Fanning et al., 2007). Fanning et al. (2007) suggested that there may have been a younger magmatic event in the Peake and Denison Inlier (Figure 4.4), at about 1550 Ma.

The youngest magmatic rocks of the Gawler Craton, at 1497 ± 13 Ma are the Spilsby Suite granites (Fanning et al., 2007). On the western margin of the Gawler Craton, the Coompana Block has only been intersected in drill holes, being obscured by the Neoproterozoic and

Phanerozoic Officer and Eucla Basins. A foliated granite from the Coompana Block has a magmatic crystallization age of 1455 ± 16 Ma (Fanning et al., 2007).

Detrital zircon sources proximal to the Willouran Trough are those areas on the Stuart Shelf that are largely under Adelaidean and younger cover. They include the Hiltaba Suite granitoids and Gawler Range Volcanics with ages between about 1590 Ma and 1560 Ma, circa 1550 Ma metamorphic rocks and Hutchison Group rocks (Figure 4.4). The Peake and Denison Inlier would supply sediment to the Willouran Trough along its axis (Figure 4.4) and so these should become common in the through-going fault stage and are considered distal. However, the Pandurra Formation, a Mesoproterozoic clastic unit that occurs on the eastern margin of the Gawler Craton, and dated at 1424 ± 51 Ma (Fanning et al., 1983) is also proximal to the Willouran Trough and may be a source of re-worked detrital zircons (Figure 4.4). A detrital zircon provenance study by Fanning and Link (2004) showed that 40 to 60% of the detrital zircons from the Pandurra Formation are from the 1580 - 1620 Ma age range, with older groups between 1640 - 1780 Ma, consistent with a Gawler Craton source.

4.2.3 The Curnamona Province.

The Curnamona Province is an approximately circular basement block to the east of the central and northern Adelaide Foldbelt (Figure 4.2). Outcrop is restricted to its southern margin in New South Wales and South Australia and to the Mt Painter and Mt Babbage inliers along its northwestern margin. Elsewhere it is covered by Neoproterozoic to Recent sediments. Rocks of the Adelaide Fold Belt lie unconformably on the Curnamona Province around the Mt Painter and Mt Babbage Inliers, and along its southern edge (Preiss, 1993).

Figure 4.3 shows that the oldest magmatic rocks recorded in the Curnamona Province are about 1710 Ma (Connor and Fanning, 2001; Raetz et al., 2002). Older Palaeoproterozoic and Archaean inherited zircons have been found in synorogenic granitoids and as detrital zircons in metasediments, with ages clustering between 2400 and 2700 Ma, and 2900 and 3000 Ma (Cook et al., 1994; Raetz et al., 2002). The youngest magmatic or high-grade metamorphic events dated are about 1550 - 1560 Ma for the Moolawatana Suite in the Mt Painter and Mt Babbage Inliers (Robertson et al., 1997).

4.2.4 The Musgrave Block

The Musgrave Block is a Mesoproterozoic amphibolite facies to granulite facies terrane cropping out in the northwestern corner of South Australia, and adjacent parts of Western Australia and the Northern Territory (Figure 4.2). It has been divided into six lithostratigraphic units (Wade et al., 2006 and references therein). The oldest rocks are the Musgravian Gneiss, which has yielded zircon crystallization ages between 1600 Ma and 1540 Ma. These comprise magmatic, volcanic and metasediments metamorphosed to amphibolite to granulite facies. Wade et al., (2006) recognized an un-named cover sequence which has a maximum age, based on zircon geochronology, of about 1400 Ma. They comprise metasediments interlayered with felsic, mafic and calc-silicate gneisses, and are interpreted to represent a metavolcanic package (Conor, 1987; Wade et al., 2006). An un-named

orthogneiss gives U-Pb zircon ages betweeen 1324 Ma and 1296 Ma (White et al. 1999). It is interpreted to be deformed granitoid intrusions. The fourth unit is the Pitjantjatjara Supersuite, which comprises granitic rocks and occurs throughout the Musgrave Block. They are both deformed and undeformed and range in age between 1200 Ma and 1140 Ma, (Major and Conor, 1993; Camacho and Fanning, 1995, Glikson et al, 1996; Scrimgeour et al., 1999; Edgoose et al., 2004). The Giles Event, which includes mafic - ultramafic layered intrusions, bi-modal volcanics, granitic intrusions and felsic dyles occurred between 1080 Ma and 1040 Ma (Sun et al., 1996; Glikson et al., 1996; Camacho et al., 2002; Close et al., 2003; Edgoose et al., 2004). It is interpreted to be part of the Warakurna Large Igneous Province, which covered much of central and western Australia (Wingate et al., 2004). Widespread felsic magmatism occurred between about 1020 Ma and 1000 Ma (Camacho et al., 2002) and this age in particular is thought be diagnostic of the Musgrave Inlier (Maidment et al., 2007).

In addition to the Musgravian Gneiss and the un-named orthogneiss, amphibolite to granulite facies metamorphism occurred during the Musgrave Orogeny. The Pijantjatjara Supersuite were intruded during and after deformation constraining the orogeny to between 1230 Ma and 1150 Ma (Wade et al., 2006).

Nelson (2005a,b,c) has dated zircons from metamorphosed amphibolite, microtonalite and tonalitic gneiss from the Madura Complex (covered by sedimentary rocks of the Eucla Basin), part of the Fraser Belt that is considered to be contiguous with the Musgrave Block. These returned ages of 1415 ± 7 Ma, 1408 ± 7 and 1407 ± 7 Ma respectively and are interpreted to be crystallization ages (Nelson, 2005a,b,c). These and zircons from the Birksgate Complex of the Musgrave Block dated from 1422 ± 8 Ma are the only zircon ages between 1450 and 1350 Ma recorded from Australia, and this period has been termed the Australian magmatic gap (Wade et al., 2007).

4.2.5 Summary: Proximal vs Distal Detrital Zircons.

At the first approximation, detrital zircons older than about 1720 Ma are most likely sourced from the Gawler Craton but distal to the Willouran Trough. Detrial zircons younger than 1350 Ma, but older than 1000 Ma, will likely have a Musgrave Block source and hence are distal. Between 1450 and 1620 Ma, the source could be the Curnamona Province in which case they are are proximal, the Musgrave Block which is distal (Figure 4.3), or the Gawler Craton, with could be either proximal or distal sources. Detrital zircons with ages between 1620 and 1720 Ma could also be sourced from either the Gawler Craton or the Curnamona Province and if the former would likely be distal and the latter, proximal (Figure 4.2). Except for zircons with ages given above, which are from areas distal to the Willouran Trough, between 1450 and 1350 Ma, there is no identified magmatic source in Australia. Between 1000 and 830 Ma, the only U-Pb zircon age is about 975 Ma, from a dolerite dyke in the Arunta Block (Wyborn et al., 1998). Neumann and Fraser (2007) suggested mafic dykes in the Musgrave Block mapped by Edgoose et al. (2004) may be related to this dyke and hence the same age. In both instances, they are distal to the Willouran Trough.

4.3 Sample Selection

Detrital zircons were separated from 10 sandstone samples. The samples were collected from the Dome Sandstone (four samples), the Recovery Formation, a sandstone megaclast from the breccia near The Dome, the Paralana Quartzite, the Humanity Seat Formation, the Emeroo Subgroup and the Skillogalee Dolomite (Figure 4.5).

The four samples from the Dome Sandstone were selected to test the correlation of the Dome Sandstone between the Euchre Pack Domain (DS1 and DS3), Stony Range Domain (DS4), and the South Hill Domain (DS5: Figure 4.5a,c). Sample DS1 is from just above the basal contact of the Dome Sandstone with the underlying breccia, whereas sample DS3 is from about 100 m below its upper contact with the Rook Tuff. It is difficult to be sure of the exact correlations between for DS4 and DS5, but DS5 is likely from nearer the base of the Dome Sandstone and DS4 nearer the top (Figure 4.5c). Sample REC1 was collected from RSds1 unit of the Recovery Formation in the Euchre Pack Domain (Figure 4.5c). A sixth sample was collected from a sandstone unit in the Boorloo Siltstone and although it had abundant zircons, all were less than 50 µm in diameter and the majority too small to analyse. Together this group of samples will determine whether the evolution of the Willouran Trough follows that predicted in the theoretical model for detrital zircon provenance in rift basins decscibed above.

The Paralana Quartzite (PQ1) sample was collected from one metre above the contact with the basement in the Mt Painter Inlier at Arkaroola and the Humanity Seat Formation sample (HSF3) was collected from near its base, also at Arkaroola (Figure 4.5b). Both samples were collected to test whether the Arkaroola area was connected to the Willouran Trough during its early development. Sample PQ1 was also selected as a comparison with DS2 for the reasons given below.The Humanity Seat Formation is correlated with the Emeroo Subgroup (Preiss, 1987), and Sample HSF3 was collected to test correlations with the Emeroo Subgroup in the Willouran Range.

Sample DS2 was collected from a sandstone clast near The Dome, in the breccia west of the outcropping Dome Sandstone (Figure 4.5a). The sample may be Dome Sandstone but as a clast within a breccia it may also be from another unit, including the Paralana Quartzite (Figure 4.5c). If its zircon spectrum is sufficiently different from the Dome Sandstone samples, and similar to sample PQ1, it will provide strong evidence of the presence of Paralana Quartzite below the Curdimurka Subgroup in the Willouran Trough.

Two Burra Group samples were collected; one from the Emeroo Subgroup (B2) about 10 m above the contact with the Boorloo Siltstone in the Trial Hole Domain and one from a sandstone unit from near the top of the Skillogalee Dolomite (B4) in the Kingston Domain (Figure 4.5a,c). They will provide constraints on continuing development of drainage patterns that feed the Willouran Trough, after deposition of the Curdimurka Subgroup, and correlations with the Arkaroola area.

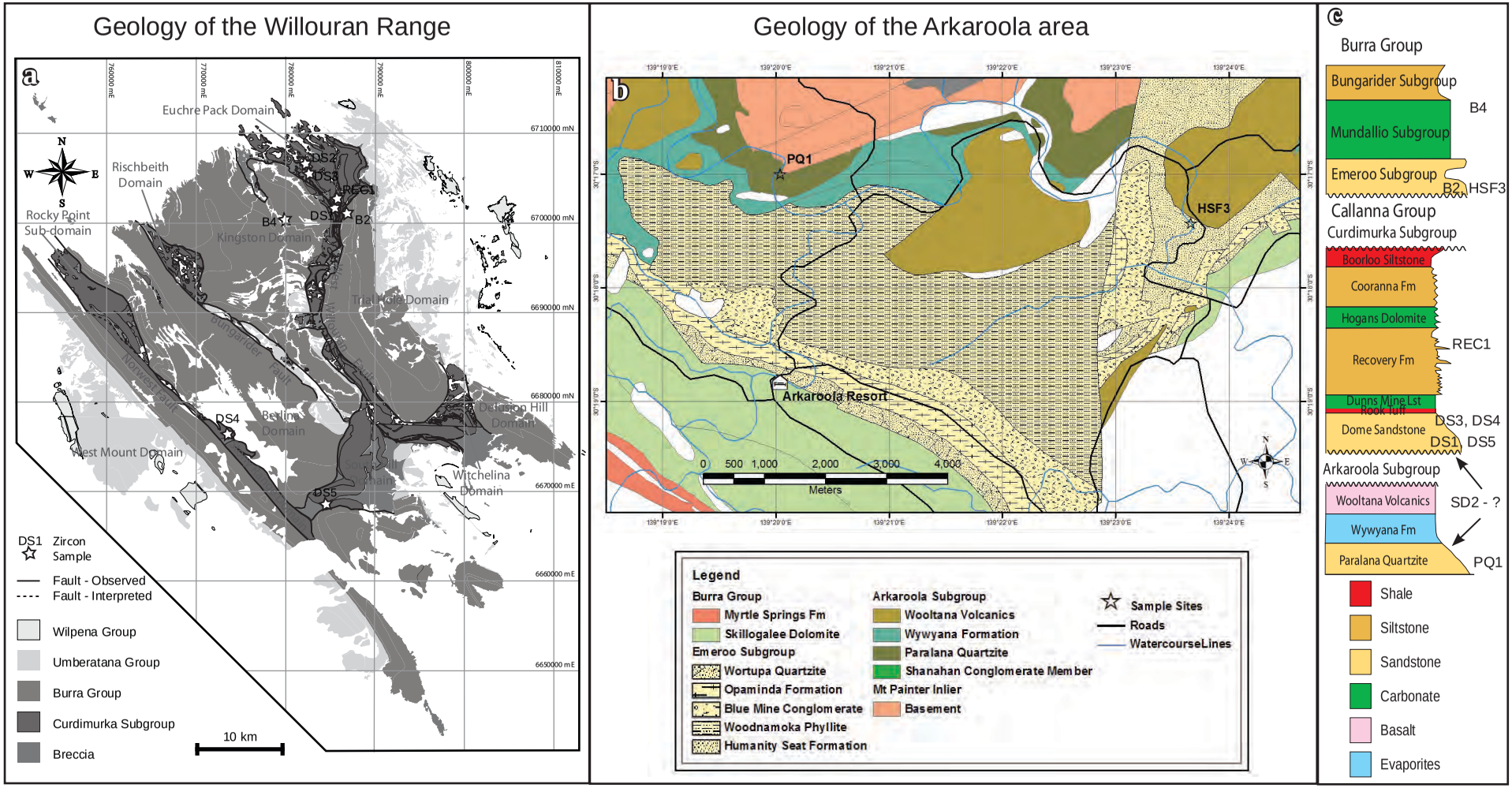

Figure 4.5. Sample locations. a) In the Willouran Range. b) Geology of the Arkaroola area, showing the sample sites for PQ1 and HSF3. c) Stratigraphic column showing the stratigraphic level of each sample. The stratigraphic level of DS2 is not known (Maps based on the PIRSA 1:100,000 GIS data)

4.4 Methodology

The samples for analysis were initially hand-crushed within a cast-iron mortar and pestle and hand-sieved through a -180 µm sieve. A minimum of 100 g of the -180 µm fraction was passed across a Wifley table and the heavy mineral tails collected. The heavy mineral separates were dried and a magnet passed over the sample to remove highly magnetic material. The remaining sample was passed through a high intensity magnetic separator, initially at 0.5 A and then the least magnetic fraction was passed through again at 1.8 A, with the least magnetic fraction containing the majority of the zircons. Zircons were hand-picked and placed on double-sided tape and then mounted in epoxy grain mounts which were polished so that the zircons were exposed at about two-thirds of their thickness.

Analysis of the zircons was by the LA-ICPMS method, using a HP4500 quadrupole ICPMS with a 213 nm New Wave Laser. Analyses were performed two hours after ignition of the mass spectrometer to enable the machine to stabilise. Four primary (Temora standard of Black et al., 2003) and two secondary glass standards (91500 standard of Wiedenbeck et al., 1995) were analysed at the beginning of the session and 12 unknown zircons. Each analysis began with a 30 second blank gas measurement followed by one minute of analysis time, when the laser was switched on. Zircons were sampled on 30 micron spots using the laser at 5Hz and a density of about 12 mJ/cm^2. A flow of He carrier gas at a rate of 0.7 litres/minute carried particles ablated by the laser out of the chamber to be mixed with Ar gas and carried to the plasma torch. Isotopes measured included ^{96}Zr, ^{178}Hf, ^{202}Hg, ^{204}Pb, ^{206}Pb, ^{207}Pb, ^{208}Pb, ^{232}Th and ^{238}U.

The analyses were done in two batches separated by several months. Over this time, the methodology was being refined and so a number of changes were made in the analysis of zircons. The first change was a shortening of the tube from the sample chamber to the ICP plasma chamber to increase the sensitivity of the analysis. Unfortunately the shorter tube resulted in less mixing of the sample and due to a probable coupling between the laser pulses and detector switching, the analysis produced a very peaky signal, with peaks in the ^{238}U count coinciding with troughs in the ^{206}Pb count and vice versa. This led to large variations in the ^{238}U:^{206}Pb ratio in about 25% of the analyses and hence large errors in the calculated ages. The probl0em was fixed by inserting a mixing chamber into the line between the sample chamber and ICP-MS, and smaller errors resulted.

In the second batch of analyses, ^{235}U was not analysed for and a shorter analysis switching frequency (0.1 seconds vs 0.2 seconds) was used. The change lowered the detection limits and improved the precision, giving lower errors. As a result, the first batch of samples have more rounded cumulative probability graphs than the second batch. All of these changes did not affect the accuracy of the results as these were checked against the zircon standard; the main affect was on the size of the errors.

Data reduction was based on the method outlined in detail by Harris et al., (2004) and modified to suit the ICPMS and laser at the University of Tasmania. The average of the background counts were subtracted from each isotope. Pb and U isotope ratios were then calculated from each 0.2 second measurement. These ratios were filtered to exclude the top

and bottom 1% to eliminate spikes and spurious data. Filtered ratios were then corrected for machine drift, downhole fractionation and mass-bias.

After the corrections were applied to the ratios, radiometric ages were calculated for each 0.2 second measurement and plotted against analysis time using an Excel spreadhseet developed at UTAS by Sebastian Meffre. An integration interval was then selected for the most stable portion of the analysis to exclude parts with contamination from inclusions. The standard errors quoted were based on the standard error of the measurements within the integration intervals and the errors on the measurement of the standards. Elemental abundances were calculated using the method outlined by Kosler (2001) using Zr as the internal standard element, assuming stoichiometric proportions and using the secondary standard 91500 to correct for mass bias.

The data was plotted against the inverse $^{238}U/^{206}Pb$ – $^{207}Pb/^{206}Pb$ isochron. An arbitrary limit of ±10% of the isochron is used and all the analyses plotting outside of this limit are rejected. Most rejected analyses plotted above the isochron at its lower age end and this effectively removed all the analyses that gave ages younger than the age of the sediments. The retained analyses are used in the final cumulative probability plots, produced using Isoplot v3.01 (Ludwig, 2003).

4.5 Results

A table with the analytical results and calculated ages is given in Appendix 1. Table 4.1 shows the major and minor zircon age populations for each sample and the major peaks. Zircon age spectra for the samples are shown in Figures 4.6 (Arkaroola area samples) 4.7 (Curdimurka Subgroup samples) and 4.8 (Burra Group samples).

4.5.1 Paralana Quartzite - PQ1.

A total of 72 zircons were analysed with 21 being rejected. The average error is 2.7%. Analytical problems encountered during the analysis of PQ1 have resulted in a broad peaks (Figure 4.6a). The major spread occurs between 1320 Ma and 1800 Ma with the major peak at 1520 Ma, a small notch at 1589 Ma and a small peak on the side of the major peak at 1405 Ma. On the young side of the major spread of data is a smaller peak with a maximum at 1260 Ma and an inflection point at 1175 Ma. There is one small peak at 2124 Ma. The youngest age is 1164 ± 36 Ma.

4.5.2 Humanity Seat Formation - HSF3.

A total of 72 zircon analyses were completed with 15 rejected. The average error is 0.6%. There is one major spread of data from about 1360 Ma to about 1980 Ma (Figure 4.6b). The highest peak is at 1557 Ma, with a lesser peak at 1499 Ma and 1463 Ma. The next highest peak is at 1725 Ma, with another peak at 1848 Ma. There are smaller peaks at 1667 Ma, 1628 Ma and 1932 Ma. At 1036 Ma, there is a peak representing two analyses and at 1091, there is a peak representing one analysis. The youngest age is 1022 Ma ± 14 Ma.

Table 4.1. Number of analyses and accepted analyses for each sample with the major and minor spread of age populations and age peaks.

Sample No	Analyses	Accepted	Major Spread	Minor Spread	Youngest (Ma)	< 1000 Ma (%)	1000 - 1350 Ma (%)	1350 - 1450 Ma (%)	1450 - 1620 Ma (%)	1620 - 1720 Ma (%)	>1720 Ma (%)	Peaks in descending order of height (Ma)
PQ1	72	51	1340 – 1800	1050 – 1340	1164 ± 36	0	14	12	55	16	4	1520, 1589, 1405 , 1260 , 1175, 1214
HSF3	72	57	1360 – 1980	990 – 1100	1022 ± 14	0	5	5	51	16	23	1557, 1449, 1463, 1725, 1848, 1667, 1036, 1091
DS1	78	63	1350 - 1850	1100 – 1300	1056 ± 33	0	14	11	56	16	3	1562, 1465, 1671, 1247, 1200
DS2	72	59	1300 – 1750	1100 – 1250	1136 ± 7	0	7	20	51	8	14	1600, 1525, 1415 1459, 1141, 1851, 2129
DS3	72	65	1300 – 1850	1100 – 1300	1016 ± 8	0	20	17	40	11	12	1516, 1455, 1149, 1601, 1718, 1234, 1794
DS4	72	51	1150 – 2000	850 – 1100	849 ± 13 861 ± 36	4	10	8	29	18	31	1500, 1641, 1447, 1315, 1818, 1014, 2074, 2532
DS5	84	72	1350 – 2000	1100 – 1250	1128 ± 16	0	10	6	19	26	41	1677, 1720, 1557, 1903, 1190, 1388, 1480, 1218, 2207
Rec1	72	58	1050 – 1360	1410 – 1900	868 ± 20	2	46	0	26	10	16	1175, 1589, 1641, 1285, 1822, 2107, 1007
B2	60	55	910 – 1350	1350 – 1700	939 ± 13	7	37	4	22	15	16	1642, 1133, 1239, 1096, 980, 1504, 1790
B4	96	54	800 – 1950	1950 – 2650	857 ± 23 866 ± 32	20	37	6	9	2	25	1014, 942, 1131, 1279, 1545, 1804, 2470, 2011

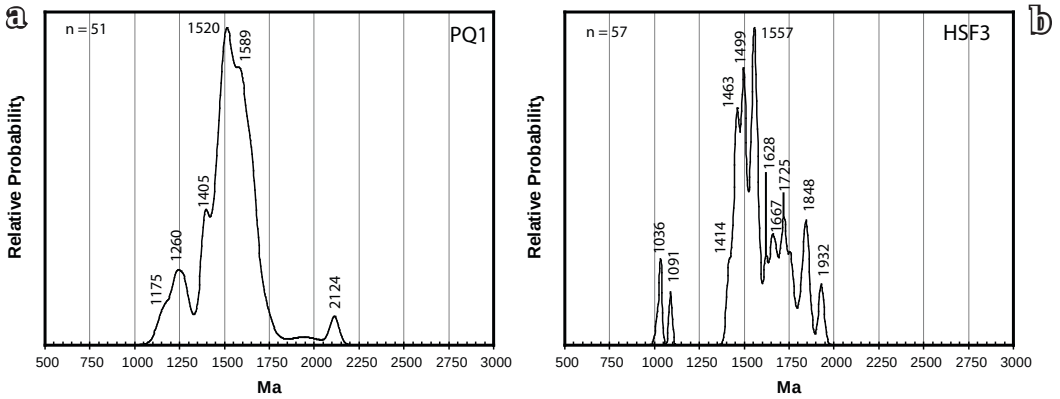

Figure 4.6. Detrital zircon age spectra from the Arkaroola area.
a) Sample PQ1, from the Paralana Quartzite, sampled about one metre above the contact with the basement of the Mt Painter Inlier. b) The Humanity Seat Formation, the lowest member of the Burra Group in that area. The numbers are the age peaks.

4.5.3 Dome Sandstone - DS1.

A total of 78 zircons from DS1 were analysed, with 15 being rejected (Figure 4.7a). The average error is 2.3%, giving broad peaks in the zircon age spectrum. The major peak occurs at 1562 Ma, with a secondary peak at 1465 Ma and an inflection in the curve at about 1671 Ma. A smaller, separate peak occurs at 1247 Ma, with a lesser peak at 1200 Ma. The broad peak begins at about 1350 Ma and concludes at about 1850 Ma. The youngest age is 1056 ± 33 Ma.

4.5.4 Dome Sandstone(?) - DS2

A total of 72 zircons were analysed with 13 being rejected. The average error is 0.9%. The age spectrum of DS2 comprises two equal peaks at 1525 Ma and 1600 Ma, with a slightly lower peak at 1415 Ma (Figure 4.7b). The majority of the data occurs between about 1300 Ma and 1760 Ma. There are smaller isolated peaks at 1141 Ma, 1851 Ma and 2129 Ma, with peaks representing single zircons above 2000 Ma. The youngest age is 1136 ± 7 Ma.

4.5.5 Dome Sandstone - DS3.

A total of 72 zircons were analysed with seven being rejected. The average error is 0.9%. The age spectrum reveals two main populations; the smaller between 1070 Ma and 1300 Ma and the larger between 1300 Ma and 1860 Ma (Figure 4.7c). The older population contains a main peak at 1516 Ma, with a lesser peaks at 1455 Ma, 1601 Ma, 1718 Ma and 1794 Ma. The younger group contains one main peak at 1149 Ma and a smaller peak at 1234 Ma. The youngest age is 1016 ± 8 Ma.

4.5.6 Dome Sandstone - DS4.

A total of 72 zircons were analysed with 21 being rejected. The average error is 4.5%. Due to the larger errors, the probability graph does not have the resolution of the above samples (Figure 4.7d). It shows a broad maxima from about 1150 Ma to about 2000 Ma, with two peaks at 1500 Ma and 1641 Ma and two lesser peaks at 1315 Ma and 1818 Ma. There is also a small shoulder on the 1500 Ma peak at 1447 Ma. The main grouping of data has a

long tail with lesser peaks at 2074 Ma and 2532 Ma. There is a small isolated peak at 1014 Ma, with a minima at about 810 Ma and a maxima at 1100 Ma. The youngest age is 849 ± 13 Ma, with a second youngest of 861 ± 36 Ma.

4.5.7 Dome Sandstone - DS5.

A total of 84 zircons were analysed with 12 being rejected. The average error is 0.8%. The major spread of the data is from about 1250 Ma to about 2100 Ma, with two peaks of equal height at 1677 Ma and 1720 Ma (Figure 4.7e). There are smaller peaks at 1557 Ma, 1903 Ma, 1388 Ma and 1480 Ma. There is a small group of data from about 1100 Ma to about 1250 Ma with one peak at 1190 Ma, a smaller peak at 1218 Ma and a small peak at 1134

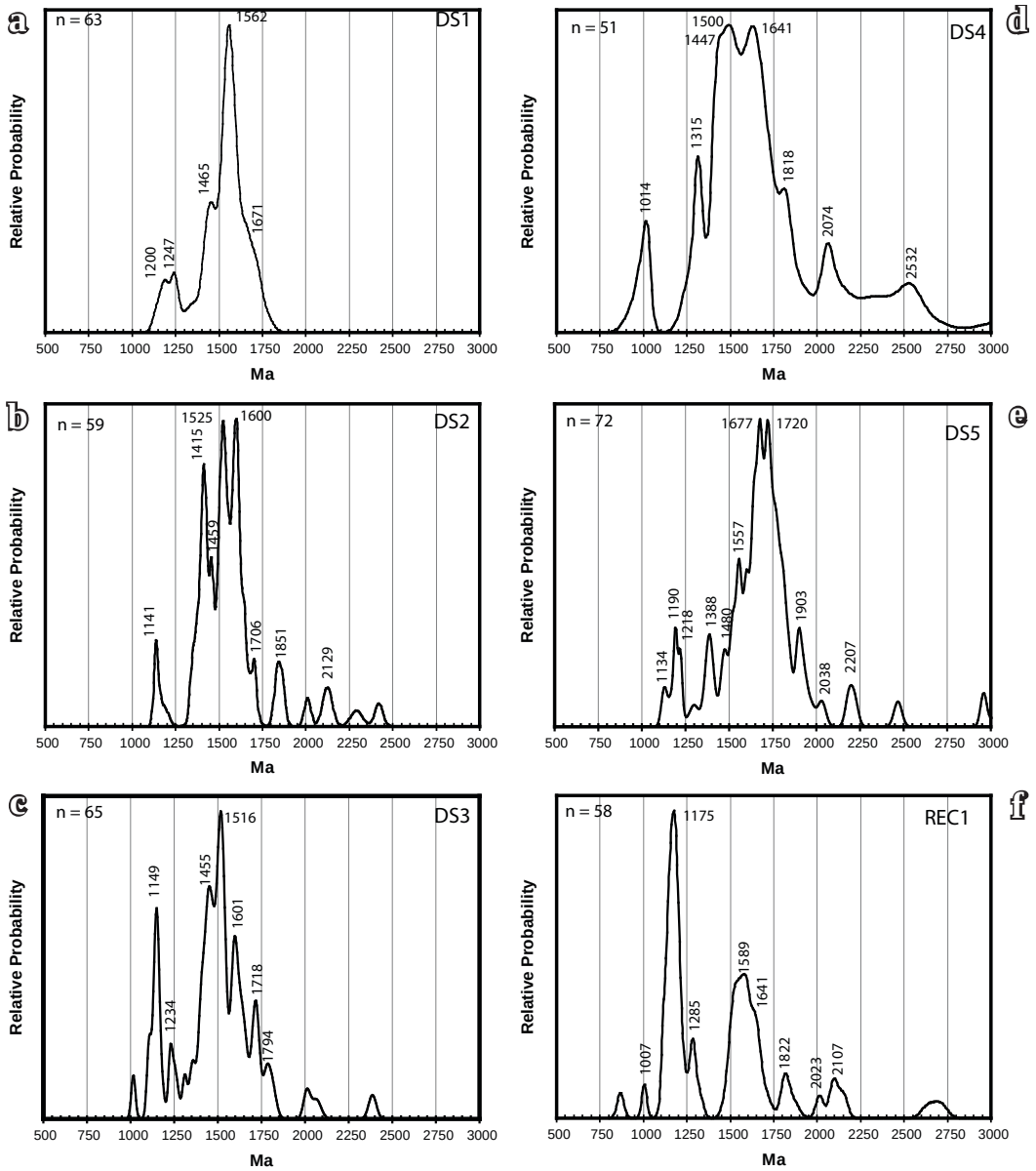

Figure 4.7. Detrital zircon age spectra from the Curdimurka Subgroup.
a) Sample DS1 from about the middle of the Dome Sandstone, b) Sample DS2 from a sandstone clast within the breccia underlying the Dome Sandstone near the Dome. c) Sample DS3 from a sandstone-conglomerate facies near the base of the Dome Sandstone. d) Sample DS4 from the Dome Sandstone in the Stony Range Domain. e) Sample DS5 from the Dome Sandstone in the South Hill Domain. f) Sample REC1, from the Recovery Formation in the Euchre Pack Domain. The numbers are the age peaks.

Ma. Above 2100 Ma, are three small peaks, the largest at 2207 Ma. The youngest age is 1128 ± 16 Ma.

4.5.8 Recovery Formation Sandstone Unit 2 - REC 1

A total of 72 zircons were analysed with 14 being rejected. The average error is 1.2%. The age spectrum has a narrow spread of data from about 1060 Ma to 1370 Ma, with the highest peak for the sample at 1175 Ma and a lesser peak at 1285 Ma, representing a total of 26 of the analyses (Figure 4.7f). The next major group, containing 21 analyses, is from about 1400 Ma to 1750 Ma with a single peak at 1589 Ma and inflection points at about 1518 Ma and 1641 Ma. There is a small peak about 1822 Ma and another series of small peaks about 2000 Ma. Single analysis peaks occur at 1007 Ma and 877 Ma. The youngest age is 868 ± 20 Ma.

4.5.9 Burra Group - B2

A total of 60 zircons were analysed with 55 analyses being accepted. The average error is 0.6%. The cumulative probability plot for B2 has two main clusters; one from about 910 Ma to about 1350 Ma and the second from about 1350 Ma to about 1700 Ma (Figure 4.8a). In the first group, there are a number of peaks with the highest peak at 1133 Ma, and lesser peaks at 1239 Ma, 1096 Ma, 980 Ma, 1191 Ma, 1028 Ma and 1298 Ma. In the second group, the highest peak for the sample is at 1642 Ma, with lesser peaks at 1504 Ma and 1419 Ma. Beyond the second grouping are a series of peaks at 1790 Ma, 1996 Ma, 2076 Ma, 2372 Ma and 2446 Ma, representing one or two zircon analyses each. The youngest age is 939 ± 13 Ma.

4.5.10 Burra Group - B4

Although this sample has abundant zircons, most are less than 50 μm in diameter and therefore near the lower limit of the size suitable for analysis using this method. A total of 96 samples were analysed with 54 accepted. Analytical problems during the first 84 analyses resulted in an average error of 4.4% whereas the last 12 analyses produced an average error of 0.7%, and the smaller errors produce sharp peaks on a more rounded graph.The bulk of the analyses occur in the interval between about 770 Ma and 1150 Ma,

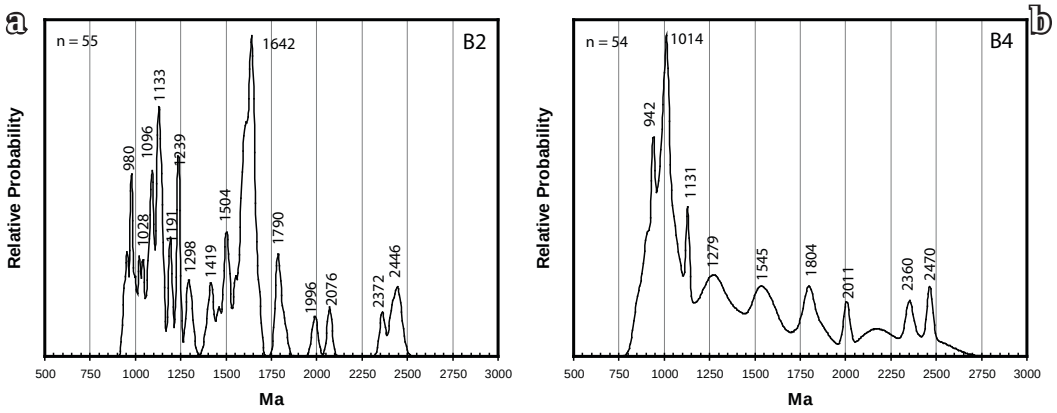

Figure 4.8. Detrital zircon age spectra from the Burra Group.
a) Sample B2 from the base of the Emeroo Subgroup. b) Sample B4 from the Skillogalee Dolomite.

with the remainder of the curve being a series of low peaks and troughs until about 2700 Ma (Figure 4.8b). In the first group, the major peak is at 1014 Ma, with lesser peaks at 952 Ma and 1131 Ma. There is an inflection point at about 911 Ma. The smaller peaks occur at 1279 Ma, 1545 Ma, 1804 Ma, 2011 Ma, 2360 Ma and 2470 Ma. The peak at 1545 Ma represents a group of five analyses and the peak at 1804 Ma represent a grouping of four analyses, otherwise these lesser peaks represent one or two analyses only. The youngest zircons give ages of 857 ± 23 and 866 ± 32.

4.6 Discussion

4.6.1 Detrital Zircon Sources.

As a first approximation, Figure 4.9 compares the detrital zircon ages with possible source areas including the Gawler Craton, Curnamona Province, Musgrave Block, as well as more distal areas that may have been linked to the Musgrave Block, the Albany-Fraser Belt and the Paterson Province (Figure 4.2). Table 4.2 is a more detailed attempt to identify zircon age spectra peaks with individual sources that have been identified in the Gawler Craton, Curnamona Province and the Musgrave Block. In the age range 1450 Ma to 1720 Ma, which could contain samples from any of these three source regions, for the majority of age peaks there is no unique solution but for several ages, about 1515 - 1525 Ma and about 1600 Ma and 1640 Ma there are only Curnamona Province sources known.

4.6.2 Curdimurka Subgroup Samples

Detrital zircon age spectra for Dome Sandstone samples DS1 and DS3, and also DS2, have similar profiles (Figure 4.7) with the bulk of the data ranging from 1300 Ma to 1750 - 1800 Ma and minor spreads between 1100 Ma and 1250 - 1300 Ma. They have matching peaks at about 1455 - 1465 Ma; DS1 and DS3 have peaks at 1234 - 1247 Ma but DS2 and DS3 are most similar with an additional four matching peaks at about 1600 Ma, 1520 Ma, 1145 Ma, and 1710 Ma. The major peak in DS1 at 1562 Ma is between the peaks in DS2 and DS3.

Considering likely distal zircons sources, i.e., younger than 1350 Ma and older than 1720 Ma, DS1 has 17% of zircons, DS2 21% and DS3 32%. These three samples, with PQ1, have the lowest proportion of Gawler Craton only age zircons, with DS1 having only three percent over 1720 Ma. In the likely proximal detrital zircon age group between 1450 and 1720 Ma, DS1 has 72% of zircons in this age range, DS2 59% and DS3 51%. Hence all three samples have over 50% of detrital zircons within the likely proximal source age group and less than a third in the likely distal source age group.

Sample DS4 has 45% of detrital zircons from a likely distal source and 47% from a likely proximal source. The detrital zircon age spectra has a major spread that is wider than DS1, DS2 and DS3, and a narrow, younger minor spread, however it shows a similar overall shape. It shares only one peak (to within 10 Myrs) with samples DS1, DS2 and DS3, at about 1450 Ma, hence although it shares a similar pattern with these samples in detail it appears to have different source areas, with more zircons sourced distally.

Abbreviations (names of orogenic events are italicized) ADS – Amata Dyke Swarm; AS – Adelaide Supergroup; BC Birksgate Complex; CB – Cariewerloo Basin; CoO – Cornian Orogeny; DeO – Delamerian Orogeny; DS – Donington Suite granitic rocks; FC – Fraser Complex; GC – Giles Complex; GDS – Gairdner Dyke Swarm; GFDS – Gnowangenup Dyke Swarm; GHS – Gawler Range Volcanics and Hiltaba Suite; grn – granite; KaO – Kararan Orogeny; KiO Kimban Orogeny; KsZ – Kalinjala Shear Zone; MBG – Mount Barren Group; ME – Miltalie Event; MiG – Miltalie Gneiss; MiO – Miles Orogeny; MlG – Malcolm Gneiss; MNG – Mount Neill Granite; MR – Mount Ragged metasedimentary rocks; MuG – Munglinup Gneiss; MWO – Mount West Orogeny; MuO – Musgravian Orogeny; NS – Ninnerie Suite; ogneiss – orthogneiss; Ole – Ooldean Event; OlO – Olarian Orogeny; Paleo – Paleozoic; PaO – Paterson Orogeny; PeO – Petermann Orogeny; pgneiss – paragneiss; PS – Pitjantatjara Supersuite; SI – Stage I of the Albany – Fraser Orogeny; SII – Stage II of the Albany – Fraser Orogeny; S&MC – Sleaford and Mulgathing complexes; SlO – Sleafordian Orogeny; SPS – St. Peter Suite; SRF – Stirling Range Formation; SS – Spilsby Suite; Ss1 – Supersequence 1 (Centralian Superbasin); Ss2 – Supersequence 2 (Centralian Superbasin); Ss3 – Supersequence 3 (Centralian Superbasin); Ss3 + 4 – Supersequence 3 + 4 (Centralian Superbasin); TG – Tarcunyah and Throssel Range groups; TG – Tollu Group; TS – Tunkillia Suite granitic rocks; WaS – Wankanki Supersuite; WDS – Wig Dyke Swarm; WLIP – Warakuna Large Igneous Province; WM – Wirku Metamorphics; WS – Willyama Supergroup; YpO – Yapungku Orogeny.

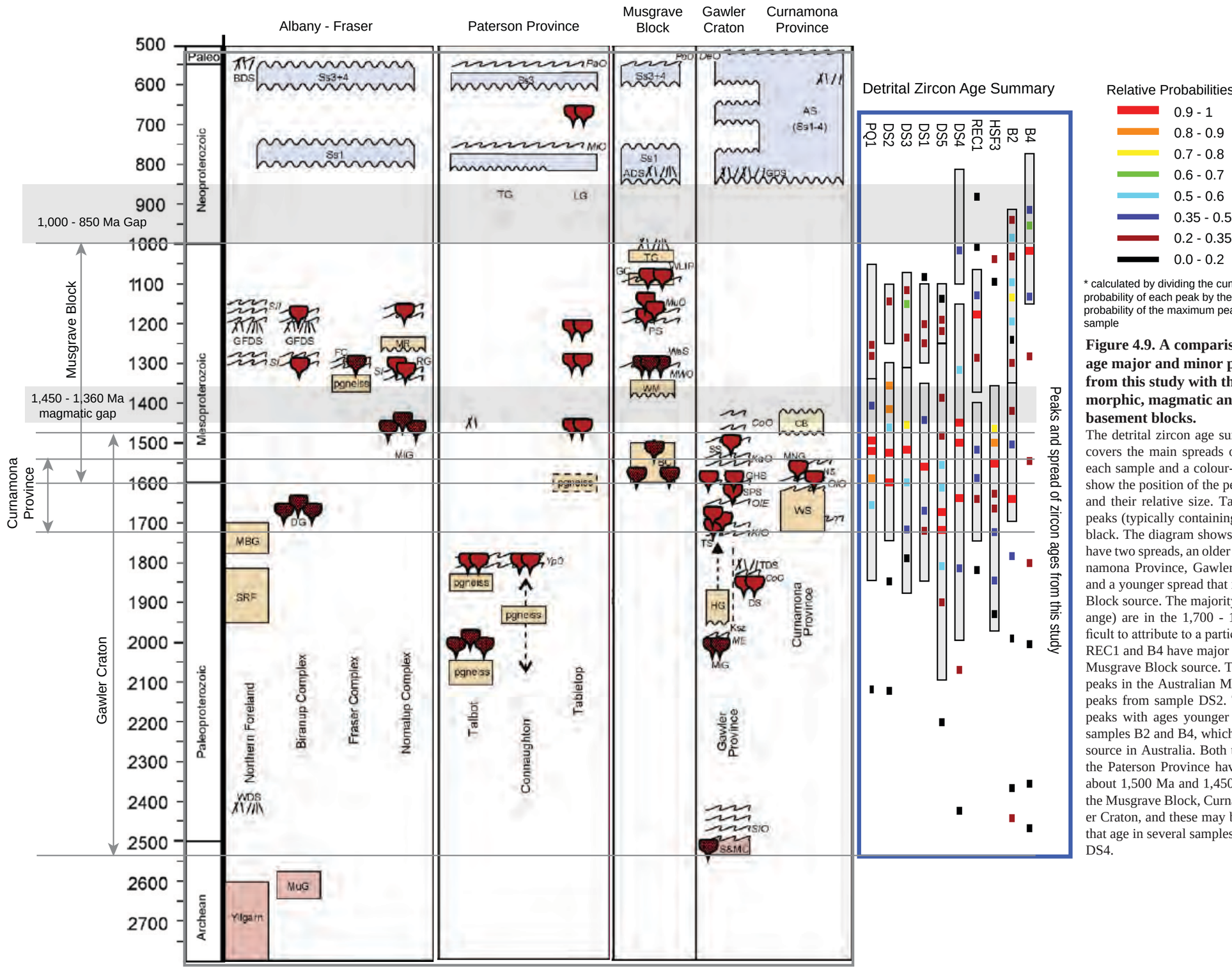

Figure 4.9. A comparison of the detrital zircon age major and minor populations and peaks from this study with the reported ages of metamorphic, magmatic and zircon ages from the basement blocks.

The detrital zircon age summary comprises a box that covers the main spreads of the zircon age spectra for each sample and a colour-coded relative probability to show the position of the peaks in the zircon age spectra and their relative size. Tallest peaks are red, smallest peaks (typically containing one or two data points) are black. The diagram shows that the majority of samples have two spreads, an older age spread that could be Curnamona Province, Gawler Craton or Musgrave Block and a younger spread that it is indicative of a Musgrave Block source. The majority of major peaks (red and orange) are in the 1,700 - 1,500 Ma period and so difficult to attribute to a particular source area but samples REC1 and B4 have major peaks that are indicative of a Musgrave Block source. There are a number of smaller peaks in the Australian Magmatic Gap, and two major peaks from sample DS2. There are also several small peaks with ages younger than 1,000 Ma, particularly samples B2 and B4, which have no recorded magmatic source in Australia. Both the Albany - Fraser Belt and the Paterson Province have magmatic events between about 1,500 Ma and 1,450 Ma that are not recorded in the Musgrave Block, Curnamona Province of the Gawler Craton, and these may be sources for small peaks of that age in several samples, and a major peak in sample DS4.

Table 4.2. Possible detrital zircon sources.
The table emphasizes the single source of detrital zircons younger than 1,350 Ma and the magmatic gap between 1,450 and 1350 Ma. It also shows the mulitple possible zircon sources between 1,500 Ma and 1, 720 Ma.

Peak	Sample	Source	Distal/ Proximal
942	B4	South China?	Distal
980	B2	Dolerite dykes, Arunta Block South China?	Distal Distal
1007,1014	Rec1,B4 DS4	Felsic magmatism, MB	Distal
1036	HSF3	Youngest Giles Event, MB	Distal
1091, 1096	HSF3,B2	Walu Granite, MB	Distal
1131,1133	B4,B2	Umutju Suite Granite, MB	Distal
1141,1149	DS2,DS3	Pitjantjatjara Supersuite Granite, MB Ayers Range Adamellite, MB	Distal Distal
1175	PQ1 Rec1	Musgrave Orogeny, MB	
1190	DS5	Pitjantjatjara Supersuite Granite, MB Musgrave Orogeny, MB	Distal Distal
1200	DS1	Metamorphism, Musgrave Orogeny, MB	Distal
1214,1218	PQ1,DS5	Metamorphism, Musgrave Orogeny, MB	Distal
1234,1239	DS3,B2	Metamorphism, Musgrave Orogeny, MB	Distal
1247	DS1		
1260	PQ1		
1279,1285	B4,Rec1		
1315	DS4	Magmatic event, MB	Distal
1388	DS5		
1405, 1415	PQ1, DS2		
1447,1449	DS4,HSF3	Granite Gneiss, Coompana Block, GC	
1455,1459, 1463,1465	DS3,DS2 HSF3,DS1	Granite Gneiss, Coompana Block, GC	Distal
1480	DS5		
1500,1504	DS4,B2	Spilsby Suite, southern GC Mafic Dykes, CP	Distal Proximal
1516,1520,1525	DS3,PQ1,DS2	Mafic Dykes, CP	Proximal
1545	B4	Metamorphic event, GC Mulga Park Domain, MB	Either
1557,1562	DS5 HSF3,DS1	Youngest Hiltaba Suite Granites GC Metamorphic event, GC Moolawatana Suite, CP Mt Painter Inlier Felsic magmatism, CP Mulga Park Domain, MB	Either Either Proximal Proximal Distal
1589	PQ1 Rec1	Gawler Range Volcanics, CP Hiltaba Suite Granite, CP Bimbowrie Suite Granites CP Mt Painter Province Granites, CP Mulga Park Domain, MB	Proximal Proximal Proximal Proximal Distal
1600,1601	DS2,DS3	Syn-orogenic intrusives, CP Olarian Orogeny, CP	Proximal Proximal
1641,1642	DS4 Rec1,B2	S-type granites, CP Pepagoona Volcanics, CP	Proximal

Peak	Sample	Source	Distal/ Proximal
1667,1671,1677	HSF3,DS1,DS5	Tunkillia Suite, GC; Zircon popl. Felsic gneiss, N. GC Clevedale Migmatite, Thorndale Gneiss, CP Rasp Ridge Gneiss CP	Distal Distal Proximal Proximal
1718,1720,1725	DS3,DS5,HSF3	Syn-orogenic granite, mafic magmatism, GC High grade metamorphism, S.GC Basso Suite, Redan Gneiss? CP	Distal Distal Proximal
1790,1794,1804	B2,DS3,B4	Myola, Tidnamurkuna Volc's GC	Distal
1818,1822	DS4,Rec1	Zircon popl., felsic gneiss, N. GC	Distal
1848,1851	HSF3,DS2	Donington Suite, GC	Distal
1903	DS5		
2011	B4	Miltalie Gneiss, GC	Distal
2074	DS4		
2107	Rec1		
2129	DS2		
2207	DS5		
2470	B4	Kiana Granite (Dutton Suite), GC Sleaford Orogeny, GC	Distal
2532	DS4	Coulta Granodiorite (Dutton Suite), GC	Distal

Sample DS5 has 51% of detrital zircons from a likely distal source and 45% from a likely proximal source. The major spread has an older upper age than DS1, DS2 and DS3, but a similar minor spread. It shares only three peaks (to within 10 Myrs) with samples DS1 - DS4, 1560 Ma, about 1675 Ma and about 1720 Ma.

Sample REC1 has 52% of zircons sourced from likely distal areas, with 46% in the 1000 - 1350 Ma age range and likely sourced from the Musgrave Block. The major age spread reflects this, being younger than the minor age spread. It shares three peaks with DS4, 1641 Ma, 1010 Ma and 1820 Ma, although the latter two are minor peaks representing only a few analyses each, and 1641 Ma is an inflexion on a larger peak in sample REC1 and may also represent a few analyses. REC1 is the only sample with no zircons in the 1350 - 1450 Ma age range.

Based on these comparisons, samples DS1, DS2 and DS3 from the Euchre Pack Domain are most similar. Samples DS4, from the Stony Range Domain, and DS5 from the South Hill Domain share the same broad source regions as the Euchre Pack Domain samples but with a larger proportion of distal zircons, particularly the older Gawler Craton zircon sources (Table 4.2). DS4 and DS5 also have a smaller proportion of detrital zircons in the 1350 - 1450 Ma age range, with DS2 and DS3 having the highest proportion of zircons in this age range. REC1 shows a greater proportion of distal zircons, particularly from the Musgrave Block with a decrease in likely proximal sources.

If the age groups about 1515 - 1525 Ma and 1600 - 1640 Ma are only sourced from the Curnamona Province (Table 4.2), variations in the proportion of zircons with ages in these ranges may provide further information on variations in source regions. DS1 has 16% of detrital zircons in this age group, DS2 22%, DS3 20%, DS4 14%, DS5 13% and REC1

10%. DS1, DS2 and DS3 have the largest proportion in these age groups agrees with these samples having the lowest proportion of distal zircons. Sample DS5 has the lowest proportion of zircons in these age ranges (with REC1) and the highest proportion of distal zircons .

4.6.3 The Burra Group in the Willouran Trough

Sample B2 has 53% of zircons sourced from likely distal areas, including 37% with Musgrave Block only ages. It shares four peaks with Curdimurka Subgroup samples; ~ 1240 Ma with DS1 and DS3, ~ 1500 Ma with DS4, ~ 1640 Ma with DS4 and ~ 1795 Ma with DS3. Sample B4 has only 11% of zircons sourced from likely proximal areas and 82% from likely distal sources. It shares the ~ 1101 peak with REC1 and DS4, the ~ 1280 Ma peak with REC1 and the ~ 1795 Ma peak with DS3, and the 1130 Ma and ~ 1795 Ma peak with sample B2. Both B2 and B4 have younger major age spreads than minor age spreads indicating the Musgrave Block is the source of the majority of detrital zircons for both samples. However, the primary peaks show a marked change, from 1642 Ma, a Curnamona Province source in B2 to 1014 Ma in B4. There is also a shift in the proportion of zircon ages less then 1450 Ma, from 48% in B2 to 63% in B4.

4.6.4 The Arkaroola Area

Samples PQ1 and HSF3 were collected from close to the Mt Painter Inlier and so it would be expected that their zircon age sprectra would record contributions from this local basement source. PQ1 has 71% of zircons with ages from likely proximal sources and 18% from distal sources. The largest peak in the zircon age spectra of PQ1, 1520 Ma, is within error of zircon ages from mafic enclaves within the Yerila Granite (1529 ± 9 and 1504 ± 29 Ma, Kromkhun and Foden, in prep) in the Mt Painter Inlier. A shoulder on the main peak occurs at 1589 Ma, which correlates with the Hiltaba Suite Granites and Gawler Range Volcanics on the Gawler Craton, and the Mundi Mundi Granite and Bimbowrie Granite from the Curnamona Province. It shares the ~ 1175 Ma and 1589 Ma peak with REC1, the ~ 1215 Ma peak with DS5, and the 1560 Ma peak with DS1. By visual comparison, sample DS2 is more similar to samples DS1 and DS3 than with PQ1, therefore it is interpreted to be a clast of Dome Sandstone rather than Paralana Quartzite.

Sample HSF3 has 67% of zircons with ages from likely proximal sources and 28% from likely distal sources, including the smallest proportion age zircon ages between 1000 Ma and 1350 Ma (Table 4.1). It shares no peaks with PQ1, and one peak, ~ 1095 Ma wih B2, but six peaks with samples from the Curdimurka Subgroup; ~ 1445 Ma with DS4, 1460 Ma with DS1, DS2 and DS3, its main peak, ~ 1560 Ma with the main peak of DS1 and a minor peak of DS5, ~ 1670 Ma with DS1 and DS5, ~ 1720 Ma with DS3 and DS5, and ~ 1850 Ma with DS2. Its highest peak at 1557 Ma corresponds with the age of felsic magmatism in the Mt Painter Inlier (e.g., Johnson, 1980; Sheard et al., 1992; Teale et al., 1995) but the

second and third peaks, 1449 Ma and 1463 Ma are within error of magmatic zircons in the Coompana Block and are distal to the Humanity Seat Formation (Table 4.2).

4.6.5 Comparison of Curdimurka Subgroup and Burra Group Results.

If the age of 797 ± 5 Ma for the Skillogalee Dolomite (Drexel, 2009; Reid 2009) was correct, one of the possible implications is that the Rook Tuff and the Skillogalee Dolomite would be about the same age. Therefore, the Emeroo Subgroup and Dome Sandstone detrital zircon spectra should be similar, as they are geographically in the same area, and within the same depositional trough. And, although the correlation is not precise, the Skillogalee Dolomite detrital zircon spectra should be similar to that of the Recovery Formation. The results from this study show that this is clearly not the case. Sample B2 shares only four peaks (out of seven identified in Table 4.2) with the Dome Sandstone samples, and although it shares the major peak of about 1640 Ma with sample DS4, the second peak of 1133 Ma, matches a small (representing only two analyses) 1134 Ma peak in sample DS5. It also has a higher proportion of detrital zircon ages from distal areas than all of the Dome Sandstone samples, except sample DS5. However, sample DS5 has the majority of distal zircons from the older age group (above 1720 Ma), whereas sample B2 has the majority in the younger distal age group (below 1350 Ma).

Sample B4 from the upper Skillogalee Dolomite shares only two peaks with sample Rec1 (from the Recovery Formation), at about 1010 and 1280 Ma, but the former is the major peak for B4 but minor for Rec1, and the latter a minor peak for both. The major peak of 1175 Ma for sample Rec1 has no match in the detrital zircon age spectra of sample B4. Both samples are dominated by distal source areas, particularly from the Musgrave Block, but sample B4 has a significant (second highest) peak below 1000 Ma, whereas sample Rec1 has a small peak (one sample) below that age. Hence the detrital zircon age spectra of the Burra Group samples are sufficiently different from their possible correlatives in the Curdimurka Subgroup to conclude that they were not deposited at the same time and are therefore not correlative units.

4.6.6 Comparison with other detrital zircon ages from the Adelaide Fold Belt.

Ireland et al. (1998) conducted a detrital zircon provenance study on four sandstone samples from the Adelaide Fold Belt (Figure 4.10). The Niggly Gap Beds are equivalent to the Recovery Formation and the zircon spectrum of Ireland et al. (1998) has a major population range of about 1500 Ma to 1900 Ma, with peaks at 1600 Ma, 1680 Ma and 1840 Ma (Figure 4.11). Its major population has a similar range to sample DS5 and the peaks are matched in several samples but no sample from this study records more than one of the three peaks. Most significantly however is the absence of zircon ages less than 1500 Ma, indicating that there was no input from the Musgrave Block, whereas in the correlative REC1, they constitute a major proportion of the sample.

The Mitcham Quartzite is from the uppermost Burra Group and so has no direct correlative to the samples from this study (Figure 4.10). Its zircon age spectrum is most similar to Dome Sandstone spectra from this study, with a major spread between about 1350 Ma and

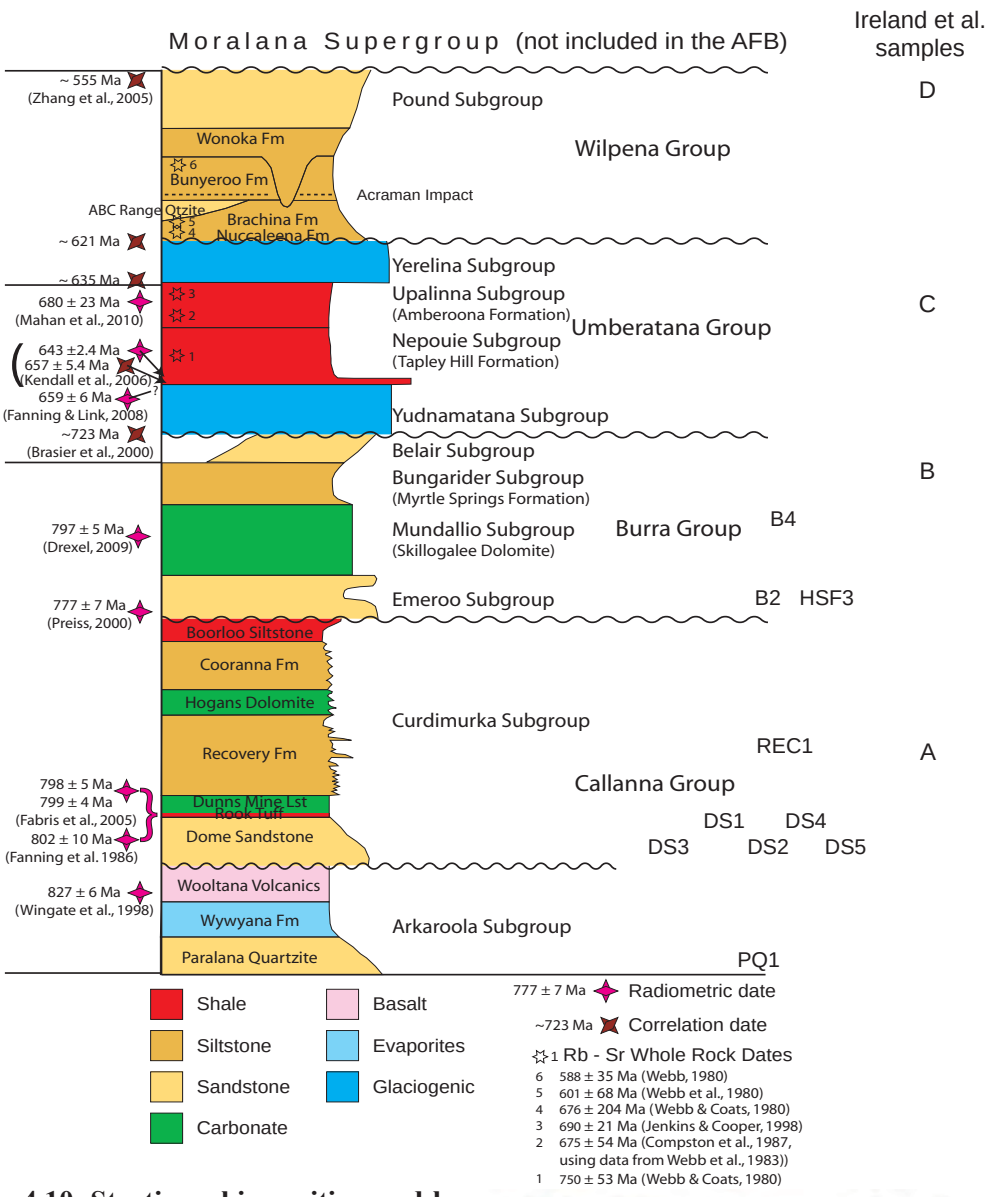

Figure 4.10. Stratigraphic position and locality of the detrital zircon samples from this study and Ireland et al. (1998).
From Ireland et al. (1998)
A - Niggly Gap Beds
B - Mitchan Quartzite
C - Marino Arkose
D - Bonney Quartzite.
From this study (locality map).
E - PQ1, HSF3
F - DS1,DS2,DS3,REC1,B2
G - DS5
H - DS4
I - B4

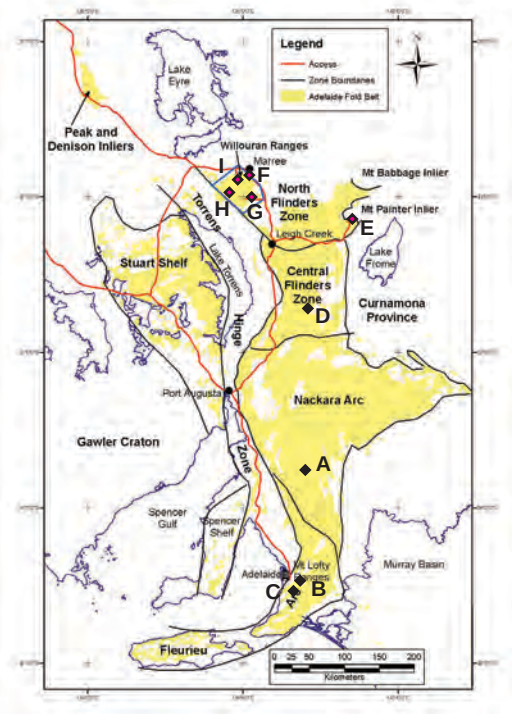

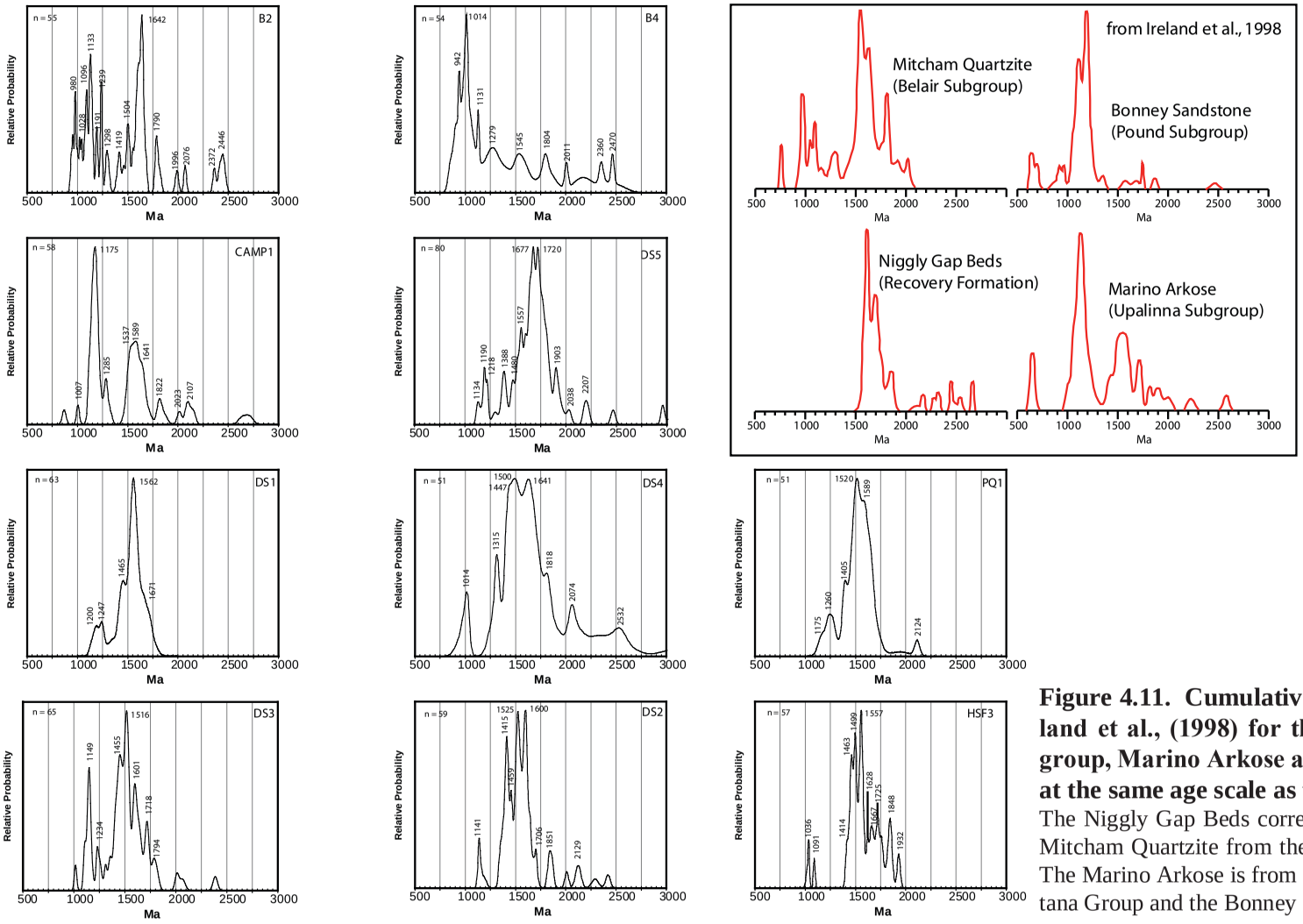

Figure 4.11. Cumulative Probability Diagrams from Ireland et al., (1998) for the Niggly Gap Beds, Belair Subgroup, Marino Arkose and the Bonney Sandstone, plotted at the same age scale as those from this study.

The Niggly Gap Beds correlate with the Recovery Formation, the Mitcham Quartzite from the Belair Subgroup of the Burra Group. The Marino Arkose is from the Upalinna Subgroup of the Umberatana Group and the Bonney Sandstone from the Wilpena Group.

2100 Ma, and a minor spread from 900 Ma to 1350 Ma (Figure 4.11). In contrast, samples B2 and B4 have younger major than minor spreads. The largest peak at about 1560 Ma matches the largest peak of DS1 and HSF3 but the second peak at about 1620 Ma is not matched in this study. The largest peak in the minor spread is at about 980 Ma, which matches a peak in B2.

The Marino Arkose is from the Umberatana Group and so has no stratigraphic correlative to the samples from this study (Figure 4.10). However, its zircon age spectrum has a similar shape to that of REC1, although with the younger peak, 1140 Ma from the Marino Arkose and 1175 Ma from REC1 (Figure 4.11). The Bonney Sandstone is from the Wilpena Group but being from the northern part of the Central Adelaide Fold Belt, is spatially closest to the samples from this study (Figure 4.10). It is dominated by zircon ages consistent with a Musgrave Block source and the peaks at 1180 Ma and 1100 Ma are recorded in samples from this study (Figure 4.11). The small 950 Ma peak in the Bonney Sandstone sample is matched by the 942 Ma peak in sample B4, but the youngest peaks are younger than the depositional age of the Skillogalee Dolomite.

4.6.7 Zircon Provenance and the Evolution of the Willouran Trough

The model detrital zircon age variation expected for sedimentation in rift environments suggests that during the initial stage of rift development, the dominant source of sediments should be from the area immediately surrounding the forming depocentre. At the lowest level sampled in the Dome Sandstone (sample DS3) to the highest (DS1), in the Euchre Pack Domain, the bulk of the detrital zircons are sourced from the Curnamona Province and/or the Gawler Craton and are likely proximal. Hence the rift shoulders were likely exposed to erosion. However there is a significant proportion of detrital zircons sourced from the Musgrave Inlier, possibly by axial drainage along the rift from the northwest. It is likely that the rift is in the through-going fault stage, corresponding to the rift maxima during deposition of the Dome Sandstone.

From the Dome Sandstone to the RSds2 (sample REC1), the detrital zircon age spectra becomes more complex, with an increased proportion of zircons less than 1350 Ma without a significant increase in zircons older than 1720 Ma. This may be a reflection of greater sediment transport from the Musgrave Inlier, a reduction in the erosion of the proximal sources as the topography adjacent to the Willouran Trough matured or a combination of both. Because there is only a minor increase in older Gawler Craton zircons which are mostly from distal sources, but a large increase in Musgrave Block sourced zircons, it is likely that axial drainage is still dominant. There is a significant proportion of proximal sourced zircons which could be from re-working of sediments within the trough or from the margins of the trough. If the latter, the rift shoulders are still exposed and the Willouran Trough is not within a sag phase. Hence according to the model developed here, the Willouran Trough is not in a sag phase at this time. With no zircons between 1450 and 1350 Ma, sedimentation from this source area has been significantly reduced. This has two possible interpretations;

1. the source is proximal and has been covered, inferring that the basin is in the sag phase according to the model proposed,

2. or the source is distal and sediments from that source are no longer reaching the Willouran Trough through sediment by-pass or stream capture directing sediments from that source elsewhere.

Because there is still a significant proportion of zircons from proximal sources, the first option is rejected and the second is favoured.

Sample DS4 has a similar zircon age spectrum to samples DS1, DS2 and DS3, suggesting that they were all draining the same area. However it has a greater proportion of zircons greater than 1720 Ma, reflecting a Gawler Cration source, likely due to its position near the western margin of the Willouran Trough. But it also has peaks at 1500 and 1641 Ma which are likely Curnamona Province sourced zircons so there is transport from the eastern side of the Willouran Trough, suggesting that it was not compartmentalized at this time. It has a similar proportion of zircons younger than 1350 Ma to DS1 and DS3, and so was likely seeing a similar proportion of Musgrave Block sourced sediments. Taking these factors into account, it is interpreted that the Willouran Trough was a full graben at this time.

Sample DS5 is significantly different, with the oldest main peak of the zircon age spectra, the highest proportion of zircons older than 1720 Ma and only 10% of zircons younger than 1350 Ma. The Gawler Craton was likely the dominant source of detrital zircons although the three highest peaks could be either the Gawler Craton or the Curnamona Province (Table 4.2). However, it also has the smallest proportion of zircons from about 1525 Ma and the 1600 - 1640 Ma age range, suggesting that the Curnamona Province provided only a small proportion of the sediments.

Sample PQ1 has 14% of detrital zircons of Musgrave Block age which, given the proximity to the basement and the results of the study by Cawood et al., (2003) is surprising. Coats and Blisset (1971) considered that the deposition of the Paralana Quartzite was controlled by faulting at the initiation of rifting whereas Preiss (2000) suggested that sedimentation began on a peneplained basement surface. If the latter is the case, it is possible that there may have been some sediment transport from the Musgrave Block prior to initiation of the rift basin. Another possibility is that they were sourced from a Grenvillean terrane no longer cropping out in South Australia, having been buried, eroded or rifted away, as proposed by Wyoczanski and Allie (2004).

With renewed rifting and deposition of the basal Burra Group, the Curnamona Province and the Gawler Craton again become the dominant suppliers of zircons in the Willouran Trough. The B2 zircon age spectrum has a similar profile to the Euchre Pack Domain Dome Sandstone samples, albeit with a greater proportion of zircons younger than 1350 Ma. These younger zircons may be sourced directly from the Musgrave Block or be re-worked from the Curdimurka Subgroup. In the Arkaroola area sample HSF3 records very few zircon ages younger than 1400 ma indicating that with the renewed rifting with the beginning of deposition of the Burra Group, sediment was locally derived, albeit with

minor input from the Gawler Craton. Furthermore it indicates that the Arkaroola area was likely separated from the Willouran Trough, if the Humanity Seat Formation does correlate with the Emeroo Subgroup.

By the time of deposition of the upper Skillogalee Dolomite, (Sample B4), the Musgrave Inlier had become the major source of sediments to the Willouran Trough with reduced input from the Curnamona Province and Gawler Craton. Sample B4 has only a minor input from the Curnamona Province, suggesting that by this time its topography may have been reduced and not undergoing significant erosion.

In summary, variations in the detrital zircon age spectra predicted by the model developed for sediment source areas are seen in both the Curdimurka Subgroup and the Burra Group. It is likely that from the Dome Sandstone was deposited in the through-going fault stage of rift development. It had been expected that the Willouran Trough had later evolved to the sag phase but sample REC1 suggests that this was not the case during deposition of the Recovery Formation, although it is likely the topography of the rift shoulders was subdued at this time. The mostly likely unit to be deposited in the sag phase, the Boorloo Siltstone did not supply sufficient zircons to fully test the model.

The change in detrital zircon age spectra from sample B2 to B4 also shows increasing complexity. Sample B4 has a small proportion of zircons from likely proximal sources suggesting that the basin was in a sag phase during deposition of the upper part of the Skillogalee Dolomite. However more detailed sampling of the Burra Group would better test this conclusion.

4.7 Other Source Areas?

As seen today, the Gawler Craton, the Musgrave Inlier and the Curnamona Province all lie adjacent to, or close to the northern Adelaide Fold Belt and so are the most likely sources of detrital zircons. However, the Adelaide Fold Belt was initiated as an intracontinental basin within the Neoproterozoic supercontinent of Rodinia (Powell et al., 1994; Preiss, 2000). At about 700 Ma, the basin probably became a passive margin (Powell et al., 1994; Preiss, 2000) but the continental land mass that rifted away is not known. Four configurations of Rodinia prior to break-up have been suggested (Figure 4.12);

- AUSWUS (Australia – Western United States), where the Willouran Trough is adjacent to southern California (Karlstrom et al., 1999; Burrett and Berry, 2000)
- SWEAT (Dalziel, 1991; Moores 1991), where the Willouran Trough is adjacent to the Yukon;
- AUSMEX, where northeastern Australia is adjacent to western Mexico and the Willouran Trough would be adjacent to an unknown land mass (Wingate et al., 2002).
- South China, with South China between Australia and Laurentia (Li et al., 1995; Li et al., 2002).

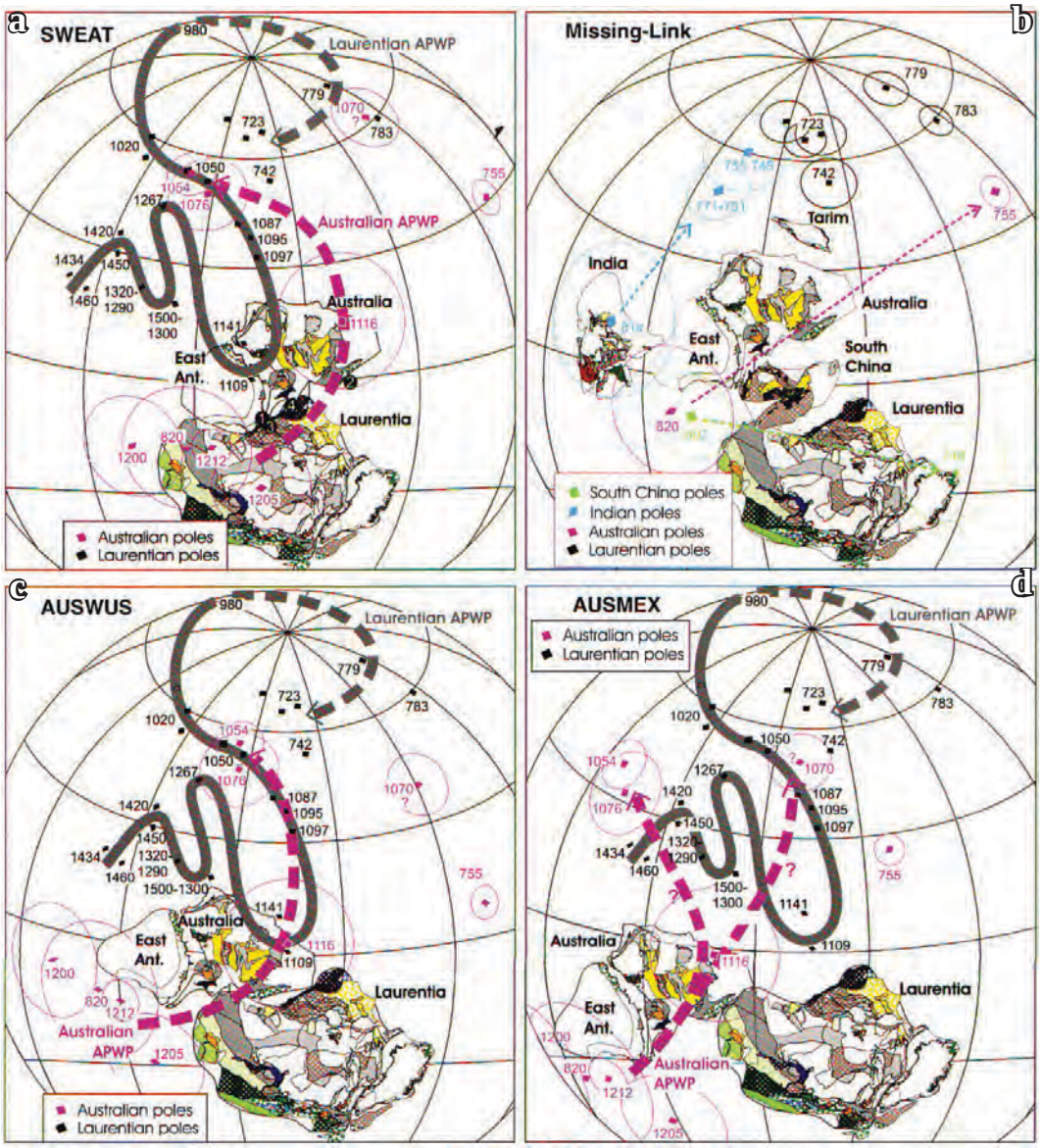

Figure 4.12. Reconstructions of Rodinia at about 780 Ma (from Li et al., 2008).
a) SWEAT; Southeastern Australia is adjacent to northwestern Canada (Moores, 1991; Dalziel, 1991. b) South China between Australia and Laurentia (Li et al., 1999; c) AUSWUS. Western United States is adjacent to southeastern Australia (Karlstrom et al., 1999; Burrett and Berry; 2000) d) AUSMEX; Southeastern Australia is adjacent to western Mexico (Wingate et al., 2002).

A fifth configuration, intermediate between SWEAT and AUSWUS, with the Willouran Trough adjacent to Idaho was suggested by Berry et al., (2001).

The results of this study may offer evidence in favour of one or another of these possibilities. A caveat is that it is unknown where the Willouran Trough was relative to the continental margin. Direen and Crawford (2003 and references therein) offered a summary of the geometry of the edge of the continent prior to the Delamerian Orogeny suggested by various authors. Relative to the Willouran Trough, it could be as close as perhaps 100 km, on the northwestern side of the Mulroona Gravity Ridge (Shaw et al., 1996) or it could be hundreds of kilometres as suggested by Direen and Crawford (2003), with the intervening continental crust having been thinned and lying beneath the Lachlan or New England Orogens. As such, the rifted continental mass may have been proximal to the Willouran

Trough, separated only by a basement high, or distal, at an unknown distance to the east. In addition, if the continental margin was at some distance from the Willouran Trough, there is no indication of the age of that continental crust and so could supply detrital zircons of ages not recorded in the Gawler Craton, Curnamona Province or the Musgrave Inlier.

4.7.1 North America

Several authors have suggested that some detrital zircons in North American units originated in Australia. Ross et al. (1992) and Ross and Villeneuve (1999) have suggested that 1590 Ma – 1600 Ma zircons in the Belt Supergroup were sourced from the Gawler Craton. Blewett et al. (1999) proposed a northern Queensland source for these same age zircons in the Belt Supergroup. Stewart et al. (2001) considered it likely that zircons in the age range of 1576 to 1578 Ma and 1605 to 1619 Ma that occur in Neoproterozoic sandstone units in the southwestern United States and northern Mexico were sourced from the Gawler Craton. They also considered that the detrital zircon populations from Neoproterozoic and Cambrian rocks in Ireland et al. (1998) show a poorly defined similarity to those in the western United States and northern Mexico. They pointed out that zircons in the range 1450 Ma to 1400 Ma are sparse in Australian arenites but common in the United States (Stewart et al., 2001). Samples DS1, DS2, DS3, DS4 and HSF3 have peaks in this range, although the major peak from Stewart et al. (2001) at 1430 Ma is between the major peak grouping of 1447 -1463 Ma and a minor peak at 1405 Ma recorded in this study. A-type granites ranging in age between 1400 Ma and 1450 Ma are common in the western United States and northern Mexico (Anderson, 1983; van Schmus et al., 1993) and a total of 38 detrital zircon ages are from that interval in this study and so the southwestern United States may have been a source for these zircons. However, the western United States zircon age spectra of Stewart et al., (2001) do not have zircon ages in the 900 Ma to 1000 Ma range and so the western United States is not thought to be the source of these zircons.

Gehrels and Ross (1998) conducted a detrital zircon age study on ten sandstone samples collected from western Canada ranging in age from Neoproterozic to Triassic. In the Neoproterozic Horsethief Creek Group, all of the detrital zircons are older than 1600 Ma, with the majority between 1600 Ma and 1950 Ma and a major peak at 1777 Ma. Of the ten samples, only one, the Carboniferous Spray Lakes Group contained zircons with an age between 1400 and 1500 Ma. Hence, it is unlikely that the Neoproterozoic sandstone was sourcing the same area as the Curdimurka Subgroup and the almost complete absence of zircons between 1400 and 1500 Ma from these samples suggests that no rocks of that age occur in the vicinity, and therefore area did not lie adjacent to the Willouran Trough at any time.

Rainbird et al. (1992) suggested that detrital zircons in the 1100 – 720 Ma Shaler Group of northern Canada, are derived from the Grenville structural province of eastern Canada. Of the 25 zircons, none have ages that match major peaks from this study and only four have ages than match minor peaks with another four having similar ages. There is one 1441 Ma zircon and no zircons younger than 1000 Ma (Rainbird et al., 1992). It is unlikely then that

the Shaler Group and the Curdimurka Subgroup were receiving sediment from the same area and therefore, the SWEAT configuration of Rodinia is unlikely.

Hence, of the three configurations of Rodinia where the Willouran Trough is adjacent to the western margin of Laurentia, only AUSWUS is supported by the detrital zircon data. However, AUSWUS does not provide a source of zircons younger than 1000 Ma.

4.7.2 South China Block

South China has been suggested by Li et al. (1995, 1996, 2002) to have been situated between Laurentia and Australia during the early Neoproterozoic, having rifted away at about 750 Ma, based on palaeomagnetic data (Figure 4.12). Wang et al. (2003) suggested that the South China Block was adjacent to Australia, based on Neoproterozoic tectonstratigraphic correlations between South China and the Adelaide Fold Belt. Z-X Li et al. (1999) used the presence of basic volcanism, attributed to a mantle plume and dated at about 825 Ma in both South Australia and southern China, to suggest the two areas were adjacent at this time. If this was so, then South China may have been a source of sediments to the Adelaide Fold Belt.

Within the South China Block, there are a series of igneous rocks dated between 1000 Ma and 800 Ma. They are attributed to magmatism during in the Sibao Orogen, which marks the amalgamation of the Yangtze and Cathaysia blocks between 1000 and 900 Ma (e.g., Chen et al., 1991; X-H Li et al., 1994; Charvet et al., 1996; X-H Li and McCulloch, 1996; Z-X. Li et al., 2002; Greentree at al., 2006; X-H Li et al., 2009); anorogenic magmatism at about 850 Ma (e.g., X-H Li et al., 2003; X-H Li et al., 2009) and; mantle plume magmatism and rifting between about 830 Ma and 780 Ma (e.g., Z-X Li et al., 1995; X-H Li et al., 2003; Z-X Li et al., 2003). There is also some debate on whether the Sibao Orogen continued to as late as 800 Ma (e.g., Z-X Li, 1999; Zhao and Cawood, 1999).

Li et al. (1994) reported a SHRIMP U – Pb zircon age of 968 ± 23 Ma for an albite granite sample that Li and Li (2003) identified as an adakite, that occurs as lenses within the NE Jiangxi ophiolite in eastern China. The Jiangxi ophiolite complex is part of the Gan-wan ophiolite belt, within the Sibao Orogen located between the Yangtze and Cathaysia blocks (Figure 4.13: Li et al., 2003). According to the Rodinia reconstruction of Li and Powell (2001), the Gan-wan ophilite belt would run approximately parallel to the eastern margin of Australia, and so could be a source for zircons (Figure 4.13). Ling et al. (2003) reported TIMS zircon ages of 950 ± 3 Ma and 895 ± 3 Ma for the upper and lower units of the Xixiang Group in the Hannan area, on the northern margin of the Yangtze Craton. The (current) northern margin of the Yangtze Craton would be the closest point of the South China Block to the Australian Craton, according to the Li and Powell (2001) Rodinia reconstruction. X H Li et al., (2009) concluded that the final amalgamation between the Yangtze and Cathaysia blocks occurred at about 880 Ma, based on the youngest U-Pb zircons ages of 891 ± 12 Ma from the Zhangcun Formation, which they interpret to be due to arc magmatism.

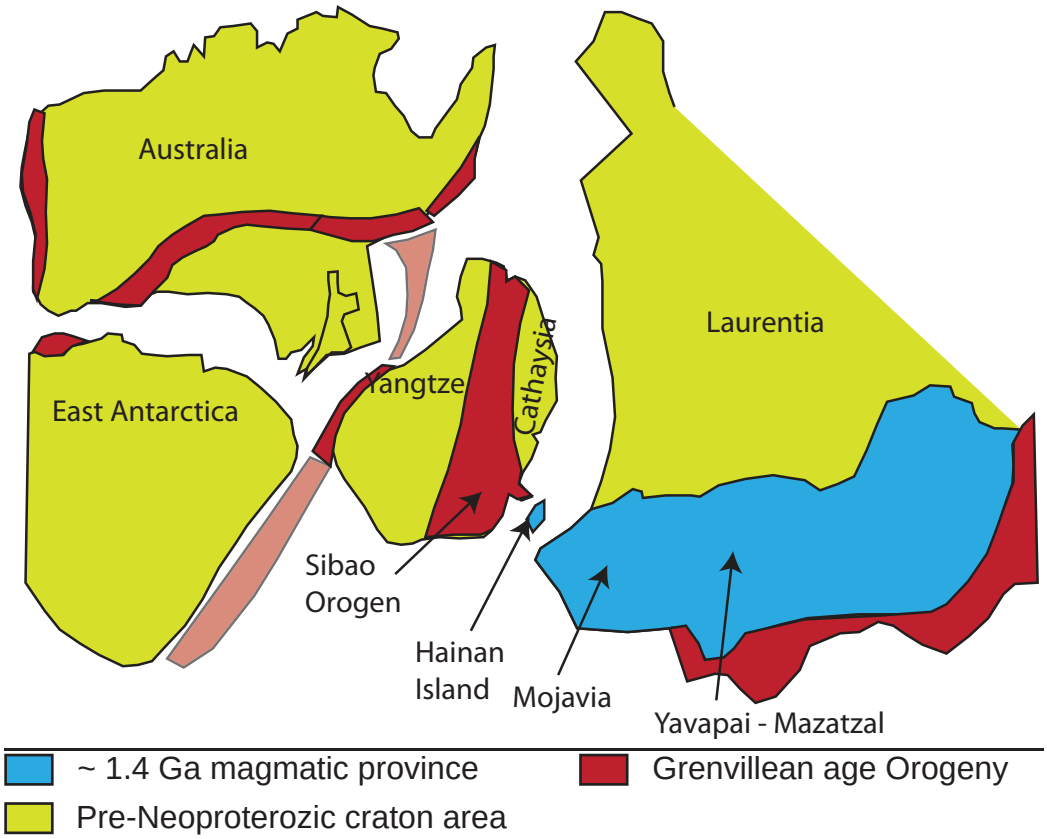

Figure 4.13. South China in Rodinia with respect to to Australia, East Antarctica and Laurentia (modified from Z-X Li et al., 2002)

The Yangtze Block is nearest the Adelaide Fold Belt, with a Grenvillean orogenic zone possibly separating it from the the AFB

Altogether, there are 18 detrital zircons with ages less than 1,000 Ma (Appendix 1), 11 from sample B4, four from B2, two from DS4 and one from Rec1. The majority have large error bars and so to claim that they are within error of a particular date is misleading, but the 940 Ma peak in B4 is within the period of the amalgamation of the Yangtze and Cathaysia blocks. In addition, the three c.a. 860 Ma ages (from B4 and Rec1) are also within error of the ca. 850 Ma magmatism in South China, Therefore South China could be a source of the 1000 - 900 Ma zircons from the Adelaide Fold Belt.

4.7.3 Antarctica

Antartica was to the south of Australia before the break-up of Rodinia up until the Early Tertiary (Figure 4.12). The Ross Orogen of Antartica is an extension of the Delamerian Orogen of southeastern Australia (e.g. Veevers, 2000; Li and Powell, 2001).

The Rayner Complex of Endersby Land and the Prince Charles Mountains of eastern Antarctica records the collision between eastern India and eastern Antarctica between 1000 Ma and 900 Ma during the Rayner Structural Episode (Sandiford and Wilson, 1984). Felsic intrusives have been dated at about 990 Ma and 910 Ma, with a metamorphic event at about 940 Ma in this area (e.g., Carson et al., 2000; Boger et al., 2000; Kelly et al. 2002). If this area was a source of detrital zircons to the Willouran Trough, they would have to be transported across the continent, a distance of thousands of kilometres. The Mitcham Quartzite has a zircon peak at 980 Ma (Ireland et al., 1998) and so by the time of the later

Burra Group, there may have been transport from Antarctica to the Northern Adelaide Fold Belt through the Southern Adelaide Fold Belt. Goodge et al., (2002) suggested on the basis of ~1400 Ma detrital zircons in the Beardsmore Group of the Transantarctic Mountains, that the trans-Laurentian anorogenic granite belt (Anderson, 1983; Windley, 1993) continued into Antarctica. If this were the case, it would place southwestern United States adjacent to the the Transantarctic Mountains, a distance of some thousands of kilometres from the Willouran Trough (although it would also depend on the orientation of Laurentia relative to Australia-Antartica) and would likely favour the SWEAT configuration of Rodinia. As such, it is unlikely that it could have supplied the large (relative to the proximal 1500 – 1750 Ma zircons) proportion of zircons of that age found in the Dome Sandstone.

Detrital zircons from the Skeleton Group (deposited between 1050 – 535 Ma) in southern Victoria Land and the central Trans-Antarctic Mountains are dominated by 1300 Ma to 950 Ma zircons with very few zircons older than 1500 Ma (Wysoczanski and Allibone, 2004). They reject the Rayner Complex as a source for these zircons, instead suggesting that potential Grenville age basement along the margin of eastern Antarctica and eastern Australia was the source of these zircons (Wysoczanski and Allibone, 2004). Their suggestion implies that to the east of the Willouran Trough was a Grenvillean terrane which was rifted away. If this were the case, it may underlie the Lachlan and New England Orogens of eastern Australia as suggested by Direen and Crawford (2003).

4.8 Minimum detrital zircon ages.

Minimum detrital zircon ages provide the maximum age of the unit they are within, and can therefore assist in refining the depositional geochronology. Chapter 2 discussed the geochronology of the Adelaide Fold Belt, and it is summarized in Figure 4.10. The minimum detrital zircon U-Pb ages from this study (Table 4.1) do not add significantly to the contentious dates identified in chapter 2, particularly the age from the porphyritic intrusion in the Skillogalee Dolomite of 797 ± 5 Ma(Drexel, 2009; Reid, 2009). All of the youngest ages from this study are older than the oldest age that has been attributed to the Adelaide Fold Belt rocks, the 827 ± 9 Ma from baddelyite of the Gairdner dyke swarm, which has been correlated with the Wooltana Volcanics (Wingate et al., 1998). Only the Paralana Quartzite lies below the Wooltana Volcanics, and so the youngest zircon from sample PQ1, with an age of 1164 ± 36 Ma provides a maximum age of the onset of deposition of the Adelaide Fold Belt. It is interesting that three samples (DS4, REC1 and B4) record five zircons from the 850 - 870 Ma period, and it could be speculated that this may represent volcanism associated with the initial development of the Adelaide Fold Belt, but it is only speculation. No magmatic source of this age is known in Australia but perhaps it has been eroded or lies hidden beneath the Adelaide Fold Belt.

4.9 Conclusions

The sources of the detrital zircons can be attributed in the main part to either the Curnamona Province, the Gawler Craton, or the Musgrave Block. Between the ages of about 1500 Ma and 1620 Ma, the zircon ages are not diagnostic of any one source from these three areas.

For zircons younger than about 1350 Ma, the Musgrave Inlier is the most likely source and for those older than about 1750 Ma, the Gawler Craton is the most likely source. There is a group of detrital zircons with ages less than 1000 Ma. These have no source in the area surrounding the Adelaide Fold Belt, but one possibility is that they are derived from the South China Block, which may have been between Australia and Laurentia until about 750 Ma. A second group of detrital zircons, with ages between 1350 and 1450 Ma have two corresponding zircon ages recorded in Australia, on the western margin of the Gawler Craton, but also correspond to the A-type granites in the southwestern United States.

The age spectra of sandstones from the Adelaide Fold Belt demonstrate a gradual decrease with time in detrital supply from of the Gawler Craton and the Curnamona Province, and an increasing supply from the Musgrave Block. This trend is apparent throughout the stratal evolution of individual groups but also at the broader stratigraphic scale. The reason for this is likely that within an individual basin phase, with rifting, the adjacent basement was exposed and supplied most of the sediment. With time, the rift phase gave way to the sag phase, subsidence decreased and the rift shoulders become covered with sediments and the topography adjacent to the rift became subdued. At the same time, sediment transport along the rift axis becomes more important in distributing (and redistributing) sediment in the basin and sources sediment from wider areas, resulting in a greater spread of ages with time.

The changes of the detrital zircon spectra from the Curdimurka Subgroup do agree with the model developed for the transition from rift to sag phase. However because it was not possible to date sufficient zircons from a sample from the Boorloo Siltstone, it wasn't tested fully. Therefore the Willouran Trough is interpreted to be a rift basin in the fault linkage stage of development during deposition of the Dome Sandstone.This continued up to deposition of the second sandstone unit of the Recovery Formation (RSds2).

It is concluded that it is unlikely that the Arkaroola area was connected to the Willouran Trough, either during deposition of the Arkaroola Subgroup or the Humanity Seat Formation. The unexpected Musgrave Block age detrital zircon from sample PQ1 is interpreted to suggest it was sourced from a separate area to the Musgrave Block, based on the sample position being one metre above the basement contact. Therefore it is suggested there may have been a Grenvillean age block east of the Curnamona Province which supplied sediment to that area. The detrital zircon age spectra from this study also provide no support for correlating Burra Group rocks with Curdimurka Subgroup rocks, which leads to a rejection of the possibility that the Rook Tuff is a correlative of the Skillogalee Dolomite, based on similar zircin U-Pb ages of volcanics rocks found in both.

The youngest zircon age recorded from the basal Paralana Quartzite is 1164 ± 36 Ma, and this provides an upper limit of the age of the Adelaide Fold Belt. Five zircons from between 850 and 870 Ma from samples DS4, REC1 and B4 are the youngest of all the zircons analysed, but these are all older than, and come from rocks that lie above the Wooltana Volcanics, and so do not provide additional information on the maximum age of the Adelaide Fold Belt.

CHAPTER 5.
CARBON AND OXYGEN ISOTOPE STUDIES OF THE CURDIMURKA SUBGROUP.

5.1 Introduction

5.1.1 Carbon and Oxygen Isotopes and Depositional Environments.

Carbon and oxygen isotope studies have been used to assist in understanding depositional settings of carbonate sedimentary rocks and may be used to differentiate between marine and lacustrine environments. Unaltered marine carbonates should plot on global isotope curves but lacustrine systems are much smaller and the $\delta^{13}C$ and $\delta^{18}O$ composition of carbonates will reflect local conditions and may be highly variable (Talbot and Kelts, 1990; Casanova and Hillaire-Marcel, 1993; Rosen et al, 1995; Wachniew and Rozanski, 1997; Duktiewicz et al., 2000; Hoefs, 2004). As such, a starting point for using stable isotope data for discriminating between marine and lacustrine conditions is by comparison with a global isotope curve.

5.1.2 Global Isotope Curves

Stable isotopes have been used in stratigrapic and sedimentological studies to correlate between outcrops within basins and globally, and to provide direct evidence of depositional environments. In the absence of fossil and geochronological data, particularly in the Proterozoic, carbon and strontium isotopes have proven useful in correlating within and between basins at the continental scale (e.g., Alveranga et al., 2004; Galindo et al., 2004; Lindsay et al., 2005). The compilation of global isotope curves assists in the correlation of rock packages. Veizer et al., (1999) produced $\delta^{13}C$, $\delta^{18}O$ and Sr isotopes curves for the Phanerozoic with the Sr curves being extended into the Neoproterozoic. Shield and Veizer (2002) further extended the isotope curves for $\delta^{13}C$, $\delta^{18}O$ and Sr ratios from 3,800 Ma to 450 Ma with a compilation based on roughly 10,000 carbonate rock samples, and Schidlowski (2001) compiled curves for $\delta^{13}C_{carb}$ and $\delta^{13}C_{org}$ back to 3800 Ma.

Researchers have produced $\delta^{13}C$ curves for the Neoproterozoic, using data from (Kaufmann and Knoll, 1995; Jacobsen and Kaufmann, 1999; Walter et al., 2000; Halverson et al, 2005; Halverson, 2006). Figure 5.1 is an example of one of these curves prepared by Halverson et al (2006), based on $\delta^{13}C$ results from widely spaced areas including northwest Canada, Svalbard, Oman and Namibia.

The ^{18}O of ancient oceans varied from about -8‰ in the Cambrian to 0‰ today (Clayton and Degens, 1959; Veizer and Hoefs, 1976; Veizer et al., 1999). Attempts to extend the curve into the Proterozoic have been limited because of doubts about its validity due to alteration of original $\delta^{18}O$ values by diagenesis and metamorphism **(**Shields and Veizer, 2002**)**. Because of these problems, particularly related to diagenesis, metamorphism and alteration, all of which have affected the Curdimurka Subgroup in the Willouran Range, the $\delta^{18}O$ results will be presented but not discussed in the context of global correlations.

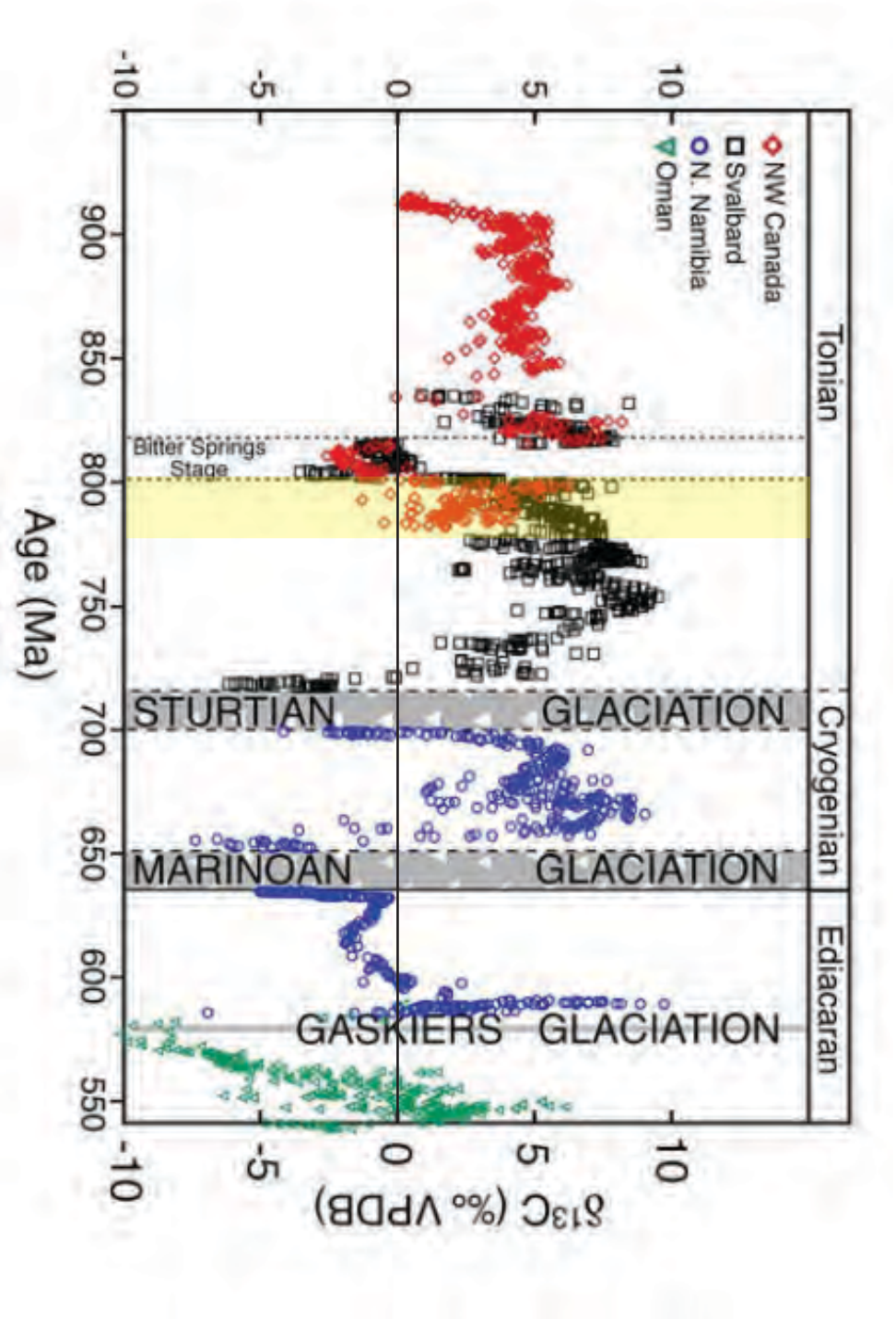

Figure 5.1. The $\delta^{13}C$ curve of Halverson et al., 2006.
The depositional period of the Curdimurka Subgroup is marked by the pale yellow rectangle. It shows that the Curdimurka Subgroup was deposited beginning just at the end of the Bitter Springs Stage, a period of global negative $\delta^{13}C$

The Neoproterozoic has been the focus of numerous carbon, oyxgen and strontium isotope studies, particularly in the past twenty years. These studies have been influenced by the debate on where to place the boundaries of its sub-division into the Cryogenic and Ediacaran periods; the Neoproterozoic glaciations and the rise of multicellular life in the Ediacaran (e.g. Kaufmann and Knoll, 1995; Jacobsen and Kaufmann, 1999; Santos et al., 2000; Walter et al., 2000; Bartley et al., 2001; Melezhik et al., 2001; Bekker et al., 2003; Ray et al., 2003; Pyle et al., 2004; Halverson et al., 2005; Lindsay et al., 2005; Halverson et al., 2006). Because of the discussion on the extent and number of Neoproterozoic glacial periods (e.g., Kaufmann et al., 1997; Hoffman et al., 1998; Kennedy et al., 1998; Schrag et al., 2002; Porter et al., 2004; Xiao et al., 2004; Halverson et al., 2005; Prave et al., 2009), many of the stable isotopic studies of Neoproterozoic rocks have concentrated on the period of the glaciogenic sediments from the Sturt glaciation at about 725 Ma to the Elatina glaciation at about 630 Ma. Negative $\delta^{13}C$ excursions in cap dolomites that overly diamictite units have been used to assist in the global correlation of the diamictites **(**e.g. Kaufmann and Knoll, 1995; Kennedy et al., 1998 **)**. The period from the end of the Elatina glaciation to the terminal Neoproterozoic and early Cambrian has also attracted attention because of the rise of multi-cellular life during this time and to assist in the correlation of the terminal Neoproterozoic globally (e.g. Ripperdan, 1994; Saylor et al., 1998; Condon et al., 2005). Considerably less work has been conducted on rocks older than 725 Ma. Hill and Walter (2000) reported $\delta^{13}C$ and $\delta^{18}O$ data from the Callanna Group and the Burra Group. Other examples include studies from the Shaler Supergroup of northern Canada (Kaufmann and Knoll, 1995; Jones et al., 2010), the Bitter Springs Formation of the Amadeus Basin (Hill et al., 2000; Hill and Walter, 2000; Lindsay et al., 2005), the Mesoproterozoic – Neoproterozoic boundary in Siberia (Bartley et al., 2000); the Tambien Group in Ethiopia (Miller et al., 2003; Miller et al., 2009); the Akademikerbreen Group of northeastern Svalbard (Halverson et al., 2007b) and the Dalradian of Scotland (Sawaki et al., 2010).

5.1.3 Australian Neoproterozoic Isotope Studies

Hill and Walter, (2000) reported $\delta^{18}O$ and $\delta^{13}C$ values for the Callanna and the Burra Groups from the northern Adelaide Fold Belt and the Peake and Denison Inlier (Figure 5.2). The Arkaroola Subgroup has mainly positive $\delta^{13}C$ compositions with a small number of negative $\delta^{13}C$ compositions whereas the Curdimurka Subgroup has mostly negative $\delta^{13}C$ compositions in both the Peake and Denison Inlier and the Willouran Range. The Burra Group only has positive $\delta^{13}C$ values up to 7.2‰ $\delta^{13}C$.

Hill and Walter (2000) and Hill et al., (2000) reported negative $\delta^{13}C$ for Units 1 and 2 of the Loves Creek Member (Figure 5.3), with a small positive excursion at the top of the section they interpret to be lacustrine. Unit 3 has only positive $\delta^{13}C$ values. Halverson et al. (2005) has termed the negative excursion the Bitter Springs Stage and correlated it with the negative $\delta^{13}C$ excursion within the Curdimurka Subgroup (Hill and Walter., 2000), placing its beginning at 802 Ma and lasting about 8 Myrs. Although termed the Bitter Springs Stage, the dating is based on the ages of the Rook Tuff (802 ± Ma, Fanning et al., 1986) and the negative $\delta^{13}C$ excursion from the Curdimurka Subgroup (Hill and Walter, 2000). Lindsay et al., (2005) also correlated the negative $\delta^{13}C$ excursion within the Bitter Springs

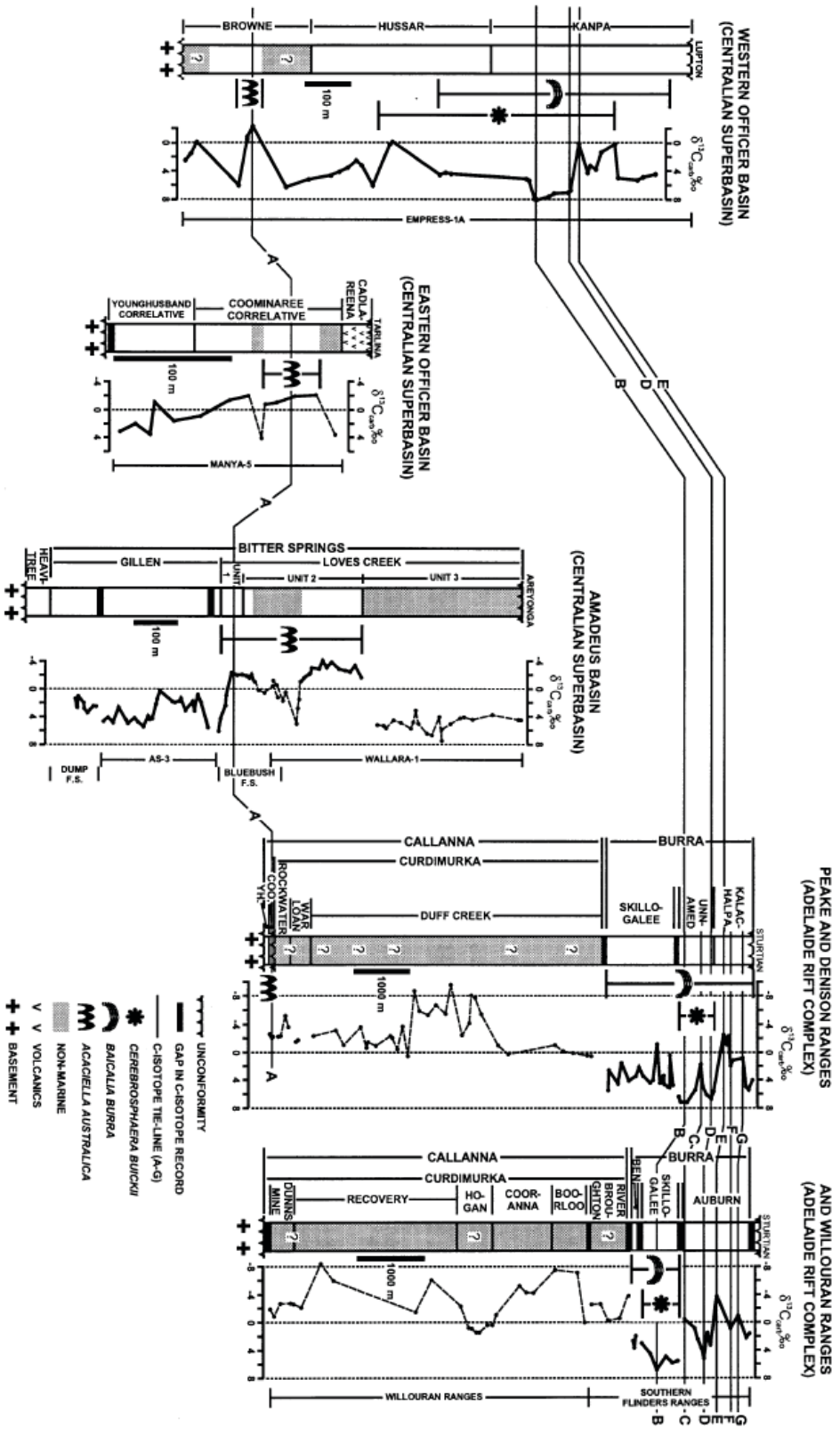

Figure 5.2. Carbon isotope curves for the Neoproterozoic of Australia from Hill and Walter, 2000.

Note that they correlated the volcanics within the Bitter Springs with the Gairdner Dyke Swarm and hence the Wooltana Volcanics whereas Lindsay et al. (2005) and Halverson et al. (2005) correlated units with the negative excursion in the Bitter Springs Formation with the negative excursion in the Curdimurka Subgroup.

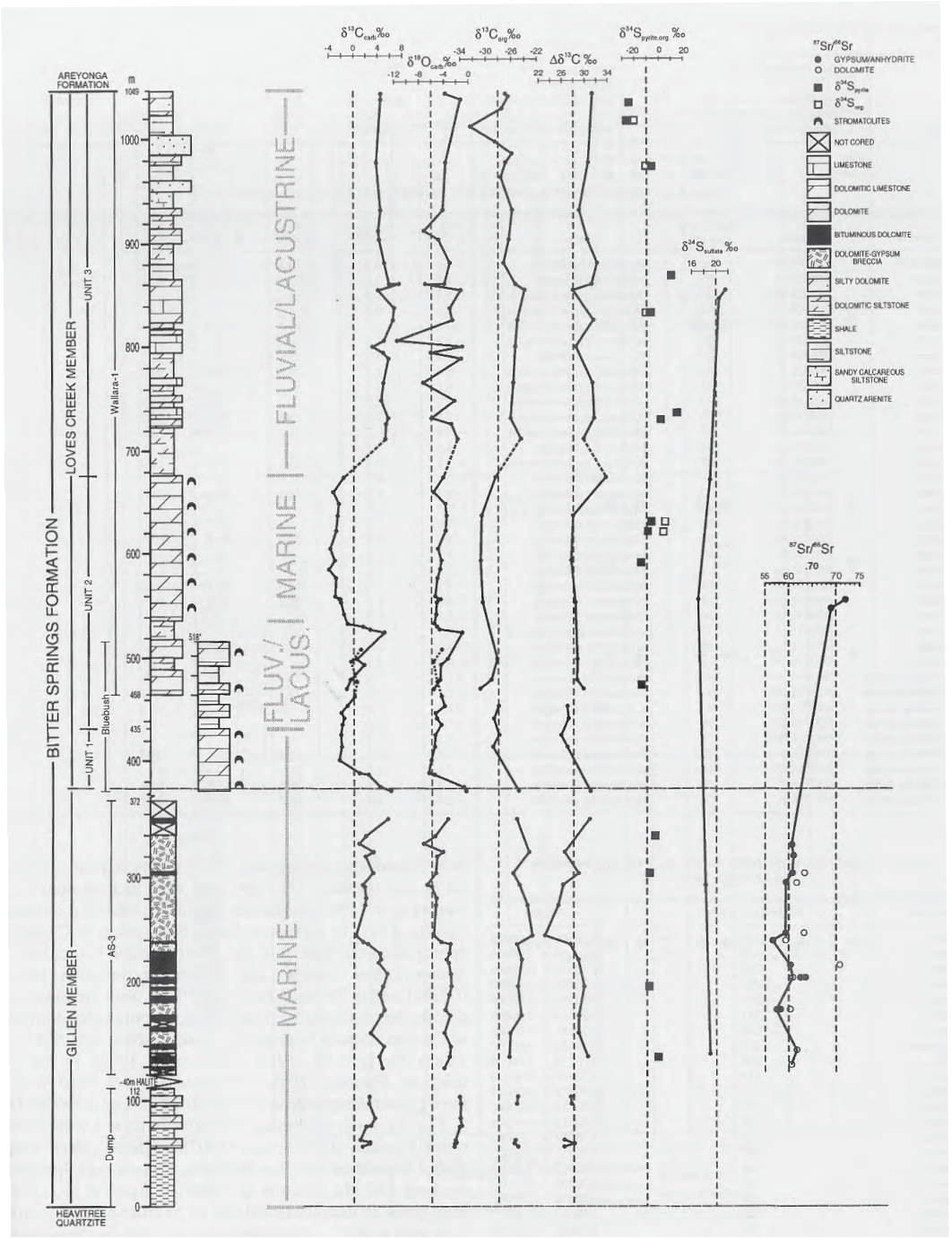

Figure 5.3. Isotope curves, lithology and interpretation of the Bitter Springs Formation (Hill et al., 2000).

Formation with the negative $\delta^{13}C$ excursion in the Curdimurka Subgroup but place the upper boundary at about 780 Ma.

5.1.4 Stable Isotopes and Depositional Environment

The isotopic compositions of primary lacustrine carbonates is dependent on the composition of the lake waters and the temperature of mineral precipitation. (Stuiver, 1970; Talbot, 1990; Gasse and Van Campo, 1994). The isotopic composition of lake waters will vary depending on the isotopic composition of the rainfall of the catchment area, its amount and seasonality, the temperature, the rate of evaporation, the relative humidity and biological activity (Talbot, 1990; Wachniew and Rozanski, 1997). $\delta^{13}C$ will vary with the difference

between isotopic enrichment of dissolved inorganic carbon (DIC) by photosynthetic activity and isotopic depletion by oxidation of organic matter (Stuiver, 1975; McKenzie, 1981; Rosen et al., 1995; Benson et al., 1996, Wachniew and Rozanski, 1997). Variations in all of these factors over periods of months to thousands of years will result in highly variable lacustrine carbonate $\delta^{18}O$ and $\delta^{13}C$.

In a closed system total dissolved inorganic carbonate (TDIC) is mainly controlled by isotopic exchanges with the atmosphere (Fontes and Gasse, 1990), and ^{12}C is removed preferentially by organisms (Casanova and Hillaire-Marcel, 1993), hence ^{13}C will become enriched in brines. As $\delta^{18}O$ and $\delta^{13}C$ vary in a systematic way, both increasing with increasing concentration of the brine, they should be correlated, and studies have identified covariance between $\delta^{18}O$ and $\delta^{13}C$ in lacustrine carbonates (e.g., Janaway and Parnell, 1989; Casanova and Hillaire-Marcel, 1993; Camoin et al., 1997). Talbot (1990) established that covariant trends typify closed basins. Typically the covariance trend should be positive but Camoin et al., (1997) also found coexisting positive and negative correlations of increasing $\delta^{18}O$ and decreasing $\delta^{13}C$, from carbonates from perennial and ephemeral carbonate lakes in the central palaeo-Andean Basin of Bolivia. They attributed the co-existing trends to changes between perennial (negative correlation) and ephemeral (positive correlation) lacustrine conditions. In the case of decreasing $\delta^{13}C$, ^{12}C is supplied from oxidation of organic matter in deeper waters (Camoin et al., 1997; Wachniew and Rozanski, 1997).

Therefore, in an open lacustrine setting, the $\delta^{18}O$ and $\delta^{13}C$ of carbonates will be highly variable as the balances between the various inputs change. In contrast, in a closed lacustrine setting, there will be a correlation between $\delta^{18}O$ and $\delta^{13}C$. If either or both of these conditions are found to occur in the Curdimurka Subgroup carbonates, this will provide supporting evidence for a lacustrine depositional environment.

5.1.5 The Aims of this Study.

In Chapter 3 sedimentological analysis of the Curdimurka Subgroup proved ambiguous in determining its depositional environment. The Dome Sandstone was deposited in a fluvial environment but from the Rook Tuff to the Boorloo Siltstone, the depositional environment varied from mud-flat to sub-wavebase, without conclusive evidence for either a marine or lacustrine setting. Although a marine origin is favoured, further evidence is sought to provide support for the conclusions of the sedimentological analysis. Stable isotopes can provide a method of determining between marine and non-marine depositional environments in two ways. Firstly, $\delta^{13}C$ of carbonate rocks may be compared with global $\delta^{13}C$ curves, and if the data does not match the curve, the carbonates were likely deposited in a lacustrine environment. Secondly, depositional factors can influence the $\delta^{13}C$ of carbonate rocks, and by comparing $\delta^{13}C$ results against those expected from lacustrine and marine environments, it may be possible to identify the depositional enivronment.

5.2 Methodology

Samples were collected from throughout the Curdimurka Subgroup, although most were collected from the two carbonate-dominant levels of stratigraphy; the Dunns Mine Limestone

and the Boorloo Dolomite (Figures 5.4). About half of the samples were collected from diamond drill core and half from outcrop. Several samples from the Burra Group were also collected from diamond drill core for comparison. One sample of a weathered rind to a carbonate vein from the Dunns Mine Limestone was sampled to determine the effects of weathering on the isotopic values. A sample of pedogenic carbonate (aragonite?) from above a black shale in the Cooranna Formation was also collected. Appendix 2 has the sample details.

A dental drill was used to grind material from a fresh surface. Samples from outcrop were first sliced to expose a fresh surface and the sample for analysis taken from that surface. Selective samples (from the matrix and clasts of breccias, veins, and individual beds) were drilled out but otherwise the samples were taken to be representative of the sample as a whole. The standard procedure of measuring C and O isotopes of carbonate rocks to determine marine isotopic composition insist on micro-sampling early diagenetic (non-luminescent) cement (e.g., Kaufman et al., 1991; Bartley et al., 2001) however, the samples collected for this study are too fine-grained to allow this. Several studies have demonstrated that whole-rock $\delta^{13}C_{carb}$ analyses can differ insignificantly from the non-luminescent phases (e.g., Aharon, 1987; Fairchild and Spiro, 1987; Kaufman et al., 1991; Melezhik and Fallick, 2003). Hence the sampling method here is considered to be valid.

CO_2 gas for analysis was extracted at the University of Tasmania Central Science Laboratory using a modification of the method of McRea (1950). Samples were reacted in sealed, evacuated pyrex glass tubes with H_3PO_4 at a controlled temperature of 50°C in a water bath for 24 hours. The CO_2 generated was separated from any traces of water vapour by passing it through a trap at the freezing point of acetone (-95°C), before collection under liquid nitrogen. The CO_2 was analysed on a Micromass Optima Stable Isotope mass spectrometer using a reference gas calibrated against NBS-19. Results are expressed relative to V-PDB (for oxygen) and V-PDB (for carbon). Analyses of the ANU-M1 calcite, used as a working standard for several years in this laboratory, show standard errors of +/-0.06 permil for $\delta^{13}C$ and +/-0.1 permil for $\delta^{18}O$.

5.3 Results

5.3.1 All Data.

The results for all the samples are shown in Figure 5.5a, divided by stratigraphy (Figure 5.5b) and mineralogy (Figure 5.5c). For the analysis of the depositional environment of the Curdimurka Subgroup, only the samples collected from carbonate beds are considered (Figure 5.6). This excludes samples collected from the Burra Group, the Arkaroola Subgroup, and weathered, vein samples, breccia and diagenetic nodules, which are discussed below.

The majority of samples from the Curdimurka Subgroup have $\delta^{13}C$ compositions less than zero, the exceptions being from the Boorloo Dolomite and the Dome Sandstone (Figure 5.6a,b). They vary from -12.3‰ to 2.3‰, with an average of -3.3‰. $\delta^{18}O$ compositions

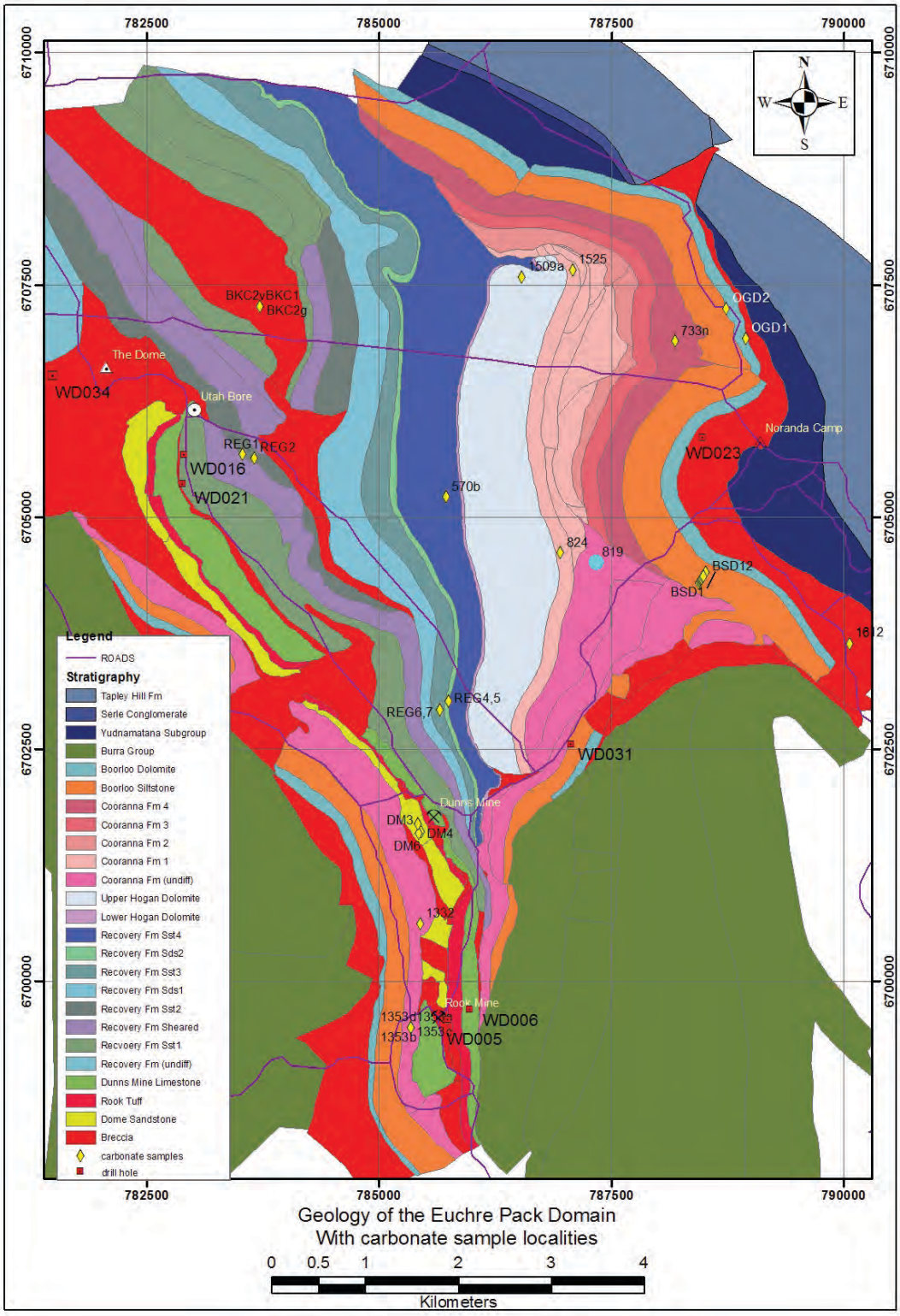

Figure 5.4a. Sample locality map for isotope analyses from the Euchre Pack Domain.

vary from -16.3‰ to -5.6‰, with average values are -12.1‰. There is no correlation between $\delta^{18}O$ and $\delta^{13}C$: the r^2 is 0.032.

To help put the Curdimurka Subgroup data into context, Figure 5.7a includes the data of Hill and Walter (2000) for samples they collected from the Callanna and Burra groups in the Peake and Denison Inlier and the northern Adelaide Fold Belt. The majority of Burra

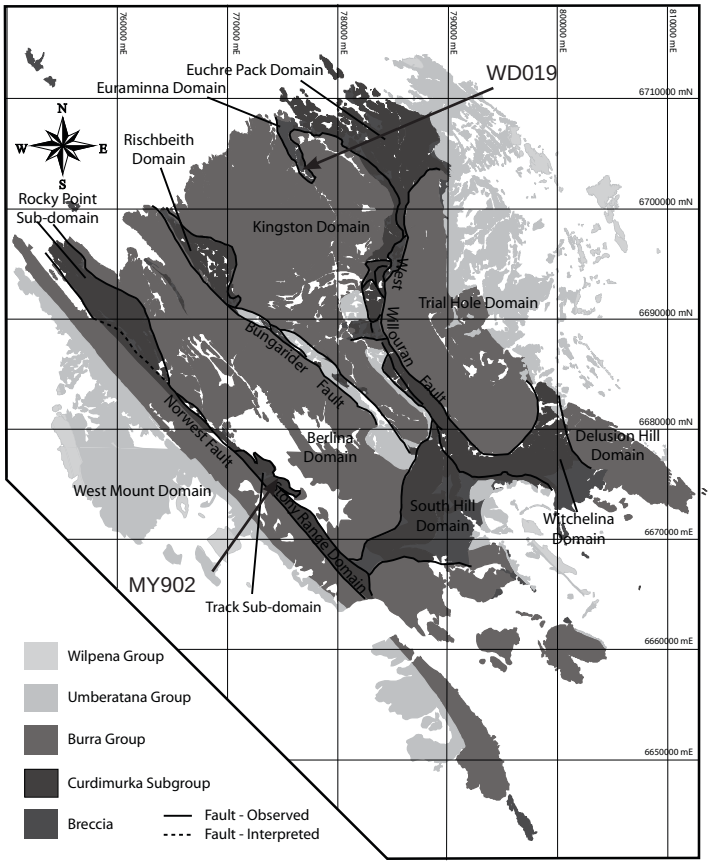

Figure 5.4b. Sample locality map for isotope analysis from the regional samples.
Drill hole WD019 drilled a breccia and Burra Group. MY902 is from an evaporitic carbonate in the Dome Sandstone, Track Sub-domain.

Group samples have positive $\delta^{13}C$ values, with $\delta^{18}O$ compositions typically heavier than the Curdimurka Subgroup (Figure 5.7b). It also emphasises that the light $\delta^{18}O$ and $\delta^{13}C$ values of the Curdimurka Subgroup are not confined to the Willouran Range, but extend to the Peake and Denison Inliers and hence are of regional extent. Figure 5.7c breaks the data into the formations of the Curdimurka Subgroup and the Burra Group subgroups. Figure 5.8 shows a comparison of the data from this study and that of Hill and Walter (2000). It shows broad similarities but they recorded positive values in the Hogan Dolomite which was not sampled in this study. Hill and Walter (2000) recorded positive values within the lower Cooranna Formation whereas this study returned negative $\delta^{13}C$ values.

To look more closely at small-scale variation in the stable isotopes and to investigate possible grain-size and mineralogical effects, two sub-sets of data were selected for closer analysis. The first is from the Dunns Mine Limestone and the second is from the Boorloo Siltstone.

5.3.2 Dunns Mine Limestone

A total of 43 samples from the Dunns Mine Limestone were analysed (Figure 5.9), comprising 24 samples for stratigraphy; three from diagenetic nodules; five for (hydrothermal?) alteration; seven from carbonate veins and four from breccias with matrix and clasts sampled. Included in the stratigraphic samples are three samples in which calcarenites and calcitic siltstone beds were sampled separately (Figure 5.10).

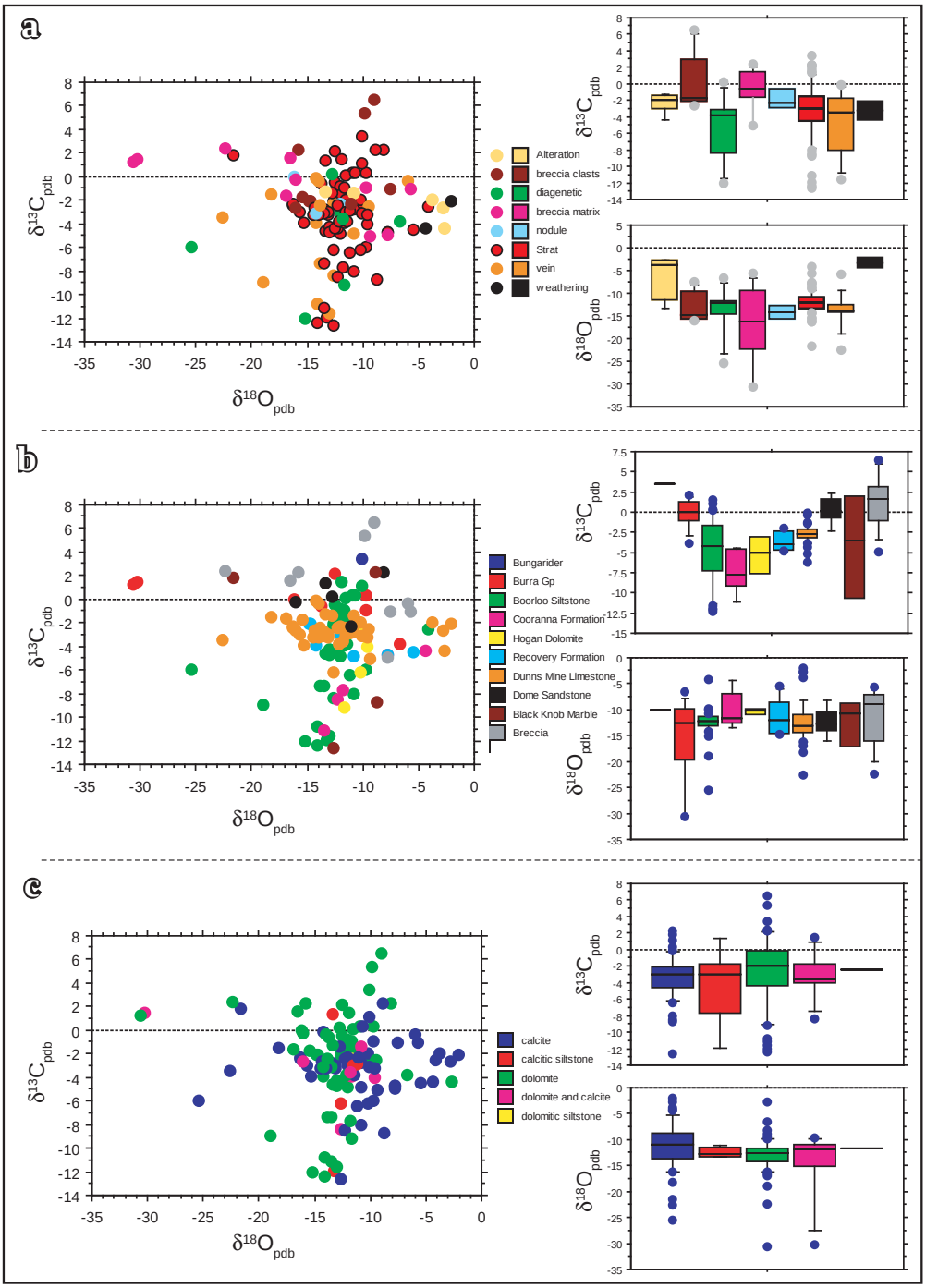

Figure 5.5 All isotope analyses results from this study.
a) Split by type of sample. b) Split by stratigraphy. c) Split by mineralogy.

The samples collected for stratigraphic purposes have $\delta^{18}O$ values between -16.3‰ and -9.6‰, with a mean of -13.0‰. The $\delta^{13}C$ values range from -1.4‰ to -6.2‰, the latter plots as an outlier however, -3.8‰ is the next lowest $\delta^{13}C$ value (Figure 5.9a,). The mean $\delta^{13}C$ value is -3.0‰. There is no relationship between $\delta^{13}C$ and $\delta^{18}O$: R^2 is 0.004. The $\delta^{13}C$ values for the other sample groups plot within the range of the stratigraphic samples except vein samples which have heavier mean and maximum values. $\delta^{18}O$ values for all but the altered and breccia clast samples have similar means to the stratigraphic samples. The altered samples have a higher mean and maximum $\delta^{18}O$ values and the calcite veins have a range of 20‰ (Figure 5.9a). However the samples with the highest $\delta^{18}O$ values (greater than -5‰)

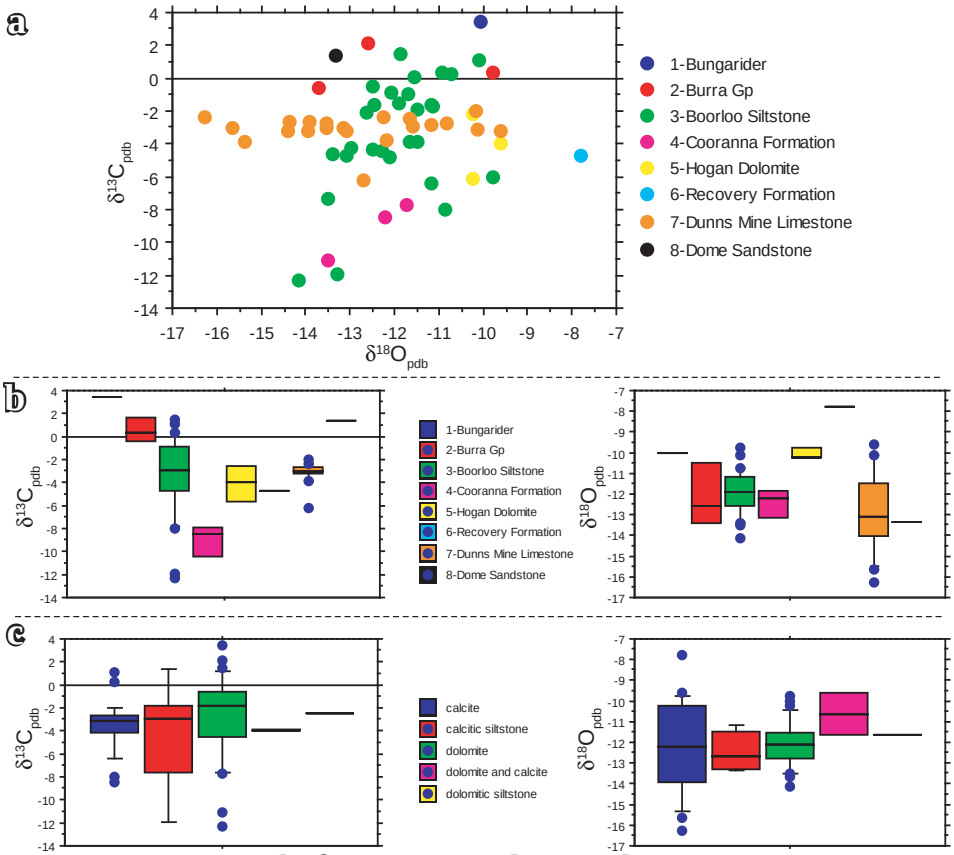

Figure 5.6. Isotope results from stratigraphic samples.
a) All data. b) Split by stratigraphy. c) Split by mineralogy.

for both the alteration and vein samples show strong weathering in hand specimen and so these high values are attributed to weathering.

Samples were divided into four grain-size categories, coarse-grained (cg), medium-grained (mg), fine-grained (fg) and siltstone (sst) (Figure 5.9b). The fifth category (na) consists of samples which were not stratigraphic samples. The results show that grain-size does not affect the $\delta^{13}C$ or $\delta^{18}O$ within statistical limits. Pairs of samples from adjacent beds, show that except for sample 630722 (Figure 5.10a), coarse-grained beds have a lower $\delta^{13}C$ than shale beds but there is no consistent variation in $\delta^{18}O$ (Figure 5.10b,c). There is no systematic variation in the $\delta^{18}O$ or $\delta^{13}C$ between calcite and dolomite (Figure 5.9c).

The results for the two drill holes samples are plotted against the drill log in Figure 5.11. These plots underline the small variation in the $\delta^{13}C$ (less than 2‰) and the larger variation in $\delta^{18}O$ (greater than 4‰). In WD16, there is no trend in $\delta^{13}C$ but $\delta^{18}O$ is lightest in the central part of the Dunns Mine Limestone, becoming heavier up and down the hole. There is a trend to lighter $\delta^{13}C$ up the hole in WD05, and perhaps to heavier $\delta^{18}O$, but there is considerable variation over short distances in $\delta^{18}O$ (Figure 5.11).

5.3.3 Boorloo Siltstone

A total of 37 samples were collected from the Boorloo Siltstone, comprising 18 samples from a measured section through the Boorloo Dolomite, 18 samples from diamond core and a calcite nodule from a surface sample. There are 29 stratigraphic, two diagenetic

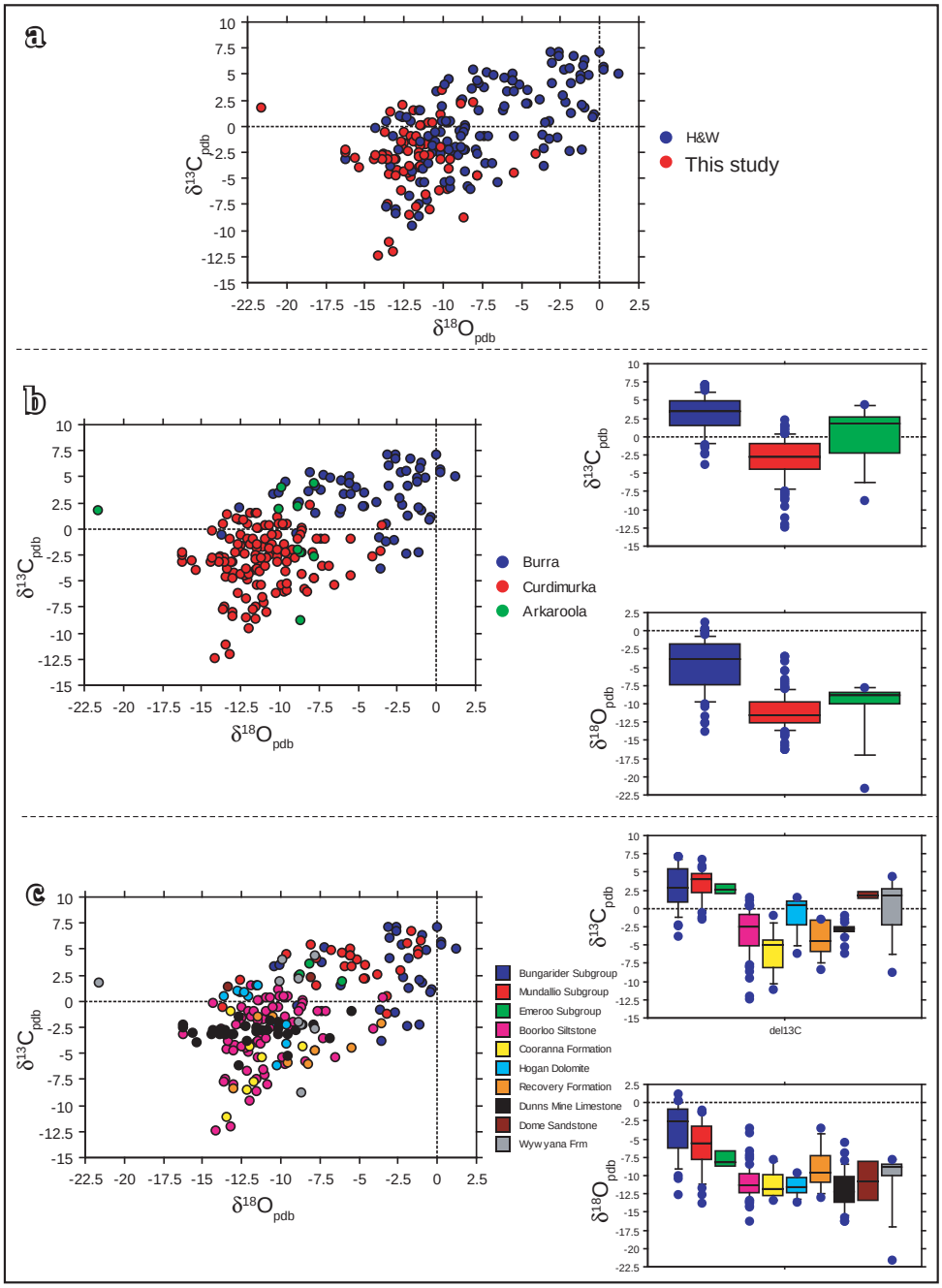

Figure 5.7. Carbon and oxygen isotope data for the Callanna Group and the Burra Group, from this study and Hill and Walter, 2000.
a) All data split by source. b) All data divided by Burra Group and Callanna Group Sub-groups and formations. c) All data split by Burra Sub-groups and Callanna Group formations.

(nodule) and six vein samples (Figure 5.12). Sample BSD9D with a $\delta^{18}O$ of -4.1‰ is a weathered sample and is not considered further.

Both the diagenetic and vein samples have lower mean $\delta^{13}C$ than the stratigraphic samples, although the vein samples do not show the same range as the stratigraphic samples. The mean $\delta^{18}O$ values for the vein and diagenetic samples are also lower than for the stratigraphic samples, and show much greater variation (Figure 5.12a).

Both $\delta^{13}C$ and $\delta^{18}O$ increase with increasing grain size (Figure 5.12b), but as the grain size increases up the section, the correlation is likely coincidental. The $\delta^{13}C$ values for calcite and dolomite are statistically similar although the mean for dolomite is higher than for

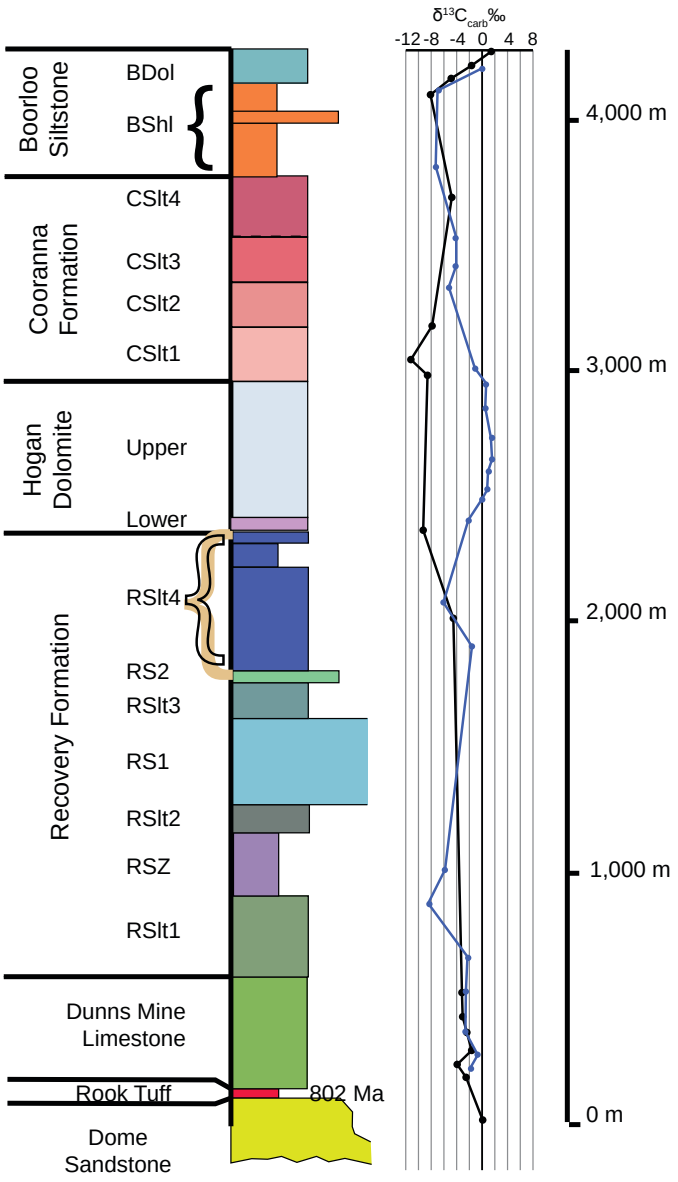

Figure 5.8. A comparison between the $\delta^{13}C$ curve from this study (black) and that of Hill and Walters (2000: blue).
There is good agreement between the two studies for the Dunns Mine Limestone and the Boorloo Siltstone. This study did not collect samples from the upper Hogan Dolomite where the Hill and Walter study returned positive ^{13}C values.

calcite. There is however a large difference in the $\delta^{18}O$, with dolomite having lower values than calcite (Figure 5.12c)

The analyses are plotted against the lithological logs for both the measured section and drill hole WR023 (Figure 5.13). Both sections show that $\delta^{18}O$ decreases slightly with depth but the $\delta^{13}C$ becomes significantly lighter down the section. A calcite nodule within a surface sample of black shale collected below the Boorloo dolomite has a light $\delta^{13}C$ value also. The common factor is that the lighter $\delta^{13}C$ are from black (organic) shales. That is, as the depositional environment goes from deeper water reduced to evaporitic and oxidised, the isotopic signature for $\delta^{13}C$ becomes heavier whereas the $\delta^{18}O$ does not vary. There is a weak correlation between $\delta^{18}O$ and $\delta^{13}C$, with R^2 being 0.231.

5.3.4 Alteration.

5.3.4.1 Diagenetic Carbonates

The samples collected to examine alteration include nodules, veins, breccias and alteration samples. Two groups of diagenetic samples are used, six nodules, two samples of dolomite

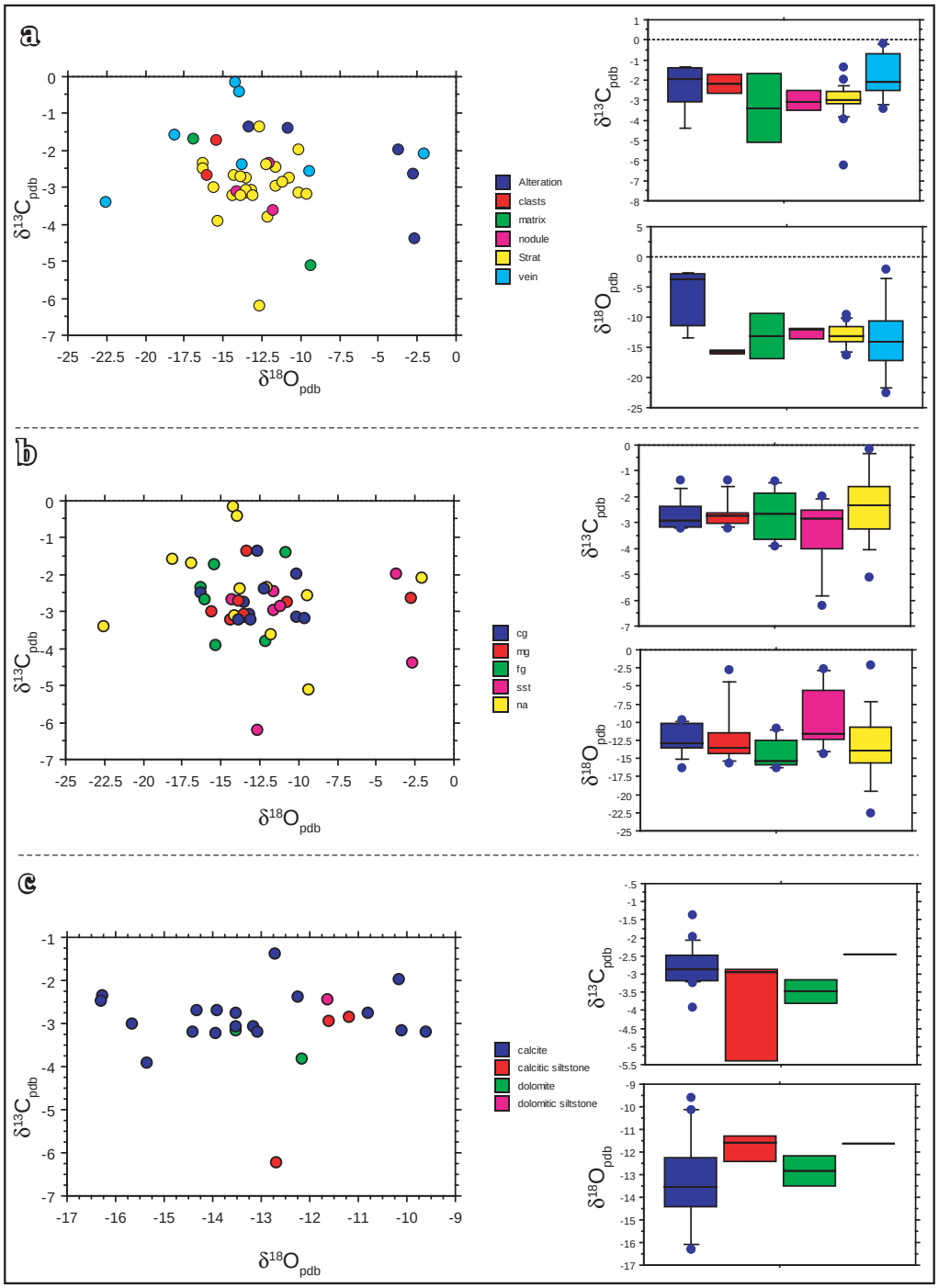

Figure 5.9. Dunns Mine Limestone $\delta^{13}C$ and $\delta^{18}O$ isotope analyses.
a) Split by sample type. b) Split by grain-size. c) Split by mineralogy (stratigraphic samples only).

pseudomorphs of gypsum and three samples of carbonate cement. For diamond drill core samples from the Boorloo Siltstone and the Dunns Mine Limestone, both the $\delta^{13}C$ and $\delta^{18}O$ compositions of nodules are similar to adjacent carbonate beds (Table 5.1, Figure 5.14a,b,c). Sample 733n is a nodule within black shale which was collected from about the middle of the Boorloo Shale. Its $\delta^{13}C$ is similar to about the middle value of stratigraphic values but its $\delta^{18}O$ is the lightest in this study. The lightest $\delta^{13}C$ values are from a nodule in the Boorloo Shale, which post-dates compaction, and the surrounding rock (sample 630518, Table 5.1). Sample 570B from the Hogan Dolomite has chickenwire texture and has a lighter $\delta^{13}C$ than stratigraphic samples from the Hogan Dolomite but similar $\delta^{18}O$ values. Sample

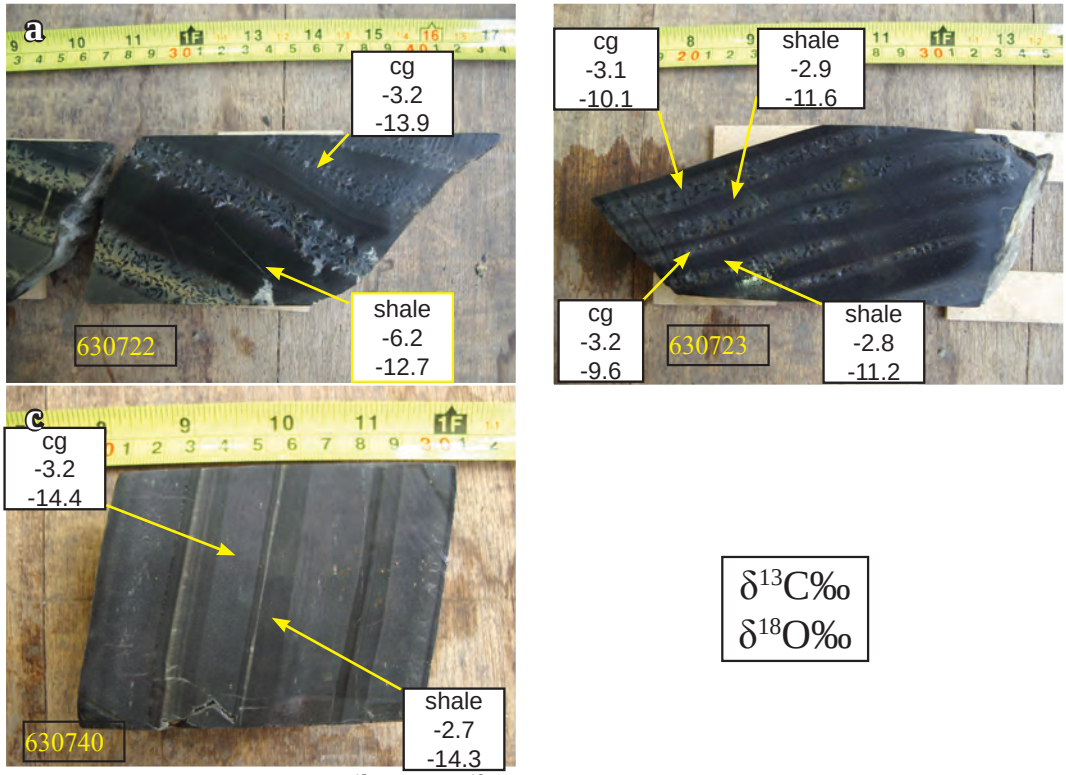

Figure 5.10. Variations in $\delta^{13}C$ and $\delta^{18}O$ between coarse-grained (cg) and shale beds, Dunns Mine Limestone.

a) Interbedded black shale and recrystallised limestone, WD005. The $\delta^{13}C$ from the shale bed is the lowest from the Dunns Mine Limestone. b) Interbedded black shale and recrystallised limestone, WD005. c) Interbedded siltstone and limestone, WD016. This sample has not undergone the same degree of recrystallisation as the samples above, and overall, the proportion of siltstone and shale is less than in WD005. These samples show that there is no consistent variation between coarser- and finer-grained beds.

My902 is also from dolomite replacing gypsum or anhydrite from the Dome Sandstone in the Stony Range Domain, whereas DomeC1 is a sandy limestone from the Euchre Pack Domain. Although the two samples are not directly comparable, they have similar $\delta^{13}C$ and $\delta^{18}O$ values. In the Burra Group, there are differences in both $\delta^{13}C$ and $\delta^{18}O$ compositions between the diagenetic samples and the surrounding rock (Table 5.1, Figure 5.14d).

5.3.4.2 Vein Carbonates

Vein samples were collected from the Dunns Mine Limestone, the Boorloo Siltstone and two from the Recovery Formation. Figure 5.15 shows examples of some of the veins in diamond drill core and the results are included in Table 5.2. Veins from the Dunns Mine Limestone included large veins over one metre wide from the surface at Dunns Mine, that have a spatial relationship to copper mineralisation and smaller veins from diamond drill core. From the Boorloo Siltstone, several small veins were sampled from diamond drill core. The veins sampled from the Recovery Formation are quartz-carbonate veins tens of metres long and up to one metre wide, from the RSZ unit.

There is a large spread of $\delta^{18}O$ values from carbonate veins in the Dunns Mine Limestone, and the $\delta^{13}C$ values are a little heavier than the stratigrapic samples. (Figure 5.9a, Table 5.2). Sample 630732, a quartz-carbonate-pyrite-chalcopyrite vein (Figure 5.15a), has a low $\delta^{18}O$ value of -22.6‰, but the $\delta^{13}C$ value is -3.4‰, about average for the Dunns Mine

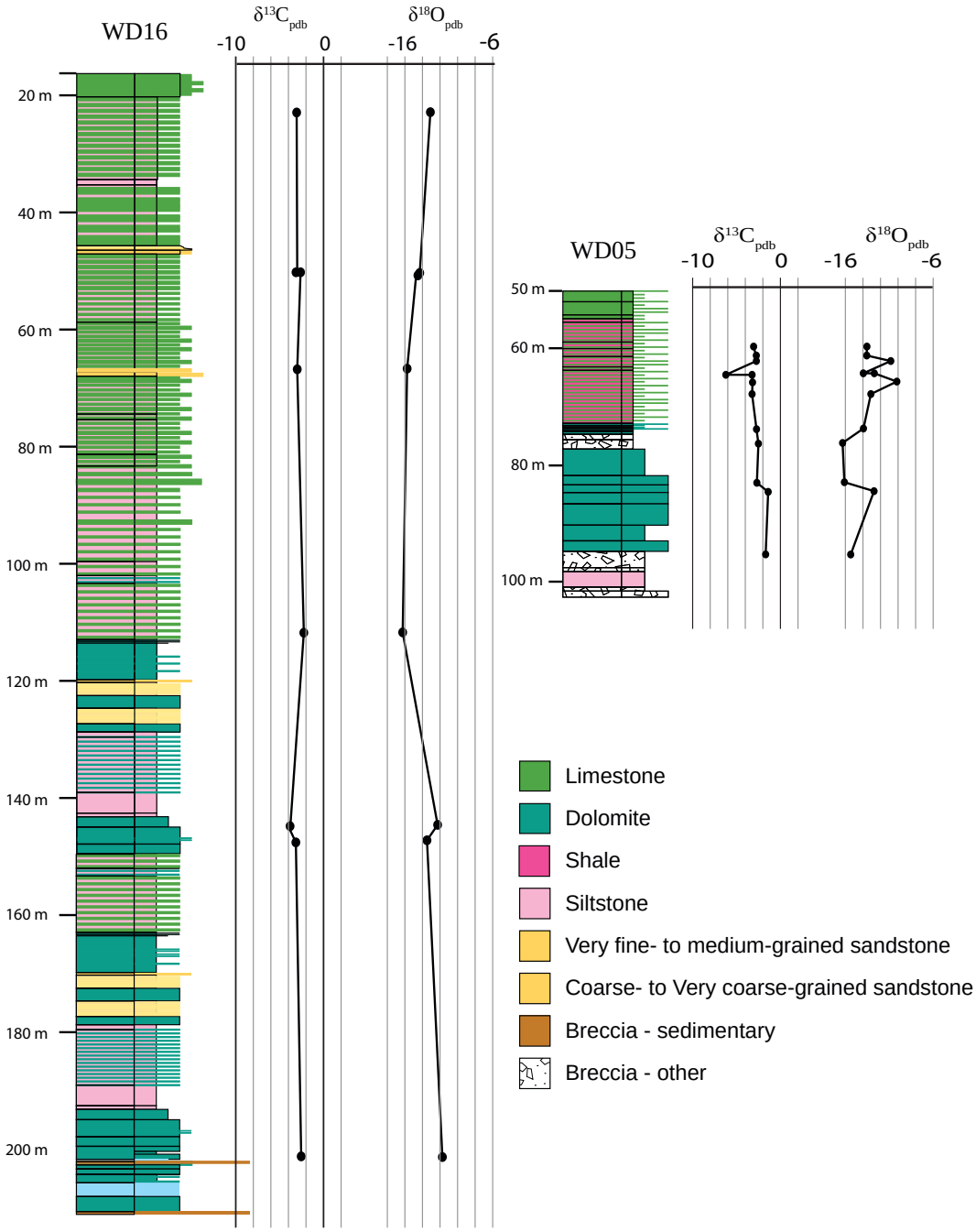

Figure 5.11. $\delta^{13}C$ and $\delta^{18}O$ isotope stratigraphy for the Dunns Mine Limestone, WD016 (left) and WD005 (right).

It is not possible to correlate between the two holes because faulting has removed an unknown thickness of Dunn Mine Limestone from the top and bottom of WD005. The $\delta^{13}C$ is reasonably constant whereas the $\delta^{18}O$ values are highly variable over short distances.

Limestone. However, a massive calcite vein with massive chalcopyrite (sample 631132) has $\delta^{18}O$ and $\delta^{13}C$ values of 16.2‰ and -0.2‰ respectively (Figure 5.15b). These veins are from different drill holes and it was not possible to establish a relationship between them, except that both are from near the base of the Dunns Mine Limestone. Another vein sampled (DM4) with similar $\delta^{18}O$ and $\delta^{13}C$ values to sample 631132, was collected from a massive quartz-carbonate vein from within the mineralised fault zone at Dunns Mine (Table 5.2). One other mineralised vein, sample DM3 returned $\delta^{18}O$ and $\delta^{13}C$ values intermediate between the mineralised veins (Table 5.2).

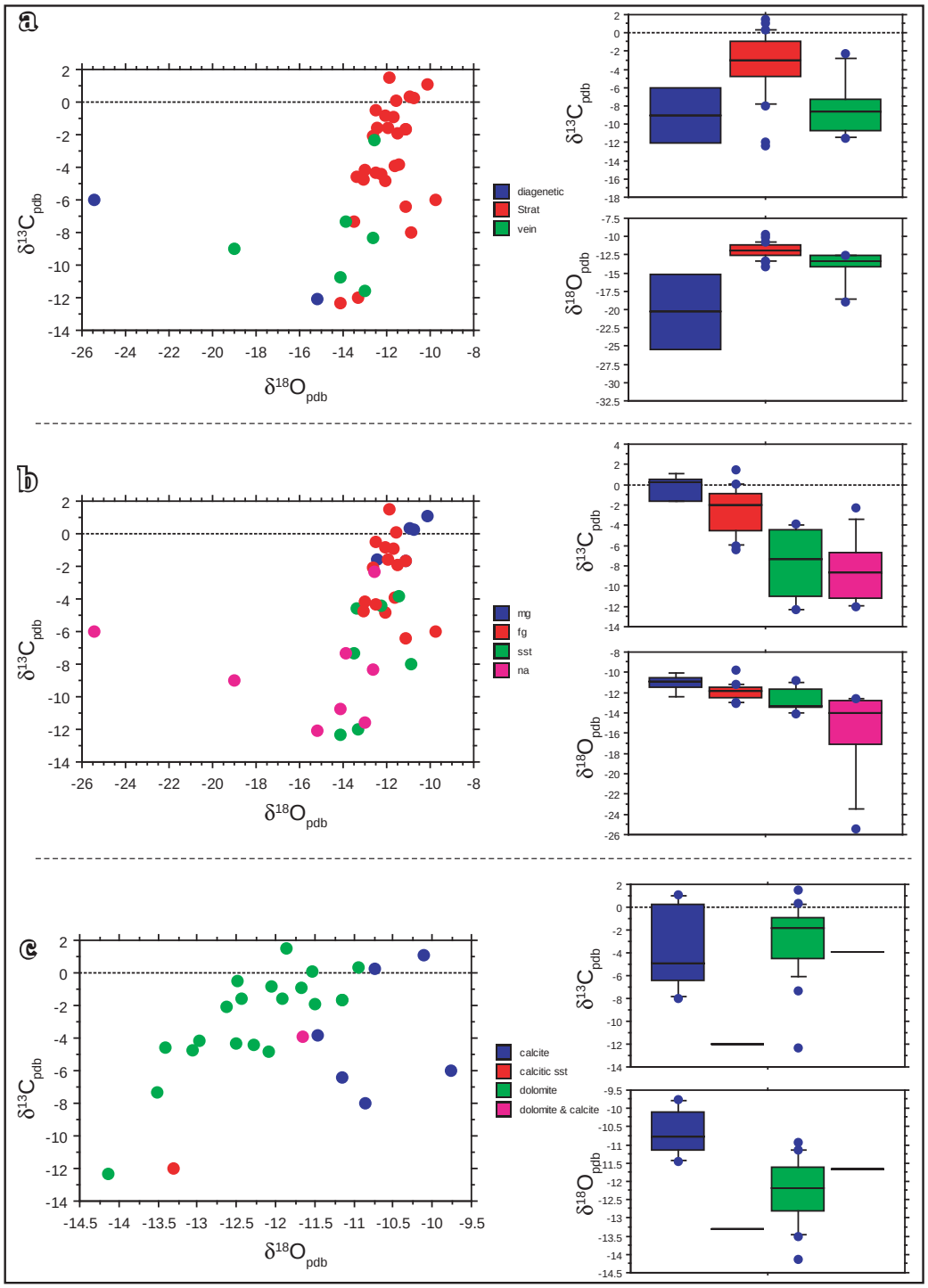

Figure 5.12. Boorloo Siltstone $\delta^{13}C$ and $\delta^{18}O$ isotope isoptope analyses.
a) Split by sample type. b) Split by grain-size. c) Split by mineralogy (stratigraphic samples only).

The veins from the Boorloo Siltstone all have similar $\delta^{18}O$ or $\delta^{13}C$ values to the adjacent country rock (Table 5.2, Figure 5.15c). Veins within the Black Shale Facies (Figure 5.15d), have strongly negative $\delta^{13}C$ values, including one that cuts across a K-feldspar alteration zone within the Boorloo Shale (Figure 5.15e). The two veins sampled from the Recovery Formation have similar $\delta^{18}O$ and $\delta^{13}C$ values to to samples collected by Hill and Walters (2000) from that unit (Table 5.2, Figure 5.6).

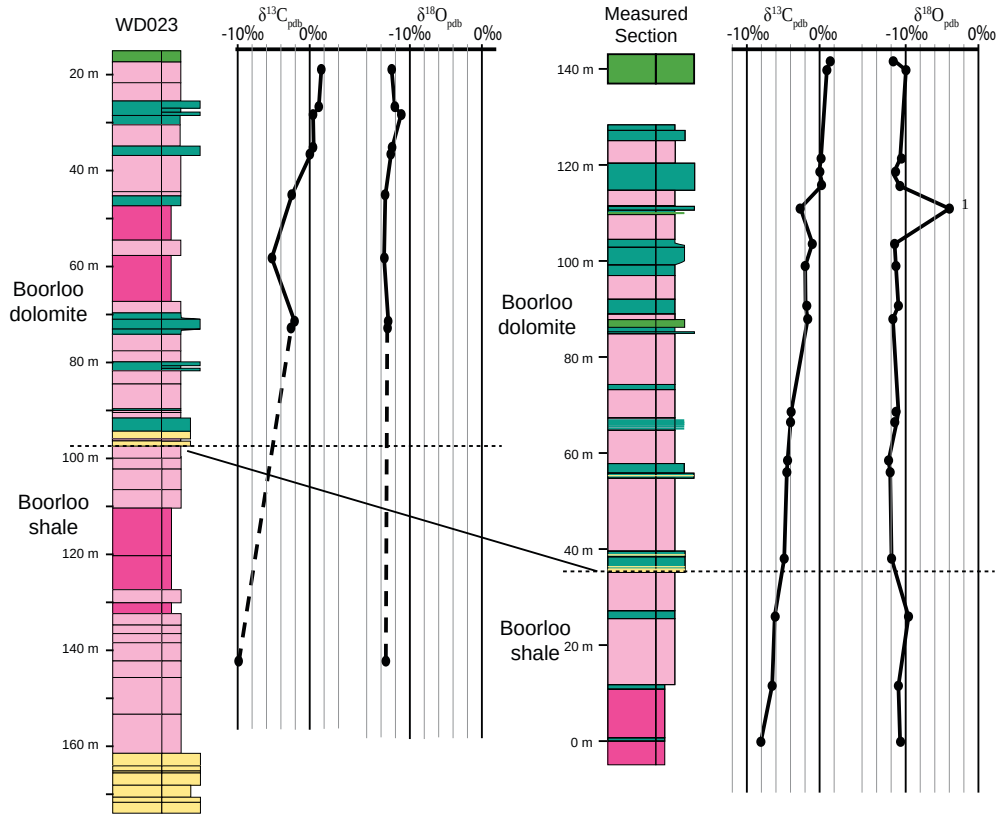

Figure 5.13. $\delta^{13}C$ and $\delta^{18}O$ stratigraphy of the Boorloo dolomite.
Left is from WD023, right is from a measured section (Figure 5.4). The point marked 1 is a weathered sample. There is a gradual increase in $\delta^{13}C$ whereas $\delta^{18}O$ stays about the same. Thin carbonate beds in the Boorloo shale likely have a component sourced from organic carbon, depleted in ^{13}C.

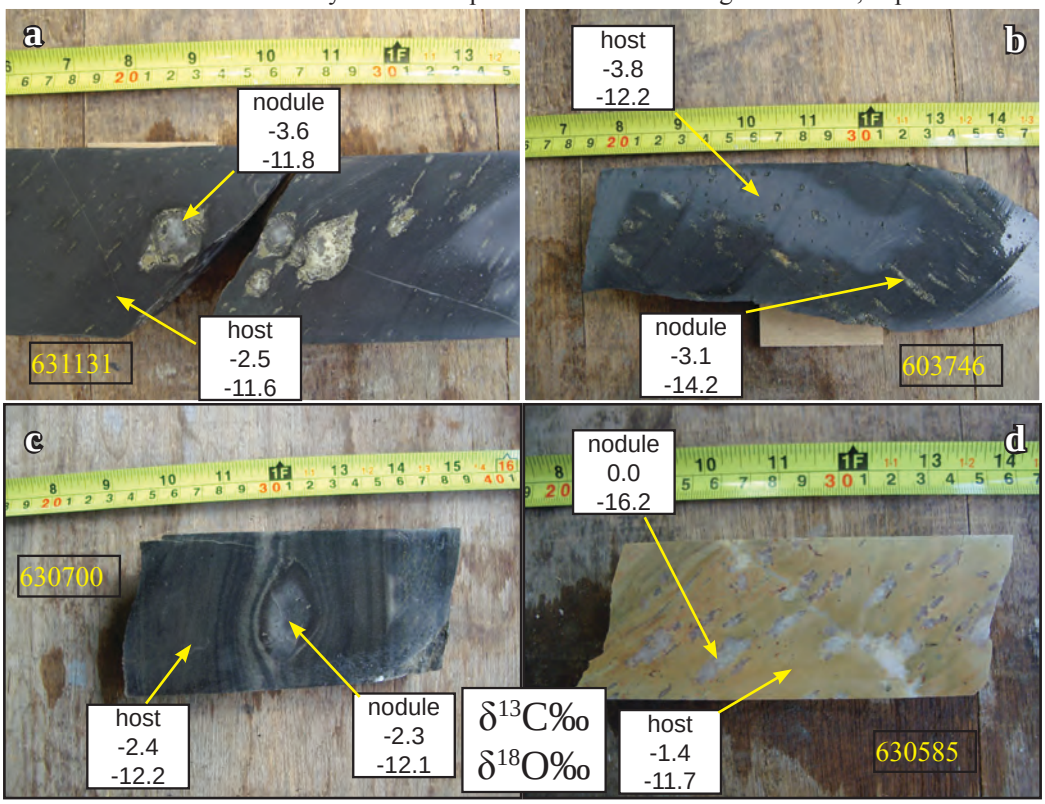

Figure 5.14 Isotope composition of diagenetic nodules and host carbonate beds.
a and b) Dolomite-quartz-sulfide nodules in the Carbonate-chert Facies, Dunns Mine Limestone. In a) the nodules are pre-compaction and elongated parallel to S_0 but in b) the nodules are parallel to S_1 (WD16). c) Calcite nodule in limestone, Interbedded carbonate-clastic facies, Dunns Mine Limestone (WD34). d) Dolomite nodules in Skillogalee Dolomite, (WD19).

5.3.4.3 Breccias.

The breccias show a wide variation in $\delta^{18}O$ and $\delta^{13}C$ values. Comparing clast-matrix pairs, in some samples, the $\delta^{18}O$ and $\delta^{13}C$ values are similar but in others there is a considerable difference between clast and matrix. In samples with two generations of matrix, there are differences between the two generations (Table 5.3, Figure 5.16a,b,c,d).

Breccias from the Burra Group occur in host-rocks with positive $\delta^{13}C$ and a heavier $\delta^{18}O$ composition than the Curdimurka Subgroup above the Dome Sandstone (Figure 5.7; Hill and Walter, 2000). Clasts have both negative (Figure 5.16a) and positive (Figure 5.16b,c) $\delta^{13}C$ values, with variable $\delta^{18}O$ values (Table 5.3), and the former may be sourced from

Table 5.1. $\delta^{18}O$ and $\delta^{13}C$ compositions of carbonate nodules and diagenetic carbonates with associated sedimentary carbonate $\delta^{18}O$ and $\delta^{13}C$ composition.

Sample No	Hole No	From	To	Strat	Type	$\delta^{13}C$	$\delta^{18}O$
630586b	WD19	260.7	260.8	Burra Gp	diagenetic	-3.8	-6.6
630586a	WD19	260.7	260.8	Burra Gp	Strat	-0.6	-13.7
630585a	WD19	228.7	228.8	Burra Gp	nodule	0.0	-16.7
630585b	WD19	228.7	228.8	Burra Gp	Strat	-1.4	-11.7
630518n	WD31	132.2	132.3	Boorloo Siltstone	nodule	-12.1	-15.2
630518g	WD31	132.2	132.3	Boorloo Siltstone	Strat	-12.4	-14.1
733n				Boorloo Siltstone	nodule	-6.0	-25.4
570b				Hogan Dolomite	diagenetic	-9.2	-11.7
1509a				Hogan Dolomite	Strat	-6.2	-10.2
REG6				Hogan Dolomite	Strat	-4.0	-9.6
REG4v				Recovery Formation	diagenetic	-3.0	-12.0
REG4g				Recovery Formation	Strat	-4.7	-7.8
630746b	WD16	159	159.2	Dunns Mine Limestone	nodule	-3.1	-14.2
630746a	WD16	159	159.2	Dunns Mine Limestone	Strat	-3.8	-12.2
630700a	WD34	29.1	29.25	Dunns Mine Limestone	nodule	-2.3	-12.1
630700b	WD34	29.1	29.25	Dunns Mine Limestone	Strat	-2.4	-12.3
631131b	WD16	169.7	169.8	Dunns Mine Limestone	nodule	-3.6	-11.8
631131a	WD16	169.7	169.8	Dunns Mine Limestone	Strat	-2.5	-11.6
MY902				Dome Sandstone (NFD)	diagenetic	0.6	-12.8
DomeC1				Dome Sandstone	Strat	1.4	-13.3

Table 5.2 $\delta^{18}O$ and $\delta^{13}C$ composition of carbonate veins.

Sample No	Hole No	From	To	Strat	mineralogy	$\delta^{13}C$	$\delta^{18}O$
630508	WD31	47.5	47.6	Boorloo Siltstone	dolomite	-9.0	-19.0
630525	WD31	131.1	131.2	Boorloo Siltstone	dolomite	-10.7	-14.1
630531v	WD23	37.4	37.6	Boorloo Siltstone	dolomite	-2.3	-12.6
630556	WD23	212.1	212.2	Boorloo Siltstone	dolomite	-7.3	-13.9
630557	WD23	216.7	216.8	Boorloo Siltstone	dolomite and calcite	-8.3	-12.6
630559	WD23	236.6	236.7	Boorloo Siltstone	dolomite	-11.5	-13.0
630732	WD6	157.2	157.3	Dunns Mine Limestone	calcite	-3.4	-22.6
631132	WD16	174.1	174.2	Dunns Mine Limestone	calcite	-0.2	-14.2
631136	WD21	119.8	119.9	Dunns Mine Limestone	dolomite	-2.6	-9.5
DM3				Dunns Mine Limestone	calcite	-1.6	-18.2
DM4				Dunns Mine Limestone	dolomite	-0.4	-14.0
DM6f				Dunns Mine Limestone	dolomite	-2.4	-13.8
REG1				Recovery Formation	calcite	-4.8	-10.8
REG2				Recovery Formation	dolomite	-3.9	-14.2

the Curdimurka Subgroup. Matrix $\delta^{18}O$ values in Burra Group breccias are highly variable, ranging from -5.7‰ to -30.7‰, whereas $\delta^{13}C$ values show a smaller variation than seen in the Curdimurka Subgroup stratigraphic samples, varying from -1.1‰ to 2.4‰ (Table 5.3). The heaviest $\delta^{18}O$ values (sample 630568, Figure 5.16a) are from two generations of matrix that have similar values for both $\delta^{18}O$ or $\delta^{13}C$, suggesting they are derived from the same fluid. However, the $\delta^{18}O$ values are similar to those associated with weathered samples and so could be altered by weathering.

Samples OGD1 and OGD2 are orange-weathering, recrystallised dolomite megaclasts from the Breaden Hill Breccia (Figure 5.4). Their $\delta^{13}C$ and $\delta^{18}O$ compositions are both heavier than the Curdimurka Subgroup and the Burra Group, the $\delta^{13}C$ being the heaviest in this study. They differ considerably from megaclasts of Black Knob Marble, both in appearance and $\delta^{18}O$ and $\delta^{13}C$ values (Table 5.3).

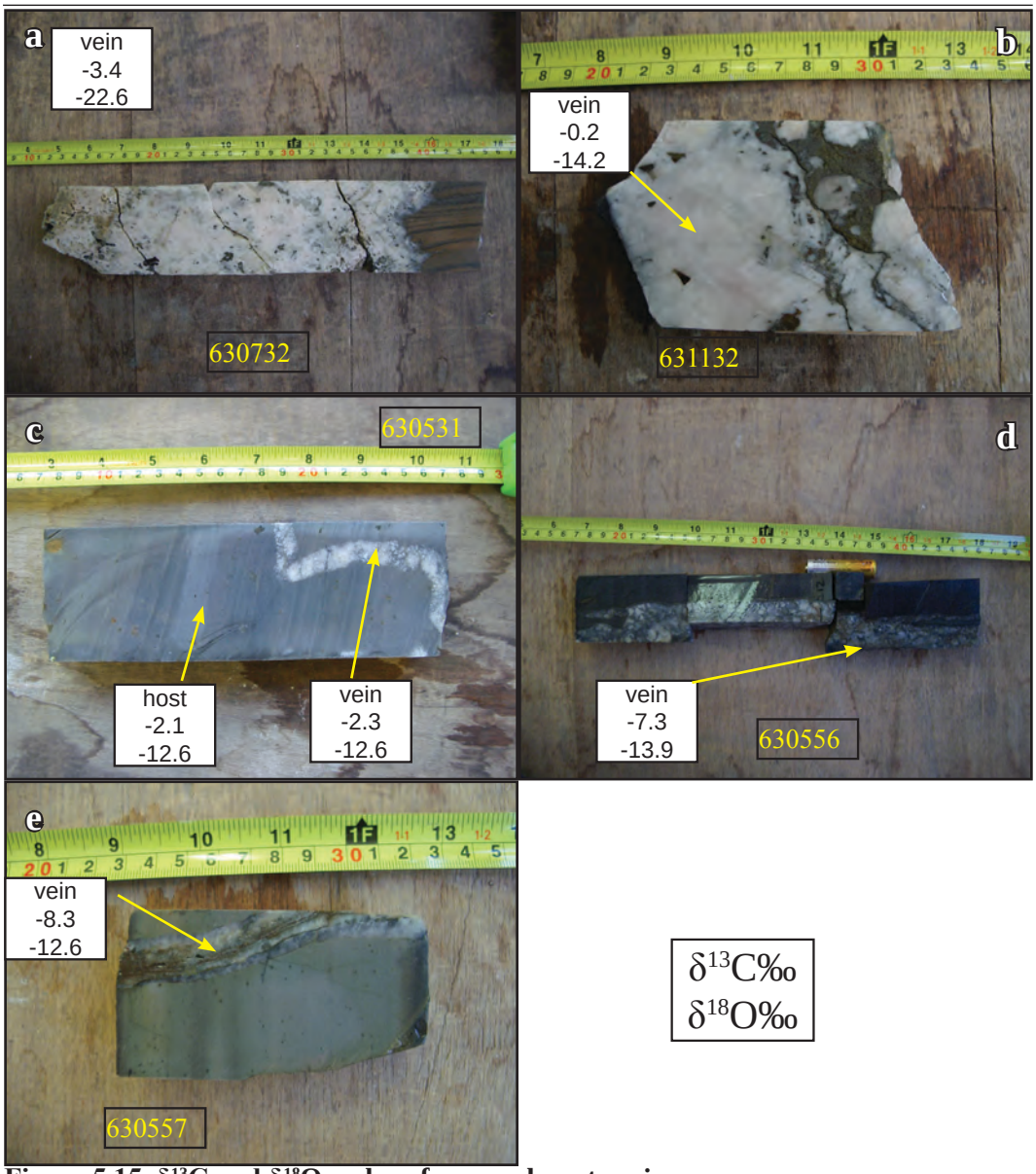

Figure 5.15. $\delta^{13}C$ and $\delta^{18}O$ values from carbonate veins.
a) Calcite-sulfide vein from a fault zone in the Dunns Mine Limestone, WD006. b) Calcite-pyrite-chalcopyrite vein, Dunns Mine Limestone, c) WD006. Calcite-quartz vein within a sandy dolomite bed, BDol, WD023. d) Quartz-dolomite vein in black shale, BShl, WD023. e) Quartz-biotite-carbonate (ank-dol-cc) vein in K-feldspar altered black shale, BShl, WD023.

Samples RF1 and RF2 are from folded carbonate-siltstone clasts from a brecciated zone within the Recovery Formation (Figure 5.4). They have negative $\delta^{13}C$ values typical of the Curdimurka Subgroup in general but are heavier than Recovery Formation samples from Hill and Walter (2000; Figure 5.7). Sample 1062 is matrix from a diapiric breccia at the base of the Recovery Formation (Figure 5.4). The breccia is matrix supported with an orange calcite matrix and large feldspar clasts after scapolite. Its $\delta^{13}C$ plots within the Curdimurka Subgroup field whereas its $\delta^{18}O$ is heavier than typical.

Samples 630731 and 630729, both brecciated Dunns Mine Limestone, underscore the complexity of the $\delta^{18}O$ and $\delta^{13}C$ variations in the breccias (Table 5.3, Figure 5.16e,f). In the former, the matrix and breccia $\delta^{18}O$ and $\delta^{13}C$ are similar whereas in the latter they differ with the matrix having lighter isotopic compositions. The clasts in both samples have similar $\delta^{18}O$ and $\delta^{13}C$ values, and the $\delta^{13}C$ are similar to the stratigraphic sample values.

5.4 Discussion

5.4.1 Alteration

Before comparing the results with the global Neoproterozoic isotope curves it is necessary to discuss whether the $\delta^{13}C$ and $\delta^{18}O$ values reflect the original composition or have been altered? Hill and Walter (2000) explained the generally lower $\delta^{18}O$ to be due to diagenetic reactions with a single groundwater system or connate basin within a restricted region, but conclude the $\delta^{13}C$ was largely unaffected. Foden et al. (2001) suggested that the entire Adelaide Fold Belt was subject to a hydrothermal event at about 586 Ma, which reset

Table 5.3. $\delta^{18}O$ and $\delta^{13}C$ compositions of breccia samples.

Sample No	Strat	Type	mineralogy	$\delta^{13}C$	$\delta^{18}O$
630566	Burra Gp	matrix	calcite	-0.9	-9.7
630576	Burra Gp	matrix	dolomite and calcite	1.4	-30.3
630582	Burra Gp	matrix	dolomite	1.2	-30.7
630568a	Breccia (Burra Gp)	matrix	calcite	-0.3	-5.9
630568b	Breccia (Burra Gp)	matrix	calcite	-1.1	-5.7
630568c	Breccia (Burra Gp)	clasts	calcite	-1.0	-7.5
630574a	Breccia (Burra Gp)	clasts	dolomite	2.2	-15.9
630574b	Breccia (Burra Gp)	matrix	dolomite	2.4	-22.3
630574c	Breccia (Burra Gp)	matrix	dolomite	1.6	-16.5
OGD1	Breccia (Breaden Hill)	clasts	dolomite	5.3	-9.8
OGD2	Breccia (Breaden Hill)	clasts	dolomite	6.5	-8.9
RFM1	Recovery Formation	clasts	dolomite	-2.0	-14.8
RFM2	Recovery Formation	clasts	dolomite	-2.1	-14.8
1062	Breccia (RSlt1)	matrix	calcite	-5.0	-7.8
630729a	Dunns Mine Limestone	clasts	dolomite and calcite	-2.6	-16.0
630729b	Dunns Mine Limestone	matrix	calcite	-5.1	-9.3
630731a	Dunns Mine Limestone	clasts	dolomite	-1.7	-15.4
630731b	Dunns Mine Limestone	matrix	dolomite	-1.7	-16.9
630704c	Dome Sandstone	clasts	calcite	-2.3	-11.1
630704b	Dome Sandstone	matrix	dolomite	-0.2	-16.1
BKC1	Black Knob Marble	Strat	calcite	2.2	-8.9
BKC2g	Black Knob Marble	Strat	calcite	-8.7	-8.7
BKC2v	Black Knob Marble	Vein	calcite	-12.6	-12.6
1612	Black Knob Marble	Strat	calcite	1.8	-21.6

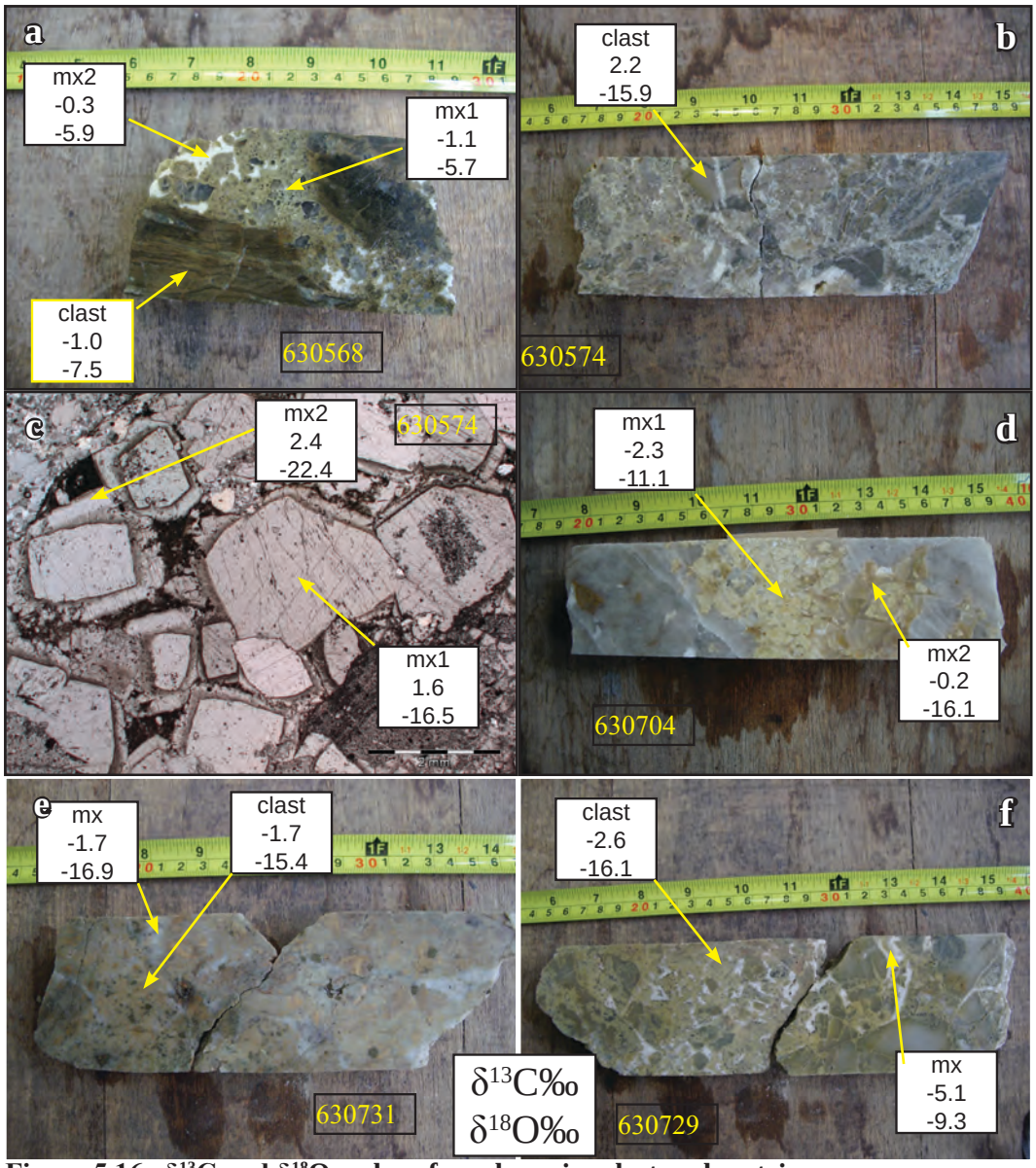

Figure 5.16. $\delta^{13}C$ and $\delta^{18}O$ values from breccias clast and matrix.
a) Breccia with clasts, an early orange dolomite matrix (mx1) with a later white calcite in-fill (mx2). b) Breccia from the Burra Group with isotope values in the clasts. c) Photomicrograph of matrix in b) dolomite lined by calcite, with differing isotopic compositions. d) Brecciated quartz vein with large dolomite crystals (mx1) with later calcite (mx2), Dome Sandstone. e) Brecciated Dunns Mine Limestone with dolomite matrix. The clast and matrix have similar $\delta^{18}O$ and $\delta^{13}C$ values. f) Brecciated Dunns Mine Limestone with calcite matrix. In this sample the $\delta^{18}O$ and $\delta^{13}C$ values of the clast and matrix differ.

the Sr^{86}/Sr^{87} ratio, and so may have affected the $\delta^{13}C$ and $\delta^{18}O$ values. The Curdimurka Subgroup was subject to several generations of alteration and has undergone lower to middle greenschist and metamorphism that will drive the $\delta^{18}O$ and $\delta^{13}C$ toward 0‰, although at low metamorphic grades this shift is minimal (Melezhik et al., 2001, 2005). Hence it is probable that the $\delta^{18}O$ and $\delta^{13}C$ values today do not reflect the initial values just after deposition.

Jacobsen and Kaufmann (1999) suggested that correlations between $\delta^{18}O$ and $\delta^{13}C$ may result from post-depositional alteration. There is no correlation between $\delta^{18}O$ and $\delta^{13}C$ in the Dunns Mine Limestone, with little variation in $\delta^{13}C$ except for one outlier, and the $\delta^{18}O$ varying considerably (Figure 5.9). Variations in the $\delta^{18}O$ and $\delta^{13}C$ composition of veins and

breccias (Tables 5.2 and 5.3) show that post-depositional fluids have passed through the Dunns Mine Limestone. Most veins within the Dunns Mine Limestone have similar $\delta^{18}O$ and $\delta^{13}C$ to the sedimentary carbonate, but one vein is has considerably heavier $\delta^{18}O$, and one vein and the matrix of a breccia have considerably lighter $\delta^{18}O$ suggesting at least two fluids have affected it (Tables 5.2 and 5.3).

In most cases, the $\delta^{13}C$ and $\delta^{18}O$ composition of the diagenetic nodules is similar to the surrounding sedimentary carbonate indicating that they formed from fluids of the same isotopic composition. The majority of nodules are pre-compaction and hence early diagenetic but a nodule in sample 630518 from the Boorloo shale formed post-compaction, and has similar $\delta^{13}C$ and $\delta^{18}O$ values to the surrounding rock (Table 5.1). The highly negative $\delta^{13}C$ values in this sample and in samples from the Boorloo shale are interpreted to indicate that the carbon is in part derived from the oxidation of organic carbon during late diagenesis. Carbonate beds in the thirty or so metres below the level of the Boorloo dolomite also show highly negative $\delta^{13}C$ compositions and are interpreted to have a similar origin. However, the more oxidised carbonate units of the Boorloo Dolomite also have negative $\delta^{13}C$ compositions until only the last one or two units record positive $\delta^{13}C$ compositions. Veins with the Boorloo Siltstone also have similar $\delta^{13}C$ and $\delta^{18}O$ values to the surrounding rock, except for sample 630508, which has a light $\delta^{18}O$ composition (Table 5.2). Most veins contain biotite and are likely metamorphic, but the similarity in isotopic composition to the host rock suggests that the carbon and oxygen was sourced locally, the light $\delta^{13}C$ suggesting that they formed in part by oxidation of organic carbon.

$\delta^{13}C$ values are typically resistant to alteration because hydrothermal waters carry more oxygen than carbon, and carbonate rocks contain considerably more carbon than meteoric waters **(**Banner and Hanson, 1990**)**. The final $\delta^{18}O$ and $\delta^{13}C$ composition of a rock reflects the $\delta^{18}O$ and $\delta^{13}C$ of the fluid and the rocks through which the fluid passes, and the ratio of water to rock involved in the interaction (Banner and Hanson, 1990). Calculations suggest that the water:rock ratios required to significantly alter the original $\delta^{18}O$ and $\delta^{13}C$ are about 10:1 and 1,000:1 respectively (Jacobsen and Kaufman, 1999). In both the Boorloo Siltstone and the Dunns Mine Limestone, the majority of veins have similar $\delta^{13}C$ values to the surrounding rock but the $\delta^{18}O$ varies in a few examples. Hence it is concluded that sufficient water (at least two fluids) has passed through the Dunns Mine Limestone to alter the $\delta^{18}O$ but not enough to alter the $\delta^{13}C$.

5.4.2 Comparison with the Neoproterozoic $\delta^{13}C$ Curve.

A comparison of the results of this study and that of Hill and Walter (2000) with the Neoproterozoic $\delta^{13}C$ curve presents difficulties because of the correlations with the Bitter Springs Formation. The Bitter Springs Formation consists of the Gillen and Loves Creek Members (Figure 5.2, 5.17). The Gillen Member overlies the Heavitree Quartzite and comprises a lower unit of black shale with interbedded grey-black shale, sandstone and thinly bedded dolomite; and an upper evaporitic unit consisting of laminated sulfate and dolomite and a dolomite-gypsum breccia. Within the evaporitic unit is a thick middle halite unit, with thinner halite units below and a number of bituminous dolomite beds. It was

deposited in a marine environment and has positive $\delta^{13}C$ values (Hill and Walter, 2000; Hill et al., 2000).

From Southgate (1991), the Loves Creek Member comprises three units;

- Unit 1; A lower most stromatolitic dolomite unit with an upper 20 m to 30 m of dolo-mudstone
- Unit 2; A central unit consisting of a series of shallowing-upward stromatolite cycles, indicating a period of gradual marine transgression (Southgate, 1991). A complete cycle includes a lower grainstone facies, a middle domical and columnar stromatolite facies and an upper thin-bedded stratiform stromatolite dolomite facies (Hill et al., 2000). Dessication cracks and cauliflower chert nodules occur in the upper dolo-mudstone.
- Unit 3; The upper unit consists of red dolomitic siltstone and red siltstone interbedded with dolomite, limestone and dolomitic siltstone (Figure 5.3).

Hill et al., (2000) interpreted that Unit 1 was deposited in a marine environment, the lower part of Unit 2 deposited in a lacustrine environment and the upper part in a marine environment and Unit 3 was deposited in a lacustrine environment. However, Gore et al., (2004) reinterpreted Unit 3 to be marine in origin and Lindsay et al., (2005) interpreted the Loves Creek Member to be wholly marine. Walter et al. (2000) suggested a distinctive $^{87}Sr/^{86}Sr$ ratio at the boundary between the Gillen and Loves Creek Member occurs at 834 Ma, based on a correlation with a similar ratio in the Shaler Supergroup.

In the Curdimurka Subgroup, up to about 3,000 m of sediment was deposited during the negative excursion whereas the total thickness of the Bitter Springs Formation that shows a negative $\delta^{13}C$ excursion is about 280 metres **(**Figure 5.17**).** Between the Curdimurka Subgroup and the Umberatana Group, there is about 6,000 m of Burra Group whereas Unit 3 of the Loves Creek Member is about 370 m thick. There was also some erosion at the top of the Loves Creek Member prior to deposition of the Areyonga Formation, which is correlated with the Yudnamatana Subgroup (Preiss, 1987). These differences in thickness may only reflect the different tectonic setting of the basins. The Bitter Springs Formation is thought to have been deposited in a sag basin, with deposition controlled by eustatic changes in sea level (Lindsay et al., 2005) whereas the Curdimurka Subgroup was deposited in a rapidly subsiding rift basin. However, both have significant thicknesses of salt beneath them, in the Gillen Member of the Bitter Springs Formation and the Arkaroola Subgroup. If the salt deposition at this time reflects the first incursion of the sea water onto the continent of Rodinia, then they may be coeval. However, just as the Wooltana Volcanics, which occur below the Curdimurka Subgroup, are correlated with the Gairdner Dyke Swarm so are the Bitter Springs volcanics (Zhao et al, 1994). These comprise widespread thin basic (spilitic) units within the Bitter Springs Formation, although their stratigraphic level is uncertain. Zhao et al (1994) suggest that they occur at a relatively constant stratigraphic horizon in the Loves Creek Member whereas Hill and Walter (2000) suggested that they occur throughout the Bitter Springs Formation. If Zhao et al (1994) are correct, Units 1 and 2 of the Loves Creek Member cannot be correlated with Curdimurka Subgroup. However, if the

Bitter Springs Volcanics are younger, then the correlation may be correct. In the absence of improved geochronology of the Bitter Springs Formation, the similar shapes of the $\delta^{13}C$ curves for the Bitter Springs Formation and the Curdimurka Subgroup do favour the correlation of the Curdimurka Subgroup with Units 1 and 2 of the Loves Creek Member, despite the major difference in thickness.

The Bitter Springs Stage of Halverson et al (2005) is based on their implied correlation of the negative excursion within the Bitter Springs Formation with the results of Hill and Walter (2000) from the Curdimurka Subgroup. The more limited curve presented by Lindsay et al. (2005) is also based on a correlation with the Curdimurka Subgroup. In effect, the results presented here would be compared with themselves. It also means that the $\delta^{13}C$ curves of Halverson et al., (2005) and Lindsay et al., (2005) tacitly assume that the Curdimurka Subgroup was deposited in a marine environment.

Halverson et al., (2005) correlated the Grusdievbreen and Svanbergfjellet Formations from Svalbard, which have negative $\delta^{13}C$ compositions, with the negative $\delta^{13}C$ excursion seen in the Bitter Springs Formation. Their data does not contain the brief positive $\delta^{13}C$ peak seen in the Bitter Springs Formation. The isotope curve of Kaufmann and Knoll (1995), which does not incorporate Australian data has a negative excursion at a slightly older age but with no support for that age. On the basis of the widespread occurrence of a negative $\delta^{13}C$ excursion in rocks of about the same age, the results from the Curdimurka Subgroup do fit the global $\delta^{13}C$ curve.

5.4.3 Depositional Environment

Hill and Walter (2000) concluded that the isotope $\delta^{13}C$ values of the Curdimurka Subgroup likely represent deposition within a lacustrine environment subject to intermittent marine incursions. The lowest $\delta^{13}C$ values they attributed to deposition from a fresh water source for dissolved inorganic carbon (Hill and Walter, 2000). They suggested that the sediments have a low total organic content, which may be true of the carbonates they sampled but is not true of most of the surrounding clastic sediments.

Evaporites are interpreted to occur at the base of the Dunns Mine Limestone in the Chert-carbonate Facies, with the water level deepening up the section hence the system is not closed (above the level of the evaporites). Therefore, there should be a negative correlation between $\delta^{18}O$ and $\delta^{13}C$ if it were a perennial lake (Camoin et al., 1997). Instead, the $\delta^{18}O$ value in the Dunns Mine Limestone is highly variable and could be attributed to a lacustrine system on this basis but the $\delta^{13}C$ decreases slightly upward and there is no correlation. If it were a lacustrine system the lake would therefore be replenished by water sources that were highly variable in $\delta^{18}O$ but with consistent $\delta^{13}C$. This may be possible if the carbon was being replenished by the weathering of an organic-rich shale (to supply the negative $\delta^{13}C$), and the water was derived from a range of different sources. However, it is significant that the results from WD016 are not as variable as those from WD005. The carbonates from WD005 have undergone strong recrystallization whereas those from WD016 have undergone minor recrystallization and so recrystallization and alteration of the carbonates may be the main cause of the highly variable $\delta^{18}O$ in the Dunns Mine Limestone. The

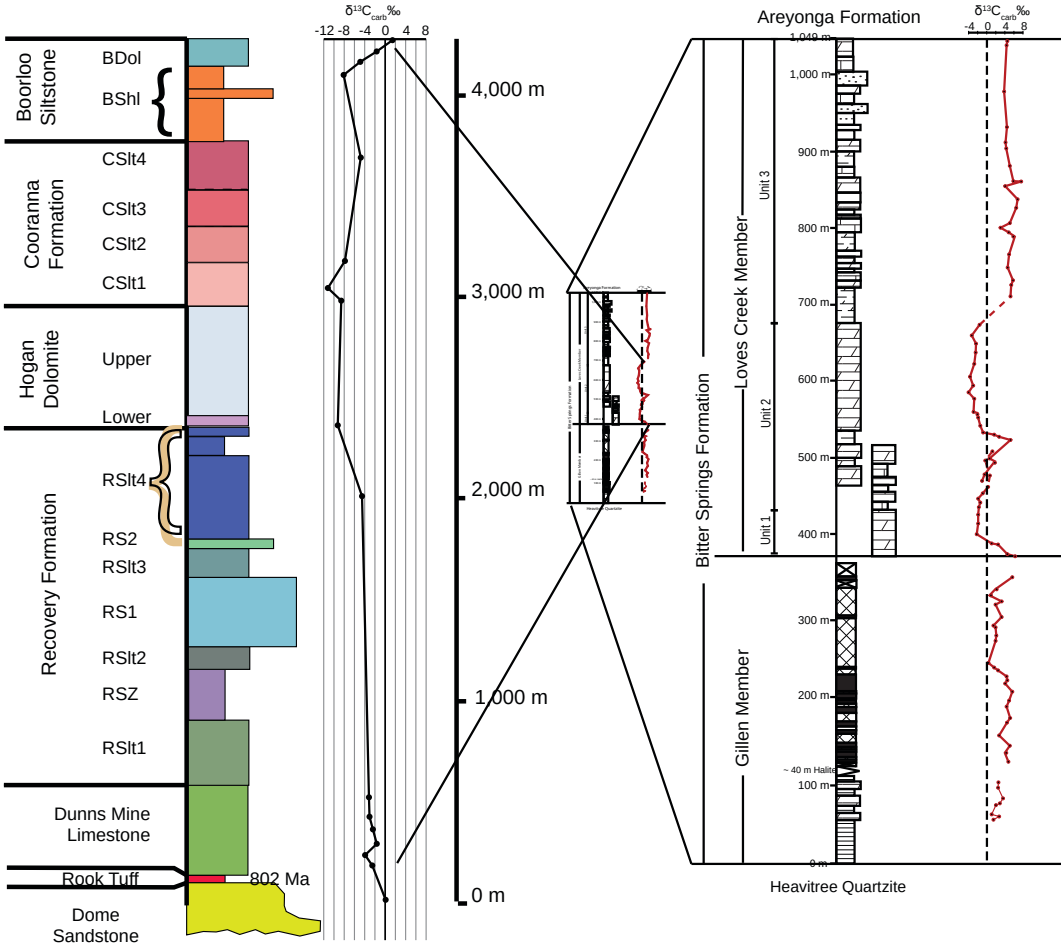

Figure 5.17. Comparison of the $\delta^{13}C_{carb}$ curve for the Curdimurka Subgroup from this study and the Bitter Springs Formation (Hill et al., 2000).
On the left is the Curdimurka Subgroup and the centre is the Bitter Springs Formation at the same scale. On the right is the Bitter Springs Formation drawn at four times the scale of the centre drawing. The negative excursion in the Curdimurka Subgroup occurs over 4,000 m whereas in the Bitter Springs Formation, it is only about 250 m thick.

small variation in the $\delta^{13}C$ occurs with increasing depth of water, which could be attributed to biological pumping (Kroopnick, 1974; Surge et al., 1997; Hotinski et al., 2004), or a reflection of increased organic matter in either a marine or lacustrine setting.

There is an increase in $\delta^{13}C$ in the Boorloo Siltstone up-section which is not matched by $\delta^{18}O$. Sedimentological evidence shows that there is a gradual shallowing from sub-wave base anoxic conditions to evaporitic conditions, so a closed system may explain this change, if the $\delta^{18}O$ has been changed by post-depositional alteration. Biological pumping may produce such a result; carbonates formed in the deeper, anoxic waters having a component of depleted (biological) carbon released by oxidation of the organic matter at the redox boundary (Kroopnik, 1974; Surge et al., 1997; Hotinski et al., 2004), but the change in the $\delta^{13}C$ of the Boorloo Siltstone is much greater than shown by either author, and is likely overshadowed by other processes. The diagenetic nodules from the Boorloo Siltstone, have $\delta^{13}C$ values of -6.0 and -12.1, suggesting that the more negative values may be due to the oxidation of organic carbon, which is incorporated into the nodules. The similar $\delta^{13}C$ of a nodule and the surrounding shale are interpreted to indicate that this is the dominant process explaining the strongly negative $\delta^{13}C$ below the level of the Boorloo

dolomite. Variations in $\delta^{13}C$ below the Boorloo dolomite are therefore interpreted to be masked by other processes. In the Boorloo doomite, there is a gradual change from negative to positive $\delta^{13}C$, with little change in the $\delta^{18}O$. This is indicative of a closed, evaporitic system, although the interbedded carbonates and siltstones suggest that there is a series of flooding and evaporitic events. Therefore the gradual change in $\delta^{13}C$ is not due to a single evaporitic event. Also the fact that the change is gradual, and not highly variable argues against a lacustrine environment. Instead it is attributed to the flooding events reflecting a gradual external change in $\delta^{13}C$ in the water on a large scale, which argues for a marine setting rather than a localized, lacustrine depositional environment.

There is no definitive stable isotope evidence for a solely lacustrine depositional environment for the Dunns Mine Limestone or the Boorloo Siltstone. Instead the $\delta^{13}C$ curve matches the global curve and so a marine environment is favoured.

5.5 Conclusions

The intention of the stable isotope analysis of carbonates from the Curdimurka Subgroup was to provide additional supporting data for interpreting the depositional environment of the Curdimurka Subgroup. On their own the results are equivocal and could be attributed to either lacustrine or marine settings. However, the negative $\delta^{13}C$ excursion seen in the Curdimurka Subgroup is seen globally which favours a marine depositional environment.

It is likely that the $\delta^{18}O$ has been at least partially re-set in the Dunns Mine Limestone, leading to the variability seen. The $\delta^{13}C$ vary only a small degree and are considered to be pristine or near pristine. In the Boorloo Siltstone, the highly negative $\delta^{13}C$ values seen in the Boorloo Shale are attributed to the oxidation of reduced carbon in organic matter during diagenesis and metamorphism. Otherwise the change in $\delta^{13}C$ up-section is interpreted to reflect depositional variations, from sub-wavebase to emergent and evaporitic in a marine setting. Moreover it likely reflects a global change, marking an end to the Bitter Springs stage negative $\delta^{13}C$ excursion and a return to positive $\delta^{13}C$ values.

CHAPTER 6
MONAZITE GEOCHRONOLOGY.

6.1 Introduction.

A series of thermal events related to magmatism and/or tectonism have affected the Northern Adelaide Fold Belt. Elburg et al. (2002) dated a series of intrusives in the Mt Painter Inlier between about 500 Ma and 485 Ma and concluded that peak metamorphism occurred at about 490 Ma. The British Empire granite intruded the Mt Painter Inlier in a series of pulses at about 450 Ma (Elburg et al. 2002). In the Peake and Denison Inliers, the Bungalina Monzonite is considered to be Cambrian in age (Morrison and Foden, 1990). In the absence of magmatic rocks in the Willouran Range, it is not possible to determine directly whether the effects of these thermal events extended to the study area, or whether the metamorphism was associated with one or both of the thermal events recognized in the Mt Painter Inlier. A monazite dating study was undertaken to test these scenario's. Post-depositional monazite growth is shown to provide a reconrd of metamorphic and other thermal events in the Willouran Range.

6.2 Monazite Geochronology.

Monazite is a Th, U, REE-bearing phosphate mineral that has been historically considered to crystallize mainly from magma or form during medium to high-grade metamorphism, and from hydrothermal fluids (Overstreet, 1966). More recently, monazite has also been found in unmetamorphosed and low-grade metamorphic rocks of sedimentary origin, having formed during diagenesis to low-grade metamorphism (e.g., Cabella et al., 2001; Rasmussen and Fletcher, 2002). It has been widely used for isotopic dating using the U – Pb geochronometer (e.g., Burger et al., 1965; Parrish, 1990; Kingsbury, 1993; Rasmussen et al., 2001; Rasmussen and Fletcher, 2002). Typically, secondary ion mass spectrometry (SIMS) and thermal ionization mass spectrometry (TIMS) methods have been used in geochronological studies using monazite, but a chemical method has been developed using electron microprobe analysis (EMPA) (e.g., Suzuki and Adachi, 1991; Montel et al., 1996; Cocherie et al., 1998; Williams et al., 1999).

Monazite is suitable for geochronological studies for a variety of reasons; 1) it is widespread, 2) it contains significant amounts of Th and U, 3) paucity of nonradiogenic Pb; 4) diffusion of major and trace components is slow; 5) it has a high closure temperature (about 750^{o}C), and 6) it has the potential to retain chemical and geochronological information through younger metamorphic events (Parrish, 1990). EMPA dating of monazite has the advantage of high spatial resolution (in the order of 5 μm or less), it provides geochemical data for elements other than U, Th and Pb, it is quick and relatively inexpensive compared with other methods, and is non-destructive (Cocherie et al., 1998). The major drawback is the lack of precision needed to tightly constrain the timing of geological events (Crowley and Ghent, 1999). This limitation is exacerbated in hydrothermal monazite because it typically has low Th and U contents (Overstreet, 1966; Smith et al., 1999). As a consequence, the

radiogenic Pb content is also low; close to or below detection limits in rocks younger than 100 Ma (Suzuki and Adachi, 1991; Montel et al., 1996).

In metamorphic rocks, most geochronological studies using monazite have concentrated on amphibolite to granulite facies rocks (e.g., De Wolf et al., 1993; Lanzirotti and Hanson, 1996; Cocherie et al., 1998; Crowley and Ghent, 1999; Williams et al., 1999; Foster et al., 2000; Rubatto et al., 2001; Engi et al., 2002; Kelsey et al., 2003) with little attention given to sub-amphibolite facies rocks. One of the reasons for this is that there has been a perception that monazite does not begin to form until amphibolite facies is reached (Smith and Barreiro, 1990; Harrison et al., 1990). However, there are a number studies that show that monazite can form at low temperatures, although for the most part, the studies are geochemical rather than geochronological. (e.g., Read et al., 1987; Milodowski and Zalasiewicz, 1991; Lev et al., 1998; Lev et al., 1999; Cabella et al., 2001). Wing et al. (2003) suggested that monazite may form within very low grade metamorphic rocks (i.e., before the formation of biotite) but once biotite begins to form, is replaced by allanite so that rocks within the biotite isograd of greenschist facies do not contain monazite. Geochronological studies of low temperature processes (i.e., diagenesis up to and including greenschist facies metamorphism, and hydrothermal events) using monazite are few but they show that monazite can be used to date these events (e.g., Evans and Zalasiewicz, 1996; Rasmussen and Fletcher, 2002).

6.3. Sample Selection and Monazite Morphology

Monazite from two heavy mineral separates, one from the Dome Sandstone (DS2), the other from the Rook Tuff, and four polished thin sections including two Dome Sandstone samples, one Dunns Mine Limestone and one from the Boorloo Dolomite were selected for EMPA to determine monazite ages. The aim was to determine the ages of metamorphism and hydrothermal events that may have affected the Curdimurka Subgroup.

Monazite is a common accessory mineral within the rocks of the Curdimurka Subgroup. In most examples, the form of the monazite and its occurrence (Figure 6.1) shows that while there may be some original sedimentary component, the euhdral form of most monazite crystals show post-depositional growth. In the Dome Sandstone, the majority of monazite is euhedral to subhedral. Figure 6.1a and 6.1b shows examples of euhedral monazite from a heavy mineral separate prepared from sample DS2. The majority of monazite from this sample is euhedral and the largest is about 200 μm in length. Figure 6.1c shows monazite growing on haematite and this in the only monazite in the Dome Sandstone that has a clear relationship with an obviously diagenetic mineral, in this case post-dating it. Figures 6.1d, 6.1e and 6f are more typical of monazite in the Dome Sandstone. Figure 6.1d is a euhedral monazite that may be entirely post-depositional whereas Figure 6.1e shows a monazite with a detrital core (De) and a post-depositional overgrowth having well-formed crystal face (Di). Figure 6.1f is an example of monazite in the Dome Sandstone initially growing on a pre-existing mineral and having well-formed crystal faces on open side. Monazite in finer grained units such as siltstone in the Dunns Mine Limestone (Figure 6.1g) and the

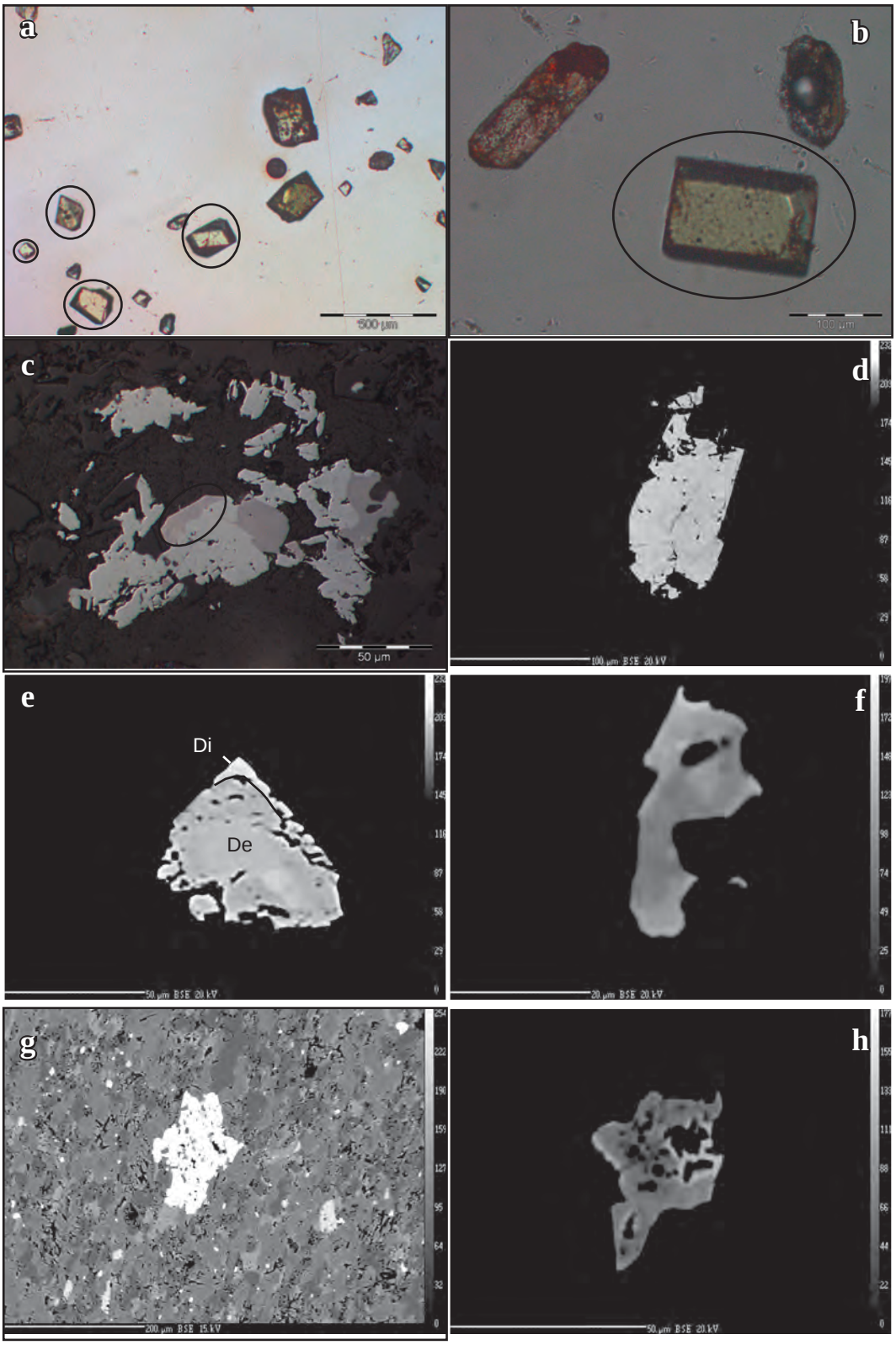

Figure 6.1 Monazite textures.
a and b) Photomicrographs of euhedral monazites (circled) from heavy mineral separates, sample DS2 (ppl). c) Photomicrograph of monazite (circled) growing on Fe-oxides sample 630713 (refl, ppl). d) BSE image of a large euhedral monazite in sample 630713. e) SEM image of a complex monazite. The solid core and surrounding zone have pre-depositional ages (De) but the paler euhedral face (Di) has a post-depositional age (see Figure 6.8 for calculated ages). f) BSE image of a suhhedral monazite from sample 630706. g) BSE image of anhedral monazite in siltstone, sample 630726. h) BSE image of anhedral monazite from sample 630694.

Boorloo Siltstone (Figure 6.1h) is poikolitic and anhedral, and typically smaller that than in the Dome Sandstone.

6.4 Methodology

The majority of samples were analysed using a CAMECA SX100 electron probe microanalyser housed in the Central Science Laboratory, University of Tasmania. The instrument is equipped with five WD spectrometers and was operated at 20kV accelerating voltage and a 100nA regulated beam current (faraday cup). A nominal spot size of 3μm was used.

All elements were acquired using a combination of TAP, LiF, and PET analysing crystals. Additional age sensitivity was achieved by using two-spectrometers for acquisition for Pb. Pb was measured on the Mβ peak to avoid the large Y overlap correction on the Mα peak.

X-ray lines were calibrated using a combination of synthetic oxides and minerals (J.M. Hanchar, pers. comm.), synthetic phosphates (Jarosewich and Boatner, 1991) and well-characterised natural minerals. Peak and background measurement positions were optimised to avoid line overlaps, and where unavoidable, were corrected using on- and off-line procedures. All lines were analysed in PHA differential mode to reduce background and high order overlaps. Data reduction and matrix corrections were performed using the PAP algorithm (Pouchou & Pichoir, 1984). Oxygen was calculated by stoichiometry.

The errors quoted in this work were estimated from counting statistics. Experiments indicated two additional sources of error that need to be considered. The Pb background is estimated using a curved background model based on points measured a long way from the Pb peak position. Experiments using pure phases indicate this adds an additional component to the background error of 0.25% of the background counts. In addition, the U background is estimated using a constant slope calculation from a measurement on only one side of the peak. This slope is dependent on the mean atomic number of the mineral analysed. Monazite varies by up to 2% in mean atomic number and experiments on pure metals indicate this produces a 1% variation in the slope of the line. These additional sources of error are included in the calculated standard deviation of Pb and U. The errors have been propagated through the age calculation using the rules for normally distributed errors (Barford 1985). They do not include any systematic errors associated with calibration, or the errors in decay constants. Instrument calibrations were checked regularly using a range of standard monazites analysed by other methods and laboratories including RGL4B (1566 ± 3 Ma, Rubatto et al. 2001) and 94-222 (467 ± 8 Ma, Hand et al. 1999). Based on these results, it is estimated that the systematic error is less than 0.5% in the ages quoted here. The systematic error has not been included in the errors, but must be considered where these ages are compared against ages from other laboratories and using other techniques. Weighted means and probability plots were calculated using ISOPLOT v3.00 (Ludwig 2003).

In addition to U, Th and Pb, Si, Fe, Ca, Y, La, Ce, Pr, Nd, Sm, Eu, Gd, Dy, Yb, Er, and P were analyzed. Additional elements Al, K and S were included to help identify contaminated

analyses. The assessment of K content for each analysis is critical, since the U analysis is very sensitive to interference from K. All analyses were screened closely based on stoichiometry, oxide totals, and contaminating elements to remove all inferior results. In addition, under the analytical conditions used, monazite grains with less than 1% Th have low radiogenic Pb and large uncertainties on the age.

Samples DS2 and RT1 were analysed using a Cameca SX50 electron probe microanalyser operating at 20kV and 100nA. The Cameca SX50 was equipped with 5 WDS spectrometers. All elements were acquired using a combination of TAP, LIF, and PET analysing crystals. Spot size was typically 5 microns. Standards are the same as with the SX100. Measurement procedure was identical except Pb was measured on one PET crystal only. The errors were calculated as for the SX100 except no additional errors were ascribed to measurement of background values. The counting errors have been propagated through the age calculation using the rules for normally distributed errors (e.g., Barford 1985). They do not include any systematic errors associated with calibration, or the errors in decay constants. The accuracy of the method was verified using a primary standard RGL04B (Rubatto et al. 2001) and range of in house standard monazites ages determined using independent isotopic methods (either SHRIMP or TIMS). The systematic error is estimated to be less than 1%. Weighted means and probability plots were calculated using ISOPLOT v3.00 (Ludwig, 2001).

The monazite ages are calculated using a series of statistical techniques. A linear probability plot is used to identify whether there is one or more age groups for each sample. Samples from a single population with a normal distribution will plot along a single linear trend whereas samples from different populations will plot above or below the trend above or below the linear trend at its lower or upper probability limits (Ludwig, 2003). Different populations are identified as having different trends.

Two methods are used to calculate the age of each population. The first is the probability density plot, which shows the cumulative probability distribution obtained by summing the probability distributions of a suite of data with normally-distributed errors (Ludwig, 2003). Peaks in the cumulative gaussian plot give the calculated age of a population, and mixed populations may have several peaks. The second method calculates the age of each population using the weighted average plot and calculation within the Isoplot program. It calculates the mean age and error based with a 95th confidence level, as well as the mean square weighted distribution (MSWD) and the probability. The CHIME method is used to show the level of support for the calculated age. In this method, isochrons are plotted for the calculated ages and plotted on a Th* versus Pb isochron diagram (Suzuki et al., 1991). A high level of support, is indicated by having multiple analyses plotting along the calculated isochron, with a wide range of Th* and Pb. A low level of support is indicated by either only having a few samples plotting on the isochron over a wide range, with a lot of scatter, or many samples with low Th* (say less than 2.0 wt% Th*).

6.5 Results

6.5.1 DS2 - Dome Sandstone

Sample DS2 is a grain mount, prepared for the zircon provenance study (Chapter 4) but with numerous monazite grains to 200 μm in diameter (Figure 6.1a,b). The monazite grains are yellow in colour with a euhedral habit. A total of 61 analyses were made on 16 monazites, with calculated ages ranging from 101 Ma to 1805 Ma. Th and Pb contents are typically low, with the highest being 6.696 wt% Th and 0.141 wt% Pb, and about 70% being less than 1 wt% Th. As a result, and because of the higher detection limits for the Cameca SX50, the errors are large, with an average one sigma error for the calculated age of ± 43%. As a first approximation, and ignoring error bars, 41 of the 61 (67%) analyses are younger than the age of the Rook Tuff, 802 ± 10 Ma (Fanning et al., 1986: i.e., interpreted as diagenetic/metamorphic in origin) and 20 are older (i.e., interpreted as detrital).

Figure 6.2 shows a linearized probability plot (6.2a), a probability density plot (6.2b), weighted average plots (6.2c) and isochron plots for the calculated ages for DS2 (6.2d). The linearized probability plot can be interpreted as indicating that there are three age groups younger than 802 Ma. Support for this division is provided by the probability density plot (and accompanying histogram) which has a peak at about 411 Ma, with a shoulder at 529 Ma, with a third peak in the histogram at about 750 Ma. The calculated weighted average ages for the three groups are; 403 ± 32 Ma (MSWD 0.064), 536 ± 63 Ma (MSWD 0.23) and 660 ± 70 Ma (MSWD 0.34). The isochron plot shows that the younger age is well defined by a range of Th* and Pb levels whereas the older ages are less-well supported, with lower variation of Th* and Pb. In particular, the 660 Ma age is calculated from a very limited Th* range, hence the relatively high calculated one sigma error.

6.5.2 630706 - Dome Sandstone

Sample 630706 is a sandstone from the Dome Sandstone, intersected in diamond core drill hole WD034. Monazites are typically euhedral, with the largest being about 40 μm in diameter, and most analysed having a diameter of about 20 μm.

A total of 16 analyses were conducted on six monazites. The ages range from 416 Ma to 1363 Ma, with 9 of the 16 (56%) younger than 802 Ma. The maximum Th content is 8.517 wt% Th, with no analysis below one wt% Th*, leading to an average one sigma error on the age of ± 5%.

Figure 6.3 shows a linearized probability plot, a probability density plot, and isochron plots for 630706. The linearized probability graph suggests that there are three groups, from 416 Ma to 691 Ma (although this group was further divided into two subgroups, a and b as the MSWD for the combined group was high; Figure 6.3c), 890 Ma to 1010 Ma and 1196 Ma to 1362 Ma but only the first group has sufficient analyses to consider further. The probability density plot has a largest peak at 494 Ma but each peak represents two or three analyses at best and so overall the analyses from 630706 by themselves are not significant.

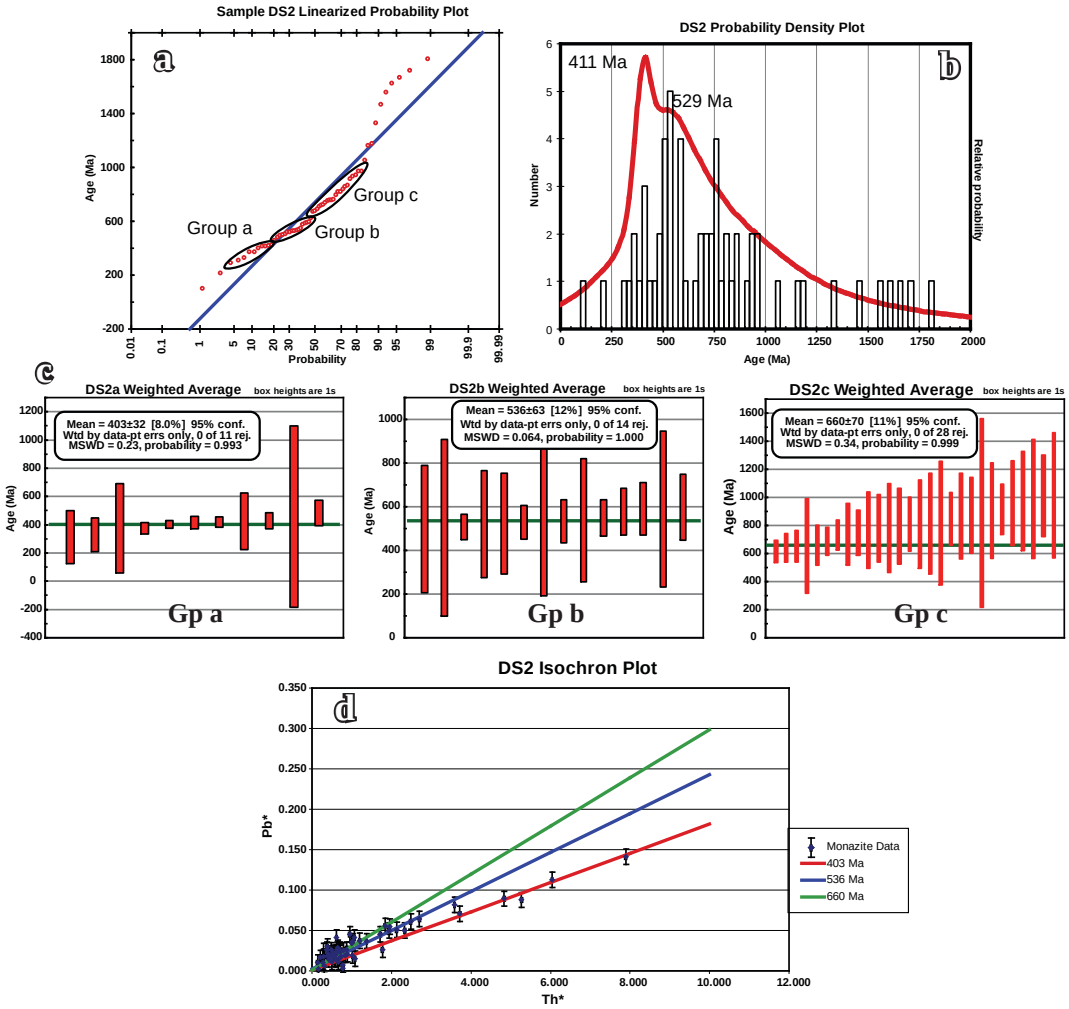

Figure 6.2. Sample DS2 Monazite age results.
a) Linear probability plot defining three age groups. b) Probability density plot. The main peak is at 411 Ma with a small peak at 529 Ma. The histogram shows a group of samples about 650 Ma that is not represented in the probability density line. c) Weighted probability plots calculated for the groups defined in a). d) Th* vs Pb isochron diagram showing that the 403 Ma age is supported by six analyses with a good range of Th* and Pb. The 536 Ma age is less-well supported although comprising eight analyses but with a limited range of Th* and Pb. The 660 Ma age is supported only by samples with low levels of Th*.

Two isochrons are calculated, for the 501 Ma and 642 Ma age calculated by the weighted average plot.

6.5.3 630713 - Dome Sandstone.

Sample 630713 is a haematitic sandstone from the Dome Sandstone, intersected in diamond core drill hole, WD016 at a depth of 292.5 m. A total of 27 analyses were completed on four monazites. Of the 27 analyses, four were discarded as bad assays.

Figure 6.4 shows a linearized probability plot, a probability density plot, weighted average plots and isochron plots for the calculated ages for 630713. The linearized probability graph shows three populations; 446 Ma – 553 Ma; 639 Ma – 796 Ma; and 1564 – 1599 Ma, with a scatter of ages between 796 Ma and 1564 Ma and an outlier at 1750 Ma. The probability density graph for 630713 has a major peak at 512 Ma, with a smaller peak at 1576 Ma, There is a smaller peak on the side of the main peak at 441 Ma, and a small peak

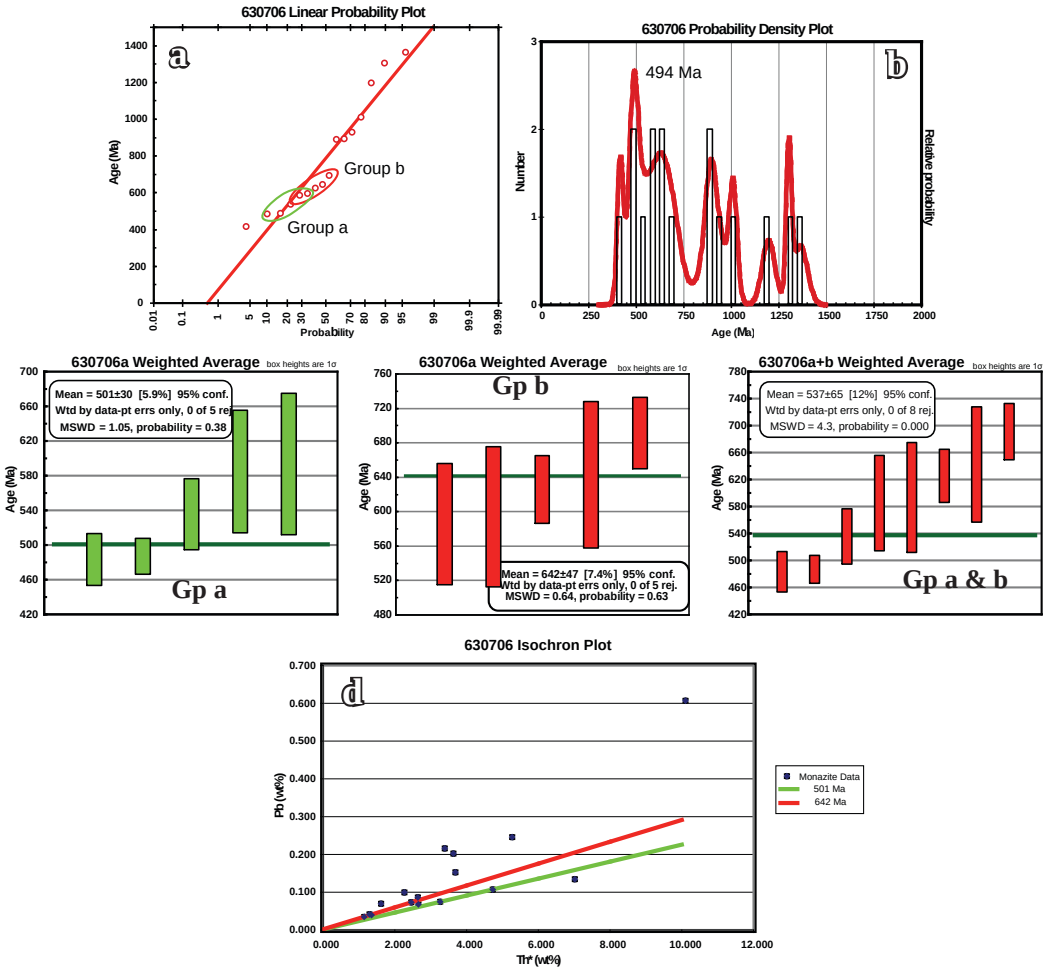

Figure 6.3. Sample 630706 monazite age results.
a) Linear probability plot. Two overlapping groups are selected; the first (green circle) from 483 Ma to 594 Ma and the second (red circle) from 536 Ma to 643 Ma. b) Cumulative probability plot. The largest peak is at 494 Ma, otherwise each peak represent only one or two analyses and are not significant. c) Weighted probability plots for the groups identified in a. The younger group (c1) has a calculated average age of 501 Ma and the older group (c2) has a calculated average age of 648 Ma. Extending the calculation to include all eight analyses (c3), gives a weighted average age of 537 ± 65 Ma, with a MSWD of 4.3. d) Th* vs Pb isochron diagram showing that the ages derived are based on only a few analyses.

at 644 Ma with a shoulder at 718 Ma. Weighted average ages of the three groups are; 511 ± 13 Ma, (MSWD 0.78 and a probability of fit of 0.64); 689 ± 35 Ma, (1.3, 0.19) and 1578 ± 25 Ma (0.39, 0.76). The calculated isochron for 510 Ma intersects six points over a range of Th* from about 2.5 wt% to about 9 wt%, providing good support for this age. There is a smaller range in Th* for the calculated 689 Ma isochron and it intersects fewer points but it appears to be valid albeit with large error bars, and the calculated 1578 Ma isochron is dominated by the four samples from which the weighted average is calculated.

6.5.4 RT1 - Rook Tuff.

Sample RT1 was prepared as two grain mounts, with 15 yellow, euhedral monazite grains to 200 μm in diameter. A total of 48 analyses were made on 11 monazites, with ages ranging from 279 Ma to 1662 Ma. Th contents are variable with a maximum of 6.307 wt% Th and 20% of assays less than 1% Th. The average one sigma error on the calculated ages is ± 17%. A total of 29 (60%) analyses are less than 802 Ma and so are likely diagenetic or

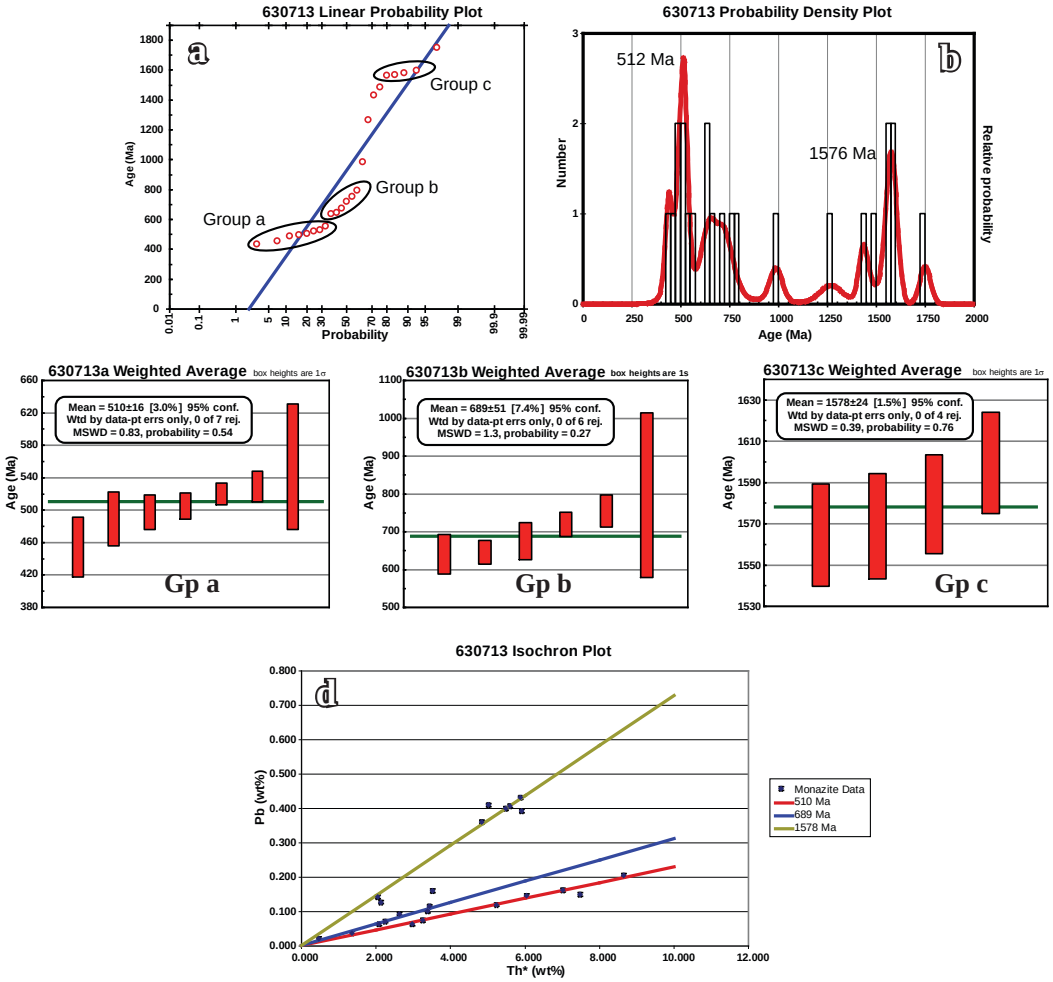

Figure 6.4. Sample 630713 monazite age results.
a) Linear probability plot defining three age groups with a scattering of ages between the second and third group, and one outlier. b) Probability density plot. The 512 Ma and 1576 Ma age peaks represent sufficient analyses to be significant whereas the remaining peaks represent scattered single analyses. c) Weighted average plots for the three age groups identified in a). d) Th* vs Pb isochron diagram showing that the calculated 510 Ma isochron intersects seven analyses with a wide range in Th* and Pb. The 1578 Ma isochron is supported by four analyses between 5 and 6 wt% Th*. The 689 Ma isochron is supported by six analyses all with Th* less than 4 wt% Th*.

related to hydrothermal or metamorphic events, the remainder being older, and are likely detrital (ignoring error bars). Of the 8 monazites with three or more analyses, two give only detrital ages with the remainder giving both detritral and post-depositional ages. None give solely post-depositional ages.

Figure 6.5 shows the statistical analysis for calculating the monazite ages for sample RT1 comprising a linearized probability plot (Figure 6.5a), a probability density plot (Figure 6.5b), weighted average plots (Figure 6.5c) and isochron plots for the calculated ages (Figure 6.5d). The linearized probability graph indicates there are at least three populations; 279 Ma – 695 Ma; 810 Ma – 963 Ma; and 1044 Ma – 1101 Ma, with a fourth group, a', containing four analyses that are interpreted to be separate from group a. There are also four points older than 1101 Ma, but these are not considered further here. The probability density plot shows a peak at 535 Ma, a second peak at 1076 Ma, with a small peak at 1641 Ma that represents two analyses. Weighted average ages of the four groups are; 514 ± 26 Ma (MSWD = 1.06, probability 0.15); 667 ± 110 Ma (0.088, 0.999); 873 ± 110 Ma (0.088,

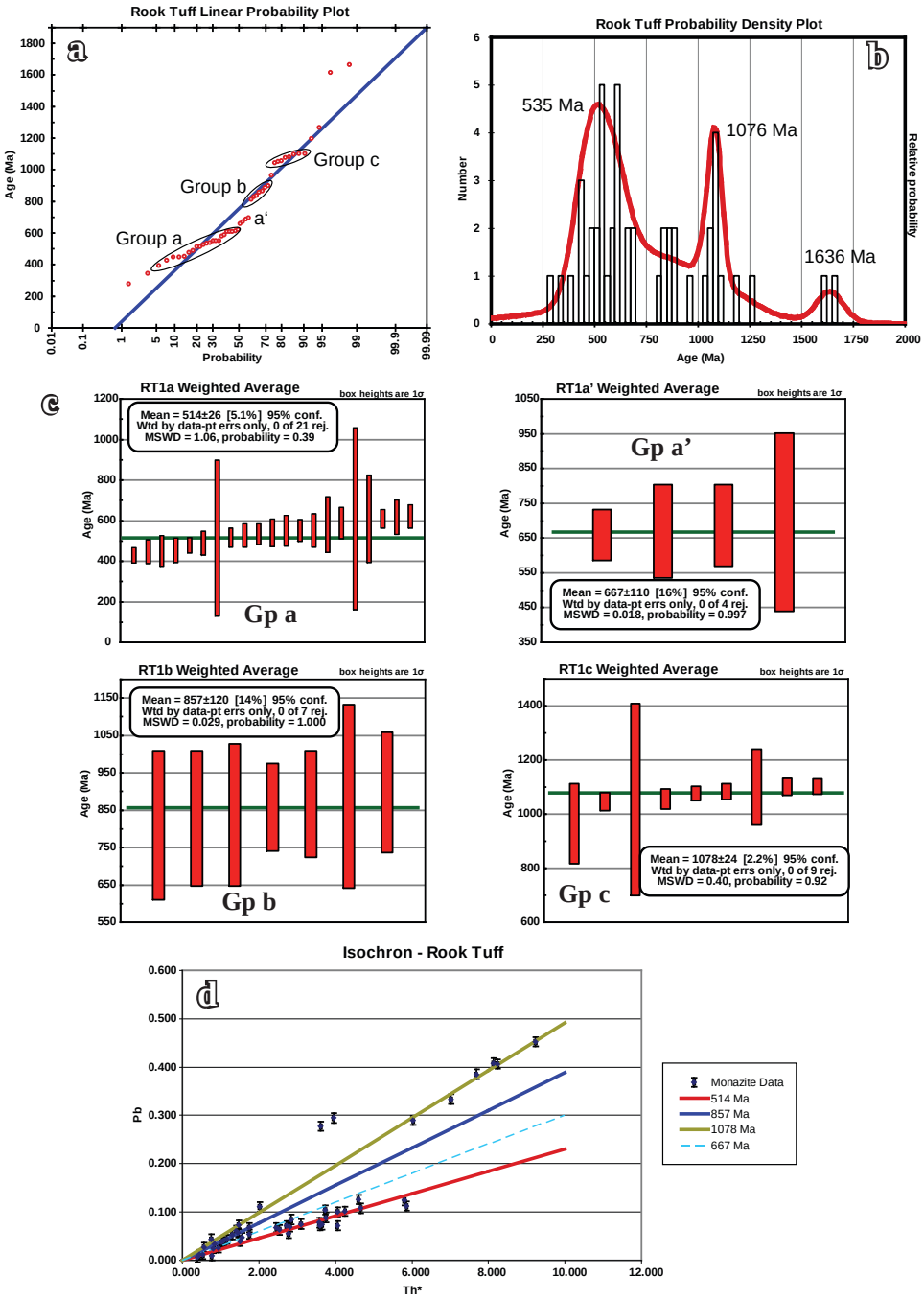

Figure 6.5. Sample RT1 Monazite age results.
a) Linear probability plot defining three age groups. b) Probability density plot shows a peak at 535 Ma and a smaller peak at 1076 Ma. c) Weighted probability plots calculated for the groups defined in a). d) Th* vs Pb isochron diagram showing that the 515 Ma and the 1079 Ma ages are supported by a number of analyses with a good range of Th* and Pb, although there is some scatterer around the 515 Ma isochron. The calculated isochrons for the 667 Ma and 857 Ma isochrons show that these are supported only by low Th* and Pb analyses.

0.999); and 1079 ± 25 Ma (0.37, 0.92). Group a' is not within error of group a and so is likely a separate population. The isochron diagram shows that the 514 Ma age has some support with a number of analyses in the range of 2 to 6 wt% Th*, although there is still a degree of scatter of the points. A wide variation in Th* and a good fit of the data to the calculated isochron for the 1078 Ma age provides good support for this age also. The 873 Ma age has limited support, with low Th* which is reflected in the large error.

6.5.5 630726 - Dunns Mine Limestone.

Sample 630726 is interlaminated limestone - siltstone from the Dunns Mine Limestone, from diamond drill hole WD34, at a depth of 99.5 m. Monazites are uncommon in this sample, and are found only in siltstone beds. They are anhedral and up to 50 μm in diameter.

A total of 21 analyses were conducted on eight monazites. There is little variation in the Th content, the maximum being 1.687wt% Th and the minimum, 0.700wt% Th. The average error to one sigma on the age is ± 0.16%. The ages are spread over about 300 Ma, with three groupings; two older ages, a group of younger ages less than 350 Ma, and in between a smearing of ages from 400 Ma to 538 Ma, with minimum error of 50 Ma.

The linearized probability plot (Figure 6.6a) shows one group of 15 ages (group b), with two older and four younger outliers (group a). The probability density plot (Figure 6.6b) has only one peak at 460 Ma. For group a the weighted average is 346 ± 68 (MSWD = 0.052, probablility = 0.99) and for group b 460 ± 33 Ma (0.44, 0.96: Figure 6.6c). For all of the ages, the weighted average is 449 ± 33 Ma (1.18, 0.26) but if the upper two ages are

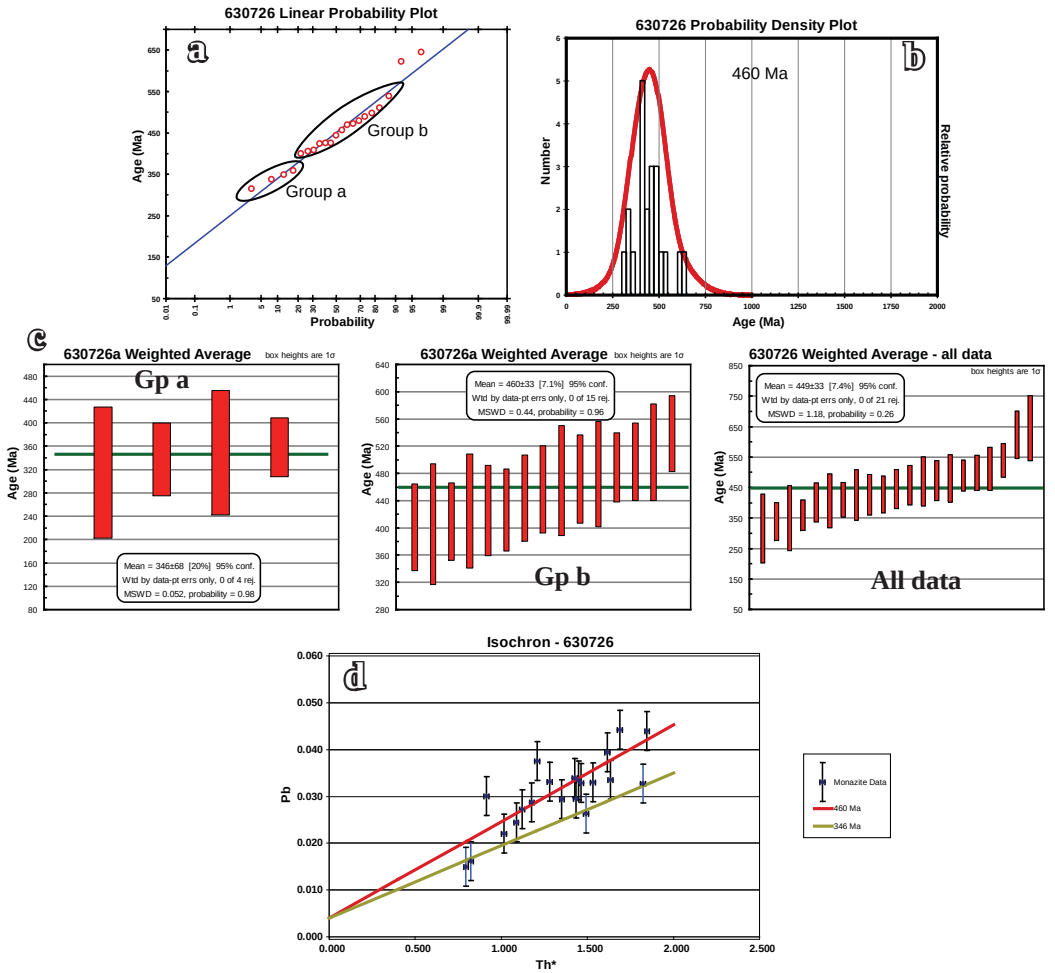

Figure 6.6. Sample 630726 monazite age results.
a) Linear probability plot showing that there is one main age group with a smaller younger group and two older outliers. b) Probability density plot showing only one peak at 460 Ma. c) Weighted average plots. The first two plots are for the groups identified and the the third includes all the data. d) Th* vs Pb isochron diagram with isochrons calculated for 460 Ma and 346 Ma. The low Th* and Pb contents give large errors, but the 346 Ma isochron is supported by the four samples in the group and the 460 Ma age is also supported by 13 analyses, but there is some overlap between the two isochrons.

excluded the weighted average age is 439 ± 30 (0.83, 0.66). The isochron diagram shows that there is only a small amount of Th* overall, with correspondingly low Pb levels. Two isochrons have been calculated; 460 Ma and 346 Ma, but with y-intercepts of 0.004 which is the average detection limit of Pb for sample 630726. It provides a better fit for both calculated isochron, the 346 Ma ischron passing through the four samples of group a (in blue) and the 460 Ma isochron passing through all but one sample of group b and suggests that there may have been common lead present at levels below detection limits (i.e., 40 ppm Pb). It is only significant in this sample because of the overall low Th, U and Pb contents.

6.5.6 630694 - Boorloo Siltstone

Sample 630694 is from the Boorloo Siltstone, from drill hole WD034 at a depth of 101.6 m. It is a siltstone from near the base of the Boorloo Siltstone, adjacent to the West Willouran Fault. There is a zone parallel to bedding with subhedral to anhedral monazites to 50 μm in diameter and outside of this are scattered anhedral monazites to 20 μm.

A total of 29 analyses from 16 monazites are reported here. The ages range from 271 Ma to 1600 Ma, with 17 of the 29 (59%) younger than 802 Ma. Highest Th reported is 6.509 wt%, with 17 below 1 wt% Th. The average error on the calculated ages is ± 22%.

The linearized probability graph indicates that there are three populations with outliers at either end (Figure 6.7a). The probability density plot (Figure 6.7b) has its major peak at 541 Ma, with smaller peaks at 871 Ma and 941 Ma. Weighted average ages for the three groups are; group a, 533 ± 27 (MSWD = 0.43 probability = 0.92); group b, 851 ± 33 Ma (0.96, 0.48); and group c, 956 ± 33 Ma (1.08, 0.36). A calculated isochron for 538 Ma passes through seven points between 1.5 and 4 wt% Th* (within the average error bars). The calculated isochron for 723 Ma intersects only two points about 1 wt% Th* and the calculated isochron for 906 Ma passes through only two points above 1 wt% Th*, providing poor support for these ages (Figure 6.7c).

6.6. Age Relationships Within Individual Monazites

The age relationships within samples and individual monazites are complex. Only sample 630726 has monazite ages that are wholly post-depositional, with monazites having grown within siltstone/shale beds. Otherwise each sample has monazites with a combination of pre- and post-depositional ages. Monazite B from sample 630713 is an example of a monazite that gives mostly pre-depositional ages with a small post-depositional overgrowth but in the same sample, monazite A gives only post-depositional ages with over 250 Myrs variation (Figure 6.8). Sample 630706 shows the complexities not only within a single sample but within individual monazite (Figure 6.9). Each monazite shown has pre- and post-depositional ages typically showing a range of ages in each monazite. The only exception is monazite b, which in-fills pore space and returns similar ages from two spots.

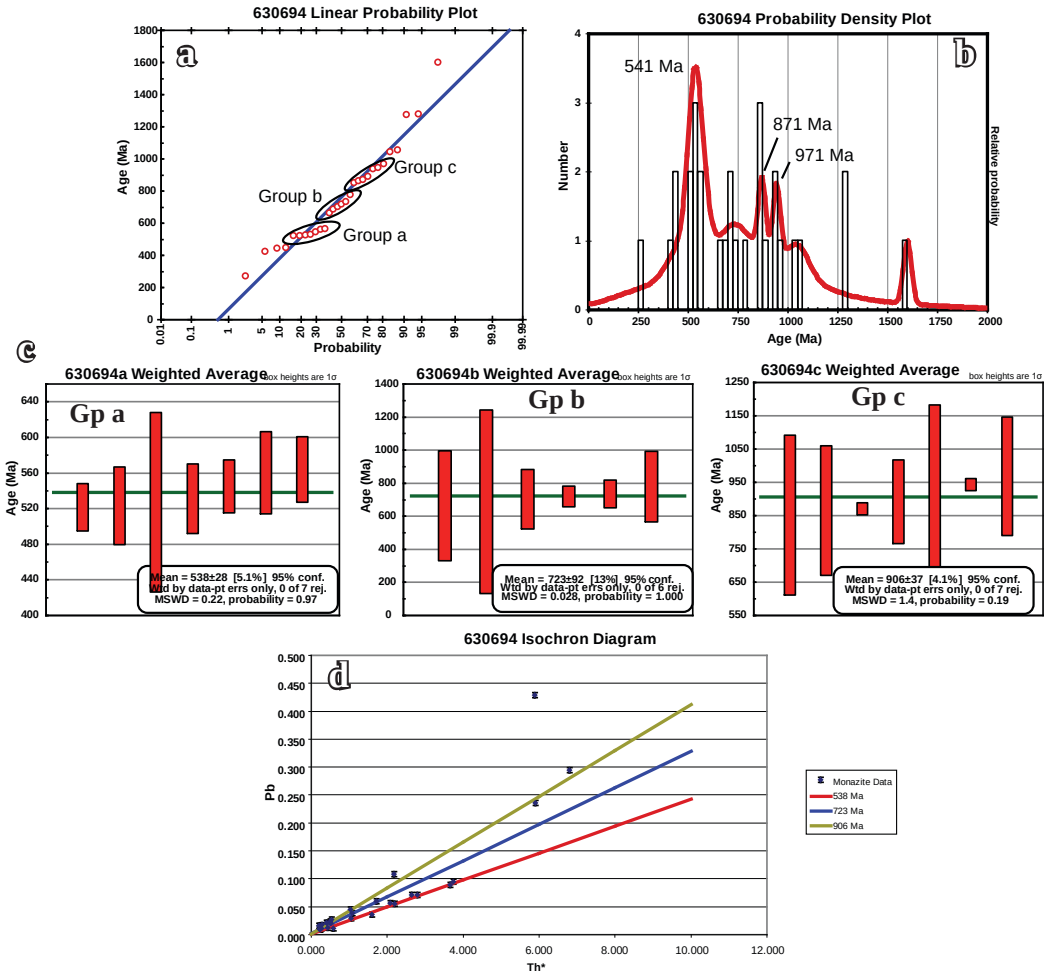

Figure 6.7 Sample 630694 monazite age results.
a) Linear probability plot showing three age groups with older and younger outliers. b) Probability density plot. The major peak is at 541 Ma with smaller peaks at 871 Ma and 971 Ma. c) Weighted probability plots for the groups identified in a). d) Th* vs Pb isochron diagram showing that the calculated isochron for the 538 Ma age passes through seven points although with a limited range of Th*. Otherwise, the 723 Ma isochron is supported only by low Th* monazites and the 906 Ma is not supported.

6.7. All Age Data Combined.

The ages calculated for the individual samples gave similar ages (Table 6.1) but most of these ages rely on a small number of sample sites which limits statistical analysis. Because the different samples have similar ages and because the rocks come from the same area and were subject to the same processes, either metamorphic or hydrothermal, combining the data may provide more precise and reliable ages. To better define the ages, all the data are combined and subject to the same analysis. The cumulative probability graph (Figure 6.10a) has a major peak at 521 Ma, and a small shoulder at 441 Ma. There are a series of small peaks at 864 Ma, 944 Ma and 1076 Ma, with another peak at 1579 Ma. The linearized probability graph (Figure 6.10b) shows five major groups; < 371 Ma; 399 Ma to 564 Ma, 577 Ma to 970 Ma; 987 Ma to 1485 Ma; and > 1564 Ma.

For each group, a linearized probability graph was prepared to see if the group all belonged to the one population or if it should be split further (Figure 6.11a). Group 1 (< 371 Ma; Figure 6.11a) contains a few outliers but otherwise it cannot be split further. The weighted

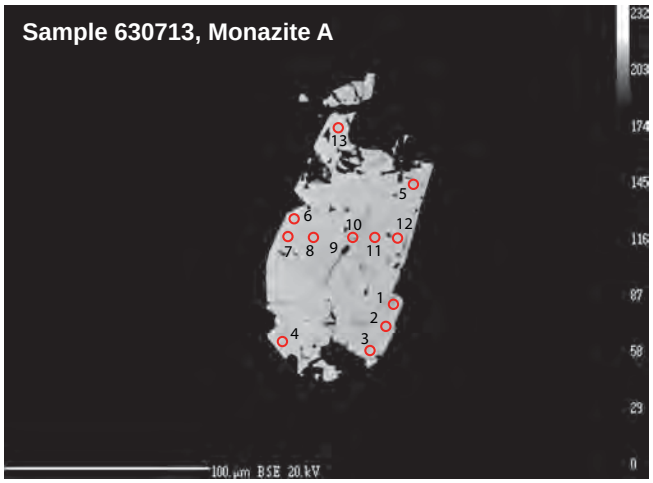

1 529 ± 19
2 497 ± 22
3 719 ± 32
4 754 ± 42
5 454 ± 37
6 504 ± 16
7 489 ± 33
8 553 ± 78
9 568 ± 46
10 796 ± 218
11 674 ± 50
12 436 ± 15
13 645 ± 32

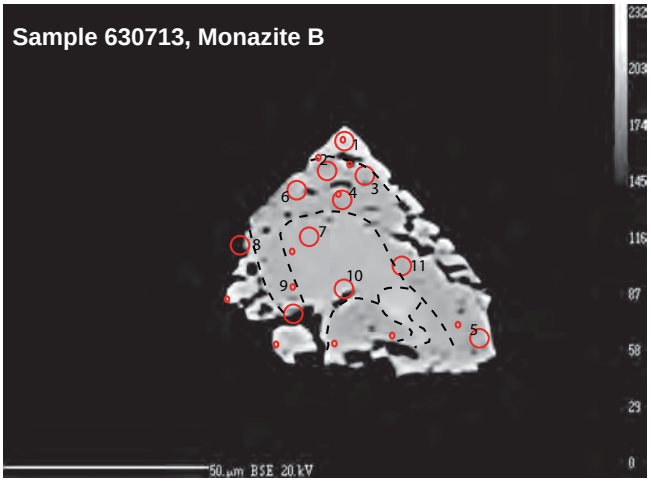

1 520 ± 14
2 1485 ± 60
3 1268 ± 57
4 1564 ± 25
5 1569 ± 26
6 1579 ± 24
7 1434 ± 22
8 bad analysis
9 bad analysis
10 810 ± 22
11 987 ± 32

Figure 6.8. Examples of variations of monazite ages in single monazites from the Dome Sandstone.

a) Both of the monazites shown here are from sample 630713. Monazite A ages indicate that it formed post-deposition, although the possibility that it contains a detrital core cannot be ruled out. Monazite B is mainly detrital with a range of ages older than the depositional age but with one post-depositional age and one age at about the time of deposition. The red circles are approximately the beam diameter.

average age for group 1 including the outliers is 348 ± 49 Ma (0.19, 0.998: Figure 6.11b). A calculated isochron for 348 Ma passes through all points on the Th* plot.

Group 2 (399 Ma – 564 Ma; Figure 6.12) likely contains two groups (2a and 2b: Figure 6.12a), and the cumulative probability density plot has two peaks, 439 Ma and 508 Ma (Figure 6.12b). A weighted average age for the entire group was calculated, which gave a result of 488 ± 11 (MSWD = 1.5, probability = 0.003). The MSWD is high, suggesting that the error is over-estimated for the entire group and so it may be split further. Using the Unmix Ages function of Isoplot (Lugwig, 2003), the optimal solution was two ages, 429 ± 9 Ma and 509 ± 5 Ma, with a relative misfit of 0.951. The probability graph suggests that the best split is between 456 Ma and 469 Ma, and the two groups return weighted average ages of 425 ± 16 Ma (0.17, 1.000) and 514 ± 10 Ma (0.35, 1.000; Figure 6.12c). These are within error of the ages calculated from the Unmix Ages function. As a final check, Th* was plotted against Pb, and isochrons calculated for each age returned by the Unmix Ages function (Figure 6.12d). Most of the data plot on either of the isochrons within analytical

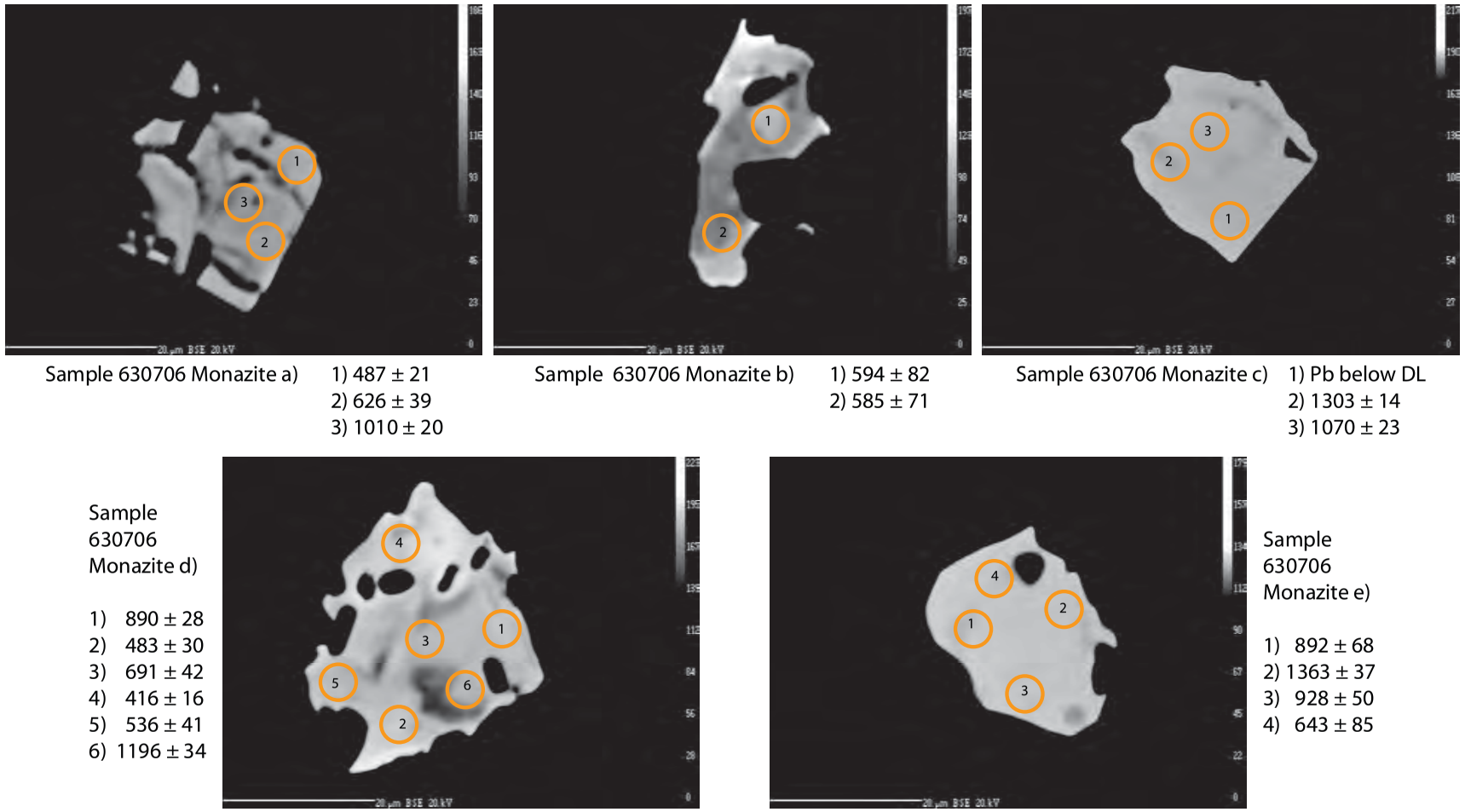

Figure 6.9. Individual monazite ages from sample 630706.
These monazites show large variations in age, except for monazite b which from its anhedral form, appearing to in-fill space may be wholly post-depositional.

Table 6.1. Comparison of calculated ages for each sample group.
All samples have weighted average ages within error of the age derived from the probability density plot. All but 630726 have a weighted average age between 494 - 535 Ma and two (different) samples have ages between 400 - 440 Ma, 660 - 690 Ma and 851 - 873 Ma.

	Probability Density Plot Peaks	Weighted Average Age	MSWD	Probability
DS2 - Dome Sandstone				
Group 1	411 Ma	403 ± 32	0.064	
Group 2	529 Ma	536 ± 63	0.23	
Group 3		660 ± 70	0.34	
630706 - Dome Sandstone				
Group 1	494 Ma	501 ± 30	1.05	0.38
630713 - Dome Sandstone				
Group 1	494 Ma	511 ± 13	0.78	0.64
Group 2		689 ± 35	1.3	0.19
Group 3		1578 ± 25	0.39	0.76
RT1 – Rook Tuff				
Group 1	535 Ma	514 ± 26	1.06	0.15
Group 2		873 ± 110	0.088	0.999
Group 3	1076 Ma	1078 ± 24	0.37	0.92
630726 - Dunns Mine Limestone				
Group 1	460 Ma	439 ± 30	0.83	0.66
630694 - Boorloo Siltstone				
Group 1	541 Ma	533 ± 27	0.43	0.92
Group 2	871 Ma	851 ± 33	0.96	0.48
Group 3	971 Ma	956 ± 33	1.08	0.36

error, with an overlap of ages and errors at the low Th* and Pb end of the graph, so this also provides support for the two ages in Group 2.

Group 3 contains 75 analyses (Figure 6.13a). It has a weighted average age of 789 ± 30 Ma (MSWD = 3.6, probability = 0.0), and the probability density plot has two peaks, 657 Ma and 869 Ma (Figure 6.13b) suggesting that it can also be split further. There is a break at about 763 Ma (Figure 6.13a) dividing the data into two groups. Group 3a returned a weighted mean average of 662 ± 22 (0.45, 0.999) and group 3b has a weighted mean average of 911 ± 20 Ma (0.59, 0.96). The Unmix Ages function gives three ages; the first with 56% of the data returns an age of 658 ± 25, the second 705 ± 53 Ma (22% of data) and the third 902 ± 11 Ma (22% of data), with a relative misfit of 0.836. There is a reasonable agreement between the weighted mean averages calculated from a straight split of the data and the Unmix Ages function, except for the 705 Ma age calculated by the Unmix Ages function. An isochron plot supports the younger and older ages and shows that the 705 Ma age takes in three moderate Th* analyses that fall between the older and younger isochrons (Figure 6.13d).

Group 4 contains 27 analyses. A linear probability plot suggests that it can be split into two groups; a tight grouping of 987 Ma – 1101 Ma, and a series of clusters between 1164 Ma and 1485 Ma (Figure 6.14a). The probability density plot has three peaks, 1077 Ma,

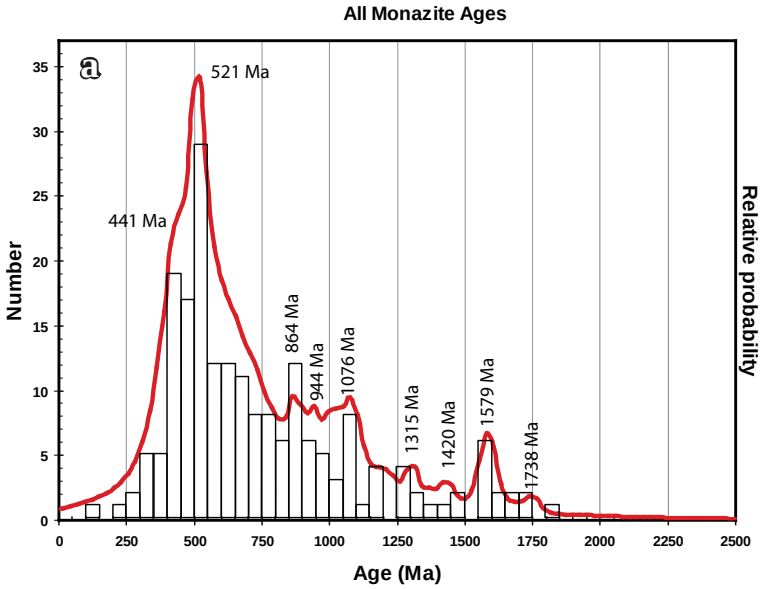

Probability Density Plot for all monazite ages.

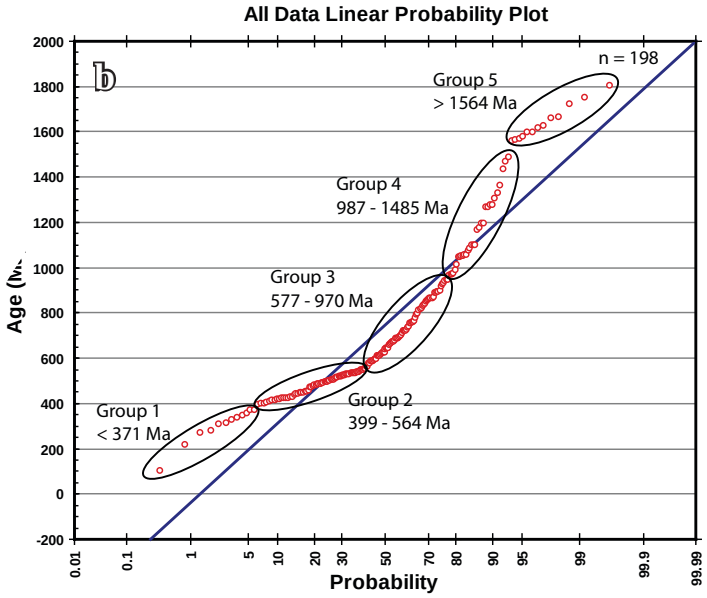

Linear Probability Diagram for all monazite ages.

Figure 6.10. All monazite ages.

a) The probability density plot has a main peak at 521 Ma, with a shoulder at 441 Ma. b) The linear probability plot identifies five age groups.

1302 Ma and 1435 Ma (Figure 6.14b). Group 4a has a weighted average age of 1053 ± 20, (MSWD = 1.3, probability = 0.20) but excluding the youngest age of 987 Ma, the weighted average age of 1060 ± 21 (0.99, 0.45; Figure 6.14c). The remaining data has a weighted mean average of 1329 ± 45 (6.0, 0.0), suggesting that this group can be split further. Two clusters from 1164 Ma to 1329 Ma when grouped together have a weighted average age of 1284 ± 26 Ma (1.05, 0.40; Figure 6.14c). The final four ages have a weighted average age of 1421 ± 66 Ma (1.3, 0.27; Figure 6.14c). The Unmix Ages function returns three ages, 1054 ± 10 Ma (62% of data), 1290 ± 12 Ma (24%) and 1429 ± 23 Ma (14%), which agrees within error with the ages calculated above. Calculated isochrons for the ages calculated by the Unmix Function diagram provides good support of the younger age and shows that the older two ages are defined only by three points each (Figure 6.14d).

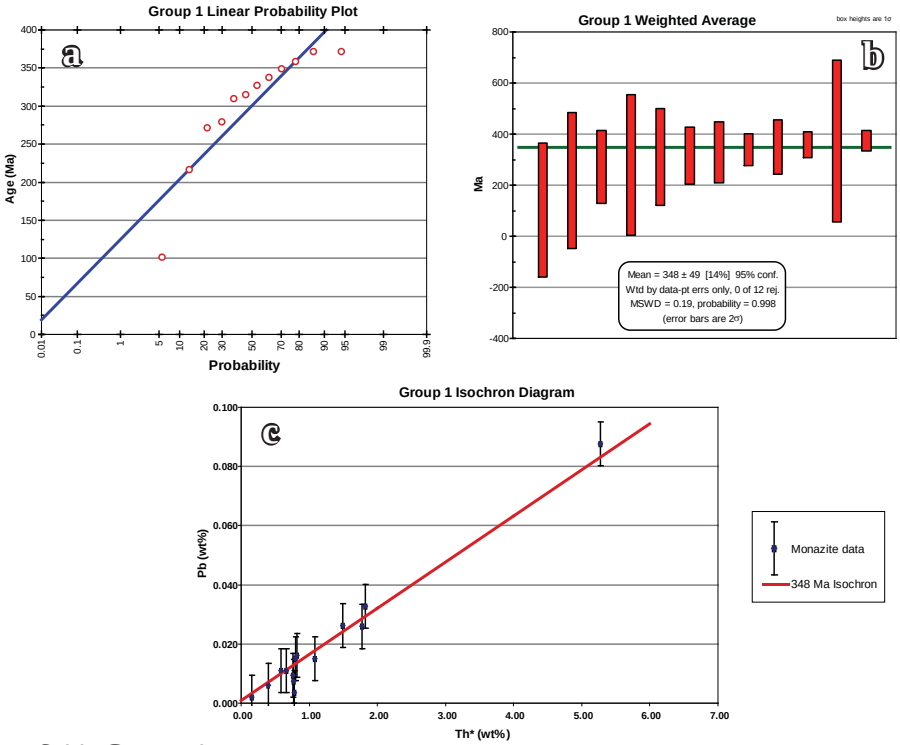

Figure 6.11. Group 1 ages.
a) The linear probability plot shows that there are two younger outliers with the bulk of the ages older than 260 Ma. b) The weighted average age is 348 ± 49 Ma. c) An isochron diagram shows good support for the 348 Ma isochron although only one sample has Th* greater than 6wt%.

The fifth group contains 13 ages, which have a weighted average age of 1607 ± 35 Ma (MSWD = 2.8, probability = 0.001). A linear probability plot (Figure 6.15a) has a group of ages from 1558 Ma to 1665 Ma (Figure 6.15a), with a weighted average age of 1587 ± 20 (0.43, 0.92) with three older outliers, group 5b, that has a weighted average age of 1754 ± 54 Ma (0.0057 0.994). The isochron diagram shows that the group 5a has good support with five analyses greater than 3 wt%Th* (Figure 6.15c). The Unmix Ages function returns two ages, 1587 ± 10 (86% of data) and 1747 ± 28 (14%), with a relative misfit of 0.865, which is in agreement with the above ages. An isochron diagram provides further support for this division.

As a final check of the ages calculated above, the ages less than 802 Ma, that is those that are post-depositional, were subject to the Unmix Ages function. It returned ages of 424 ± 9 (22% of data), 514 ± 6 (62%) and 671 ± 15 (16%), which, except for the younger ages of group 1, is within error of the ages calculated in groups 1, 2 and 3 (Table 6.2). For the ages older than 802 Ma, which are likely detrital, the Unmix Ages function returned six ages; 906 ± 12 (29%), 1052 ± 11 (40%), 1290 ± 14 (10%), 1427 ± 25 (4%), 1585 ± 10 (15%) and 1747 ± 28 (2%), all of which agree closely with the ages calculated in groups 3, 4 and 5 (Table 6.2).

6.8. Discussion

The discussion will focus on ages less than 802 Ma, which reflect monazite growth after deposition, during diagenesis and metamorphism. Post-deposition, the Curdimurka Subgroup has been affected by a number of tectonic events (Figure 6.16). These include

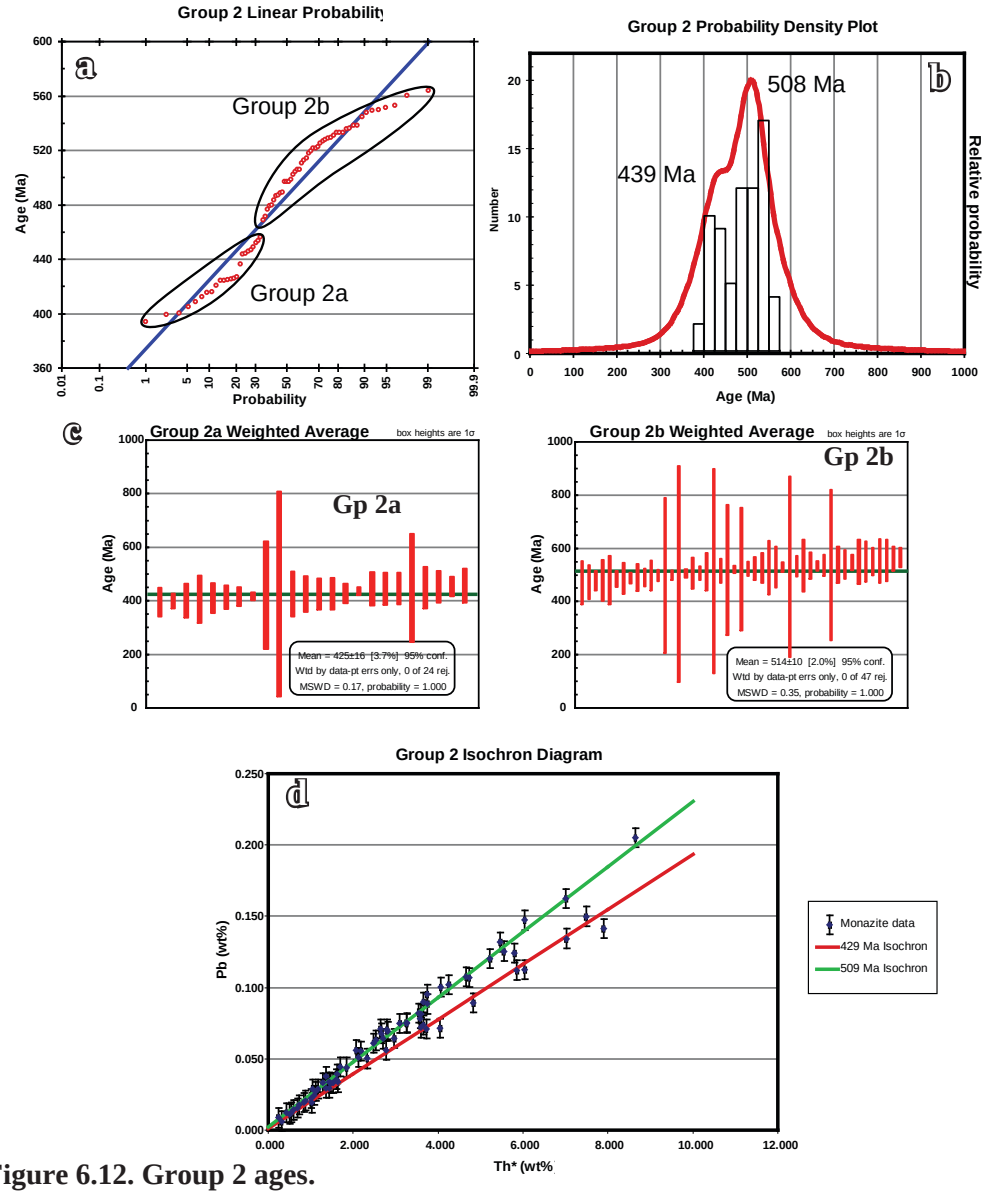

Figure 6.12. Group 2 ages.

a) The linear probability plot suggests that group 2 may be broken down into two subgroups with the division at about 460 Ma. b) A probability density plot for Group 2 shows a main peak at 508 Ma with a shoulder at 439 Ma. c) Weighted average plots for subgroups 2a and 2b. d) The isochron diagram shows that there is good support for each age with a wide range in Th* and Pb.

extension at the beginning of deposition of the Burra Group at about 777 Ma, extension at the beginning of deposition of the Umberatana Group at about 725 Ma (based on age comparisons with Sturt glacial rocks elsewhere), extension at the beginning of deposition of the Wilpena Group at about 600 Ma and finally compression during the Delamerian Orogeny, from about 530 Ma to 500 Ma. At Arkaroola, the British Empire Granite was intruded at about 450 Ma (Elburg et al., 2002). Further afield, the Petermann Orogeny which affected the Musgrave Block occurred at about 560 Ma, and the Alice Springs Orogeny which affected the Arunta Block and the remnants of the Centralian Superbasin (the Amadeus Basin, the Georgina Basin, the Ngalia Basin and the Wiso Basin) occurred in three stages between about 450 Ma to 310 Ma (Hand et al., 2001). In addition, based on Sr isotopes, Foden et al, (2001) suggested that the Adelaide Fold Belt was subject to a basin-wide fluid flow event at 586 ± 30 Ma, which they attributed to rift development at that time.

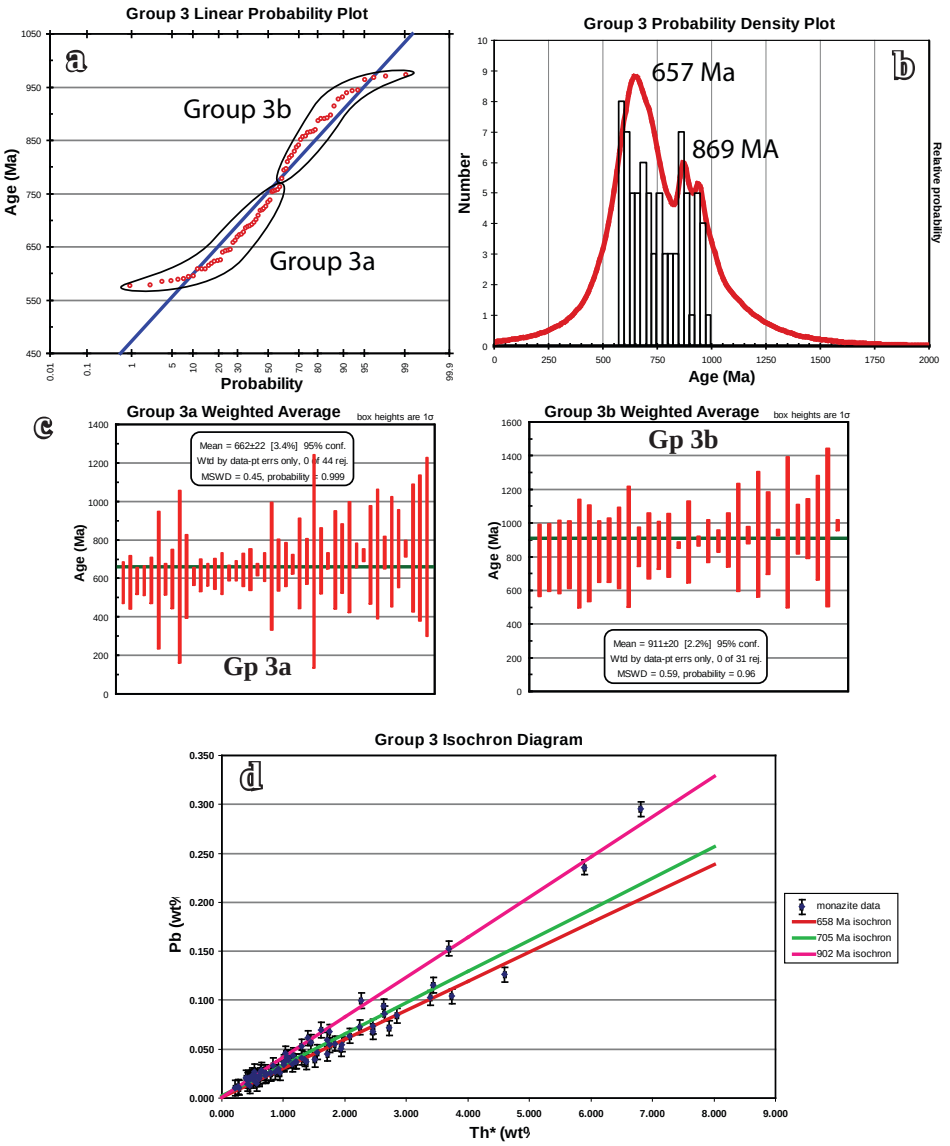

Figure 6.13. Group 3 results.
a). Linear probability plot showing that group 3 may be divided into two sub-groups at about 765 Ma. b) Probability density plot showing two peaks, the larger at 657 Ma and the smaller at 869 Ma. c) Weighted average plots for the two sub-groups, give ages of 662 ± 22 Ma and 911 ± 20 Ma. d) Isochron diagram with isochrons calculated for ages determined using the Unmix program. Most of the support for the 658 Ma and 705 Ma isochrons come from low Th* analyses but there is some support for the 902 Ma isochron over a range of Th*.

The monazite ages calculated here then can be ascribed to several events. The youngest age (348 ± 49) Ma is within error of a period of moderate cooling between 330 – 325 Ma, obtained by McLaren et al. (2002b) from K-feldspar thermal modelling of K-Ar and Ar-Ar dating, on feldspars from pegmatites at Arkaroola. Gibson and Stuwe (2000) suggested that the Southern Adelaide Fold Belt cooled through temperatures greater than between 90° – 120°C at about 350 Ma, based on apatite fission track dating. They proposed that this cooling is related to exhumation in the last stages of basin inversion during the Delamerian Orogeny. Hartley et al. (1998) and Mitchell et al. (1998) also found evidence of cooling in the Broken Hill region and the Curnamona Province at about this time, which they attributed to the waning stages of the Alice Springs Orogeny.

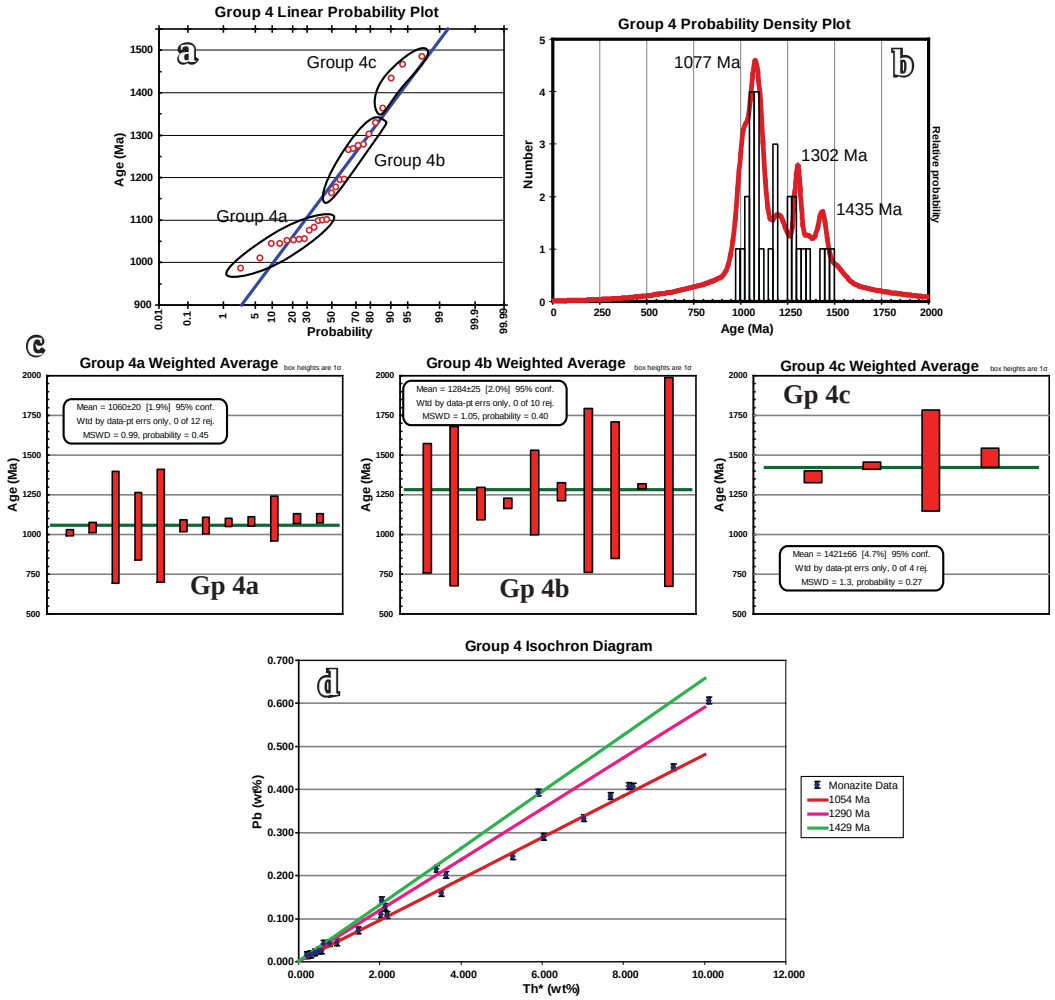

Figure 6.14. Group 4 results.
a) The linearized probability plot shows that the data could be divided into three sub-groups. b) The probability density plot shows three peaks, at 1077 Ma, 1302 Ma and 1435 Ma. c) Weighted average diagrams for the three subgroups gives ages of 1060 ± 20 Ma, 1284 ± 25 Ma and 1421 ± 66 Ma. d) Isochron diagram showing calculated isochrons for ages calculated using the Unmix function. The 1054 Ma age has good support with a range of wide range of Th*, but the 1290 Ma and 1429 Ma isochron have limited support from a few analyses.

Elburg et al. (2002) dated a series of Palaeozoic igneous, metamorphic and hydrothermal events in the Mt Painter Inlier near Arkaroola. The British Empire Granite intruded at 449 ± 2 Ma (S-type) and 455 ± 4 Ma (I-type), and quartz and diopside-sphene veins were deposited along faults in the basement (449 ± 4 Ma; Elburg et al., 2002). The British Empire Granite is thought to have formed from a mix of melts sourced from a range of rock-types in the mid-crust (McLaren et al., 2002a) and may reflect a regional heat anomaly that could drive fluid flow within the metasedimentary rocks of the now deformed Adelaide Fold Belt. McLaren et al. (2002b) recorded hornblende and K-feldspar apparent ages (K-Ar and Ar-Ar dating) of about 430 Ma which they consider to reflect the beginning of a period of rapid cooling from a temperature of about 475° – 450°C. Groves et al. (2003) dated Zn mineralisation at the Beltana mine, southeast of Leigh Creek at about 435 Ma (437 ± 5 Ma and 430 ± 5 Ma) using the K- Ar method on coronadite. They considered this to be the age of mineralisation, which they attributed to hydrothermal fluid flow during a period of cooling, possibly related to an igneous intrusion at depth (quoting N. Reynolds as a pers comm., 2002). The calculated monazite ages here are slightly younger than those

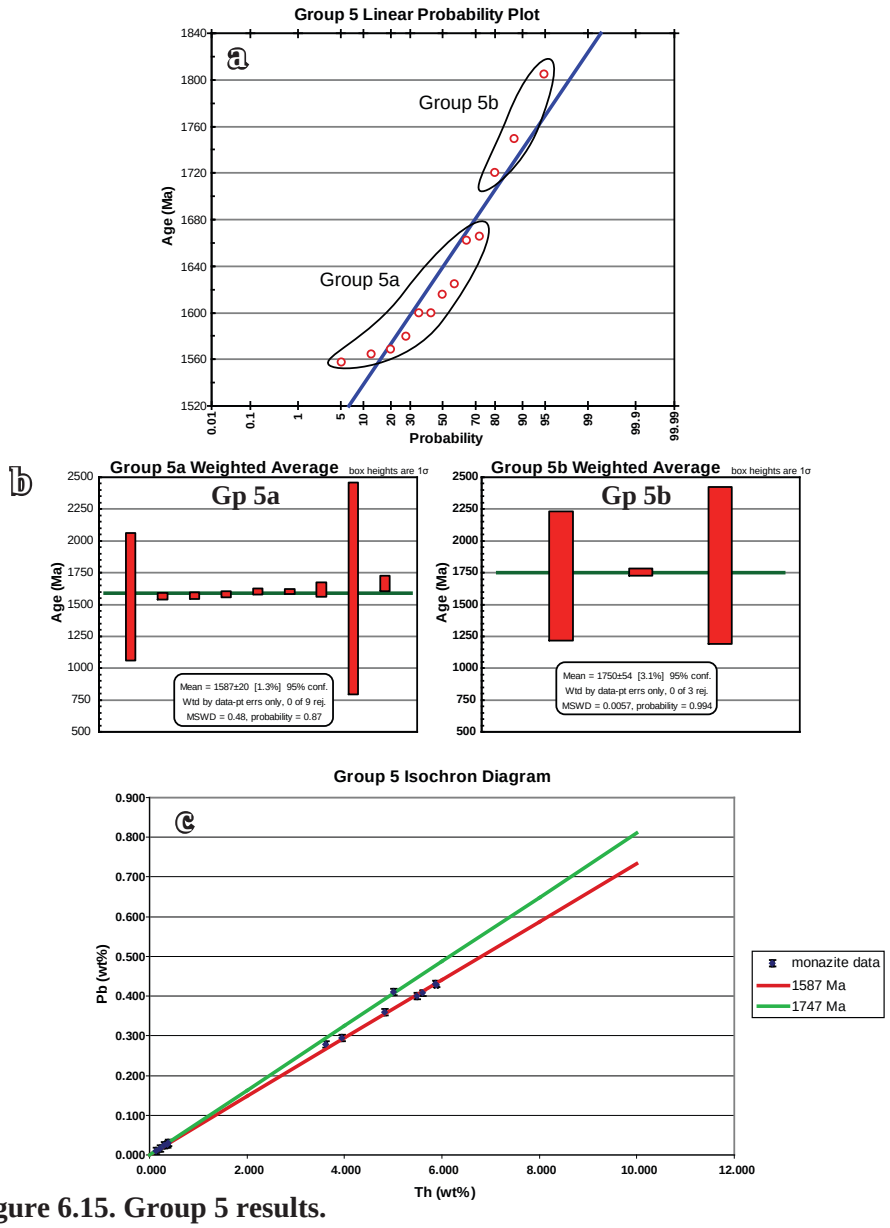

Figure 6.15. Group 5 results.
a) Linearized probability plot showing the group contains a close grouping up to about with three older outliers. b) Weighted average diagrams for the main grouping and the three outliers return ages of 1587 ± 20 Ma and 1750 ± 54 Ma. c) Isochron diagram for ages calculated by the Unmix Ages function. The 1587 Ma isochron has good support with five points about 3 wt% Th* but the 1747 Ma isochron is supported by only one analysis about 1 wt% Th*.

of the granites and veins in the Mt Painter Block but within error of the cooling and zinc mineralisation at Beltana. Hence it is likely that monazite formation occurred as a response to the increased heat flow due at this time.

Rocks of the the Adelaide Fold Belt were deformed in the Delamerian Orogeny between 514 – 485 Ma. In the Arkaroola region, peak metamorphism occurred at about 490 Ma (Elburg et al., 2002). Deformation within the basement was confined to shear zones and faults which formed pathways for pegmatitic and A-type granite intrusions dated at 496 ± 2 Ma (Sm-Nd garnet-whole rock isochron, Elburg et al., 2002). Monazites in shear bands within the basement formed at 485 ± 2 Ma (Elburg et al., 2002). The Bungalina Monzonite which intrudes the Adelaide Fold Belt metasediment rocks in the Peake and Denison Inlier is also considered to be Cambrian in age (Morrison and Foden, 1990). In the southern Adelaide

Table 6.2. Comparison of monazite ages calculated as weighted average ages for groups selected from probability diagrams and by the Unmix Ages function of Isoplot.

	From – To (Ma)	Weighted Average Age, based on Probability Diagram (Ma)	MSWD	Probability of Fit	Age Calculated by Unmix Ages function (Ma)	Percent of data included	Relative Misfit
Group 1	< 371	348 ± 49	0.19	0.998			
Group 2	399 – 564	425 ± 16 514 ± 10	0.17 0.35	1.00 1.00	429 ± 9 509 ± 5	25 75	0.951
Group 3	577 – 970	654 ± 24 892 ± 21	0.35 0.68	1.00 0.93	658 ± 25 705 ± 53 902 ± 11	56 22 22	0.836
Group 4	987 – 1485	1060 ± 21 1284 ± 26 1440 ± 42	0.99 1.05 0.33	0.45 0.40 0.72	1054 ± 10 1290 ± 12 1429 ± 23	62 24 14	0.484
Group 5	> 1564	1587 ± 20	0.43	0.92	1587 ± 10 1747 ± 28	86 14	0.865
< 802 Ma					424 ± 9 514 ± 6 671 ± 15	22 62 16	0.901
> 802 Ma					906 ± 12 1052 ± 11 1290 ± 14 1427 ± 25 1585 ± 10 1647 ± 28	29 40 11 4 15 2	0.252

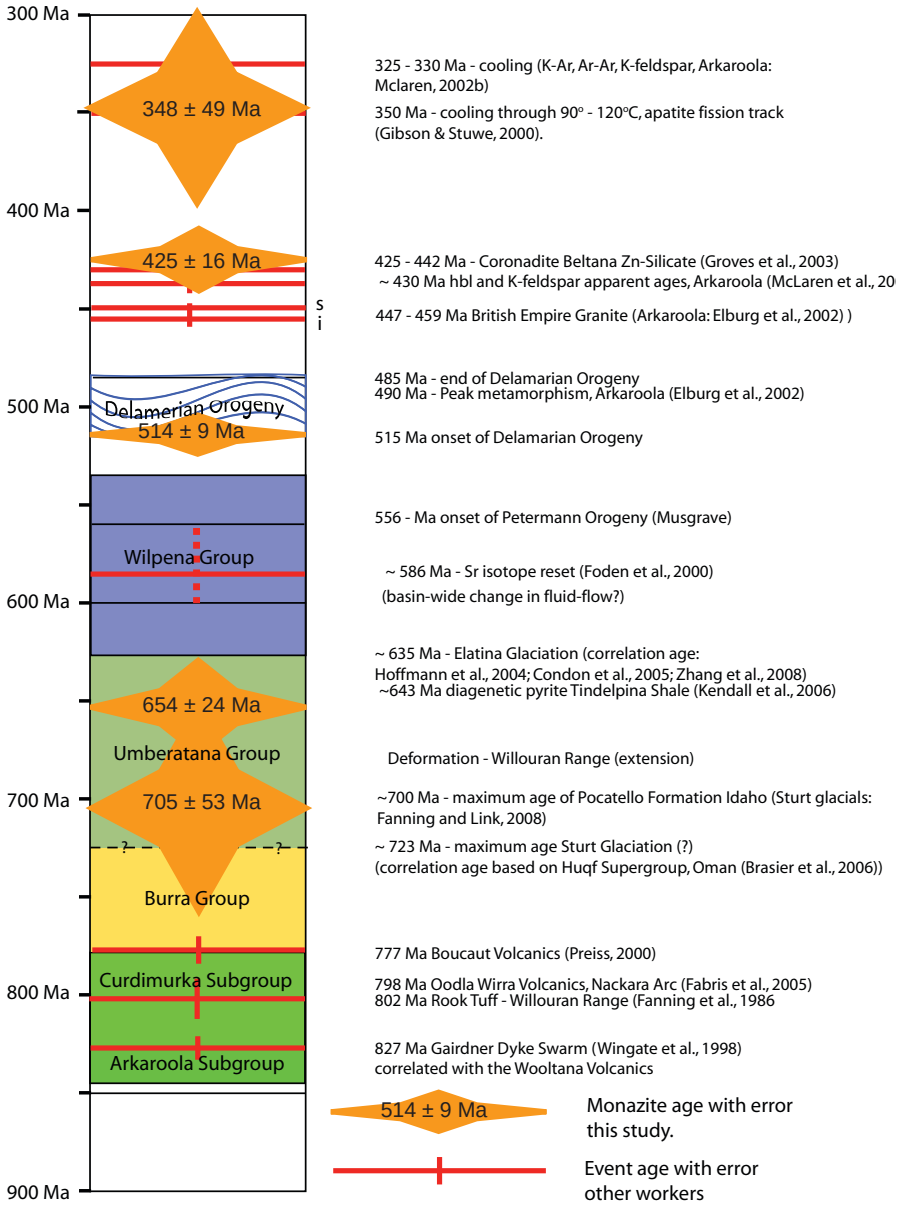

Figure 6.16. Event diagram showing the major events to have affected the Adelaide Fold Belt identified by other workers (see text for references) and the post-depositional monazite ages calculated in this study.

It shows that within errors, there is agreement between ages calculated here, the onset of the Delamarian Orogeny, a hydrothermal event responsible for Zn mineralization at Beltana and posssibly some unidentified uplift at about 350 Ma that caused regional cooling. The 654 Ma and 705 Ma ages are speculative and poorly defined but may record a hydrothermal event associated with deformation during deposition of the Umberatana Group, and identified in this study as D_1 (Chapters 8 and 9).

Fold Belt, the syn-tectonic Tanunda Creek Gneiss and Rathjen Gneiss were intruded at 513 ± 5 Ma (Heinisch and Foden, 2002) and 514 ± 5 Ma (Foden et al., 1999), respectively. Up-pressure metamorphism occurred in the interval 509 Ma – 512 Ma from Kangaroo Island shear zones but near Victor Harbor, metamorphism occurred at 498 ± 5 Ma (Webb et al., 2002). The monazite ages recorded here are at the beginning of the Delamerian Orogeny and likely reflect metamorphism at about 500 – 515 Ma.

The next oldest age calculated, about 640 – 670 Ma is about equivalent age to the Sturt glaciation (750 – 720 Ma) and predates the Elatina glaciation (about 635 Ma; Hoffman et al., 2004; Condon et al., 2005; Zhang et al., 2008). It is within error of the Re-Os age from

diagenetic pyrite from the Tindelpina Shale of 643 ± 2.4 Ma (Kendall et al., 2006), which is interpreted to be close to a depositional age. Deposition of the Umberatana Group marks a period of rapid extension and salt tectonism in the Willouran Trough (Chapters 7 - 9), that eventually led to the formation of a passive margin along the eastern margin of the Adelaide Fold Belt (Powell et al., 1994; Preiss, 2000). Monazite growth recorded in the ages here may have occurred as a response to a regional fluid flow event that marks the transition from an intracontinental, essentially closed basin to a more open passive margin.

The next age of 705 Ma is doubtful but if it is real, it reflects a similar situation to the 655 Ma event in that it falls within the period of rapid extension during deposition of the Umberatana Group. This age may therefore represent the onset of deposition of the Umberatana Group. Fanning and Link (2008) concluded that the Sturt glacial section of the Pocatello Formation in Idaho has a maximum age of 701 ± 4 Ma based on U-Pb zircons ages from volcanic clasts. The error bars on this age take it from before the onset of deposition of the Umberatana Group to the 655 Ma event.

6.9 Conclusions.

A total of 201 EPMA analyses were conducted on monazites from seven samples, two from heavy mineral separates and five from polished thin sections. Ages were calculated from the Th, U and Pb contents of the analyses and combined for each sample and as a combined group. Using several statistical techniques a series of pre- and post-depositional ages were identified.Post-depositional ages are considered to record the timing of major fluid-flow and metamorphic events that have affected the Curdimurka Subgroup.

The statistical analysis indicates five post-depositional ages; 348 ± 49 Ma, 429 ± 9 Ma, 509 ± 5 Ma, 658 ± 25 Ma and 705 ± 53 Ma. These are identified with; cooling and exhumation of the Adelaide Fold Belt, related to the last stages of the Delamerian Orogeny, the waning stages of the Alice Springs Orogeny. Coeval granite intrusion and hydrothermal activity associated with Zn mineralization at Beltana at about 430 Ma have been recognised in the northern Adelaide Fold Belt by several workers and the 429 ± 9 Ma monazite event corresponds to this. Delamerian metamorphism occurred at about 510 Ma, and this is recorded in the Curdimurka Subgroup. The remaining two ages of 658 ± 25 Ma and 705 ± 53 Ma, have not been recognised by other workers in the Adelaide Fold Belt but they correspond to periods of rapid extension in the Adelaide Fold Belt; during the beginning of deposition of the Umberatana Group and about the time of deposition of the Amberoona Formation.

CHAPTER 7.
STRUCTURE OF THE CURDIMURKA SUBGROUP.

7.1 Introduction.

Most of the published literature concerning the structural relationships of the Adelaide Fold Belt has been based on observations made in the Central Flinders Zone, and the arcuate structural domains that constitute the southern Adelaide Fold Belt (Figure 7.1). These works have concentrated on the deformation history of the Nackara Arc (Marshak, 1988; Marshak and Flöttmann, 1996) and the Fleurieu Arc (Mancktelow, 1990; Flöttmann and James, 1997; Direen et al., 2005), where classical fold and thrust belt structural styles are developed. In these areas, deformation occurred in at least two phases of the Late Cambrian – Early Ordovician Delamerian Orogeny. Within the Fleurieu Arc, deformation was thick-skinned and accompanied by sillimanite-grade, high-T, low-P metamorphism, migmatisation and granite intrusion (Jenkins and Sandiford, 1992; Sandiford et al., 1995; Oliver and Zakowski, 1995; Marshak and Flöttmann, 1996; Direen et al., 2005). In contrast, in the Nackara Arc, the structural style is thin-skinned, involving decoupling along a shallow dipping thrust surface that is coincident with evaporitic strata of the Callanna Group (Marshak and Flöttmann, 1996). An exception is along the southern margin of the Curnamona Province (Figure 7.1), where the deformation was thick-skinned (Berry et al., 1978; Clarke and Powell, 1989; Paul et al., 1999). In the Central Flinders Zone, the structural style is characterised by dome and basin fold interference, a manifestation of the two shortening events of the Delamarian Orogeny (Preiss, 1987).

In the northern Adelaide Fold Belt, the Delamerian Orogeny also produced dome and basin interference patterns. They are ellipse-shaped with the long axis changing orientation from northwest in the Willouran Range, to east - west in the vicinity of Leigh Creek to north-northeast adjacent the Mt Painter Inlier (Preiss, 1987; Paul et al., 1999: Figure 7.2). The change in orientation is attributed to the initial geometry of the basin and variations in sediment thickness (Sandiford et al., 1998; Paul et al., 1999). Deformation was thick-skinned with reverse displacements on prior extensional faults (Paul et al., 1999).

Workers in the northern Adelaide Fold Belt have recognized structures that preceded the Delamerian Orogeny (Sprigg, 1949; Murrell, 1977; Rowlands et al., 1980; Parker, 1983; Forbes, 1990; Paul et al., 1999; Selley and Bull, 2002). The deformation has a markedly different structural style to that produced by the Delamerian Orogeny and has been attributed to a number of different causes by the different authors including extension (e.g., Rowlands et al., 1980 Paul et al., 1999; Selley and Bull, 2002), compression (e.g., Sprigg, 1949; Murrell, 1977; Parker, 1983) and halokinesis (Dyson, 2004).

The present study aims to contribute to this debate via detailed and systematic structural analysis of the Curdimurka Subgroup strata in the Willouran Range and integration of

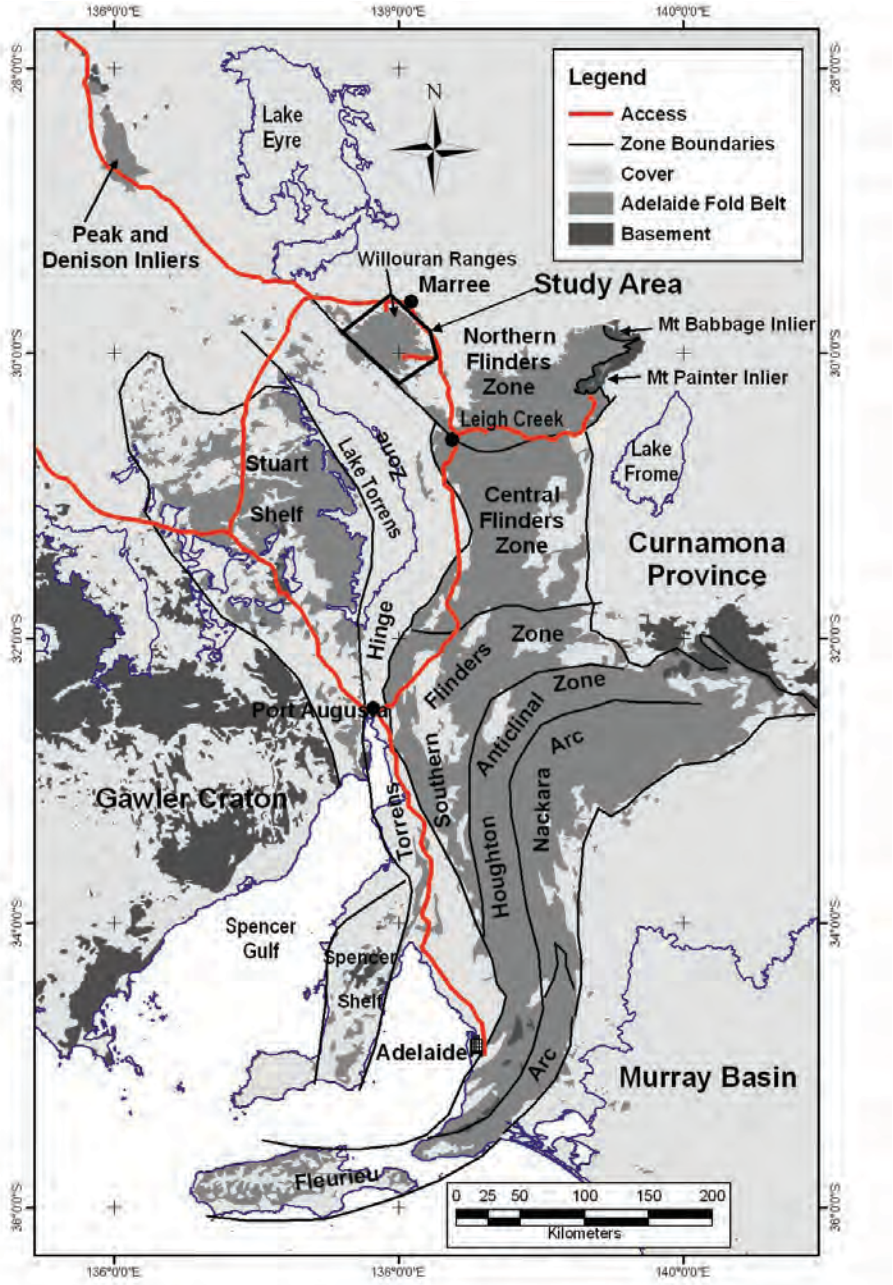

Figure 7.1. The Adelaide Fold Belt showing the structural elements and the study area.

these data with photo interpretation of the structure of the Burra and Umberatana groups supplemented with field data. The Willouran Range has the only extensive exposure of these three stratigraphic levels, providing a unique opportunity to understand the history of deformation that affected the lower stratigraphic levels of the Adelaide Fold Belt.

Data will be presented and interpreted in two chapters. In this chapter, the structure of the Curdimurka Subgroup in its type area, the Euchre Pack Domain, will be examined. Initially an overview of the Euchre Pack Domain structure will be presented before detailed analysis of the fold and fault history. Temporal constraints on the deformation history in the Euchre Pack Domain will be discussed. The next chapter deals with the regional structural framework of the Willouran Range, integrating aerial photography supplemented by field observations and modeling of gravity data.

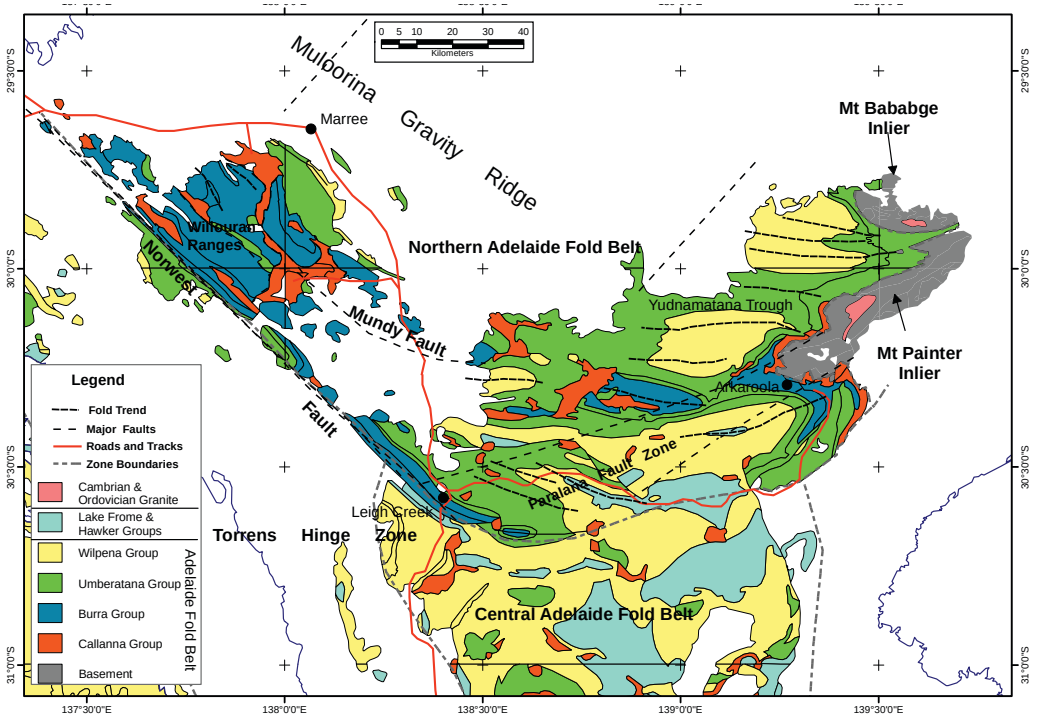

Figure 7.2. Geology of the northern Adelaide Fold Belt.
Structures in the western half trend NW, in the south they trend E - W and in the east they trend ENE (PIRSA 1:250,000 GIS Dataset).

7.2 Previous Work.

Sprigg (1949) was the first to recognise that along the northwestern margin of the Adelaide Fold Belt, the lower portion of the Adelaide Fold Belt stratigraphy had been deformed in a different manner to elsewhere. He compared the dome and basin folding seen in the Central Adelaide Fold Belt with the thrust dominated deformation seen in the Willouran Range, describing the latter as erratic (Sprigg, 1949). The structure of the Curdimurka Subgroup in the Rocky Point Sub-domain and the South Hill Domain, Sprigg (1949) interpreted as sinistral and dextral tear faults respectively, and the contact with the Burra Group adjacent to the Witchelina Domain (Figure 7.3) is interpreted to be a thrust. Collectively, he interpreted these structures as resulting from thusting with dominant movement of top or east block to the southeast (within the framework of vertical tectonics).

Murrell (1977) suggested that there were two generations of deformation prior to the Delamerian Orogeny. In the first, rocks of the Callanna Group were chaotically folded (and possibly metamorphosed) prior to deposition of the Burra Group. Folds within the Curdimurka Subgroup in the Stony Range Domain (Figure 7.3) but which are not repeated in the overlying Burra Group were attributed by Murrell (1977) to a pre-Burra Group deformation of the Callanna Group. The second deformation Murrell (1977) interpreted from a high-angle unconformity between the Burra Group and overlying Umberatana Group west of the Bungarider Fault in the Berlina Domain (Figure 7.3). Parker (1983) suggested that there was a period of folding and thrusting prior to or during early deposition of the Burra Group, based on the observation that first generation folds of the Delamerian Orogeny overprint a generation of very tight to isoclinal folds in the Rischbeith Domain

(Figure 7.3). He concluded that the earliest deformation produced west-directed reverse fault movement affecting the Callanna Group, with the Burra Group deposited in the footwall of these faults (Parker, 1983).

The above interpretations have been based on compressional deformation but other authors have identified extension to be the main deformation mechanism prior to the Delamerian Orogeny. The earliest proposed timing for deformation is during deposition of the Curdimurka Subgroup, which was favoured by Rowlands et al. (1980), who suggested that rifting during deposition of the Curdimurka Subgroup resulted in the formation of the olistostromes within the Willouran Range (Rowlands et al., 1980). Paul et al. (1999) showed that there was normal movement on the Norwest and Mundy Faults (Figures 7.2, 7.3) during deposition of the upper Burra Group, indicated by thickness variations of the upper Burra Group and lower Umberatana Group. Selley and Bull (2002) attributed the high angle unconformity between the Burra and Umberatana Group described by Murrell

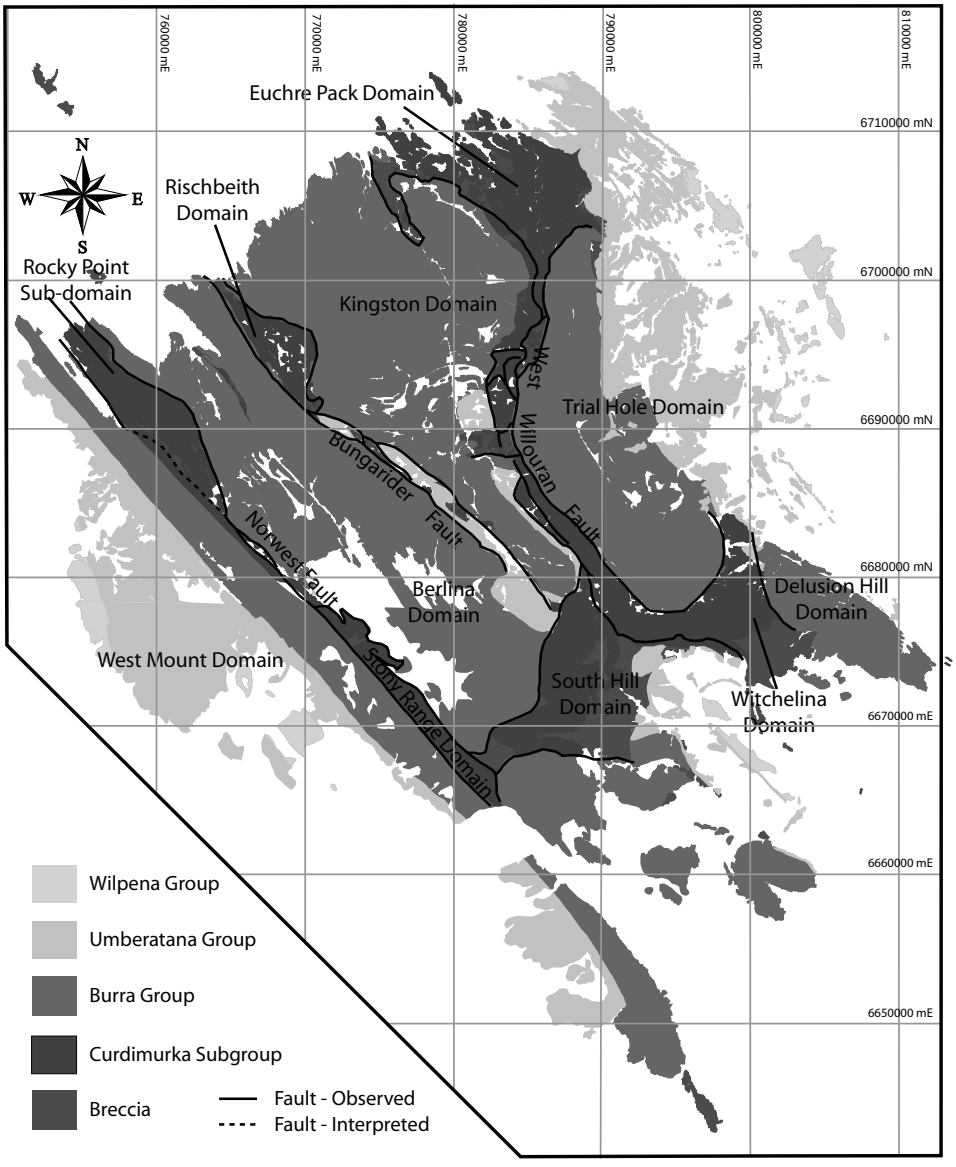

Figure 7.3. Domains of the Willouran Range.

(1977, see above) as being due low-angle extension and block rotation of the Burra Group during deposition of the lower Umberatana Group.

Another strand of evidence for deformation prior to the Delamerian Orogeny has been from studies of salt tectonics throughout the northern and central Adelaide Fold Belt. Stratigraphic relationships have been used to show that there was a period of salt tectonism that began with the onset of deposition of the Umberatana Group (e.g., Coats, 1973; Mount, 1975; Lemon, 1985; Selley and Bull, 2002) or possibly earlier (Dyson, 2004). These studies have demonstrated that peripheral sinks and salt withdrawal basins developed adjacent to breccia bodies interpreted to be diapiric in origin. The majority of the studies have been conducted in the central Adelaide Fold Belt, where the relationships between the interpreted diapirs and the surrounding sedimentary rocks are best preserved. Similar breccia bodies in the northern Adelaide Fold Belt are interpreted to represent the root zones of diapirs and so record different stratigraphic relationships between the breccia bodies and the surrounding rocks to those observed in the central Adelaide Fold Belt (Lemon, 1985).

In summary, converging evidence for pre-Delamarian deformation has been recognized by several workers based principally on contrasting structural styles between the Callanna Group rocks and younger units. However, interpretations of the driving mechanisms are varied, with compressional deformation, extensional deformation and salt tectonics all being given as possible causes.

7.3 Methodology.

The methodology applied to understanding the structure of the Curdimurka Subgroup was mapping at several scales. Aerial photographic interpretation, constrained with field traversing, was used to map at the smallest scales of approximately 1:80,000 or 1:40,000. The traverses were mapped using commercially available aerial photographs (from the Department of Primary Industry and Resources of South Australia) at either about 1:80,000 (Marree and Curdimurka map sheets) or about 1:40,000 (Andamooka and Copley map sheets).

Mapping targeted the major structures, including faults and folds with the aim of describing their orientation and geometry, and the upper and lower contacts of the Curdimurka Subgroup. Previous workers have indicated that the Curdimurka Subgroup is always bounded by faults (Preiss, 1987; Forbes, 1990), and the mapping intended to examine further the geometry and kinematics of the contacts. At the outcrop scale, structural data collected including bedding orientation, facing, fold plunges and axial plane orientations, the presence of cleavage and its orientation, and fault orientations. From the data gathered, it is intended to determine the overall geometry of the main structures, their sense of movement and their relative timing.

After completing a series of traverses across the Curdimurka Subgroup in the Stony Range, South Hill, Rischbeith and Euchre Pack domains (Figure 7.3), it was decided to concentrate mapping in the latter. The reasons for this are:

- it offers the most complete, intact and established stratigraphy of the Curdimurka Subgroup so that correlations across structures would present fewer problems than areas where the stratigraphy has not been established, allowing efforts to concentrate on structural and not stratigraphic problems;
- boundaries of the Curdimurka Subgroups with both the Burra and Umberatana groups are clearly defined
- evidence for early, possibly syn-depositional deformation of the Curdimurka Subgroup has been previously recognised in this domain (Murrell, 1977; Rowlands et al., 1981)

Mapping in the Euchre Pack Domain was conducted at a scale of about 1:20,000 in the southern half of the Euchre Pack Domain (approximately south of Dunns Mine) and 1:10,000 in the northern half, based on blown-up 1:80,000 aerial photographs. Later, when detailed imagery became available on GoogleEarth, this was also used to aid interpretation.

7.4 The Euchre Pack Domain.

7.4.1 An Overview of the Euchre Pack Domain.

The regional dip of bedding in the Euchre Pack Domain is sub-vertical to steep towards the east or northeast, and facing is to the northeast (Figure 7.4). Two exceptions are the central part of the domain where the Recovery Formation faces southwest and on the southwestern edge of the area, the Cooranna Formation and the Boorloo Siltstone face west. These localized changes in stratigraphic facing direction reveal dismembered macroscopic anticlinal geometries, the cores of which contain bodies of breccia facies.

7.4.1.1 Contact Relationships.

The margins of the Euchre Pack Domain are ubiquitously faulted, or defined by breccia bodies. To the north, youngest Curdimurka Subgroup strata (the Boorloo Siltstone) are in fault contact with basal Umberatana Group strata (Yudnamutana Subgroup), separated by a narrow breccia. However, from about 788170 E (Point A in Figure 7.4), where the trend of the contact turns to the south-southeast, these units are separated by the Breaden Hill Breccia. Both the faulted and brecciated contacts are sub-parallel to bedding in the Curdimurka and Umberatana groups.

South from Breaden Hill, the contact of the Euchre Pack Domain with the Burra Group transgresses Curdimurka Subgroup stratigraphy, cutting progressively downsection from the Boorloo Siltstone to the basal Recovery Formation to the south (Figure 7.4). It also cuts down through the Burra Group in the Trial Hole Domain at a high angle, from the upper part of the Skillogalee Dolomite to the basal Emeroo Subgroup at about 6701750N (Point B in Figure 7.4), where the contact once more trends south and is sub-parallel to bedding in the Burra Group (Figure 7.4).

The southwestern contact is between southwest-facing Boorloo Siltstone and Skillogalee Dolomite of the Burra Group in the Kingston Domain, separated by a brecciated zone of

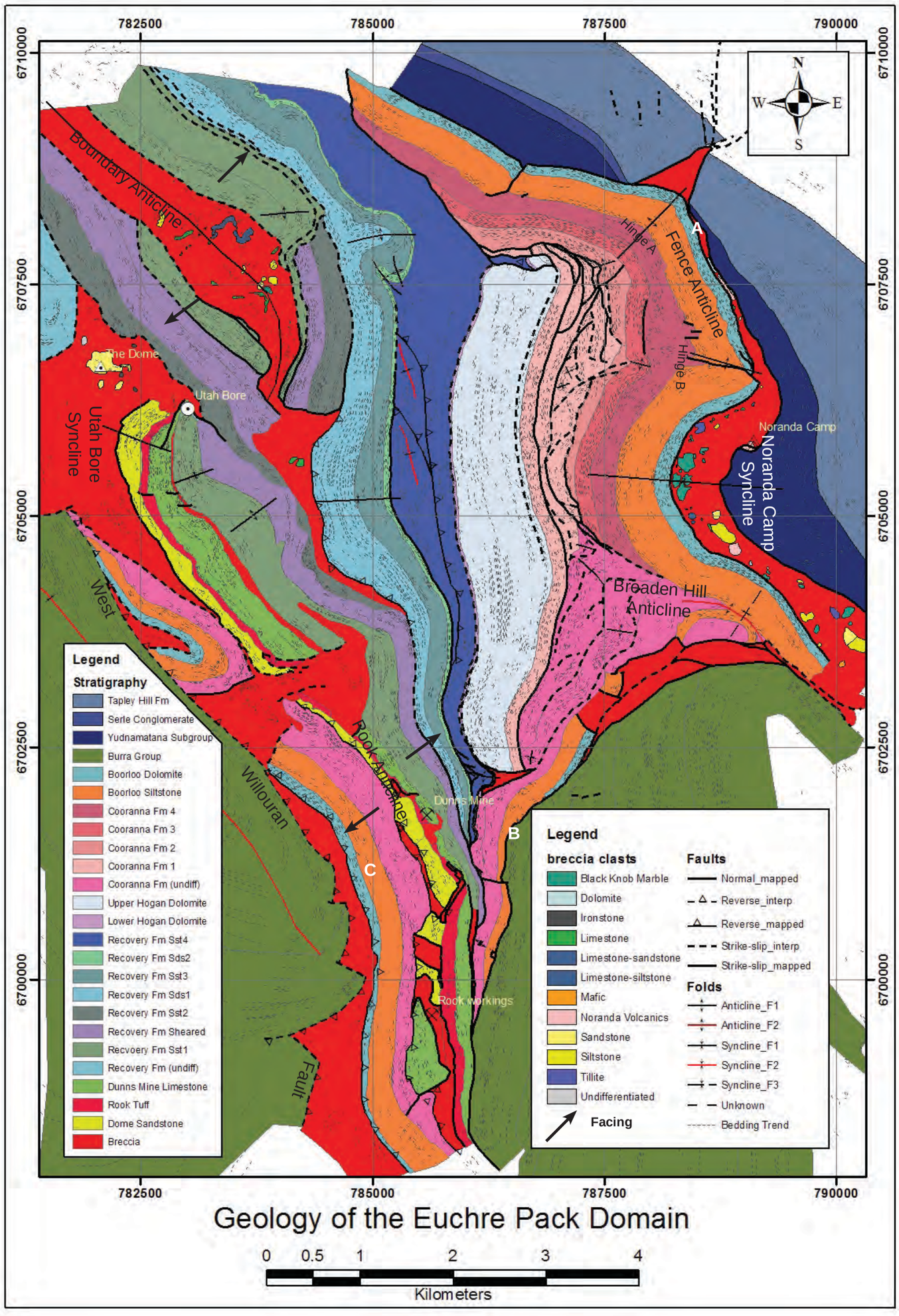

Figure 7.4. Geological map of the Euchre Pack Domain.

variable width (Figure 7.4). From the south it initially trends north for about two kilometres before changing to a northwest trend at about 6701810N (Point C in Figure 7.4).

7.4.1.2 Folds.

There are five major macroscopic folds in the Euchre Pack Domain (Figure 7.4). In the northeast, the Fence Anticline/Noranda Camp Syncline pair is defined by folded upper Cooranna Formation and Boorloo Siltstone. The Boundary Anticline in the northwest has breccia at its core and is flanked by Recovery Formation. Southwest facing Cooranna Formation and Boorloo Siltstone adjacent to east facing Dome Sandstone and Dunns Mine Limestone define the Rook Anticline, although the hinge has been faulted out. The Utah Bore Syncline, in which strata from the Dome Sandstone to RSlt2 are folded into a broad syncline which tightens toward Utah Bore and is cut-off by a fault against southwest facing RSlt1. A fifth, slightly smaller fold is the Breaden Hill Anticline in the Boorloo Siltstone, affecting upper Cooranna Formation strata in the east of the area.

7.4.1.3 Faults.

A network of fault zones that consist primarily of layer sub-parallel faults and subordinate high angle (to layering) faults affect the middle and upper portions of the Curdimurka Subgroup. The majority of faults have accommodated apparent strike-slip movement (in their present sub-vertically dipping configuration) but a small number show evidence for initial strike-slip movement with reactivation as dip-slip faults. Most strike-slip faults record dextral (i.e., east block, or top stratigraphy, to south) displacement, but a significant minority are sinistral. From stratigraphic relationships, layer sub-parallel faults have displacements of hundreds to thousands of metres, whereas the high angle structures typically have displacement measured in metres to tens of metres. A single fault or fault zone can have both layer sub-parallel and high angle (to layering) segments, giving a stepping pattern. At scales of tens to hundreds of metres the same fault zone may repeat or remove stratigraphy but at the macro-scale of the Euchre Pack Domain all the layer parallel fault zones remove stratigraphy.

7.4.1.4 Breccias.

Stratabound and cross-cutting breccias occur within the Euchre Pack Domain. Based on texture, there are two broad types. The first type is carbonate-matrix supported, and contains a wide range of clast lithologies and clast sizes. The second category is typically clast supported, with a quartz or carbonate matrix, the clast assemblage being typically derived from the immediately surrounding wall rock. Both breccia types occur at scales from centimetres to kilometres, and interfinging relationships between the two were observed.

Stratabound breccias of the first type occur at four stratigraphic levels: (i) structurally below the base of the Dome Sandstone, (ii) between the Dunns Mine Limestone and the Recovery Formation, (iii) structurally below RSs1, and (iv) between the Boorloo Siltstone and the Umberatana Group. Cross-cutting breccias of the first type cut up section from the base of the Dome Sandstone as high as the base of RSs1.

The second type of breccia is associated with fault zones, with examples in the Recovery and Cooranna formations. An example of a breccia body containing both types is the breccia along the West Willouran Fault at the southwestern margin of the Euchre Pack Domain (Figure. 7.4).

7.4.2 Fold Styles.

In this section, each of the fold generations will be described in order of their interpreted relative timing. The relative timing has been determined by overprinting relationships at a few key localities, which will be presented in the relevant sections. Fault styles will be discussed in the next section, again according to their relative timing.

7.4.2.1 F_1

F_1 folds have features that suggest they can be grouped together and are likely the one generation. Although they have variable absolute orientations, relative to bedding axial planes are consistently at low angle to bedding, with the exception of the rare upright detachment folds. These relationships are characteristic at all scales, from microscopic to macroscopic. At the mesoscopic scale they occur as stratabound trains of folds but also rarely cross-cutting stratigraphy. They typically have a common vergence, dominantly to the south to southeast with a minority showing north to northwest vergence. Hence, this style of folds is interpreted to be of one generation.

F_1 folds are partitioned into certain stratigraphic levels throughout the Curdimurka Subgroup, from the Dunns Mine Limestone to the Boorloo Siltstone. The folds vary in profile from short wavelength, high amplitude, isoclinal folds (Figure 7.5a, b), to trains of long wavelength, low amplitude folds (Figure 7.5c, d). They include isoclinal folds with sheared-out limbs (Figure 7.5a, b), asymmetric fold trains (Figure 7.5d,e) and rare box folds (Figure 7.5e). Complex fold geometries can occur due to layer-parallel movement within and between fold hinges (Figure 7.5f). Disharmonic folding occurs in limestone units with thin though variable bed thickness (Figure 7.5g) and in interbedded limestone-siltstone units (Figure 7.5h). Fold hinges are typically rounded. Rarely, a fanning penetrative cleavage is developed within the hinges of the largest examples (Figure 7.5c).

Axial surfaces may be straight and sub-parallel to the regional bedding (Figure 7.5a,b) or curving from a high angle to bedding in the base of an individual fold to a low angle to bedding toward the structural top of that fold (Figure 7.5c,d; Figure 7.6a,b,c). The strike of axial surfaces and fold plunges thus vary depending upon local and regional variations in the strike of layering. Despite this variation in fold geometry, asymmetric profiles possess a consistent clockwise-, or Z-vergence (Figure 7.5d, e), indicative of stratigraphic-top-to-S and top-to-E senses of shear in parts of the Euchre Pack Domain where regional bedding strikes N and E, respectively.

---

this locality; RSst1. g) Disharmonic F_1 fold in a limestone unit, Cooranna Formation. h) An F_1 fold hinge showing carbonate beds deforming in a ductile manner, RSst1.
Annotation line colours. S_0 - blue, S_1 red, F_1 green, Shear - yellow

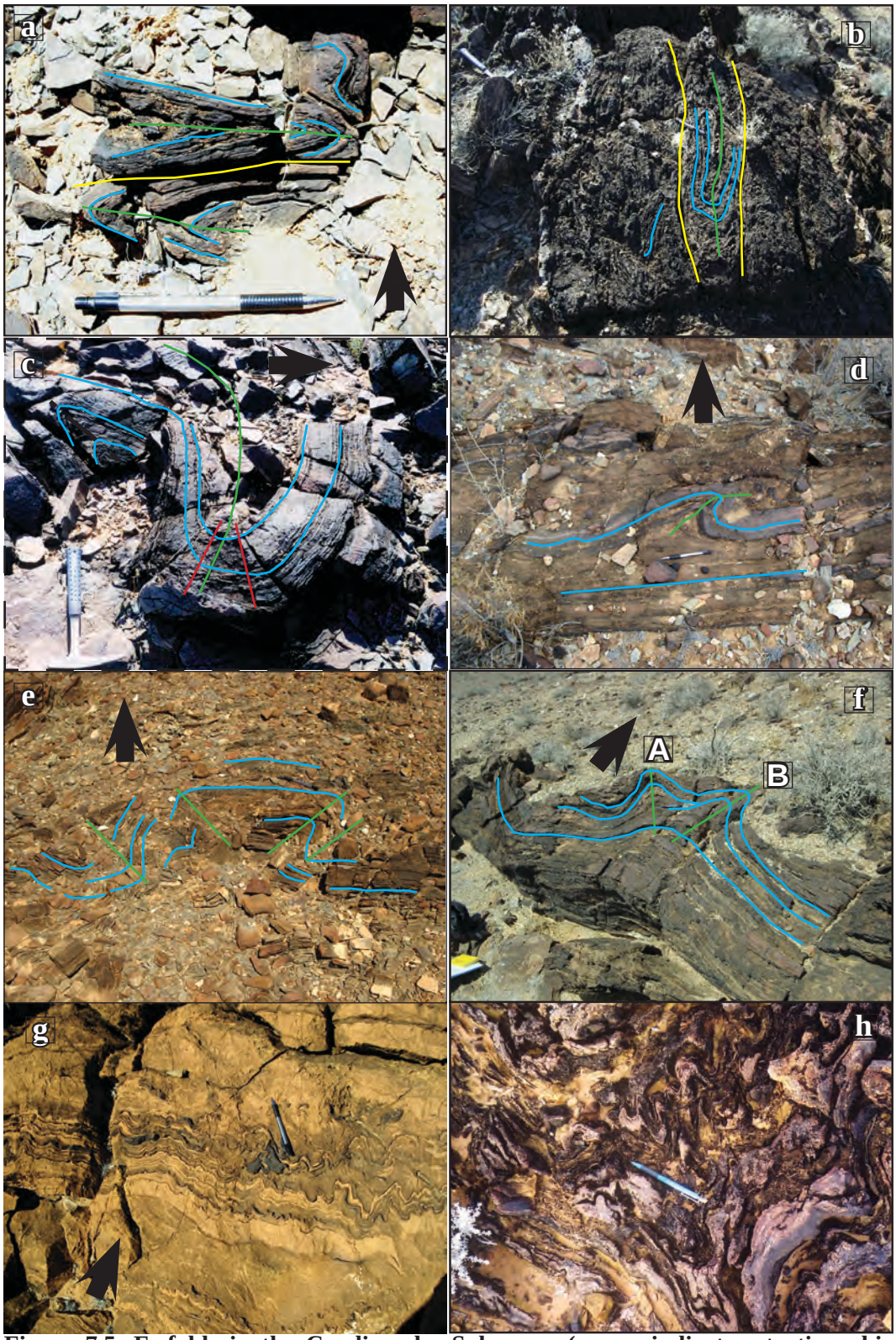

Figure 7.5. F_1 folds in the Curdimurka Subgroup (arrow indicates stratigraphic younging direction).

a) Short wavelength, high amplitude folds with limbs sheared out, Lwr Dolomite unit, BShl. b) Short wavelength folds with sheared out limbs in interlaminated shale/siltstone, Dunns Mine Limestone c) A metre-scale F_1 fold showing a curving axial plane, Lwr Dolomite Unit, BShl d) A decimetre-scale F_1 fold with an axial plane rotating to sub-parallel with the surrounding bedding, Bdol. 7.4c has the same relationship to the surrounding bedding but at a larger scale. e) A box-fold in the sandstone unit, BShl. f) A two-hinged fold resulting from layer-parallel movement transporting hinge A up the limb of hinge B above an open anticline-syncline pair which reflect the dip of the enclosing strata at

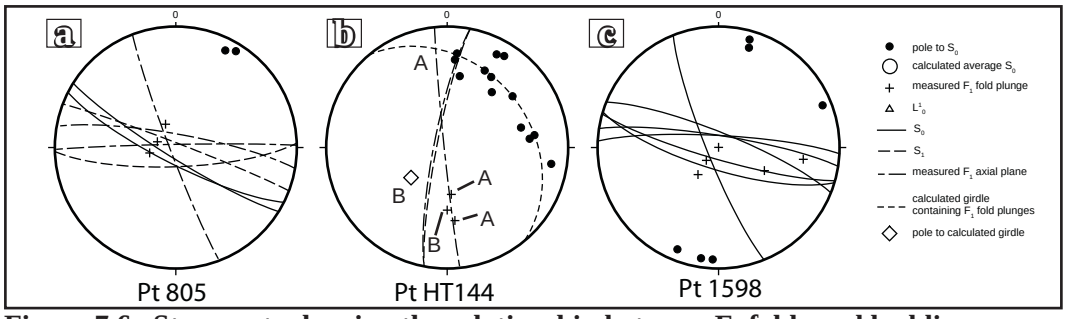

Figure 7.6. Stereonets showing the relationship between F_1 folds and bedding.
a) Pt 805 (Figure 7.5c), fold plunges are steep to the northwest quadrant, being within 15° of the dip of the enclosing strata. The axial plane curves through about 73°, from at a high angle to bedding near the base of the fold to sub-parallel in the fold hinge. The variation in the S_1 orientation is due to it being a fanning cleavage. b) PtHT144 (Figure 7.5f) the poles to bedding are from the open-folded strata stratigraphically below the two fold hinges marked A and B. The two closures have similar plunges also at a small angle to the dip of the less deformed strata stratigraphically below the folds. Letters refer to the fold hinges in Figure 7.5f. c) Pt 1598 is from an outcrop with a series of F_1 folds. Here there is a larger variation in the fold plunges but all are at a low angle to the dip of the enclosing strata.

The majority of folds observed in outcrop have formed by flexural folding (Donath and Parker, 1964). Thinly interbedded carbonate and siltstone units deform by flexural flow (Figure 7.5h), whereas the medium to thickly bedded carbonates and sandstone deform by flexural slip. (Figure 7.5c).

Most F_1 folds occur at the mesoscopic scale but several occur at macroscopic scale. Two of the larger examples are discussed in more detail below but Figure 7.7 is an example of one of these folds in the Cooranna Formation. It has a long northern limb and short southern limb, with an open synclinal hinge and a tight anticlinal hinge. The axial surface dips steeply to the west and is at a low angle to the surrounding bedding, and the syncline plunges at 66°/110° (calculated from bedding). Although the fold's geometry is compatible with that of other folds described above, thus forming the basis for its F_1 classification, it is unusual in that it possesses an anticlockwise- or S-vergence. The sense of shear indicated by this structure is thus stratigraphic top-to-N.

Refolding of mesoscopic F_1 folds occurs in a few outcrops up to 20 cm across (Figure 7.8). The interference pattern produced ranges between type 2 and type 3, the variation likely reflecting differences in orientation of the small folds after D_1, from oblique to perpendicular between the two axial surfaces. It is interpreted to indicate inclined folds being re-folded by upright folds.

Several macroscopic folds are attributed to F_1 based partly on their steep plunges but also on the spatial and genetic association with D_1 shear zones (see below), and their involvement of strata that contain mesoscopic F_1 folds. Two are discussed here; the Fence - Noranda Camp Anticline – Syncline pair and the Boundary Anticline (Figures 7.4).

The Fence Anticline - Noranda Camp Syncline

The Fence Anticline and Noranda Camp Syncline pair (Figure 7.9) deform the Boorloo Siltstone and the upper two units of the Cooranna Formation, as well as the Breaden Hill Breccia and the Yudnamatana Subgroup. Near the base of the Boorloo Siltstone it has

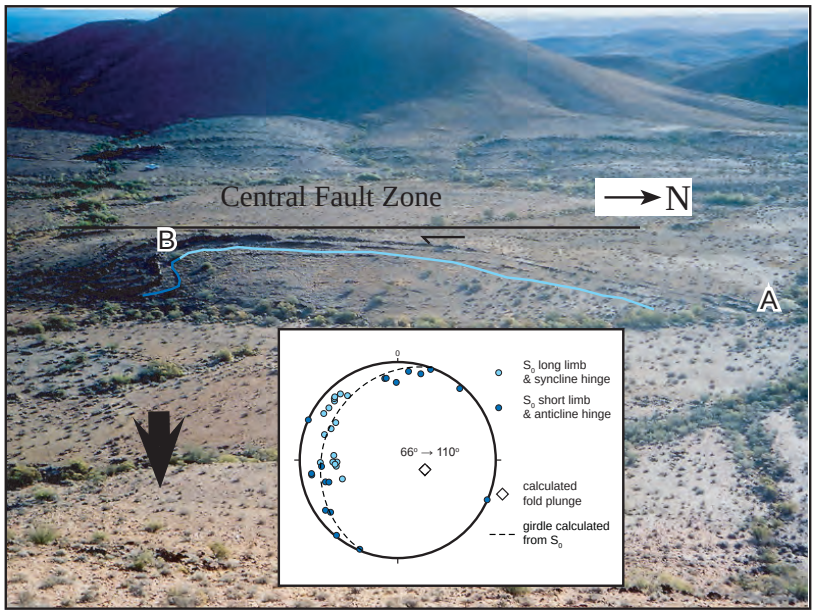

Figure 7.7. A macroscopic F_1 fold in east-facing Cooranna Formation.
The scale of this fold is unusual being about 100 m from A to B, but its form and moderately steep plunge is typical of F_1 folds. West of the fold is the Central Fault Zone, and east (just out of the bottom of the picture) is the Eastern Fault Zone. The colours of the points in the stereonet refer to the section of the fold where the dip measurement was taken. Light blue points were taken along the long limb and syncline hinge, dark blue from the short limb and anticline hinge.

an amplitude of 350 m and a wavelength of 1 km. It comprises two discrete anticlinal hinges. The northern most (hinge A) is open and rounded, and has a plunge calculated from bedding of 58°/125°, (Figure 7.10a) and the southern anticline hinge (hinge B) is close with a calculated plunge of 61°/113° (Figure 7.10b). Axial planes of both hinges dip steeply but in hinge 1, it trends to the northeast, dipping northwest and in hinge B it trends to the east-southeast, dipping north-northeast. Hinge B has been disturbed by a strike-slip fault with about 50 m sinistral displacement (Figure 7.9). A series of small dextral strike-slip faults deform the Upper Boorloo Dolomite also. The Noranda Camp Syncline has a calculated plunge of 59°/108° and a steeply dipping, east striking axial plane (Figure 7.10c).

Many of the mesoscopic F_1 folds described above occur in the Boorloo Siltstone along the limbs of the Fence Anticline and Noranda Camp Syncline. Mesoscopic F_1 folds on the north limb of hinge A have measured plunges that are spread over about 80°, plotting on a calculated girdle that dips 81°/184° (Figure 7.10e). Fold axes, S_1 and layer-parallel shears dip at a steep angle to the north to northeast and south to southeast (Figure 7.10f). On the central limb, the F_1 fold plunges from the lower dolomite are spread over about 90°, defining a girdle that dips at 88°/061° (Figure 7.10h).

To illustrate the relationship of F_1 and S_1 to bedding, the data are rotated such that the average S_0 is horizontal (Figure 7.10i,k). Two rotations are used; the first rotates the plunge of Hinge A to 0°, and the second rotates the average S_0 on each limb to horizontal. This is a purely geometric rotation and shows that the fold plunges are shallow to the north-northwest and southeast on the north limb, with the axial planes, S_1 and layer-parallel shearing having shallow to moderate dips to the northeast, shallow dips to the southwest. On the central

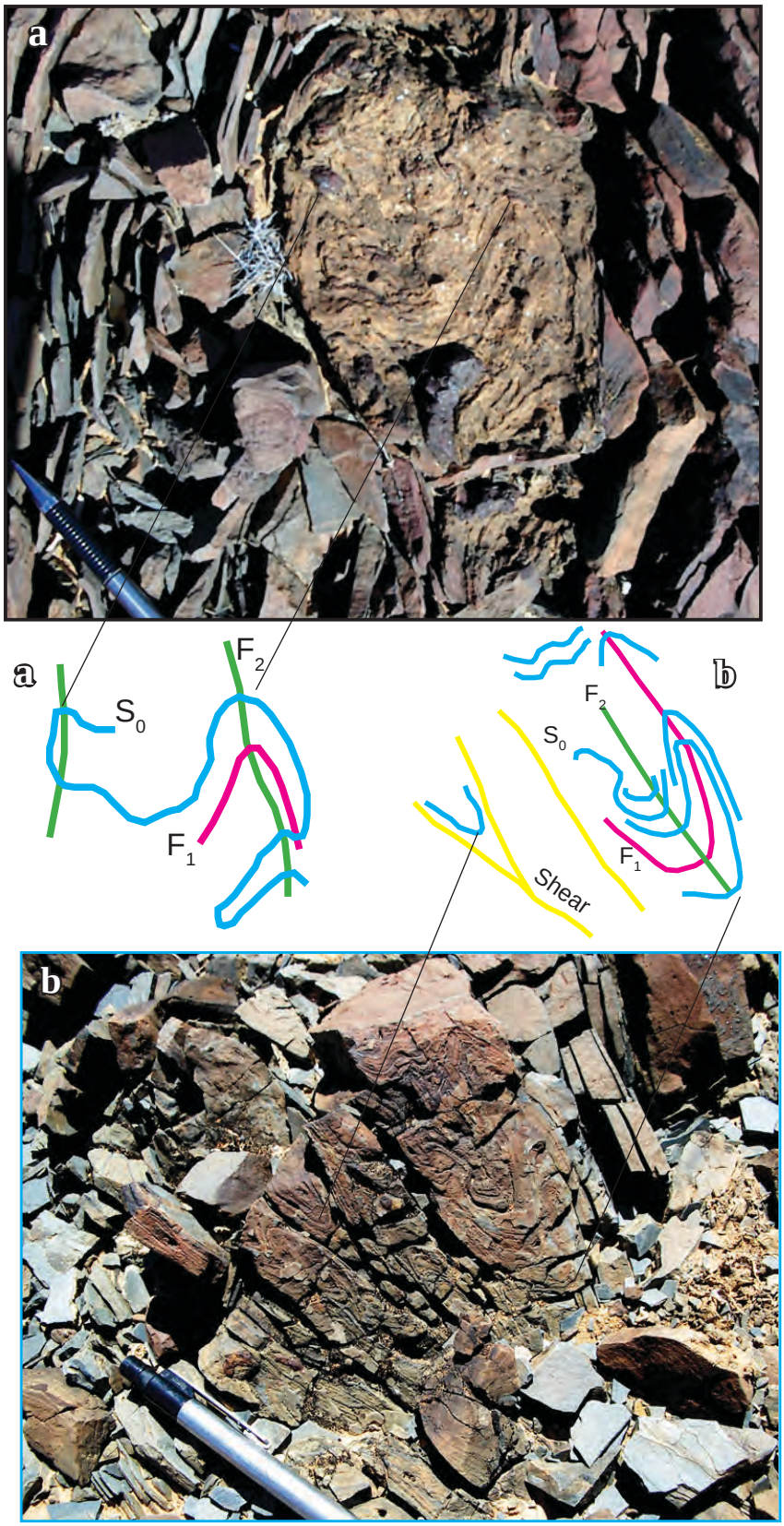

Figure 7.8. Interference folds within dolomite beds, Lower Boorloo Dolomite.
a) Outcrop from the Central Limb, Fence Anticline, with a type 3 fold interference pattern. b) From the Northwest Limb, Breaden Hill Anticline with a type 2 fold interference pattern. The difference in shape between the two interference patterns results from a different orientation of the F_1 folds when refolded by F_2. F_1 in 7.8b is at a more oblique angle to F_2 than in 7.8a.

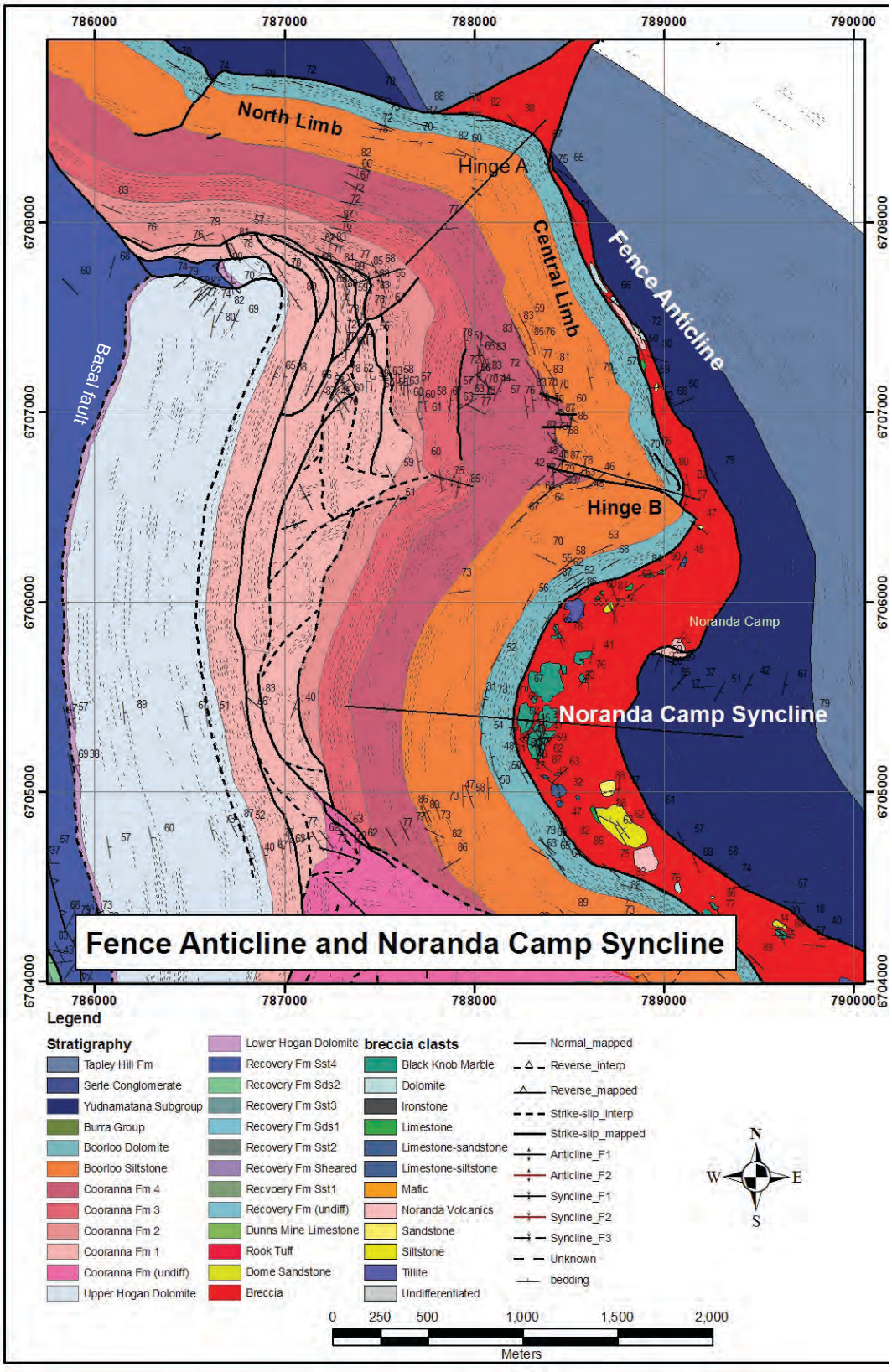

Figure 7.9. The Fence Anticline and Noranda Camp Syncline.
The Fence Anticline is a double-hinged anticline formed by the thrusting of the Boorloo Siltstone and Cooranna Units 2 - 4 over a complex fault zone at the base of the Hogan Dolomite and in Cooranna Unit 1.

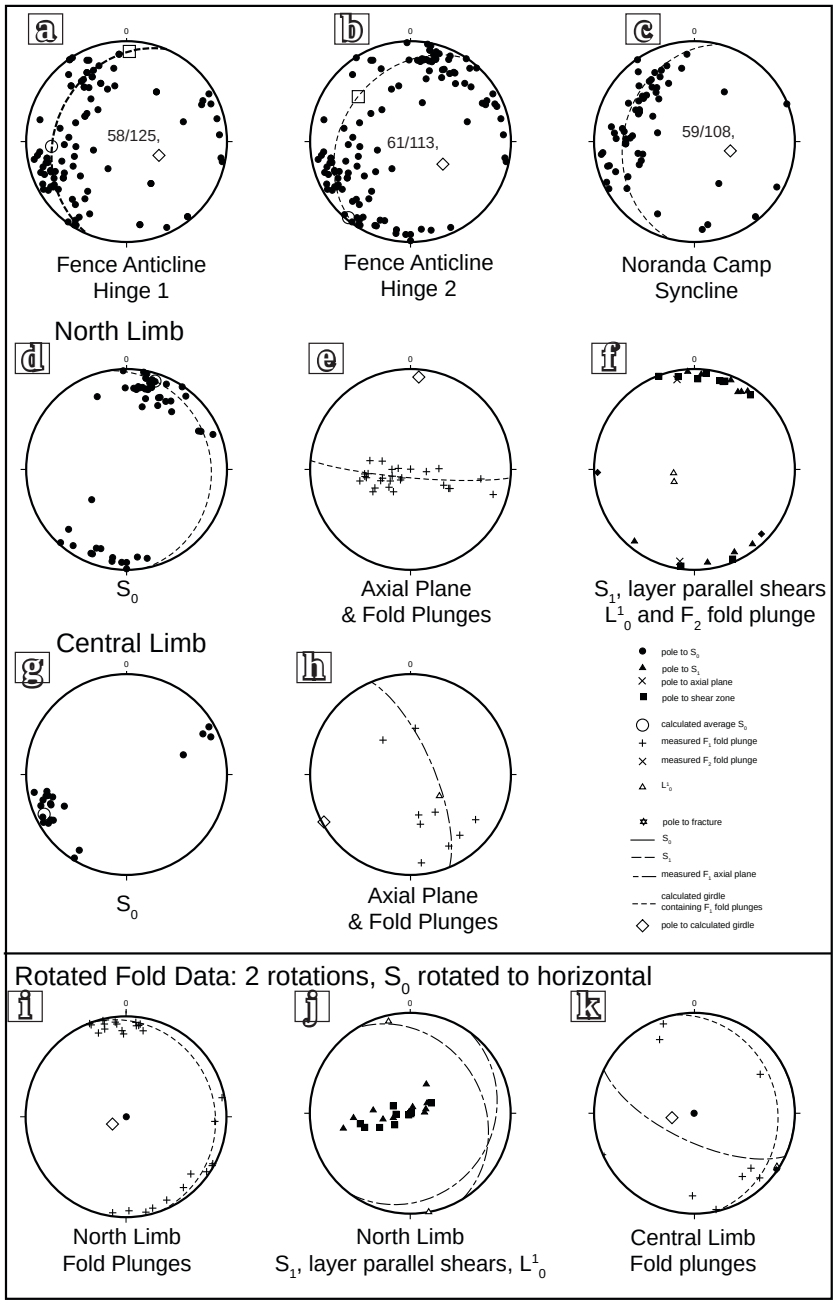

Figure 7.10. Stereonets of structural data from the Fence Anticline and Noranda Camp Syncline.

a, b, c) Poles to S_0 around Hinge A, Hinge B and the Noranda Camp Syncline respectively. All three hinges have similar calculated fold plunges, moderately steep to the ESE. d) Poles to S_0 along and across the North Limb. The main variation is about the vertical. e) Measured plunges of mesoscopic folds on the North Limb plot around a calculated girdle with a steep dip to the south. f) Other measured data from the north limb. L^1_0 have a similar plunge to the folds but S_1 and measured shears associated with F_1 have similar orientations to S_0. One F_2 fold has a shallow plunge to the south. g) Poles to S_0 on the Central Limb show is has a sub-vertical dip to the NE. h) Measured fold plunges are shallow to moderate to the SE and NW, with L^1_0 plunging at a moderate angle to the SE. The one axial plane has a steep dip to the NE. i) Rotated fold plunges and axial planes of mesoscopic folds on the north limb (see text for rotations). It shows the rotated fold plunges are close to horizontal and the axial planes dips at a shallow angle to the N to NW. j) Rotated L^1_0, axial planes and layer-parallel shears. Axial planes dip at a shallow angle to the east and S_1 and layer-parallel shears dip at shallow to moderate angles to the ENE and SSW. k) Rotated fold plunges and axial planes on the east limb. The fold plunges are sub-horizontal to the southeast and northwest. The axial plane dips at a moderately steep angle to the southwest.

limb, rotated fold plunges are shallow to the southeast and northwest with one having a shallow plunge to the northeast.

The amplitude of the Fence – Noranda Camp Anticline – Syncline pair diminishes progressively westward, the structure ultimately rooting into a layer-subparallel shear zone positioned close to the Recovery Formation-Hogan Dolomite interface (Figure. 7.8). A complex array of imbricate and duplex structures extends upsection from this basal shear zone, having led to macroscopic dismemberment of the Hogan Dolomite and structural slicing of the lower Cooranna Formation. The eastern, or higher-level parts of the fault zone are largely unaffected by the Noranda Camp Syncline, which exists as a gentle closure at lower Cooranna Formation levels. However, the same structures are clearly folded about the northern hinge of the Fence Anticline, the latter having apparently nucleated along a ramp that soles into the basal shear zone and terminates the central lozenge of Hogan Dolomite (Fig. 7.8). Aspects of this geometry, in particular the angular, multi-hinged character of the Fence Anticline, and the position of its northern hinge at the "top" of a major ramp, are analogous to classical fault-bend-fold morphologies (Fig. 7.11) of thrust environments (e.g. Suppe, 1983).

From the interpretation of the Fence Anticline and Noranda Camp Syncline as a fault bend fold, the Central Limb would be sub-horizontal whereas the northern limb would be inclined. To rotate the fold data to its pre-D_2 geometry, one rotation is used to bring the calculated average S_0 on the east limb to horizontal (Figure 7.12). In this orientation, S_0 on the north limb dips at a a moderate angle to the north to northwest with F_1 plunging at a shallow angle to the west and northeast. F_1 fold axes and layer parallel shears dip at a moderate to steep angle to the northwest. On the central limb, the rotated axial planes dip at a steep angle to the south and fold plunges are shallow but with large variation in plunge direction.

The Boundary Anticline

The Boundary Anticline is a dismembered, breccia-cored closure that affects the Recovery Formation and Dunns Mine Limestone strata (Figure 7.13a). On the southwestern side of the breccia, the Recovery Formation is facing to the southwest and on the northeastern side, the Recovery Formation faces to the northeast. The fold limbs are steeply dipping to overturned, and the hinge is faulted out and partly transgressed by breccia. The plunge of the fold calculated from limb S_0 is moderately steep to the south (Figure 7.13b).

In the centre of the breccia is a megaclast of Black Knob Marble and several megaclasts of Dome Sandstone. South of these is a zone of strongly foliated black shale and volcanic rock (possibly Noranda Volcanics) and then a largely intact limestone unit. Between the limestone unit and the Recovery Formation, the rock is strongly attenuated and the outcrop is poor. It is likely that the black shale is the Rook Tuff, and the limestone unit is the Dunns Mine Limestone. S_0 in the core of the fold is chaotic (Figure 7.13c) and measured F_1 fold plunges have highly variable orientations (Figure 7.13d). However Figure 7.13e

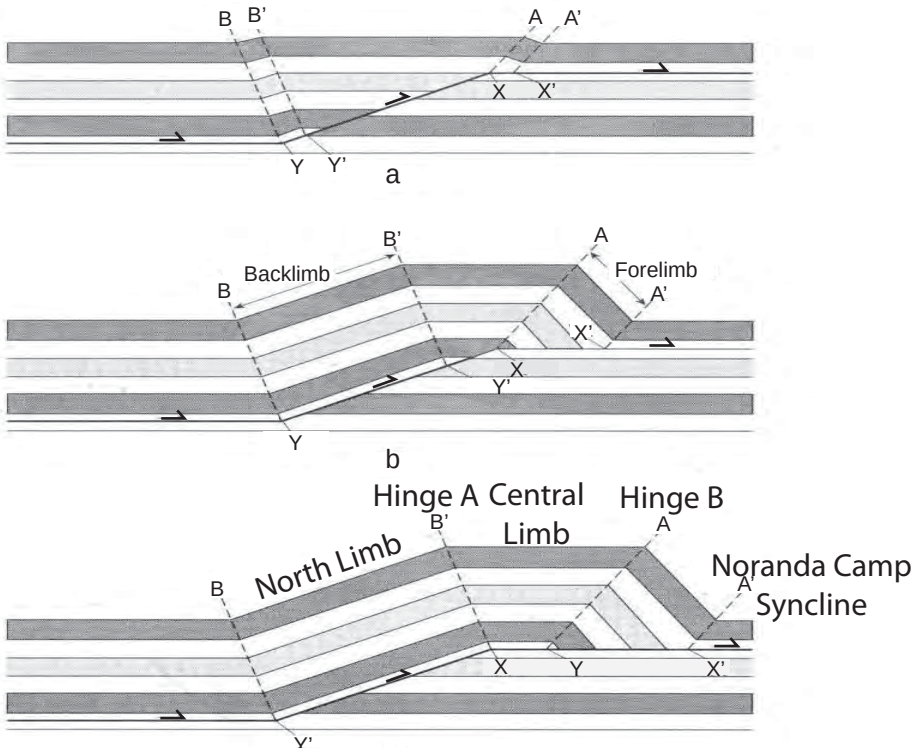

Figure 7.11. Interpretation of the Fence Anticline and Noranda Camp Syncline.
Based on its morphology, the Fence Anticline and Noranda Camp Syncline is interpreted to be a fault bend fold (Suppe, 1983). The Noranda Camp Syncline is modified by D_2 and the basal detachment is part of a listric fault.

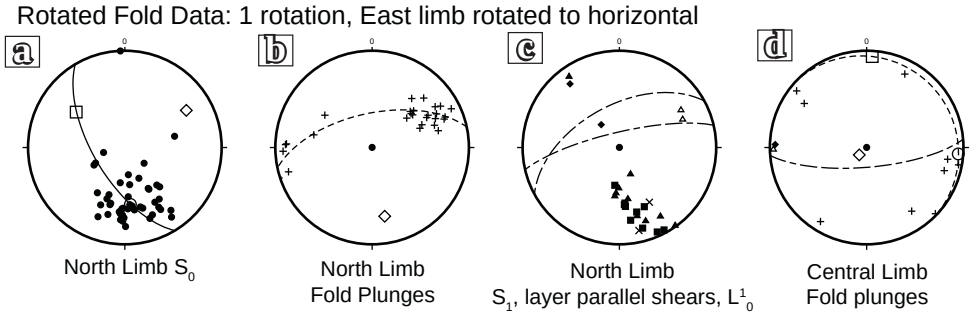

Figure 7.12. Geometry of the Fence Anticline and Noranda Camp Syncline prior to D_2.
a) After rotation, S_0 on the north limb dips at a moderate angle to the northwest. b) Fold plunges on the north limb plunge at a moderate antle to the northeast with a few folds plunging at a shallow angle to the west. c) The majority of S_1, axial planes and shears dip at varying angles to the northwest. d) On the east limb, the axial plane dips at a steep angle to the south, with the mesoscopic folds plunging at a shallow angles but with considerable variation.

is a stereonet from an individual fold which can be traced over hundreds of metres has a cylindrical profile, and suggests that this folding may have preceded the brecciation.

7.4.2.2 F_2 and F_3

In the Euchre Pack Domain, F_2 folds occur at a range of scales from meso- to macroscopic. At the scale of the Willouran Range they are the dominant fold generation, as discussed further in the next chapter. Two examples of F_2 and F_3 folds are examined here. The first, the Breaden Hill Anticline, provides evidence for three deformations at the macroscopic

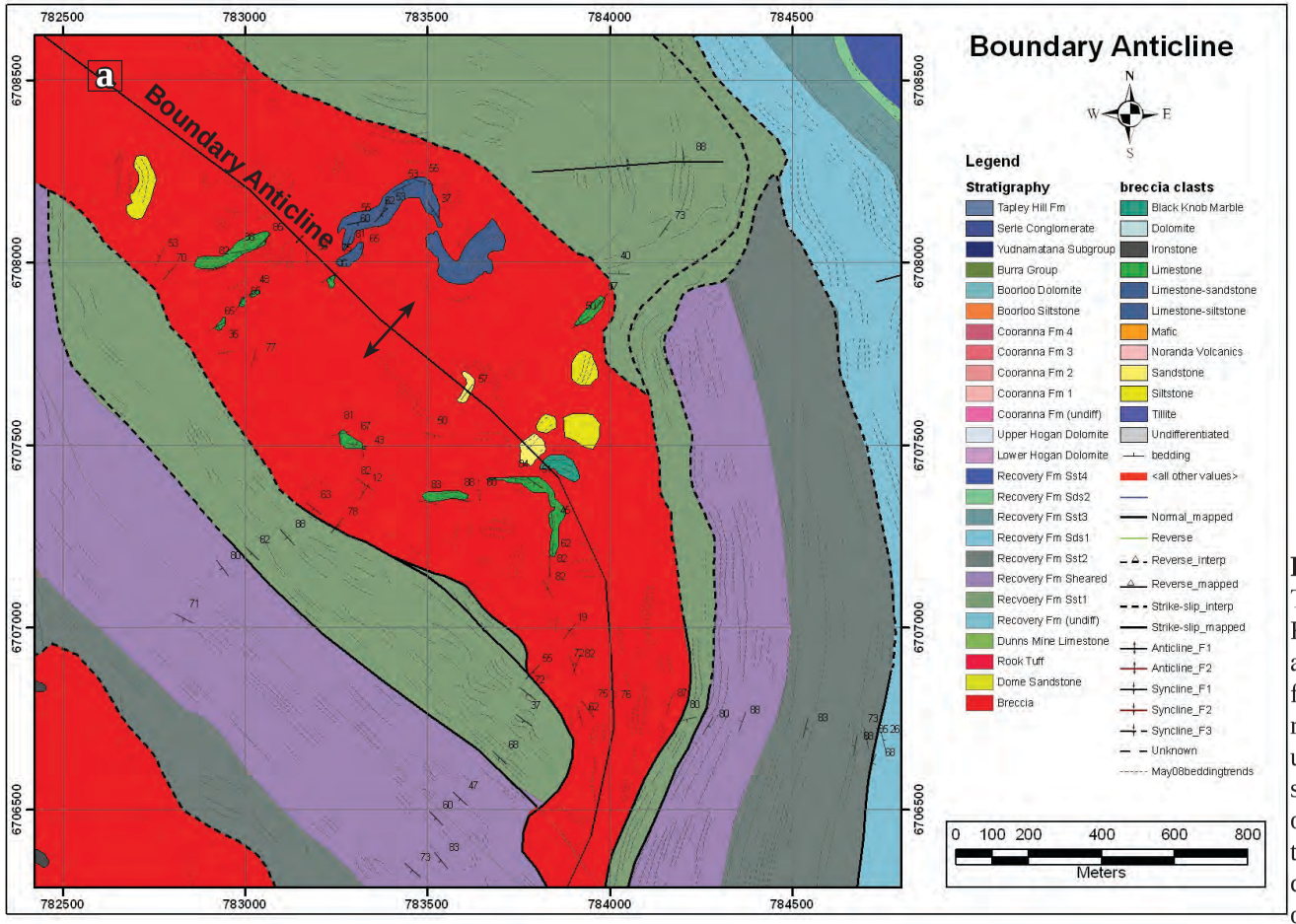

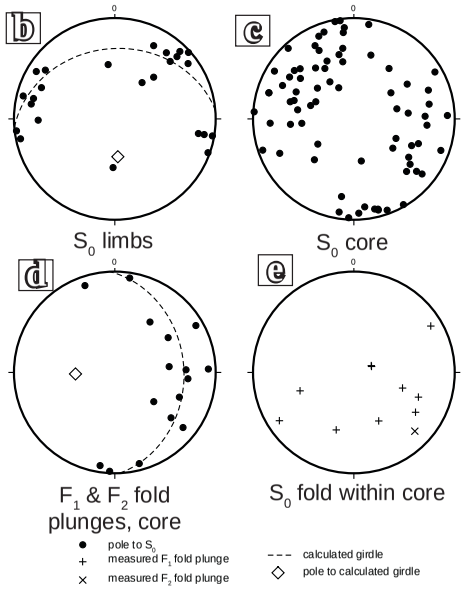

Figure 7.13. The Boundary Anticline.
The Boundary Anticline is defined by the Recovery Formation facing southwest on the southwest side and northeast on the northeast side, albeit modified by faulting. In the core is a breccia including clasts of Noranda Volcanics, Dome Sandstone and strongly attenuated limestone interpreted to be Dunns Mine Limestone. b) S_0 measurements taken around the margins of the anticline, show the calculated plunge is steep to the south.c) S_0 measurements within the centre breccia show chaotic bedding. d) S_0 measurements along one horizon of limestone has a calculated plunge of 58°/277° .e) Measured mesoscopic fold plunges are highly variable, reflecting the chaotic brecciation.

scale. The second, the Drill Pad outcrop shows evidence of two deformation events at the mesoscopic scale, without the complications of D_1.

The Breaden Hill Anticline

The Breaden Hill Anticline is a doubly plunging anticline that results from the interference of F_2 and F_3 fold generations in the east of the Euchre Pack Domain (Figures 7.14, 7.15). It folds the Boorloo Siltstone, and in particular it can be traced by following the lower dolomite unit, into an upright anticline with faulted and brecciated Cooranna Formation in the core. There is an area of poor outcrop to the south of the anticline which is interpreted to be a syncline with a basin morphology. The faulted contact with the Burra Group cuts across the stratigraphy in this area but the fault zone is also folded into an upright anticline, interpreted to be the same fold generation as the main anticline (Figure 7.15). On the northern limb of the Breaden Hill Anticline, the Breaden Hill Breccia and Umberatana Group dip steeply to the NE (Figures 7.14, 7.15). The F_2 axis has been folded about a open, SSW– NNE trending fold interpreted to be F_3 (Figure 7.14).

Significantly, F_1 folds are folded about the principal F_2 closure providing unequivocal temporal relationships between the fold generations. F_1 folds in the lower dolomite unit of the Boorloo Siltstone, can be traced from the NW limb of the anticline, around the western hinge into the SW limb. On the NW limb, S_0 is steep to overturned, and forms an open fold with a steep plunge to the northwest (Figure 7.16a). F_1 folds have moderate to steep plunges to the north to northwest, with sub-vertical axial surfaces varying in strike around the curve of the fold limb. There is an fanning axial planar cleavage, S_1 that dips steeply to the north and south in the hinge of one fold and steeply to the east in another due to the curve of the limb (Figure 7.16a).

On the SW limb S_0 is also folded into an open fold, but with variable orientation and an estimated steep plunge to the southeast, before it is cut-off by the faulted contact with the Burra Group. F_1 folds on this limb have moderate to steep plunges from the northwest to the southeast, with axial surfaces dipping to the south (Figure 7.16b).

On the NE limb, S_0 dips steeply to the northeast or is overturned, dipping steeply to the southwest. F_1 fold plunges are moderate to the northwest and southeast, with northwest striking axial planes dipping steeply to the northeast and moderately steeply to the southwest (Figure 7.16c). The lower dolomite unit can be traced for a short distance along the SE limb until it is cut-out by the contact with the Burra Group (Figure 7.14) but the outcrop is poor and no structural data was collected.

The hinge of the Breaden Hill Anticline is divided into western and eastern hinges based on the two outcrops of the lower dolomite unit, a reflection of the double-plunge of the anticline (Figure 7.14). Most of the structural data (Figure 7.16d) are from the eastern hinge, and from S_0, the calculated plunge is shallow to the northwest. From outcrop pattern, the western hinge has a shallow plunge to the southeast. F_1 fold plunges are shallow to the northwest, and the one F_2 fold plunge measured was also shallow to the northwest. F_1 axial

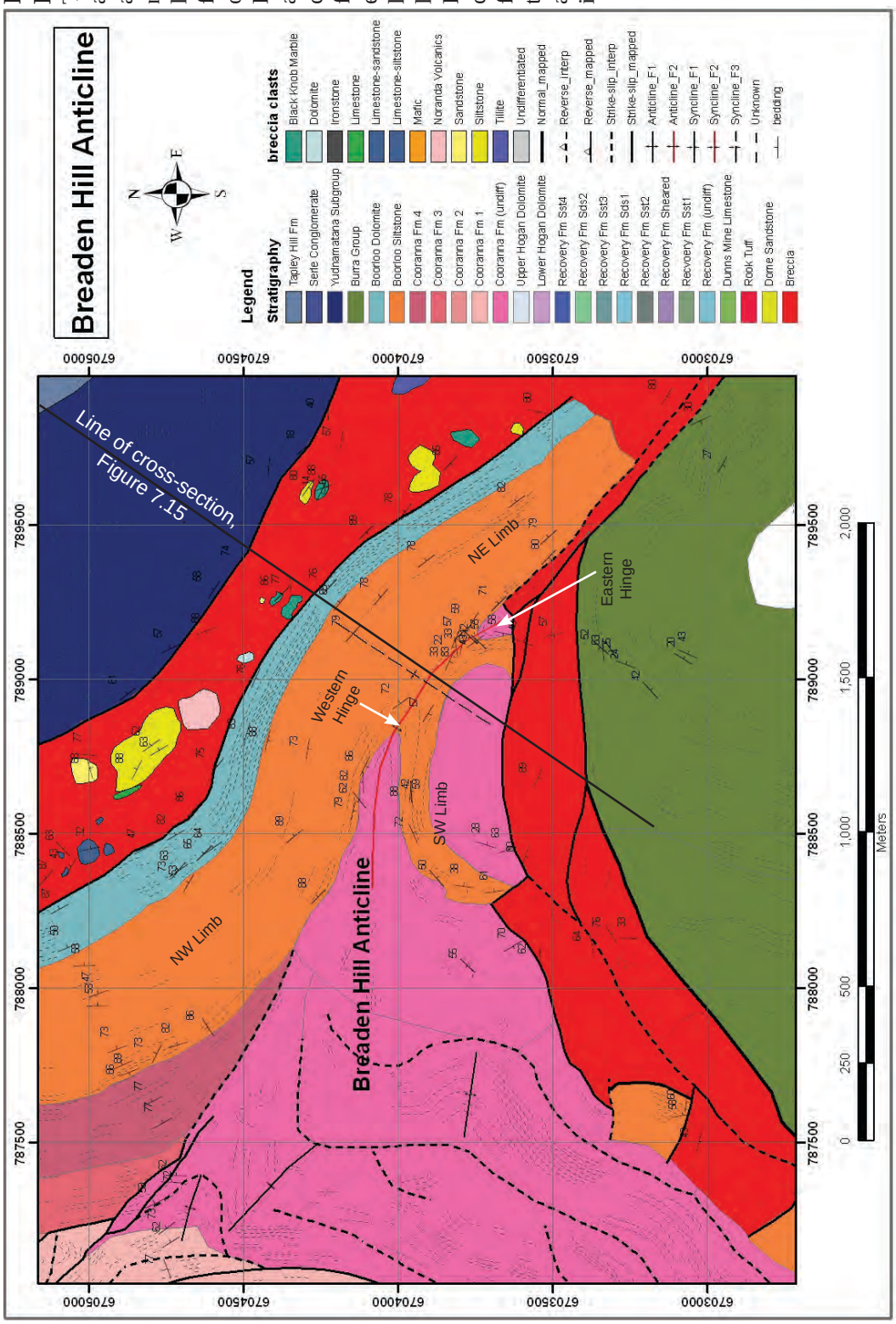

Figure 7.14 The Breaden Hill Anticline. The Breaden Hill Anticline is an upright, double-plunging anticline, folding the Cooranna Formation and the Boorloo Siltstone. Mesoscopic F_1 folds with clockwise rotation occur in the Lower Booloo Dolomite on the northwest and southwest limbs, with no change in rotation around the fold hinge. They have moderately steep plunges on the limbs of the anticline but shallow plunges in the fold hinge. Hence the Breaden Hill Anticline is interpreted to be an F_2 fold. The axial trace of the anticline has been folded around a NNE trend in an open fold interpreted to be F_3.

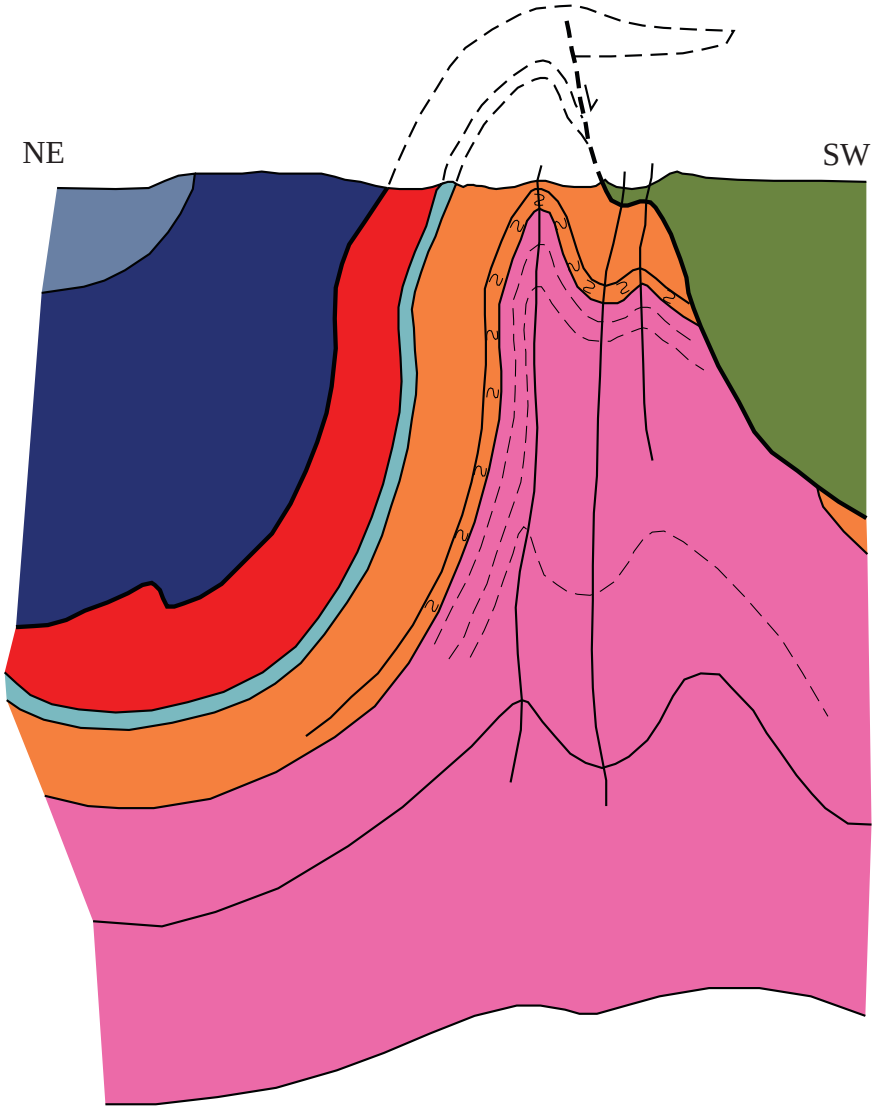

Figure 7.15. Cross-section through the Breaden Hill Anticline.
The Breaden Hill Anticline folds not only the Boorloo Siltstone but also the contact between the Burra Group and Curdimurka Subgroup to the SW and Umberatana Group and the Curdimurka Subgroup to the NE. Unit colours the same as in Figure 7.12.

N. b) On the SW limb, S_0 dips at a moderate to steep angle to the E to S reflecting F_3 folding. F_1 folds have variable plunges but are mainly to the SE to SW. F_1 axial planes dips at a steep angle to the S to SE with one dipping W. c) All structural measurements on the NE limb. S_0 has a sub-vertical dip, striking NW. F_1 axial planes also strike NW with sub-vertical dips to the NE and SW and F_1 folds plunge at shallow angles to the NW and SE. d) In the hinge of the Breaden Hill anticline, S_0 ranges from horizontal to vertical has a calculated plunge of 06º/323º. The calculated NW plunge reflects the majority of the data being collected from the SE hinge of the double-plunging anticline. F_1 axial planes dip at shallow angles to the NE, with the majority of F_1 fold plunges being shallow to the NW. Note that majority if the fold data is from isolated F_1 folds from the Lower Boorloo Dolomite on the E hinge of the fold and so reflects only a small part of the fold hinge. e) All the structural data collected around the Breaden Hill Anticline shows a large variation in S_0, brought about by the complex deformation. F_1 axial plane orientations are highly domainal and reflect the position around the fold from which they were collected. The calculated plunge of F_2 from the axial planes is 10º/298º, which is similar to the calculated plunge of F_2 from S_0 around the fold hinge. F_1 fold plunges are also domainal but taken as a whole, they are spread around a great circle with a calculated orientation of 88º/º065, reflecting F_2, with a calculated plunge of 02º/245º.

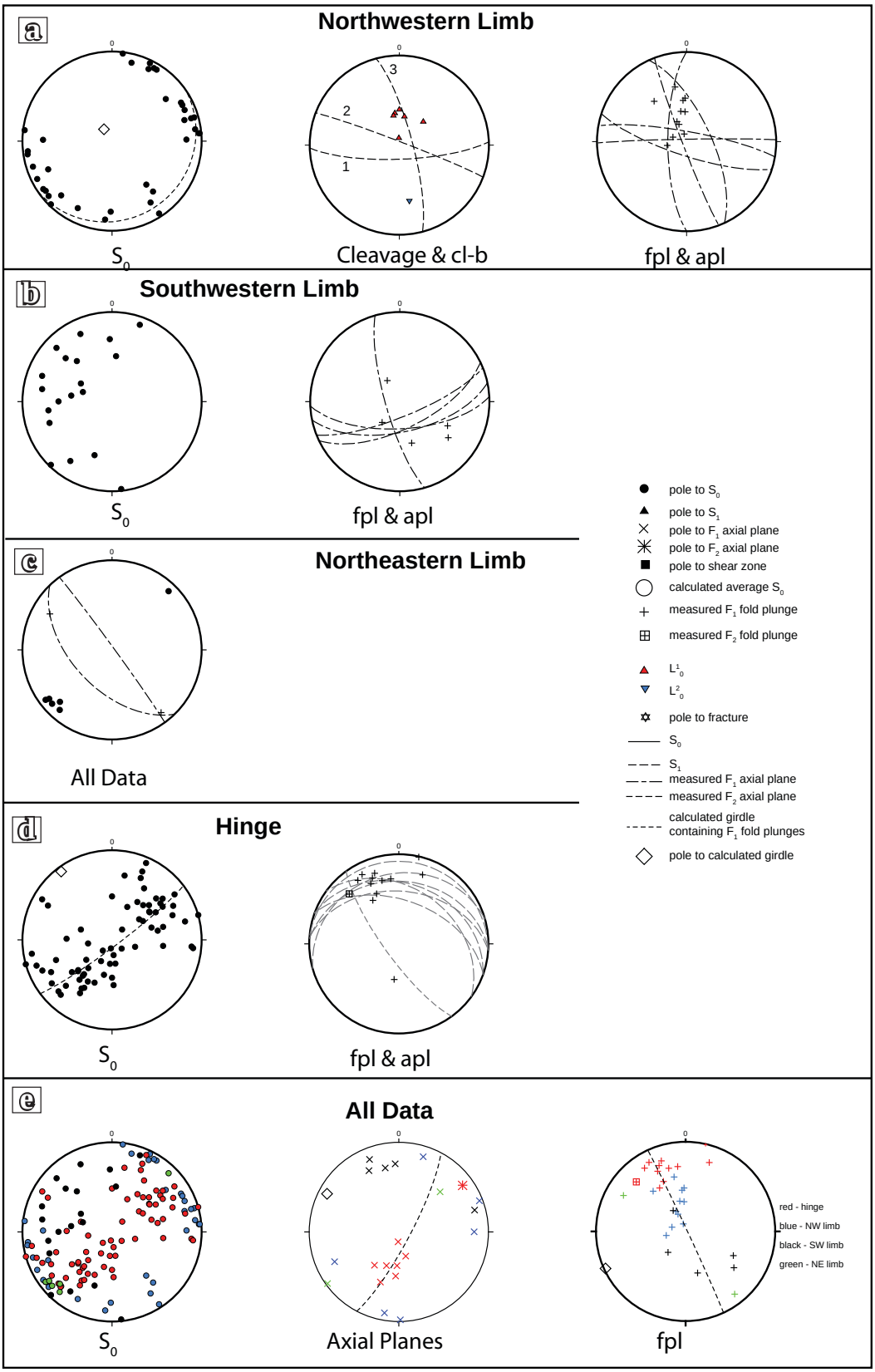

Figure 7.16. Stereonets of structural data around the Breaden Hill Anticline.
a) NW Limb. S_0 dips sub-vertically to overturned to the NE and SW. The variation in strike is attributed to F_3 with a calculated plunge to the NW S_1 has variable strike and dip, partly reflecting it being a fanning cleavage with *1* and *2* being from an F_1 fold hinge and partly due to it being rotated by F_3, with *3* being from an outcrop NW of where 1 and 2 were measured. L^1_0 plunges at a moderate to steep angle N whereas L^3_0 plunges at a moderate angle S. Axial planes all have steep dips, with the strike varying around the hinge. F_1 fold plunges are moderate to steep to the between the W and

surfaces are sub-horizontal (Figure 7.17) to shallow plunging to the NNE. The F_2 axial surface dips at a steep angle to the SW (Figure 7.16d). Mesoscopic F_2 folds are rare in the fold hinge but Figure 7.18 is an example of such a fold. It shows a tight fold (in situ the fold was upright) with a train of smaller folds and thrusts that show a dextral sense of movement which does not change around the fold hinge. These are interpreted to be D_1 structures that have been deformed by D_2.

Figure 7.18 illustrates an important point about F_2 at this locality; there is very little development of cleavage associated with F_2. There is a weak cleavage-bedding intersection L^2_0 developed at a few localities (Figure 7.19a,b), which is shallow to either the SE or NW, but the most prominent linear features are D_1 structures produced by the small folds and faults seen in Figure 7.18 and which is not a cleavage-bedding intersection.

The third deformation, D_3, has folded F_2 from the outcrop pattern about a north-northeast trend (Figure 7.14). In the absence of a strong S_2, or F_2 fold plunges or axial surfaces which can show the effects of F_3 on F_2, the geometry of F_3 can only be deduced from its effects on S_0 and F_1. On the NW limb, this is further complicated by the proximity the Noranda Camp Syncline. However in the area of the fold hinge, there is a dome and basin morphology developed. As F_1 structures are largely layer-parallel and hence sub-horizontal prior to D_2, the dome and basin morphology is an interference pattern between northwest trending F_2 and north-northeast trending F_3, with both fold generations being upright, with shallow plunges. F_1 fold plunges lend support for F_3; plotting on a great circle girdle giving a calculated plunge shallow to the southwest (Figure 7.16e).

The initial orientation of F_1 folds have been calculated by two rotations (Figure 7.20a). F_2 is thought to trend at about 210°, and so to remove the effects of F_3, each locality with F_1 fold data, the first rotation rotates the strike of S_0 at that outcrop to 300°, keeping the dip constant and bringing it into the pre-D_3 orientation. Then to remove the effects of F_2, S_0 is rotated to horizontal along a 300° trending horizontal axis (Figure 7.20a). These show that on the NW limb, F_1 folds plunge at a shallow angle to the north and south at shall, with the axial surfaces dipping at a shallow to moderate angle to the west and east (Figure 7.20b). On the NE limb, F_1 folds plunged at a shallow angle to the southeast and northwest, with axial surfaces dipping at a moderate to shallow angle to the east to northeast (Figure 7.20c). Rotated F_1 folds on the SW limb plunge at moderate angles to the north and south, and at a shallow angle to the southwest, with axial surfaces dipping at moderate angles to the northeast and southwest, and shallow to the southwest (Figure 7.20d). All the F_1 plunge data plotted together (Figure 7.20e) shows that it is widely scattered although mainly plunging at moderate to shallow angle to the north and south. This is a similar distribution of F_1 fold plunges as seen at the Fence Anticline after rotating S_0 to horizontal (Figure 7.10i,k). The rotated F_1 axial surfaces dips at shallow to moderate angles to the west and east to northeast (Figure 7.20f), which agrees with the few rotated F_1 axial surfaces from the Fence Anticline (Figure 7.10i,k).

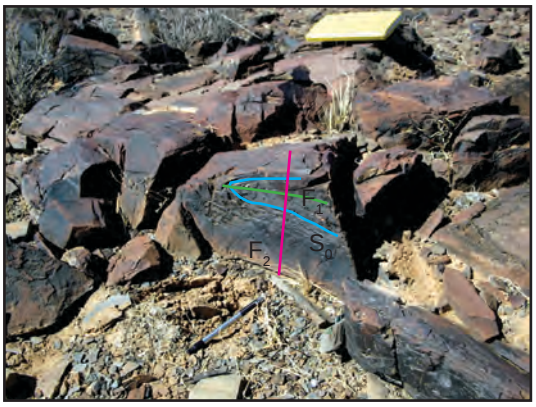

Figure 7.17. An isoclinal recumbent F_1 fold in the eastern hinge of the Breaden Hill Anticline. F_1 is re-folded by an open upright fold, F_2.

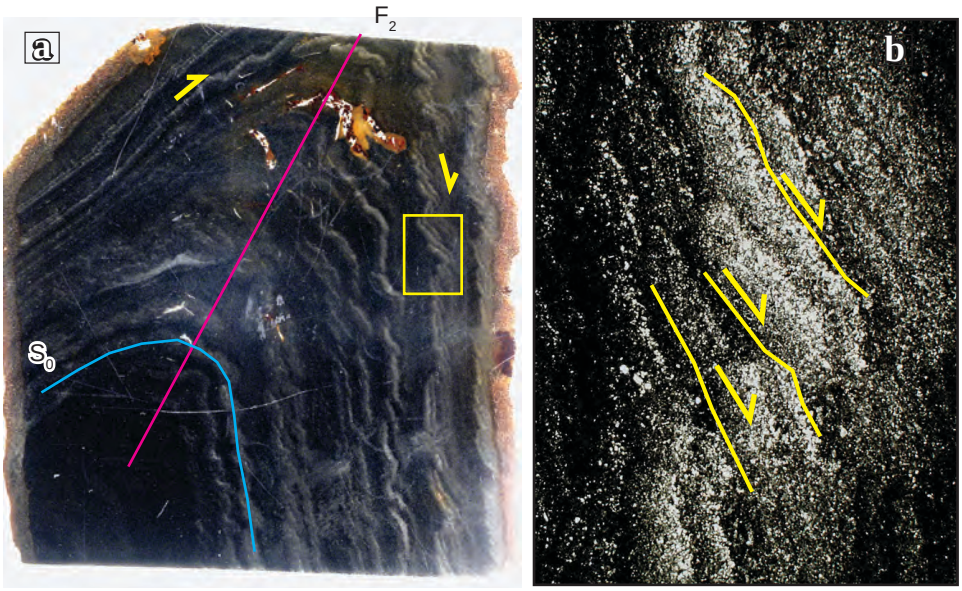

Figure 7.18. Breaden Hill Anticline, F_2 Fold Hinge.
a) Scanned image of a thin section showing an F_2 anticline in the hinge. Around the F_2 fold are F_1 structures, small thrusts and folds that show the same sense of movement around the fold, indicated by yellow arrows. f.o.v 45 mm. b) Photomicrograph of the boxed area showing the small-scale thrusts. *ppl, f.o.v*

Figure 7.19. Lineations in the Breaden Hill Anticline.
a) L^2_0 with a shallow plunge to the west in fine-grained sandstone in the anticline hinge and L^3_0 is present but barely visible. The prominent linear features are small D_1 structures similar to those in Figure 7.17, and not cleavage-bedding intersections.b) L^2_0 on the northwestern limb of the anticline. Again the prominent steeply plunging features are F_1 structures similar to those in Figure 7.17 and not a true cleavage-bedding intersection lineation.

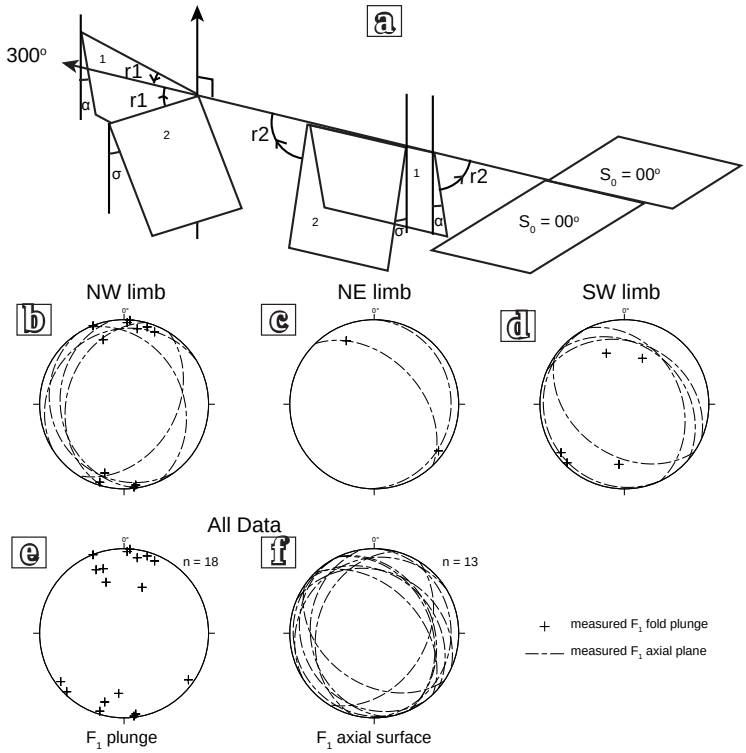

Figure 7.20. Rotated F_1 fold data for the limbs of the Breaden Hill Anticline.
a) Rotations used; r1 rotates the strike of S_0 at that point to 300°, around a vertical axis moving it into the pre-F_3 orienation; r2 rotates S_0 to horizontal, removing F_2. b) On the NW limb, rotated fold plunges are shallow to the north and south, with axial planes shallow to the west and east. c) On the NE limb, the rotated fold plunges are shallow to the NW and SE, with axial planes dipping shallow to the E and moderate to the NE. d) On the SW limb, rotated fold plunges are moderate to the N and shallow to the SW and S, and axial planes dip at moderate to shallow angles to the NE and SW. e) All the rotated fold plunges plunge at shallow to moderate angles but with a large variation plunge direction. f) All rotated axial planes have moderate to shallow dips to the W to NE and SW.

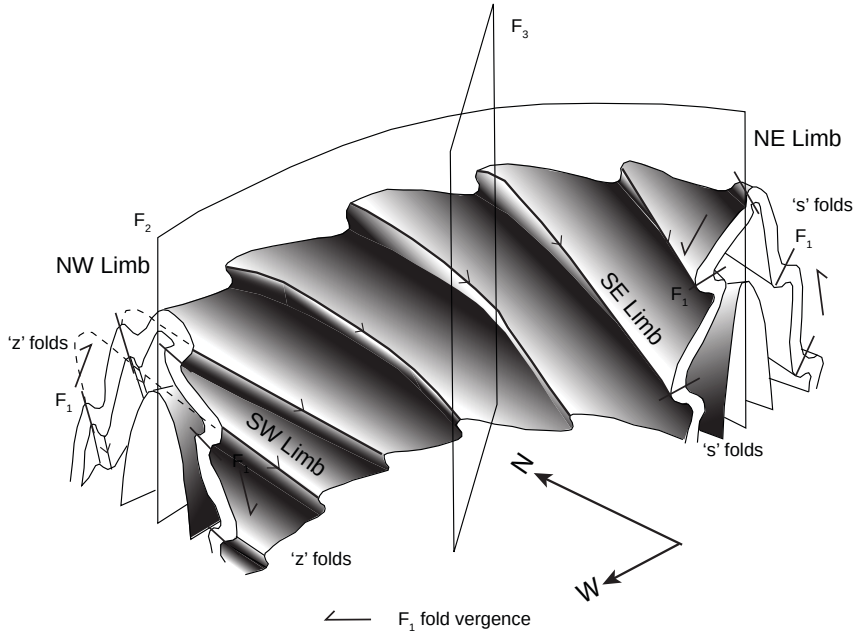

Figure 7.21 Interpretation of the Breaden Hill Anticline.
F_1 folds have south vergence, forming 'z' folds on the NW and SW limbs and 's' folds on the NE and SE limbs of the anticline. They have been folded around an upright fold F_2, the Breaden Hill Anticline, with an oblique angle between the two fold generations. F_2 has been folded around the SW trending F_3.

The main features of the Breaden Hill Anticline are shown in Figure 7.21;

- F_3 is an open fold that have folded F_2 about a NE trending axial surface,
- F_2 is a tight, upright fold that prior to F_3 trended NW and had a shallow to horizontal plunge
- F_1 has been folded about F_2, with the folds verging to the southeast.

The Drill Pad Outcrop.

The Drill Pad outcrop occurs over an area of about 50 m by 40 m in which the Dunns Mine Limestone, consisting of calcitic sandstone, siltstone and limestone, is folded into a series of tight to isoclinal, non-cylindrical folds, with variable plunges (Figure 7.22). The area was mapped at a scale of 1:200, noting fold plunges, cleavages and cleavage–bedding intersection lineations which are plotted on stereonets in Figure 7.23. Domain 3, an area of particular complexity, was mapped at a scale of 1:40 (Figure 7.22b).

No folds typical of F_1 occur at this outcrop hence the interpretation of the folding to be F_2 and F_3 and for clarity, this terminology will be used. Two cleavages are identified; S_2 which is axial planar to F_2 and it typically has a spacing of about one millimetre and S_3 which is weakly developed and typically occurs at a high angle to S_0. Both have an associated cleavage - bedding intersection, L^2_0 and L^3_0 but nowhere was a cleavage - cleavage intersection noted.

The dominant structural grain changes from southeast to west-northwest, from southern half to the northern half of the outcrop, and the interpreted affect of F_3 (Figure 7.22a). All of the structural data from the Drill Pad outcrop is shown in Figure 7.23. Contoured S_0 data describe a great circle with orientation of 28°/081°, with a calculated plunge of 62°/261°, with an estimated axial plane dipping at 70°/306°. S_2 varies around a great circle with a calculated plunge of 62°/156°. L^2_0 data cluster in two orientations, shallow to the southeast and shallow to moderate to the northwest, plotting on a calculated great circle with an orientation of 63°/236°, giving a calculated plunge of 27°/056°. Measured F_2 fold plunges are concentrated in two clusters but may plot around a small circle with an estimated orientation of 78°/048° with an alpha of about 60° and an axis plunging at 12°/227°. S_3 data plot around a great circle with an orientation of 22°/063° and L^3_0 is spread around a great circle of 73°/296°.

Together, all of the data have produced variable results, particularly with regard to the geometry of F_3-related structures, both directly measured and calculated from F_2 structures. To assist in the understanding of the relationship between F_2 and F_3, the outcrop was divided into eight domains based on the orientation of bedding (Figure 7.22). In five of these domains (Domains 1, 2, 3, 6 and 8) there are abundant mesoscopic folds, whereas in three (Domains 4, 5 and 7) mesoscopic folds are lacking and the structural style is characterized by uniformly striking and dipping layering. Stereoplots of structural data from each domain are shown in Figures 7.23b - i.

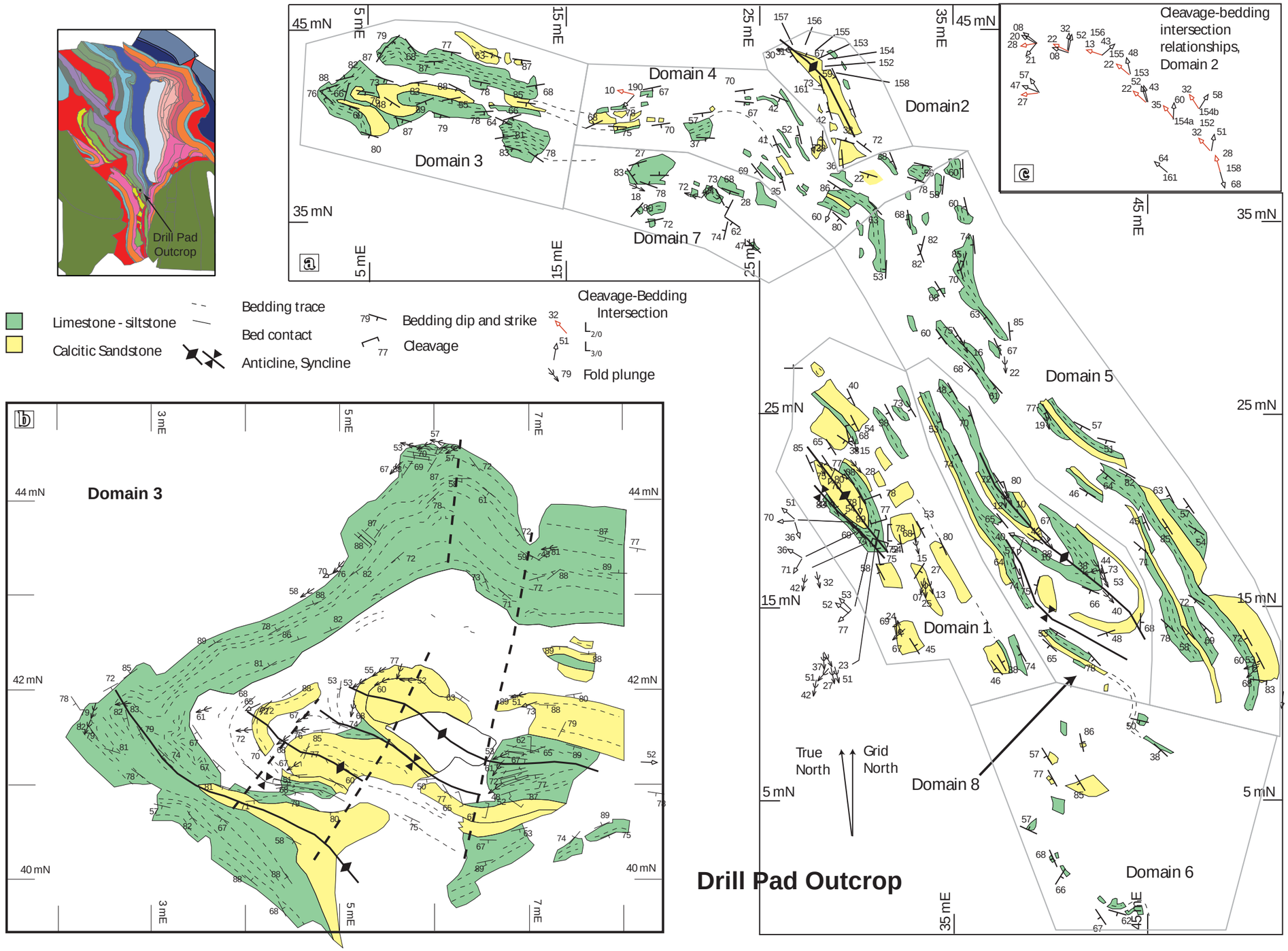

Figure 7.22. D2 and D3 deformation at the Drill Pad outcrop.
a) The Drill Pad outcrop comprises interbedded limestone-siltstone and calcitic sandstone that is tightly folded with the strike changing from NNW to WNW. It has been divided into 8 domains b) A detail of Domain 3. c) Cleavage-bedding intersection relationships in Domain 2.

a All Data	b Domain 1	c Domain 2	d Domain 3	e Domain 4	f Domain 5	g Domain 6	h Domain 7	i Domain 8
S_0 n = 396 70° to 308° contours, 1%, 2%, 3% 4%, 5%.	S_0 n = 82	S_0 n = 49	S_0 n = 158. contours 1%, 2%, 3%,4%, 5%, 6%, 7%, 8%	S_0 n = 23	S_0 n = 47	S_0 n = 35	S_0 n = 20	S_0 n = 28
Poles to S_2 n = 18 L^2_0 n = 25 Poles to S_3 n = 11 L^3_0 n = 44	S_2 n = 5 L^2_0 n = 7 S_3 n = 3 L^3_0 n = 9	S_2 n = 3 L^2_0 n = 12 S_3 n = 2 L^3_0 n = 18	S_2 n = 7 L^2_0 n = 2 S_3 n = 4	L^3_0 n = 2	S_3	S_2 n = 1 L^2_0 n = 2 L^3_0 n = 3	L^2_0 n = 1 L^3_0 n = 1	S_2 n = 2 S_3 & L^3_0 n = 12
F_2 n = 77 est small circle 78° → 048° ά ~ 60° F_3 n = 10	F_2 n = 25	F_2 n = 4	F_2 n = 30	F_2 n = 2		F_2 n = 11	F_2 n = 3	F_2

Legend

- pole to S_0
- pole to S_2
- pole to S_3
- pole to F_2 axial plane
- L^2_0
- L^3_0
- measured F_2 fold plunge
- measured F_3 fold plunge
- S_0
- S_2
- S_3
- measured F_2 axial plane
- calculated girdle
- pole to calculated girdle

All stereonets lower hemisphere projection Equal Area Stereonets

Figure 7.23 Stereoplots of structural data from the Drill Pad outcrop.
a) All Data. S_0 is spread around a great circle with an orientation of 28/081 and a calculated plunge of 62°/261°, with an estimated axial plane of 70°/307°. This is interpreted to be the orientation of the axial plane of F_3. Poles to S_2 are scattered but the majority plot around a calculated great circle of 28°/336°, with a calculated plunge of 62°/156° and an estimated axial plane of 76°/221°. L^2_0 is spread around a calculated great circle of 63°/236° with a calculated plunge of 27°/056°. An estimated axial plane is northeast striking and sub-vertical. S_3 varies considerably around a calculated great circle 22°/063° and plunge of 68°/243°. L^3_0 is spread around a great circle of 73°/296°. Measured F_2 fold plunges are concentrated in two clusters but may plot around a small circle with an estimated orientation of 78°/048° with an alpha of about 60° and an axis plunging at 12°/227°. An estimated axial plane would strike northeast with a steep dip to the southeast. Measured F_3 fold plunges are scattered but the majority are steep to the south-southeast.
b) Domain 1. S_0 is scattered but plots around a great circle with a calculated plunge of 21°/163°. S_2 strikes roughly north - south and is sub-vertical. L^2_0 plunges at a moderately steep angle to the northwest and southeast, reflecting the orientation of the bedding planes they were measured on. S_3 strikes roughly east - west but with up to 60° variation in dip. L^3_0 plot on a great circle with an orientation of 69°/257°. As these were all measured on S_0, this is interpreted to be S_3. F_2 fold axes plunge at a shallow to moderate angle to the south.
c) Domain 2. Poles to S_0 in Domain 2 plot of a great circle and have a calculated plunge of 60°/133°. The strike of S_2 varies in orientation from north to northwest, with a steep dip. The variation in dip in the northwest striking S_2 is attributed to it being a fanning cleavage. The intersection of these three planes is at a moderate angle to the southeast and so is the likely plunge of F_3. L^2_0 plot around a great circle with a pole at 63°/134°. S_3 strikes northeast with a moderate to steep dip to the northwest. L^3_0 data are scattered with most having a moderate plunge to the northwest to northeast. The F_2 fold that forms the centre of the domain has a variable plunge from shallow to the northwest to moderate to the west.
d) Domain 3. S_0 in Domain 3 is scattered around a great circle with a calculated orientation of 20°/063°, giving a calculated plunge of 70°/243°, which is interpreted to be the plunge of the F_2 fold on which Domain 3 is centred. S_2 dips steeply to the south, wth one sub-vertical S_2 striking northwest. Only two L^2_0 lineations were measured, both plunging steeply to the west-southwest. S_3 dips at a moderately steep angle to the west. Measured F_2 fold plunges vary from moderately steep to steep to the southwest to northwest, with an average of 63°/254°.
e) S_0 in Domain 4 is scattered about a great circle with a calculated orientation of 42°/070°, giving a plunge of 48°/250°. L^3_0 plunges at a moderate angle to the south to southwest and F_2 plunges at a shallow angle to the south.
f) S_0 in Domain 5 is scattered around a great circle with a calculated orientation of 28°/052°, giving a plunge of 62°/232° and the one measured S_3 dips at a steep angle to the south-southwest.
g) S_0 in Domain 6 is scattered around a great circle with an a calculated orientation of 77°/350°, giving a plunge of 13°/170°. The one measured S_2 dips at a steep angle to the east and L^2_0 plunges at a moderate angle to the north-northwest. L^3_0 plunges at a moderately steep angle to the southwest and at a moderate angle to the northeast, and F_2 plunges at a shallow angle to the south and north.
h) S_0 in Domain 7 shows too much variation to calculate reliable statistics although there is a concentration dipping steeply to the south to west. The one L^2_0 measured plunges at a shallow angle to the west-northwest, and the one measured L^3_0 has a sub-vertical plunge to the west-southwest. Measured F_2 fold plunges are variable, from steep to the north and northeast to shallow to the southeast.
i) In Domain 8, S_0 are scattered around a great circle with a calculated orientation of 33°/171°, giving a plunge of 57°/351°. S_2 dips at a steep angle to the west to southwest and S_3 dips at a steep angle to the south-southwest. L^3_0 is scattered around a great circle with calculated orientation of 71°/296°. F_2 plunges at a shallow to moderate angle to the south to southeast.

Within Domain 1, there are a series of tight anticlines plunging at a shallow angle to the southeast (Figure 7.22). From bedding, the calculated plunge of the folds is 21°/163°, and from measured fold plunges, the average plunge is 26°/175° (having removed several outliers: Figure 7.23b). Anticlines have rounded hinges, whereas synclines have angular profiles (Figure 7.24a,b). Axial planes dip steeply to the southwest (Figure 7.24b) and there is a fanning axial plane cleavage. Axial traces vary slightly, from trending southeast to east-southeast. Carbonate units are characterised by considerable thinning in fold limbs and thickening in the hinge regions (Figure 7.24c). A weak cleavage (S_3) cuts across bedding at a high angle, striking north-northeast – south-southwest. On the flanks of the anticlines, two cleavage-bedding intersections are present. The first, L^2_0, has a shallow plunge to the southeast, with a spacing of one to two millimetres whereas the second is more widely spaced, has a steep plunge to the south west and is due to the intersection of S_3 and S_0 (L^3_0) (Figure 7.23b).

Domain 2 is centred on a prominent non-cylindrical anticline with a gently curving axial trace (Figure 7.22a, 7.25a). The trend of the anticline changes from northwest to west, with shallow plunges to those directions. Poles to bedding define a girdle, the pole to which (F_2) is 30°/312° (Figure 7.23c), with an axial plane dipping at 85°/040°. At the tip of the fold, the plunge, calculated from bedding is 40°/282°. On fold limbs, bedding is steeply dipping to overturned, with gentle undulations of the bedding surface recording deformation about a sub-vertical axis. S_2 has a steep dip, varying in strike direction with F_2 strikes at a high angle to bedding (Figure 7.23c). Two prominent lineations are present (Figure 7.25b). L^2_0 has a moderately shallow plunge to the north-northwest in the southeast of the domain to west in the northwest. L^3_0 has a variable plunge, dependent on the bedding plane (Figure 7.23c) but compared with L^2_0 on the same bedding plane, it is steeper and at a moderately high angle to the axis of the fold, to the northwest to west.

The overall structure of Domain 3 is a tight anticline defined by an outer carbonate unit with several anticline and syncline pairs in the centre of the larger fold, all steeply plunging to the west (Figures 7.22a,b, 7.23d). Calculated from bedding, the overall plunge is 71°/243° and from measured fold plunges, the average plunge is 66°/248° (Figure 7.23d). The anticlines have rounded profiles and the synclines are angular (Figure 7.26a). S_2 is a fanning cleavage with an average dip to the south (Figure 7.26b). The dominant S_0 trend on the northern limb of the fold and S_2 are folded into open folds with north trending axial plane interpreted to be F_3 (Figure 7.22b). There is a weak cleavage, S_3 that fans around the F_3 fold roughly perpendicular to bedding, and cutting S_2 at a high angle (Figure 7.23d).

Domain 4 is between Domains 2 and 3 (Figure 7.22a). S_0 changes strike from north to northwest, defining an open fold with a roughly north trending axial trace interpreted to be F_3. Dip is moderate to steep to the south to southwest. Calculated from bedding, the plunge of the F_3 fold is 48°/250° (Figure 7.23e). F_2 fold closures are not prominent with two measured fold plunges being shallow to the south. L^3_0 is shallow to moderate to the south (Figure 7.23e).

Bedding in Domain 5 trends north-northwest, with a steep dip to the west-southwest (Figure 7.22a). No F_2 fold closures were noted in Domain 5. There is some minor folding of bedding attributed to F_3 (Figure 7.22a). Calculated from bedding, the plunge of F_3 is $62^o/232^o$ (Figure 7.23f). S_3 dips steeply to the south, striking at a high angle to S_0 (Figure 7.23f).

Domain 6 is at the southern end of the outcrop, along strike from Domains 1 and 8 (Figure 7.22a). The outcrop is poorer, with only a few scattered low areas of rock poking above the surface and no folds on the scale seen in Domain 1 are seen. S_0 is spread around a great circle with a calculated plunge of $13^o/170^o$ (Figure 7.23g). No large S_2 folds occur in the domain but there are a number of small F_2 folds with shallow plunges to the south and north. S_2 dips at a steep angle to the west and S^2_0 has a shallow plunge to the north. L^3_0 plunges to the southwest and northeast (Figure 7.23g).

Domain 7 is an area of poor outcrop, adjacent Domain 4 and along strike form Domain 3 (Figure 7.22a). S_0 is scattered although mainly dipping to the southwest at moderate to steep angles (Figure 7.23h). A few small F_2 folds were mapped with variable plunges, steep to the northeast and northwest, in the western half of the domain and shallow to the southwest in the eastern half (Figure 7.23h). One L^2_0 was measured, plunging at a shallow angle to the west-northwest, and one L^3_0, plunging steeply to the southwest (Figure 7.23h).

Domain 8 is centred on an anticline and syncline pair between Domains 1 and 5 (Figure 7.22a). As calculated from bedding, F_2 in Domain 8 plunges at $33^o/171^o$ (Figure 7.23i). F_2 folds have measured plunges shallow to moderate to the south-southeast, with an average plunge of $33^o/160^o$ (Figure 7.23i). S_2 dips at a a steep angle to the west to southwest and S_3 cuts across bedding, F_2 and S_2 at a high angle (Figure 7.27), dipping steeply to the south-southwest and L^3_0 plunges are scattered, plunging at moderate to steep angles to the southwest and shallow to the northwest (Figure 7.23i).

The Drill Pad outcrop displays two deformations (Figure 7.28). It shows a curving dome and basin interference pattern, which corresponds to a modified type 1 pattern (Ramsay, 1967). This geometry reflects interference of non-coplanar, upright fold generations. The first deformation at this outcrop, D_2 produced folds F_2, with a fanning axial plane cleavage S_2. The best examples of these occur in Domains 1, 2 and 3. In Domains 1, the folds plunge at a shallow angle to the southeast, in Domain 2 the plunge has changed direction to shallow to the northwest but steepening and changing direction to the west over the five metres of outcrop within the domain. Finally, at the western end of Domain 3, these same folds plunge steeply to the west. It is not certain whether F_2 folds were originally cylindrical nor non-cylindrical at this outcrop. The present fold geometry could be produced by either cylindrical or non-cylindrical folds being re-folded by F_3. In the first case, the change in F_2 fold plunge is attributed soley to F_3 whereas in the second, F_3 may be exaggerating the variable plunge of non-cylindrical folds.

The axial planar cleavage associated with these folds varies in strike from north - south in Domain 1 to northwest in Domain 2 to east - west in Domain 3. L^2_0 should parallel F_2

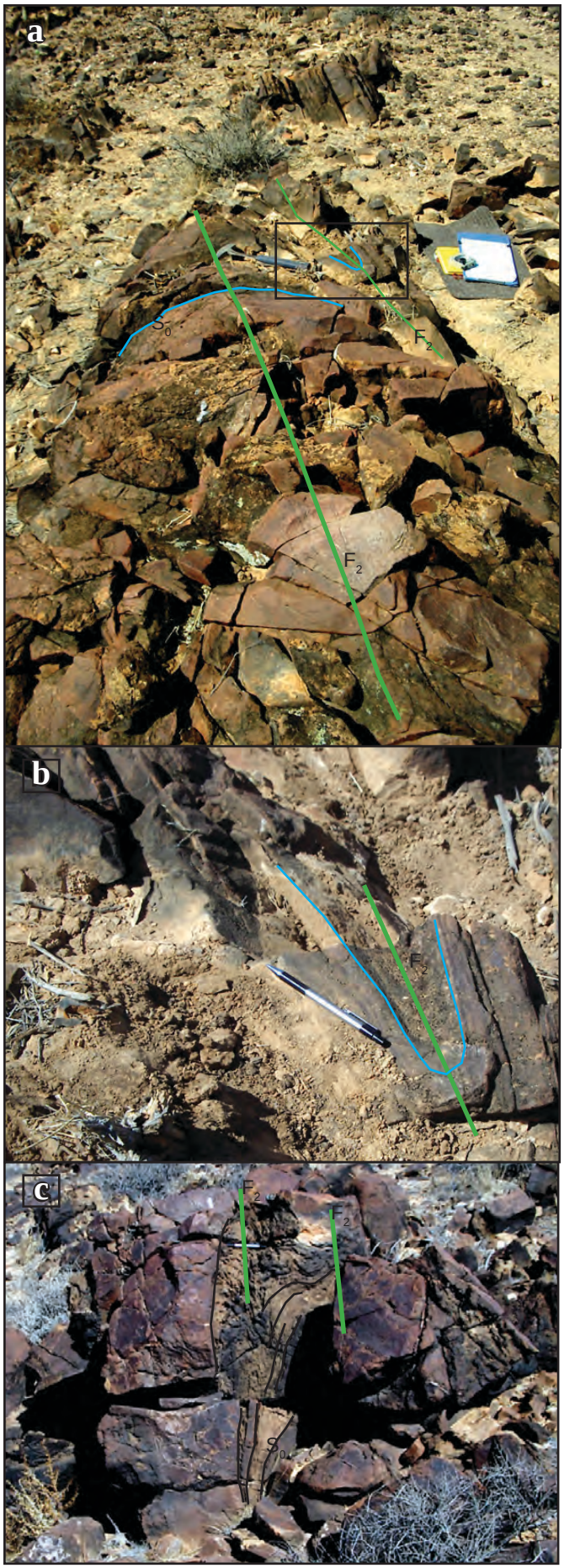

Figure 7.24. D_2 at the Drill Pad Outcrop, Domain 1, Dunns Mine Limestone.
a) Domain 1; looking SE, down the plunge of a D_2 anticline and syncline, showing slight overturning of a limb. b) Domain 1; detail of the area highlighted in 7.16a, showing slight overturning of the southwestern limb of the syncline. c) Domain 1; a D_2 fold showing extreme thinning of the carbonate bed in the limb and thickening in the fold hinge.

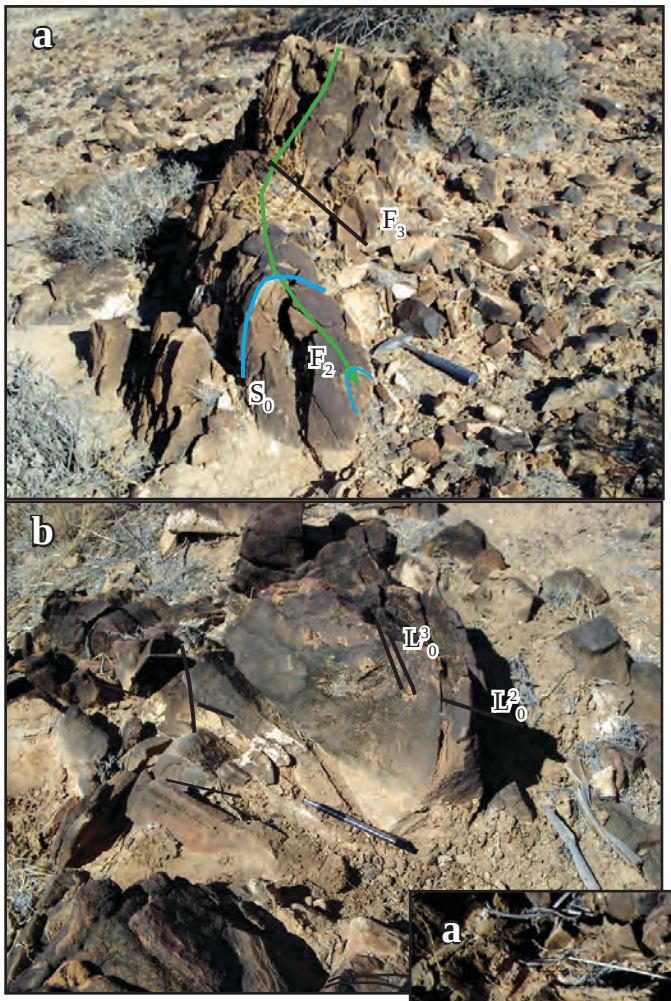

Figure 7.25. D_2 and D_3 in Domain 2, Drill Pad Outcrop; Dunns Mine Limestone.
a) Looking ENE along a F_2 fold. The F_2 fold, folded by F_3. The plunge is initially shallow to the northwest, steepening slightly and changing to the west in the foreground. b) Bedding - cleavage intersection lineations L^2_0 and L^3_0 on the northern limb of the fold in 7.24a.

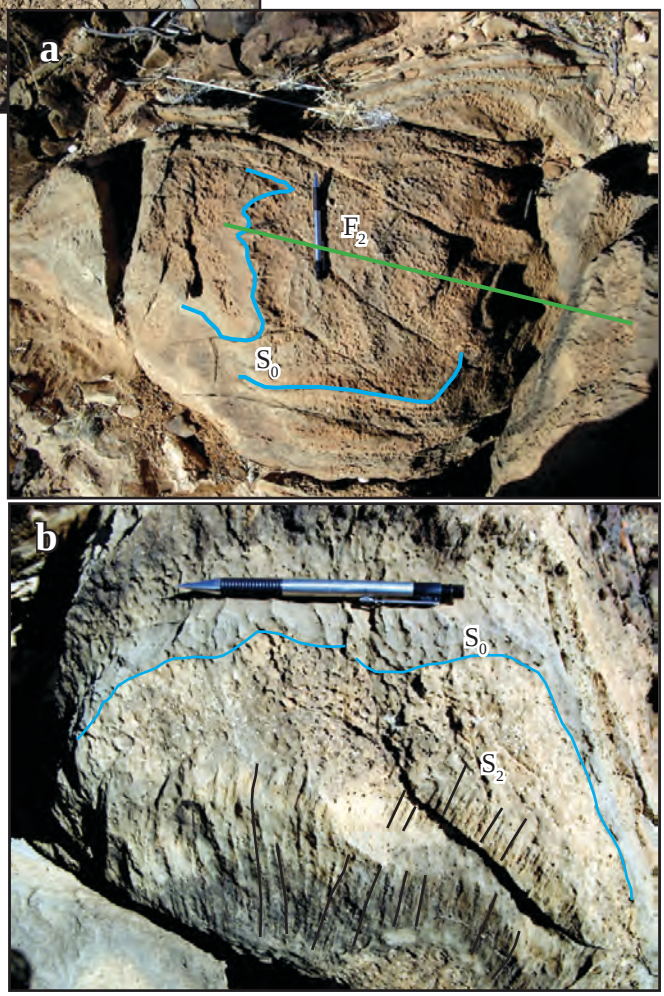

Figure 7.26. Steeply plunging F_2 folds in limestone; Drill Pad outcrop, Domain 3.
a) An F_2 fold in limestone showing thickening in the hinges and thinning in the limbs. b) An F_2 fold in limestone with a fanning axial plane cleavage.

Figure 7.27. The relationship between F_2 and S_3, Domain 7.
F_2 plunges at a shallow angle to the SE and S_3 cuts across S_0 at a high angle giving L^3_0 a variable plunge to SW

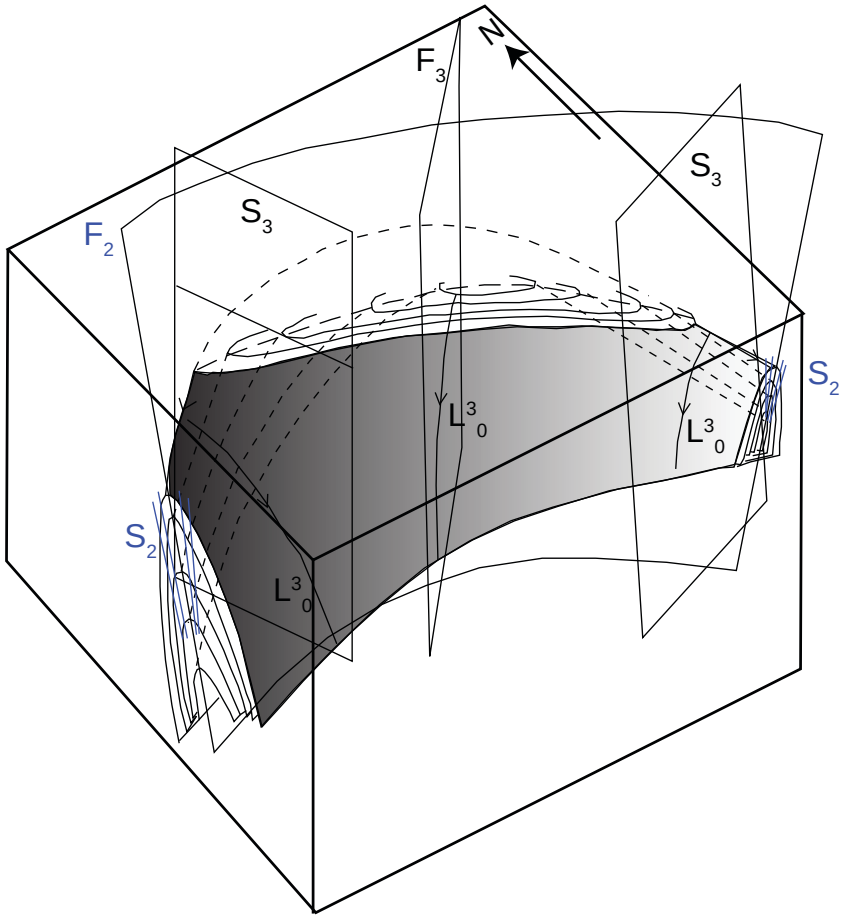

Figure 7.28 Interpretation of the Drill Pad Outcrop.
S_0 is folded by F_2 into tight folds with a fanning axial cleavage, S_2. F_3 has folded F_2 and S_2 about a SW trending axis with S_3 at a high angle to S_0.

fold plunges and broadly they do follow the same pattern, from shallow plunging to the southeast, shallow but variable to the north to west in Domain 2 and steep to the west in Domain 3. The change in the general strike of S_0, the plunge of F_2 folds, S_2 and L^2_0 define F_3.

At the Drill Pad outcrop, D_3 is therefore seen as open folding that has folded S_2 from striking southeast to west from Domain 1 to Domain 3. The calculated plunge from all S_2 data is steep to the southeast, with an axial plane that has an estimated steep dip to the southwest. However F_2 fold plunges plot on a great circle with a plunge at a moderate angle to the northeast and an estimated axial plane of 65°/145°, which is similar to the results from all the L^2_0 data. S_3 is always at a high angle to S_0 and S_2, not only at this outcrop but at other outcrops where S_3 is seen. In effect it is a fanning cleavage and their intersection will be the plunge of F_3, which is steep to the southwest and close to the majority of measured F_3 fold plunges. L^3_0 will vary depending on which limb of the F_2 fold it was measured but there are two clusters, one with plunges to the northwest to northeast and a second with steep plunges to the southwest. These clusters represent measurements on the northern and southern limbs of the S_2 fold respectively. Taking all of these factors into account, F_3 is interpreted to be open folds with a moderately steep plunge to the southwest and a sub-vertical axial plane striking roughly northeast. It has an associated spaced cleavage S_3 that is always at a high angle to S_0 and has an associated cleavage - bedding intersection lineation L^3_0 (Figure 7.28).

7.4.3 Fault Styles

7.4.3.1 Introduction

Just as there are a range of fold styles, there are several different fault styles, distinguished on the bases of their orientation, both absolute and relative to bedding, and kinematics. The dominant fault type occurs at a low angle to bedding with apparent strike-slip movement. Faults of this type are mainly dextral (i.e., east block south) with a few showing sinistral (i.e., east block north) movement. A second fault type also has apparent strike-slip movement but is oriented at a high angle to bedding, and involves inconsistent senses of displacement. The third major fault type involves high-angle reverse faults, with no consistent relationship to bedding. It will be shown that the high-angle reverse faults post-date the faults with apparent strike-slip movement.

7.4.3.2 Low Angle Faulting with apparent strike-slip movement.

The majority of faults in the Euchre Pack Domain have apparent strike-slip movement, most at a low angle to bedding. They affect all stratigraphic units of the Curdimurka Subgroup but at the scale of the Euchre Pack Domain, three major fault systems at low angle to bedding are identified (Figure 7.29);

- the Eastern Fault Zone at the upper contact of the Curdimurka Subgroup;

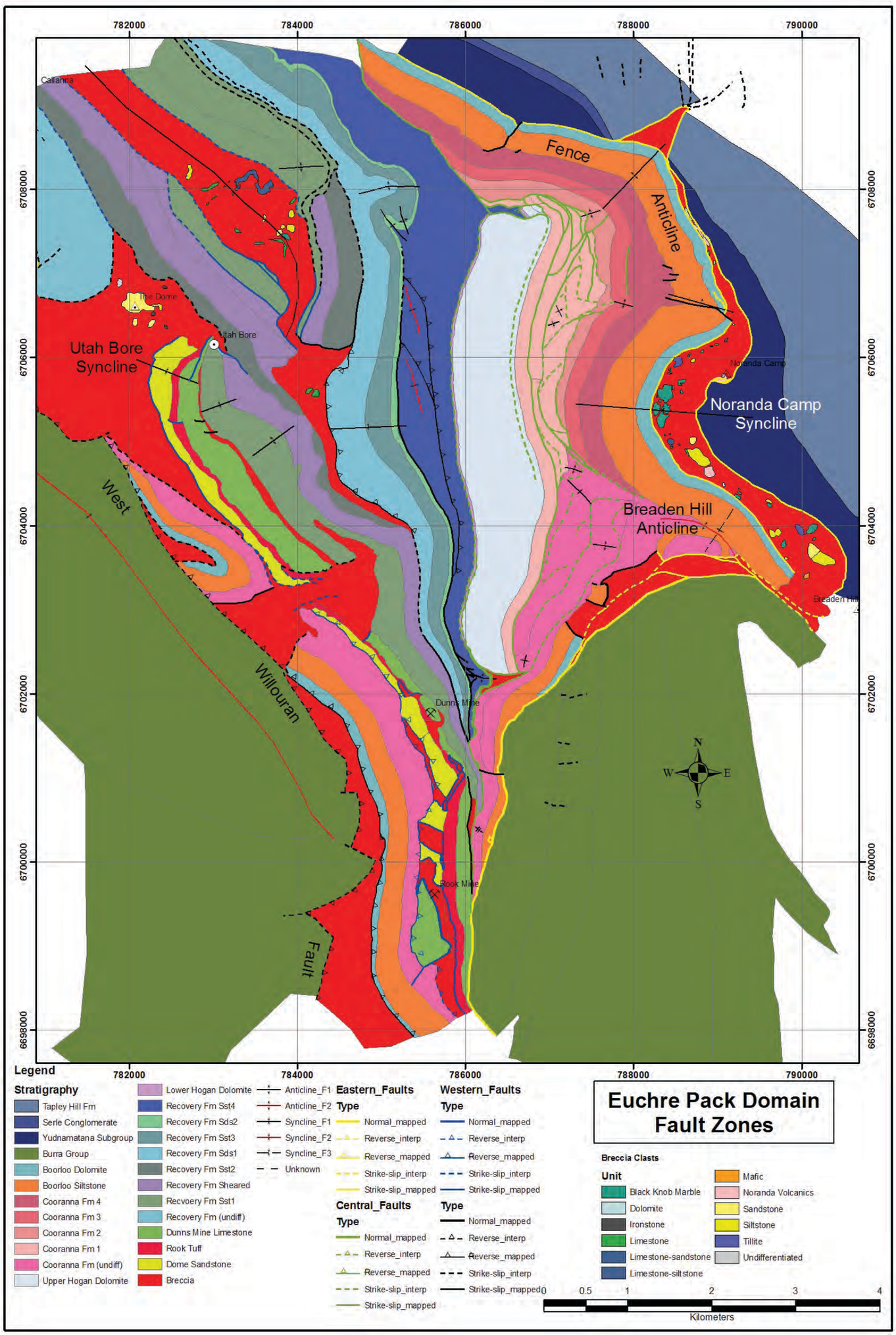

Figure 7.29. Major faults and fault zones in the Euchre Pack Domain.
The Euchre Pack Domain has many faults but three main groupings of strike-slip faults are recognized; Eastern Fault Zone (yellow), Central Fault Zone (green) and Western Fault Zone (Blue). The West Willouran Fault is another major fault zone that forms the western boundary of the Euchre Pack Domain. Other, smaller faults are un-named.

- the Central Fault Zone, which is a complicated system extending from the base of the Hogan Dolomite to the middle of Cooranna Formation ultimately merging with the Eastern Fault Zone in the southern Euchre Pack Domain, and,
- the Western Fault Zone which affects units stratigraphically below the Recovery Formation.

The Eastern Fault Zone.

The Eastern Fault Zone separates the Boorloo Siltstone from the Umberatana Group in the northern half of the Euchre Pack Domain, and from the Burra Group in the southern half (Figure 7.30). It is complicated by the Breaden Hill Breccia between the Boorloo Siltstone and the Umberatana Group and by reactivation as a reverse fault.

The northern fault termination of the fault zone is in the Umberatana Group, near the upper contact of the Amberoona Formation (Figures 7.30, 7.31). It splits into two, along either side of a triangular breccia body northeast of hinge 1 of the Fence Anticline (Figure 7.30, 7.31). In the hanging wall of the northwestern branch, the Yudnamatana Subgroup is folded into a rollover anticline. The Boorloo Siltstone is not affected by this fault, and although it could not be confirmed due to poor outcrop, it is interpreted that the fault continues along the contact between the Boorloo Siltstone and the Umberatana Group. From the presence of the rollover anticline, the fault movement is interpreted to be sinistral (Hamblin, 1965).

The fault on the eastern margin of the breccia is largely constrained to the Breaden Hill Breccia, rarely cutting down stratigraphy into the upper-most Boorloo Siltstone (Figure 7.30). It is exposed in several outcrops, mainly in a narrow gully in the north – south striking segment where sub-vertical shear zones cut clasts within the breccia (Figure 7.32a,b). Along this segment, clasts of tillite are entrained in the breccia, and have been deformed with it (Figure 7.32c,d). Where the Breaden Hill Breccia widens shearing is constrained to the breccia and is strongest nearer the contact with the Umberatana Group. Here muscovite is developed on shear planes and there is rotation of rock fragments (Figure 7.32e). Movement is sub-parallel to the contact. Structurally a few metres above the top of the Boorloo Dolomite, several megaclasts contain zones of weak shearing sub-parallel to the contact of the breccia (Figure 7.32f).

South of the Breaden Hill Anticline the fault zone is between the Curdimurka Subgroup and the Burra Group (Fig. 7.30). It initially trends southwest, cutting across the stratigraphy from the Boorloo Siltstone to the Cooranna Formation of the Curdimurka Subgroup, and the Skillogalee Dolomite to the Emeroo Subgroup of the Burra Group. At about 6701700 mN, the fault zone returns to a north – south strike, between the Emeroo Subgroup to the east and Curdimurka Subgroup to the west (Point A, Figure 7.30). The dip of bedding in the Emeroo Subgroup and the Boorloo Siltstone are roughly parallel across the contact. It crops out in a gully where a shallow-plunging isoclinal fold within the shear zone indicates sub-vertical movement (Figure 7.33). On either side of the shear zone is a narrow zone of brecciation, giving the fault zone a total thickness of about 20 m at this locality.

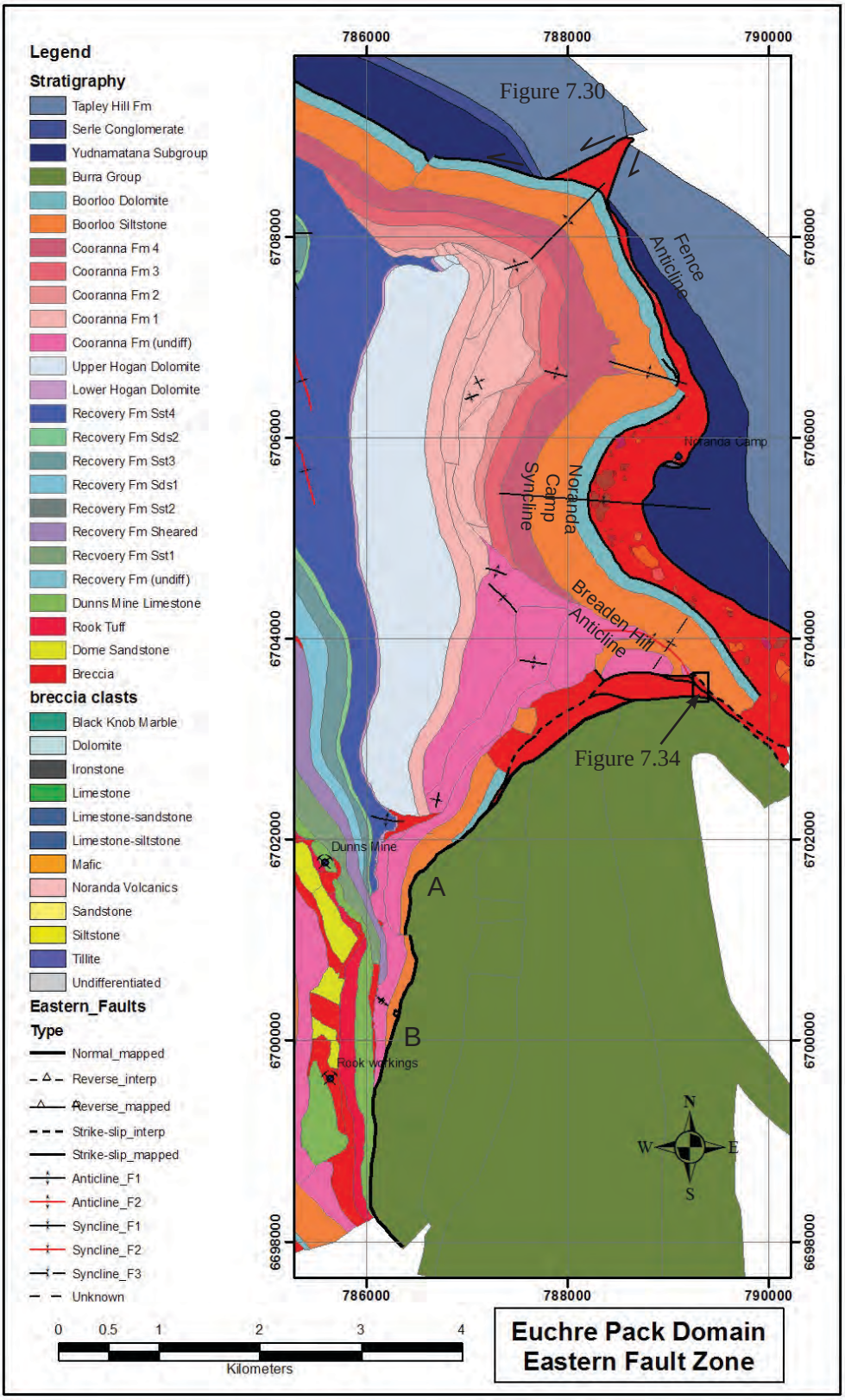

Figure 7.30. The Eastern Fault Zone.
The Eastern Fault Zone separates the Boorloo Siltstone from the Umberatana Subgroup north of about 67023600 N, although with the Breaden Hill Breccia between, and from the Burra Group south of there. It dips steeply to the east, sub-parallel to bedding in the Umberatana Group, cutting down stratigraphy of the Burra Group to about point A, then sub-parallel to bedding in the Burra Group. South of point B, it cuts down through the Curdimurka Subgroup to the level of the Dunns Mine Limestone.

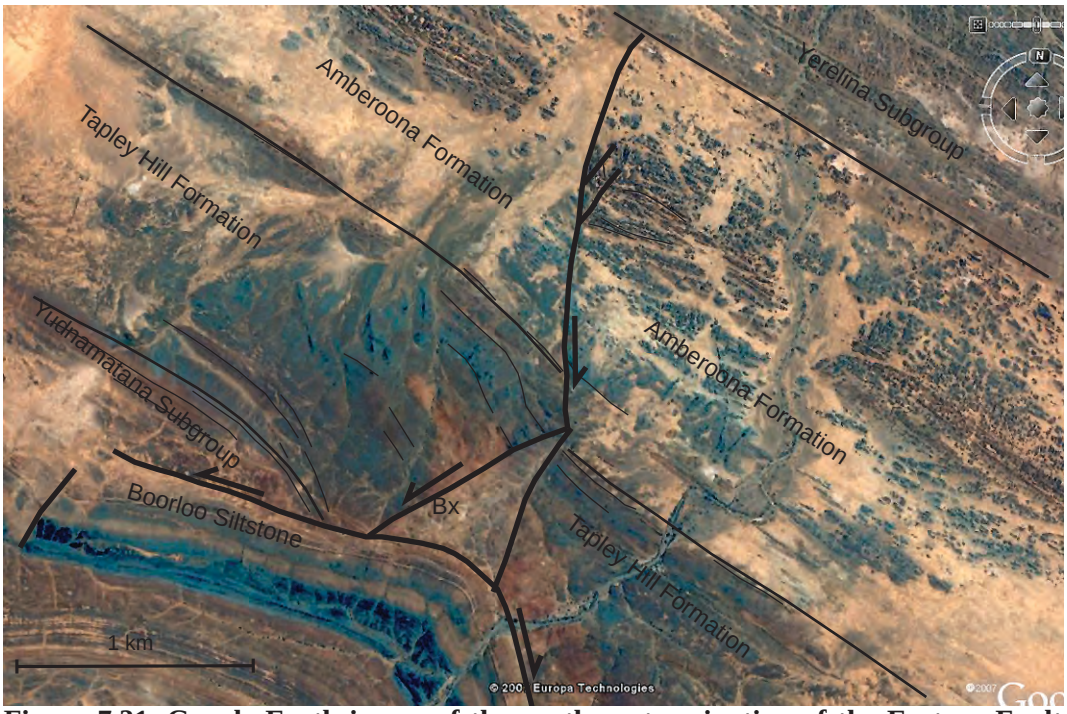

Figure 7.31. Google Earth image of the northern termination of the Eastern Fault Zone.

The Fault extends into the Umberatana Group, displacing the Tapley Hill Formation. On the western side, the Yudnamatana Subgroup and overlying Tapley Hill Formation is folded into a roll-over anticline.

The fault zone cuts down through the Boorloo Siltstone, then the Cooranna Formation until it merges with the Central Fault Zone and the Burra Group is in contact with the Dunns Mine Limestone (Figure 7.30). In this section, the fault is obscured by scree but adjacent to the fault zone, the thick sandstone units of the Emeroo Subgroup are typically brecciated (Figure 7.34).

At one locality south of the Breaden Hill Anticline (Figure 7.30), the fault zone crops out in a creek bed over 160 m (Figure 7.35). The protolith is interbedded siltstone-sandstone, with minor carbonate beds within the Skillogalee Dolomite. Structural measurements show that the fault zone is folded (Figure 7.36), and to help understand the folding, the fault zone was divided into seven domains, based on the degree of shearing and shear orientation (Figure 7.35, 7.36). On the southern margin of the fault zone (Domain 1), the rock is brecciated, from polygonal fracturing in more massive units to erosion of clast edges to minor rotation of clasts (Figure 7.37a,b,c). Fractures strike northwest but have variable dips (Figure 7.36a). Thinly bedded sandstone and siltstone is weakly sheared, with no development of muscovite on shear planes which have variable orientation (Figure 7.36a). In Domain 2 shearing intensifies but the protolith retains its basic structure; thin sandstone beds within interbedded siltstone-sandstone beginning to break apart and massive sandstone beds are brecciated. There is some folding of the shear zone, with Figure 7.36b showing that poles to shears could be fitted to either a great or a small circle girdle, but both indicate a shallow plunge to the northwest.

Toward the centre of the fault zone (Domains 3 and 4), the shearing becomes more organized, with two and rarely three shear planes developed. The relationship between multiple shear

Figure 7.32. Shearing in the Breaden Hill Breccia.
a) Sheared Noranda Volcanics; the top of the Boorloo Siltstone is 10 m to the west (right) of the photograph. b) A sheared dolomite clast close to the Umberatana Group contact. c) A clast of tillite (under hammer) within a dolomite clast. d) Tillite (white outline) within folded dolomite clast. e) Sheared sandstone a few metres below the Umberatana Group contact. Rotation and fracturing of blocks indicates dextral movement. f) Fractured and sheared tillite within the Breaden Hill Breccia. Weak shear planes are marked in black and fractures in clasts are black and white dashed lines. The top of the Boorloo Siltstone is about 20 m to the right of the photograph.

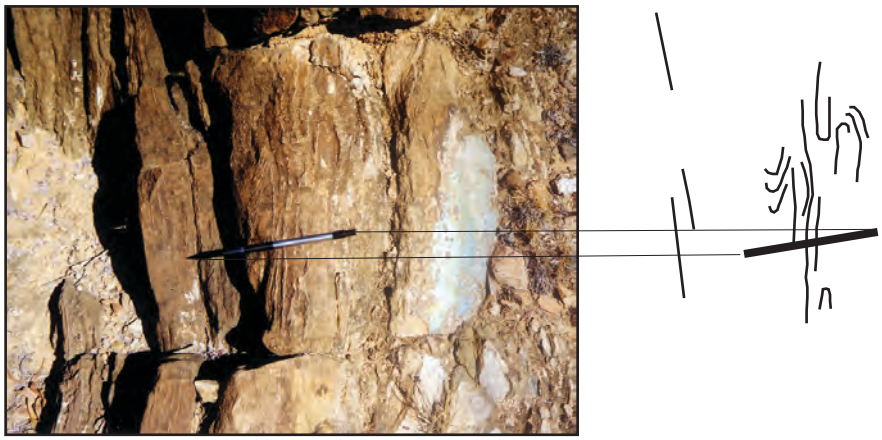

Figure 7.33. A shear zone along the contact between the Boorloo Silstone and the Emeroo Subgroup.
The Boorloo Siltstone is to the right of the picture and the Emeroo Subgroup to the left. Shearing has formed isoclinal folds within what was originally Emeroo Subgroup sandstone and shale. In the right of the photograph is brecciated sandstone-siltstone.

Figure 7.34. Fractured Emeroo Subgroup sandstone adjacent the Eastern Fault Zone.
The fracturing is sub-parallel to the faulted contact, which is to the right of the photograph but covered by scree.

planes follows no particular pattern. In some cases they may have similar strikes with differing dips, in other cases there may be two bounding shears with the same orientation and two opposing shears between. Shear sense indicators from rotated clasts and strain tails show that the main movement is dextral although sinistral movement is also indicated (Figure 7.37d). Measurements of the dominant shear planes in Domain 3 and mesoscopic folding of the dominant shear plane in Domain 3 show that the fault zone folded into an open, upright fold (Figure 7.37e). The calculated and measured plunges are shallow plunge to the northwest (Figure 7.36c). There is also a weak shear plane – axial plane cleavage intersection lineation, which also has a shallow plunge to the northwest (Figure 7.36c). In Domain 4, the shears strike northwest with steep dips to the northeast and a few dipping to the southwest (Figure 7.36d). The northeast dipping shears plot in two clusters representing main and oblique shears (Figure 7.36d).

Where shearing is most intense (Domains 5 and 6), the shear planes become better defined, with well developed ‘s’ and ‘c’ bands (Figure 7.37f). There is a gradual change in shear strike, from north-northwest in Domain 5 to north in Domain 6 with dips being steep to the

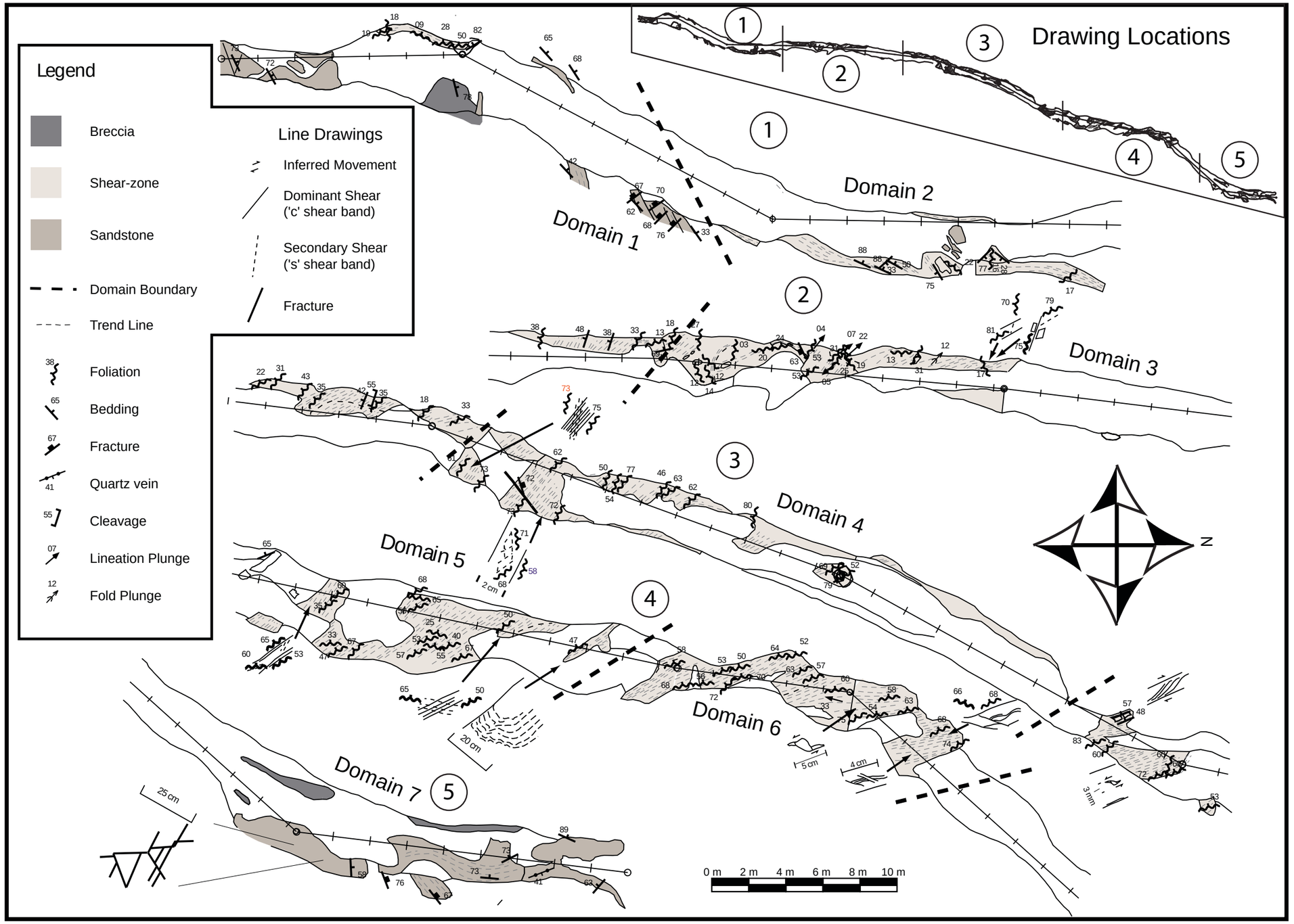

Figure 7.35. A shear zone at the contact between the Burra Group and the Curdimurka Subgroup.
Stereonets for each domain are given in Figure 7.36. The shear zone is part of the Eastern Fault Zone. Both margins are brecciation country rock and the shearing is most developed in Domain 6, with the development of s and c bands. It has been folded into an open upright fold with the main fold hinge in domains 2 and 3. In domains 5 and 6, it dips steeply to the northeast. The locality of Figure 7.35 is shown in Figure 7.30.

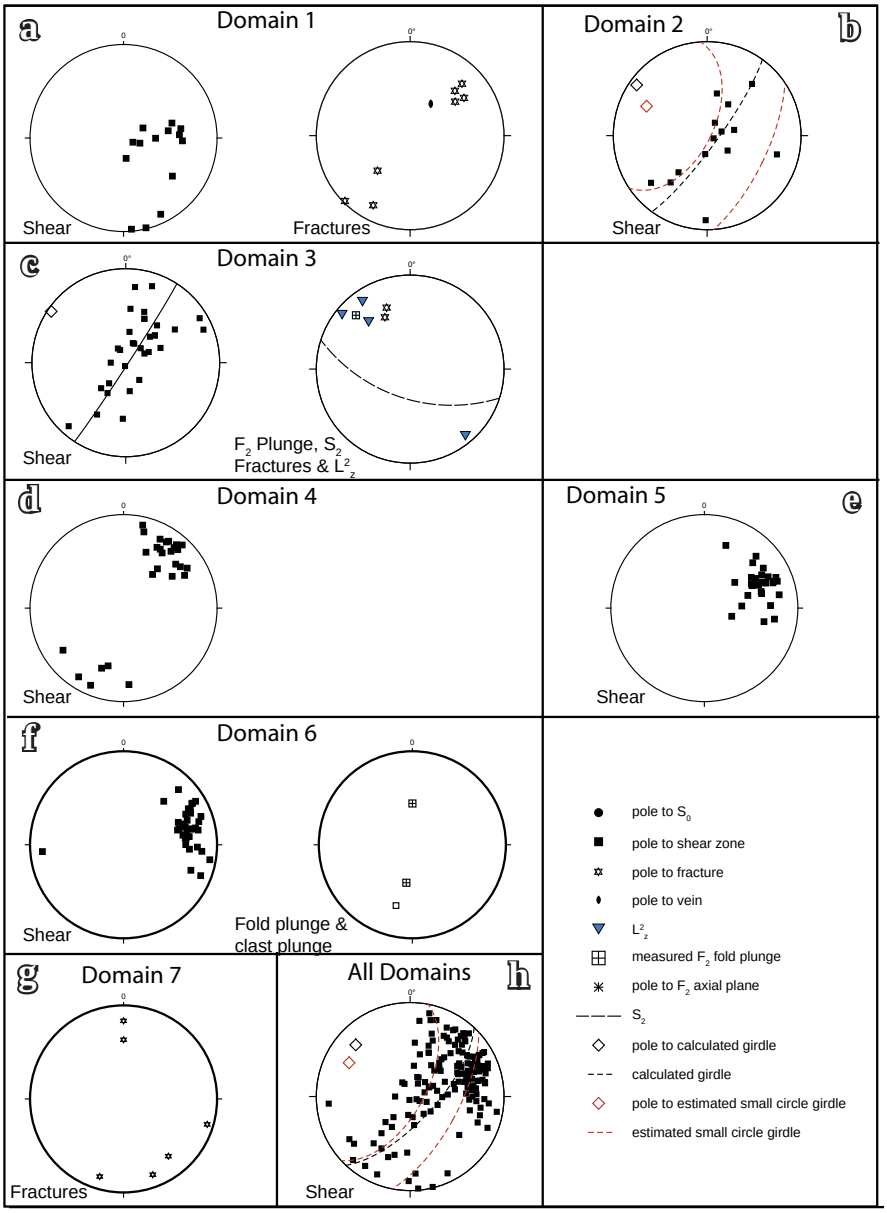

Figure 7.36. Stereonets for the Eastern Fault Zone shear zone.
a) In Domain 1, the main shears dip at a shallow angle to the E, with minor sub-vertical shears. Poles to fractures occur in a mixture of conjugate fractures (A & B). b) In Domain 2, the shear planes are spread around a great circle with a calculated plunge 09º/306º. However, a group of points also plot on a small circle with an estimated orientation of 61º/116º, with an α angle of 64º. c) In Domain 3, the shear zone is folded into an open fold with a calculated plunge of 02º/303º. A measured plunge is shallow to the NW, and a lineation formed by the intersection of the cleavage and S2 plunges at a shallow angle to the NW and SE. S_2 dips at a steep angle to the SW. d) In Domain 4, there are two main clusters of poles about 24º apart, representing a main and oblique shear planes dipping steeply to the SW. e) In Domain 5, the main shear plane dips steeply to the WSW. f) In Domain 6 there are several shear planes developed; a main shear, oblique and minor S-C shears. There are several clasts with isoclinal faulting in Domain 6, with measured plunges at moderate angles to the south and north. A carbonate clast has a long axis that plunges at a moderate angle to the south, in the plane of the shear zone where it was measured. g) Domain 7 has a polygonal fracturing, all of which are steeply dipping. h) All shear planes from this outcrop plot on a calculated great circle with an orientation of , giving a plunge shallow plunge to the NW. However the data may better fit and small circle with an estimated orientation of an axis plunging at a shallow angle to the NW and an α angle of 74º. In either case, the calculated plunges and upright folds are typical of F_2 folds.

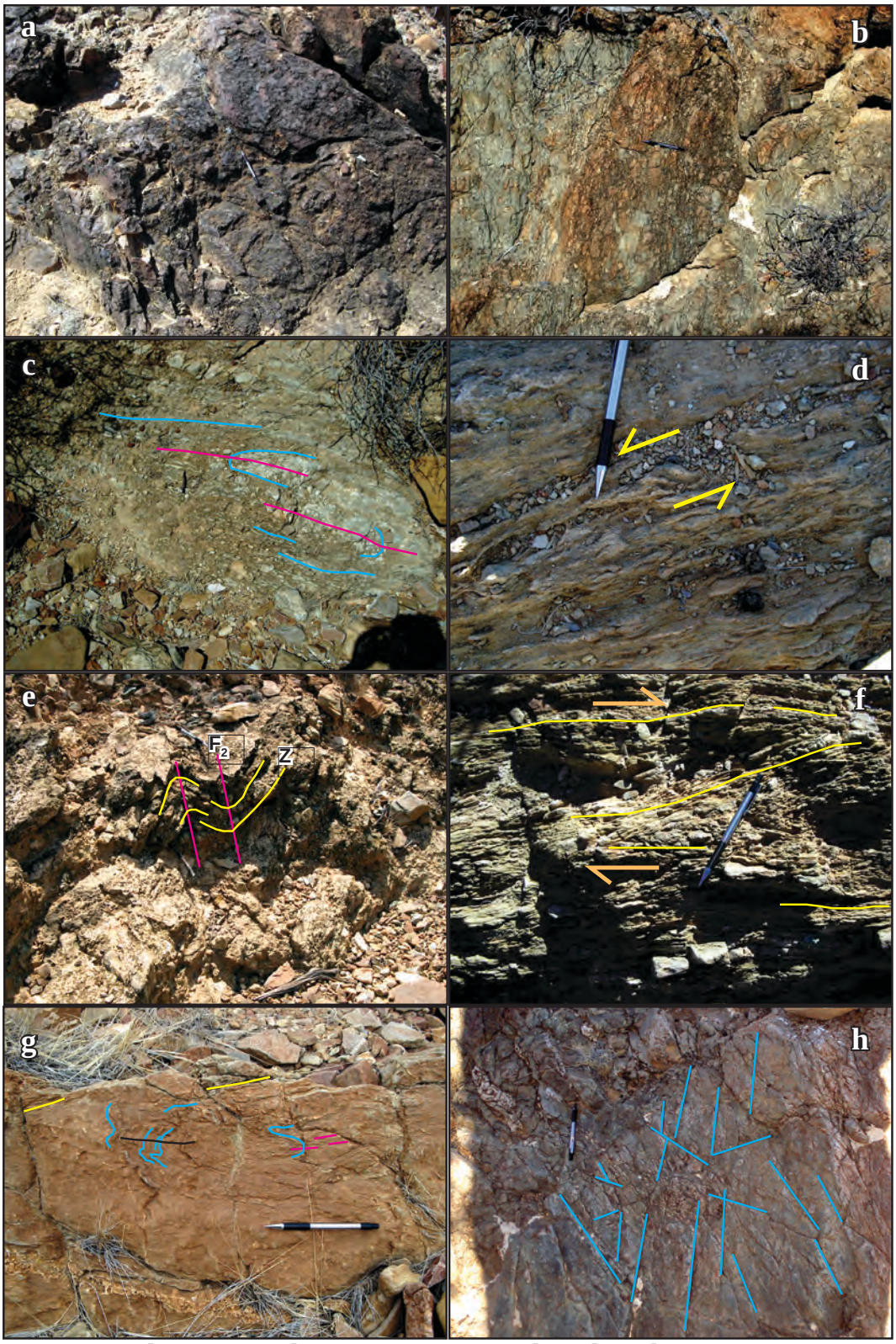

Figure 7.37. Shear zone at the Burra Gourp - Curdimurka Subgroup contact.
a) Brecciated sandstone in Domain 1 of the shear zone. b) Brecciation of sandstone on the margins of the shear zone, Domain 1. c) Siltstone - sandstone beginning to deform, with sandstone beds starting to pull apart within the eastern edge of the shear zone, Domain 2. The apparent isoclinal folding is due to the outcrop being sub-parallel to bedding. d) Shear movement indicators in Domain 4, from the tail development, the sandstone clast shows sinistral movement. e) Upright folding affecting the shear zone, Domain 3. f) A main and oblique foliation within the shear zone, Domain 6. g) A carbonate clast within Domain 6 showing isoclinal folding. h) A polygonal fracture pattern in sandstone, Domain 7.

east-southeast (Figure 7.36e,f). Clasts are rotated, and movement indicators show dominant dextral movement (Figure 7.36f). Large carbonate clasts form rare boudins, some of which contain isoclinal folds (Figure 7.37g) which plunge at moderate angles to the north and south (Figure 7.36f).

The northern edge of the shear zone is marked by fracturing and brecciation of massive sandstone (Figure 7.35). Fracturing is mainly polygonal with one set of conjugate fractures and a third orientation at a high angle to the conjugate pair (Figures 7.36g, 7.37h).

Figure 7.36h plots poles of all of the shears from this outcrop. They can be plotted on either great or small circle girdles but both have calculated plunges that are shallow to the northwest. The form of the fold seen in outcrop and its orientation are typical of F_2 folds, showing that the shear zone has been folded by F_2 and hence precedes D_2.

The sense of movement along the Eastern Fault Zone is dextral, east block to the south, but with likely sub-vertical reactivation. Evidence is mainly stratigraphic, from the relative movement of the Tapley Hill Formation at the northern end. At the mesoscopic scale movement indicators are dominantly dextral but sinistral indicators are also present and so does not provide definitive proof of movement. Evidence for vertical movement on the Eastern Fault Zone is mainly from folding within the shear zone. The majority of folds are upright with steeply dipping axial planes sub-parallel to the shearing.

Total displacement cannot be known with certainty. At the northern end, the Tapley Hill Formation has been displaced less than 50 m (Figure 7.30) but in the southern half of the fault zone, the displaced eastern block of the Boorloo Siltstone does not crop out within the mapped area, indicating a displacement of greater than 2,000 m.

The Central Fault Zone.

The Central Fault Zone is a broadly north – south striking fault zone that offsets middle portions of the Curdimurka Subgroup stratigraphy from the top of the Recovery Formation to the Cooranna Formation (Figure 7.38). Although fundamentally it removes stratigraphy, at its widest section it encloses the Hogan Dolomite in a complex compressional duplex zone that propagates into the Cooranna Formation (Figure 7.38, 7.39). The fault zone accommodates local shortening by reverse faulting and the generation of F_1 folds.

It varies considerably in width from about 20 m in the north to a maximum thickness of about two kilometres in the centre of the area to about 10 m in the south. Its northern end is obscured by Recent sediments but it extends from the Umberatana Group, splits either side of the Hogan Dolomite, and merges with the Eastern Fault Zone adjacent to the Rook Prospect (Figure 7.38). The majority of faults within the fault zone are sub-parallel to bedding, with small sections cutting across bedding at high angles. In the lower Cooranna Formation individual faults are marked by breccias or gullies (Figure 7.40a,b) but in more carbonate-rich packages, the carbonate beds accommodate movement by folding and shearing (Figure 7.41a). Rarely, carbonate units along the fault zone have been silicified and brecciated (Figure 7.41b)

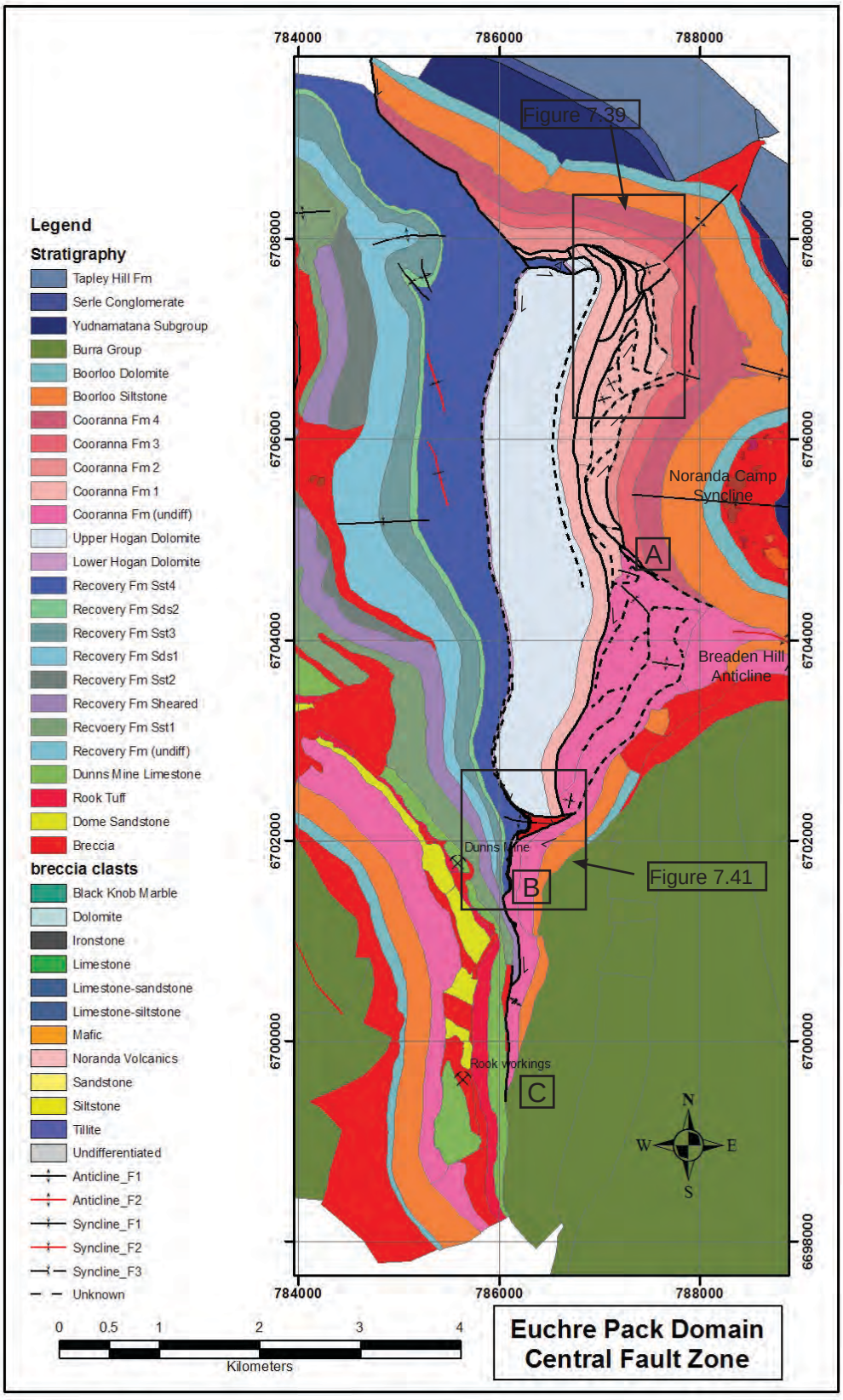

Figure 7.38. The Central Fault Zone of the Euchre Pack Domain.
The northern end of the Central Fault Zone juxtaposes the Boorloo Siltstone with the Recovery Formation before splitting either side of the Hogan Dolomite. The eastern branch forms a series of fault duplex in Cooranna Formation 2. South of about (point A) the fault zone is difficult to trace in a zone of complex faulting and folding, merging with the western branch at point B. The western branch is poorly defined and may be discontinuous within the Lower Hogan Dolomite and top of the Recovery Formation. South of point B, it cuts down the stratigraphy juxtaposing the Cooranna

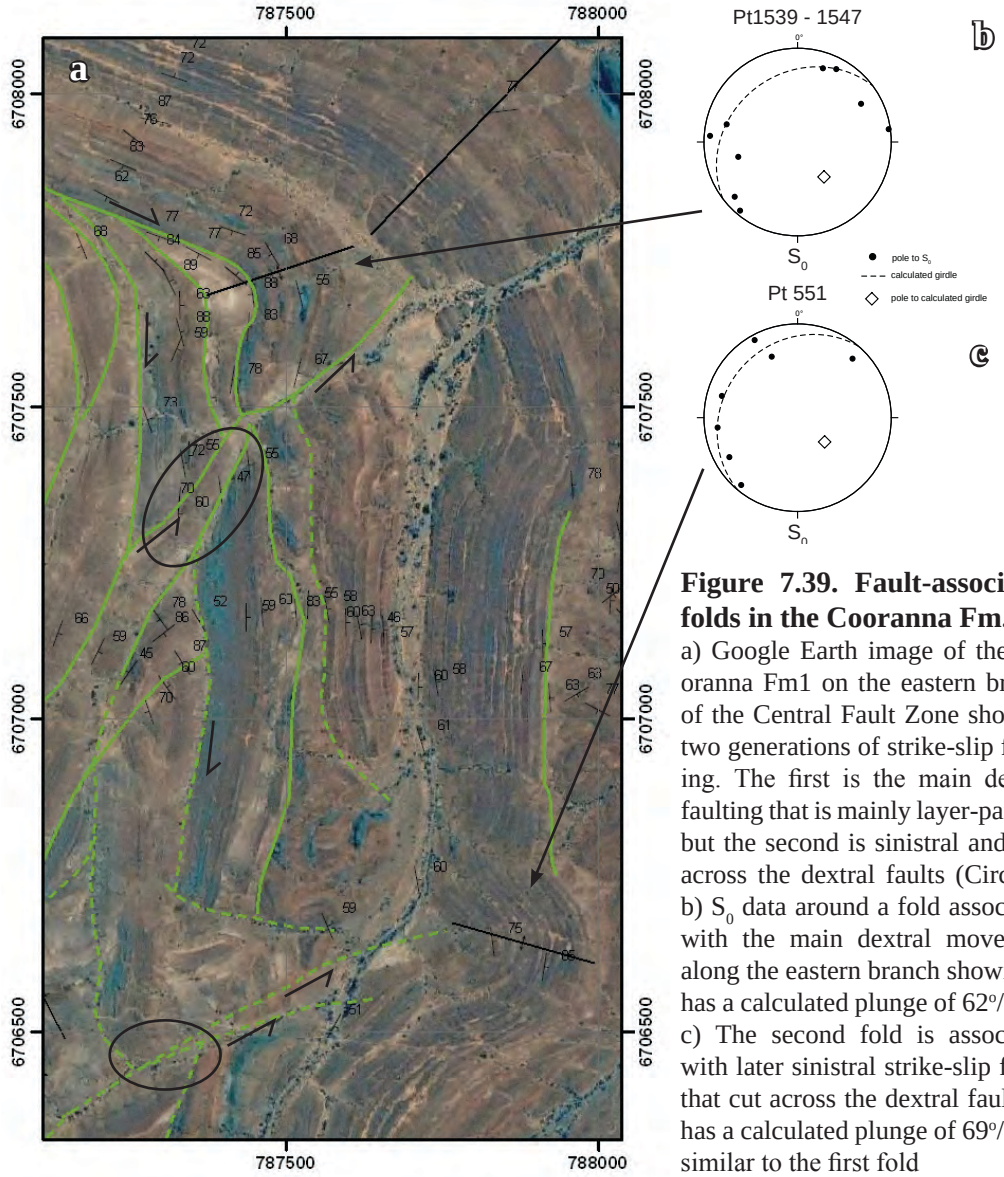

Figure 7.39. Fault-associated folds in the Cooranna Fm.
a) Google Earth image of the Cooranna Fm1 on the eastern branch of the Central Fault Zone showing two generations of strike-slip faulting. The first is the main dextral faulting that is mainly layer-parallel but the second is sinistral and cuts across the dextral faults (Circled). b) S_0 data around a fold associated with the main dextral movement along the eastern branch showing it has a calculated plunge of 62°/145°. c) The second fold is associated with later sinistral strike-slip faults that cut across the dextral fault but has a calculated plunge of 69°/130°, similar to the first fold

Fault movement is broadly dextral, with the eastern block moving south relative to the western block (Figure 7.38). Dextral movement is deduced from stratigraphic offsets and the geometry of meso- and macroscopic folds. In the north, the Boorloo Siltstone is juxtaposed against the Recovery Formation, a displacement of about 1,000 m and indicating dextral movement (Figure 7.38). The interpretations of a fault duplex east of the Hogan Dolomite and the Fence and Noranda Camp Anticline – Syncline pair as an associated fault bend fold suggest dextral movement also. However, there is also evidence of a second, later sinistral movement. Within the Cooranna Formation, there are several fault-tip folds at the tips of faults that off-set the duplex faults (Figure 7.38, 7.39). The plunge of one of these folds is steep to the northeast (Figure 7.39c), typical of F_1 folds in that area.

The two branches of the Central Fault Zone re-join at the southern end of the outcrop of the Hogan Dolomite and the Central Fault Zone merges with a series of layer-parallel faults in the Recovery Formation, bringing the Cooranna Formation into contact with the RSh unit.

Formation with the Recovery Formation, until it merges with the Eastern Fault Zone at point C. The dominant movement on the Central Fault Zone is dextral but at several localities there are late sinistal strike-slip faults.

Figure 7.40. The Central Fault Zone in the Cooranna Formation.
a). A panoramic view of the Cooranna Formation looking south showing the approximate position of faults following gullies. b) Breccia from an individual fault in the Cooranna Formation.

Figure 7.41. The Central Fault Zone south of the Hogan Dolomite.
a) A dolomite unit showing beds having been sheared out and the development of en echelon dolomite veins. Line drawing shows the shear directions and several of the veins. b) A silicified breccia from the fault zone.

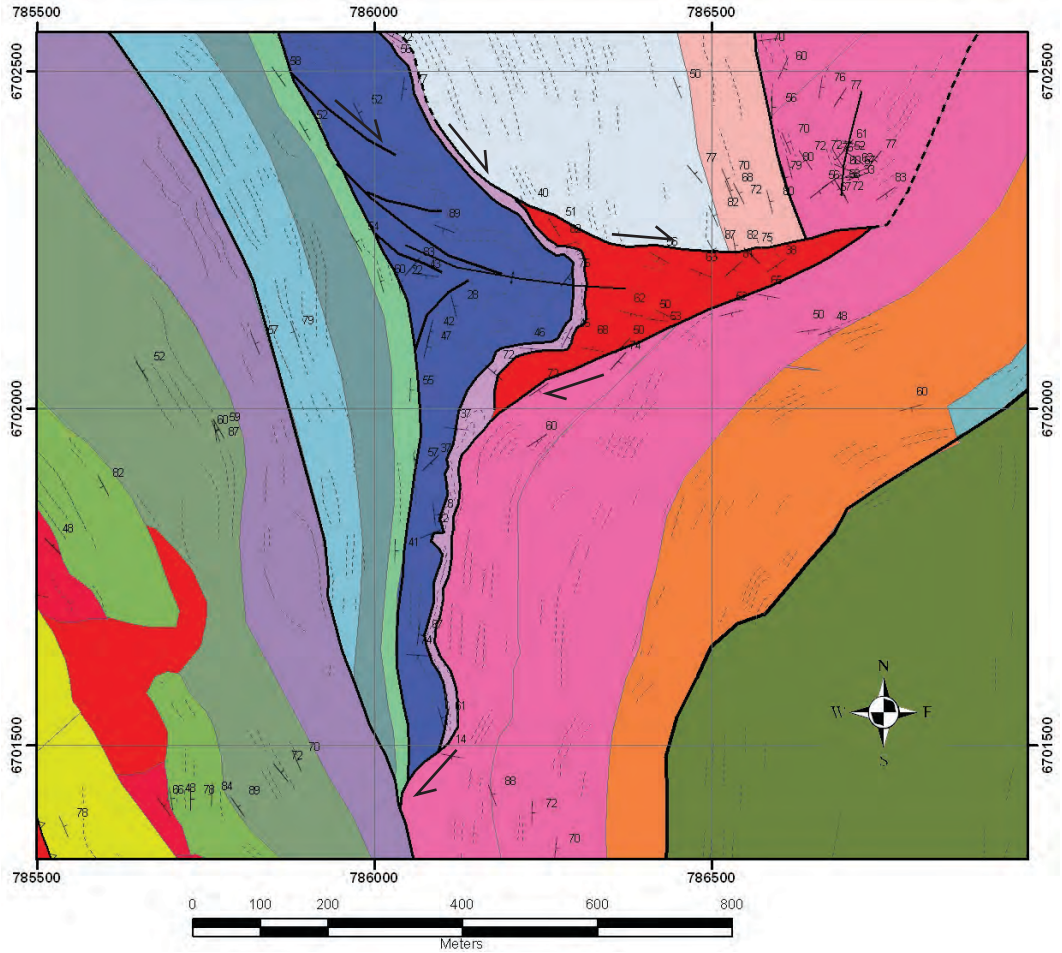

Figure 7.42. The Central Fault Zone at the southern end of the Hogan Dolomite.
The eastern and western branches of the Central Fault Zone re-join in an area of complex faulting and associated folding (See Figure 7.38 for legend).

On the western branch of the Central Fault Zone, layer-parallel faults occur at the top and bottom of the Lower Hogan Dolomite. A fault splay cuts across bedding at a high angle, cutting out the Upper Hogan Dolomite but the Lower Hogan Dolomite continues until it is terminated where the eastern and western branches re-join. Beneath the Lower Hogan Dolomite, the RSSt4 unit has been deformed by a series of fault splays emerging from a layer-parallel fault at the base of this unit. The majority are dextral strike slip but there are several smaller sinistral stirke-slip faults, with the fault splays having associated fault-propogation folds. This faulting is restricted to the RSSt4 unit but in response, the Lower Hogan Dolomite has been folded into an anticline. Above the anticline is a breccia between the Cooranna Formation and the Upper Hogan Dolomite (Figure 7.42).

South of the detachment fold, the Central Fault zone changes its orientation relative to bedding and removes stratigraphy from the Lower Hogan Dolomite to RSlt3. (Figure 7.38). At the southern end of the Central Fault Zone, upper Cooranna Formation is juxtaposed against the Dunns Mine Limestone, indicating roughly 2,000 m of stratigraphy has been removed. Because the Hogan Dolomite is not repeated within the mapped area, the minimum displacement is five kilometres.

The Western Fault Zone.

The Western Fault Zone runs from the northern to the southern end of the Euchre Pack Domain and affects strata from the base of the Dome Sandstone to the base of the RSS1 (Figure 7.43). It can be divided into three sections; a northern section from the north of the Euchre Pack Domain to about the level of the Utah Bore, including the Boundary Anticline; a middle section from the level of Utah Bore to a breccia body that cross-cuts the stratigraphy (pt A in Figure 7.43) and a southern section, and from the breccia body to the southern end of the Euchre Pack Domain. In the northern and middle section, the fault zone has a breccia to its west whereas in the southern section, southwest facing Cooranna Formation and Boorloo Shale is west of the fault zone.

In the northern section, the Western Fault Zone is at the base of the Recovery Formation with the brecciated hinge of the Boundary Anticline in the footwall of the fault (Figure 7.43). It separates southwest facing Recovery Formation from breccia and east facing Recovery Formation in the vicinity of Utah Bore. The Boundary Anticline has been discussed above but the pertinent point here is that the Dunns Mine Limestone in the breccia has been strongly attenuated and the Dome Sandstone is only present as megaclasts. In the basal Recovery Formation, a layer parallel cleavage is strongly developed just above the fault southwest of the anticline. No movement indicators were found and the thickness of the fault zone is about 2,000 m, from the base of the Dome Sandstone to the base of the Recovery Formation.

In the central section of the Western Fault Zone, a breccia lies west of the fault zone, with Dome Sandstone to the east (Figure 7.43). The breccia contains megaclasts of Dome Sandstone, Black Knob Marble and Noranda Volcanics as well as ironstone which may be from the basement (pers. comm.; A. Goode, 2002). South of about 6705000 mN (Pt B), the megaclasts within the breccia contain more intact stratigraphy with little breccia between, whereas to the north the megaclasts are typically not in contact and the outcrop resembles the Breaden Hill Breccia. The West Willouran Fault is on the western side of the breccia (Figure 7.43). Close to the fault, the Dunn Mine Limestone is strongly attenuated and displays both compressional and extensional features. Siltstone units are pulled apart whereas carbonate units tend to flow and re-crystallize (Figure 7.44a,b), thin siltstone beds may also be folded into isoclinal to inclined folds (relative to surrounding beds) similar to F_1 folds (Figure 7.44c). Rotated chert nodules within recrystallized carbonates provide evidence for layer-parallel dextral shear (Figure 7.44d), whereas evidence for layer-parallel attenuation is provided by metre-scale sandstone boudins enclosed in interlaminated limestone-shale (Figure 7.44e)

In the southern section, the Western Fault Zone separates northeast facing basal Curdimurka Subgroup from southwest facing upper Curdimurka Subgroup (Figure 7.43). The basal Curdimurka Subgroup has been brecciated to varying degrees with blocks of intact stratigraphy to the level of the Recovery Formation separated by zones of brecciation. Breccias include both fractured and fragmented Dome Sandstone with no apparent matrix, and matrix-supported breccia with exotic clasts. A block of east facing Dunns Mine

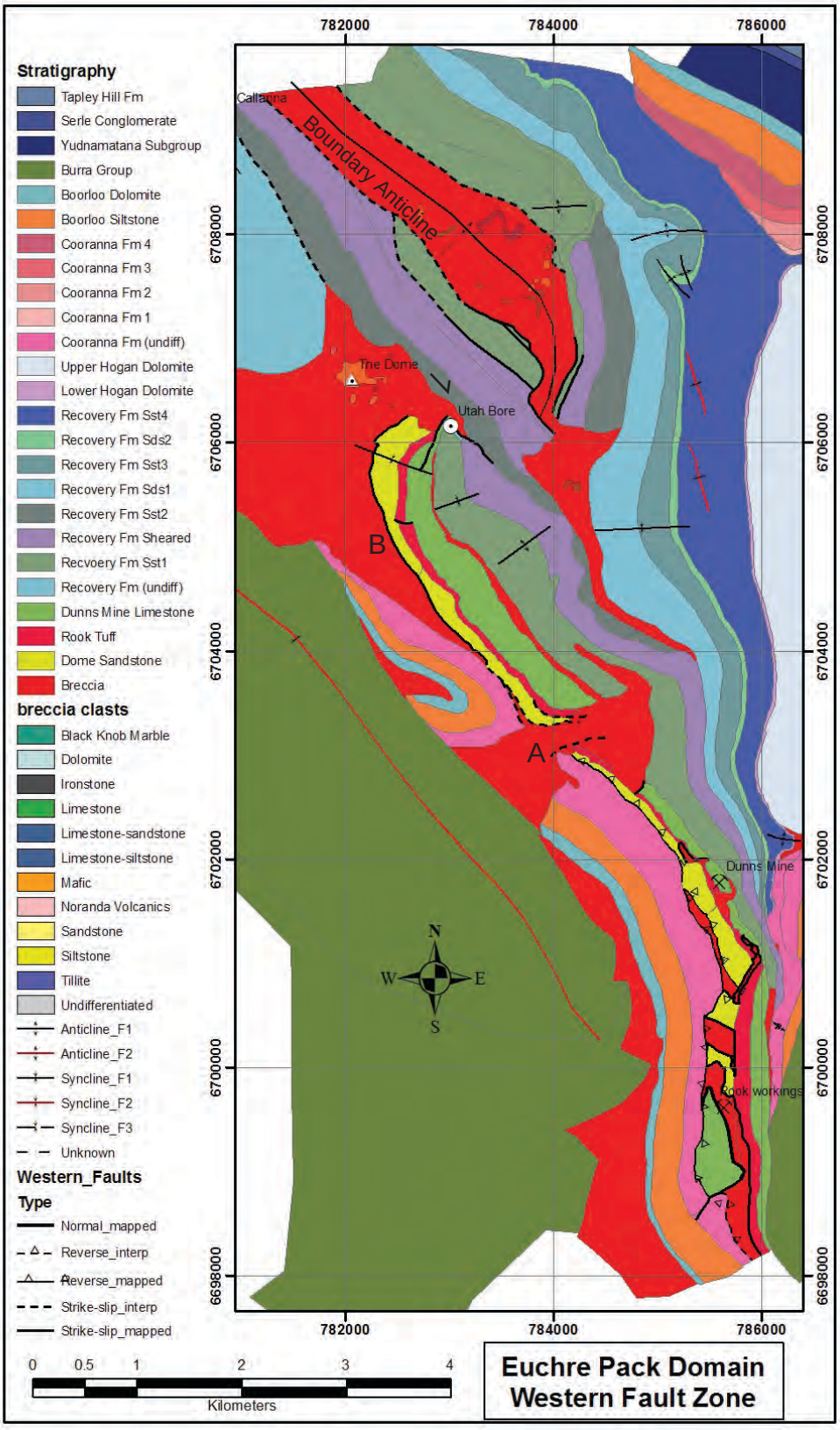

Figure 7.43. The Western Fault Zone.
The Western Fault Zone affects stratigraphy between the top of the Dunns Mine Limestone and the base of the Dome Sandstone. It is mainly parallel to bedding and south of point A the Dome Sandstone is broken-up along its length with breccia intruding up to the level of the Recovery Formation. The brecciated core of the Boundary Anticline is part of the Western Fault Zone.

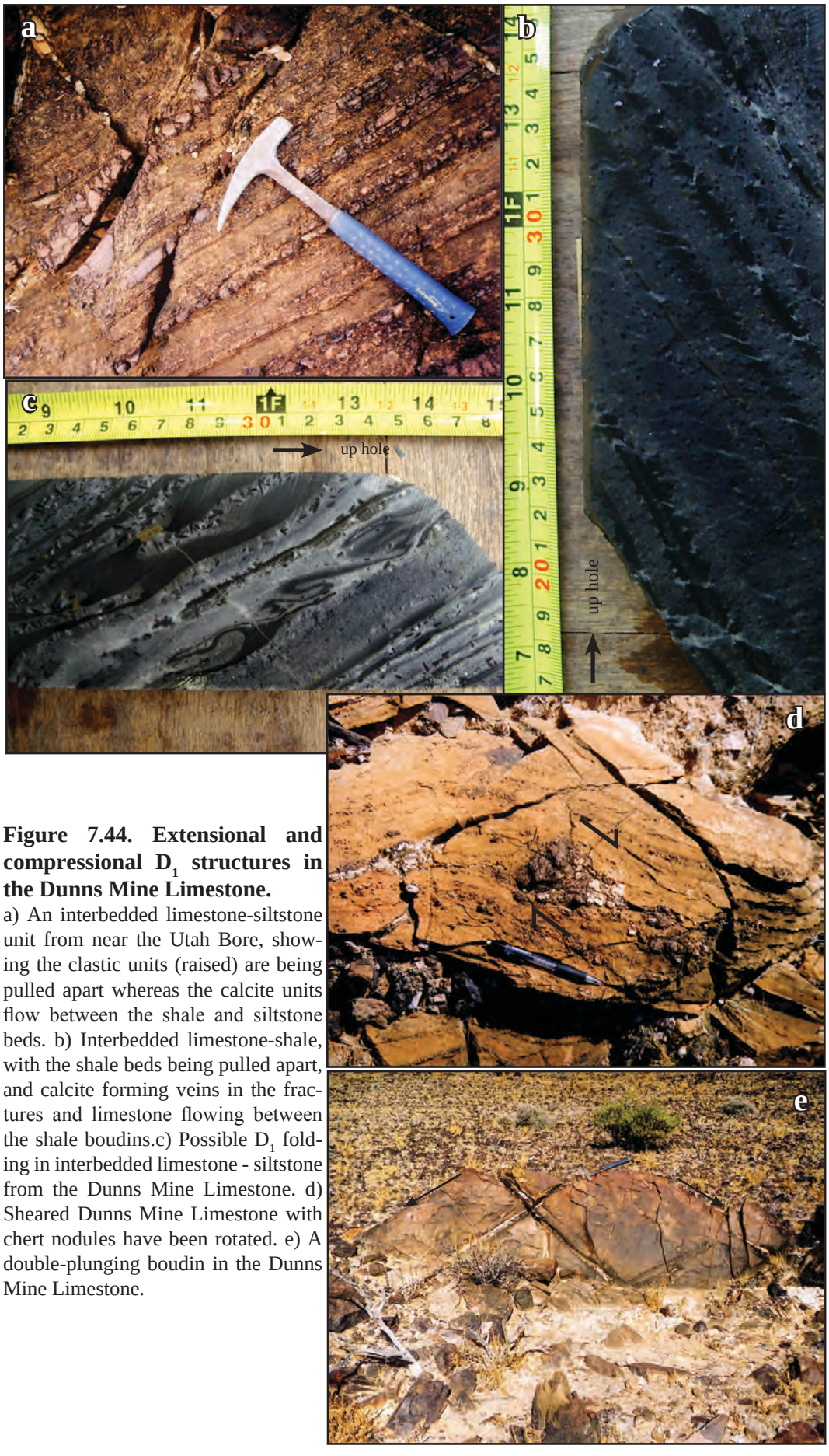

Figure 7.44. Extensional and compressional D_1 structures in the Dunns Mine Limestone.
a) An interbedded limestone-siltstone unit from near the Utah Bore, showing the clastic units (raised) are being pulled apart whereas the calcite units flow between the shale and siltstone beds. b) Interbedded limestone-shale, with the shale beds being pulled apart, and calcite forming veins in the fractures and limestone flowing between the shale boudins.c) Possible D_1 folding in interbedded limestone - siltstone from the Dunns Mine Limestone. d) Sheared Dunns Mine Limestone with chert nodules have been rotated. e) A double-plunging boudin in the Dunns Mine Limestone.

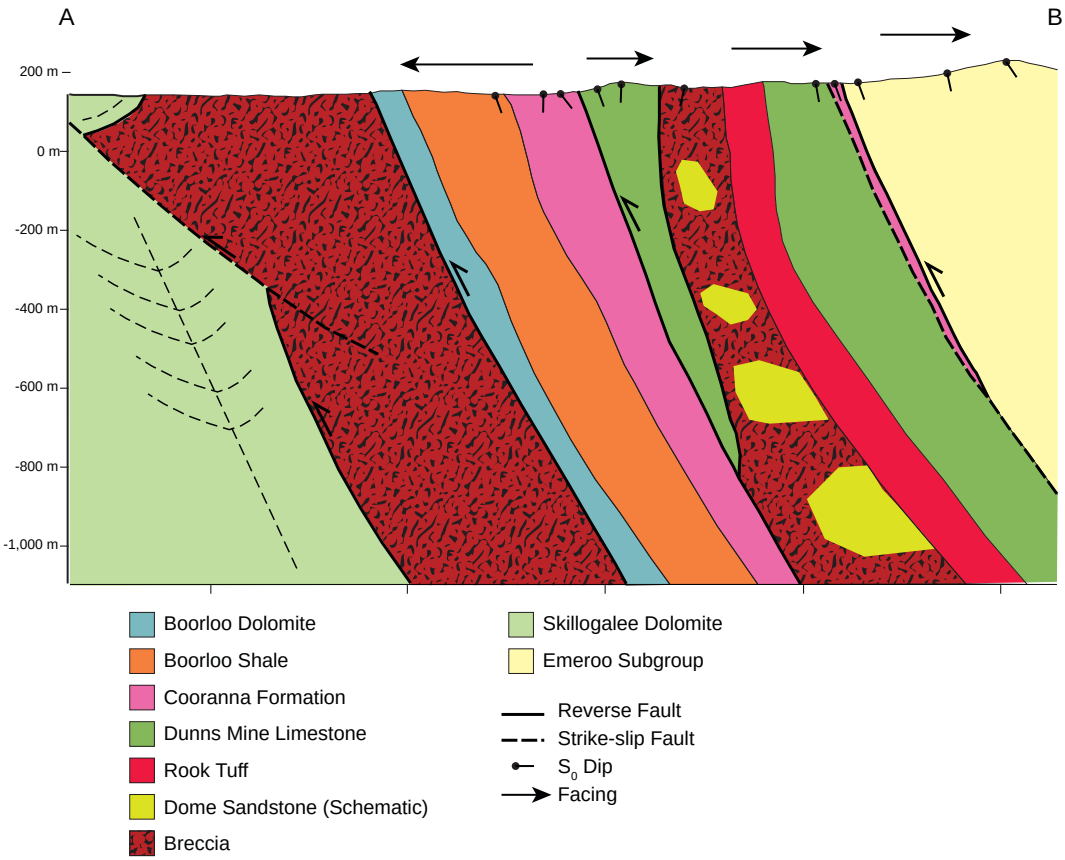

Figure 7.45. Cross-section through the south of the Euchre Pack Domain.

Limestone is in contact with west-facing Cooranna Formation within the fault zone in the region of the Rook workings area (Figure 7.43, 7.45). Here the fault zone is about 300 m wide. Movement indicators were not found along this section of the fault.

Movement on the Western Fault Zone can only be inferred from large-scale folding. The folding of the Dome Sandstone relative to the fault at Utah Bore suggests dextral movement that is eastern block moving southward.

Other Strike-Slip Faults.

Above, the three major fault zones are described but there are a number of smaller strike slip faults with movement measured in metres to possibly hundreds of metres throughout the Curdimurka Subgroup (Figure 7.29, Figure 7.46). They typically do not show the complexity of the major fault zones, and the majority are layer parallel but there are a few that cross-cut bedding at a high angle.

The layer parallel faults display many of the features described above in the fault zones; mesoscopic stratabound fold trains, dominant dextral movement but with a few showing later sinistral movement, brecciation and macroscopic fault-related folds, with moderate to steep plunges to the eastern quadrant. They may also change orientation to cut across stratigraphy at a high angle, removing stratigraphy, or more rarely, result in structural thickening before resuming a layer-parallel form. Fault thicknesses are typically less than ten metres.

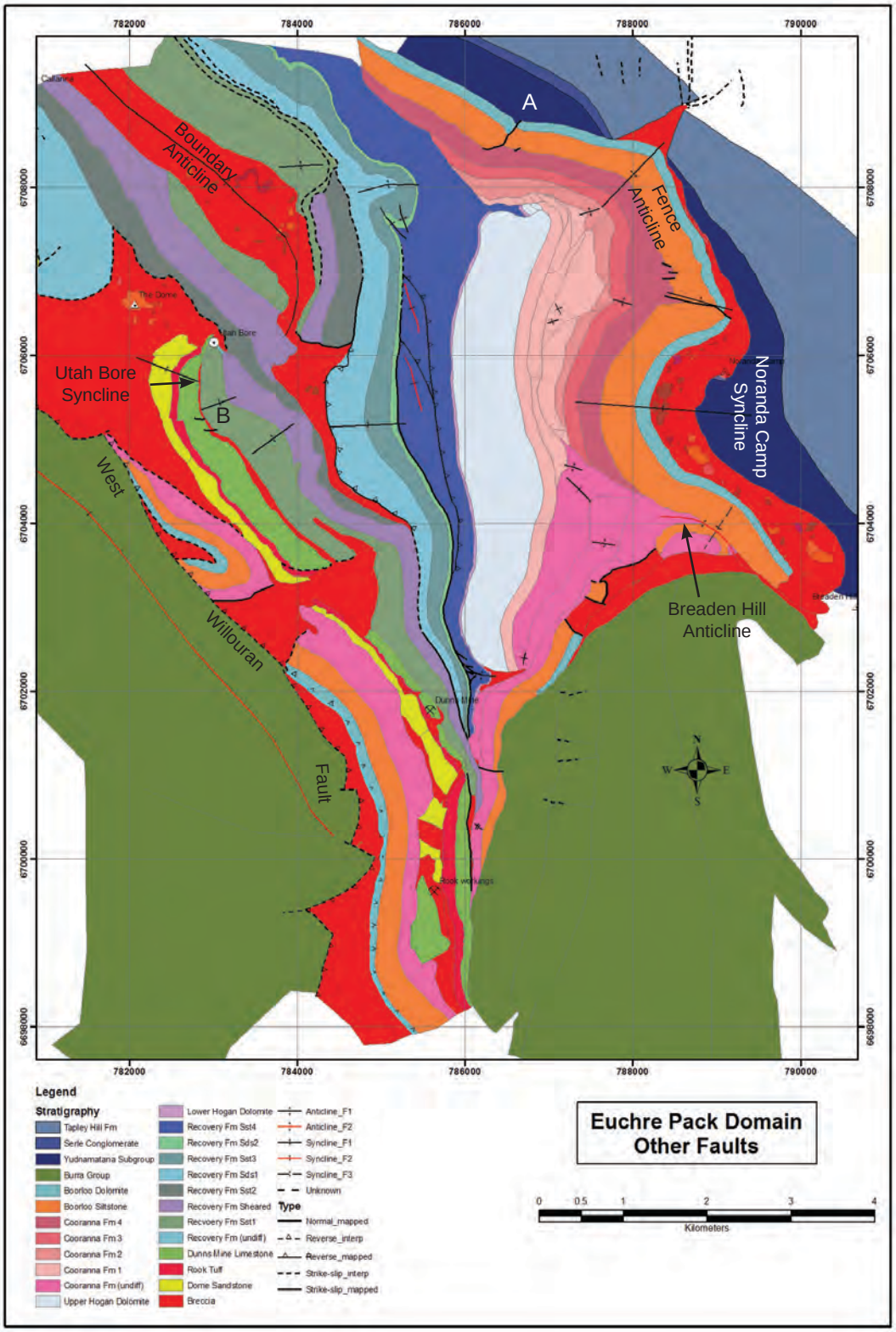

Figure 7.46. Other Fault Zones.
In addition to the Eastern, Central and Western Fault zone, there are a number of other faults. They range from major regional faults such as the West Willouran Fault to faults too small to show at this scale.

Cross-cutting strike-slip faults not associated with layer-parallel faults occur mainly within the Boorloo Dolomite where there are a series of steeply dipping faults at a high angle to bedding with apparent dextral or sinstral strike-slip movement (Figure 7.47). They occur in sets up to 200 m along strike of the Boorloo Siltstone, and each individual fault is less then 40 cm wide, with displacements up to about 15 m. A few individual faults offset the Boorloo Siltstone by up to 100 m, such as at Point A in Figure 7.46. A high angle fault offsets the Dome Sandstone and Rook Tuff near Utah Bore by about 120 m (marked B in Figure 7.46). Relative to bedding these are normal faults.

7.4.4.3 Reverse Faults

Reverse faults define the southwestern, southern and eastern margins of the Euchre Pack Domain. Fault zones are rarely exposed and their presence is determined by the juxtaposition of different stratigraphic levels. Breccias are common, reaching a maximum thickness of 500 m on the western margin of the Euchre Pack Domain.

The West Willouran Fault is the major reverse fault in the area of the Euchre Pack Domain (Figure 7.46). It extends beyond the southern boundary of the study area and likely continues north under Recent sedimentary cover. Between it and the Western Fault Zone is a breccia up to 500 m wide. It juxtaposes southwest-facing Boorloo Siltstone and southwest-facing Skillogalee Dolomite, cutting across what is interpreted from aerial photographs to be a F_1 fold (Figure 7.46). In the hanging wall is the Curdimurka Subgroup and in the footwall is the Burra Group, which has been folded into a footwall syncline. From the juxtaposition of the Skillogalee Dolomite with the Boorloo Siltstone, the movement on the fault is approximately 2 km. It dips steeply to the southwest and has rotated the strata in the hanging wall to subvertical. The regional aspects of the West Willouran Fault will be discussed in more detail in Chapter 8.

A second reverse fault occurs between southwest facing Cooranna Formation and Boorloo Siltstone and east facing Dome Sandstone, from the southern margin of the area to about 6702600 mN (Figure 7.45). Within this fault zone is a large block of east-facing Dunns

Figure 7.47. Strike-slip faults off-setting dolomite beds in the Boorloo Dolomite. Maximum offset is about 11 m.

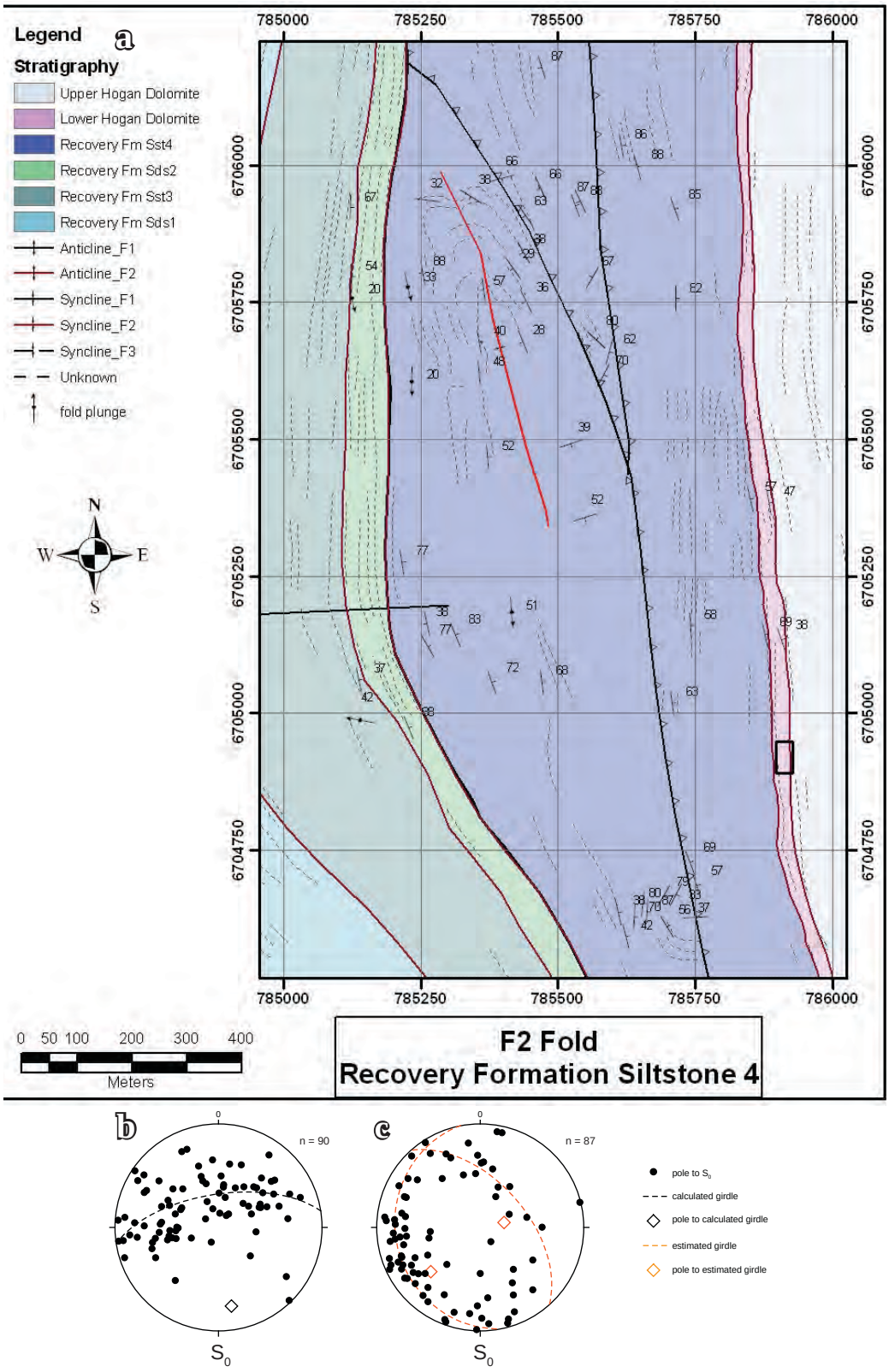

Figure 7.48. A reverse fault in the RSlt4 unit of the Recovery Formation.
a) A map of a thrusting and associated hanging wall syncline in RSSt4. It trends NNW and is one of a series of fault splays from a fault that passes on the eastern side of unit RSs2. b) Stereonet of poles to S_0 from the core of the syncline. The calculated plunge of the syncline is 24º/171º. c) A stereonet of poles to S_0 from an area of complex deformation at the base of RSSt4. There are two trends interpreted; the first with the most data plot on a great circle, giving an estimated plunge of 71º/079º, with a second group of points plotting on a great circle that gives an estimated plunge of 19º/159º. The first is interpreted to be due to F_1 folds and the second may be F_2.

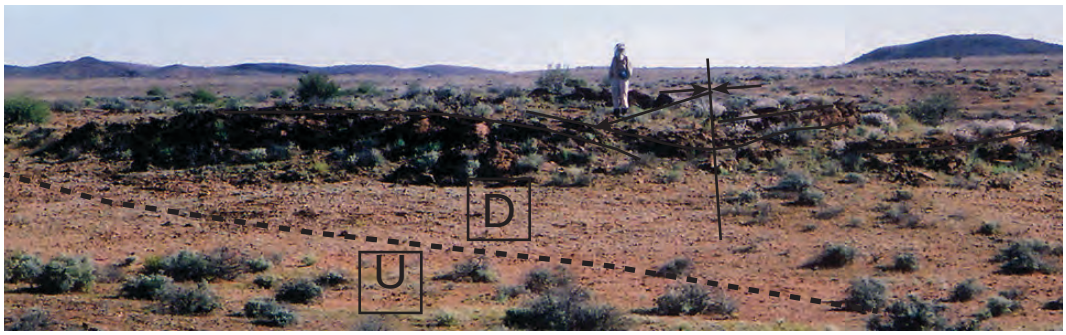

Figure 7.49 A photograph showing the footwall syncline in Figure 7.47.
The fault splay passes approximately along the line marked and the main fault is behind the rise.

Mine Limestone. The movement is parallel to bedding, and the amount of movement is unknown.

In the Eastern Fault Zone, movement indicators suggest that there has been reverse movement on the fault between the Burra Group and the Boorloo Siltstone (Figure 7.33). The movement indicators have not been affected by the strike-slip faulting and the reverse movement post-dates the strike-slip movement.

Other small reverse faults occur in the Recovery and Cooranna Formations. An example from the RSst4 unit has a reverse fault emerging as a splay from a fault zone developed east of (i.e. stratigraphic top) the RSds2 unit (Figure 7.48). The fault surfaces are not seen at this locality but there position is marked by a change in facing over one or two metres. There is an associated footwall syncline (Figures 7.48, 7.49) that is upright with a shallow plunges to the south (Figure 7.48b). The fault zone along the top of the RSds2 unit is likely a D_1 fault zone reactivated during D_2. Bedding is chaotic and the sparse outcrop does not allow tracing of individual beds over tens of metres but poles to bedding are spread about two great circles (Figure 7.48c). The first defines a steep fold plunge to the south which is a typical F_1 fold orientation and the second has a shallow plunge to the southwest, which may be a F_3 orientation. Here displacement is difficult to determine as the folding is confined to a predominantly siltstone unit. In most examples of this style of faulting the faults are sub-parallel to bedding and their presence is only indicated by the shallow-plunging footwall synclines or reversal of facing, but the fault strike is north to northwest.

7.5 Interpretation of the Structure of the Euchre Pack Domain.

7.5.1 D_1 Revealed.

Displacement on the West Willouran Fault has resulted in rotation of strata and earlier layer sub-parallel rotated D_1 structures in the Euchre Pack Domain to sub-vertical. From the relationship to bedding, it can be seen that the F_1 structures were originally shallow plunging, inclined to recumbent folds as can be seen in the hinge of the Breaden Hill Anticline, where bedding is sub-horizontal. Within the group of what are now seen as strike-slip faults, relative to bedding they consist of thrusts, low-angle normal faults, reverse faults and normal faults.

The Eastern Fault Zone is interpreted to have had listric normal fault geometry prior to D_2 shortening that ramps down-section through the Umberatana Group strata at a high angle and soles out into the Breaden Hill Breccia and the Boorloo Dolomite (Figure 7.30). It has been folded by D_2 and D_3 around the Breaden Hill Anticline (Figure 714). and has a ramp and flat morphology south of there.

The Central Fault Zone has a more complex geometry but also can be explained in terms of a pre-D_2 listric normal fault geometry. At its northern end, it is a modified extensional duplex, with the Fence Anticline being a fault bend fold, but overall it too is a low-angle normal fault (Figure 7.38). It is at a low angle to bedding within the Recovery Formation in the footwall and so is a listric normal fault, with a considerable amount of rotation of the Cooranna Formation and Boorloo Siltstone in the hanging wall. As it meets the Hogan Dolomite, it becomes (locally) a thrust, repeating the lower Cooranna Formation. South of the Hogan Dolomite, it again removes stratigraphy, including the Hogan Dolomite and the Cooranna Formation, and is thus a normal fault but being parallel to bedding for much of its length. It too has a ramp and flat character (Figure 7.38).

The Western Fault Zone is interpreted as a pre-D_2 decollement at the base of the Dome Sandstone that is linked with other faults up to the level of the top of the Dunns Mine Limestone. Above the decollement, the Boundary Anticline formed initially as a thrust nappe or fault propagation fold (Figure 7.50a) that was breached by the thrust (Figure 7.50b). Movement on the thrust changed from southeast directed to northwest, which transported the southwest facing block of Recovery Formation to the northwest, leading to the current geometry (Figure 7.50c). The Dome Sandstone behaved in a brittle manner above the decollement, becoming brecciated but the siltstone and carbonate-rich Dunns Mine Limestone and lower Recovery Formation deformed in a ductile manner.

The ramp and flat morphology may be a response to different modes of fracturing (Ferrill and Morris, 2003) due to one unit fracturing in tension and the other failing in shear. Or, it may be due to each unit having differing co-efficients of friction (Mandl, 2000). In the Euchre Pack Domain, carbonate and siltstone units have accommodated extension by shearing whereas other units have fractured in tension. The Dome Sandstone is the primary example of the latter, but the Hogan Dolomite has also behaved in this manner. At the mesoscopic scale, interbedded carbonate-clastic units display the same behaviour. It should be noted however that in most cases, those units that have deformed by shearing and so have layer-parallel deformation, have eventually failed and are cut-out as happens to the Boorloo Siltstone, Cooranna Formation and Recovery Formation.

Although this study has identified three major D_1 fault zones, strain has been distributed throughout the Curdimurka Subgroup, producing similar structures from the microscopic to the macroscopic scale. This pervasive internal deformation is typical of gravity spreading which is described as being gravity driven lateral extension and vertical contraction (Schultz-Ela, 2001). In addition, it is deforming above a decollement below the Dome Sandstone. It is not possible to determine if the decollement has formed in reaction to the

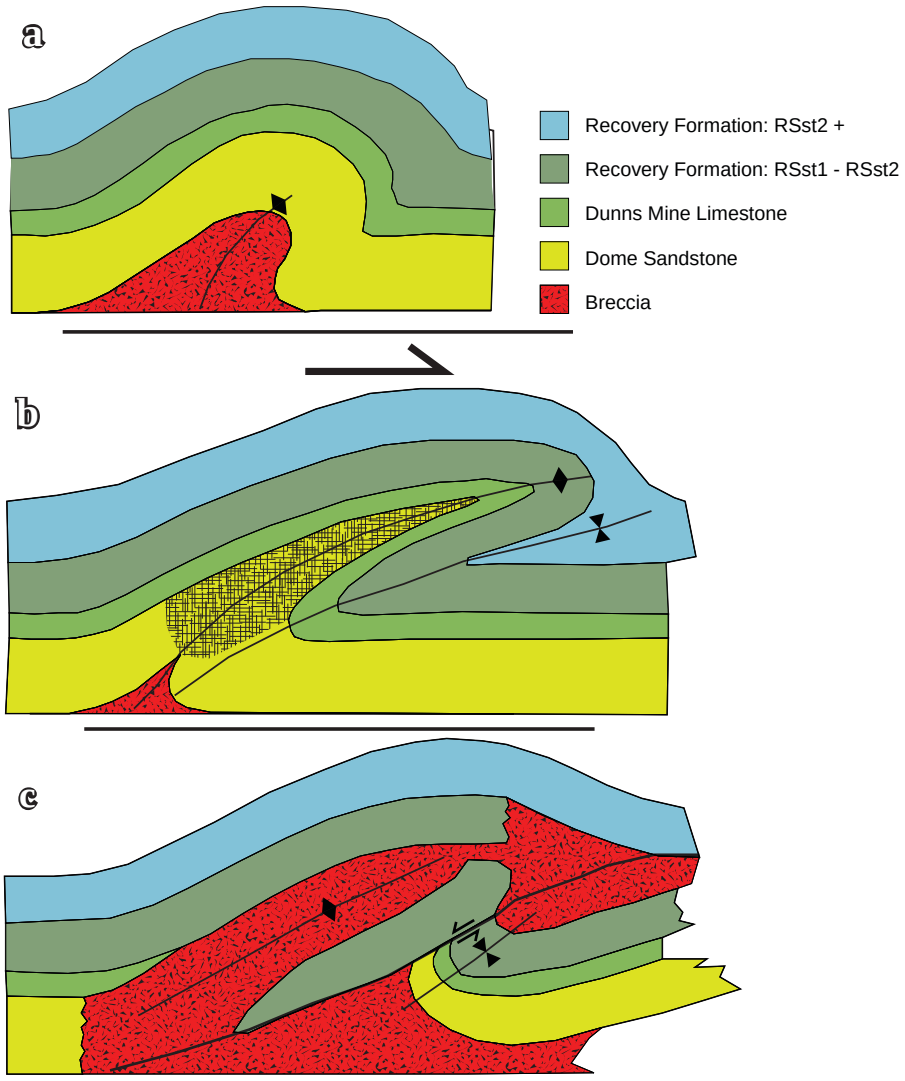

Figure 7.50. Interpretation of the Boundary Anticline.
a) The Boundary Anticline and Utah Bore Syncline were initiated as a detachment fold above a decollement at the base of the Dome Sandstone. b) With continuing movement, the hinge of the anticline rotated in a clockwise direction becoming sub-parallel with bedding. Within the hinge of the Boundary Anticline, the Dome Sandstone deforms in a brittle manner brecciating in the centre of the anticline whereas the siltstone, shale and carbonate-dominated Rook Tuff, Dunns Mine Limestone and basal Recovery Formation deform plastically, extending and thinning in the core of the anticline. c) With continued deformation, the Dome Sandstone, Rook Tuff and Dunns Mine Limestone become totally brecciated within the hinge of the Boundary Anticline. A fault that may have been initiated in the Utah Bore Syncline as a thrust undergoes low-angle normal movement, moving the lower limb of the anticline to the north. The Dome Sandstone in the Utah Bore Syncline has brecciated under tension.

gravity spreading alone or whether there is a component of gravity gliding, although the latter is favoured. Evidence for gravity spreading is seen at the level of the Dunns Mine Limestone where tablet-shaped boudins and two dimensional extension fractures suggest that extension was bi-directional. The variable F_1 fold plunge directions also suggests that deformation was multi-directional. However at the macroscopic scale the transport direction was to the southeast quadrant, although this may be a factor of outcrop which is essentially two dimensional.

A general model of deformation due to gravity spreading within the Curdimurka Subgroup is shown in Figure 7.51. A sub-vertical σ^1 causes the Curdimurka Subgroup to undergo gravity spreading above a decollement below the Dome Sandstone (Figure 7.51a). Strain is accommodated by the more ductile units flowing whereas more brittle units fracture producing boudins (Figure 7.51b). Eventually some ductile units also break vertically, leading to fault linkage and forming the ramp and flat fault morphology, which in turn leads to the loss of stratigraphy (Figure 7.51c).

Gravity spreading addresses the inhomogenous nature of the deformation but a component of gravity gliding can explain the consistent transport direction of the larger fault sheets

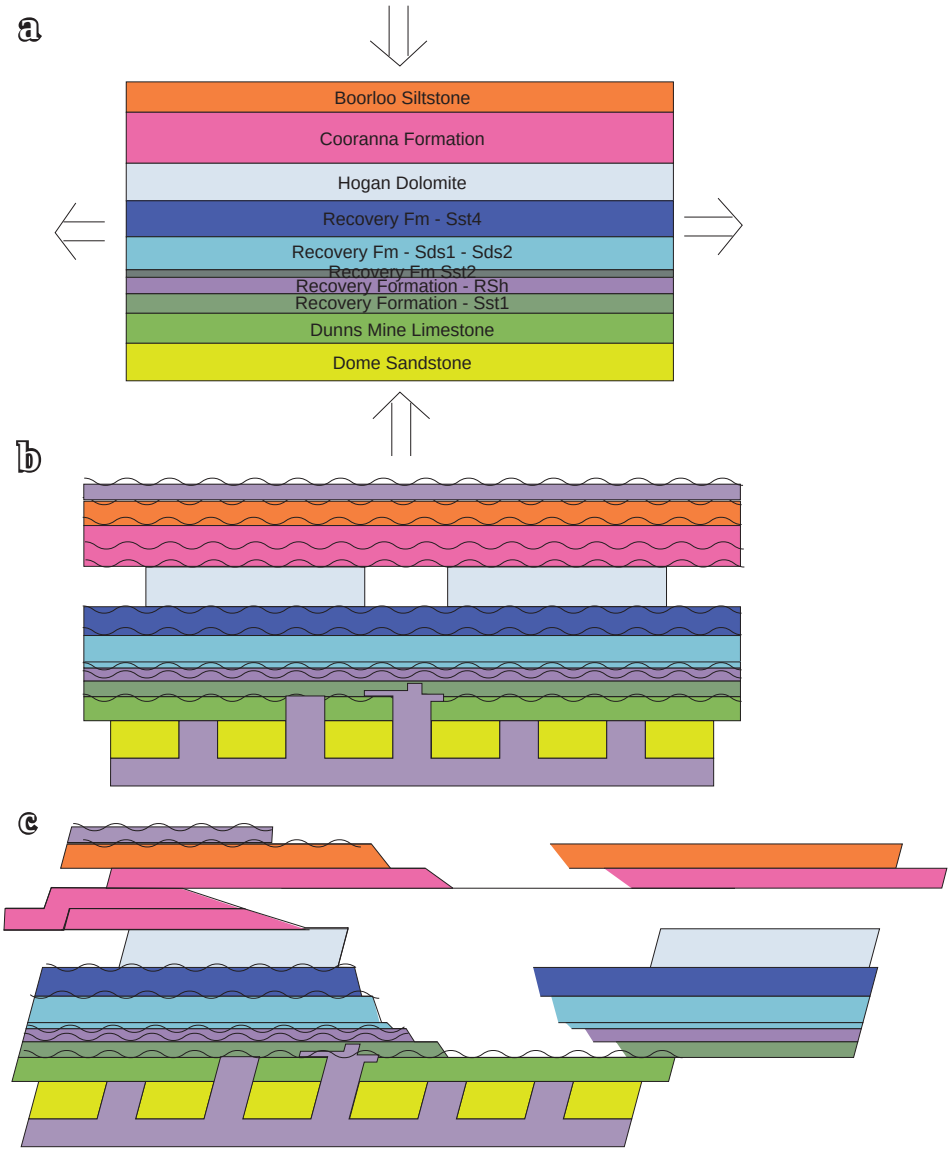

Figure 7.51. Schematic model for the deformation of the Curdimurka Subgroup during D_1.
a). The Curdimurka Subgroup is subject to a vertical σ^1. b) Strain is accommodated by layer-parallel shearing in carbonate and siltstone units and by brecciation or boudinage in brittle units. c) With continuing deformation, eventually units deforming by shearing break-apart, developing the ramp and flat fault morphology.

and the several bedding parallel faults within it. The Tapley Hill Formation thickens to the south suggesting that this rotation may have occurred during its deposition.

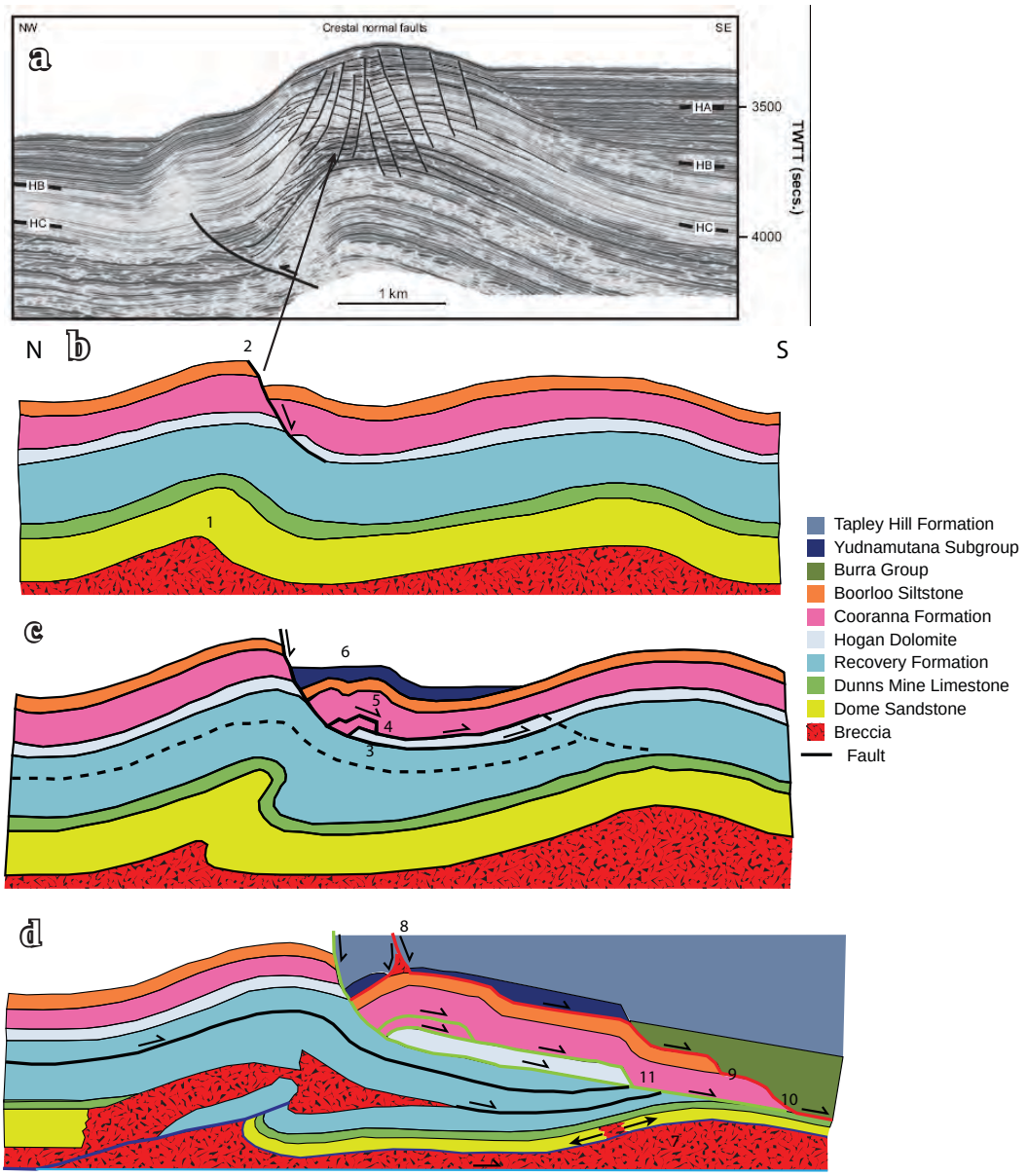

Figure 7.52. Development of the Euchre Pack Domain.

a) A seismic image of crestal normal faults forming in the crest of an anticline from a sedimentary basin in SE Asia (Morley, 2007). b) The structural development of the Euchre Pack Domain begins as the Boundary Anticline begins to form as a detachment fold above a decollement below the Dome Sandstone (the Western Fault Zone). A high angle normal fault (the Central Fault Zone) forms in the crest of the anticline, becoming parallel to bedding at the base of the Hogan Dolomite. c) With further clockwise rotation of the Boundary Anticline, the initial normal fault of the Central Fault Zone is steepened and movement continues. The western branch at the base of the Hogan Dolomite cannot accommodate all of the movement and the Cooranna Formation and Boorloo Siltstone are thrust over it (the eastern branch) beginning to form the Fence Anticline and Noranda Camp Syncline. The dashed lines are faults that may have existed in the Recovery Formation at this time. There is likely deposition of the Yudnmatana Subgroup in the hanging wall of the Central Fault Zone and in front of the developing Fence Anticline. d) With continued rotation of the Boundary Anticline the initial fault of the Central Fault Zone has steepened further and the entire hanging wall block rotated a few degrees clockwise (exaggerated here), causing further movement along the fault. The rotation may have been increased by collapse of the breccia below the Dome Sandstone which has been extended and brecciated by continuing movement on the Western Fault Zone allowing breccia between blocks of sandstone. The hanging wall of the Central Fault Zone continues to move to the south and the Eastern Fault Zone begins to form above the Fence Anticline, cutting down through the stratigraphy, possibly due to the influence of the overlying Burra Group until it merges with the Central Fault Zone, cutting it out. The Central Fault Zone ramped downward, cutting out the Recovery Formation,

and the configuration of the Curdimurka Subgroup in the Euchre Pack Domain. It requires a component of southeast directed transport above a decollement, with the deformation moving up-section (Figure 7.52). The model is based on the observation that the high angle section of the Central Fault Zone lie structurally above (i.e., east of) the Boundary Anticline, and the high angle section of the Eastern Fault Zone lies structurally above (i.e., northeast of) Hinge 1 of the Fence Anticline. Both the Curdimurka Subgroup and Burra Group have deformed above the Western Fault Zone decollement. As the Boundary Anticline forms, the section above becomes gravitationally unstable as the strata below are folded into the Utah Bore Syncline. A normal fault forms above the hinge of the anticline, flattening into the base of the Hogan Dolomite. The Hogan Dolomite was pulled apart by this movement, and with continued movement, a duplex develops above its northern end, leading to the formation of a fault bend fold, the Fence Anticline and Noranda Camp Syncline. A second gravitational instability is caused above the fault bend fold, leading to the development of the high angle section of the Eastern Fault Zone. The Central Fault Zone cuts out the faults below it and is itself cut-out itself cut-out by the Eastern Fault Zone, reflecting the sequential development of the fault zones, from deepest to shallowest. Morley (2007) has shown that normal faults may form in the crest of developing upright folds as a result of gravitational instability. In the examples of Morley (2007), the anticlines are upright and the faults do not sole-out into detachment faults and are straight to slighty concave in cross-section and so it is not an exact analogy, however the general principle is applied here in sediments that have a series of layer-parallel weaknesses caused by the presence of interbedded ductile and brittle rocks.

7.5.2 Timing of D_1

The timing of D_1 can be demonstrated by it folding the Yudnamatana Subgroup in the Fence Anticline and Noranda Camp Syncline. Figure 7.53 is a palinspastic projection of data from the Euchre Pack Domain from the middle of the Amberoona Formation to the Hogan Dolomite, interpreted from aerial photographs. From this map, true thicknesses of the Tapley Hill Formation to the Boorloo Siltstone have been calculated using bedding dips from this study, Selley and Bull (2002) and Krieg and Anthony (1992) and unfolded, using the base of the Amberoona Formation as the datum. Note that the aerial photographs were not geo-rectified and so the thickness measurements are not accurate although the errors are not sufficiently large to place doubt on the conclusions. Figure 7.53 shows that the Yudnamatana Subgroup is folded by the F_1 Fence Anticline and Noranda Syncline which formed as a fault bend fold in response to movement along the Central Fault Zone. The amplitude of the fold decreases structurally upward, indicating that the Yudnamatana Subgroup are growth strata deposited in front of the developing Fence Anticline (Suppe et al., 1992; Verges et al., 2002). Deformation continued possibly into deposition of the Tapley Hill Formation. However, bedding traces suggest that there may have been two phases of folding separated by extension. The second unit from the base recognized does not thin over the hinge of the anticline but thins toward the normal fault and into the Noranda Camp Syncline. This may be the result of extensional movement on the Eastern Fault

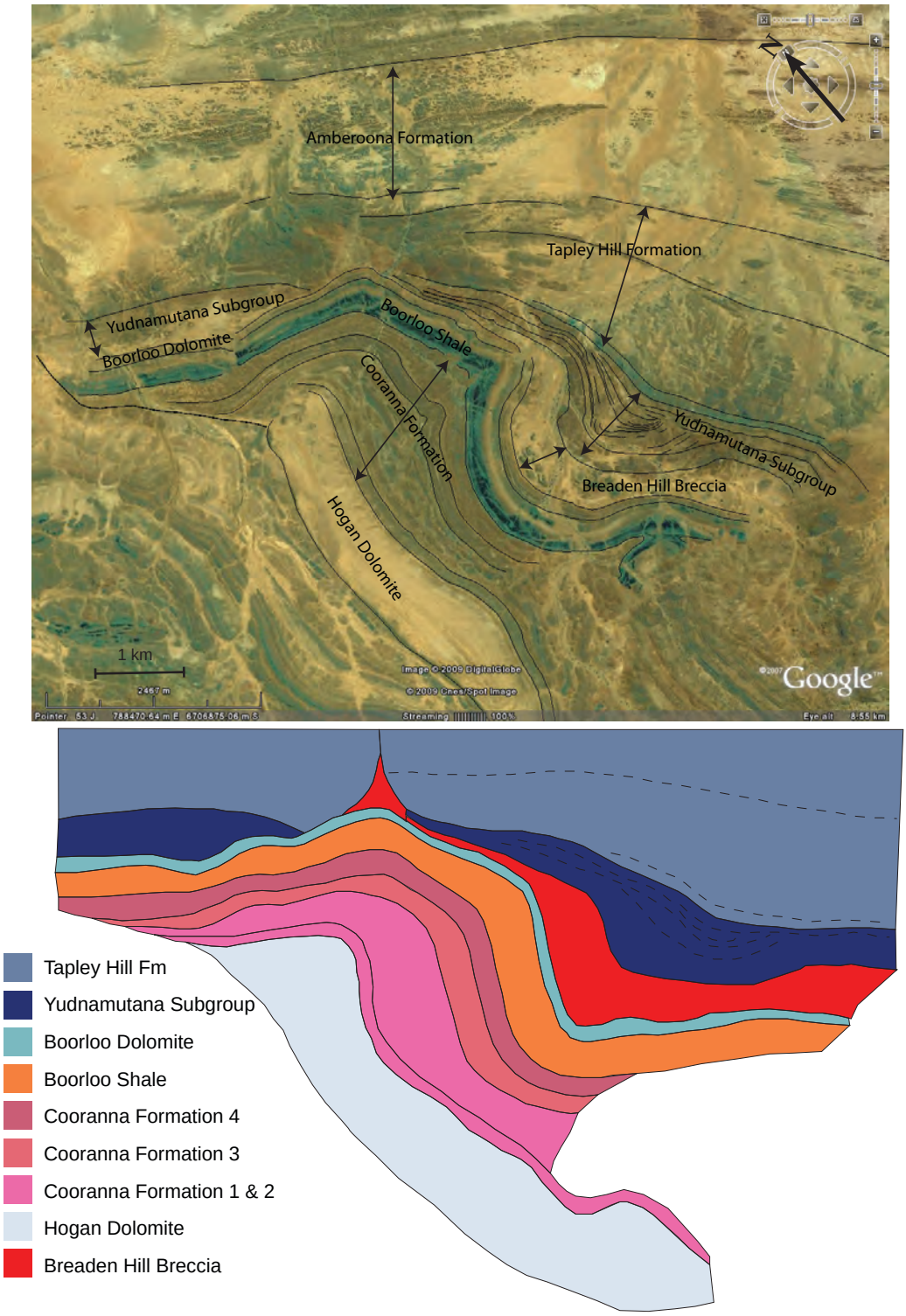

Figure 7.53. Map showing the true thickness of the Hogan Dolomite to the top of the Tapley Hill Formation, measured from the base of the Amberoona Formation.
It shows that the Yudnamutana Subgroup has been affected by the same folding as the Curdimurka Subgroup, as the Boorloo Siltstone was folded into the fault-bend fold. Within the Yudnamutana Subgroup are a number of unconformities which show a decrease in folding upward. The basal Tapley Hill Formation is weakly folded. It can also be seen that there are two normal faults that were active at this time, centred on the triangular breccia. To the west of the breccia, the Yundamatana Subgroup and the Tapley Hill Formation are folded into a roll-over anticline, whereas to the east, it gradually thickens to the southeast. The faults can be traced into the Breaden Hill Breccia. Note that the breccia has moved into the space between the two faults, above the fault-bend fold, interpreted as the normal faulting and the fault-bend folding are related.

Zone, whereas the Fence Anticline is forming in response to movement on the Central Fault Zone.

Figure 7.53 also shows that the Tapley Hill Formation thickens to the southeast from the triangular breccia at Hinge 1 of the Fence Anticline. Selley and Bull (2002) mapped conglomerates within the Tapley Hill Formation at this locality, consistent with pulses of movement along bounding faults, showing that the northern tip of the Eastern Fault Zone was active at this time. As D_1 occurs during deposition of the lower Umberatana Subgroup, and there is no evidence for deformation of the Curdimurka Subgroup prior to D_1 as proposed by Murrell (1977), Parker (1983) and Dyson (2004).

7.5.3 D_2 and D_3.

D_2 produced folding and reverse faulting and was responsible for the rotation of the hanging wall of the West Willouran Fault to sub-vertical. It produced upright, tight folds F_2, with an initial northwest trending hinge line and a sub-horizontal plunge, and an axial planar cleavage. The folding may have been non-cylindrical to produced the extreme change in fold plunges seen in the Drill Pad outcrop, and the fit of poles to some F_2 folded surfaces to small circles, such as in the folded shear zone. It re-activated some D_1 faults, particularly layer-parallel sections striking between north and northeast.Where the Eastern Fault Zone is oriented roughly north - south it was reactivated, but where it is oriented east - west it was folded but shows no reverse movement. The example from the RSst4 unit (Figure 7.48) also shows this relationship, displaying a footwall syncline with a shallow plunge to the south. Paul et al. (1999) showed that the main basin inversion re-activated northwest trending normal faults as reverse faults during the Delamerian Orogeny.

D_3 folded F_2 structures around a northeast trending hinge line. It produced a spaced cleavage S_3 at a high angle to bedding and a bedding cleavage intersection, S^3_0 but overall, its effect was minimal in the Euchre Pack Domain. Both of these deformations are best observed at the scale of the Willouran Range and are discussed further in the next chapter.

7.5.4 Relationship between the Curdimurka Subgroup and the Burra Group

The field relationships in the Euchre Pack Domain provide further evidence that the age of 797 ± 5 Ma is a depositional age of the Skillogalee Dolomite (Drexel, 2009; Reid, 2009) is incorrect. If it were correct, either the upper Skillogalee Dolomite would be of the same age as the Rook Tuff and therefore correlatives, and the units from the Dunns Mine Limestone to the Boorloo Siltstone would be equivalent to the upper part of the Burra Group, from the uppermost Skillogalee Dolomite to the Bungarider Subgroup (and possibly the Belair Subgroup). If this were the case, the contact between the Emeroo Subgroup and the Boorloo Siltstone would be a reverse fault with the Emeroo Subgroup being thrust over the Curdimurka Subgroup, along the Eastern Fault Zone, bringing it in contact with the Boorloo Siltstone. This could be the case, if the movement along the Eastern Fault Zone was sinistral, with the Burra Group being transported to the north. However, as has been shown, the first and most significant movement was a dextral strike-slip movement as seen

today, with the Burra Group being transported to the southeast. There was minor sinistral movement on the Central Fault Zone, but this was late and of less than 100 metres. Hence prior to D_1, the Burra Group overlay the Curdimurka Subgroup, and was not along strike (i.e. equivalent to it).

The other area in the Euchre Pack Domain where this correlation is tested is on either side of the Western Fault Zone, where southwest facing Skillogalee Dolomite is separated from southeast facing Boorloo Siltstone by breccia within the fault zone (Figure 7.43). This juxtaposition infers that the northeast dipping West Willouran Fault is a normal fault, if the deposition age of the Skillogalee Dolomite was correct. However, the field evidence presented here, and in the next chapter indicate that it is a reverse fault, with the Skilligalee Dolomite occuring within a footwall syncline to the fault. Hence, once again the structural relationship shows that the Curdimurka Subgroup is not equivalent to the Burra Group.

7.6 Conclusions

Mapping of the Curdimurka Subgroup in its type area, the Euchre Pack Domain has shown that it has been subject to three deformations. These are:

- D_1, which produced moderate to steeply plunging inclined folds and strike-slip faulting initially with the transport to the southeast, then to the northwest.

- D_2, which produced upright, northwest – southeast trending folds with a penetrative axial plane cleavage and large southeast directed reverse faults, and

- D_3, which folded axial surfaces of D_2 folds into open, southwest trending folds, with a spaced cleavage at a high angle to bedding.

D_1 was contemporaneous with the deposition of the basal Yudnamutana Subgroup, and possibly the lower part of the Tapley Hill Formation. D_1 structures were rotated by D_2 and so the apparent strike-slip faults seen today originally formed as normal faults having a ramp and flat morphology and thrusts. D_1 folds were inclined to recumbent prior to their rotation to sub-vertical during D_2.

D_1 was likely initiated by a vertical σ^1 which produced layer parallel deformation in siltstone and carbonate units but caused coarse-grained clastic units such as the Dome Sandstone to fail in a brittle manner. Gravity spreading was the likely mechanism of deformation although there may also have been a component of gravity sliding above a decollement below the level of the Dome Sandstone.

Field relationships demonstrate also that the correlation between the Curdimurka Subgroup and the Burra Group, as implied by the similar ages of intrusives in the Skillogalee Dolomite and Rook Tuff, does not hold. Therefore, the 797 ± 5 Ma age attributed to the Skillogalee Dolomite is considered to be incorrect.

CHAPTER 8.
STRUCTURE OF THE WILLOURAN RANGE.

8.1 Introduction

The previous chapter showed that the timing of D_1 in the Euchre Pack Domain was during deposition of the Yudnamutana Subgroup and Tapley Hill Formation. It concentrated on a small area of the Willouran Range and so in this chapter, the focus moves out to show that D_1 was a major regional deformation, affecting the whole of the Willouran Range. It will do this by examining the kilometre-scale structure of the Willouran Range, using traverse mapping, aerial photograph interpretation and aeromagnetic data.

To assist in the description of the geology of the Willouran Range, it has been divided into a series of structural domains identified in this work (Figure 8.1). The definition of structural domains is based on them having different styles and geometries than in the adjacent areas and each will be discussed below. Sub-domains are defined on the basis of individual domains having broadly the same features but differing in detail in the differnt sub-domains. Domainal boundaries are all faulted whereas sub-domain boundaries are transitional along strike. By discussing the structure and stratigraphy of each structural domain a broad picture of the structure of the Willouran Range will be developed.

Regional gravity data will be used to create a 2.5D gravity model of a cross-section and a long section to better understand the geology at depth, and to test the geological interpretation. The results of this work will be combined with the conclusions of the previous chapter to understand the the structural development of the Willouran Trough.

8.2 The Curdimurka Subgroup

8.2.1 The Stony Range Domain

A total of eight traverses were mapped across the Stony Range Domain (Figure 8.2a). Its southwestern edge is the Norwest Fault, although nowhere is the fault seen in outcrop, and the northeastern edge is the faulted contact with the Burra Group. To assist in describing the main features of the domain, two sub-domains; the Rocky Point, and Track Sub-domains have been defined based on their more complex structure than other sections of the Stony Range Domain. The main rock unit cropping out is Dome Sandstone, which includes a ridge-forming sandstone overlain by interbedded siltstone and sandstone with minor dolomite (Krieg and Anthony, 1992). It is repeated by strike-slip faulting in the Rocky Point and the Track Sub-domains (Figure 8.2a). Breccia bodies occur in both sub-domains, with megaclasts within the Rocky Point Sub-domain including blocks of interbedded siltstone and sandstone, epidote-bearing amygdaloidal basalt. Murrell (1977) also reported a megaclast of Black Knob Marble in the Rocky Point Sub-domain. A series of folds which plunge at about $60^o/110^o$ (Murrell, 1977), with ENE striking axial planes occur in the southeast part of the domain (Figure 8.2a).

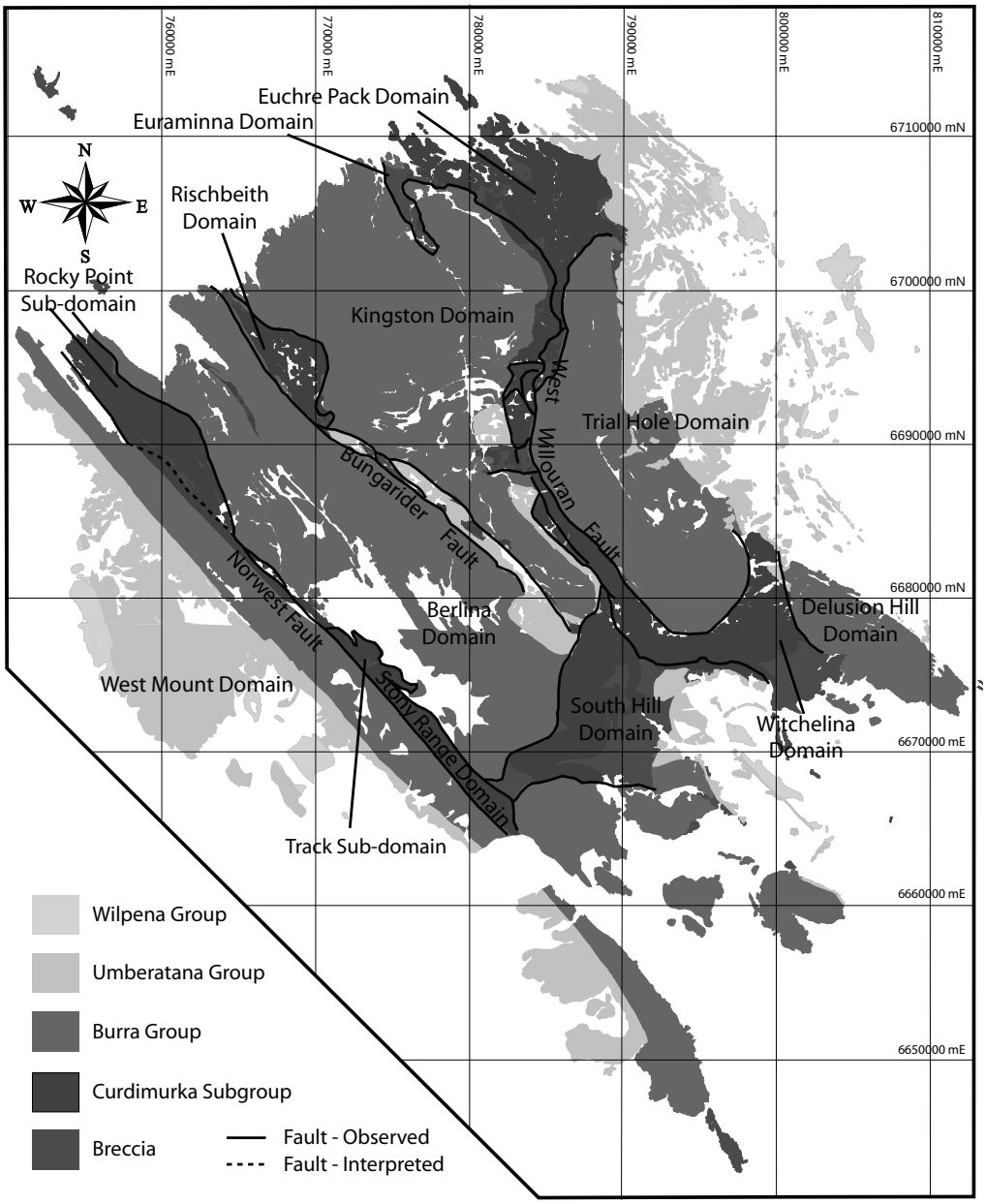

Figure 8.1. Structural domains of the Willouran Range.
All domain boundaries are faulted. The Rocky Point and Track sub-domains are part of the Stony Range Domain.

The general dip of the Dome Sandstone in the Stony Range Domain is steep to the northeast, with stratigraphic facing in that direction. In the Rocky Point Sub-domain, strata between the two northeast-facing blocks of Dome Sandstone are folded into a tight syncline, with a moderately steep plunge to the north (Stereonet *i*, Figure 8.2a). The axial plane strikes approximately northwest, sub-parallel to the strike of the Dome Sandstone. Sprigg (1949) interpreted the Rocky Point Sub-domain to have formed as the result of sinistral strike-slip movement of the Norwest Fault. Here the repetition of the Dome Sandstone in the Rocky Point Sub-domain is interpreted to be a dextral strike-slip fault in its present orientation. By comparison with similar structures in the Euchre Pack Domain, it is interpreted to be a D_1 structure, with the syncline forming as a footwall syncline (Figure 8.2b).

In the Track Sub-domain the Dome Sandstone is folded and faulted into a complex structure associated with breccia. North of the Andamooka - Farina track, north-east facing Dome Sandstone crops out in two ridges with folded siltstone, shale minor carbonate and breccia between. South of the track, to the east is a ridge of east-facing Dome Sandstone separated by a fault from a syncline of Dome Sandstone, plunging at a moderate angle to the northwest. A fourth ridge of Dome Sandstone crops out in the immediate hanging wall of the Norwest Fault, and it separated from the syncline by a fault. Both faults are interpreted to be strike-slip faults. The structure is interpreted to have formed by an initial dextral movement followed by sinistral movement (Figure 8.2c). The calculated plunge of folds from a traverses across the structure north of the track is 30°/319° (Stereonet *iii*, Figure 8.2a) and for the syncline south of the track, the calculated plunge is 57°/319° (Stereonet *iv*, Figure 8.2a).

8.2.2 The South Hill Domain

The South Hill Domain is a north – south trending block of folded Curdimurka Subgroup, comprising ridge-forming sandstone units with interbedded siltstone and sandstone on the slopes, that Krieg and Anthony (1992) mapped as Dome Sandstone (Figure 8.3). Stratigraphic facing is to the east and the domain as a whole dips steeply to the eastern quadrant. The Dome Sandstone is folded into an east-plunging tight anticline with breccia, including several large (tens of metres across) clasts of Black Knob Marble, in the core. On the western side, at the northern and southern ends of the domain the Dome Sandstone is folded into close to tight anticlines.

At the southeastern end of the Domain, a sub-vertical fault separates the Dome Sandstone on the western side from a second quartz arenite unit. The fault is marked by quartz veining and brecciation, and is sub-parallel to bedding. A thin sandstone unit near the top of the Curdimurka Subgroup within a syncline in the northern half of the South Hill Domain may be the same unit (Figure 8.3).

A breccia crops out at the southern end of the South Hill Domain (Figure 8.3). It consists of several large (hundreds of metres across, not shown separately here) blocks of folded siltstone with minor sandstone and dolomite, tightly folded and separated by fault zones. At several localities a breccia with a carbonate matrix occurs within the fault zone. It was not possible to identify which unit or units these faulted blocks belong to. They resemble the siltstone units stratigraphically above the ridge-forming sandstone of the Dome Sandstone but they are also similar to siltstone units in the Burra Group.

No field work was conducted on the northeastern side of the South Hill Domain and this area on the map is an aerial photograph interpretation. It is interpreted to be a breccia with megaclasts up to 2,000 m in diameter (Figure 8.3). From comparison with mapped areas, the majority of the blocks are interpreted to be siltstone-sandstone-carbonate units although one has an outcrop typical of ridge-forming sandstone. Areas between these blocks may be breccia matrix or siltstone-shale only. One block located on the southeastern part of

a

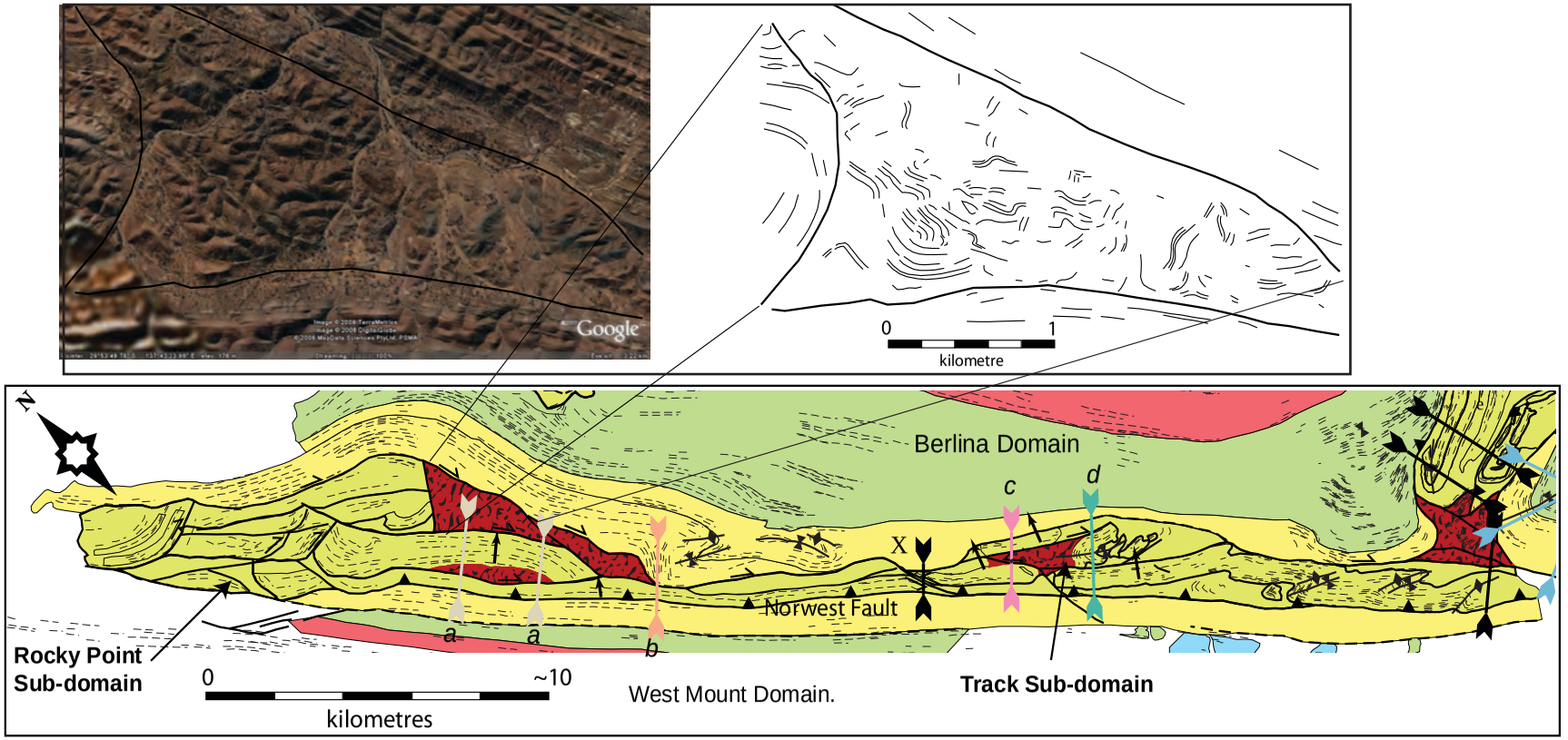
Google
0
1
kilometre
N
Berlina Domain
c
d
X
Norwest Fault
a
a
b
Rocky Point
Sub-domain
0
~10
kilometres
West Mount Domain.
Track Sub-domain
Dome Sandstone
Breccia
Myrtle Springs Formation
Skillogalee Dolomite
Emeroo Subgroup
mapping traverse
Bedding Trend
Anticline
Syncline
Fold hinge - facing not known
Normal Fault
Reverse Fault/Thrust
Strike-slip fault
Fault - inferred
i)
ii)
iii)
iv)

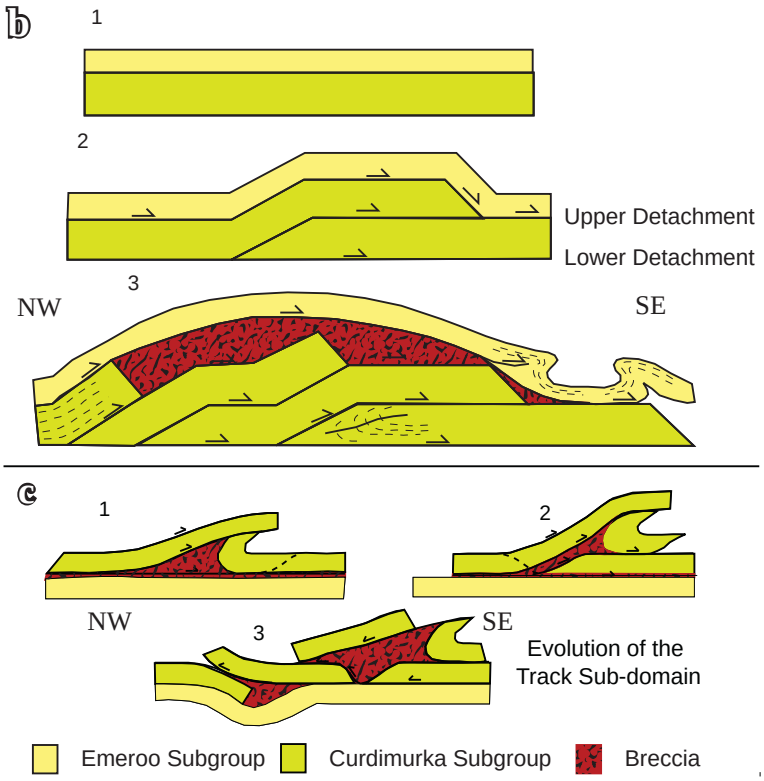

Figure 8.2. The Stony Range Domain.
a) Aerial photograph interpretation of the Curdimurka Subgroup along the Norwest Fault. The entire outcrop is the Stony Range Domain but within this are the Rocky Point and Track Sub-domains. The Rocky Point Sub-domain is interpreted to be a thrust stack, with the Dome Sandstone being thrust over itself to the southeast. In the footwall of the thrust is a syncline with a moderately steep plunge to the northwest (stereonet i). South of the Rocky Point Sub-domain, the Curdimurka Subgroup occurs as only a single strike ridge until the Track Sub-domain where it is again repeated by thrusting with a series of thrusts, back thrusts and a footwall syncline. Folding associated with the thrusting plunges at a moderate angle to the northwest (stereonets iii and iv). Between the Rocky Point Sub-domain and the Track Sub-domain is a small backthrust (X). No mapping was conducted in the southeastern part of the Stony Range Domain but in this area are the drag folds of Murrell (1977), which verge to the southeast. A traverse across the Burra Group at position (b) shows that it is folded, with a steep plunge to the southeast, with a second fold possibly associated with the back-thrust (stereonet ii). Breccias occur in the Rocky Point Sub-domain and the Track Sub-domain although these are not shown. Above is a GoogleEarth image of the southeastern Rocky Point Domain with line interpretation showing the chaotic folding in the breccia.

b) Evolution of the Rocky Point Sub-domain and deformation of the Emeroo Subgroup.
The Rocky Point Sub-domain formed as a antiformal thrust stack with detachments above and below the Curdimurka Subgroup. The Emeroo Subgroup is folded by gravity collapse on the upper detachment. In D_2, the thrust stack was rotated by reverse movement on the Norwest Fault to its present orientation.

c) Evolution of the Track Sub-Domain.
1) The structure of the Track Sub-domain developed initially at a southeast directed thrust with an associated footwall syncline. 2) A second thrust developed to the southeast of the first, transporting the initial structure to the southeast. 3) With the reversal of movement on the basal thrust, the upper sheet was dragged to the northwest and the reverse thrust at X was formed.

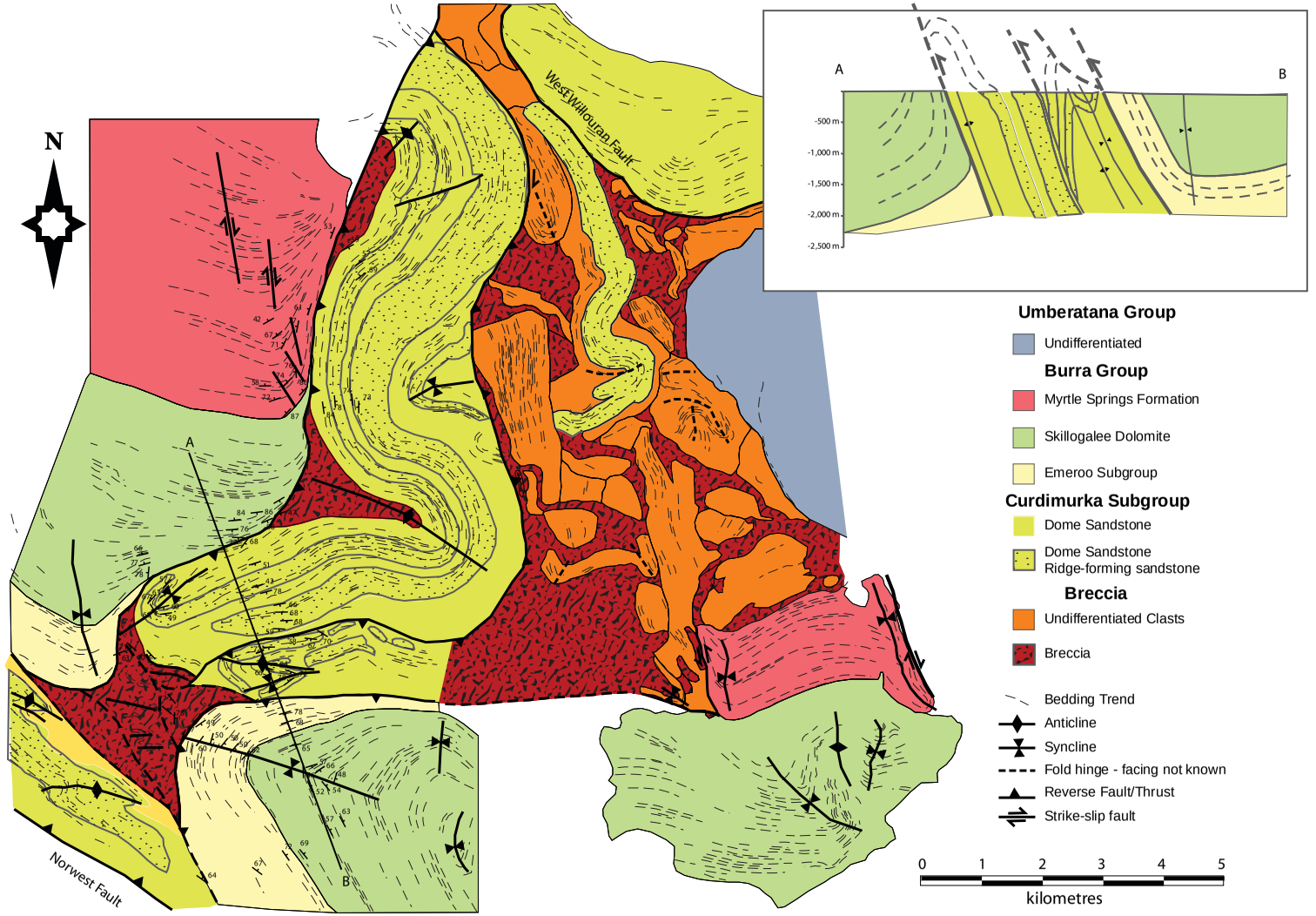

Figure 8.3. Geology of the South Hill Domain.
The South Hill Domain consists of ridge-forming, east-facing Dome Sandstone. Its western margin is a faulted contact with the Burra Group, with breccia in the fault zone. The southeastern margin is also a faulted contact with the Burra Group. Breccia with megaclasts to two kilometres in diameter occur in the northeastern third of the domain. Megaclasts are interpreted to be mainly siltstone-sandstone-carbonate with one sandstone-dominant megaclast that has a similar appearance to Dome Sandstone in aerial photographs. The Umberatana Group lies unconformably on the South Hill Domain along eastern margin. The West Willouran Fault lies along the contact with the Witchelina Domain to the north. The inset shows a cross-section of the South Hill Domain along the line marked. It shows that the South Hill Domain dips steeply to the southeast and has been thrust to the northwest, over the Burra Group.

the domain has a similar structure and outcrop appearance to that of the Myrtle Springs Formation on the western side of the South Hill Domain.

On the western side of the South Hill Domain, the west-facing Burra Group is overturned with dips sub-parallel to those in the adjacent Dome Sandstone (Figure 8.3). The contact is a fault zone, marked by a zone of brecciation and quartz veining over a width of up to 50 metres. It has a steep dip to the east, and cuts across the stratigraphy of the Burra Group from the Emeroo Subgroup in the south to the Myrtle Springs Formation in the north. Not shown in Figure 8.3 but discussed below, the Umberatana Group is west of the Curdimurka Subgroup at the northwestern end of the South Hill Domain.

A cross-section of the South Hill Domain shows that the Dome Sandstone has been thrust across the Burra Group from east-southeast to west-northwest, along a steeply dipping fault plane (Figure 8.3).

8.2.3 The West Willouran and Witchelina Domains.

Only reconnaissance mapping was conducted in these domains and the following is based on aerial photograph interpretation, previous mapping (Krieg and Anthony, 1992; PIRSA 1:100,000 GIS database) and a few field observations. South of the Euchre Pack Domain in the West Willouran Domain, the Curdimurka Subgroup is broken into a number of fault blocks, none of which have a complete Curdimurka Subgroup stratigraphy (Figure 8.4). In one block, Boorloo Siltstone is separated from Dome Sandstone by Hogan Dolomite, another comprises a section from the Recovery Formation to Cooranna Formation, including Hogan Dolomite, and only Boorloo Siltstone in another block and so on (Figure 8.4). In total there are five separate fault blocks separated by faults with or without breccia. Breccia may occur above or below the fault blocks also. Within the southern-most fault block, the Hogan Dolomite and Cooranna Formation is folded into a south-verging ‘z’ fold. From aerial photograph interpretation, the fold appears to have a moderately steep plunge to the south, and an axial plane dipping steeply to the northeast.

The West Willouran Fault forms the boundary between the South Hill Domain to the west and the Witchelina Domain to the east (Figures 8.4 and 8.5). Tightly folded Curdimurka Subgroup and breccia crops out in the Witchelina Domain (Figure 8.5; PIRSA 1:100,000 GIS database). From reconnaissance mapping thick units of ridge-forming quartz arenite are likely Dome Sandstone and not Recovery Formation as shown in the PIRSA map. They are folded into a series of anticlines and synclines, modified by faulting. Limited data from a traverse across the centre of the domain suggests that the fold plunges are shallow to the northwest (Figure 8.5), with upright axial planes. In the west of the domain, low ridges of sandstone separated by siltstone units may be Recovery Formation. In the middle of the domain, between sandstone ridges is white silicified siltstone and fine-grained sandstone with abundant halite and gypsum pseudomorphs, which could be correlated with either the Recovery Formation or the Cooranna Formation. Minor silicified dolomite beds to one metre thick occur interbedded with the siltstone and sandstone units. In the southeast corner of the domain, just above the West Willouran Fault is an area of breccia, with folded

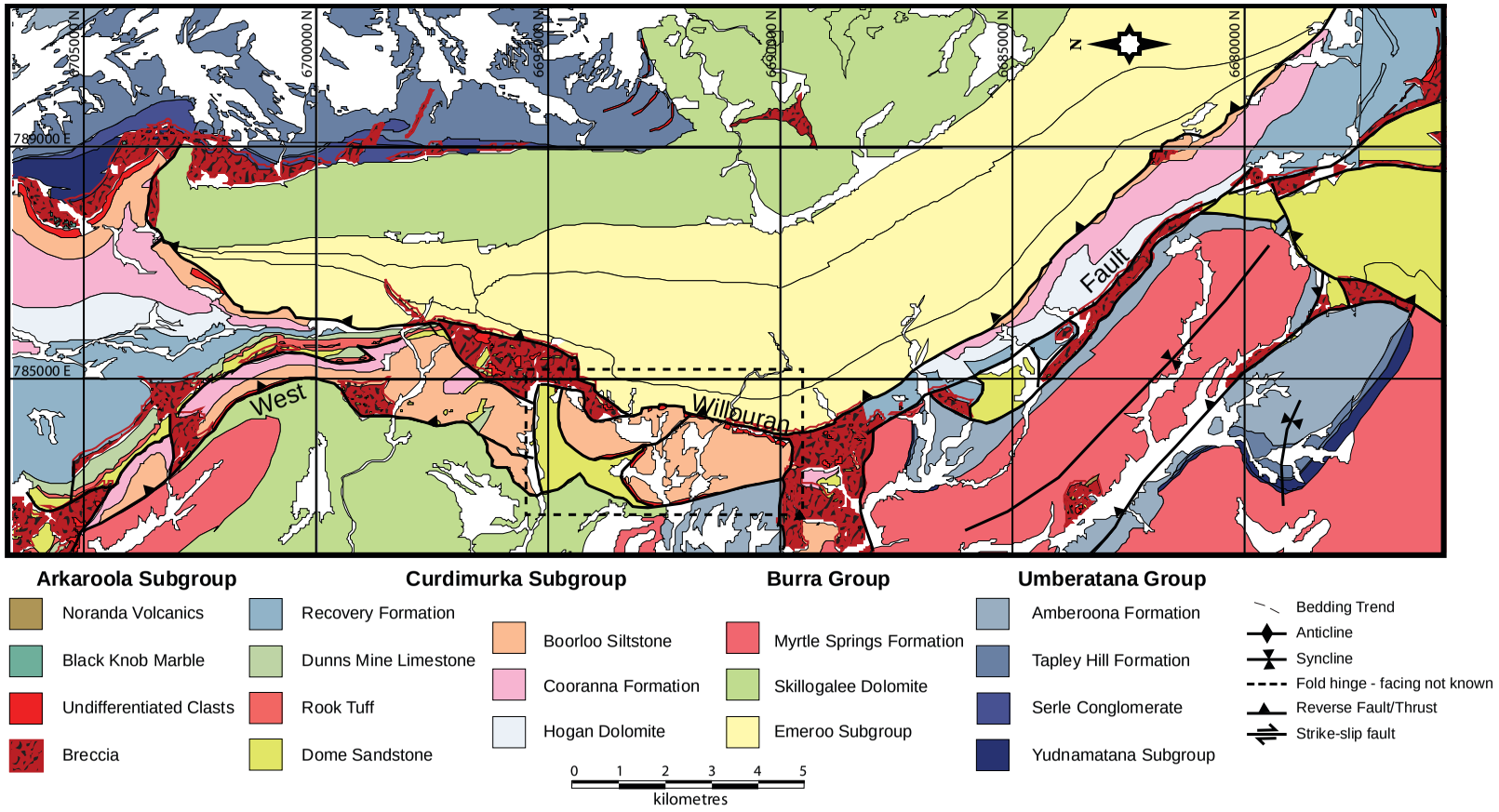

Figure 8.4.The Curdimurka Subgroup along the West Willouran Fault (PIRSA 1:100,000 GIS Geological Map).
East-facing Curdimurka Subgroup crops out in a series of fault blocks within the West Willouran Faut zone, between east-facing Emeroo Subgroup to the east and west-facing Umberatana Group and Burra Group in the west. There are also breccia bodies between the fault blocks of Curdimurka Subgroup. In the dashed box, Boorloo Siltstone is mapped in contact with Dome Sandstone. If this is the black shale facies within the Rook Tuff, the complete stratigraphy is preserved within the West Willouran Fault zone, from its base in the north to the Boorloo Siltstone in the south.

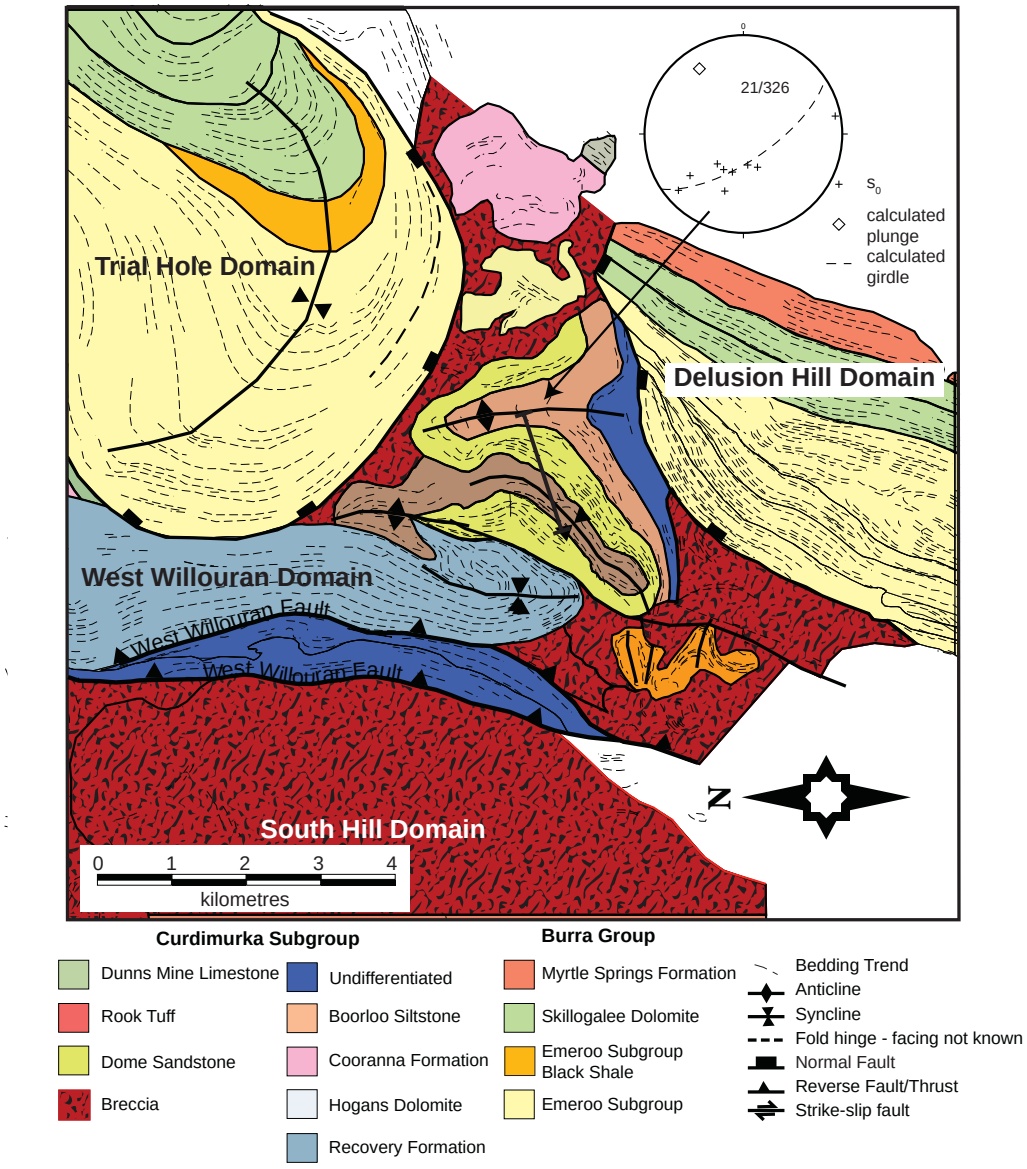

Figure 8.5. Aerial photograph interpretation of the Witchelina Domain.
The bulk of the domain consists of folded but otherwise intact Curdimurka Subgroup. In the centre is a ridge-forming quartz arenite unit with siltstone and carbonate stratigraphically above and below, that is likely the Dome Sandstone. Breccia forms only a small proportion of the domain, along the margins and at the eastern end. The stereonet shows poles to bedding and the calculated plunge from bedding taken along the marked traverse across one fold hinge.

megaclasts. Cooranna Formation also occurs in the eastern part of the domain, and possibly in contact with the Umberatana Group. Breccia is mapped between the blocks of intact strata. Both the northern and southern contacts with the Burra Group are normal faults with steep dips to the north and south respectively.

8.3 The Burra and Umberatana Groups.

8.3.1 The West Mount Domain.

The West Mount Domain is positioned in the footwall (i.e. western block) of the Norwest Fault (Figure 8.6). Immediately adjacent to the fault is a near complete southwest facing succession of Burra Group rocks up to about 2,000 m in thickness (Belperio, 1990).

The overlying Umberatana Group show considerable variation in thickness in the West Mount Domain. The Yudnamutana Subgroup varies in thickness from 850 m near West Mount to 1080 m at Screech Owl Creek, 20 km along strike to the northwest (Murrell, 1977). The Tapley Hill Formation varies in thickness from 0 m just north of the Witchelina – Mulgaria track to about 1,100 m on the western edge of the Andamooka 1:250,000 map sheet (Murrell, 1977; Preiss, 1987). The Amberoona Formation varies in thickness from about 380 m to about 1080 m (Murrell, 1977). From the western to eastern limb of the West Mount Dome it varies in thickness from 720 m to 380 m, prompting Murrell (1977) to suggest that the eastern limb saw a period of non-deposition. The base of the Amberoona Formation cuts down section into the Yudnamutana Subgroup between points A and B in Figure 8.6 and, as in the Willouran Range, contains a series of slump breccias (Murrell, 1977; Preiss, 1987).

The Umberatana Group has been folded into an upright, northwest – southeast trending anticline in the West Mount Dome. Further west, outside of the area under discussion here (see below), the Umberatana and Wilpena Groups have been folded into a series of broad, upright anticlines and synclines, until the Lake Arthur Fault, which marks the boundary between the Torrens Hinge Zone to the east and the Stuart Shelf to the west.

8.3.2 The Berlina Domain.

The Berlina Domain is in the hanging wall of the Norwest Fault, with the strata dipping steeply to the northeast (Figure 8.7). It is separated from the Curdimurka Subgroup by a reverse fault at the base of the Emeroo Subgroup. There is a complete succession of Burra Group from the Emeroo Subgroup to the Myrtle Springs Formation, with a thin succession of the Umberatana Group preserved in a small area in the footwall of the Bungarider Fault (Figures 8.7 and 8.8). Belperio (1990) estimated a total thickness of between 6,000 m and 8,000 m of the Burra Group in the Berlina Domain.

The Emeroo Subgroup varies in thickness in outcrop from being absent adjacent the Track Sub-domain of the Stony Range Domain, to over 1,420 m thick east of the Rocky Point Sub-domain (Figure 8.7). However, the base is not seen and thickness variations may only be a reflection of the post-depositional structure. The Skillogalee Dolomite thickens from 1,510 m in the northwest to 3,921 m in the centre of the domain (Belperio, 1990). The upper contact of the Myrtle Springs Formation is not seen except where it approaches the South Hill Domain, where it is erosional, with angular unconformity between it and the overlying Umberatana Group. A narrow sliver of Curdimurka Sub-group rocks occurs within the Skillogalee Dolomite above the Rocky Point Sub-domain (Figure 8.7). It deforms the surrounding rocks, with faults at its tips and the underlying dolomite folded into a syncline.

Northeast of the Rocky Point Sub-domain, the Emeroo Subgroup is folded into a large-scale open anticline with a moderate to steep plunge to the northeast (interpreted from aerial photographs and Krieg and Anthony (1992). From the steep plunge and the relationship with the underlying deformation with the Rocky Point Sub-domain, it is interpreted to

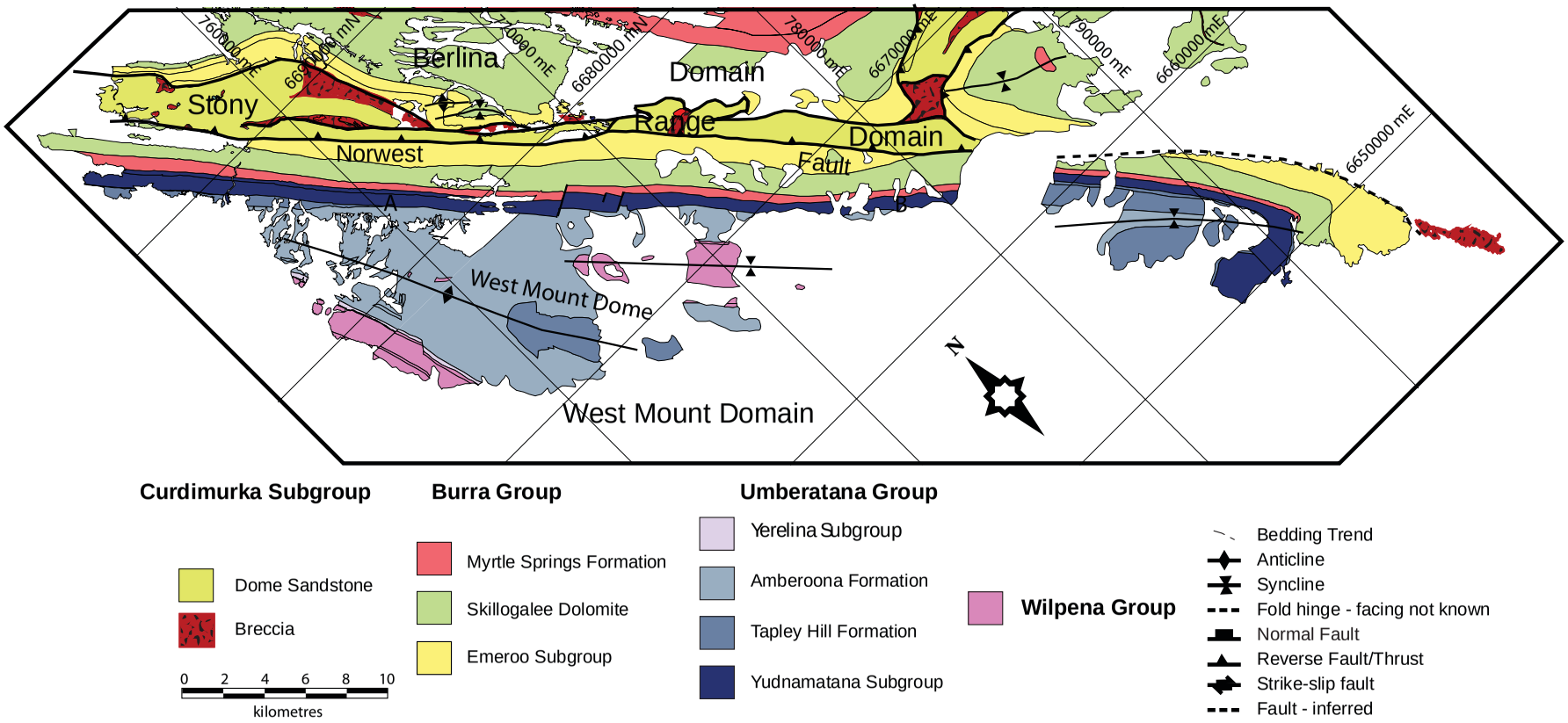

Figure 8.6. The West Mount Domain.
The West Mount Domain contains outcrop from the Emeroo Subgroup to the Wilpena Group. It is in the footwall of the Norwest Fault and is dominated by NW - SE trending upright folds. The Amberoona Formation cuts down the stratigraphy until sits on the Myrtle Springs Formation. (PIRSA 1:100,000 GIS database).

have formed during D_1. Close folding between the Rocky Point Sub-domain and the Track Sub-domain has a moderate plunge to the southeast (Stereonet b, Figure 8.7). Closer to the Bungarider Fault, the Myrtle Springs Formation is folded into a broad syncline that was examined in two traverses. Calculated plunges from bedding across the synclines are 08°/151° and 28°/137° (stereonets f and g, Figure 8.8) but photograph interpretation suggests that they are regionally doubly plunging, with a shallow plunge to the northwest also (Figure 8.7). Outcrop-scale folds and layer-parallel faults with anomalous vergence (to these folds) and transport direction show that the syncline has re-folded earlier structures. The Myrtle Springs Formation was affected by a fold and faulting event prior to D_2.

The Umberatana Group crops out in a small area at the intersection of the Bungarider Fault and the South Hill Domain (Figure 8.8). It comprises a thin succession of Yudnamutana Subgroup and Tapley Hill Formation, with a thicker succession of Amberoona Formation, all of which are folded into a broad syncline. Murrell (1977), and Selley and Bull (2002) interpreted the basal contact as an angular unconformity. Selley and Bull (2002) reported that the lower Umberatana Group wedges out on either margin of the syncline. The contact between the Amberoona Formation and the Tapley Hill Formation is an unconformity. Within the Amberoona Formation are a number of megabreccia deposits (Figure 8.8) interpreted to be slump deposits by Murrell (1977). Selley and Bull (2002) concluded that the Amberoona Formation was deposited within a series of steep-sided canyons that locally cuts down through the lower Umberatana Group into the Myrtle Springs Formation.

8.3.3 The Kingston Domain

In the Kingston Domain, there is a complete succession of the Burra Group from the Emeroo Subgroup to the Myrtle Springs Formation (Figure 8.9). Belperio (1990) calculated a maximum thickness for the Burra Group of about 3,000 m in the Kingston Domain. Outcrop of the Emeroo Subgroup is restricted to an anticline with the Curdimurka Subgroup in its core in the Rischbeith and Euraminna Domains. The Skillogalee Dolomite crops out northwest of a northeast trending line beginning approximately at the southern end of the Rischbeith Domain, with Myrtle Springs Formation southeast of this line, folded into a tight syncline. The Myrtle Springs Formation also crops out against the northern margin of the Rischbeith Domain and in the core of a syncline between the Euraminna Domain and the West Willouran Fault. The upper contact between the Rischeith Domain and the Burra Group was considered to be an on-lap surface by Murrell (1977) but here it is interpreted to be a structural contact. An apparent on-lap surface is due to broad, open folds being cut at a low-angle to bedding by a later high angle reverse fault.

The Umberatana Group crops out in the Kingston Domain, adjacent to the Bungarider Fault and in the footwall of the West Willouran Fault (Figure 8.9). Adjacent to the Bungarider Fault, only the Yudnamutana Subgroup and Tapley Hill Formation crop out in a thin succession, that thickens into the Berlina Domain as described above. In the footwall of the West Willouran Fault, it has a similar outcrop pattern to that described in the Berlina Domain, with a thin or absent basal succession and a much thicker Amberoona

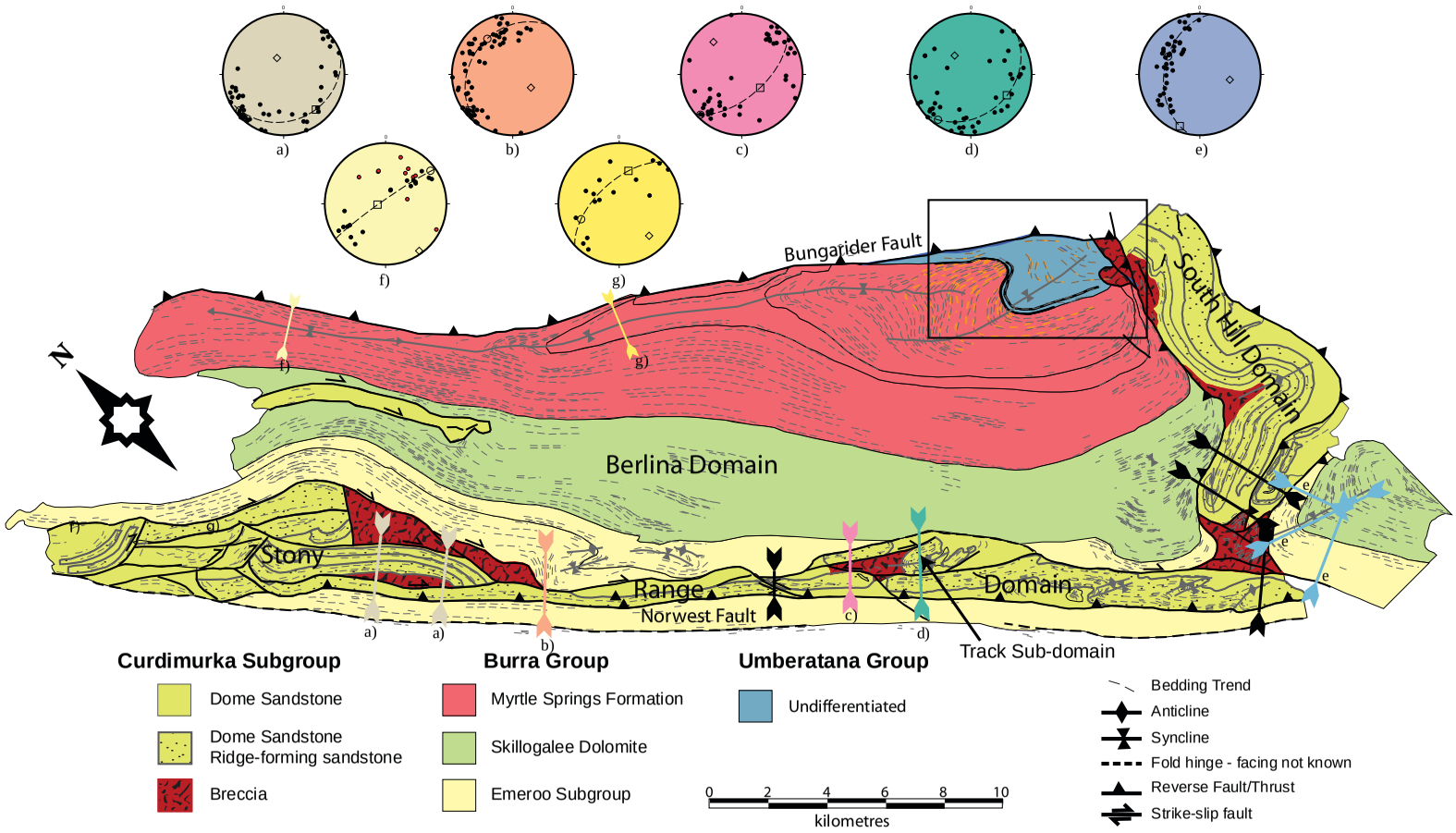

Figure 8.7. The Berlina Domain and the Stony range Domain.
Stereonets show poles to bedding taken on traverses marked; b, e, f and g are from the Burra Group, and the remaindera re from the Curdimurka Subgroup across the Stony Range Domain. Stereonet b is from a an anticline - syncline in the Emeroo Subgroup, whereas f and g are across the top of the Myrtle Springs Formation, in the footwall of the Bungarider Fault. Whereas the former has a moderately steep plunge to the SE and is interpreted to be F1, f and g have shallow plunges to the SE and are interpreted to be D2. Stereonet e is from folded Burra Group between the South Hill Domain and Norwest Fault, and has a moderately steep plunge to the east.

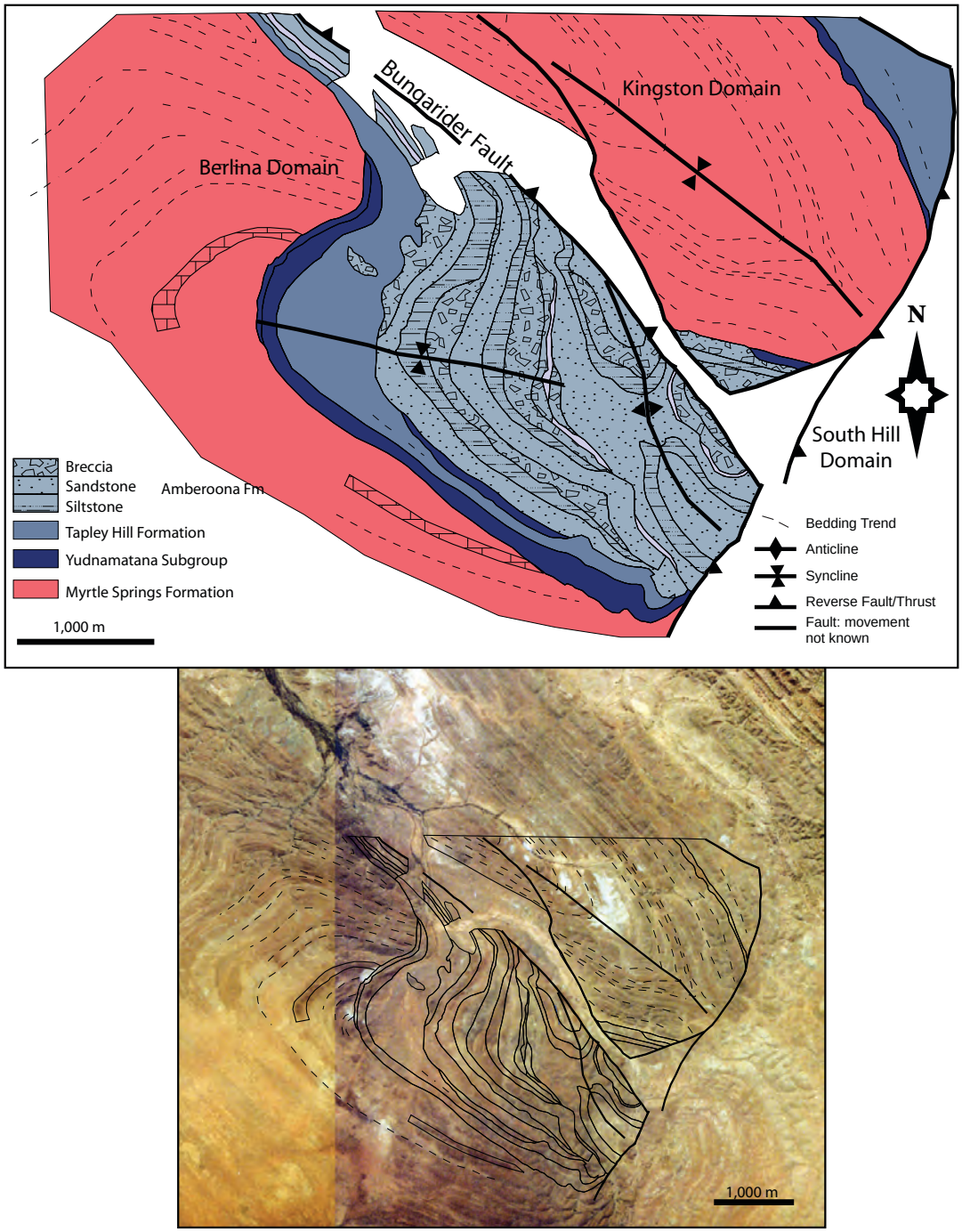

Figure 8.8. The Umberatana Group in the Berlina Domain.
The Umberatana Group lies unconformably on the Myrtle Springs Formation. It comprises a thin Yudnamatana Subgroup and Tapley Hill Formation and a thicker Amberoona Formation. The Amberoona Formation has within it a series of sedimentary breccia units interpreted to be slump deposits by Murrell (1977). It has also been folded but the severity of the folding decreases up the stratigraphy. There are also a number of unconformities within the Amberoona Formation indicating that the deformation was syn-depositional. The outcrop pattern shown here is repeated in several other outcrops of Umberatana Group in the Willouran Range. (modified from Murrell, 1977). The line work from the drawing is overlain on a composite aerial photograph to show the relationship between the geology and topography.

Formation. There is an angular unconformity between the Myrtle Springs Formation and the Umberatana Group.

At the largest scale, the structure of the Kingston Domain is a broad, open anticline and syncline verging to the southeast, which divides the domain into three sub-domains (Figure 8.9). The first is in the area of outcrop of the Emeroo Subgroup and the Skillogalee Dolomite, which is the anticlinal hinge of the broad fold. Dome and basin folding is the main structural style, with domes elongate to the northwest – southeast and having a minor axis trending west-northwest – east-southeast. The second sub-domain is the syncline of the broad fold, with Myrtle Springs Formation in the core. It has been folded into a tight syncline between the Bungarider and West Willouran faults interpreted to be a footwall syncline to the latter. A third sub-domain is southwest of the Euchre Pack Domain, where the Skillogalee Dolomite and the Myrtle Springs Formation are folded into a footwall syncline to the West Willouran Fault. Tight east-southeast trending folds also occur at the boundary between the first and second sub-domains.

8.3.4 The Trial Hole and Delusion Hill Domains.

The Trial Hole and Delusion Hill Domains occur in the hanging wall of the West Willouran Fault. Both the Burra Group (Figure 8.10) and Umberatana Groups (Figure 8.11) crop out in these domains and they join north of the Witchelina Domain, which separates them at the level of the Burra Group. In the Trial Hole Domain, the Emeroo Subgroup reaches a maximum thickness of over 4,000 m (Belperio, 1990). It has a faulted basal contact with the Curdimurka Subgroup as described in Chapter 7. It thickens from the northwest to the southeast but at least part of this thickening is structural. On-lap surfaces are interpreted from aerial photographs at the northern and southern end of the domain toward the top of the Emeroo Subgroup (Figure 8.10). At the northern end, is a fault block with apparent reverse movement (relative to bedding) with the upper unit of the Emeroo Subgroup thickening towards the fault.

The Skillogalee Dolomite has a similar thickness across the Trial Hole Domain, thickening in a fault block near the centre of the domain. In the northern half of the domain the Skillogalee Dolomite is overlain by breccia and the Umberatana Group and in the southern half, it is overlain by a thin Myrtle Spring Formation. Between the Emeroo Subgroup and the Skillogalee Dolomite in the southern end of the domain is a thin black shale unit.

In the Delusion Hill Domain, the basal units of the Emeroo Subgroup are on-lapped by the upper unit (Figure 8.10). From the outcrop pattern, the Emeroo Subgroup thins toward the Witchelina Domain, although there is also structural thickening. The Skillogalee Dolomite, although thinner than in the Trial Hole Domain remains at a constant thickness. It appears to overlap the Emeroo Subgroup but this may be due to later faulting along the contact with the Curdimurka Subgroup. The Myrtle Springs Formation retains a constant thickness also, with a similar thickness to that at the southern end of the Trial Hole Domain but is does not extend across the Witchelina Domain.

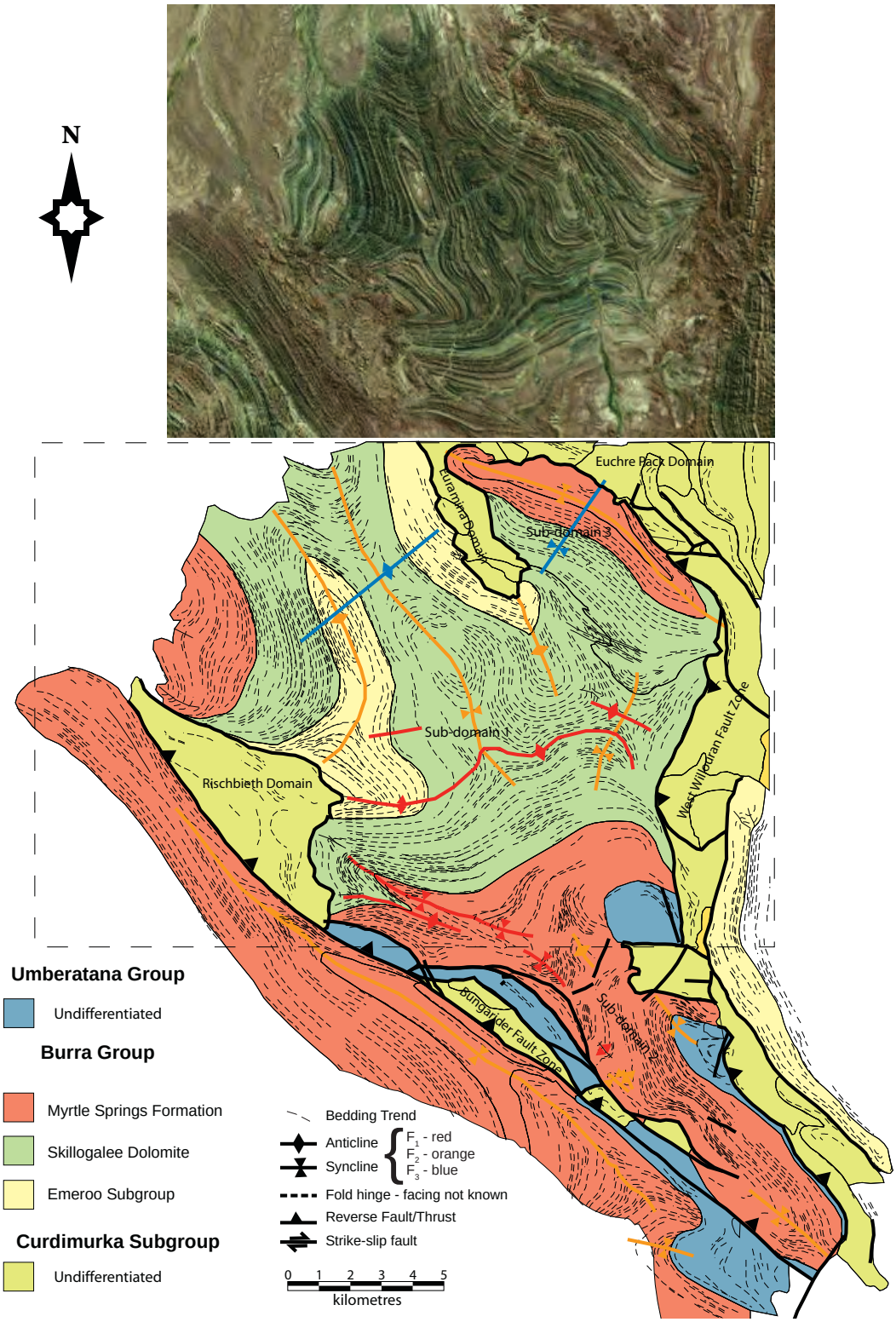

Figure 8.9. The Kingston Domain.
The Kingston Domain is within the hanging wall of the Bungarider Fault Zone and the footwall of the West Willouran Fault Zone. The Burra Group is the dominant unit within this domain with smaller outcrops of the Umberatana Group along the Bungarider Fault Zone and in the immediate footwall of the West Willouran Fault Zone. The Curdimurka Subgroup crops out within the Bungarider Fault Zone and the West Willouran Fault Zone but otherwise does not occur within the Kingston Domain. The Kingston Domain is most notable for the folding in its northern half, where three fold events can be seen. Above is a an image from Google Earth of the northern half, showing the spectacular folding and below is an aerial photograph interpretation of the domain.

The Umberatana Group is continuous from the Trial Hole Domain to the Delusion Hill Domain (Figure 8.11). The Yudnamutana Subgroup is a few hundred metres thick at the most but the Tapley Hill and Amberoona formations reach their maximum thickness within the Willouran Range area in the Trial Hole Domain. From a normal fault above the fault bend fold in the Euchre Pack Domain, the Tapley Hill thickens to the south, reaching its thickest adjacent to the faulted block of Skillogalee Dolomite. Conglomerate lenses are mapped within the Tapley Hill Formation adjacent to this structure (Figure 8.11), indicating that it was active during deposition of the Tapley Hill Formation. The Amberoona Formation also thickens from the normal fault into the Trial Hole Domain. Then, both formations thin to the south until the Yerelina Sub-group lies on Myrtle Springs Formation just north of the northern edge of the Copley 1:250,000 map sheet.

8.3.5 North of the Euchre Pack Domain.

North of the Euchre Pack Domain, the Adelaidean sediments crop out poorly or are overlain by a thin Mesozoic to Recent cover (Krieg and Anthony, 1992). To investigate whether the Burra Group occurs north of the mapped area, PIRSA regional aeromagnetic survey data for the over this area was examined. Only on the Curdimurka 1:250,000 map sheet does the available data have sufficient resolution to be able to interpret shallow structures, using the first vertical derivative (Figure 8.13). The magnetic texture of the units was first identified where there is outcrop (Table 8.1) and then these were then extrapolated to those areas without outcrop.

The Norwest, Bungarider and West Willouran Faults are all interpreted to continue to the northwest, retaining the same basic structure identified in the Willouran Range. However the Bungarider Fault trend changes to north-northwest for approximately 10 km beyond the Rischbeith Domain. The Norwest Fault becomes more complex about 15 km northwest of the Rocky Point Sub-domain, with the Curdimurka Subgroup thickening in a structure analagous to the Rocky Point Sub-domain. The West Mount Domain continues to the northwest with little change until about 6712000mN where the Emeroo Subgroup is interpreted to define a footwall syncline to the Norwest Fault.

The Berlina Domain continues to the north but with more some variation in the apparent variation in thickness. A thicker Umberatana Group than seen within the mapped Berlina Domain is interpreted in a structure similar to that shown in Figure 8.9, based on Krieg and Anthony, (1992) and the aeromagnetic image. There is also a zone of complex magnetics within is uninterpreted between the Umberatana Group and the Bungarider Fault. Further north, there is a syncline of interpreted Umberatana Group up to the level of the Yerelina Subgroup which may be a footwall syncline to the Bungarider Fault.

The Kingston Domain continues to the northwest, with the Myrtle Springs Formation adjacent the Bungarider Fault, a narrow Emeroo Subgroup in the footwall of the West Willouran Fault and Skillogalee Dolomite between. A thickening of the Curdimurka Subgroup and/or breccia surrounded by the Emeroo Subgroup divides the continuation of the Kingston Domain almost in two, centred on 6730000 mN. There may be a continuation

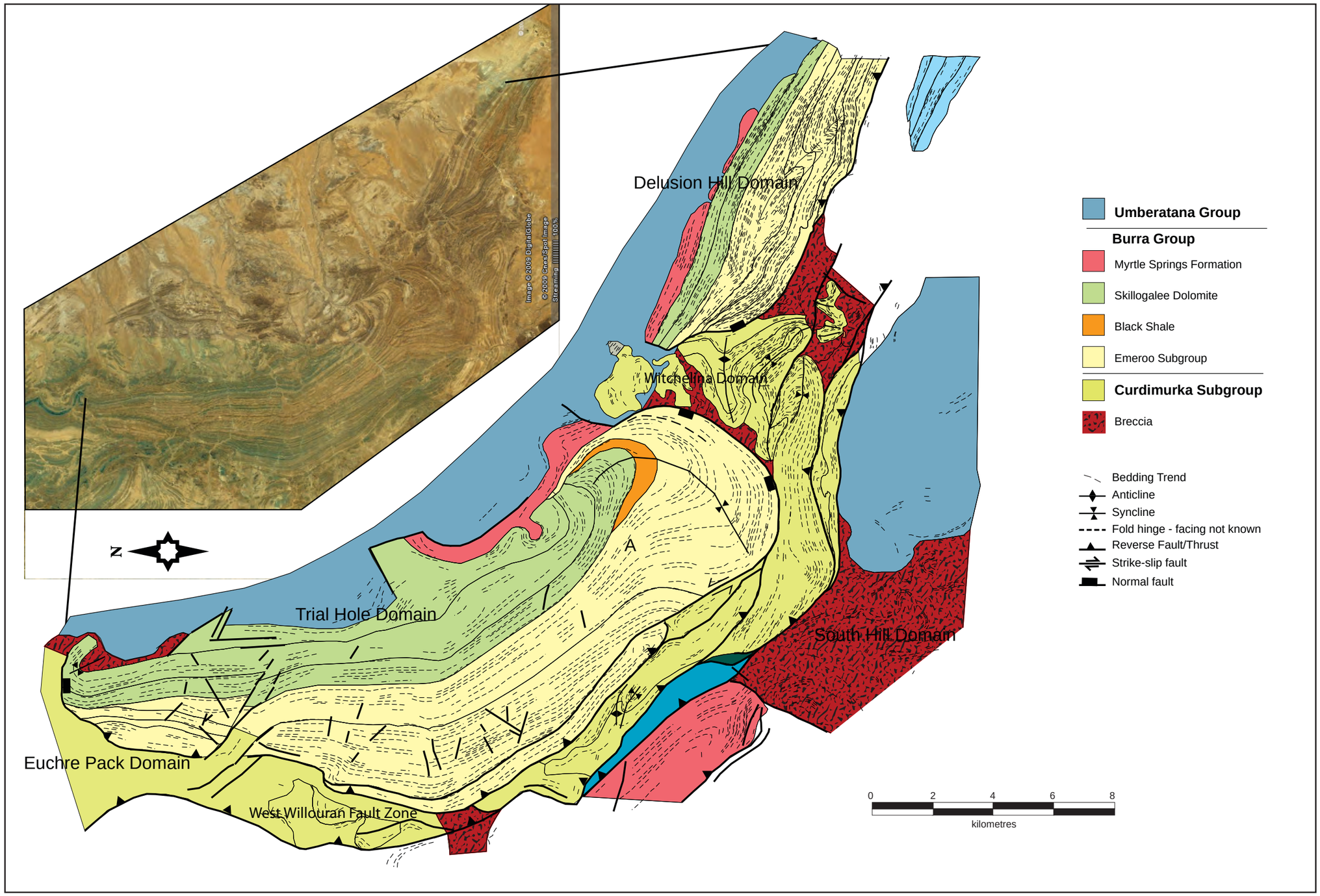

Figure 8.10. Aerial photography interpretation of the Trial Hole and Delusion Hill Domains.
In these domains, the Emeroo Subgroup is unusually thick compared with the Kingston, Berlina and West Mount Domains. The Myrtle Springs Formation is absent from the northern Trial Hole Domain. The Skillogalee Dolomite forms a pop-up structure in the middle of the Trial Hole Domain. An on-lap surface occurs near the top of the Emeroo Subgroup in both the Trial Hole and Delusion Hill Domains, and a thin black shale unit occurs between the Emeroo Subgroup and Skillogalee Dolomite in the Trial Hole Domain. These indicate short-lived uplift of the Curdimurka Subgroup in the Witchelina Domain. A roll-over anticline in the basal Emeroo Subgroup (A) suggests a listric normal fault that soled out in the Curdimurka Subgroup may have controlled the uplift.

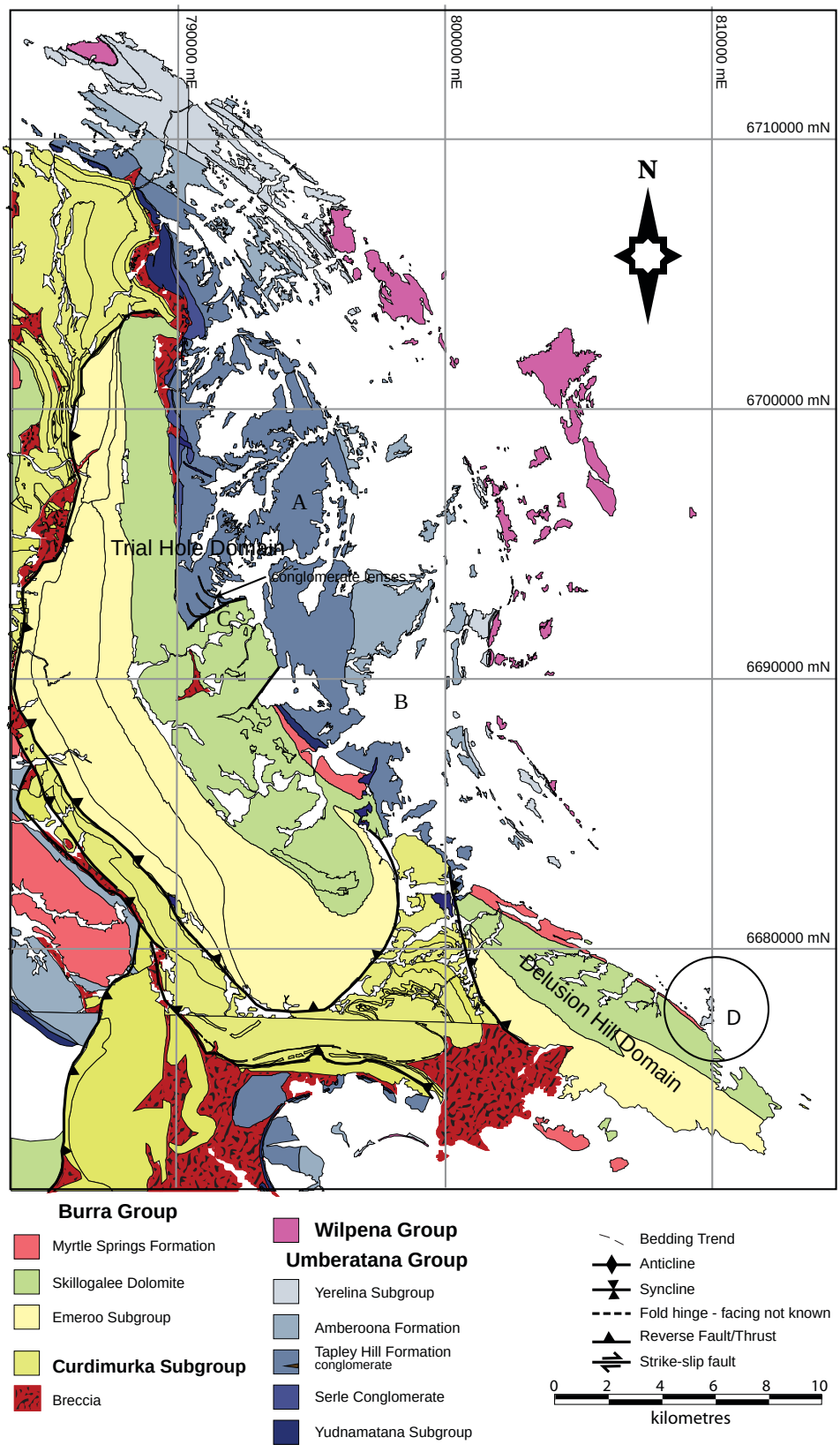

Figure 8.11 The Umberatana Group in the Trial Hole and Delusion Hill Domains. Note the Yudnamatana Subgroup is thickest above the Euchre Pack Domain. The Tapley Hill Formation reaches its thickest point at A and the Amberoona Formation reaches its thickest point at B, but both then thin toward the south until the Yerelina Subgroup sits on top of the Burra Group in the Delusion Hill Domain (circled). Note also the conglomerate lenses (brown) adjacent to the up-faulted block of Skilogalee Dolomite at C, indicating that the fault block was being uplifted during deposition of the Tapley Hill Formation. (from PIRSA 1:100,000 GIS geology)

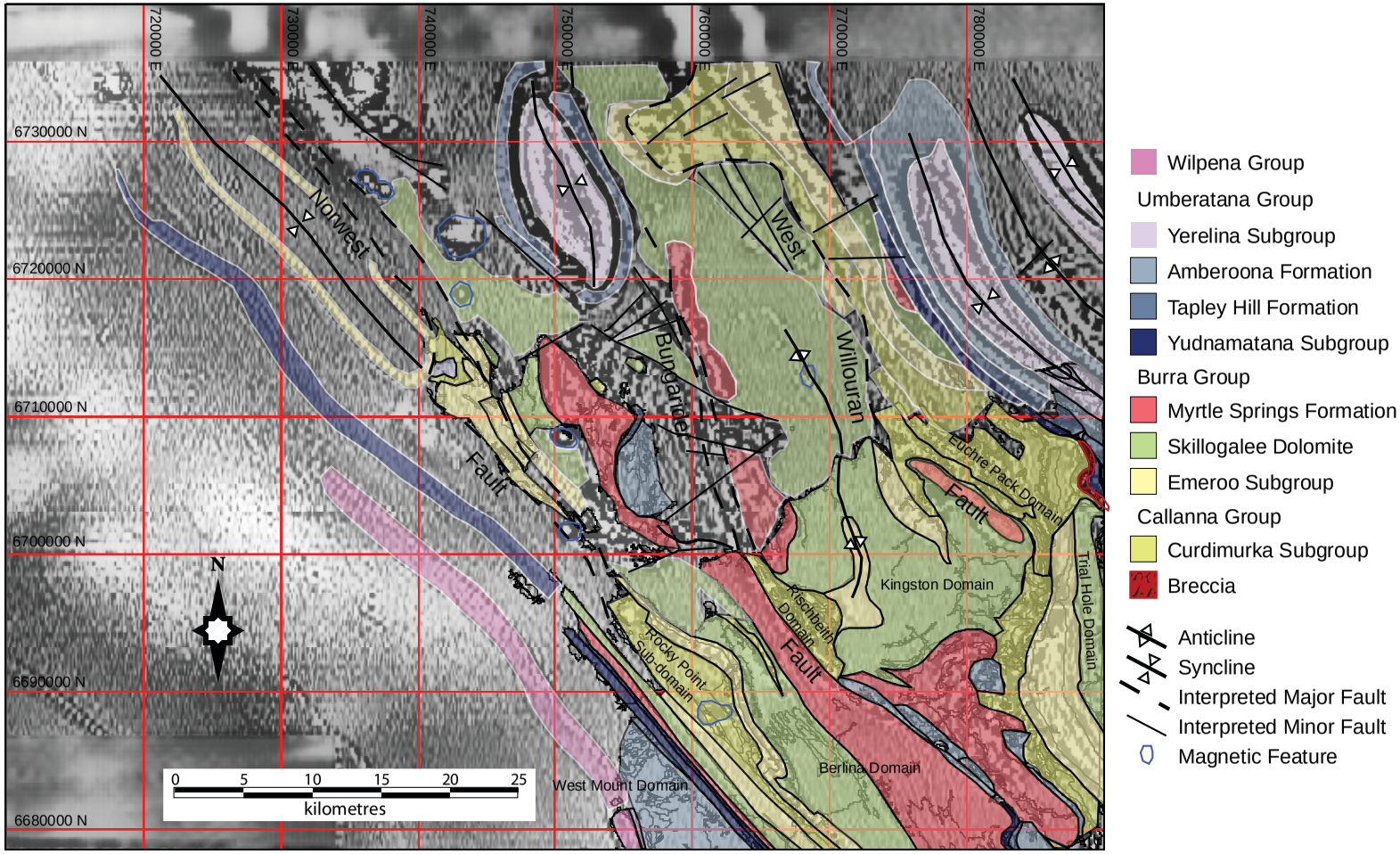

Figure 8.12. Geological interpretation of the first derivative magnetic intensity over the northern Willouran Range area.
Geology from the PIRSA 1:100,000 GIS geology with solid black outlines, interpreted geology with white outlines.

Table 8.1. Magnetic characteristics of units

Unit	Magnetic Characteristics
Wilpena Group	Moderate to low, bedded
Yerelina Subgroup	High intensity, thick bedded
Amberoona Formation	Low to high intensity
Tapley Hill Formation	Low intensity
Yudnamutana Subgroup	High intensity
Myrtle Springs Formation	Moderate to low intensity, bedded
Skillogalee Dolomite	Low intensity,
Emeroo Subgroup	High Intensity
Curdimurka Subgroup	Variable depending on unit
Breccia	Variable with highs on volcanic clasts

of the northwest-trending anticline in the centre of the Kingston Domain which brings the Emeroo Subgroup close to the surface in an area of moderate magnetic intensity (Figure 8. 12).

The Euchre Pack Domain continues to the northwest, rapidly thinning but thickening again at about 6728000 mN. It is interpreted to be overlain by the Burra Group which is cut-out by the Umberatana Group just north of the outcropping Euchre Pack Domain in a manner analagous to that seen either side of the Witchelina Domain. The Umberatana Group in the Trial Hole Domain continues to the north, folded into a series of curving, northwest to north-northwest trending anticlines and synclines (Figure 8.12).

8.4 Deep Structure of the Willouran Trough

8.4.1 Gravity Model of the Willouran Trough

An image of the gridded bouger gravity anomaly is shown in Figure 8.13, with the margins of the Willouran Trough. From this data set, a subset of the South Australian gravity data base specific to the area of the Willouran Trough was taken. The data varies widely in their density, from high data density in the area of the Leigh Creek Coal Field to very low-density regional data set, with a spacing of about nine kilometres. In areas of widely spaced data, there may also be concentrations of more closely spaced data following roads and tracks. To account for the wide variation in data density, the point data was gridded using Surfer, with a final grid spacing of one kilometre square. The griding algorithm used was a standard kriging algorithm. Grid data was then exported to the Potent potential- field modelling program.

Two gravity profiles were modelled across the Willouran Trough. The first is a section oriented transversely with respect to the long axis of the trough, beginning at 174000 mE, 6642000 mN, with an azimuth of 038.5^{o}, and extending for about 100 km (Figures 8.13, 8.14). The second is oriented parallel to the long axis of the trough, beginning at about, with an azimuth of 134.7^{o}, extending for about 60 km (Figures 8.13, 8.15). Geological constraints for the gravity model are from the 1:250,000 Curdimurka, Copley and Andamooka map

sheets, and the 1:100,000 digital geological data set for the Marree 1:250,000 map sheet. Additional data from fieldwork done as part of this study was used to better define the structure. In areas of no outcrop along the line of the section, geological contacts and structures were extrapolated from areas of outcrop, with the assistance of the gravity data image and the South Australia state magnetic data image.

Rock density data collected by Utah Development Corporation as part of a gravity survey they undertook in the early 1980's (Rowlands et al., 1981) were used when assigning bulk densities to stratigraphic blocks used in the model. Basement bulk densities for granodiorite, granite and other possible basement lithologies were taken from Kearey and Brooks (1991). Bulk densities for evaporitic sediments were estimated using data from Barrows and Fett (1985). Densities used for the blocks modelled are listed in Table 8.1. The densities used for the lower Wilpena Group were varied to model individual short-wavelength features. No attempt was made to model the Jurassic to recent sediments that obscure the Adelaidean sediments east and west of the Willouran Range; they are less than 200 m thick. A background density of 2.67 t/m^3 and a regional value of –20.348 mgal are used. Details of each model are included in Appendix 4.

8.4.2 Gravity Cross-Section.

Three possible solutions were modelled for the cross-section (Figure 8.14). There is good agreement in the upper part of the density model (above about 8,000 m) with the interpreted geology. The position of the Norwest Fault matches the deep, narrow gravity low, and the shape and position of the Burra Group bodies matches the mapped and interpreted geology. The small peaks or inflections in the regional field on the Torrens Hinge Zone and east of the Willouran Trough coincide with the position of known or interpreted fold closures.

The long wavelength features reflect the deeper geology, a deep trough filled with mostly low-density sediments bounded by steadily rising higher density basement. Deep level strata are inferred to comprise the Arkaroola Subgroup. Although highly fragmented in the Willouran Trough, its stratigraphic components and architecture can be inferred from clast-types in diapiric breccias, and exposures in the Mt Painter and Peak and Denison Inliers. These are the Paralana Quartzite overlain by the carbonate/evaporite package of the Wywyana Formation, which is overlain by the Wooltana Volcanics. From the distribution of clasts in breccias, the presence of basalt (the Noranda Volcanics) is inferred to be widespread at depth, the thickness of which is estimated to be about 1,000 m, based on the outcrop of Wooltana Volcanics around the Mt Painter Inlier (Preiss, 1987). From the Mt Painter Inlier, quartzite equivalent to the Paralana Quartzite is inferred, although it has not been definitely identified in breccias. Around the Mt Painter Inlier its thickness is variable and fault controlled, but it may be up to 1,000 m thick. Breccias are thought to be diapiric and sourced from the Wywyana Formation and so the distribution of the breccias is inferred to represent the initial distribution of a carbonate/evaporite succession.

In the first model (Figure 8.14a), a basement bulk density of 2.72 t/m^3 is used, this figure being from the upper end of average values for granodiorite (Kearey and Brooks, 1991).

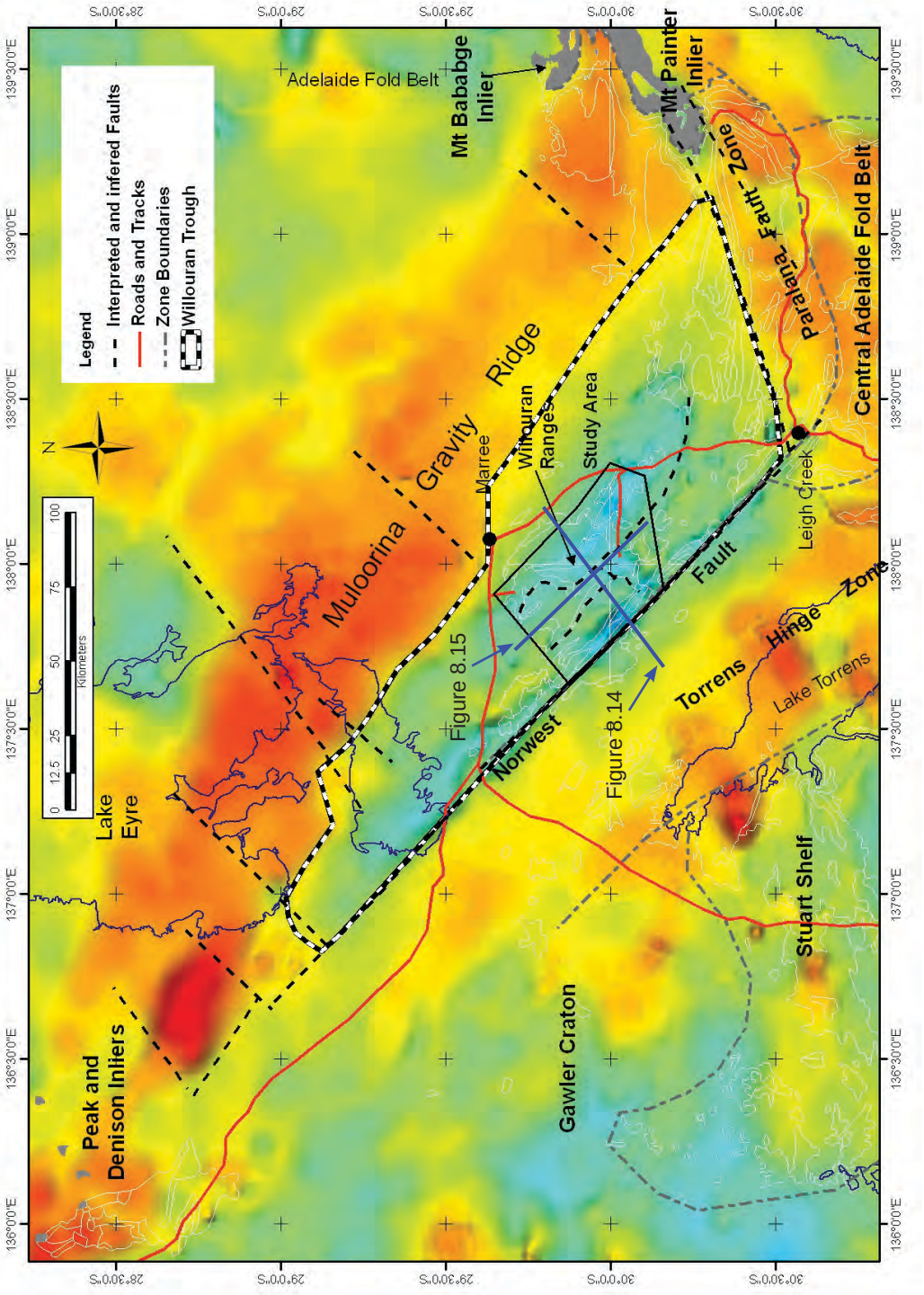

Figure 8.13. Gridded Bouger gravity anomaly image of the Willouran Trough and surrounding area with major structures interpreted. The position of the cross-section (Figure 8.14) and long section (Figure 8.15) are shown in blue.

Table 8.2 Densities applied to blocks in preparing the gravity models.

Unit	Density (t/m^3)
Basement (granodiorite)	2.72
Basement – Hiltaba Suite Granite	2.62
Paralana Quartzite	2.67
Evaporites (salt-rich)	2.30
Basalt	3.00
Breccia - South Hill Domain	2.68
Dome Sandstone - South Hill Domain	2.62
Dome Sandstone - Other	2.60
Curdimurka Subgroup (siltstone)	2.58
Emeroo Subgroup (sandstone)	2.65
Skillogalee Dolomite (siltstone-carbonate west of Norwest Fault)	2.68
Skillogalee Dolomite (dolomite-rich, elsewhere)	2.72
Myrtle Springs Formation (i/b carbonate – siltstone)	2.65
Umberatana (undifferentiated)	2.65
Tapley Hill Formation (siltstone)	2.62
Lower Wilpena (siltstone-, sandstone-, carbonate-dominated)	2.62, 2.65, 2.70
Upper Wilpena	2.70

The source's for the densities are given in the text.

The gravity model suggests that to balance the high-density basement and basalt, about 1,500 m of lower density material is required. As field evidence suggests that the source of diapirs in the Willouran Trough is the Arkaroola Subgroup (see below) the first model has an evaporite sheet at depth (represented by the Wywyana Formation). The narrow deep gravity low along the Norwest Fault requires the presence of a narrow body of low-density material approaching the surface. A salt diapir is modelled to account for the gravity low. Although there are no diapirs exposed on the section, diapiric breccias have been mapped along the Norwest Fault to the northwest and southeast.

The second model excludes a thick salt sheet at depth (Figure 8.14b). That is, the salt that caused the diapirism has been removed by salt evacuation and dissolution. Salt may still be present in diapirs however. To account for the long wavelength gravity lows, a block of low-density basement beneath the Willouran Trough is introduced. The density for this material was taken from the published density of the Hiltaba Granite Suite (2.62 t/m^3: Gow et al., 1993), which occur in the Gawler Craton, west of the Willouran Trough (Figures 8.16, 8.17). Although the low density basement can explain the long wavelength gravity low, the shorter wavelength, high amplitude gravity low along the Norwest Fault requires a narrow body of low density material. As in the case of the first model,this anomaly is explained by a remnant saly body at depth.

The third model is based on an interpretation of a steep basin-bounding fault on the northeastern margin of the Willouran Trough, adjacent the Muloorina Gravity Ridge. It is based on thickness variations of the Emeroo Subgroup across the Willouran Trough

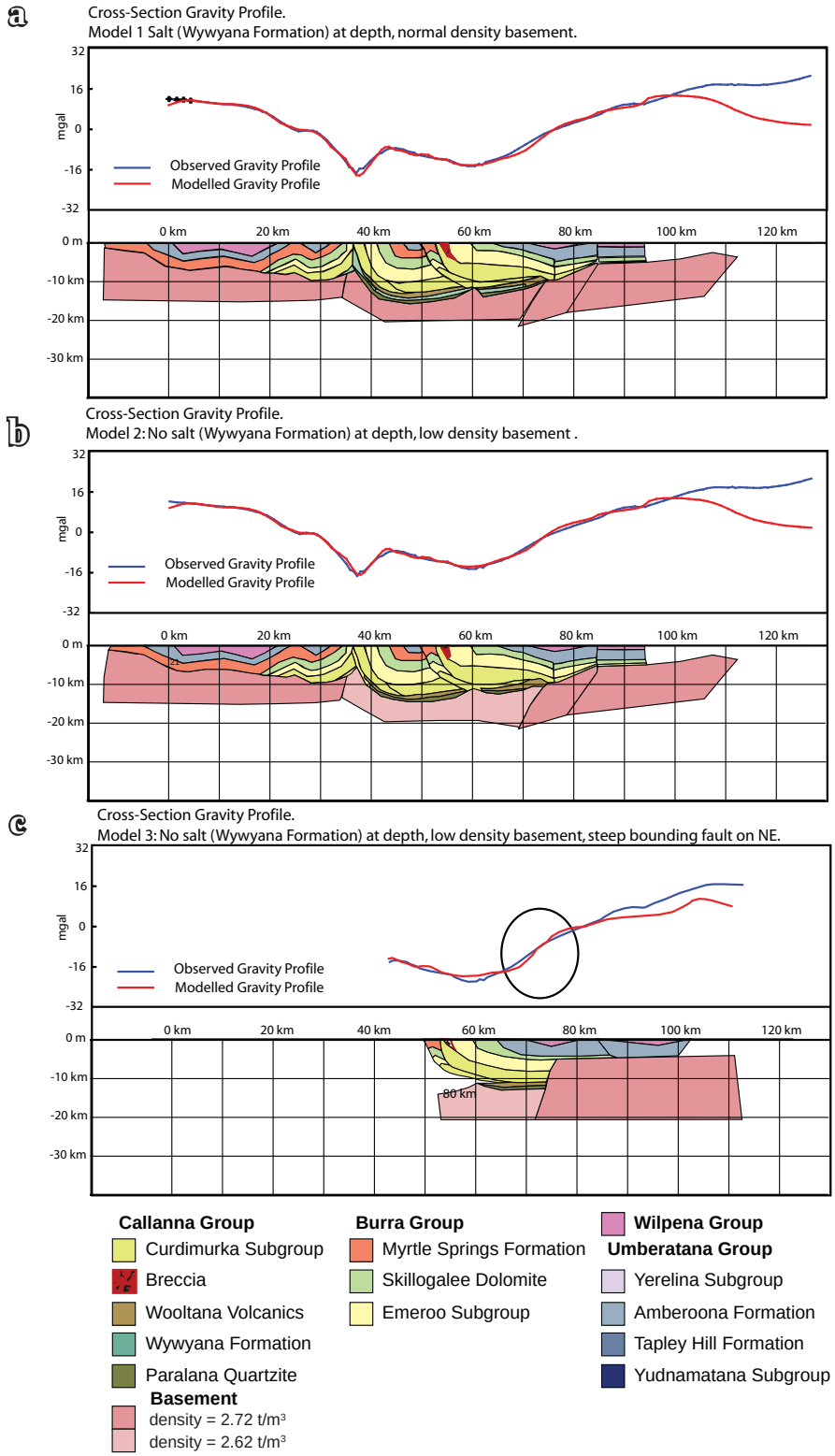

Figure 8.14. Gravity models for a cross-section of the Willouran Trough.
a) An evaporite layer is modelled below the Wooltana Volcanics, b) No salt is modelled and a block of lower density basement is modelled (density 2.62 t/m3). Both models explain the the low mass along the trace of the Norwest Fault to be due to a sub-surface salt body (density 2.30 t/m^3). c) The NE end of a third model based on Model 2. Here a steep normal fault controlling deposition of the Burra Group is modelled. This configuration cannot match the slope of the modelled curve with that of the observations (circled); the slope of the model curve is controlled by the slope of the top of the basement block. Densities for the stratigraphic blocks are given in Table 9.1 and the position of the cross-section is shown in Figure 8.13.

being interpreted to reflect deposition in a half-graben controlled by a fault on the northeast margin at that time. Only the northeastern section of the model is shown to focus on the area of interest. It was not possible to fit the slope of the model above the intepreted fault geometry to the observed data (Figure 8.14c). Assuming a steep fault angle at the basin margin, the modelled gravity slope is too steep to fit the observed data. Hence the geometry of the basement - Adelaide Fold Belt contact is interpreted to be at a moderate angle to the southwest.

8.4.3 Long Section Models

Three gravity profiles were modelled along the Willouran Trough (Figure 8.15). The gravity data are consistent with a block of low density material below the South Hill Domain, with a block of high density material to the southeast. In all three models the short wavelength features are consistent with a section prepared from the mapped geology and so this is not changed between models. Northwest of the South Hill Domain, the geology and the gravity profile match well, although a low density basement block with the Hiltaba Suite Granite density is required to match the long-wavelength feature. The South Hill Domain is interpreted to be two thrust sheets of Dome Sandstone with salt bodies on the thrust surfaces. A salt pillow with a narrow diapiric salt body is modelled below and area of brecciation and faulting southeast of the South Hill Domain. The Curdimurka Subgroup in the South Hill Domain comprises mainly Dome Sandstone and so a higher density (2.62 t/m^3) was assigned. Breccia within the South Hill Domain was originally assigned a lower density but the profile suggests that the breccia is of higher density than the surrounding sandstone and so to fit the curve, a density of 2.68 t/m^{3}was assigned, consistent with a greater proportion of dolomite, but basalt may also be present. The differences are in modelling the long wavelength features and the deep structure of the South Hill Domain.

In the first model, a horst block of basement is modelled beneath the southeastern margin of the South Hill Domain, with the Paralana Quartzite on-lapping the basement. A decollement occurs below the Noranda Volcanics, with the South Hill Domain being a series of two thrust sheets. No basalt occurs at depth below the South Hill Domain, the basalt sheet having been breached by the intrusion of salt from below.

In the second model, the basement rises slightly below the South Hill Domain but the rise in the gravity data is accounted for by a continuous basalt unit, thickening to 2,000 m over five kilometres. There is a continuous sheet of salt that thins below the thickened basalt and the Paralana Quartzite is continuous across the area. Thin salt bodies are present in the South Hill Domain along the major thrusts but they are not connected (in section) to the main salt body. Although this model fitted the gravity low, it could not fit the high precisely.

In the third model, a similar basement configuration is used as in the second model, with the exception of having a higher density block below the South Hill Domain. The basalt is a continuous unit beneath the South Hill Domain, thickening slightly to the southeast.

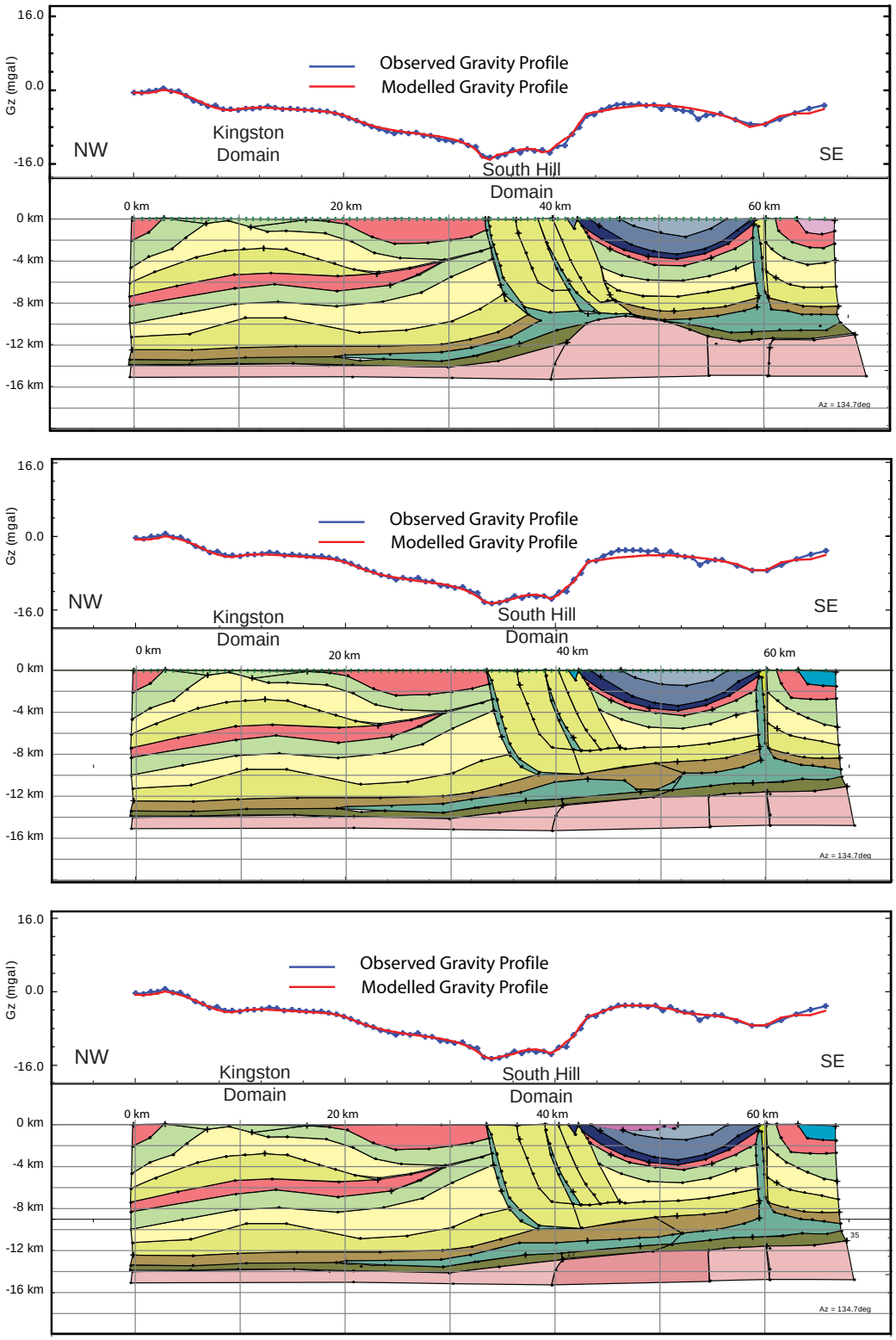

Figure 8.15. Long section gravity models.
a) A block of higher density basement lies below the South Hill Domain with no basalt. A decollement lies below the level of the Noranda Volcanics. b) The basement rises to the southeast but there is no isolated high density block below the South Hill Domain. A thickened area of Noranda Volcanics lifts the gravity model to match the gravity high southeast of the South Hill Domain. c) A higher density body of basement lies beneath the South Hill Domain and the Noranda Volcanics are thickened but there is not large fault block beneath the South Hill Domain.
See Figure 8.14 for legend.

8.4.4 Confidence of the Models.

When fitting the model curves to the observed gravity curves, several points should be noted. Because the geological units modelled are a series of sub-parallel sheets with widely varying densities from salt to basalt, varying the thickness of one requires varying the thickness of one or more other bodies. In the upper part of the model, outcrop provides good control on the thickness and structure but in areas of poor outcrop, the thickness variations in the Skillogalee Dolomite are balanced by varying the the thickness of the Curdimurka Subgroup in particular, but also the Emeroo Subgroup. At depth, a thicker basalt unit raises the calculated profile above the observed but can be balanced by a thicker salt layer, which requires lowering the basement to accommodate the extra stratigraphy, or thinning the overlying stratigraphy. Or, a thicker basalt layer could be balanced by decreasing the density of the basement, without the addition of a salt layer. The lower part of the model remains speculative but the assumptions made regarding the thickness of the basalt, the presence or absence of salt, and the thickness of the Paralana Quartzite are reasonable and so the model is accepted.

Evidence, albeit circumstantial, in favour of there being low-density basement beneath the Willouran Trough comes from three sources. Gow et al., (1993) interpreted a regional gravity low on the Stuart Shelf to be due to a body of Hiltaba Suite Granite, intruded into metagranite beneath an eroded caldera complex filled with Gawler Range Volcanics (Figures 8.16, 8.17). The width of the anomaly is about 50 km, a similar size to the anomaly associated with the Willouran Trough, and it too has a central high between two lows. Selley (2000) also suggested that a pronounced gravity low beneath the Spencer Gulf is related to Hiltaba Suite Granites. A weak gravity low also occurs over the Mt Painter Block (Figure 8.16), in which radiogenic Palaeoproterozoic to Mesoproterozoic granites and metamorphic rocks crop out (Coats and Blisset, 1971; Elburg et al., 2001).

8.5 Cross-section and Long Section of the Willouran Range.

8.5.1 Cross-section of the Willouran Range.

Figure 8.18 is a cross-section of the Willouran Range developed from surface mapping, the PIRSA 1:100,000 GIS database, 1:250,000 geological maps and the gravity modelling. The cross-section follows the line of the gravity model (Figure 8.14).

The Arkaroola Subgroup is mainly confined to the Willouran Trough, and salt is present at depth, extending on to the adjacent Torrens Hinge Zone.Salt is present at depth and along the Norwest Fault but it also extends onto the Torrens Hinge Zone. No basalt is shown in the Torrens Hinge Zone, which may be attributed to erosion prior to deposition of the Burra Group. It shows the the Curdimurka Subgroup is mainly confined to the Willouran Trough but does extend on to Torrens Hinge Zone. There is also an assumption that the Curdimurka Subgroup thickens to the northeast, which may be due to;

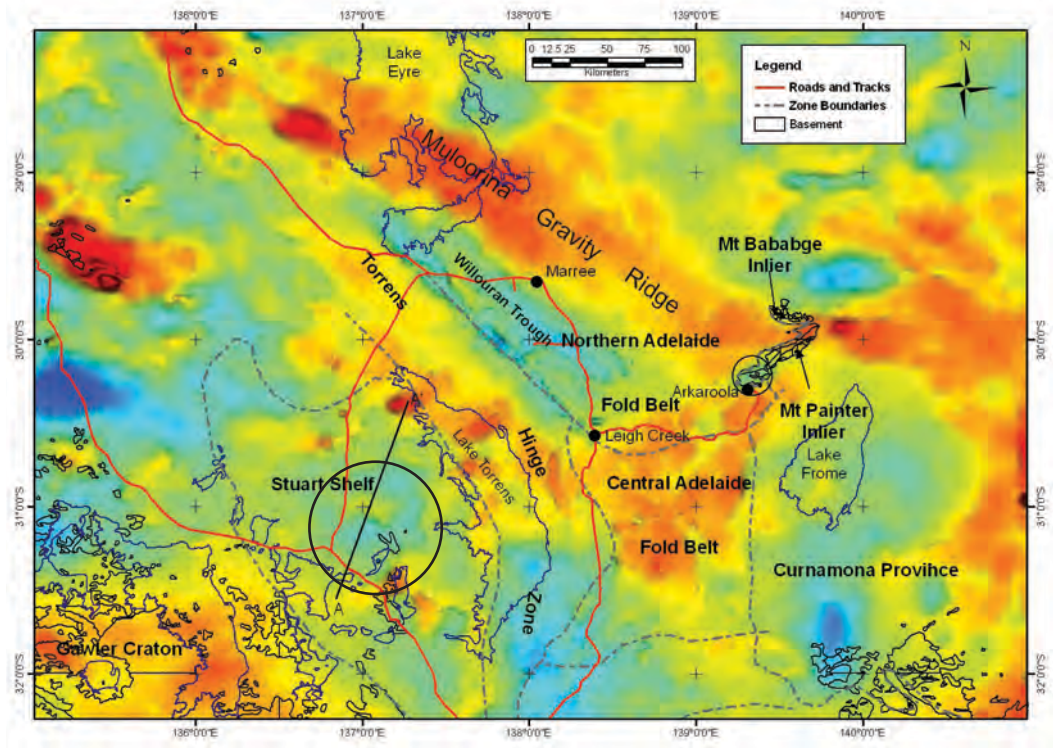

Figure 8.16. Regional Bouger gravity anomaly image of north-central South Australia.

The Willouran Trough is a large NW trending gravity low. A gravity low underlies the Mt Painter Inlier, and a broad gravity low (circled) on the Stuart Shelf is modelled to be a Hiltaba Suite granitoid body by Gow et al (1993) as shown in Figure 8.17. The line marked A - A' is the gravity line modelled by Gow et al. (1993).

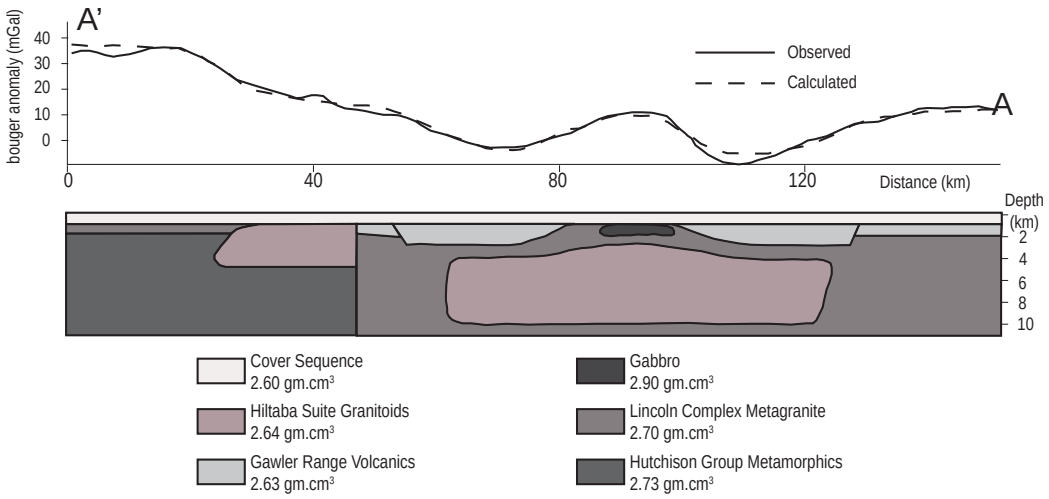

Figure 8.17. Bouger gravity anomaly profile with a 2.5- dimensional model of a cross-section through the central Stuart Shelf regional gravity low from Gow et al., (1993).

They have modelled the geology as an eroded caldera complex with a central dome. The anomaly is of a similar shape and size to the Bouger gravity anomaly over the Willouran Range (Figure 8.13), and so the long-wavelength features may reflect a body of Hiltaba Suite granitoid at depth.

- structural thickening which accommodates the extension seen in the Euchre Pack and West Willouran Trough.
- sedimentological thickening as has been discussed in Chapter 3.
- a combination of both.

The Burra Group is thickest in the Willouran Trough but it also occurs on the Torrens Hinge Zone, and the Skillogalee Dolomite overlaps the Emeroo Subgroup and is in turn overlapped by the Myrtle Springs Formation. It thins gradually to the northeast. The Umberatana Group is thinnest within the Willouran Trough but maintains an approximately constant thickness on the Torrens Hinge Zone. In the northeast, it may also have a roughly constant thickness but there is insufficient information to be certain. The preserved levels of the Wilpena Group are thickest on the Torrens Hinge Zone.

The structure is dominated by a series of northeast-dipping thrusts. There are two types; those that sole-out into a basal thrust (Lake Arthur Fault), and those that are confined to the Willouran Trough. The Arthur Fault crops out west of the study area and is the boundary between the Torrens Hinge Zone and the Stuart Shelf, marking the western boundary of the Adelaide Fold Belt. The Norwest Fault is the next major thrust and marks the boundary between the Torrens Hinge Zone and the Northern Adelaide Fold Belt, as well as being the western boundary of the Willouran Trough. Between these two faults are two blind thrusts with associated fault propagation folds, which are shown on the Andamooka 1:250,000 geological map (Ambrose, 1983). Two basement thrusts are intepreted intersecting the surface east of about 74,000 m. The position of these thrusts is based on the 1:100,000 PIRSA GIS database and interpretation of regional aeromagnetic and gravity data.

The second thrust type includes the Bungarider and West Willouran Faults, and the fault along the northeastern margin of the Stony Range Domain. These branch from the un-named basement fault and are confined to the Callanna Group as low angle faults which ramp upward, cutting the Burra Group at a high angle.

Both thrust types produce footwall synclines and hanging wall anticlines which trend parallel to the thrusts. From their plan view, they trend roughly northeast and in cross-section, they are upright to slightly inclined to the northeast. Field evidence indicates that they have shallow plunges either to the northwest or southeast. Hence this group of folds and associated reverse faults are interpreted to be D_2, from comparisons with D_2 folds in the Euchre Pack Domain. However, the Norwest Fault was shown to be active as a normal fault during deposition of the Burra and Umberatana Groups, and so this fault was reactivated as a reverse fault during basin inversion (Paul et al., 1999).

8.5.2 Long Section of the Willouran Range.

The long section (Figure 8.19) emphasises the structure of the South Hill Domain. It shows that the Curdimurka Subgroup has been thrust to the northwest, over the Burra Group as shown above. The breccia is interpreted to result from a series of smaller thrusts that have

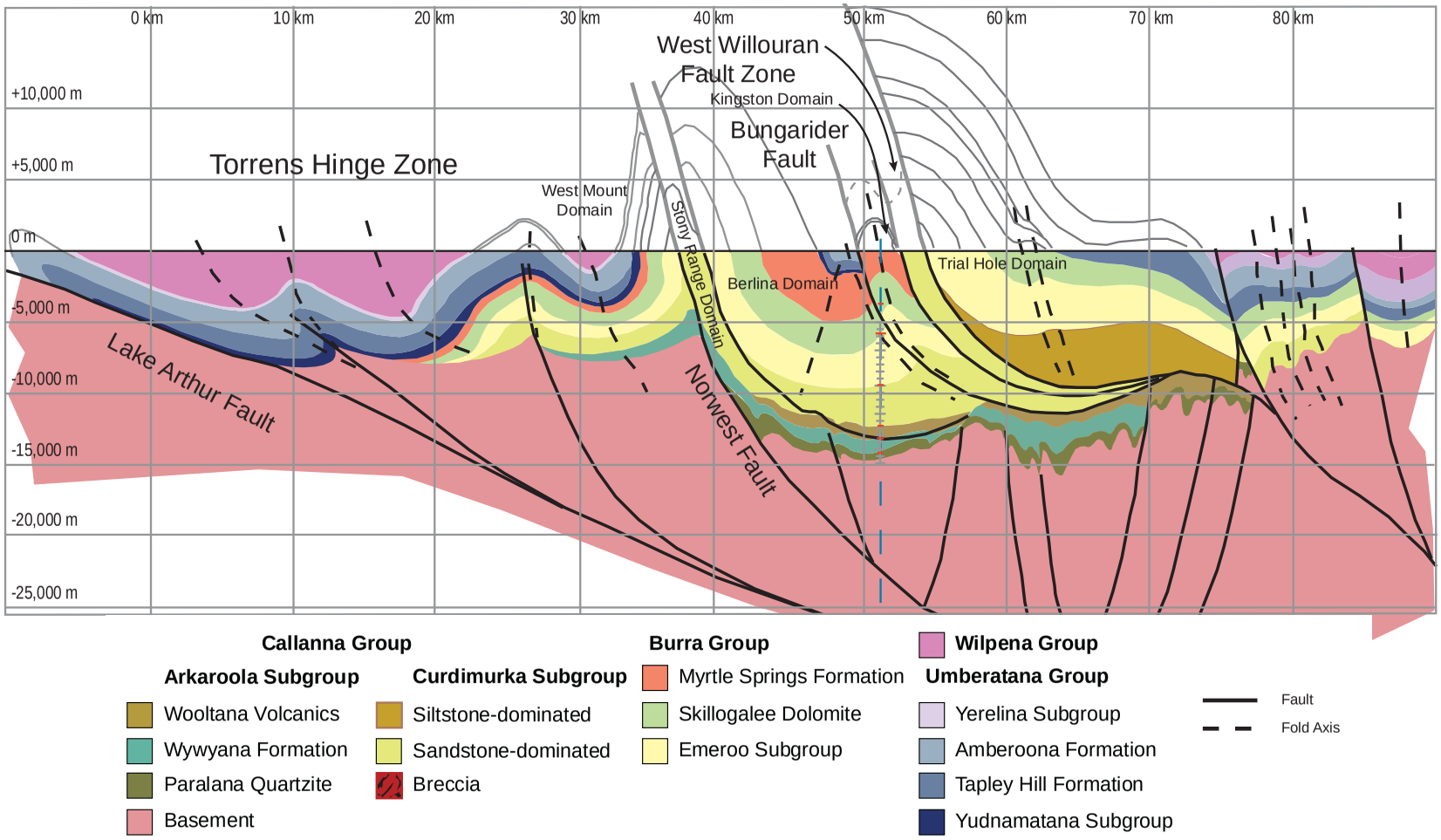

Figure 8.18. Cross-section of the Willouran Trough.
See Figure 9.8 for the line of the section. Based on the PIRSA 1:100,000 GIS Data Set, 1:250,000 map sheets, field work conducted as part of this study and modeling of gravity data.

dismembered the Curdimurka Subgroup above the level of the Dome Sandstone. A narrow salt body is interpreted to be present in the footwall of the main thrust, below the Dome Sandstone. This was likely a factor in the development of the structure of the South Hill Domain but the role of salt tectonics will be expanded upon in the next chapter. A basement high is also interpreted to be situated to the southeast of the South Hill Domain.

Northwest of the South Hill Domain, the structure of the Rocky Point Sub-domain is interpreted to continue at depth below the Rischbeith Domain. An anticline in the Burra Group in the Kingston Domain has the Curdimurka Subgroup in its core, and there are a series of smaller anticlines and synclines developed in the Burra Group. These have a long northwestern hinge and a short southeastern limb and verge to the southeast. They also occur below the Bungarider Fault.

8.6 Discussion.

8.6.1 The Curdimurka Subgroup.

Chapter 7 has shown that three deformations affected the Curdimurka Subgroup in the Euchre Pack Domain. D_1 produced both extensional and compressional structures, but the extensional listric normal faults formed above compressional folds. The dominant transport direction was to the south to southeast with a second, smaller reversal of movement along some faults. In the Stony Range Domain, macroscopic structures show features similar to those identified as D_1. Folds are inclined with calculated plunges being moderately steep to the northwest. Axial planes dip steeply to the northwest but in folds in the southeast of the domain, they curve, convex upward to become inclined to the general strike, and folds verge to the southeast. Dextral strike-slip faults dominate but as in the Euchre Pack Domain, there is a reversal of movement, with some faults having sinistral movement. All of these features were identified as being typical of D_1 in the Euchre Pack Domain. However all of the structures identified in the Stony Range Domain are compressional with no extensional structures noted.

The West Willouran Domain has many structures that, from aerial photograph and map interpretations, are typical of D_1. Folds are interpreted to have moderately steep plunges and there are detachment folds with curving axial planes relative to the general bedding, verging to the southeast. The Curdimurka Subgroup is dismembered and thinned considerably, suggesting that the main movement was extensional. If the identification of the stratigraphic succession being from the Dome Sandstone in the northwest to the Cooranna Formation in the southeast is correct, this would indicate dextral movement along the West Willouran Fault Zone, smearing out the Curdimurka Subgroup. This is speculative however and would need further work to confirm. Structures observed in the West Willouran Fault zone are similar D_1 structures in the Euchre Pack Domain.

The South Hill Domain contains a breccia-cored detachment fold which is a fold style typical of D_1, but except for the steep plunge, its orientation is atypical. The Curdimurka

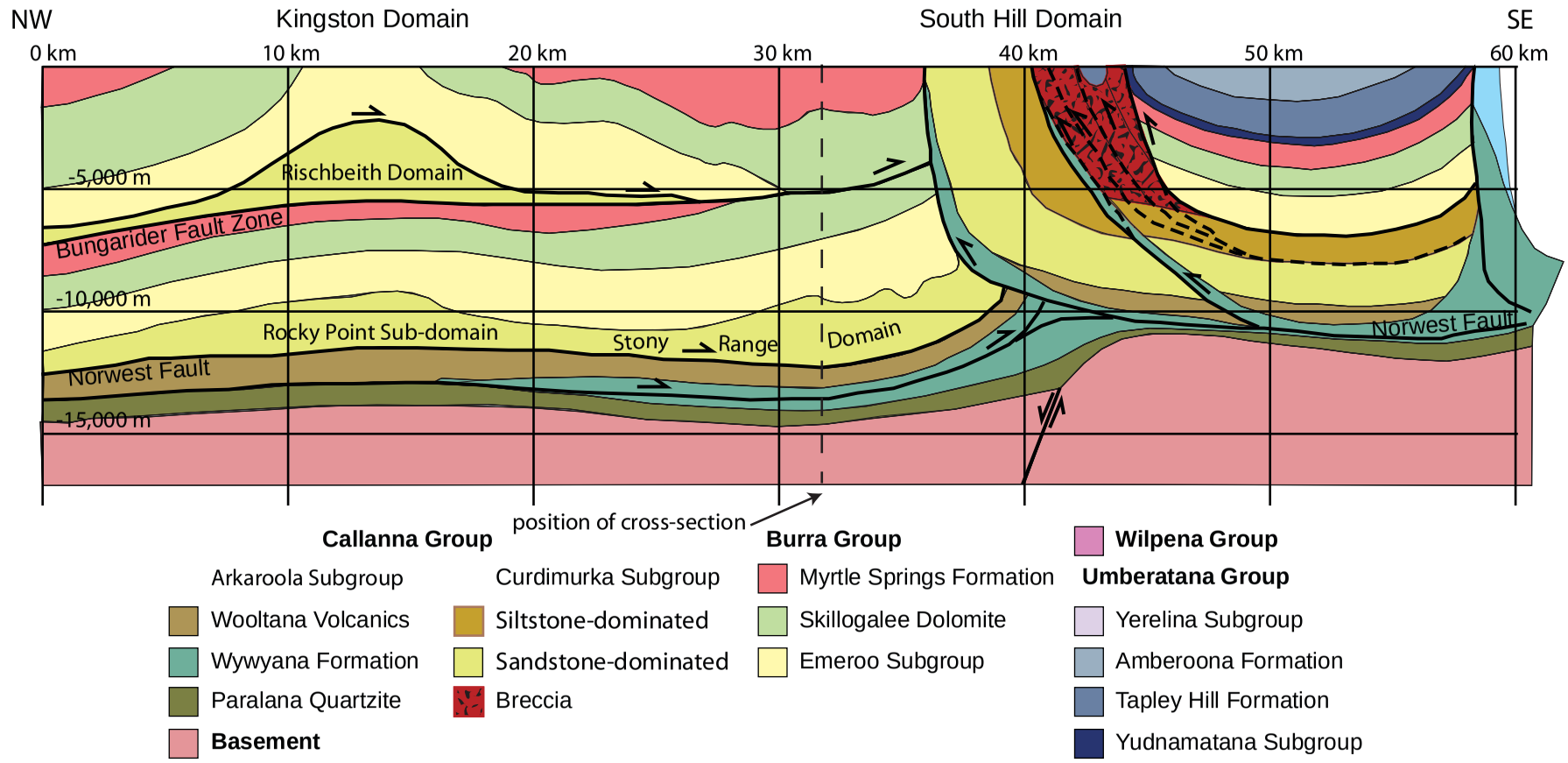

Figure 8.19. Long-section of the Willouran Trough. See Figure 8.13 for the line of the section.
Up to about 45 km, the geological control is good but beyond that point, outcrop is poor. The section shows that the South Hill Domain is a thrust, with the Curdimurka Subgroup being thrust to the northwest over the Burra Group. The Bungarider Fault has rotated about the South Hill Domain. Gravity modelling suggests that there is a low-desity body below the South Hill Domain, interpreted to be salt (density used 2.30 t/m3) and below the area from about 50 km. At about 58 km, breccia is mapped on the Copley 1:250,000 geological map. Gravity modelling suggests that a higher density block of basement lies below the South Hill Domain.

Subgroup has been thrust to the northeast, which corresponds to the indicated transport direction of the sinistral strike-slip fault movement seen in the Euchre Pack and Stony Range Domains. It does not have the correct orientation to be a D_2 structure and so it is interpreted to be D_1.

Insufficient mapping was completed in the Witchelina Domain to understand the structure fully. The interpreted folds in the Dome Sandstone trend between roughly north - south to NNW - SSE and have shallow plunges and so may be D_2 refolded by D_3.

8.6.2 Deposition of the Burra Group

Murrell (1977), Preiss (1987), Belperio (1990) and Dyson (2004) considered that the Burra Group was deposited in a series of sub-basins, bounded by the Norwest, Bungarider and West Willouran Faults with syn- and post-depositional diapirs formed along the sub-basin margins. Dyson (2002, 2004) suggested also that the Burra Group in the Trial Hole Domain was deposited in a separate sub-basin. Murrell (1977) also posited a fourth normal fault, the East Willouran Fault, between the Burra Group and the Umberatana Group in the Trial Hole Domain. Dyson (2004) interpreted the fault to be an unconformity and the breccia interpreted by Murrell (1977) to be related to a fault is a salt glacier deposited on the Skillogalee Dolomite.

Murrell (1977) suggested that the Norwest Fault was a hinge zone during deposition of the Emeroo Subgroup. From the gravity model and cross-section developed from it, the Emeroo Subgroup thickens across the Norwest Fault, but it does not reach the same thickness as in the Trial Hole Domain. The rift sedimentation and structure model of Gawthorpe and Leeder (2000) shows that in a half-graben, the thickest clastic unit would be adjacent the active fault and so the thick Emeroo Subgroup in the Trial Hole Domain suggests that the faulted margin is on the eastern side of the Willouran Trough during its early development. The gravity model does not indicate a rapid change in depth to basement in this area, and the Emeroo Subgroup is modelled to thin gradually to the northeast. A possible solution is a marginal fault on the northeastern side of the basin but it does not connect to the basement, soling out into the Callanna Group. A second, related solution is that the normal fault controlling deposition of the Emeroo Subgroup is the faulted contact between the Trial Hole and Witchelina Domains, soling out into the West Willouran Fault. The on-lap surface near the top of the Emeroo Subgroup in the Trial Hole Domain and a roll-over anticline in the basal Emeroo Subgroup suggests that the fault may have been active as a normal fault at this time. However, the timing of the movement is during deposition of the upperpart of the Emeroo Subgroup and there is no indication of fault movement prior to this time. More work is required in the Emeroo Subgroup to determine which alternative is more likely.

Murrell (1977) concluded that the polarity of the basin changed during deposition of the Skillogalee Dolomite, with the Norwest Fault becoming the major active fault at that time. Belperio (1990) demonstrated this by comparing the thickness of the Skillogalee Dolomite across the fault. This study uses the same information and so agrees with Belperio (1990) on the role of the Norwest Fault. It is also likely that it was the dominant fault during

deposition of the Myrtle Springs Formation also (Paul et al., 1999). The measured sections of Belperio (1990) showed that at its thickest in the Berlina Domain, the Myrtle Springs Formation is over 3,000 m thick whereas in the West Mount Domain it reaches a maximum thickness of about 600 m.

The sedimentological and stratigraphic evidence that Belperio (1990) presented for the Bungarider and West Willouran Faults being active, and dividing the basin into sub-basins during deposition of the Skillogalee Dolomite is not conclusive. These features could instead be attributed to clastic input from the northeast and sediment bypass in the west allowing the deposition of shallow water carbonates in a broad half-graben. Thickening of the Curdimurka Subgroup in the Euchre Pack and Rischbeith Domains and the Rocky Point Sub-domain suggests that at D_1, the basin was not sub-divided. All of these domains occur along a north-northeast trending line and may have formed as a single linear structure above the decollment at the base of the Dome Sandstone. As a D_1 structure, it formed after deposition of the Burra Group, and has been dissected by faulting along the major D_2 reverse faults. If the Burra Group had been deposited within a series of northwest – southeast trending sub-basins, the bounding faults would have disrupted the Curdimurka Subgroup breaking it into separate fault bound blocks that could not have formed a single structure.

8.6.3 Deposition of the Umberatana Group.

Selley and Bull (2002) suggested that the Willouran Range area was the site of extreme extension at the onset of deposition of the Yudnamutana Subgroup, with fault blocks of the Burra Group undergoing large degrees of rotation. Such a scenario is consistent with a supradetachment basin, in which the amount of extension is significantly greater than the accommodation created and so the basin formed would only be one to two thousand metres deep (Friedmann and Burbank 1995). Chapter 7 showed that faults that cut the Umberatana Group at a high angle rapidly become low-angle faults within the Curdimurka Subgroup, hence a supradetachment style basin is possible. Selley and Bull (2002) showed that the Bungarider and West Willouran Fault were active at this time, as listric faults (Figure 8.21).

Whether there was significant movement on the Norwest Fault during the deposition of the Yudnamutana Subgroup is uncertain. The preserved thickness of Umberatana Group is greater in the West Mount Domain, on the footwall of the fault than within the adjacent Berlina Domain in the hanging wall. It is possible that the preserved section adjacent to the Bungarider Fault is a remnant of a much thicker section that was removed during basin inversion in the Delamerian Orogeny. Or, there may never have been a great thickness deposited; the Willouran Range not being the site of significant basin development during the deposition of the Umberatana Group. During this period, the main depocentre within the Adelaide Fold Belt shifted to the east, where there is over 5,000 m of the Yudnamutana Subgroup west of the Mt Painter Inlier (Preiss, 1987; Paul et al., 1999). Paul et al. (1999) showed that in the vicinity of Leigh Creek, the Norwest Fault was not active during the

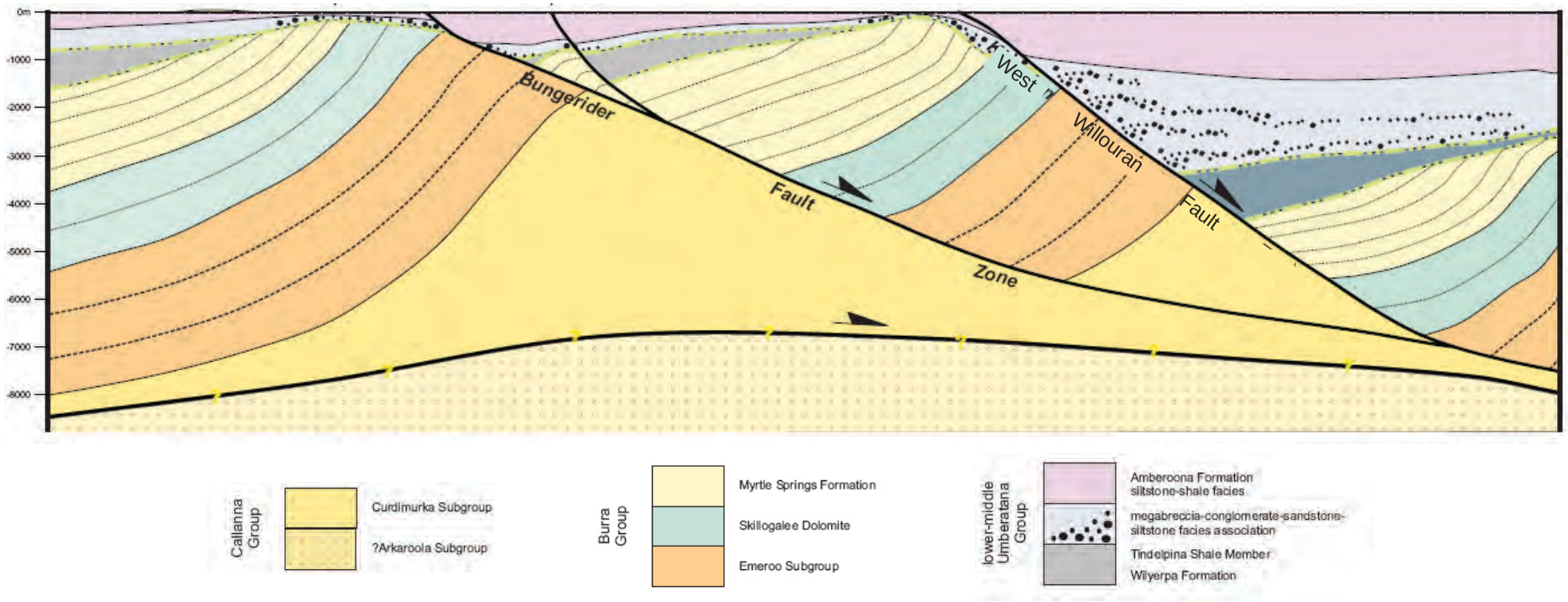

Figure 8.20. Figure 8 from Selley and Bull (2002) showing their interpretation of the deposition of the Umberatana Group in the Willouran Range. It is a simplified cross-section of the Berlina to Trial Hole Domains, across the Bungerider and West Willouran Fault Zones (Kingston Fault Zone in Selley and Bull, 202), restored to middle Umberatana Times. They interpret the Umberatana Group to have been deposited in a supradetachment basin formed above shallow-dipping normal faults that sole out in the Callanna Group.

deposition of the Umberatana Group, which thicken only slightly in the centre of the basin. Instead, the opening of the Yudnamutana Trough was controlled by movement along the Paralana Fault Zone, inferring north - south to northwest - southeast directed extension (Paul et al., 1999).

8.6.4 D_1

In this chapter, evidence has been presented that supports the three deformations to have affected the Willouran Range. In the Burra Group, D_1 has produced open to tight inclined folds with variable plunges in the Emeroo Subgroup in the Berlina and Kingston Domains. Within the Myrtle Springs Formation, D_1 folds are open, with a long wavelength and low amplitude, verging to the southeast. In addition, the Burra Group is folded into open folds above the Rocky Point and Rischbeith sub-domains. Murrell (1977) interpreted folds in the Burra Group east of the Rischbeith Domain as growth folds formed by differential movement of the Curdimurka Subgroup during deposition of the Emeroo Subgroup. It assumes that the Curdimurka Subgroup formed two fault blocks between which the basin was subsiding. However, no on-lap surface is interpreted between the Skillogalee Dolomite and the Emeroo Subgroup and no differential movement is interpreted. The trend of the folds considered to be pre-D_1 by Murrell (1977) is consistent with D_2 folds also.

One of the arguments that Murrell (1977) and Parker (1983) put forward as evidence for a pre-Burra Group deformation is the differing deformation styles in the Burra Group and Curdimurka Subgroup. Although the deformation styles are different, the geometry of southeast-verging folds with steep plunges are similar. The differences can be attributed to the different rheology and position relative to the major decollement. The Curdimurka Subgroup lies on a major decollement, with evaporitic and silty units throughout, whereas the Emeroo Subgroup is mainly arenite and rests upon the Curdimurka Subgroup. Most of the strain is accommodated by the deformation of the Curdimurka Subgroup but the Burra Group deforms above a detachment at the contact. Sherkati et al. (2005) showed that gravity collapse structures may develop above secondary detachments on the flank of rising salt-cored anticlines producing folds with different morphologies.A similar process is suggested here for the Burra Group; as the antiformal thrust stack in the Rocky Point Sub-domain rises, the Emeroo Subgroup slides down the front of the structure above a secondary detachment (Figure 8.2b). Deformation intensity decreases up-stratigraphy in the Burra Group with the Myrtle Springs Formation having been folded into long wavelength, low amplitude folds.

It was shown that the South Hill Domain has been thrust to the north to northwest. Selley and Bull (2002) suggested that this occurred during deposition of the Umberatana Group, with deposition of the Amberoona Formation in the Berlina Domain being syn-deformation. This is later than the movement on the Euchre Pack Domain, which Chapter 7 has shown to be during deposition of the Yudnamutana Subgroup and Tapley Hill Formation. However, the sinistral movement noted on strike slip faults in the Stony Range and Euchre Pack Domains post-dates the dextral and indicates northwest movement on these faults. Hence

the northeast thrusting of the South Hill Domain and the sinistral movement likely occurred at the same time and are the same event. Together, they are different phases of D_1.

Paul et al. (1999) suggested that the main extension was north - south to north-northwest - south-southeast whereas Selley and Bull (2002) suggested it was controlled by northwest-trending faults. They suggested that there was a second order basin growth about a northeast trending basin axis, which they attribute to gravitational collapse of the Burra Group into the underlying Callanna Group (Selley and Bull, 2002). This study has shown that the major transport direction during D_1 was to the southeast, which is consistent with Paul et al. (1999). However, the deformation is complex and there are indications of it being three dimensional as shown in Chapter 7.

8.6.5 D_2 and D_3

D_2 re-activated the northwest trending fault zones as reverse faults, resulting in the inversion of the Willouran Trough. It produced northwest-trending folds, F_2, that are upright to inclined at a steep angle to the northeast and may have an axial planar cleavage, as noted in Chapter 7. The folds typically have shallow plunges but due to D_2 overprinting F_1 folds as in the Berlina Domain, and possibly the Kingston Domain, they are double plunging. Figure 8.12 shows a series of these folds intepreted from aeromagnetic data in the Umberatana Group north of the Euchre Pack Domain. Figure 8.19 shows that buried faults on the Torrens Hinge Zone and the Lake Arthur Fault were also re-activated in D_2, producing the open to tight folds west of the Willouran Trough. The timing of D_2 is therefore after deposition of the Wilpena Group. All workers attributed structures of this orientation to be Delamerian in origin (e.g., Murrell, 1977; Preiss, 1987; Paul et al., 1999).

Murrell (1977) concluded that the Delamerian imposed a northeast - southwest directed stress field, which tightened existing structures. The major northwest trending folds attributed to D_2 here, Murrell (1977) interpreted to be syn-depositional in origin, formed by differential movement of basement blocks during deposition of the Burra Group in particular. However, it has been shown that there was only one deformation event prior to the Delamerian Orogen and the folds attributed by Murrell (1977) to be syn-depositional do not have the correct geometry to be D_1, but have D_2 geometries, hence are D_2.

In the vicinity of Leigh Creek, the dominant Delamerian fold axis trends east - west and adjacent the Paralana Fault Zone folds trend northeast (Preiss, 1987; Paul et al., 1999). Paul et al. (1999) attributed this change in orientation to north – south compression reflecting an overall left-lateral transpressional regime in the Delamerian Orogeny. They suggested that in this orientation, both the Norwest Fault and the Paralana Fault were reactivated as strike-slip faults (Paul et al., 1999). But movement on the Norwest Fault and other northwest trending faults was reverse and not strike-slip. Instead movement is consistent with northeast - southwest shortening, which would also result in strike-slip movement on the Paralana Fault Zone as shown by Paul et al. (1999).

D_3 folded D_2 fold axes into open folds with northeast trending axial surfaces. The best examples are those described in Chapter 7 in the Euchre Pack Domain, and in the Kingston Domain. They are consistent with northwest - southeast shortening, and as shown in Chapter 7, they produced a weak cleavage. No reverse faults that are consistent with this stress field orientation were noted but this orientation may re-activate existing northeast trending faults as reverse faults. The Paralana Fault Zone is the most signicant fault with this orientation, and its reactivation could produce the northeast trending folds adjacent the fault zone. Preiss (1987) interprets the work of Richert (1976) to indicate that meridional folds were the first generation, with a second generation trending east to east-northeast.

In the central Flinders Ranges, folding has produced a dome and basin structure, with the dominant north-northwest trending axial planes attributed to (there) D_1 and a minor east-northeast fold trend, attributed D_2 (Mendis, 2002). Around the Weekeroo (Talbot, 1967) and the Outalpa (Berry et al., 1978) basement outliers on the southern margin of the Curnamona Province, two interfering fold directions were mapped. The first trends north-northwest to northwest and is overprinted by the second east-northeast regional folds. Further south, in the Nackara Arc, Preiss (1987) interprets a first generation of folds trending meridional folds with a second northeasterly trending overprint.

Marshak and Flottmann (1996) interpreted the arcuate shape of the southern Adelaide Fold to result from northwest directed compression. In the Willouran Range, this stress direction would produce D_3 folds. D_2 has reactivated normal faults that controlled the deposition of the Burra Group and the Umberatana Group during basin inversion and reflects southwest-directed compression. The plate margin closest to the Willouran Range at this time may have been on the northeastern side of the Mulroona Gravity Ridge and it is what was happening on this margin that had a greater influence in the northern Adelaide Fold Belt than in the southern Adelaide Fold Belt.

8.6.6 Relationship between the Curdimurka Subgroup and the Burra Group

As in the Euchre Pack Domain, filed relationships at the scale of Willouran Range underline the point that the Curdimurka Subgroup cannot be correlated with the Burra Group, and hence does not support the 797 ± 5 Ma depositional age of the Skillogalee Dolomite (Drexel, 2009; Reid, 2009). The structural development of the Rocky Point sub-domain by itself, does not exclude the possibility that the Emeroo Subgroup is equivalent to the Curdimurka Subgroup, and has been thrust over the top to the southeast in D_1. However, the only allowable movement of the Burra Group to the Curdimurka Subgroup in the Euchre Pack Domain, if they were equivalent is to the northwest. Therefore, the two possible transport directions that would allow the thrusting of the Emeroo Subgroup over an equivalent basal Curdimurka Subgroup are opposed, in the Euchre Pack Domain and the Rocky Point sub-domain. The relationship between the Curdimurka Subgroup in the Stony Range Domain and the Emeroo Subgroup in the West Mount Domain does not provide evidence either way, as the major movement along the Norwest Fault is D_2.

In the areas where the Burra Group overlies the Curdimurka Subgroup; the Stony Range and Berlina domains, the Rischbeith and Kingston domains and the South Hill Domain, the 4,000 m of the middle and upper part of the Burra Group is absent from above the Curdimurka Subgroup. Only in the Euchre Pack Domain is the thickness of the Curdimurka Subgroup above the Dome Sandstone roughly equivalent to that of the Burra Group above the level of the Emeroo Subgroup. Therefore, about 4,000 m of Burra Group would have to be removed from above that part of the Emeroo Subgroup (Dome Sandstone). And yet that entire thickness occurs in that part of the Burra Group which overlies it. Hence, it is unlikely that the Burra Group and Curdimurka Subgroups are stratigraphic equivalents, based on the outcrop patterns in the Willouran Range.

8.7 Conclusions.

The three deformations initially identified within the Curdimurka Subgroup in the Euchre Pack Domain, have been found to have affected the Burra Group and the lower part of the Umberatana Group. D_1 does not have the same intensity within the Burra Group or Umberatana Group as a result of strain partitioning close to the main decollement below the level of the Curdimurka Subgroup. A secondary detachment between the Curdimurka Subgroup and the Burra Group also assisted in isolating the latter from the stronger deformation in the former. The Burra Group did deform during D_1, producing structures with typical D_1 orientations but it was as a reaction to the formation of D_1 structures in the Curdimurka Subgroup. The basal Umberatana Group, from the Yudnamutana Subgroup to the Tapley Hill Formation was deposited during D_1. This produced syn-depositional folding within the Umberatana Subgroup, with the development of a series of unconformities in the Yudnamutana Subgroup and conglomerates within the Tapley Hill Formation, adjacent to D_1 structures. D_1 likely continued to the end of the deposition of the Amberoona Formation with decreased intensity, and the northward movement of the Delusion Hill Domain, marking the end of D_1. There is no evidence for deformation prior to D_1.

Deposition of the Burra Group occurred within a northeast – southwest extending basin which may have changed polarity from the Emeroo Subgroup to the Skillogalee Dolomite. During deposition of the Emeroo Subgroup, the main controlling fault was likely to the northeast of the current outcrop in the Willouran Range, but the Norwest Fault became the controlling fault with the deposition of the Skillogalee Dolomite. The Bungarider and West Willouran Faults were not major features at this time. There may have been some uplift of the Curdimurka Subgroup in the Witchelina Domain during deposition of the upper part of the Emeroo Subgroup but this was short-lived and not regionally significant.

There is no evidence for the deposition of a thick Umberatana Group within the Willouran Range area. Evidence to the south suggests that there may have been some thickening of the Umberatana Group relative to the adjacent areas but the major basin bounding faults were not active at this time. Instead, the major depocentre for the Umberatana Group developed to the east, adjacent to the Mt Painter and Mt Babbage Inliers (Paul et al., 1999).

The major basin inversion event in the Willouran Range was the Delamerian Orogeny. It comprised two deformations; D_2 that resulted in the reactivation of the Norwest, Bungarider and West Willouran Faults as reverse faults, with northwest – southeast trending folds, and D_3 that folded F_2 fold axes along north-northeast – south-southwest fold axes.

Finally, there is no support for the Curdimurka Subgroup being a correlative of the Burra Group. The structural scenario which may allow for the Emeroo Subgroup to correlate with the Dome Sandstone, and be thrust over it requires opposed directions of fault movement during D_1 in the Euchre Pack Domain and the Rocky Point sub-domains. Also the absence of a thick correlative of the middle to upper Burra Group overlying the Dome Sandstone in the Stony Range and South Hill domains, particularly with the contact between the latter and the Emeroo Subgroup being faulted, is also interpreted to indicate that the Curdimurka Subgroup and the Burra Group are not correlatives. Hence there is no support for the ca. 797 Ma depositional age of the Skillogalee Dolomite.

CHAPTER 9.

SALT TECTONICS IN THE WILLOURAN TROUGH

9.1 Introduction

Breccias were first recognized in the Willouran Range by Mawson (1927) but it was in the Central Adelaide Fold Belt, that a link was first made between breccias and salt diapirs (e.g., Webb, 1960; Coats, 1965; Dalgarno and Johnson 1968). Not all workers have agreed with the interpretation of the breccias as being related to salt diapirism and other suggested origins include carbonatites (White, 1983), tectonic breccias (e.g., Preiss, 1987: Krieg, 1993; Mendis, 2002) and sedimentary breccias deposited in graben foundering (Rowlands et al., 1980). Today there is a general consensus that salt tectonics gave rise to the formation of the diapirs and breccias of much of the central and northern Adelaide Fold Belt (e.g., Mount, 1975; Lemon, 1985; Preiss, 1987; Dyson, 1998, 1999, 2002, 2004). However, the term diapir has a specific meaning and implies a specific origin, whether as salt, shale or an igneous body. The term "diapir" was first used by Mrazec (1907) from studies of domal salt intrusions in the Carpathians fold and thrust belt. The definition of a diapir is "an intrusion which domes the overlying cover after piercing the lower layers" (Whitten and Brook 1972). From this definition, the term diapir should only be used where there is evidence of vertical movement of a ductile mass through an overlying rock mass. Salt tectonics is a broader term that encompasses a series of structures and their related mechanisms, of which diapirism is only a part. In the context of the Adelaide Fold Belt, where the salt is no longer present, the term diapir should only be applied if those features associated with diapirs can be proven. Otherwise the term breccia should be applied, it being purely descriptive with no genetic meaning. But, it should be remembered that there may also be some overlap between salt tectonics and normal tectonic processes, an example being evaporitic layers forming a decollement as suggested for the Nackara Arc (e.g., Preiss, 1987; Marshak and Flottmann, 1996).

From stratigraphic relationships and sedimentology, the timing of salt tectonism within the Central Adelaide Fold Belt has been shown to begin during deposition of the mid Umberatana Group, continuing into the Cambrian (e.g., Mount, 1975; Lemon, 1985; Dyson, 1999) with possibly some Quaternary movement (Lemon, 1985). Coats (1973) suggested that in the northern Adelaide Fold Belt, salt tectonism began with the onset of deposition of the Umberatana Group. Lemon (1985) suggested that salt tectonism may have controlled the deposition of the Triassic Leigh Creek Coal Measures within in a salt withdrawal basin. Dyson (2002, 2004) used stratigraphic relationships, changes in unit thickness and the relationship of breccias to the surrounding sedimentary rocks to suggest that salt tectonics began within the Willouran Range area as early as during deposition of the Curdimurka Subgroup. He considered that the Burra Group in the hanging wall of the West Willouran Fault formed in a salt withdrawal mini-basin, adjacent to the Witchelina Diapir (used in the historical sense).

In this chapter, the role of salt tectonics in the Willouran Range is examined. The first section introduces some of the basic principles of salt tectonics which are applied to the Willouran Range in subsequent sections.

9.2 Salt Tectonics

9.2.1 Regional Salt Tectonics.

Most of the studies aimed at understanding salt tectonics have dealt with passive margin environments, such as the Gulf of Mexico (e.g McBride et al., 1998; Camerlo and Benson, 2006), the Kwanza Basin on the central/west African margin (Spathopolous, 1996; Mauduit, 1997; Rouby et al., 2003; Fort et al., 2004; Hudec and Jackson, 2002, Jackson and Hudec, 2005) and the Brazilian coast (e.g. (Mohriak et al., 1995; Cobbold et al., 1995; Gemmer et al., 2005). From these studies, the main driving mechanisms of salt tectonics have been identified as differential loading (Vendeville and Jackson, 1992a; Gemmer et al., 2004; Vendeville, 2005) or basin tilting (Hudec and Jackson, 2004). From analogue experiments, local salt evacuation may occur by either differential subsidence of the proximal overburden and inflation of the distal salt, or gravity spreading where the surface slope of the sedimentary wedge causes a gravity instability (Figure 9.1a), forcing the overburden to spread over the weak salt layer, or a combination of both (Vendeville, 2005). In the former, the salt body moves down slope and the overburden moves vertically in response, but in the latter, the salt remains at approximately the same level but the overburden moves, creating an upslope extensional zone, a central region where overburden is translated oceanward and a downslope compressional zone.

Tectonic (basin) tilting of salt layers and overburden can also generate gravitational instability, leading to downslope migration of salt and gliding of overburden (Figure 9.1b Mauduit et al., 1997; Hudec and Jackson, 2004). It produces many of the same structural features, and a similar downslope zonation in structural style to differential loading models in analogue models based on the Angolan margin (Hudec and Jackson, 2004). Vendeville (2005) argued that on many passive margins, salt and overburden movement has been up-slope indicating that differential loading is responsible.

The more descriptive studies of Bishop et al. (1995) and Maudit et al. (1997), although not directly arguing for either differential loading or basin tilting, suggested that a combination of sediment loading and basin tilting may act as driving mechanisms for salt tectonics. Bishop et al. (1995) suggesed that sediment loading acts as the initial mechanism for movement of Zechstein salt in the Triassic, but thereafter movement is a reaction to sediment loading and regional tilting. Mauduit et al. (1997) suggested from analog modeling based on the Gulf of Guinea that the basin slope is the initial driving force but thereafter differential loading modifies the structures produced.

On passive margins, salt tectonics produces a consistent zonation of structural styles, from an up-slope extensional zone, a down-slope compressional zone with an intermediate translational zone (e.g, Spathopolous, 1996; Mauduit et al., 1997; Fort et al., 2004; Gemmer

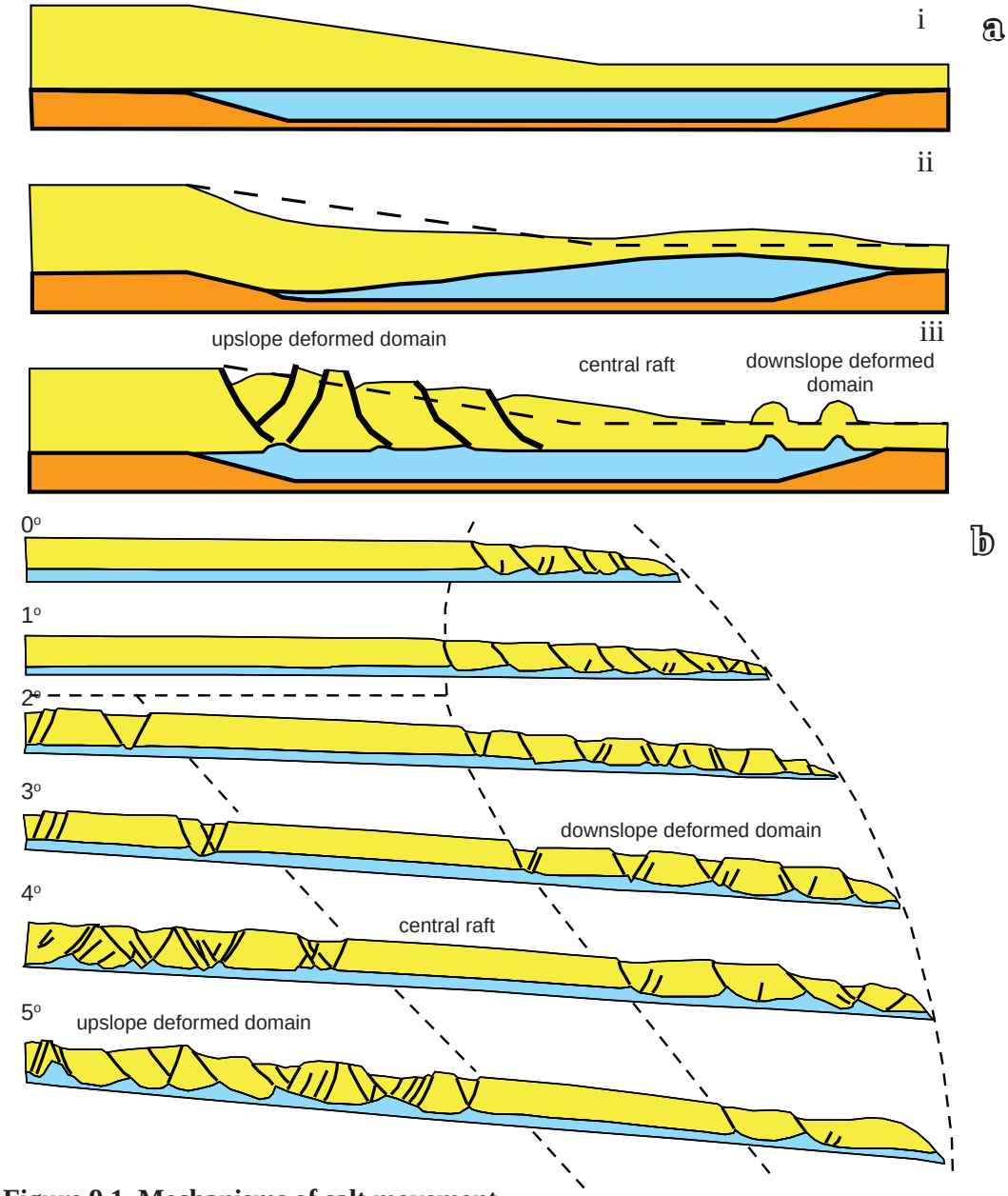

Figure 9.1. Mechanisms of salt movement.
a) (top). Potential structural responses to the loading of a salt layer (blue) by a sediment wedge (yellow). i initial stage, assuming instantaneous overburden deposition. ii) differential subsidence of the proximal overburden and inflation of the distal salt. iii) Gravity spreading of the overburden causing proximal extension, midslope distal translation and distant contraction. (from Gaullier and Vendeville, 2005). b). Analog model showing the effect of tectonic tilting on structures produced by downslope movement of post-salt sediments on a salt base. (from Mauduit et al., 1997). Note the similar structural domains produced by the different mechanisms. The differing structural styles in the downslope deformation domains reflects the different initial salt geometry.

et al., 2005; Camerlo and Benson, 2006: Figure 9.1). The extensional zone is the site of salt ridges and diapirs. Within the compressional zone, compression is accommodated by symmetric box-folding if the source layer is evaporitic (Rowan et al., 2004) or lateral shortening and vertical inflation of existing salt bodies (Vendeville, 2005).

In compressional settings with associated fold and thrust belts, salt layers act as decollement surfaces, above which thrusting and folding may occur (Figure 9.2: Brun and Fort, 2004; Rowan, 2004; Sherkati et al., 2005). Symmetrical detachment folds commonly develop above decollements formed above viscous layers whereas asymmetric thrusts develop

above frictional decollements (Figure 9.2a: e.g., Rowan, 2004; Higuera-Diaz et al., 2005; Sherkati et al., 2005). From analogue modeling, Brun and Fort (2004) showed that in compressional regimes, strong shortening is characterized by pinched synclines of post-salt sediments, pinched anticlines that may give rise to compressional diapirs and possible salt extrusion, and thrust faults (Figure 9.2b,c). In areas of moderate shortening, double wavelength folds may form and there may be squeezing of diapirs formed in extensional zones with tightening of adjoining synclines (Figure 9.2d). Extrusion of salt by compression may lead to the formation of salt canopies (Brun and Fort, 2004). Disharmonic folding in the Zagros Fold and Thrust belt is attributed by Sherkati et al., (2005) to diapirism in a compressional setting, with salt being mobilized into diapirs below thrusts (Figure 9.2e).

9.2.2 Diapirs.

Earlier studies and analogue modeling of salt tectonics was concerned with the formation of individual diapirs (Vendeville and Jackson, 1992a,b) and the sedimentary response to the forming diapir (e.g., Lemon, 1985; Vendeville and Jackson, 1992a,b; Kennedy, 1993; Shelley and Lawton, 2005). Figure 9.3a shows the stages of diapir formation. During the early phases of diapir amplification, normal faults form in the overburden to the salt, forming grabens, beneath which salt rises reactively (Vendeville and Jackson, 1992a). As the diapir continues to rise, the overburden may become thin enough for it to be breached as the fluid pressure of the salt exceeds the strength of the overburden. Vendeville and Jackson (1992a) referred to this stage as active diapirism. Salt flow becomes unrestrained and may continue even if extension ceases (Vendeville and Jackson, 1992a). The final stage of diapir growth is passive diapirism. During this stage, diapir growth continues by downbuilding, as the head of the diapir crest remains near the surface while the source layer sinks. Without continued sedimentation, the diapir cannot increase in height and it will spread laterally, forming salt glaciers (Vendeville and Jackson, 1992a) .

If extension continues, the diapir may begin to fall as it widens by viscous flow to fill the increasing gaps between fault blocks (Figure 9.3b: Vendeville and Jackson, 1992b). The salt supply becomes depleted or restricted and the diapir begins to sag. A graben forms above the falling diapir which fills quickly with sediment and is termed a salt withdrawal basin. The crest of the diapir becomes indented by the base of the graben and if all the salt is removed, the graben may rest upon the basement (Vendeville and Jackson, 1992b).

One of the conclusions of the work of Vendeville and Jackson (1992a) is that in the absence of extension, salt cannot pierce a thick overburden and so diapirs will not form. From analogue modeling, Stewart (1995) suggested that at least 20% extension is required before diapirism can be initiated.

From the work of Vendeville and Jackson (1992a, b) it is clear that in the area above and adjacent to diapirs, sedimentation is controlled by the rise and fall of the diapir (Figure 9.3). There have been many studies on the relationship between sedimentation and salt tectonics, using analogue modeling (Vendeville and Jackson, 1992a,b), field relatonships (e.g., Lemon, 1985; Kennedy, 1993; Aschoff and Giles, 2005; Shelley and Lawton, 2005) and in seismic sections (e.g., Kossow and Krawczyk, 2002). In the reactive phases, sedimentation occurs

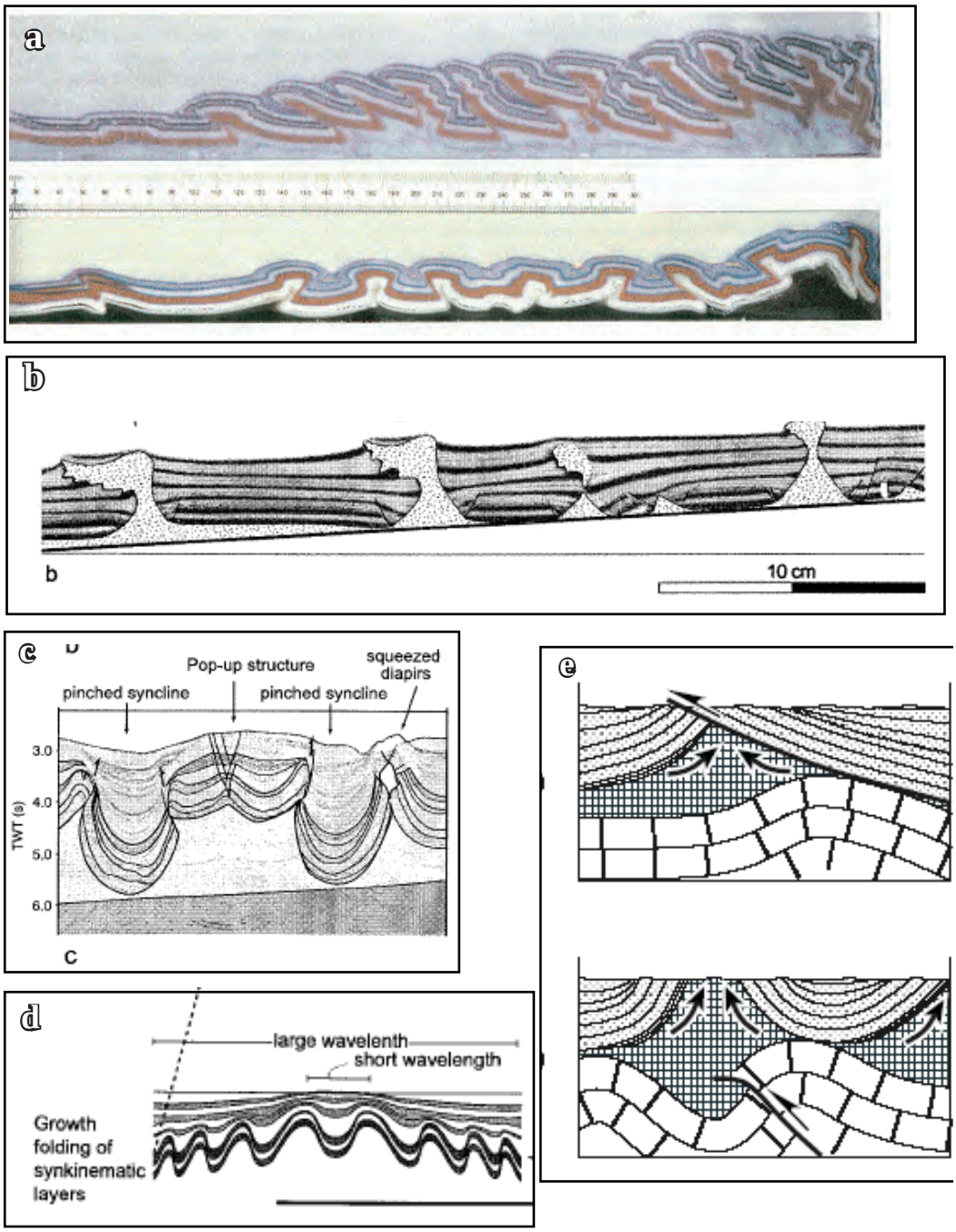

Figure 9.2 Structures formed by salt tectonics in compressional settings.
a) The effect of decollement rheology on structural style. In the upper image, frictional detachments result in asymmetric imbricate fault geometries. In the lower image, a viscous decollement produces symmetrical detachment folds with minor faulting of limbs. (From Rowan et al., 2004, experiments carried out by B. Vendeville.) b) Pinched extensional diapirs in a zone of moderate compression. c) A seismic section showing structures formed in a zone of strong compression. d) Double wavelength folds formed in a zone of moderate compression. (b,c,d from Brun and Fort, 2005). e) Disharmonic folding in the Zagros Fold and Thrust Belt. A syncline forms above an anticline as initially a thrust forms on a detachment above salt. With the thinned cover above the salt, salt begins to move upward, forming a compressional diapir with a pinched syncline on either side (Sherkati et al., 2005).

in the crestal anticline above the diapir. During the active phase, the crestal graben is still present and so sedimentation is still restricted to the crest of the diapir. In the passive phase, because the diapir crest stays at about the same level while the basin subsides, the crestal anticline does not form and the crest is an area of little or no sedimentation (Vendeville and Jackson, 1992a). Field studies show that in marine settings, sediments above the crest of a passive rising diapir are typically shallower water relative to the sediments on either side of the diapir (e.g., Lemon, 1985; Kennedy, 1993; Shelley and Lawton, 2005). During salt withdrawal, sedimentation occurs within the graben formed above the falling diapir (Vendeville and Jackson, 1992b).

9.3 The Structure of the Willouran Range and Salt Tectonics.

9.3.1 Introduction.

The above studies provide a veriety of structural frameworks within which to examine the role of salt tectonics in the Willouran Range. In doing so, two points are pertinent:

- the Willouran Trough was not a passive margin but an intracontinental basin, separated from the continental margin by an unknown distance up to the deposition of the Umberatana Group. Thereafter, the Adelaide Fold Belt was likely a passive margin but the Willouran Trough was still within the continental margin; and
- the area has been subject to three deformations and so early-formed structures that may be related to salt tectonics have been modified by later deformation.

Because of these points, it is apparent that no complete model may be applied with certainty and it is necessary to examine the individual features to arrive at an understanding of the role of salt tectonics and its driving mechanism.

The hanging wall of the West Willouran Fault provides the most extensive evidence of salt tectonics. Historically, the Witchelina Domain was termed the Witchelina Diapir and the Breaden Hill Breccia has been interpreted to be related to a diapir (Coates, 1973; Murrell, 1977; Preiss, 1987; Forbes 1990; Dyson, 2002, 2004). The Burra Group in the Trial Hole Domain was interpreted by Dyson (2002, 2004) to have been deposited in a salt withdrawal basin. Dyson (2004) also considered that breccias in the Euchre Pack Domain offer evidence of the earliest salt movement in the Adelaide Fold Belt.

9.3.2 The Witchelina Domain

If by the Witchelina Diapir, Coates (1973) meant to infer that it formed by diapiric processes, then it should be identifiable as such through comparisons with the models for diapir formation given above. The previous chapter showed that there was uplift of the Curdimurka Subgroup on the faulted contact with the Burra Group which stopped at the end of deposition of the Emeroo Subgroup. In addition, a small area of black shale also crops out at the margin between the Emeroo Subgroup and the Skillogalee Dolomite, which is limited to the area near to the Witchelina Domain. The formation of a salt pillow within the Callanna Group is one way in which the Curdimurka Subgroup may have been

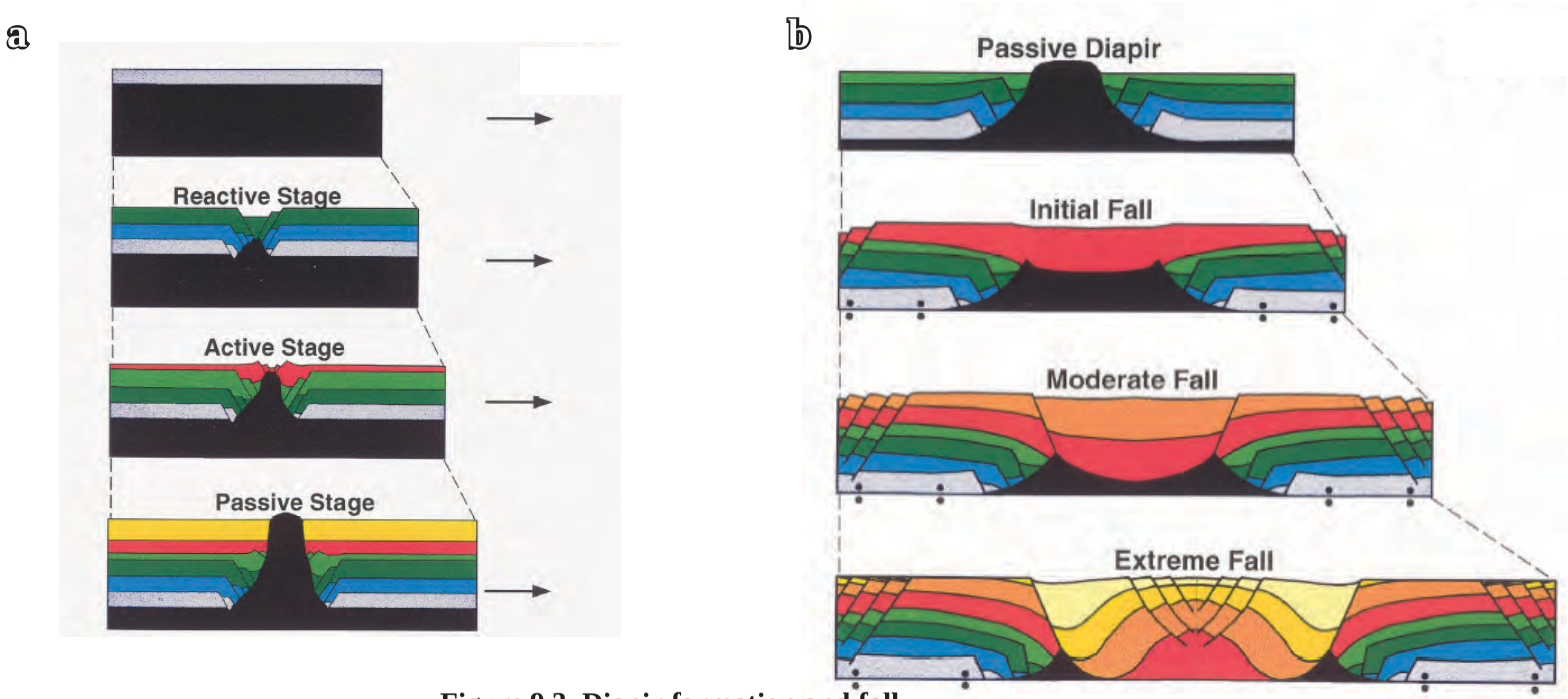

Figure 9.3. Diapir formation and fall.

Figure 9.3a. Stages of Diapir Formation. With extension, a graben forms and below, salt begins to rise. With continued extension, if sedimentation cannot match the rise of the salt, the force of the rising salt may overcome the strength of of the overburden and break through to the surface. In the passive stage, the diapir rises by down-building with the crest of the diapir remaining close to the surface. Sedimentation occurs above the crest of the diapir in the crestal graben, widening in the active stage to the margins of the diapir. In the passive stage, because the crest of the diapir is close to the surface, sedimentation is limited to a thin veneer with a low possibilty of preservation (Vendeville and Jackson, 1992a).

Figure 9.3b. Stages of Diapir Fall. With continued extension, the salt may become depleted or otherwise restricted. The crest of the diapir begins to fall as the salt flows to fill the space created. Eventually the sediment-fill in the salt withdrawal basin may sit on the presalt unit. Sediment deposition occurs in the withdrawal basin above the falling diapir, reaching a maximum thickness initially above the crest but in later stages, thickening at the margins of the basin. (Vendeville and Jackson, 1992b).

uplifted within the framework of salt tectonics, with the black shale being deposited within a periphery basin.

If a salt pillow did form and then the salt was withdrawn from the structure, a salt withdrawal basin would form above the site of the falling diapir (Figure 9.4). The Skillogalee Dolomite does not appear to thicken in the vicinity of the Witchelina Domain, the Myrtle Springs Formation thickens to the southeast, in the Delusion Hill Domain and the Tapley Hill Formation is thinning to the southeast also (Figure 9.4). Hence, a salt withdrawal basin did not form structurally above the Witchelina Domain and so, despite some doming during deposition of the Emeroo Subgroup, a diapir did not develop in the area of the Witchelina Domain. If a salt pillow did form then it remained stable until deposition of the Umberatana Group or removal of the salt was matched by the movement into the structure of the Curdimurka Subgroup, but as has been shown, it was not subject to deformation until D_1, also at the time of deposition of the Umberatana Group. Hence if it formed as a salt pillow, it remained stable until the deposition of the Umberatana Group.

9.3.3 The Breaden Hill Breccia and the Euchre Pack Domain.

The Breaden Hill Breccia (Figure 9.5) has the characteristics of being the remnants of a salt body; it contains clasts of Arkaroola Subgroup, the clasts are poorly sorted by range in scale to hundreds of metres, and it may be matrix-rich, although this may be a factor of outcrop. It proves that salt has moved from the likely source in the Arkaroola Subgroup to the top of the Curdimurka Subgroup, a vertical distance of roughly 6,000 m. Dyson (2002, 2004) considered it to have been formed as a salt glacier deposited onto the surface of outcropping Boorloo Siltstone prior to the deposition of the Umberatana Group but this interpretation is rejected on three grounds. Firstly it contains megaclasts of tillite indicating that the tillite must have been lithified at the time of inclusion within the salt. Chapter 7 showed that the tillite clasts have similar structures and structural orientations to the underlying Boorloo Siltstone shown to be D_1, so their inclusion is either pre-, or syn-D_1. Secondly there is no erosion of the Boorloo Siltstone beneath the breccia. Finally, its shape relative to the Fence Anticline and Noranda Camp Syncline suggests that it was intruded at about the time of the formation of the folds. The breccia is thinnest on the upper surface of the anticline where stress was greatest and thickest in the syncline where stress was least. It also forms a triangular body in the footwall of the normal fault formed above the first hinge of the Fence Anticline (Figure 9.5). Where it may have formed as a salt glacier was in front of the propagating fault bend fold, onto the surface of Skillogalee Dolomite at the southern end of the breccia. PIRSA mapping shoes that the western contact of the breccia is with the Skillogalee Dolomite, and thus interpreted to have been deposited on it. The Yudnamutana Subgroup was then deposited on the breccia (Talbot, 1994; Fletcher et al., 1995) or the Umberatana Group was up to a few hundred metres thick when the breccia was intruded into the unlithified sediments (Nelson and Fairchild, 1989). From this, the timing of salt movement is during deposition of the Yudnamutana Subgroup with extrusion at about the onset of deposition of the Tapley Hill Formation.

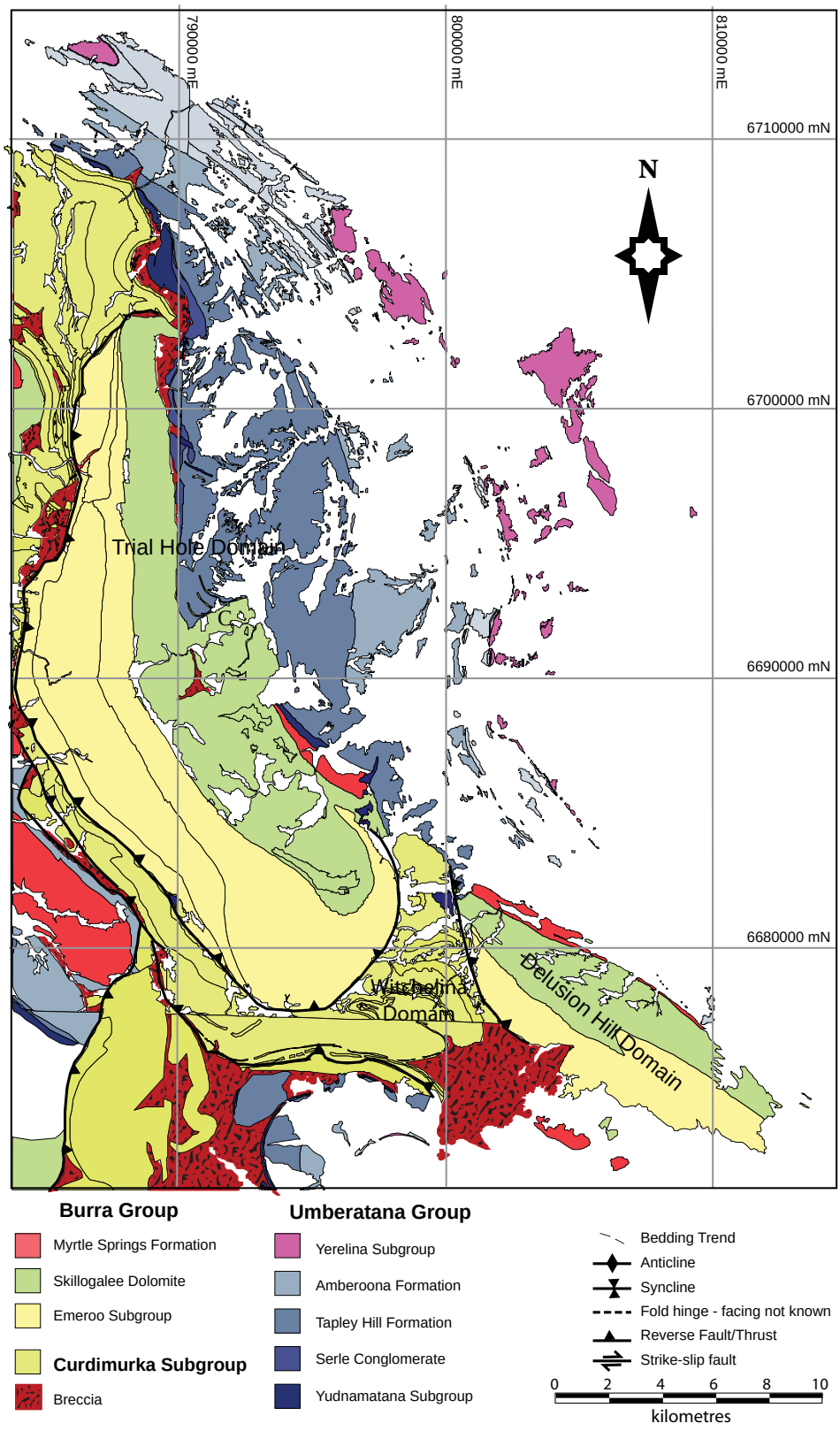

Figure 9.4. The Witchelina Domain and diapirism.
The Witchelina Domain has been interpreted to be a diapir (Coates, 1973), however the sedimentary relationships of the surrounding and overlying rocks do not support this. There is no evidence of either a crestal graben having formed above it during deposition of the Burra Group or sedimentation above a falling diapir (compare with Figure 9.3). Geology from the 1:100,000 PIRSA GIS data set.

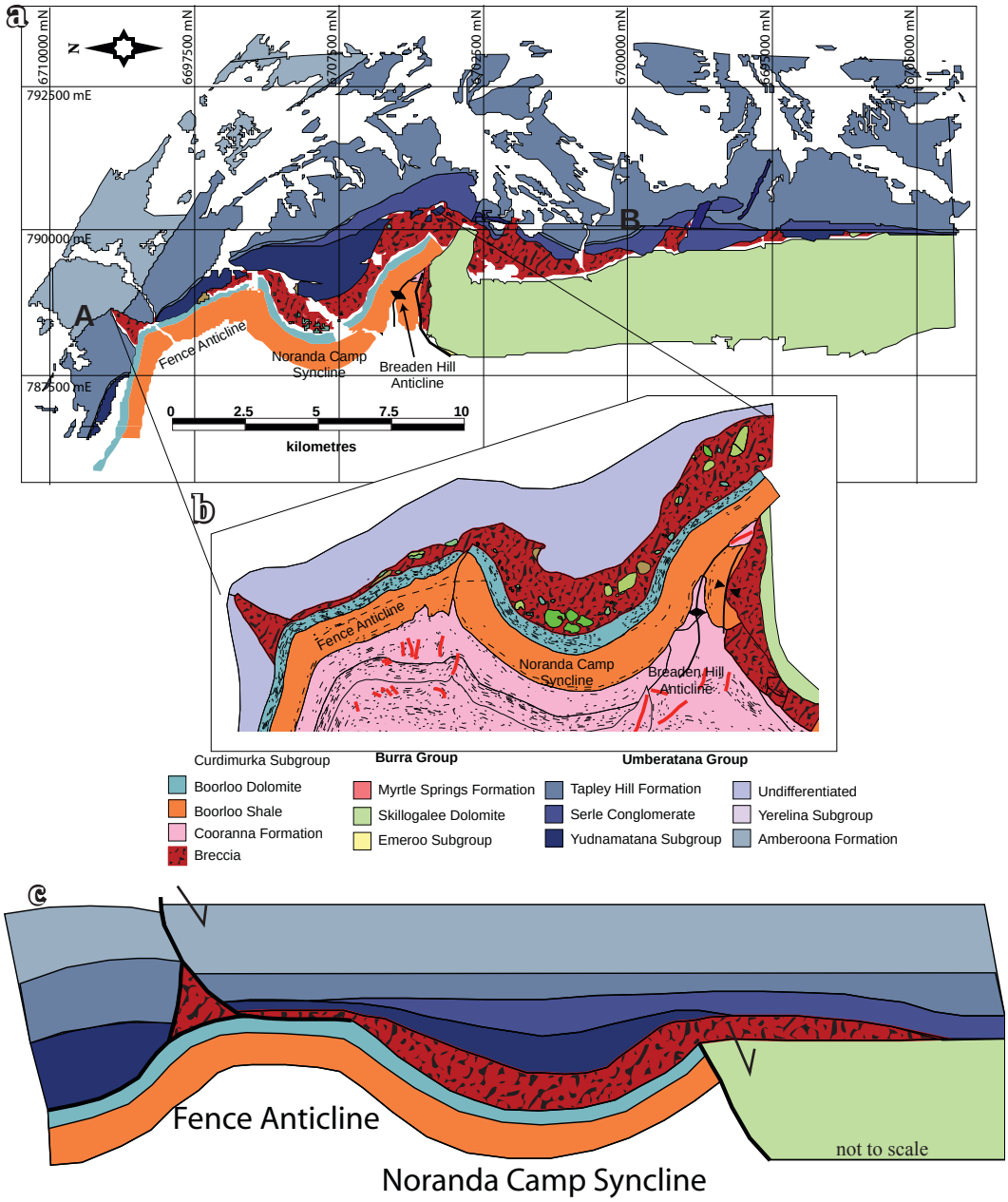

Figure 9.5. The Breaden Hill Breccia.
a) The Breaden Hill Breccia extends from pt A, along the upper surface of Boorloo Siltstone through the Fence Anticline and Noranda Camp Syncline, along the hinge of the Breaden Hill Anticline, and along the upper surface of the Skillogalee Dolomite to point B. It sits below the lower surface of the Umberatana Group, with a sheared contact. There is no erosion of the upper surface of the Boorloo Dolomite. b) A detail of the breccia showing the largest megaclasts occur where the breccia is thickest, in the Noranda Camp Syncline. c). A simplified drawing of the Breaden Hill Breccia relative to the main structures. It has been intruded between the Boorloo Dolomite and the Yudnamatana Subgroup, but extruded in front of the fault bend fold onto the surface of the Skillogalee Dolomite, with the Serle Conglomerate deposited on top. The salt has intruded from out of the plane of the figure.

Dyson (2005) considered that the first movement occurred just prior to deposition of the Recovery Formation. He interpreted a narrow band of breccia above the Dunns Mine Limestone as being a salt glacier, with the Recovery Formation on-lapping it. However, the contact is not sedimentary and the breccia has intruded along a zone of weakness above the Dunns Mine Limestone. Near Utah Bore, where Dyson interprets the on-lap there are two layers of breccia above the Dunns Mine Limestone, with deformed siltstone between.

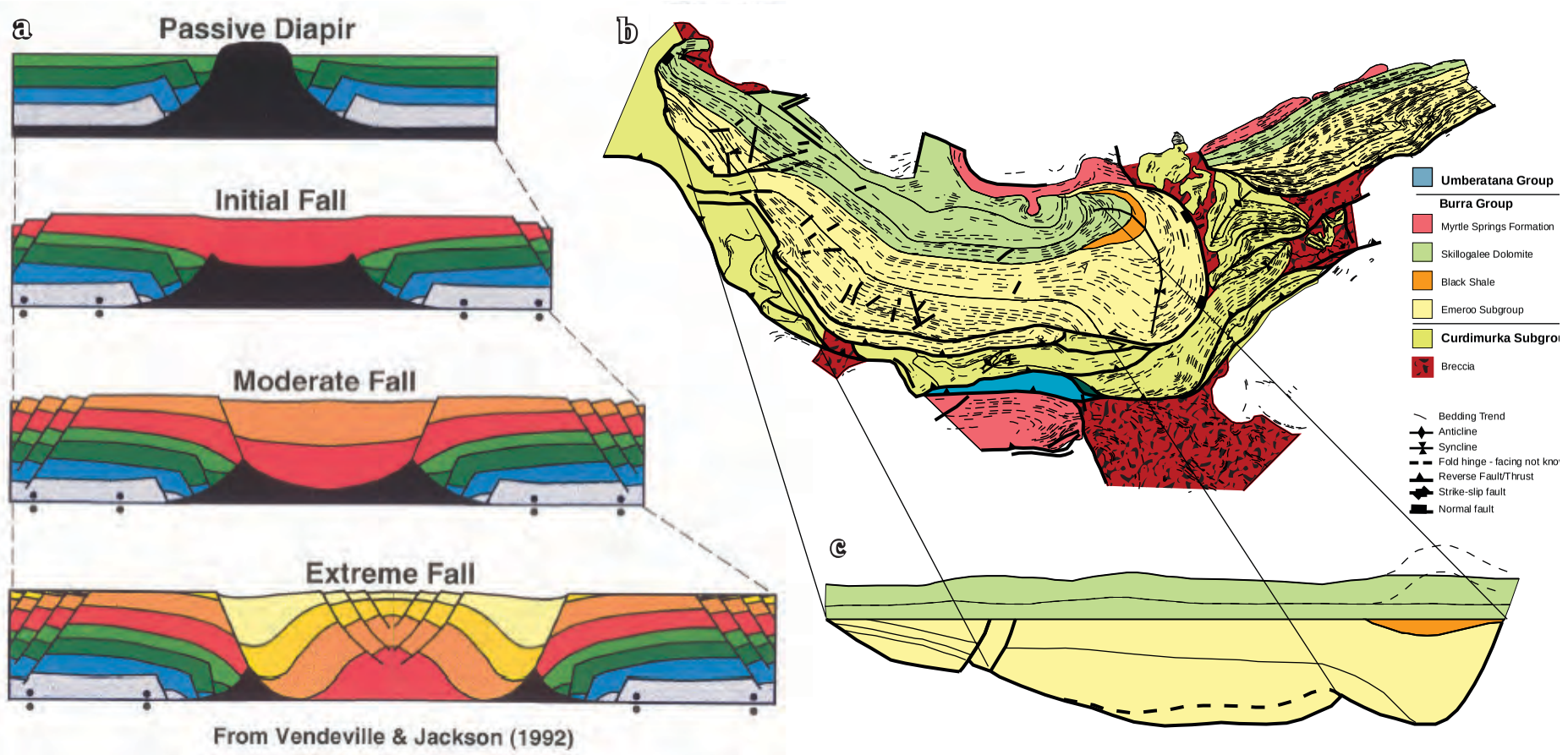

Figure 9.6. Comparison of a model showing expected geometry of sediments associated with deposition during salt withdrawal and the Burra Group in the Trial Hole and Delusion Hill Domains.

Although there are some similarities, with some up-turning of the Burra Group at the margins. The Curdimurka Subgroup is present beneath the Burra Group and the normal faults at the edges at the margins of the salt withdrawal basin are absent. The Myrtle Springs Formation is also absent whereas accordiing to the model, it should be thickened at the edges of the basin.

The lower breccia crops out poorly here but intrusion of the upper breccia, has deformed the surrounding siltstone. The breccia is also a branch of a larger body that intrudes the Recovery Formation up to the level of Sandstone 1. As part of his evidence Dyson (2005) also considered that the Curdimurka Subgroup in this area was deposited in a salt withdrawal basin. Where it is thickest, Dyson (2005) interpreted to be the sub-basin, thinning over a diapir in the vicinity of Dunns Mine. As has been shown, the Curdimurka Subgroup thins considerably in this area but the primary reason for the thinning is removal of stratigraphy by low-angle normal faults. There are no structures above the suggested position of the diapir indicative of either diapir formation or collapse.

9.3.4 The Burra Group.

Salt mobilization during the Burra Group is favoured by several authors with two mechanisms invoked. Preiss (1987) and Belperio (1990) concluded that salt walls developed along the lines of the Norwest, Bungarider and West Willouran Faults, dividing the Willouran Trough into several sub-basins. The previous chapter addressed this with the conclusion that the facies variations mapped by Belperio (1990) are consistent with a single half-graben.

Preiss (2000) and Dyson (2002, 2004) suggested that deposition of the Burra Group in the Trial Hole Domain occurred in a salt withdrawal minibasin. If this is correct, the outcrop pattern of the Burra Group should resemble analogue models or examples of salt withdrawal basins in seismic sections. Comparing models of diapir fall (e.g., Vendeville and Jackson, 1992b), and assuming moderate to extreme diapir fall, although there are some similarities, the Burra Group does not have the correct geometry (Figure 9.6). Instead the outcrop pattern resembles a half-graben, with the controlling fault being a listric normal fault, with the sub-vertical portion on the southeastern boundary of the Trial Hole Domain, soling out into the Curdimurka Subgroup. A second analogue model (Vendeville and Jackson, 1992b) showed that the Curdimurka Subgroup should form isolated blocks separated by salt and should be absent from beneath the Burra Group. Although it does thicken and thin significantly, the Curdimurka Subgroup is never absent from beneath the Burra Group despite being strongly distended. Instead, it appears that the Burra Group itself has been subject to extension and block rotation, indicating that salt movement occurred after deposition of the Burra Group. The on-lap surface within the upper Emeroo Subgroup indicates that there was some vertical movement on either side of the Witchelina Domain Dyson (2004) linked the on-lap to rising salt in the Witchelina Domain, however there is no other evidence to support the link, which could otherwise be attributed to normal movement on the West Willouran Fault.

9.3.5 The Stony Range and South Hill Domains.

Breccias occur in areas of complex deformation, where there is repetition by faulting of the Dome Sandstone such as in the Rocky Point Sub-domain and in the cores of anticlines (Figure 9.7). The breccias contain megaclasts of Arkaroola Subgroup and so are inferred to have the same source as the breccias attributed to salt tectonics. In the Rocky Point Sub-domain, the breccias occur between thrust sheets of Dome Sandstone and have been deformed by the thrusting. They occur stratigraphically below the Dome Sandstone in the

South Hill Domain, in the core of an anticline (Figure 9.7). The mass of megabreccia in the northeast of the South Hill Domain is interpreted, from the gravity long-section, to be in a separate structure, possibly a series of thrusts. Hence, there is no indication of significant vertical movement of salt to levels higher than the base of the Dome Sandstone in either the Stony Range or South Hill Domains. A sub-vertical salt body was inferred in the gravity cross-section below the Stony Point Domain but this is in the plane of the Norwest Fault and is not interpreted to cross-cut the Dome Sandstone.

It was noted in the previous chapter that the dominant structural style in both the Stony Range and South Hill Domains is compressional. In compression, salt acts as a lubricant, forming a decollement upon which the supra-salt package slides. Rowan et al., (2004) demonstrated the differences between structural styles developed above a viscous ductile decollement such as salt, and a frictional substrate (Figure 9.2a). The structure of the Curdimurka Subgroup most closely resembles that of thrusting above a viscous ductile substrate (Figure 9.2a, cf. Figure 9.7) Salt-cored anticlines may form as detachment anticlines and this is seen in the South Hill Domain. The long-wavelength asymmetric folds seen in the Burra Group are similar to the North Sea Basin, which were interpreted to result from gravity sliding above an evaporite layer (Stewart and Coward, 1995) and this interpretation is favoured here (Figure 9.7b).

9.4 Salt Source

To place these features into a salt tectonics framework a source of salt and a mechanism for mobilizing the salt is required. The source of the salt is either the Wywyana Formation or the Curdimurka Subgroup. Coats and Blisset (1971) suggested that the Wywyana Formation is the source of salt for diapiric breccias adjacent to the Mt Painter Block. Given the absence of the Curdimurka Subgroup in that area, it is likely the case. Preiss (1985) considered that the Curdimurka Subgroup contributed to the formation of intrusive breccias in the Worumba Anticline, and Dyson (2005) wrote that salt from the Curdimurka Subgroup may have contributed to salt movement in the Willouran Range.

There are two arguments against the Curdimurka Subgroup being the source of salt mobilized by salt tectonics: 1) within the Euchre Pack Domain, there may have been some salt deposited in either or both of the Recovery Formation and the lower Cooranna Formation but there does not appear to be a major stratigraphic interval missing or a stratiform breccia not associated with faults in these units. 2) the stratigraphic equivalent along strike to an evaporite body is an unconformity (Warren 2000) and so there should be a major unconformity within the Euchre Pack Domain, which there is not. Further west in the Stony Range and South Hill Domains, the only indication of salt deposition are minor halite and gypsum pseudomorphs in the Dome Sandstone and the siltstone immediately above. Hence, the Curdimurka Subgroup cannot be a source of the salt.

The level of the decollement is below the Dome Sandstone and not below the Noranda Volcanics. There may be two reasons for this. The first is that there may have been an evaporite unit deposited at that level but the only evidence for this is the level of the

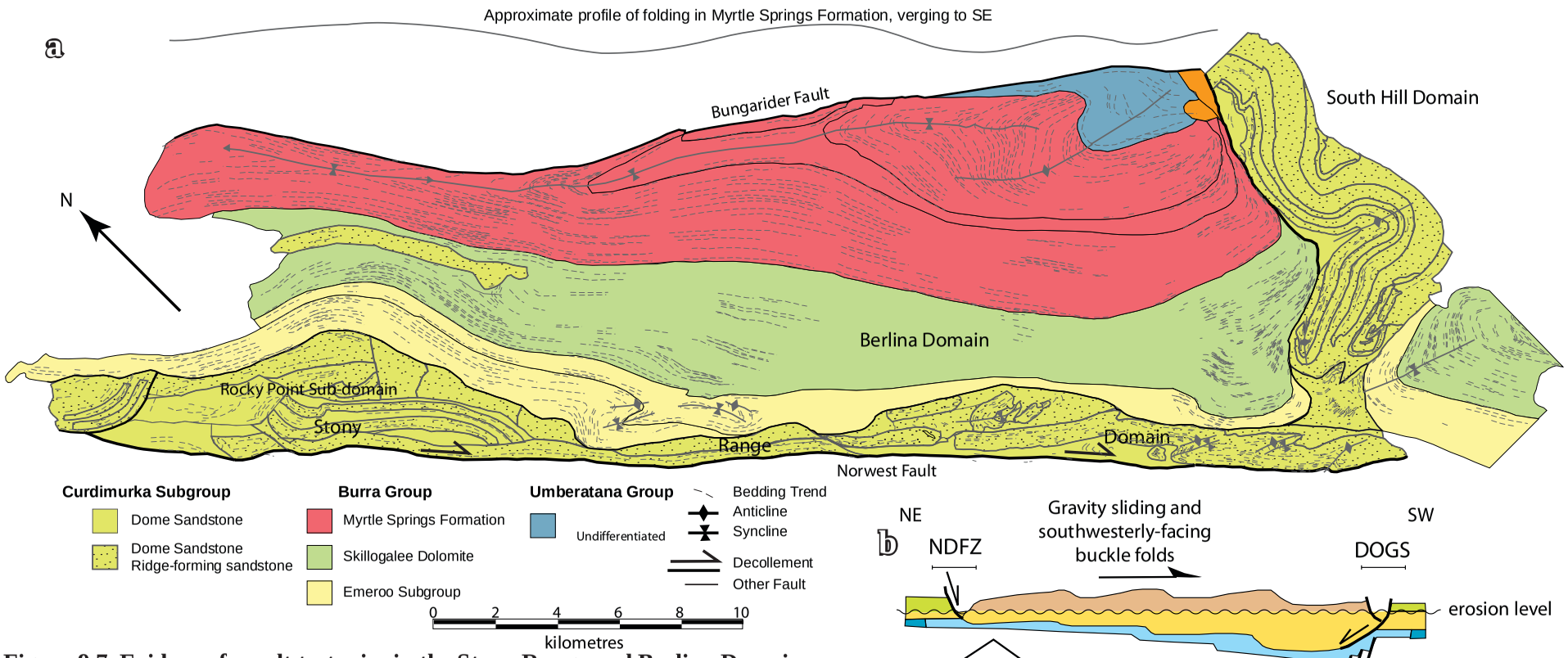

Figure 9.7. Evidence for salt tectonics in the Stony Range and Berlina Domains.
a) The Stony Range Domain has deformed above a decollement. It has deformed by thrusting in the Rocky Point sub-domain, and by detachment folds at the southeastern end. Compare with the analog models of folding and thrusting in Figure 10.3. Above is an approximate profile of D_1 folding in the Myrtle Springs Formation, verging to the southeast. Note also the breccia cored detachment folds in the northwestern end of the South Hill Domain. b) A cartoon of gravity sliding from the southern North Sea (from Stewart and Coward, 1995). It shows similar features to the Berlina Domain, with buckle folds verging toward the deeper part of the basin.

decollement. Otherwise, the salt may be allochthonous, having risen from below the Noranda Volcanics. The mechanism for salt sheet emplacement of Talbot (1993) and Fletcher et al., (1995), suggests that it occurs at the sediment-water interface as salt glaciers, implying salt movement prior to deposition of the Dome Sandstone (Figure 9.8a). This interpretation is rejected as the Dome Sandstone was deposited in a continental environment and not at some depth below sea level in a low energy environment as in the northern Gulf of Mexico. Nelson and Fairchild (1989) suggested that salt emplacement may occur within a few hundred metres of the sediment-water interface as sills (Figure 9.8b). In this model, there is good potential for the preservation of the salt. Both of these mechanisms would indicate salt movement during deposition of the Dome Sandstone. However, analogue models show that if salt did penetrate the Wooltana Volcanics at this time, there should be a greater variation in thickness in the Dome Sandstone than is inferred from its outcrop. On this basis, it is unlikely that salt did penetrate the Wooltana Volcanics prior to or during deposition of the Dome Sandstone. A third model based on the North Sea Basin is illustrated by Stewart et al., (1995; Figure 9.8c). In this model, a salt wing develops when salt from a diapir spreads laterally between two units, causing delamination of the lower unit. The Wooltana Volcanics may have delaminated from the Dome Sandstone, facilitated by the large difference in density and rheology between the two units. On the evidence available, it is not possible to determine between the two alternatives for a salt source: either salt is sourced from a layer between the Wooltana Volcanics and the Dome Sandstone, or it moved into this position at some time after deposition of the latter.

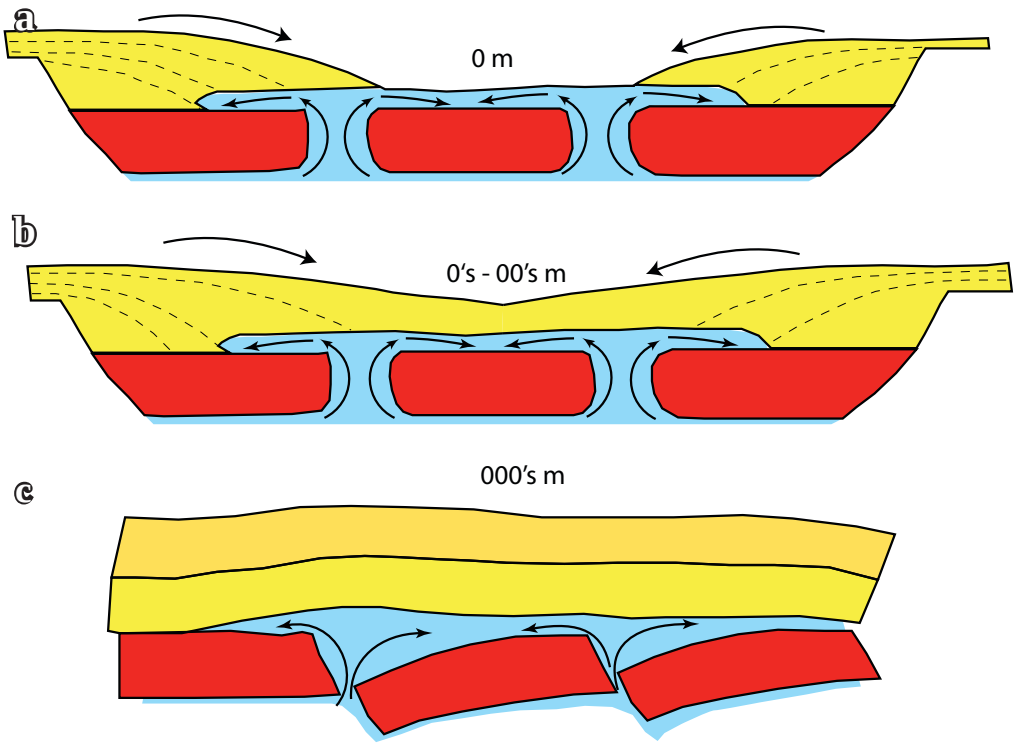

Figure. 9.8. possible origin of salt (blue) between the Dome Sandtone (yellow) and the Wooltana Volcanics (red).
a) Salt extruded onto the surface of the Wooltana Volcanics at the surface with deposition of the Dome Sandstone onto the salt. b) Salt extruded during sedimentation of the Dome Sandstone, below a cover of tens to hundreds of metres. c) Extrusion of salt at some time after deposition of the Dome Sandstone, with hundreds to thousands of metres of sediments above.

9.5 Mechanisms and Timing of Salt Movement

Salt movement typically begins a short time after deposition, but it can be delayed for several hundred million years. In the Dneiper-Donets Basin, diapirism began with as little as 400 m overburden above the Frasnian salt series (Stovba and Stephenson, 2002), whereas in the Persian Gulf Basin, the Hormuz Salt is late Neoproterozoic in age but salt movement did not begin until the Permian, approximately 250 million years after deposition (Edgell, 1995). Salt deposition within the Kwanza Basin ended in the Aptian and movement began when the overlying Albian – Early Cenomanian carbonate platform was only a few hundred metres thick (Spathopoulos, 1996;) and in the Permian Basin of northern Europe, the Zechstein was deposited in the Late-Permian and diapirism initiated by late Triassic extension (e.g., Coward and Stewart, 1996; Scheck et al., 2003), although Buchanan et al. (1996) suggested that salt swells had begun to form in the Early Triassic.

Coats (1973) concluded that salt movement in the Willouran Trough began during deposition of the lower Umberatana Subgroup. Dyson (2004) considered that the first salt movement begain during deposition of the Recovery Formation, roughly 75 million years before deposition of the Umberatana Subgroup. Evidence presented here indicates the major salt movement began during deposition of the Yudnamutana Subgroup, although there may have been some movement during deposition of the upper Emeroo Subgroup. If this is the case, the major salt movement was initiated over 100 million years after deposition.

When considering the timing of salt movement, time is not the limiting factor; it is the forces discussed above that intiate salt movement. But in considering these forces a third factor has to be added, space for salt to move into (e.g., Vendeville, 2005). The importance of free space is illustrated in the Canyonlands National Park, Utah where grabens began to form in a suprasalt layer after the Colorado River cut through this layer, exposing the salt and removing the restraints to overburden extension (Schultz-Ela and Walsh, 2002).

The Willouran Trough is bounded on three and possibly four sides and so of these three factors, space may be absent. Futhermore, if the Wywyana Formation was the source of the salt, the Wooltana Volcanics were deposited rapidly above the salt layer, forming a one kilometre thick seal that the salt may not have been able to penetrate. Thus, the Willouran Trough did not have an open side and space had to be created before the salt could move. Extension creates space, hence there are three periods when the salt could move; at the beginning of deposition of the Curdimurka Subgroup, the Burra Group and the Umberatana Group.

The previous chapter concluded that the Curdimurka Subgroup was deposited in a rift basin formed in the aftermath of the eruption of the Wooltana Volcanics, with greatest subsidence on the northeastern margin. It has not been possible to estimate the amount of extension during deposition but during deposition of the Dome Sandstone, subsidence was slow, with about 1,400 m deposited in 25 million years between the Wooltana Volcanics and the Rook Tuff. It is possible that at this time, there was insufficient extension to breach the basalt and so vertical salt movement was limited. Subsidence increased markedly during deposition

of the remainder of the Curdimurka Subgroup with about 4,000 m deposited in the next 25 million years and so this likely marks the time of greatest extension. Differential loading may not have been significant during deposition of the Curdimurka Subgroup as in contrast to passive margins, where sediment input is largely unidirectional from the landward margin, in a continental rift, sediment may enter the basin from any side. However, the basin would tilt to the northeast, encouraging salt movement in that direction. Analogue models (Vendeville and Jackson, 1992a) show that if there was extension at this time, the basalt should develop a series of grabens within which the Dome Sandstone was deposited and with salt rising below. There is no indication in the Willouran Range of the Dome Sandstone having a configuration that would arise from this situation.

As the rate of subsidence increased after the deposition of the Dome Sandstone, there may have been greater tensional stress on the basalt and Dome Sandstone, particularly in the northeast. It is at this time that salt movement would be most likely and Dyson (2002, 2005) suggested this based on field evidence, but is rejected here for the reasons given above.

There is evidence for limited salt movement during deposition of the Burra Group as discussed above. Both the Mundy and Norwest Faults were active as normal faults (Paul et al. 1999) and from facies variations (Belperio, 1990) sediment supply was likely dominated from the northeast. Sedimentary loading was at a maximum in the Trial Hole Domain and minimal in the Berlina Domain. Basin tilting may have occurred but the extent and direction of tilting is unknown and dependent of the relative amounts of movement of the Norwest and Mundy Faults. By the end of deposition of the Skillogalee Dolomite, the potential for differential loading was reduced as the sediment thickness at this time was approximately equal across the Willouran Trough (Belperio, 1990). Despite these favourable features, salt tectonics was not active during this time.

Evidence from the Breaden Hill Breccia, the centre of the Willouran Range (Selley and Bull, 2002) and elsewhere in the northern Adelaide Fold Belt (e.g., Coates and Blisset, 1971; Coates, 1973; Preiss, 1987) indicates that the time of maximum salt movement was during the deposition of the of the Tapley Hill Formation. It was during this time that extension may have been at its maximum as the Adelaidean Basin underwent a change from an intercontinental rift to a passive margin (Powell et al., 1994). It was a time of maximum extension and space was being created within the Willouran Trough. It was also thick-skinned, extending to the southwest across the Torrens Hinge Zone, so the combination of thick-skinned extension and the amount of extension was sufficient to breach the up to 12 km thick cover above the salt layer. Despite this the Willouran Trough, at the level of the Arkaroola Subgroup, was confined to the northeast by the Mulroona Ridge and the southwest by the Norwest Fault. So, although the major extension at this time was directed to the northeast – southwest, from fold orientations the mass of the basin fill from the base of the Dome Sandstone to the top of the Burra Group was moving to the south to southeast. Basin tilting is interpreted to have been the main mechanism, with normal fault movement below the South Hill Domain. Differential loading may also have been important. The area to the northwest of the Willouran Range is largely obscured by Mesozoic to Recent sediments but aeromagnetic and gravity interpretation suggests that the Umberatana Group

is thicker there than in the Willouran Range. It was also a time of glaciation and so ice formation may also have played a role in differential loading.

9.6 Conclusions.

Salt tectonics has played an important role in the evolution of the Willouran Trough. The salt was sourced from the Wywyana Formation and the best evidence of the timing of the salt movement shows that it occurred during deposition of the Yudnamutana Subgroup and particularly during deposition of the Tapley Hill Formation. Previous chapters showed that the structures formed at this time are D_1 in the Willouran Trough.

The majority of structures that are related to salt tectonics formed as compressional features. In the Stony Range and South Hill Diapirs, salt has facilitated movement by forming a decollement at the base of the Dome Sandstone. Above the decollement, the Dome Sandstone has been folded in to detachment folds and formed an antiformal thrust stack in the Rocky Point Sub-domain. A decollement also occurs beneath the Dome Sandstone in the Euchre Pack Domain, with the Boundary Anticline being a salt-cored anticline that formed during D_1. Movement was to the southeast and was likely facilitated by basin tilting and possibly differential loading of the Umberatana Group and may be also glaciers.

The Breaden Hill Breccia was intruded into areas of lower stress as the Fence Anticline formed during D_1. Presumably the salt was sourced from a diapir outside the plane of the outcrop. The continuation of the breccia onto the contact between the Skillogalee Dolomite and the Tapley Hill Formation was formed as a salt glacier as the salt was forced forward of the Fence Anticline. Tillite megaclasts in the breccia show that the Yudnamutana Subgroup had been deposited and lithified prior to the introduction of the salt.

Evidence from other sedimentary basins suggests that salt tectonics should have become active somewhat earlier than is apparent in the Willouran Trough, relative to the time of deposition. The main reason for the delayed onset is the Willouran Trough being an intracontinental basin and there was no free side for salt to move into. Other factors may have been that differential loading was not possible as sediments could enter the basin from any side and extension was limited in the period after deposition of the Wywyana Formation and the Wooltana Volcanics. It is also possible that the thick basalt layer could not be breached by the salt until the basin underwent a large amount of extension as the Adelaide Fold Belt changed from an intracontinental rift to a passive margin. The affect of the basalt on the underlying salt and its role in salt tectonics requires further investigation.

CHAPTER 10.
DISCUSSION AND CONCLUSIONS: THE EVOLUTION OF THE WILLOURAN TROUGH.

10.1 Introduction.

The most complete model for the evolution of the Adelaide Fold Belt was published by Preiss (1987). In this publication, the development of the Adelaide Fold Belt as a whole was discussed and in subsequent publications, Preiss (1993, 2000) provided summaries of the evolution of the Adelaide Fold Belt, modified by additional information that became available in the intervening years. Other authors who have discussed the development of the Adelaide Fold Belt include von der Borch (1980), Jenkins (1990) and Powell et al., (1994).

The concensus view is that basin growth in the Adelaide Fold Belt developed in an intracontinental rift setting some time after the end of the Musgrave Orogeny, evolving to a passive margin as a land mass drifted away in the Neoproterozoic. Most authors favour the timing of the transition to a passive margin during deposition of the Umberatana Group (e.g., Powell et al., 1994; Preiss, 2000) , although Veevers et al. (1997) and Foden et al. (2001) suggested the transition occurred at about 580 Ma. Deposition then continued to the earliest Cambrian, when a change to compression led to the development of the overlying Arrowie and Hawker Basins before sediment deposition ceased in the Late Cambrian Delamarian Orogeny. However within this concensus view there are still areas of dispute concerning the processes and timing involved. The previous chapters have considered the sedimentology and structure of the Willouran Trough, concentrating on the Curdimurka Subgroup, but extending up to the level of the Umberatana Subgroup. In this chapter, the intention is to synthesise these data and interpretations ti develop a model for the evolution of the Willouran Trough.

10.2 Prior to Initiation of the Willouran Trough.

At the initiation of the Willouran Trough, east of the Willouran Trough was a landmass which, from detrital zircon evidence presented here, was likely the South China Block (Figure 10.1: Li et al., 1999; Li et al., 2002). South of the Adelaide Fold Belt, Antarctica was attached to the southern Australian margin until the Mesozoic (Veevers et al., 1991). The Gawler Craton and the Curnamona Province were likely contiguous (Glen et al., 1977; Rutland et al., 1981). To the north was the Grenvillean Musgrave Orogeny, and there may have been a Grenvillean age orogenic belt to the east of the Curnamona Province (Wysoczanski and Allibone, 2004). Recent deep seismic surveys in northern Queensland are interpreted to show the presence of Grenvillean-age crust underlying the Palaeozoic Thompson Orogeny and yournger sedimentary basins (Korsch et al., 2009). Hence it was possible there was a Grenvillean age orogenic belt along the eastern margin of the continent (Figure 10.1). The area had been geologically stable for perhaps 150 million years, with the

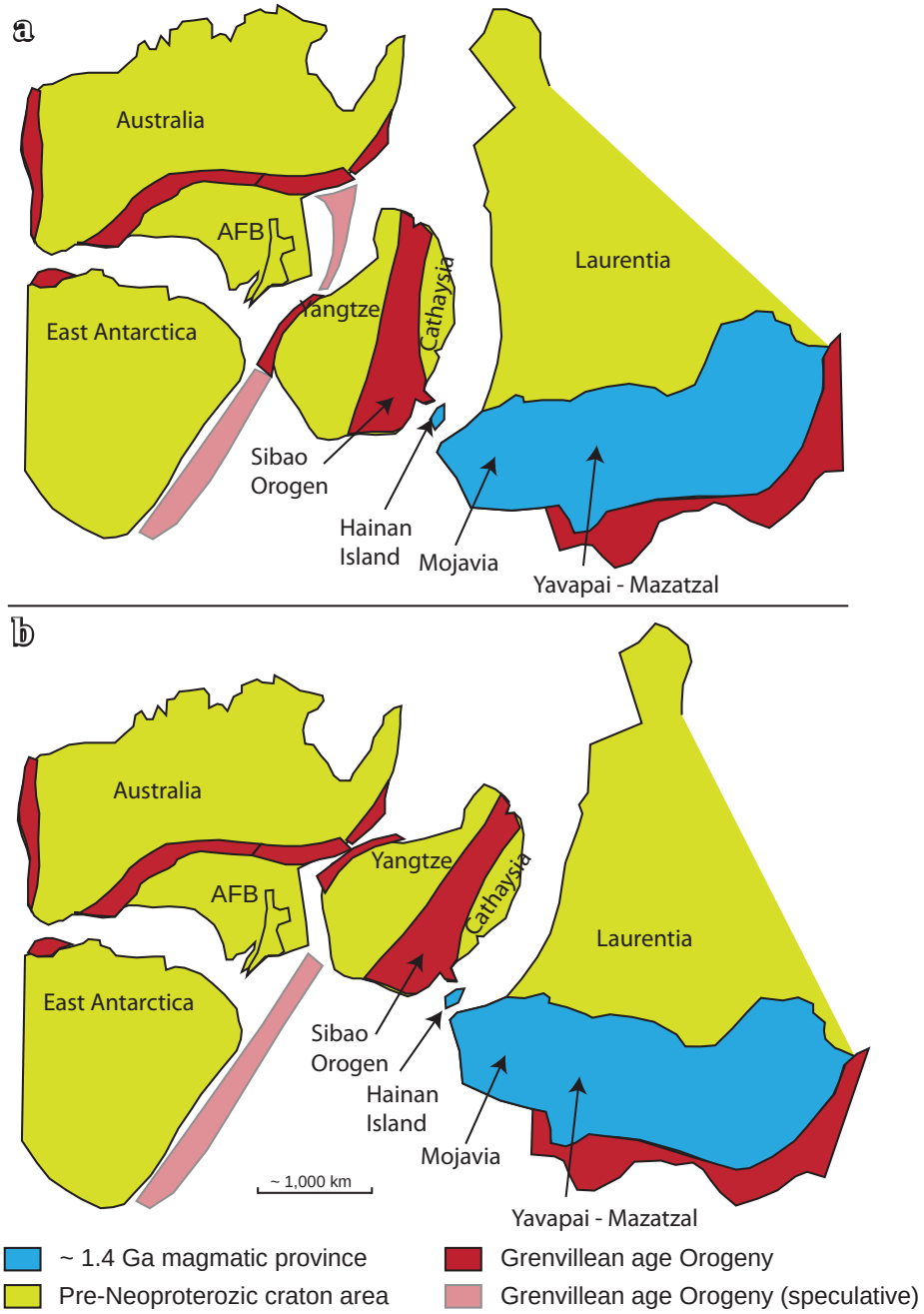

Figure 10.1. Rodinia prior to the initiation of the Adelaide Fold Belt.
a) Rodinia in the Neoproterozoic with South China adjacent to the Adelaide Fold Belt (modified from Li et al., 2002). b) In this configuration, South China is moved north, and with Laurentia rotated 20° clockwise to fit in the indent in the northeast Australian margin, and match the Grenvillean belt on it eastern edge with the Grenvillean belt on the eastern margin of Australia. Speculative Grenvillean Orogenic belts are based on Wysoczanski and Allibone (2004) and results of this study.

exception of tectonism in the South China Block between about 970 Ma and 890 Ma (Li et al., 1994; Ling et al., 2003).

10.3 Initiation of the Willouran Trough: The Callanna Group.

10.3.1 Introduction

The tectonic setting during deposition of the Callanna Group has been interpreted by the majority of authors to be an intracontinental rift (Rowlands, 1980; von der Borch, 1980;

Rutland, 1982; Jenkins, 1990; Powell et al, 1994). In the majority of these papers, there has been little differentiation between the Arkaroola and Curdimurka subgroups, when considering the initial formation of the Adelaide Fold Belt. Rowlands et al. (1980) and von der Borch (1980) suggested that initial development of the Adelaide Fold Belt had similarities to the East African Rift Valley. Hilyard (1990) suggested that the Arkaroola Subgroup was deposited in a broad sag basin prior to the eruption of the Wooltana Volcanics, and the Curdimurka Subgroup was deposited in a rift basin. Preiss (2000) arrived at a similar interpretation based on the absence of conglomerate and sedimentary breccias in the Paralana Quartzite.

10.3.2 Rift Location.

The locality of rifts may be controlled by pre-existing weaknesses and branch around stronger cratons, which include orogenic belts, mechanical anisotropy of the mantle, thermal disturbances and base lithosphere pre-existing topography (Keranen and Klemperer, 2008 and references therein). There is no indication that there was an orogenic belt or mechanical anisotropy in the area of the Adelaide Fold Belt as it is thought that the Curnamona Province and Gawler Cratons were continuous prior to rifting (Glen et al., 1977; Rutland et al., 1981). Sandiford and McLaren (2002) and McLaren et al. (2002) suggested that thermal anomalies produced by high heat producing granites that are common within the Gawler Craton and Mt Painter and Mt Babbage Inliers may have weakened the crust sufficiently to allow rifting. As was discussed in Chapter 8, there may be a high heat producing granite beneath the Willouran Trough that contributed to the location of rift nucleation.

10.3.3 The Arkaroola Subgroup.

Deposition within the Adelaide Fold Belt was initiated at some time prior to ca. 827 Ma, the age of the Gairdner Dyke Swarm and by inference (but see below) the Wooltana Volcanics (Wingate et al., 1998). The youngest detrital zircon age from the Paralana Quartzite, sampled from one metre above the basement at Arkaroola, is 1164 ± 36 Ma, giving the maximum age of formation of the northern Adelaide Fold Belt.

Coats and Blisset (1971) concluded that deposition of the Paralana Quartzite was fault controlled within a rift basin and Preiss (1987) suggested that it was deposited in an intracontinental rift. Where it crops out around the southern half of the Mt Painter Inlier, the thickness is fault-controlled, with Coats and Blisset (1971) having showed that the faulting was syn-depositional. However, except for a narrow and limited outcrop length of the Shanahan Conglomerate on the western margin of the Mt Painter Inlier (Coats and Blisset 1971), the anticipated conglomerates are absent. Based on the absence of conglomerates and sedimentary breccias, Preiss (2000) suggested that the Paralana Quartzite was deposited on a gradually subsiding peneplained stable craton and not within a rift zone. Detrital zircon ages from the Paralana Quartzite show that a proportion of the sediment was sourced from areas other than the Curnamona Province and Gawler Craton. The most likely source is the Musgave Block, which is consistent with rifting which captures a pre-existing stream

draining the Musgrave Block or a gradually subsiding peneplained craton in which there is significant transport and mixing of sediments.

Within the Willouran Trough, the presence of the Arkaroola Subgroup can only be inferred from the outcrop of the diapiric breccias sourced from the evaporitic equivalent of the Wywyana Formation. The breccias only occur within the bounds of the trough but the extent of diapirism does not necessarily correspond with the extent of the original deposition of salt. For example, in the Permian Basin of northern Europe salt diapirism occurs in the centre of the basin but thick salt units are present along southern the margin without associated diapirism (e.g., Zeigler, 1990; Scheck-Wenderoth et al.,2008). Conversely, the Louann Salt of the Gulf of Mexico shows that allochthonous salt can be transported some distance from the original site of deposition by components of lateral and vertical migration (e.g., Rowan, 1995; McBride et al., 1998; Rowan et al., 1999). The gravity model presented here suggests that salt was largely confined to the Willouran Trough, however remnants appear to extend onto the trough margins.

It is not possible to say with certainty that the Paralana Quartzite was deposited in the Willouran Trough. But if the Paralana Quartzite was deposited in a gradually subsiding basin (Preiss, 2000), it is likely to have been widespread, and if the Willouran Trough developed as a rift at this time, then it would have been deposited along the margins of the rift. Hence the Paralana Quartzite is likely present at depth and the gravity models shown in Chapter 9 assume this.

In the northern Adelaide Fold Belt, the Wooltana Volcanics crop out around the Mt Painter Inlier (Coats and Blisset, 1971). They are interpreted to correlate with the Beda Volcanics, which inter-tongue with sandstone of the Backy Point Beds, the basal unit of the Adelaidean on the Stuart Shelf (Mason et al., 1978). Mason et al. (1978) suggested on petrological grounds that the Gairdner Dyke Swarm were feeders to the Beda Volcanics. Other correlatives include the Cadlareena Volcanics in the Peake and Denison Inlier and the Wilangee Basalt in the Barrier Ranges of western NSW (Preiss, 1987). Mafic volcanic mega-clasts are also common in diapiric breccias throughout the northern and central Adelaide Fold Belt and the Nackara Arc (Dalgarno and Johnson, 1968; Preiss, 1987; Hilyard, 1990). Including the Gairdner Dyke Swarm with the Wooltana Volcanics and correlative volcanic units, Hilyard (1990) estimated that the Willouran Basic Province covered about 210,000 square kilometres. Hence they underlie at the very least, the northern three quarters of the Adelaide Fold Belt, and the occurrence of the correlative Beda Volcanics on the Stuart Shelf shows that they were not confined to possible early rifts such as the Willouran Trough.

At this point, it is not possible to conclude from the available data whether or not the Willouran Trough was a significant feature during the deposition of the Arkaroola Subgroup. However, the interpretation of the eruption of the Wooltana Volcanics and the intrusion of the Gairdner Dyke Swarm as being the result of a mantle plume (Hilyard, 1990) requires some examination of the relationship between mantle plumes and rifting, and may help in understanding the early development of the Willouran Trough.

10.3.4 The Willouran Basic Province: Its role in the development of the Willouran Trough.

The term Willouran Basic Province was first introduced by Crawford and Hilyard (1990) and Hilyard (1990). It comprises the Wooltana Volcanics, correlative volcanic units, and the Gairdner Dyke Swarm, and was interpreted by to have resulted from a mantle plume (Crawford and Hilyard, 1990; Hilyard, 1990). Zhao et al. (1994) concluded from geochemical data that the Gairdner Dyke Swarm and the coeval Amata Suite in the Musgrave Block formed from the decompressional melting of a large-scale mantle plume. In Australia, the diameter of the plume is in excess of 1,000 km, from the Adelaide Fold Belt to the central Australia. They suggested that the plume may have been responsible for large-scale crustal extension and thinning, leading to the formation of the Centralian Superbasin (Zhao et al., 1994). Von der Borch (1980), Zhao et al. (1994), and Williams and Gostin (2000) placed the plume head below a postulated triple point centred in the vicinity of Leigh Creek. Li et al. (1999) suggested that the break-up of Rodinia was initiated by a mantle plume beneath South China, which they placed adjacent to the Adelaide Fold Belt at this time (Figure 10.2). Mafic and ultramafic intrusives in South China have been dated at 828 ± 7 Ma (Li et al., 1999), the same age as the Gairdner Dyke Swarm (Wingate et al., 1998).

A mantle plume originating from the core – mantle boundary will have a head with a final diameter of about 1,000 km, which at the top of its ascent flattens, forming a disc with a diameter about twice the size of the head (Campbell and Griffiths, 1990). A broad dome may develop over the plume head, with a maximum elevation of about 1,000 to 1,500 m and a diameter of 1,000 – 1,500 km (Griffiths and Campbell, 1991; Campbell, 2001; Sengor, 2001). Uplift begins 20 – 30 Myr prior to volcanism (Campbell, 2007) and evidence from East Greenland (Dam et al., 1998; Ukstins Peate et al. 2003) shows that in a marine environment, there will be a shallowing upward and eventual removal of sediments prior to the onset of volcanism. Hence, if the North Adelaide Fold Belt was subject to doming, a thin Paralana Quartzite deposited as a veneer across a peneplain would likely be removed as the dome developed. However it is preserved in the Arkaroola area which suggests that it was deposited in an area undergoing subsidence as the area as a whole is being domed.

Apical extensional zones may develop over the plume head as the rising crust produces extension perpendicular to the dome (Burke and Dewey, 1973; Sengor, 1995; Sengor, 2001). Therefore if the mantle plume was centred below the northern Adelaide Fold Belt (von der Borch, 1980; Zhao et al., 1994, Williams and Gostin 2000), the Willouran Trough may have formed as an apical extensional zone. Furthermore the margin of the dome would extend to the Officer Basin in the west, and the Amadeus Basin to the north (Figure 10.2a, 10.3a). Lindsay (2002) concluded that the Centralian Superbasin was initiated as a thermal sag basin above a mantle plume beginning about 900 Ma. If the plume was situated below the Northern Adelaide Fold Belt, these basins may have formed as a result but at the margins of the domal uplift and not as a result of thermal decay as proposed by Lindsay (2002). Sengor (2001) suggests that a sag basin may form above the plume head prior to the main period of uplift as mantle lithosphere becomes detached, entraining a part of the overlying

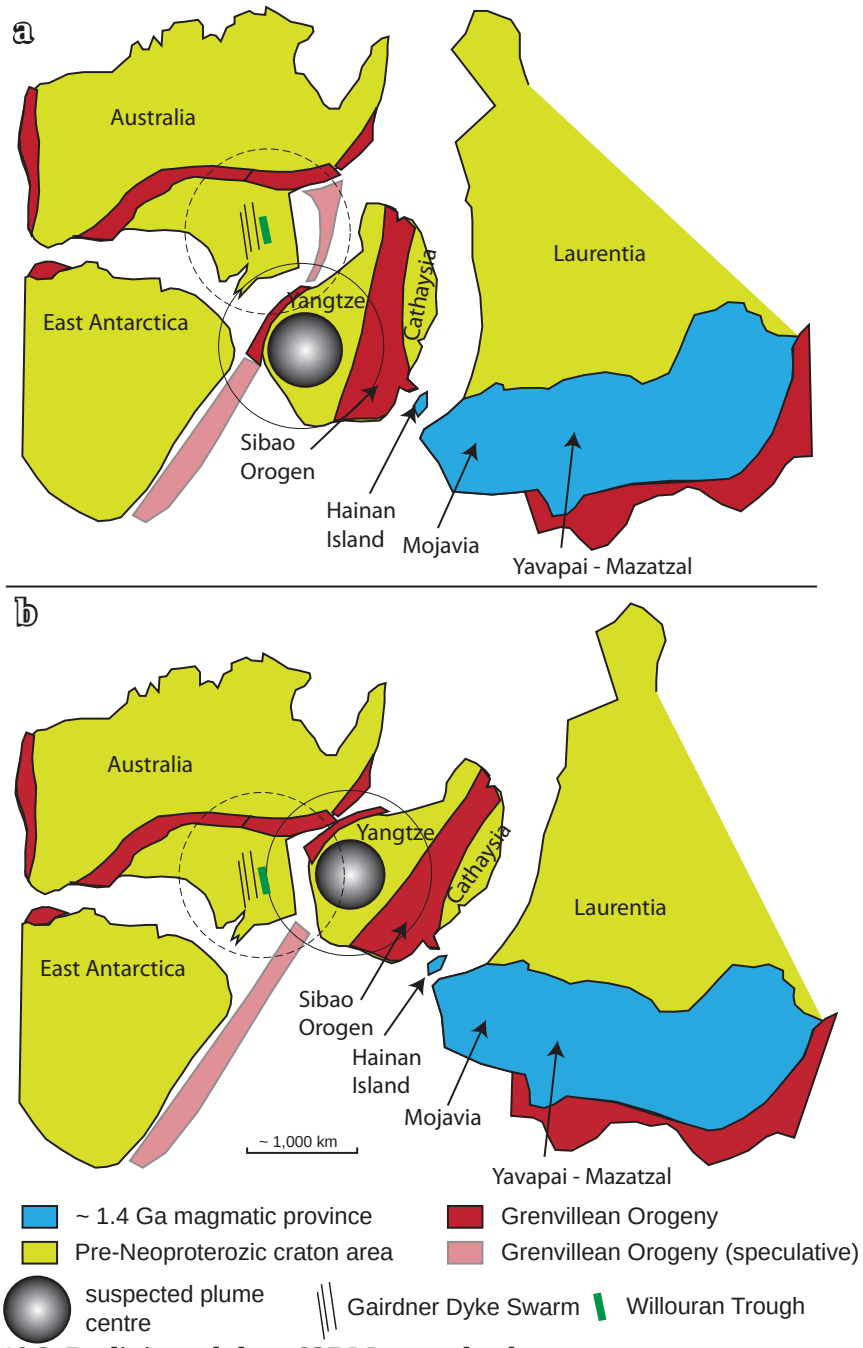

Figure 10.2. Rodinia and the ~ 827 Ma mantle plume.
The position of the centre of the mantle plume is based on Li et al. (2003). The solid circle is 1,500 km in diameter, centred on the mantle plume. a) If the mantle plume was centred in South China in a position south of Australia, it would be too far away to influence the Centralian Superbasin, and if centred on the northern Adelaide Fold Belt, it would not influence South China. b) With South China east of Australia, a mantle plume centred there would influence the northern Adelaide Fold Belt and vice versa.

crust. However the dimensions of such a sag basin are hundreds of kilometers and not of the same scale as the Centralian Superbasin (Sengor, 2001).

Li et al. (1999, 2003) place South China to the southeast of the Adelaide Fold Belt at about 800 Ma and suggest that the Gairdner Dyke Swarm is radial to the plume centre (Figure 10.2a). Dyke swarms are not necessarily radial to the plume centre but can intrude along pre-existing weaknesses (Mege and Korme, 2004) or, if there are existing far-field

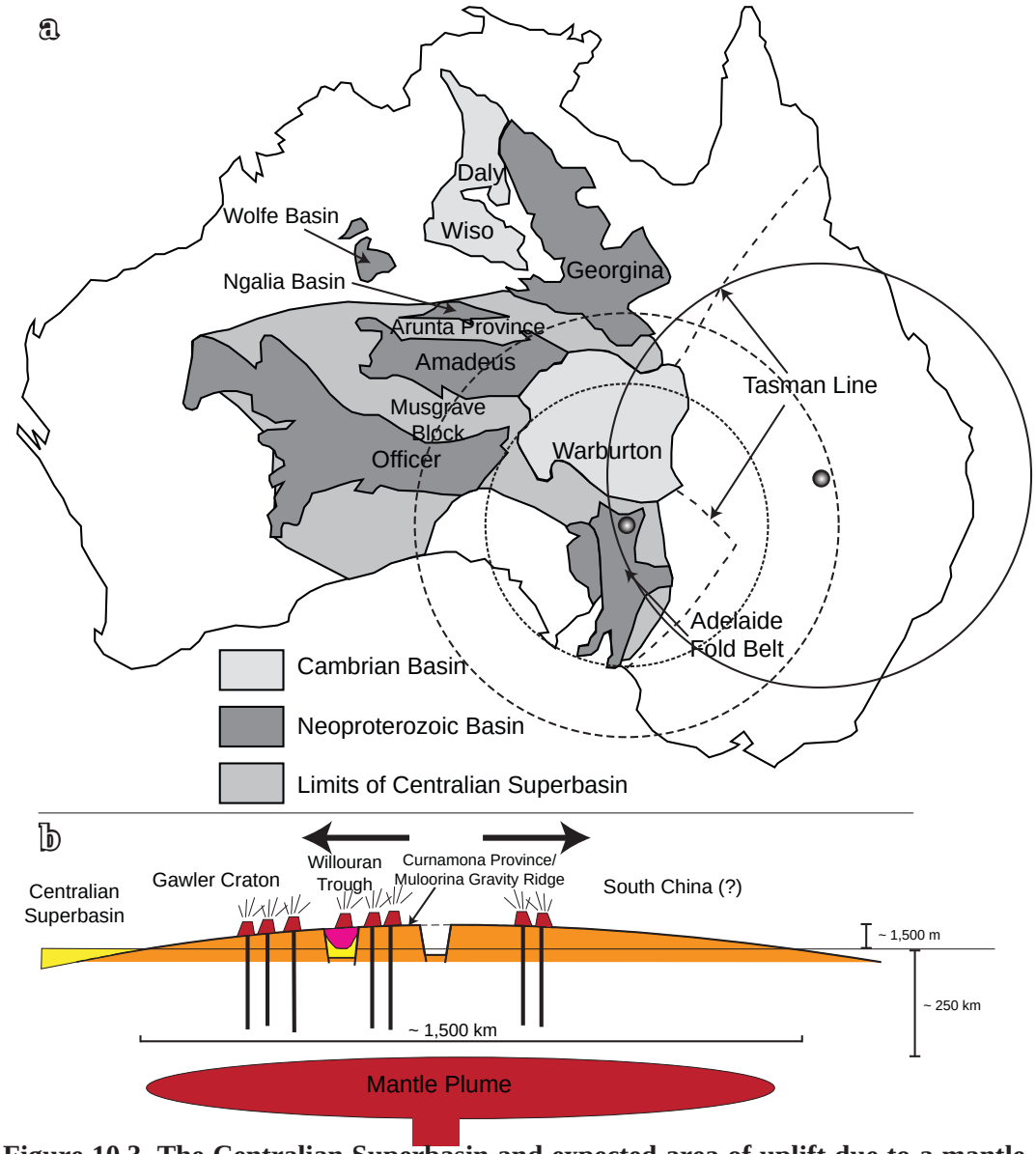

Figure 10.3. The Centralian Superbasin and expected area of uplift due to a mantle plume.

a) The Centralian Basin with a 1,500 km diameter circle centred on a mantle plume in South China (solid circle). Two other mantle plume positions are shown; centred on the northern Adelaide Fold Belt with a 1,000 km dome (inner dashed circle) and a 1,500 km dome (outer dashed circle). b) Diagrammatic cross-section across the area of doming associated with a mantle plume centred east of the Willouran Trough.

extensional stresses, they may intrude perpendicular to that stress direction (Hooper, 1990; Campbell, 2001; Menzies et al., 2001). Therefore, if the Willouran Trough has already been initiated by far-field extension, the geometry of the Gairdner Dyke Swarm may reflect this stress regime rather than tensional forces localized about a plume head. If the plume was centred as shown in Figure 10.2a, it may be too distant from the Northern Adelaide Fold Belt to have any influence on the development of the Centralian Basin. However, given the alternative position for South China given in Li et al. (1999) to the east of the Northern Adelaide Fold Belt, the plume would have been centred east of the Curnamona Province, and thus sufficiently close to the northern Adelaide Fold Belt to influence its development (Figure 10.2b).

10.3.5 The Curdimurka Subgroup.

10.3.5.1 The Dome Sandstone.

Deposition of the Curdimurka Subgroup in the Willouran Trough occurred after the eruption of the Wooltana Volcanics, but the area was likely still under the influence of a mantle plume. The area of the plume head may undergo subsidence after the eruption of flood basalts or as the over-riding plate moves away from the plume (Campbell, 2001; Sengor, 2001). There are two phases of subsidence; rapid subsidence above the plume head related to extraction of melt from the mantle, and gradual subsidence as the thermal anomaly declines (Campbell, 2001). The rapid subsidence leads to deposition of clastic deposits in canyons and alluvial fans radiating away from the apical zone (e.g., Dam et al., 1998; Xu et al., 2004). The Dome Sandstone shows no evidence of having been deposited in a period of rapid subsidence, with about 1,400 m being deposited in about 25 M yrs, based on the bracketing ages of the Gairdner Dyke Swarm (Wingate et al., 1998) and of the Rook Tuff (Fanning et al., 1986). Therefore the Willouran Trough was likely not directly over the plume head.

As rapid subsidence over the plume head can be ruled out, the tectonic environment of deposition of the Dome Sandstone may have been;

- a sag basin in the thermal relaxation phase of the mantle plume (Griffiths and Campbell, 1991; Campbell, 2001; Sengor, 2001).
- a rift basin in the fault linkage stage (Gawthorpe and Leeder, 2000), with the rift having formed earlier, either in a single phase beginning with deposition of the Arkaroola Subgroup or rifting was initiated after the eruption of the Wooltana Volcanics and this early stage is not seen.

As was noted in Chapter 3, the conglomerates and sedimentary breccias expected to occur in a basal rift sandstone are absent but that may be because the edges of the basin are not seen, and the outcropping sandstone may be from near the centre of the basin. The thickness of the Dome Sandstone appears not to vary significantly along the Stony Range Domain. In the South Hill Domain, the Dome Sandstone is interpreted to gradually thicken from the southwest to the northeast. Greater thickness variation is expected if it was deposited in the early stages of a rift basin, that is before it had reached the fault-linkage stage of Gawthorpe and Leeder (2000). Instead it appears to have a sheet-like form, which could be attributed to deposition within a thermal sag basin or the fault linkage stage, where the observed outcrop is parallel to the controlling normal faults. A third option is that deposition of the Dome Sandstone occurred within a half graben, and the continuous outcrop seen in the Stony Range Domain is due to this being the hinge zone of a half graben. The controlling normal fault of the half graben is therefore on the opposite side of the trough, adjacent the Muloorina Gravity High (Figure 10.4a). As both the Dome Sandstone and the Curdimurka Subgroup as a whole thicken to the northeast, this third option is preferred.

The Dome Sandstone was deposited in a continental environment. Detrital zircon ages show that the rift zone was well developed and sourcing sediment from the Musgrave Block by well-developed axial drainage, although transverse drainage was dominant at this time (Figure 10.4b). It was likely a closed basin, isolated from the Central Adelaide Fold Belt by uplift along the Paralana Fault Zone

10.3.5.2 Middle and upper stratigraphic levels of the Curdimurka Subgroup.

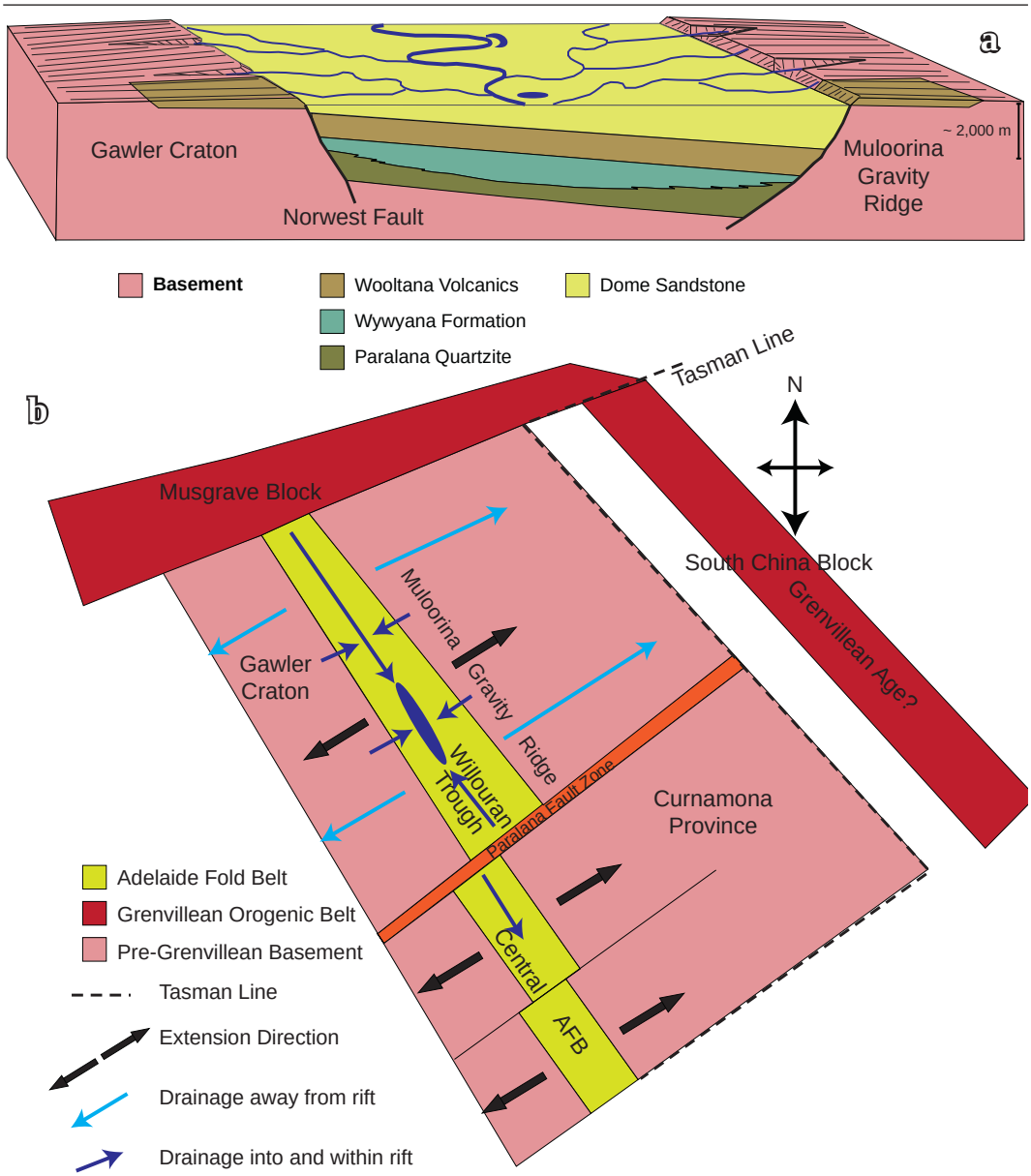

Figure 10.4. The Willouran Trough during deposition of the Dome Sandstone.
a) Oblique view of the Willouran Trough showing the Dome Sandstone was deposited in a half graben controlled by a normal fault adjacent the Muloorina Gravity Ridge. Wooltana Volcanics outcrop on the shoulders of the rift.
b) Plan of the Willouran Trough and Central Adelaide Fold Belt showing the regional context. Uplift on the shoulders of the rift provides transverse drainage into the basin but most drainage is directed away. Axial drainage is well developed, delivering sediment from the Musgrave Block. The Paralana Fault Zone is likely an area of positive relief, isolating the Willouran Trough from the Central Adelaide Fold Belt.

Above the Dome Sandstone, 4,000 m thick of a siltstone dominated package, deposited in about 25 Myrs, is preserved in the Euchre Pack Domain. Although there is some variation in depositional setting from below wave-base to emergent, overall the setting remained shallow marine for most of this time, suggesting that the supply of sediment kept pace with subsidence. Sedimentological changes are gradual, indicating gradual subsidence, with three significant transgressions marked by the deposition of black shale; the Rook Tuff, the top of the Recovery Formation and the black shale facies of the Boorloo Siltstone.

It is unclear whether a depositional history similar to that recorded in the Euchre Pack Domain occurred in other parts of the Willouran Trough. While elements of the stratigraphy are preserved in the Witchelina, Stony Range and Rischbeith domains, (principally a lower sandstone sequence with local presentations of carbonate and shale at higher levels), the Curdimurka Subgroup in the area is complexly deformed and less completely preserved.

There are four possibilities to explain the greater thickness of the Curdimurka Subgroup in the Euchre Pack Domain relative to the Stony Range and South Hill Domains;

- It is an original deposition feature with a gradual deepening of the basin to the northeast (Figure 10.5a);
- It is an original depositional feature but with a distinct deeper sub-basin in the northeast (Figure 10.5b);
- It is structural with the upper Curdimurka Subgroup being removed by faulting in the centre to southwest (Figure 10.5c);
- It is erosional, with the upper part of the Curdimurka Subgroup being removed by erosion in the southwest (Figure 10.5d).

A gradual deepening of the basin to the east would form the basis for the interpretation of a half-graben with a controlling fault on the eastern side and a hinge line at about the position of the Norwest Fault (Figure 10.5a). Movement on the Norwest Fault would be minor. Evidence from the preserved lithological variations from the Rocky Point Sub-domain, the Rischbeith Domain and the Euchre Pack Domain, also suggests deepening to the northeast.

Evidence for the first possibility may also be applied to the second listed, and so it may not be possible to distinguish between them. Faulting controlling the sub-basin would cut through the Dome Sandstone and there is no evidence of this across the South Hill Domain. Therefore if a sub-basin did develop, the fault zone on the northern margin of the South Hill Domain may have been the western margin of a small sub-basin, re-activated as the West Willouran Fault Zone.

A structural interpretation of the distribution of the upper Curdimurka Subgroup requires it to have been removed by faulting. One scenario would be a single low-angle fault dipping to the southwest cutting through the Curdimurka Subgroup from the top of the Boorloo Siltstone in the northeast to the top of the Dome Sandstone in the southwest (Figure 10.5c).

A similar style of faulting is seen in the Euchre Pack Domain, where the Eastern Fault Zone brings the Burra Group into contact with the Dunns Mine Limestone over a few kilometres. However, the direction of movement on that fault is to the southeast and not southwest.

In the final scenario the upper Curdimurka Subgroup is removed by erosion (Figure 10.5d). To achieve this scenario a two step process is needed. In the first, reverse movement occurs on the Norwest Fault, lifting the upper Curdimurka Subgroup above baselevel and it is therefore eroded. This would need to occur prior to deposition of the Emeroo Subgroup. In the second step, the Emeroo Subgroup is deposited in a half-graben with the bounding normal fault adjacent the Muloorina Gravity Ridge (see Section 10.4 for discussion on the Burra Group). The eroded material would therefore be re-deposited in the Emeroo Subgroup. Although the second step of this scenario is interpreted to occur, there is no evidence for reverse faulting prior to deposition of the Burra Group. Hence, this possibility is also rejected. To conclude, of the four options given for the distribution of the stratigraphy of the Curdimurka Subgroup, only the first two are possible. Here the simplest explanation is favoured, that the stratigraphic distribution is an original depositional feature, and the

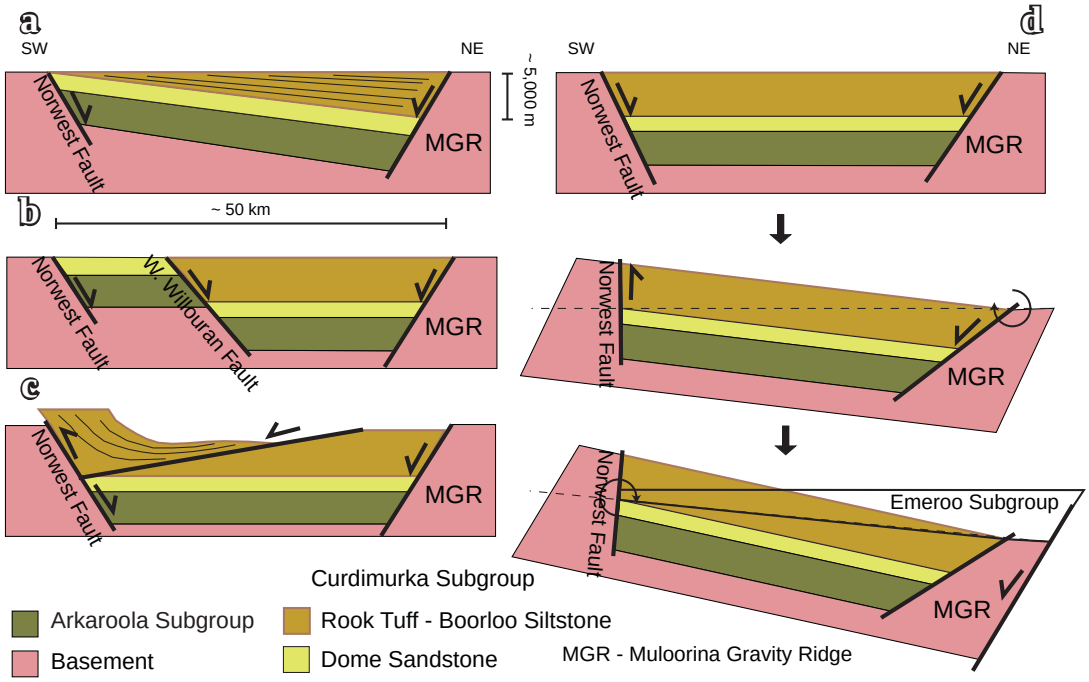

Figure 10.5. Four possibilities to explain the distribution of the Curdimurka Subgroup in the Willouran Range, with only the Dome Sandstone present adjacent the Norwest Fault to a full thickness of about 6,000 m in the NE adjacent the Muloorina Gravity Ridge.

a) The upper Curdimurka Subgroup (Rook Tuff to Boorloo Siltstone is deposited in a half graben. b) The upper Curdimurka Subgroup is deposited within a sub-basin on the eastern side of the Willouran Trough. c) A full thickness of the Curdimurka Subgroup is deposited but a low-angle normal fault dipping SW develops. The strata in the hanging wall move to the southwest but impeded by the Norwest Fault they can only move upward, and hence are eroded. d) To remove the upper Curdimurka Subgroup by erosion, first the basin is tilted to the NE about a centre of rotation in the NE by reverse movement on the Norwest Fault, lifting the western part of the Curdimurka Subgroup up for it to be eroded. Then normal movement on a basin-bounding fault adjacent the Muloorina Gravity Ridge about a hinge line near the Norwest Fault creates accommodation space in which the Emeroo Subgroup is deposited.

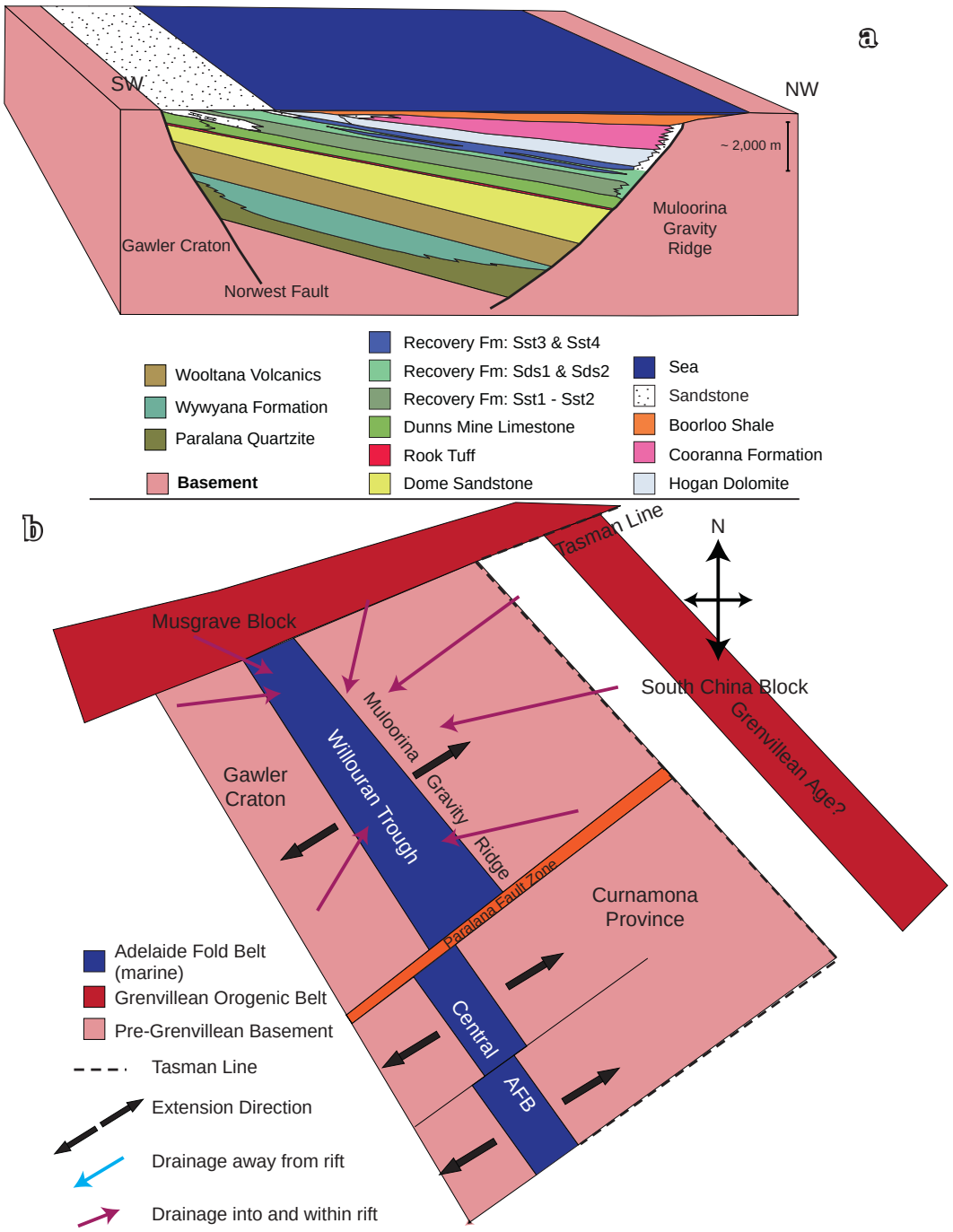

Figure 10.6. The Willouran Trough during deposition of the Boorloo Shale.
a) Cross-section of the Willouran Trough showing it continued to develop as a half graben, controlled by the normal fault against the Muloorina Gravity Ridge. The southwestern side of the trough was a hinge zone.
b) Plan view showing the regional context. The ocean has invaded the trough, creating a long, narrow gulf. The Paralana Fault Zone is likely still a positive feature, limiting transport of material between the Willouran Trough and Central Adelaide Fold Belt. Drainage has extended beyond the margins of the trough, sourcing a wide area.

Curdimurka Subgroup as a whole was deposited within a half graben controlled by subsidence on a fault adjacent the Muloorina Gravity Ridge (Figure 10.6a). It is a continuation of the interpretation of deposition of the Dome Sandstone and in the absence of evidence to the contrary, or evidence in favour of the other possibilities it is preferred.

Regionally, the northern Adelaide Fold Belt was undergoing continued northeast - southwest directed extension (Figure 10.6a). However by the time of deposition of the RSst2 unit, sediment was being transported from a wider area, although the margins of the rift were still exposed. Figure 10.6a and b are drawn for the period of deposition of the Boorloo Shale and show the area covered by a sea that extends a short distance onto the Muloorina Gravity Ridge, with the shoulders of the rift now covered.

10.4 The Burra Group

The Burra Group was deposited in a second extensional phase of the Willouran Trough. Over the period of about 50 Myrs (~ 777 to ~ 725 Ma), more than 6,000 m of sediments were deposited in the Willouran Trough, deposition rates similar to that of the Curdimurka Subgroup in the Euchre Pack Domain.

From Belperio (1990) thickness variations across the Willouran Range may indicate that initially the eastern fault was more active during deposition of the Emeroo Subgroup, with the Norwest Fault becoming the dominant fault during deposition of the Skillogalee Dolomite and Myrtle Springs Formation. However forward modelling of gravity data in Chapter 8 showed that the geometry of the top of the basement on the northeastern margin of the Willouran Trough dips at a moderate angle to the southwest. This geometry is not consistent with a steep normal fault as would be expected of a major basin-bounding fault. Instead the Burra Group, including the Emeroo Subgroup is interpreted to on-lap the Muloorina Gravity Ridge, which would be consistent with the Norwest Fault being the main basin-bounding fault throughout the period of deposition of the Burra Group (Figure 10.7). More detailed structural and sedimentological mapping of the Burra Group throughout the Northern Adelaide Fold Belt is necessary to understand the tectonic setting and controls on its deposition.

At this time extension continued to be northeast - southwest directed but was over an increasing area (Figure 10.7b). Normal faulting extended onto the Torrens Hinge Zone (Figure 10.7a, b: Preiss, 1987) and in the northern Adelaide Fold Belt the Norwest Fault remained the dominant extensional structure (Paul, 1999). From the gravity model, the Torrens Hinge Zone formed the shoulder to the Willouran Trough, on-lapped by the Burra Group. The mechanism causing the renewed rifting is unclear. It was not restricted to the Willouran Trough with the Burra Group being widespread throughout the Adelaide Fold Belt. In the southern Adelaide Fold Belt, the Burra Group was deposited directly on the basement (Preiss, 1987). Across the Adelaide Fold Belt the thickness of the Burra Group varies considerably, reaching over 6,000 m in the Willouran Trough, the Nackara Arc and the Southern Adelaide Fold Belt (Preiss, 1987). Hence there is nothing unusual in the thickness of the Burra Group in the Willouran Trough and no need to apply mechanisms that are specific to that area such as salt tectonism (e.g. Preiss, 1987; Dyson, 2002; 2005).

The most unusual feature of the Burra Group in the Willouran Range is the northwest-directed extension implied in the Trial Hole Domain. Several authors have suggested that

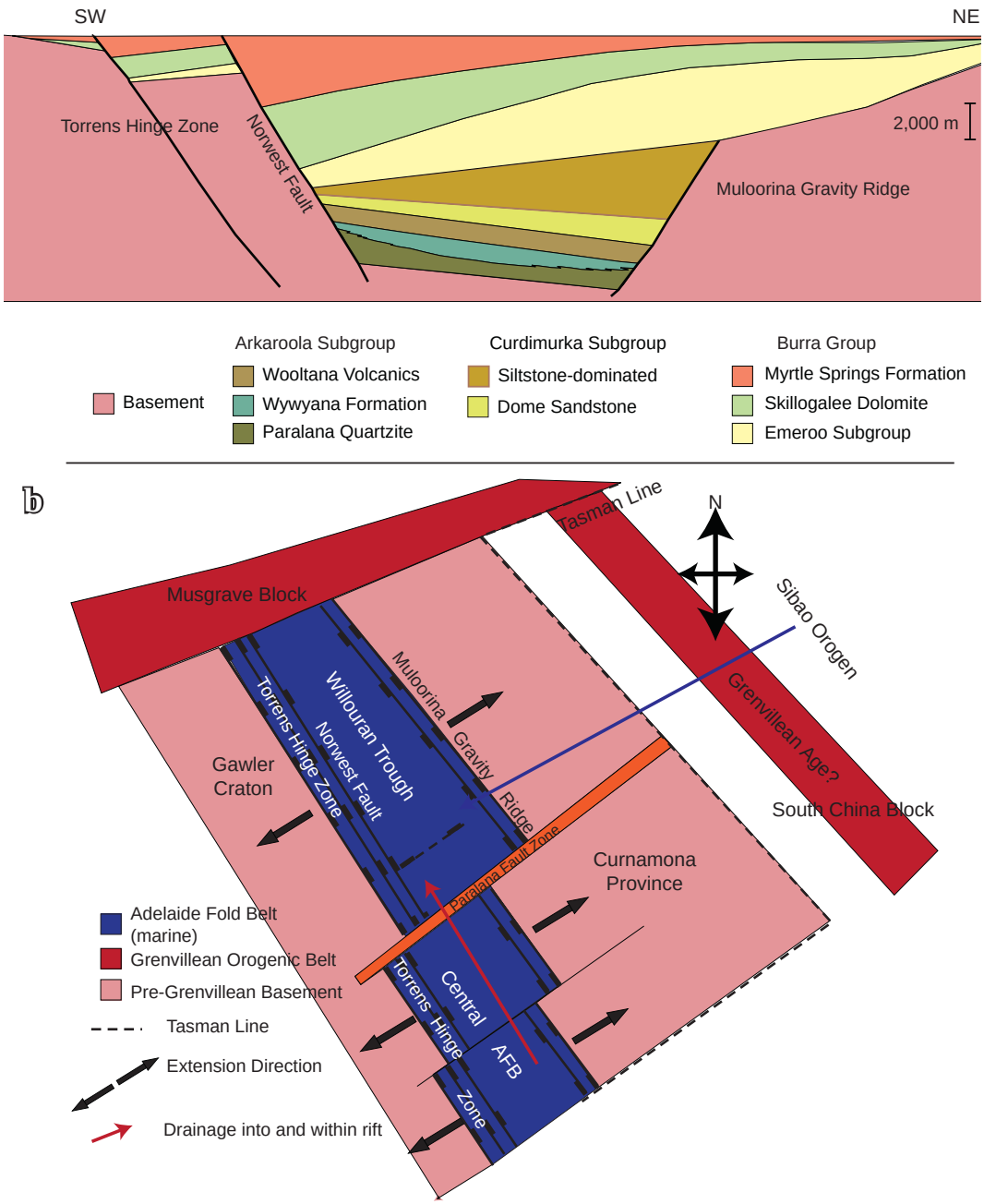

Figure 10.7. The Burra Group.
a) Cross-section of the Willouran Trough. Burra Group unit thicknesses are based on Belperio (1990). They are interpreted to show that during deposition of the Emeroo Subgroup, deposition was controlled by movement on the NE margin. The movement switched to the Norwest Fault at about the time of the start of deposition of the Skillogalee Dolomite.
b) Plan view showing the regional context. NE - SW directed extension continued, with faulting extending to the Torrens Hinge Zone. For the first time, the Central Adelaide Fold Belt was connected to the Willouran Trough, allowing Musgrave Block age zircons to move south of the Paralana Fault Zone. Zircon detrital age data also suggests sediment sourced from the South China Block.

deposition of the Burra Group in the Willouran Trough was influenced to greater or lesser degrees by diapirism. Preiss (1987) suggested that it was deposited in a peripheral sink to the Witchelina Diapir. Dyson (2002, 2005) concluded that the Burra Group in the Trial Hole Domain was deposited between rising salt walls in the Euchre Pack Domain and the Witchelina Domain. Belperio (1990) concluded that diapirs formed along the major

northwest-trending faults, dividing the Willouran Trough at this time into a series of sub-basins to explain the thickness variations. This interpretation is largely rejected in this study. An on-lap surface is mapped from aerial photography interpretation at the top of the Emeroo Subgroup on either side of the Witchelina Domain and south of the Euchre Pack Domain. It is interpreted to result from some upward doming of the underlying stratigraphy, perhaps forming a turtle structure but above and below this level, there appears to be little variation in bed thickness.

The 797 ± 5 Ma age that Drexel (2009) attributes to the deposition of the Skillogalee Dolomite, based on his interpretation of a zircon U-Pb age from an intrusive igneous rock at the Burra mine is rejected here. One inference from that age is that it correlates with the Rook Tuff, dated at 802 ± 10 Ma (Fanning et al., 1986), but field studies presented here show that this is not the case. A second option, that both units dated are intrusive, and therefore both the Skillogalee Dolomite is older than 797 Ma, making the Curdimurka Subgroup somewhat older than that (but younger than the 827 ± 6 Ma age of the Gairdner Dyke Swarm (Wingate et al., 1998), and by correlation the Wooltana Volcanics (Hilyard, 1990). However, this interpretation is also rejected on the basis of volcanic rocks of the Oodla Wirra Volcanics in the Mt Grainger Diapir being dated at 798 ± 5 Ma, and 799 ± 4 Ma (Fabris et al., 2005). These volcanic rocks are therefore of the same age as the Rook Tuff and the dated igneous intrusive within the Skillogalee Dolomite, and occur as megaclasts within a diapiric breccia. Hence it is suggested that Drexel (2009) has wrongly interpreted the field relationships of the dated rocks at the Burra mine, and that they are clasts with a diapiric breccia that has intruded the Skillogalee Dolomite.

10.5 D_1 and Deposition of the Umberatana Group.

Deposition of the Burra Group ended prior to about 720 - 700 Ma, based on correlation of the Yudnamutana Subgroup with other Sturt glaciogenic units that have been dated (Brassier et al., 2000; Allen et al., 2002; Kilner et al., 2005). Paul et al. (1999) showed that the depocentre in the northern Adelaide Fold Belt moved from the Willouran Trough eastward to the Yudnamutana Trough during deposition of the Lower Umberatana Group (Figure 10.8). The Yudnamutana Trough is a west-northwest trending depositional trough in which up to 6,700 m of the Yudnamutana Subgroup was deposited (Preiss, 1993). Preiss (1987) divided the Sturt glaciogenic sediments into younger and older, with the older being deposited primarily in the Yudnamutana Trough and the younger being much more widespread, including in the Willouran Range. Hence at the time of deposition of about 6,000 m in the Yudnamutana Trough, the Willouran Range was an area of non-deposition, with uplift and erosion in the east, i.e., nearer the Yudnamutana Trough.

The main features of the Willouran Trough during deposition of the Umberatana Group are shown in Figure 10.9. At depth, the Curdimurka Subgroup has been thickened by folding and thrusting (Figure 10.9a). The Euchre Pack and Rischbeith Domains, and the Rocky Point Sub-domain are aligned and interpreted to be part of the same structure. In the South Hill Domain, the Curdimurka Subgroup has been thrust to the northwest, over the Burra

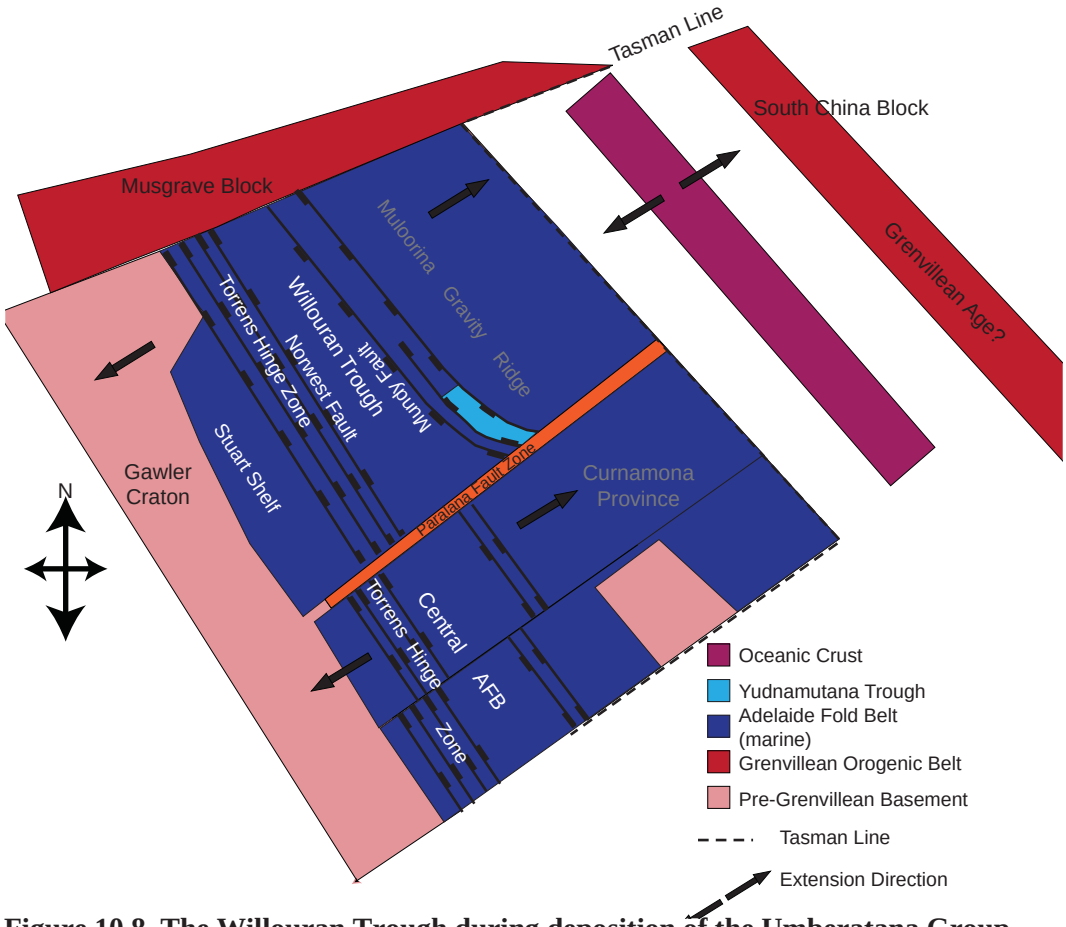

Figure 10.8. The Willouran Trough during deposition of the Umberatana Group. At this time, the South China Block began to move away from Australia. It was the initial time that the ocean moved onto the undeformed cratonic areas of the Gawler Craton and the Curnamona Province. The Yudnamutana Trough opened adjacent the Muloorina Gravity Ridge. Dextral strike-slip movement along the Paralana Fault Zone rotated the southern end of faults anti-clockwise, giving the WNW trend of the Yudnamutana Trough.

Group (Figure 10.9a). In the Berlina Domain the Burra Group is folded, with inclined folds verging to the southeast whereas in the Trial Hole Domain it has been divided into fault-bounded blocks with Curdimurka Subgroup between the blocks. The Umberatana Group above the Yudnamutana Subgroup reaches several thousand metres thickness in the Trial Hole Domain whereas in the Berlina and Kingston Domains, it is less than 1,000 m thick, and the Tapley Hill Formation in particular is considerably thinner than in either the Trial Hole or West Mount Domains. Also its outcrop is restricted to areas in front of D_1 folds in the Curdimurka Subgroup (Euchre Pack Domain) or Myrtle Springs Formation (Berlina and Kingston Domains).

Regionally at this time the overall tectonic regime is interpreted to be extensional (Figure 10.8: e.g., Preiss, 1987; Powell et al., 1994; Paul et al., 1999; Preiss, 2000). Most authors consider this to be the time of transition from a rift to a passive margin in the Adelaide Fold Belt (Preiss, 1987; 2000; Powell et al., 1994). However the majority of structures mapped in the Willouran Range are compressional, including in the Euchre Pack Domain where the development of the extensional Central and Eastern Fault zones are attributed to gravitational instability in the hinge of a developing detachment anticline. Therefore the

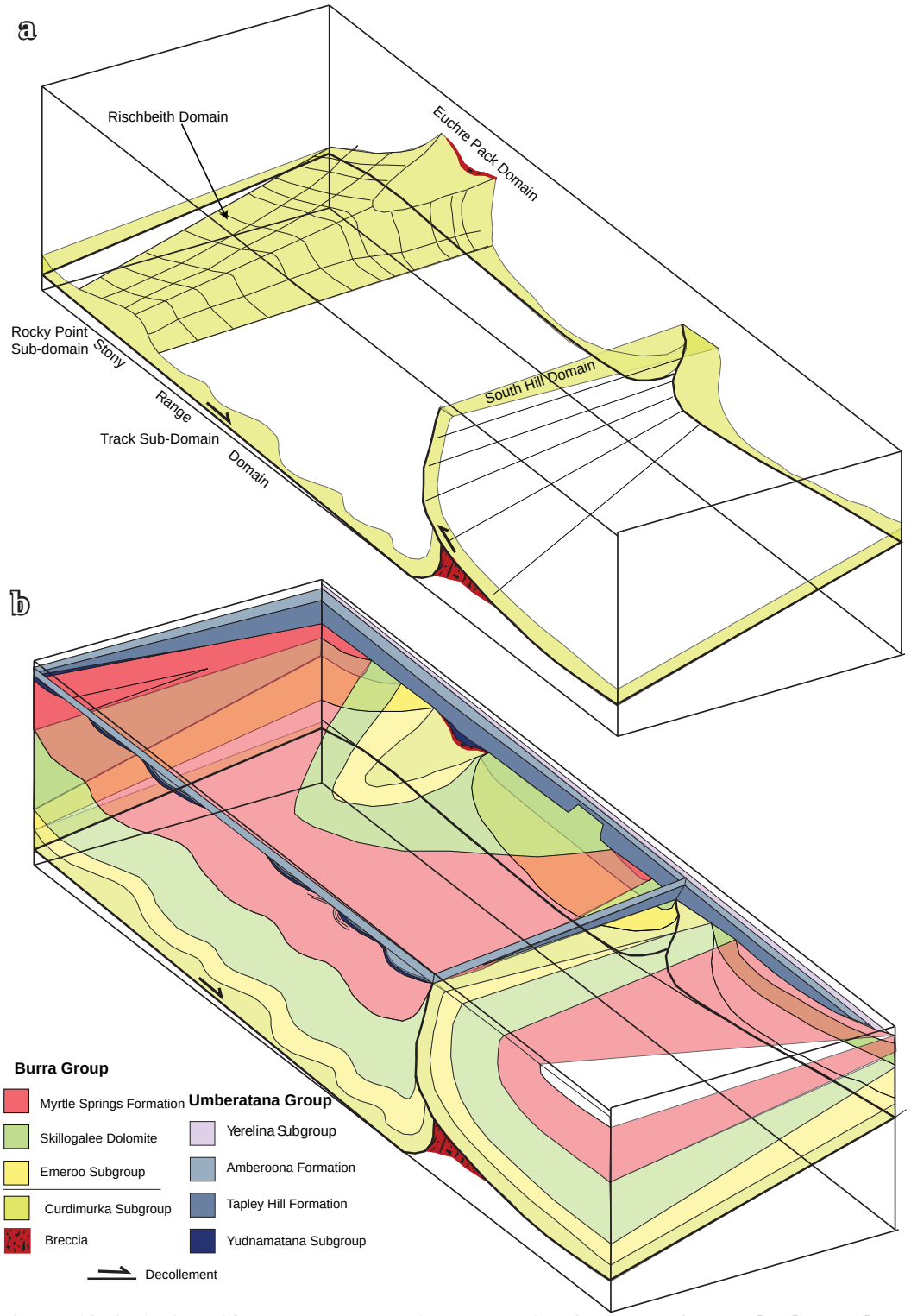

Figure 10. 9. A simplified cartoon showing the major features of D_1 and relationships between structures between the NE and SW margins of the Willouran Trough.
a) The effect of D_1 on the Curdimurka Subgroup, emphasising the relationship between the Rocky Point Sub-domain, the Rischbeith and Euchre Pack Domains. b) A simplified block diagram showing the structural and stratigraphic variations across the Willouran Trough. Whereas the Burra Group is intact on the SW side of the trough, on the NE it has been divided into fault-bound blocks. Uplift in the NE has removed the Burra Group. On the NE side, the Umberatana Group reaches several thousand metres in thickness whereas in the centre and SW, it is less than 1,000 m thick and restricted to small areas adjacent D_1 folds.

development of D_1 compressional features need to be placed within a regional extensional setting.

Fold and thrust belts are developed on passive margins on the west African coast, where they are attributed to both salt tectonics and downslope movement of over-pressured delta-fan sediments, and the Gulf of Mexico, where they are attributed to salt tectonics. In the Gulf of Mexico and the west African Kwanza Basin, the decollement is a salt layer whereas in the Niger delta region of west Africa (Morley and Guerin, 1996; Corredor et al., 2005), gliding is caused by overpressure in purely brittle siliciclastic sediments (Mourgues and Cobbold, 2006). These all occur on passive margins, with the fold and thrust belt verging toward the basin centre. At the time of D_1, the Adelaide Fold Belt is interpreted to be in transition from a rifted to a passive margin (Preiss, 1987; 2000; Powell et al., 1994) but the Willouran Trough is interpreted to be within the continental margin (i.e., the continental margin is beyond the Muloorina Gravity Ridge and the Curnamona Province: Figure 10.8). Furthermore the folding and thrusting verge between parallel to oblique but away from the basin centre. The Central Graben of the North Sea provides an example of compressional structures forming in an extensional environment, in a basin with no open side, similar to the setting of the Willouran Trough. Here folding is interpreted to be caused by gravity sliding above a salt layer. Normal faulting within the basement below the basin tilts the basin with the rock mass sliding towards the area of faulting, with folding verging in that direction (Stewart and Coward, 1995). This model is interpreted to apply in the Willouran Trough during D_1.

In map view, folding verges to the southeast but the plunge of F_1 folds indicates that there is a component of out of section movement toward the southwest, and their pre-D_2 vergence is interpreted to be between the south to southeast. Folds and faulting verge toward the Norwest Fault and the South Hill Structure, which is interpreted to be underlain by a basement high. Compressional deformation is balanced by extensional movement upslope of the fold and thrust belt (Figure 10.10). For the Willouran Trough, this would be to the north to northwest. In the extensional areas, a large thickness of Yudnamutana Subgroup to Tapley Hill Formation sediments would have been deposited. Northwest to north of the Willouran Range these strata are under-cover but the interpretation of the aeromagnetic data suggests a greater thickness of Umberatana Group, including the Yerelina Subgroup, than in the Willouran Range, and to the north may be an extension of the Yudnamutana Trough. The inferred vergence of the folding is roughly in the extensional direction of the Yudnamutana Trough, further indicating a link between its development and D_1 as seen in the Willouran Range.

10.6 The Wilpena Group.

In the Willouran Range, there are no Wilpena Group sedimentary rocks preserved and it is not clear whether any were deposited at all. There is no evidence of erosion of the Umberatana Group; it's upper contacts within the the Berlina and Kingston Domains are tectonic. However the Wilpena Group was deposited in the Trial Hole, Delusion Hill

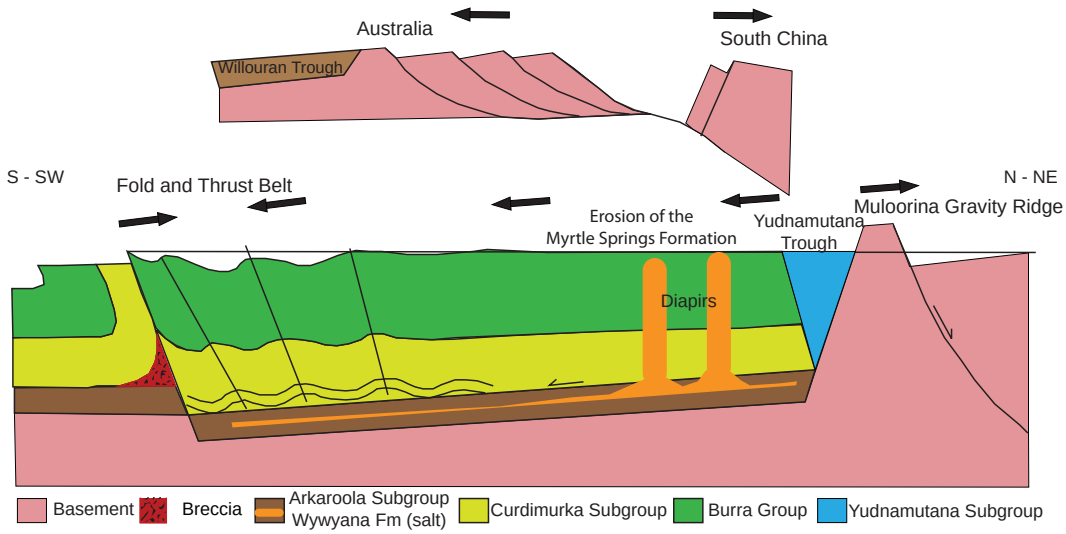

Figure 10.10. Interpretation of the causes of the compressional structures seen in the Willouran Range.
Uplift in the northern quadrant caused by normal faulting north of the Muloorina Gravity Ridge tilts the Willouran Trough to the southern quadrant. In response, the rocks of the Willouran Trough above a decollement at the base slide to the south. The northern end is in extension and the Yudnamutana Trough opens in response whereas at the southern end, the trough cannot move beyond a basement high below the South Hill Domain, causing compression. In the extensional zone, diapirs may develop.

Domains and the West Mount Domain and westward on the Torrens Hinge Zone. There are two possibilities; the Willouran Range area was an area of non-deposition at this time, or the basin inversion during the Delamerian Orogeny caused the erosion of the Wilpena Group. It is not possible to conclude which of these two options is correct from the available data.

10.7 D_2 and D_3: The Delamerian Orogeny

Deposition within the Adelaide Fold Belt ceased in the earliest Cambrian and was succeeded by deposition in two smaller basins, the Arrowie and Stansbury Basins (Preiss, 1987). The Arrowie Basin is interpreted to be a foreland basin developed in front of the Delamerian Orogen and hence marks a change from extension to compression (Haines and Flottman, 1998). Deposition of the Kanmantoo Group in the southern part of the Stansbury Basin occurred in a rapidly subsiding basin that has been interpreted as a rift (Haines and Flottman, 1998), or a tear (pull-apart) basin (Foden et al., 2002).

The Delamerian Orogeny began at about 515 Ma, continuing to about 490 Ma in the Northern Adelaide Fold Belt (e.g., Preiss, 1987; Jenkins and Sandiford, 1992, Oliver and Zakowski, 1995; Foden et al., 1999; Foden et al., 2002). The Willouran Range was an area of uplift, with reverse movement on the Norwest, Bungarider and West Willouran Faults, as well as north to northwest trending faults on the Torrens Hinge Zone and east of the Willouran Range (Figure 10.11a). The majority of these faults were extensional faults formed prior to or during deposition of the Umberatana Group and underwent re-activation during the Delamerian Orogeny. In the Willouran Trough, the Norwest Fault was reactivated as a normal reverse fault, linked to a basal thrust within the basement

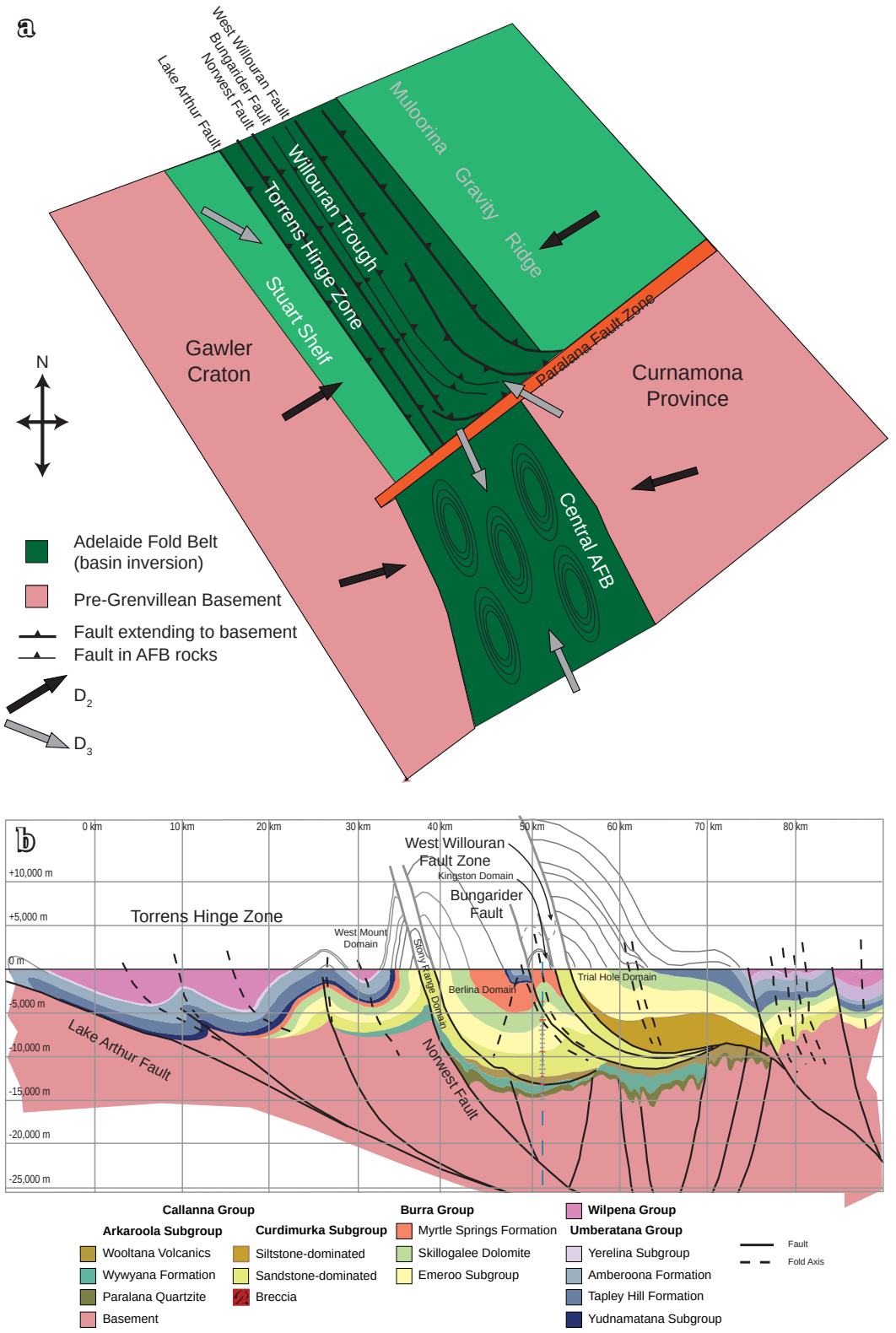

Figure 10.11. The Willouran Range in the Delamerian Orogeny.
a) Diagrammatic plan view showing the direction of faulting and interpreted compression directions in the northern Adelaide Fold Belt from this study and the Central Adelaide Fold Belt (Preiss, 1987). b) Cross-section of the Willouran Range from Chapter 9 showing major D_2 structures of reverse faults and associated folds.

(Figure 10.11b). The Bungarider and West Willouran Faults are interpreted to be normal faults soling-out into the Curdimurksa Subgroup that were also reactivated as reverse faults (Figure 10.11b). Movement on these faults rotated the Curdimurka Subgroup and the Burra Group into their present geometry in the Willouran Range.

Paul et al. (1999) attributed the Delamerian folding in the Willouran Range to north - south directed shortening, within a left-lateral transpressional regime. It was thick-skinned and the major extensional faults were re-activated. Most of the shortening strain was localized across the Norwest and Paralana Faults (Paul et al., 1999). Overall this produced the folding pattern seen in the northern Adelaide Fold Belt, with folds changing trend from northwest to south to northeast from the northwest to south to northeast (Figure 10.12). This study is in agreement with the re-activation of normal faults as reverse faults in the Delamerian. However northeast - southwest shortening is favoured here. It is broadly in agreement with the shortening directions inferred from the north-northwest trending fold directions in the Central Adelaide Fold Belt (Preiss, 1987). Several F_2 folds in the Willouran Range (not re-folded by F_3) trend almost north - south, being influenced by D_1 fault orientations. These would re-activate as reverse faults for a northeast - southwest directed compression but not for north - south directed compression, under which they would likely be re-activated as strike slip faults. Similarly D_2 structures within re-activated north - south trending faults show approxiamately dip-slip movement and not oblique or strike-slip D_2 movement. The east - west trending folds in the south of the northern Adelaide Fold Belt are interpreted to result from;

- re-activation of pre-existing structures in that orientation and/or
- transcurrent movement along the Paralana Fault Zone, which rotated the folds into the fault zone (Figure 10.12).

In both of these instances, the required shortening direction is northeast - southwest, sub-parallel to the Paralana Fault Zone.

D_3 re-folded F_2 structures along a north-northeast trend,into open folds with a weak cleavage at a high angle to bedding. These imply northwest - southeast directed shortening, which may re-activate northeast trending faults as reverse faults, including the Paralana Fault Zone, and so may produce the northeast trending folds. It is also sub-parallel to the second generation of folds seen within the Central Adeliade Fold Belt.

10.8 Post-Delamerian Development.

The Willouran Trough continued to develop after the Delamerian Orogeny. Monazite electron microprobe analysis (chemical) ages are interpreted to show that at about 450 Ma a thermal event affected the Northern Adelaide Fold Belt. It was widespread, with the intrusion of the British Empire Granite and diopside-sphene veins at Arkaroola at this time (Elburg et al., 2002) and the formation of the Beltana Zn deposit (Groves et al., 2003). Monazite ages of 425 ± 16 Ma from dating by electron microprobe analyses in this

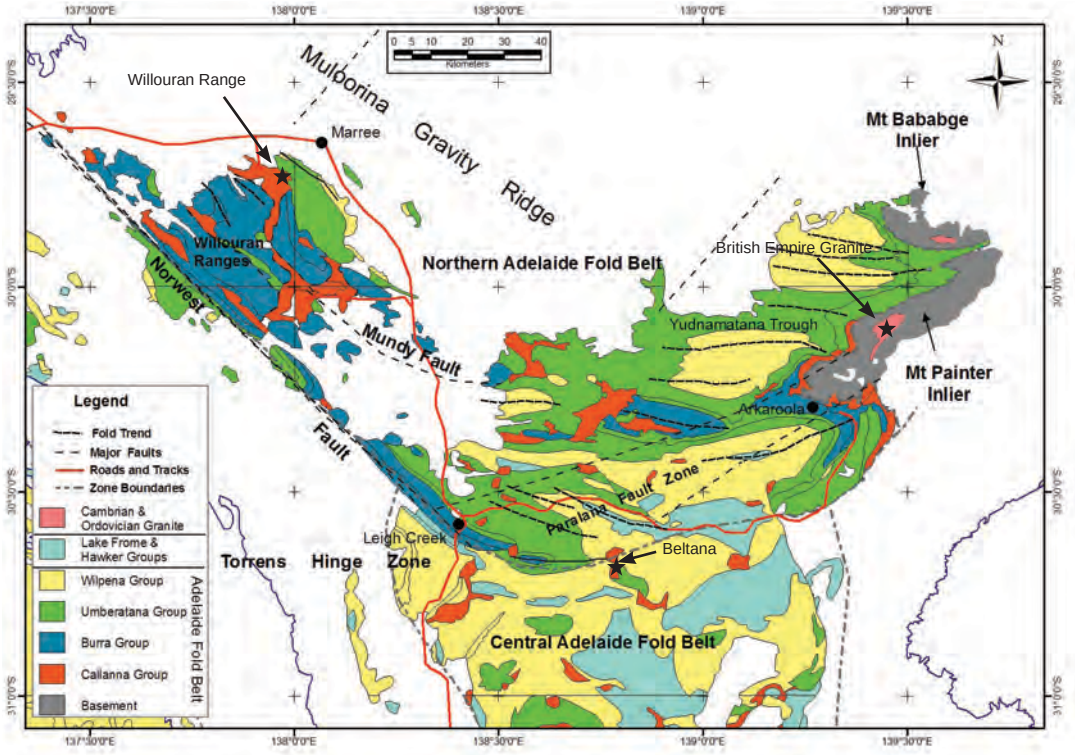

Figure 10.12. The northern Adelaide Fold Belt. Folds change trend from northwest to east - west to northeast from the northwest to south to northeast.
Marked by circles are areas where post-Delamerian thermal events are recorded. These are monazite ages from the Willouran Range from this study, the British Empire Granite in the Arkaroola area (Elburg et al., 2002) and the Beltana Zn deposit (Groves et al., 2003).

study are inferred to be due to a hydrothermal event showing that this thermal event was widespread, having affectedbeing from the northeastern, southern and northwestern limits of the North Adelaide Fold Belt (Figure 10.12).

10.9 Conclusions.

The Willouran Trough is a northwest trending depositional centre identified as a deep gravity low in the northern Adelaide Fold Belt. It was initiated at some time prior to 828 Ma as an intracontinental rift. Much of the Willouran Trough is obscured by Mesozoic to Recent sedimentary rocks but it crops out in the Willouran Range. Research focused on the lower most units within the Willouran Trough, the Callanna Group (comprising the Arkaroola and Curdimurka Subgroups) which crops out in a series of fault blocks in the Willouran Range.

Deposition began with the Arkaroola Subgroup, which only outcrops as megaclasts within breccias throughout the Willouran Range. Those breccia are interpreted to have originated as salt tectonic features, the salt being sourced from the Wywyana Formation. The uppermost unit of the Arkaroola Subgroup in the Willouran Range, the Noranda Volcanics are correlated with the Wooltana Volcanics which crop out in the Arkaroola area. These are interpreted to be continental flood basalts deposited at about 828 Ma as a result of a mantle plume centred east of the Willouran Trough, possibly in the South China Block. It is not thought that the Willouran Trough (and the associated extension) was initiated by the

mantle plume. Instead the mantle plume impinged on the early phase of its development and the associated dykes and volcanics were intruded along pre-existing weaknesses.

Deposition of the Curdimurka Subgroup began after the extrusion of the Wooltana Volcanics. The tectonic setting at this time was a half graben with the basin controlling fault adjacent the Muloorina Gravity High, although there may have been some movement on the Northwest Fault. Deposition was initially in a continental environment, in braided streams along the subsiding floor of the half graben. At this stage, axial drainage was likely dominant with sediment being sourced from the immediate area but also with a significant component from the Grenvillean-age Musgrave Block. As subsidence continued, the depositional environment changed at about 802 Ma, to a marine setting which continued for the remainder of the deposition of the Curdimurka Subgroup. During this time, subsidence and deposition were approximately in balance although there were periods of sub-wave base deposition of black shales and emergent periods with deposition of thin evaporitic beds in a sabkha environment.

Deposition of the Curdimurka Subgroup finished at about 777 Ma with a final regression at the top of the Boorloo dolomite. It was followed by the deposition of the Burra Group. Everywhere the contact between the Curdimurka Subgroup and the Burra Group is tectonic, and the base of the latter is not seen so the nature of the change in not known. However, from unit thickness variations it is interpreted that movement on the major fault adjacent the Muloorina Gravity Ridge was renewed, with the thick sandstone-dominated Emeroo Subgroup being deposited. Toward the top of the Emeroo Subgroup there was a change in the tectonics and movement of the basin controlling fault ceased, switching instead to the Norwest Fault on the western margin of the Willouran Trough. Also at about this time, there was minor uplift of the Curdimurka Subgroup, possibly due to the development of a turtle structure that led to the development of an on-lap surface near the top of the Emeroo Subgroup, and deposition of a thin black shale unit. This may have been the first stirrings of salt tectonics in the Willouran Trough.

With the switch of movement to the Norwest Fault, the Skillogalee Dolomite and Myrtle Springs Formation thicken in that direction, with over 3,000 m of each recorded in the hanging wall of the fault. On the footwall the units of the Burra Group crop out but are much thinner than within the Willouran Trough.

Deposition of the Burra Group ceased at about 725 Ma. In the northeastern Willouran Range, the absence of the Myrtle Springs Formation suggests that this area underwent uplift and erosion just prior to, or at the beginning of deposition of the overlying Umberatana Group. Elsewhere within the Willouran Range, the contact between the Burra and Umberatana Groups is unconformable, reflecting a period of deformation that began at the beginning of deposition of the Umberatana Group and continued until possibly the deposition of the Amberoona Formation, a period of about 50 million years. The deformation is the first to have affected the basal Curdimurka Subgroup and here is termed D_1. Although D_1 occurred within an overall extensional setting, in the Willouran Range the majority of structures are

compressional. They include layer-parallel shearing, thrusting and reverse faults, inclined to recumbent folding (relative to the enclosing bedding) with the development of a weak layer-parallel cleavage, S_1. In the Euchre Pack Domain, there are large low-angle normal faults that have resulted in the loss of stratigraphy but even these are interpreted to be caused by gravitational instability in weak sedimentary rocks above developing anticlines.

The ultimate cause of D_1 is uplift associated with extension to the east of the Willouran Trough that heralds the onset of the final break-up of Rodinia. Uplift to the north of the Willouran Trough tilted the basin causing the sedimentary pile to glide to the southern quadrant. This produced extension to the north, reflected in the development of the Yudnamutana Trough and the development of a fold and thrust belt in the Willouran Range area. There was likely a component of gravity spreading as well, resulting in the inhomogeneity of D_1 structures seen in the Curdimurka Subgroup. As a result deposition of the basal units of the Umberatana Group, the Yudnamutana Subgroup and Tapley Hill Formation took place in a complicated setting of sub-basins in front of developing folds and thin extensional supra-detachment sub-basins.

In the area of the centre of the Willouran Range, there was likely a thin development of the Umberatana Group (less than 1,000 m) but to the east it quickly thickens to several thousand metres, reflecting the tilting of the basin. On the Torrens Hinge Zone, there was about 2,000 metres of the Umberatana Group deposited but here too there was uplift and erosion of its lower part, to the level of the Burra Group at about the time of onset of deposition of the Amberoona Formation.

There is no record of deposition of the upper most unit of the Umberatana Group, the Yerelina Subgroup in the Willouran Range, nor of the overlying Wilpena Group. Although it cannot be ruled at that there was some deposition of these units that was subsequently removed by erosion in the Delamerian Orogeny, it is intepreted here that the area of the Willouran Range was an area of non-deposition. The depocentres had moved to the west, onto the Torrens Hinge Zone, and to the east, adjacent the Paralana Fault Zone.

Deposition in the Adelaide Fold Belt ceased in the early Cambrian and the basin underwent orogenesis in the Delamerian Orogeny between about 515 - 490 Ma. In the Willouran Trough the Delamerian Orogeny produced two deformations D_2 and D_3. D_2 re-activated northwest trending normal faults as reverse faults. It produced upright northwest trending folds (F_2) with shallow plunges to the northwest and southeast and an axial planar cleavage, S_2. D_2 is interpreted to be the result of northeast - southwest directed shortening. D_3 has re-folded D_1 and D_2 structures about a north-northeast trend, producing a dome and basin structure in the central Willouran Range. The folds F_3 are open and it has an associated weak cleavage S_3, that is at a high angle to bedding where seen.

A regional thermal event is recorded in the re-setting of monazite in the Willouran Range at about 430 Ma. Elsewhere in the northern Adelaide Fold Belt, this thermal event is recorded by granite intrusion in the Mt Painter Inlier and the zinc mineralization in the southern part of the northern Adelaide Fold Belt.

REFERENCES

Aharon, P., and Dickinson, W. R., 1987, On the nature and origin of strata-bound massive magnesites; a neglected problem of sedimentary geology, Abstracts with Programs - Geological Society of America, 19, p. 568.

Allen, P. A., Bowring, S. A., Leather, J., Brasier, M., Cozzi, A., Grotzinger, J. P., McCarron, G., Amthor, J. E., 2002. Chronology of Neoproterozoic Glaciations: New Insights from Oman. The 16th International Sedimentological Congress, Abstract Volume, Johannesburg, South Africa, pp. 7 –8.

Allen, J. R. L., Principles of physical sedimentology, Allen and Unwin, Boston, 272p.

Allen, S. R., Simpson, C. J., McPhie, J. and DalAy, S. J., 2003, Stratigraphy, distribution and geochemistry of widespread felsic volcanic units in the Mesoproterozoic Gawler Range Volcanics, South Australia, Australian Journal of Earth Sciences, v. 50, p. 97-112.

Alveringo, C. J. S., Santos, R. V. and Dantas, E. L., 2004, C-O-Sr stratigraphy of cap carbonates overlying Marinoan-age glacial diamictites in the Paraguay Belt, Brazil, Precambrian Research, v. 131, p. 1 – 21.

Ambrose, G. J., Flint, R. B., and Webb, A. W., 1981, Bulletin - Geological Survey of South Australia, v. 50, 71p.

Amthor, J.E., Grotzinger, J.P., Schroder, S., Bowring, S.A., Ramezani, J., Martin, M.W., and Matter, A., 2003, Extinction of Cloudinia and Namacalathus at the Precambrian – Cambrian boundary in Oman, Geology, v. 31, p. 431 - 434.

Anderson, J. L., 1983, Proterozoic anorogenic granite plutonism of North America, in Medaris, L. G., Jr., Byers, C. W., Mickelson, D. M., and Shanks, W. C., eds., Memoir - Geological Society of America, vol.161, p. 133-154.

Annels, A. E., 1984, The geotectonic environment of Zambian copper-cobalt mineralization, Journal of the Geological Society of London, v. 141, p. 279 – 289.

Aschoff, J. L. and Giles, K. A., 2005, Salt diaper-influenced, shallow marine sediment dispersal patterns: Insights from outcrop analogs, American Association of Petroleum Geologists, v.89, p. 447-469.

Baas, J. H., 1999, An empirical model for the development and equilibrium morphology of current ripples in fine sand: Sedimentology, v. 46, p. 123-138.

Banner, J. L., and Hanson, G. N., 1990, Calculation of simultaneous isotopic and trace element variations during water-rock interaction with applications to carbonate diagenesis: Geochimica et Cosmochimica Acta, v. 54, p. 3123-3137.

Barford, N. C., 1985, Experimental measurements: precision, error and truth, Wiley, Chichester, 159p.

Barovich, K. M. and Foden, K. M., 2000, A neoproterozoic flood basalt province in southern-central Australia; geochemical and Nd isotope evidence from basin fill, Precambrian Research, v. 100, p. 213-234.

Barrows, L. and Fett, J. D., 1985, A high precision gravity survey in the Delaware Basin of southeastern New Mexico, Geophysics, v. 50, p. 825-833.

Bartley, J. K., Knoll, A. H., Grotzinger, J. P., and Sergeev, V. N., 2000, Lithification and fabric genesis in precipitated stromatolites and associated peritidal carbonates, Mesoproterozoic Billyakah Group, Siberia: Special Publication - Society for Sedimentary Geology, v. 67, p. 59-73.

Bartley, J. K., Semikhatov, M. A., Kaufman, A. J., Knoll, A. H., Pope, M. C., and Jacobsen, S. B., 2001, Global events across the Mesoproterozoic-Neoproterozoic boundary; C and Sr isotopic evidence from Siberia: Precambrian Research, v. 111, p. 165-202.

Bekker, A., Karhu, J. A., Eriksson, K. A., and Kaufman, A. J., 2003, Chemostratigraphy of Paleoproterozoic carbonate successions of the Wyoming Craton; tectonic forcing of biogeochemical change?: Precambrian Research, v. 120, p. 279-325.

Belperio, A.P., 1990, Palaeoenvironmental interpretation of the Late Proterozoic Skillogalee Dolomite in the Willouran Ranges, South Australia. In Jago, J.B. and Moore, P.S. (eds), The evolution of a late Precambrian - early Palaeozoic rift complex: the Adelaide Geosyncline. Geological Society of Australia, Special Publication 16, 85-104.

Benison, K. C. and Goldstein, R. H., 2001, Evaporites and siliciclastics of the Permian Nippewalla Group of Kansas, USA; a case of non-marine deposition in saline lakes and saline pans, Sedimentology, v. 48, p. 165-188.

Benson, L. V., White, L. D., and Rye, R. O., 1996, Carbonate deposition, Pyramid Lake Subbasin, Nevada; 4, Comparison of the stable isotope values of carbonate deposits (tufas) and the Lahontan lake-level record: Palaeogeography, Palaeoclimatology, Palaeoecology, v. 122, p. 45-76.

Berry, R. F., Flint, R. B., and Grady, A. E., 1978, Deformation history of the Outalpa area and its application to the Olary Province, South Australia: Transactions of the Royal Society of South Australia, v. 102, p. 43-53.

Berry, R. F., Jenner, G. A., Meffre, S., and Tubrett, M. N., 2001, A North American provenance for Neoproterozoic to Cambrian sandstones in Tasmania?: Earth and Planetary Science Letters, v. 192, p. 207-222.

Black, L. P., Kamo, S. L., Allen, C. M., Aleinikoff, J. N., Davis, D. W., Korsch, R. J. and Foudoulis, C., 2003, TEMORA 1; a new zircon standard for Phanerozoic U-PB geochronology, Chemical Geology, v. 200, p. 155-170.

Blewett, R. S., Black, L. P., Sun, S. S., Knutson, J., Hutton, L. J. and Bain, J. H. C., 1998 U-Pb zircon and Sm-Nd geochronology of the Mesoproterozoic of North Queensland: implications for a Rodinian connection with the Belt Supergroup of North America, Precambrian Research, v. 89, p. 101-127.

Blisset, A. H., Creaser, R. A., Daly, S., Flint, D. J. and Parker, A. J., 1993, Gawler Range Volcanics, in Drexel., J. F., Preiss, W. V. and Parker, A. J. (eds), The geology of South Australia, Volume 1, the Precambrian. Geological Survey of South Australia, Bulletin 54, Adeliade, p. 107-131.

Boger, S. D., Carson, C. J., Wilson, C. J. L. and Fanning, C. M., 2000, Neoproterozoic deformation in the Radok Lake region of the northern Prince Charles Mountains, east Antarctica; evidence for a single proracted orogenic event, Precambrian Research, v. 104, p. 1-24.

Bradley, W. H., 1964, Geology of the Green River Formation and associated Eocene rocks in southwestern Wyoming and adjacent parts of Colorado and Utah, US Geoogucal Survey Professional Paper, Report: P 0496A, p. A1-A86.

Bradley, W. H., and Eugster, H. P., 1969, Geochemistry and paleolimnology of the trona deposits and associated authigenic minerals of the Green River Formation of Wyoming.

Brasier, M., McCarron, G., Tucker, R., Leather, J., Allen, P. and Shields, G., 2000. New U-Pb zircon dates for the Neoproterozoic Ghubrah glaciations and for the top of the Huqf Supergroup, Oman, Geology, v. 28, p. 175-178.

Brun, J. P. and Fort, X., 2004, Compressional salt tectonics (Angolan margin), Tectonophysics, v. 382, p. 129-150.

Buchanan, P. G., Bishop, D. J., and Hood, D. N., 1996, Development of salt-related structures in the central North Sea; results from section balancing: Geological Society Special Publications, v. 100, p. 111-128.

Burger, A. J., von Knorring, O. and Clifford, T. N., 1965, Mineralogical and radiometric studies of monazite and sphene occurrences in the Namib Desert, South-West Africa, Mineralogical Magazine, v. 35, p. 519-528.

Burke, K. and Dewey, J. F., 1973, Plume-generated triple junctions: key indicators in applying plate tectonics to old rocks, Journal of Geology, v. 81, p. 406-433.

Burret, C. and Berry, R., 2000, Proterozoic Australia-Western United States (AUSWAS) fit between Laurentia and Australia, Geology, v.28, p. 103-106.

Cabella, R., Lucchetti, G., and Marescotti, P., 2001, Authigenic monazite and xenotime from pelitic metacherts in pumpellyite-actinolite-facies conditions, Sestri-Voltaggio Zone, central Liguria, Italy: The Canadian Mineralogist, v. 39, p. 717-727.

Calver, C. R., Black, L. P., Everard, J. L. and Seymour, D. B., 2004, U-Pb zircon age constraints on late Neoproterozoic glaciations in Tasmania, Geology, p. 893-896.

Camacho, A. and Fanning, C. M., 1995, Some isotopic constraints on the evolution of the granulite and upper amphibolites facies terranes in the eastern Musgrave Block, central Australia, Precambrian Reseearch, v. 71, p. 155-181.

Camacho, A., Hensen, B. J. and Armstrong, R., 2002, Isotopic test of a thermally driven intraplate orogenic model, Australia, Geology, v. 30, p. 887-890.

Camerlo, R. H. and Benson, E. F., 2006, Geometric and seismic interpretation of the Perdido fold belt: Northwestern deep-water Gulf of Mexico, American Association of Petroleum Geologists, v. 90, p. 363-386.

Camoin, G. F., Casanova, J., Rouchy, J.-M., Blanc-Valleron, M.-M., and Deconinck, J.-F., 1997, Environmental controls on perennial and ephemeral carbonate lakes; the central palaeo-Andean Basin of Bolivia during Late Cretaceous to early Tertiary times: Sedimentary Geology, v. 113, p. 113-126.

Campbell, I. H., 2001, Identification of ancient mantle plumes, In Ernst, R. E., (Ed), Mantle plumes; their identification through time, Geological Society of America, Special Publication, v. 352, p, 5-22.

Campbell, I. H., 2007, Testing the plume theory, Chemical Geology, v. 241, p. 153-176.

Campbell, I. H. and Griffiths, R. W., 1990, Implications of plume structure for the evolution of flood basalts, Earth and Planetary Science Letters, v. 99, p. 79-93.

Carson, C. J., Boger, S. D., Fanning, C. M., Wilson, C. J. L., and Thost, D. E., 2000, SHRIMP U-Pb geochronology from Mount Kirby, northern Prince Charles Mountains, East Antarctica: Antarctic Science, v. 12, p. 429-442.

Casanova, J., and Hillaire-Marcel, C., 1993, Carbon and oxygen isotopes in African lacustrine stromatolites; palaeohydrological interpretation: Geophysical Monograph, v. 78, p. 123-133.

Catlos, E. J., Gilley, L. D., and Harrison, M. T., 2002, Interpretation of monazite ages obtained via in situ analysis, Chemical Geology, v. 188, p. 193-215.

Cawood, P. A., Nemchin, A. A., Freeman, M., and Sircombe, K., 2003, Linking source and sedimentary basin; detrital zircon record of sediment flux along a modern river system and implications for provenance studies: Earth and Planetary Science Letters, v. 210, p. 259-268.

Cawood, P. A. and Korsch, R. J. 2008, Assembling Australia: Proterozoic building of a continent, Precambrian Research, v. 166, p. 1-35.

Changsong. L, Eriksson, K., Sitian, L., Yongxian, W., Jianye, R and Yanmei, Z., 2001, Sequence architecture, depositional systems and controls on development of lacustrine basin fills in part of the Erlian Basin, Northeast China, American Association of Petroleum Geologists Bulletin, v. 85, p. 2017-2043.

Charvet, J., Shu, L., Shi, Y., Guo, L., Faure, M., 1996a. The building of south China: collision of Yangzi and Cathaysia blocks, problems and tentative answers. Journal of South East Asian Earth Science, v.13, p.223–235.

Chen, J., Foland, K. A., Xing, F., Xu, X., Zhou, T., 1991. Magmatism along the southeastern margin of the Yangtze block: Precambrian collision of the Yangtze and Cathysia blocks of China. Geology, v.19, p. 815–818.

Christie-Blick, N., Dyson, I. A. and von der Borch, C. C., 1995, Sequence stratigraphy and the interpretation of Neoproterozoic earth history, Precambrian Research, v. 73, p. 3-26.

Clarke, G. L. and Powell, R., 1989, Basement-cover interation in the Adelaide Foldbelt, South Australia: the development of an arcuate foldbelt, Tectonophysics, v. 158, p. 209-226.

Clayton, R. N. and Degens, E, T., 1959 Use of carbon isotope analyses of carbonates for differentiating fresh-water and marine sediments, Bulletin of the American Association of Petroleum Geologists, v. 43, p. 890-897.

Close, D. F., Edgoose, C. J. and Scrimgeour, I. R., 2003, Hull and Bloods Range Special, Northern Territory 1:100,000 geological map series explanatory notes. Northern Territory Geological Survey, Darwin.

Coats, R.P., 1964, The geology and mineralization of the Blinman Dome Diapir. Report of Investigations, Geological Survey of South Australia, v. 26, p.53.

Coats, R. P., 1965, Diapirism in the Adelaide geosynclines, Australian Petroleum Explorers Association Journal, v. 5, p. 98 - 102.

Coats, R.P. (Compiler), 1973, Copley map sheet. Geological Survey of South Australia, Geological Atlas 1:250,000 Series, sheet SH54-9, 38p.

Coats, R. P., and Blissett, A. H., 1971, Regional and economic geology of the Mount Painter Province, Bulletin - Geological Survey of South Australia, v. 43, p. 426.

Coats, R. P. and Dalgarno, R., 1983, Large-scale slumping in the Umberatana Group, Willouran Ranges in In Adelaide Geosyncline sedimentary environments and tectonic settings symposium, Adelaide, 1983, Abstracts of the Geological Society of Australia, v. 10, p. 63-64.

Cobbold, P. R., Szatmari, P., Santiago Demercian, L., Coelho, D., and Rossello, E. A., 1995, Seismic and experimental evidence for thin-skinned horizontal shortening by convergent radial gliding on evaporites, deep-water Santos Basin, Brazil, in Jackson, M. P. A., Roberts, D. G., and Snelson, S., eds., AAPG Memoir, vol.65, p. 305-321.

Cocherie, A., Legendre, O., Peucat, J. J., and Kouamelan, A. N., 1998, Geochronology of polygenetic monazites constrained by in situ electron microprobe Th-U-total lead determination; implications for lead behaviour in monazite: Geochimica et Cosmochimica Acta, v. 62, p. 2475-2497.

Condon, D., Zhu, M., Bowring, S., Jin, Y., Wang, W. and Yang, A., 2005, From the Marinoan glaciations to the oldest bilaterians: U-Pb ages form the Doushantou Formation, China, Science, v. 308, p. 95 - 98.

Conor, C. H. H., 1987, The geology of the Eateringinna 1:100,000 sheet area eastern Musgrave Block, South Australia, MSc Thesis, The University of Adelaide (unpublished).

Conor, C. H. H., and Fanning, C. M., 2001, Geochronology of the Woman-in-White Amphibolite, Olary Domain: MESA Journal, v. 20, p. 41-43.

Cook, N. D. J., Fanning, C. M. and Ashley, P. M., 1994, New geochronological results from the Willyama Supergroup, Olary Block, South Australia, In Australian Research on Ore Genesis Symposium, Adelaide, Australian Mineral Foundation, p. 19.1-19.5

Corredor, F., Shaw, J. H. and Bilotti, F., 2005, Structural styles in the deep-water fold and thrust belts of the Niger Delta, American Association of Petroleum Geologists Bulletin, v. 89, p. 753-780.

Coward, M. P., 1976, Large-scale Palaeozoic shear zone in Australia and present extension to the Antarctic Ridge, Nature, v. 259, p. 648-649.

Coward, M. and Stewart, S., 1995, Salt-influenced structures in the Mesozoic-Tertiary cover of the southern North Sea, in Jackson, M. P. A., Roberts, D. G. and Snelson, S. (eds), Salt tectonics; a global perspective, American Association of Petroleum Geologists, Memoir, v. 65, p. 229-250.

Crawford, A.J. and Hilyard, D., 1990, Geochemistry of Late Proterozoic tholeiitic flood basalts, Adelaide Geosyncline, South Australia, In Jago, J.B. and Moore, P.S. (eds), The evolution of a late Precambrian - early Palaeozoic rift complex: the Adelaide Geosyncline. Geological Society of Australia, Special Publication 16, 49-67.

Creaser, R. A., 1996, Petrogenesis of a Mesoproterozic quartz latite-granitoid suite from the Roxby Downs area, South Australia, Precambrian research, v. 79, p. 371-394.

Crowley, J. L., and Ghent, E. D., 1999, An electron microprobe study of the U-Th-Pb systematics of metamorphosed monazite; the role of Pb diffusion versus overgrowth and recrystallization: Chemical Geology, v. 157, p. 285-302.

Dalgarno, C. R., 1982, Andamooka map sheet, South Australian Geological Survey, Geological Atlas 1:250,000 series, sheet SH53-12, 38p.

Dalgarno, C. R., and Johnson, J. E., 1968, Diapiric structures and late Precambrian-early Cambrian sedimentation in Flinders ranges, South Australia: Memoir - American Association of Petroleum Geologists, v. 8, p. 301-314.

Daily, S.J., 1970, Curdimurka map sheet, South Australian Geological Survey, Geological Atlas 1:250,000 series, sheet SH53-8, preliminary edition.

Dalrymple, R. W., 1992, Tidal depositional systems, in Walker, R. G., and James, N. P., (eds) Facies models: response to sea level change, Geological Association of Canada, p. 239-15-218.

Daly, S. J., Fanning, G. M. and Fairclough, 1998, Tectonic evolution and exploration potential of the Gawler Craton, in: Hodgson, I. and Hince, B. (Eds) Geology and mineral potential of major Australian mineral provinces, AGSO Journal of Australian Geology and Geophysics, v. 17, p. 145-168.

Dalziel, I. W. D., 1991, Pacific margins of Laurentia and East Antarctica-Australia as a conjugate rift pair: evidence and implications for an Eocambrian supercontinent, Geology, v. 19, p. 598-601.

Dam, G., Larsen, M. and Sonderholm, M., 1998, Sedimentary response to mantle plumes: implications from Paleocene onshore successions, West and East Greenland, Geology, v. 26, p. 207-210.

Dewar, G. J. and Hatcher, M. I., 1975, The geology and mineralization of Copley Diapir, northern Flinders Ranges, South Australia, Australian Institute of Mining and Metallurgy, Conference Series, v. 4, p. 483-493.

De Wolf, C. P., Belshaw, N. and O'Nions, R. K., 1993, A metamorphic history from micron-scale 207Pb/206Pb chronometry of Archean monazite, Earth and Planetary Science Letters, v. 120, p. 207-220.

Dickinson, S.B., 1944, The structural control of ore deposition in some Australian copperfields. Bulletin - Geological Survey of South Australia, v. 21, p. 66.

Dickinson, W. R., 1988, Provenance and sediment dispersal in relation to paleotectonics and paleogeography of sedimentary basins, in Kleinspehn, K. L., Paola, C., and Bouma, A. H., eds.: New York, Springer-Verlag.

Dickinson, W. R., and Suczek, C. A., 1979, Plate tectonics and sandstone compositions: AAPG Bulletin, v. 63, p. 2164-2182.

Direen, N. G., and Crawford, A. J., 2003, The Tasman Line; where is it, what is it, and is it Australia's Rodinian breakup boundary?: Australian Journal of Earth Sciences, v. 50, p. 491-502.

Direen, N. G., Brock, D. and Hand, M., 2005, Geophysical testing of balanced cross-sections of fold-thrust belts with potential field data: an example from the Fluerieu Arc of the Delamerian Orogen, South Australia, Journal of Structural Geology, v. 27, p. 964-984.

Donath, F.A., and Parker, R.B., 1964. Folds and Folding. Geological Society of America Bulletin, v. 75, p. 45-62.

Drexel, J. F., Preiss, W. V. and Parker, A. J., 1993, The Geology of South Australia, Volume 1, The Precambrian, South Australia Geological Survey Bulletin 54.

Drexel., J. F., 2009, Review of the Burra Mine project, 1980 – 2008 – a progress report, South Australia , Department of Primary Industries and Resources, Report Book 2008/16, 40p.

Dunn, P. R., Plumb, K. A. and Roberts, H. G., 1966, A proposal for time-stratigraphic subdivision of the Australian Precambrian, Journal of the Geological Society of Australia, v. 13, p. 593-608.

Dutch, R.A., Hand, M. and Clark, C., 2005, Cambrian reworking of the southern Australian Proterozoic Curnamona Province: constraints from regional shear-zone systems, Journal of the Geological Society, v. 162, p. 763-775.

Dutkiewicz, A., Herczeg, A. L., and Dighton, J. C., 2000, Past changes to isotopic and solute balances in a continental playa; clues from stable isotopes of lacustrine carbonates: Chemical Geology, v. 165, p. 309-329.

Dyson, I.A., 1998, The "Christmas Tree Diapir" and salt glacier at Pinda Springs, central Flinders Ranges, MESA Journal, v. 10, p. 40-43.

Dyson, I. A., 1999, The Beltana Diapir; a salt withdrawal minibasin in the northern Flinder Ranges: MESA Journal, v. 15, p. 40-46.

Dyson, I. A., 2002, Adelaidean sedimentation and the timing of salt tectonics in the East Willouran Ranges, in Preiss, V. P., ed., Abstracts - Geological Society of Australia, vol.67, p. 380.

Dyson, I. A., 2004, Geology of the eastern Willouran Ranges; evidence for the earliest onset of salt tectonics in the Adelaide Geosyncline, MESA Journal, v. 35, p. 48-56.

Edgoose, C. J., Scrimgeour, I. R. and Close, D. F., 2004, Geology of the Musgrave Block, Northern Territory, Northern Territory Geological Survey, Report 15.

Edgell, H. S., 1996, Salt tectonism in the Persian Gulf Basin, Geological Society of London, Special Publications, v. 100, p. 129-151.

Elburg, M. A., Bons, P. D., and Brugger, J., 2002, Palaeozoic events around Arkaroola, northern Flinders Ranges, South Australia, in Preiss, V. P., ed., Abstracts - Geological Society of Australia, vol.67, p. 167.

Engi, M., Cheburkin, A. K., and Koeppel, V., 2002, Nondestructive chemical dating of young monazite using XRF; 1, Design of a mini-probe, age data for samples from the Central Alps, and comparison to U-Pb (TIMS) data, in Poitrasson, F., Schaltegger, U., and Hanchar, J. M., eds., Chemical Geology, 191, p. 225-241.

Eugster, H. P., and Hardie, L. A., 1978, Saline lakes, in Lerman, A., ed.: New York, Springer-Verlag.

Evans, J., and Zalasiewicz, J., 1996, U-Pb, Pb-Pb and Sm-Nd dating of authigenic monazite; implications for the diagenetic evolution of the Welsh Basin: Earth and Planetary Science Letters, v. 144, p. 421-433.

Fabris, A., Constable, S., Conor, C., Woodhouse, A., Hore, S and Fanning, M., 2005, Age, origin, emplacement and mineral potential of the Oodla Wirra Volcanics Nackara Arc, central Flinders Ranges: Mesa Journal, v. 37, p. 44-52.

Fairchild, I. J., and Spiro, B., 1987, Petrological and isotopic implications of some contrasting late Precambrian carbonates, NE Spitsbergen: Sedimentology, v. 34, p. 973-989.

Fanning, C. M., 1997, Geochronological synthesis of Southern Australia, Part II, The Gawler Craton, South Australia Department of Mines and Energy, Open File Envelope 8918 (unpublished).

Fanning, C. M., Ludwig, K. R., Forbes, B. G. and Preiss, W. V., 1986, Single and multiple grain U-Pb zircon analyses for the Adelaidean Rook Tuff, Willouran Ranges, South Australia, in 8th Australian Geological Convention, Adelaide, Abstracts of the Geological Society of Australia, v. 15, p. 71-72.

Fanning, C. M. and Link, P. K., 2004, Detrital zircon provenance of the Mesoproterozoic Pandurra Formation, South Australia; Gawler Craton derived age spectra and implications for the source of the Belt Supergroup, USA: Abstracts - Geological Society of Australia, v. 73, p. 155.

Fanning, C. M. and Link, P. K., 2008, Age constraints for the Sturtian Glaciation; data from the Adelaide Geosyncline, South Australia and Pocatello Formation, Idaho, USA, Geological Society of Australia Abstracts, v. 91, p. 57-62.

Fanning, C. M., Reid, A. J. and Teale, G. S., 2007, A geochronological framework for the Gawler Craton, South Australia, South Australia Geological Survey Bulletin 55, pp. 258.

Ferrill, D. A. and Morris, A. P., 2003, Dilational normal faults, Journal of Structural Geology, v. 25, p. 183-196.

Ferris, G. M., 2001, The geology and geochemistry of grantioids in the CHILDARA region, western Gawler Craton, South Australia; implications for the tectonic history of the western Gawler Craton and the development of lode-style gold mineralization at Tunkillia, Universtiy of Tasmania, MSc Thesis (unpubl), 175 pp.

Ferris, G. M. and Schwartz, M. P., 2003, Proterozoic gold province of the central Gawler Craton, MESA Journal, v. 30, p. 4 - 12.

Figueiredo, A. M. F., Braga, J. A. E., Zabalaga, J. C., Oliveira, J. J., Aguiar, G. A., Silva, O. B., Mato, L. F., Daniel, L. M. F., Magnavita, L. P. and Bruhn, C. H. L., 1994, Reconcavo Basin, Brazil: a prolific intracontinental rift basin, in Landon, S. M., (Ed.) Interior rift basins, American Association of Petroleum Geologists Memoir 59, p 157-203.

Fletcher, R. C., Hudec, M. R., and Watson, I. A., 1995, Salt glacier and composite sediment-salt glacier models for the emplacement and early burial of allochthonous salt sheets, in Jackson, M. P. A., Roberts, D. G., and Snelson, S., eds., AAPG Memoir, vol.65, p. 77-107.

Flint, R. B., Rankin, L. R. and Fanning, C. M., 1990, Definition; the Palaeoproterozoic St Peter Suite of the Western Gawler Craton, Quartely Geological Notes – Geological Survey of South Australia, v. 114, p. 2-8.

Flottman, T., Gibson, G. and Kleinschmidt, G., 1993, Structural continuity of the Ross and Delamerian orogens of Antarctica and Australia along the margin of the palaeo-Pacific, Geology, v 21, p. 319 - 322.

Flottman, T., James, P.R., Menpes, R., Cesare, P., Twining, M., Fairclough, M., Randabell, J and Marshak, S., 1995, The structure of Kangaroo Island (South Australia): strain and kinematic partitioning during Delamerian basin and platform reactivation, Australian Journal of Earth Sciences v. 42, p. 35-49.

Flottman, T. and James, P., 1997, Infuence of basin architecture on the style of inversion and fold-thrust belt tectonics – the southern Adelaide Fold Belt, South Australia, Journal of Structural Geology, v. 19, p. 1093 – 1110.

Foden, J., Sandiford, M., Dougherty-Page, J., and Williams, I., 1999, Geochemistry and geochronology of the Rathjen Gneiss; implications for the early tectonic evolution of the Delamerian Orogen: Australian Journal of Earth Sciences, v. 46, p. 377-389.

Foden, J., Barovich, K., Jane, M., and O'Halloran, G., 2001, Sr-isotopic evidence for late Neoproterozoic rifting in the Adelaide Geosyncline at 586 Ma; implications for a Cu ore forming fluid flux: Precambrian Research, v. 106, p. 291-308..

Folk, R. L., 1973, Evidence for Peritidal Deposition of Devonian Caballos Novaculite, Marathon Basin, Texas: The American Association of Petroleum Geologists Bulletin, v. 57, p. 702-725.

Forbes, B. G., 1963, Geology of the Marree 1:250,000 map area. Geological Survey of South Australia, Report of Investigations, v. 28, 47p.

Forbes, B.G., 1978, The Boucaut Volcanics, Quarterly Geological Notes - Geological Survey of South Australia, v. 65, p. 6-10.

Forbes, B.G., 1990. Geology of the Willouran Ranges. In Jago, J.B. and Moore, P.S., The evolution of a late Precambrian - early Palaeozoic rift complex: the Adelaide Geosyncline. Geological Society of Australia, Special Publication 16, 68-84.

Forbes, B. G., Murrell, B., and Preiss, W. V., 1981, Subdivision of lower Adelaidean, Willouran Ranges: Quarterly Geological Notes - Geological Survey of South Australia, v. 79, p. 7-16.

Fort, X., Brun, J. P. and Chauvel, F., 2004, Salt tectonics on the Angolan margin, synsedimentary deformation processes, American Association of Petroleum Geologists, v. 88, p. 1523-1544.

Foster G., Kinny, P., Vance, D., Prince, C. and Harris, N., 2000, The significance of monazite U-Th-Pb age data in metamorphic assemblages: a combined study of monazite and garnet chronometry, Earth and Planetary Science Letters, v. 181, p. 327-340.

Frank, T. D. and Fielding, C. R., 2003, Marine origin for Precambrian carbonate-hosted magnesite? Geology, v. 31, p. 1101-1104.

Freidmann, S. J. and Burbank, D. W., 1995, Rift basins and supradetachment basins: intracontinental extensional end-members, Basin Research, v. 7, p. 109-127.

Galindo, C., Casquet, C., Rapela, C., Pankhurst, R. J., Baldo, E., and Saavedra, J., 2004, Sr, C and O isotope geochemistry and stratigraphy of Precambrian and lower Paleozoic carbonate sequences from the western Sierras Pampeanas of Argentina; tectonic implications: Precambrian Research, v. 131, p. 55-71.

Gasse, F., and Van Campo, E., 1994, Abrupt post-glacial climate events in West Asia and North Africa monsoon domains: Earth and Planetary Science Letters, v. 126, p. 435-456.

Gaullier, V. and Vendeville, B. C., 2005, Salt tectonics driven by sediment progradation: Part II-Radial spreading of sedimentary lobes prograding above salt, American Association of Petroleum Geologists, v. 89, p. 1081-1089.

Gawthorpe, R. L. and Leeder, M. R., 2000, Tectono-sedimentary evolution of active extensional basins: Basin Research, v. 12, p. 195-218.

Gehrels, G. E., and Ross, G. M., 1998, Detrital zircon geochronology of Neoproterozoic to Permian miogeoclinal strata in British Columbia and Alberta: Canadian Journal of Earth Sciences = Journal Canadien des Sciences de la Terre, v. 35, p. 1380-1401.

Gemmer, L., Ings, S. J., Medvedev, S. and Beaumont, C., 2004, Salt tectonics driven by differential sediment loading: stability analysis and finite-element experiments, Basin Research, v. 16, p. 199-218.

Gemmer, L., Beaumont, C. and Ings, S. J., 2005, Dynamic modeling of passive margin salt tectonics: effects of water loading, sediment properties and sedimentation patterns, Basin Research, v. 17, p. 383-402.

Gibson, H. J. and Stuewe, K., 2000, Multiphase cooling and exhumation of the southern Adelaide fold belt revealed from apatite fission track data and thermal history modelling, Abstracts - Geological Society of Australia, vol.58, p. 117-119.

Glaessner, M.F., 1958, The oldest fossil faunas in South Australia, Geology Rundschau, v. 47, p. 522-531.

Glen, R. A., Laing, W. P., Parker, A. J. and Rutland, R. W. R., 1977, Tectonic relationships between the Proterozoic Gawler and Willyama orogenic domains, Australia, Journal of the Geological Society of Australia, v. 24, p. 125-150.

Glikson, A. Y., Stewart, A. J., Ballhaus, C. G., Clarke, G. L., Feeken, E. H. J., Sheraton, J. W. and Sun, S. S., 1996, Geology of the western Musgrave Block, central Australia, with particular reference to the mafic-ultramafic Giles Complex, AGSO Bulletin v. 239, p. 41-68

Goodge, J. W., Myrow, P., Williams, I. S., and Bowring, S. A., 2002, Age and provenance of the Beardmore Group, Antarctica; constraints on Rodinia supercontinent breakup: Journal of Geology, v. 110, p. 393-406.

Goodge, J. W., Williams, I. S., and Myrow, P., 2004, Provenance of Neoproterozoic and lower Paleozoic siliciclastic rocks of the central Ross Orogen, Antarctica; detrital record of rift-, passive-, and active-margin sedimentation: Geological Society of America Bulletin, v. 116, p. 1253-1279.

Gore, A. P. K., Shields, G. A., and Hill, A. C., 2004, A re-interpretation of marine versus non-marine environments in the Bitter Springs Formation of central Australia utilising "molar-tooth" structures: Abstracts - Geological Society of Australia, v. 73, p. 232.

Gornitz, V. M., and Schreiber, B. C., 1981, Displacive halite hoppers from the Dead Sea; some implications for ancient evaporite deposits: Journal of Sedimentary Petrology, v. 51, p. 787-794.

Gostin, V. A., Haines, P. W., Jenkins, R. J. F., Compston, W and Willians, I. S., 1986, Impact ejecta horizon within late Precambrian shales, Adelaide Geosyncline, South Australia, Science, v. 233, p. 198-200.

Gow, P. A., Wall, V. J., and Valenta, R. K., 1993, The regional geophysical response of the Stuart Shelf, South Australia, in Odins, J. A., and Facer, R. A., eds., Exploration Geophysics, v. 24, p. 513-519.

Greentree, M. R., Li, Z. X., Li, X. H., Wu, H., 2006, Late Mesoproterozoic to earliest Neoproterozoic basin record of the Sibao orogenesis in western South China and relationship to the assembly of Rodinia, Precambrian Research, v.151, p. 79–100.

Griffiths, R. W. and Campbell, I. H., 1991, Interaction of mantle plume heads with the Earth's surface and onset of small-scale convection, Journal of Geophysical Research, v. 96, p. 18295-18310.

Groves, I. M., Carman, C. E. and Dunlap, W. J., 2003, Geology of the Beltana willemite deposit; Flinders Ranges, South Australia: Economic Geology and the Bulletin of the Society of Economic Geologists, v. 98, p. 797-818.

Haines, P., 1988, Storm-dominated mixed carbonate/siliciclastic shelf sequence displaying cylces of hummocky cross-stratification, late Proterozoic Wonoka Formation, South Australia, Sedimentary Geology, v. 58, p. 237-254.

Haines P. W. and Flöttman, T., 1998, Delamerian Orogeny and potential foreland sedimentation: a review of age and stratigraphic constraints. Australian Journal of Earth Sciences, v. 45, p. 559-570.

Halverson, G. P., Hoffman, P. F., Schrag, D. P., Maloof, A. C., and Rice, A. H. N., 2005, Toward a Neoproterozoic composite carbon-isotope record: Geological Society of America Bulletin, v. 117, p. 1181-1207.

Hamblin, W.K., 1965. Origin of "reverse drag" on the down-thrown side of the normal faults: Geological Society of America Bulletin, v 76, p. 1145 – 1164.

Hand, M., Bendall, B., and Mawby, J., 2001, The metamorphic expression of the Alice Springs Orogeny, in Davidson, G., and Pongratz, J., eds., Abstracts - Geological Society of Australia, vol.64, p. 72-74.

Harms, J. C., Southard, J. B., Spearing, D. R. and Walker, R. G., 1975, Depositional environments as interpreted from primary sedimentary structures and stratification sequences, Society of Economic Palaeontologists and Mineralogists, Short Course 2, 161p.

Harms, J. C., Southard, J. B. and Walker, R. G., 1982, Structures and sequences in clastic rocks: Society of Economic Palaeontologists and Mineralogists, Short Course 9, 851p.

Harris, N. B., 2000, Evolution of the Congo rift basin, West Africa, an inorganic geochemical record in lacustrine shales, Basin Research, v. 12, p. 425-445.

Harris, N. B., Freeman, K. H., Pancost, R. D., White, T. S., and Mitchell, G. D., 2004, The character and origin of lacustrine source rocks in the Lower Cretaceous synrift section, Congo Basin, West Africa: AAPG Bulletin, v. 88, p. 1163-1184.

Harrison, T. M., Kingsbury, J., Miller, C. F., 1990, Prograde thermochronology; U-Pb dating of monazite growth, V. M. Goldschmidt conference; program and abstracts.

Hartley, M. J., Foster, D. A. and Gray, D. R., 1998, The significance of younger thermal events in the Willyama Inliers; using 40Ar- 39Ar thermochronology, in Noble, W. P., ed., Abstracts - Geological Society of Australia, vol.52, p. 19-20.

Heinisch, E. R., and Foden, J., 2002, The field relations within the Tanunda Creek Gneiss and the Kanmantoo Group and its evolution, in Preiss, V. P., ed., Abstracts - Geological Society of Australia, vol.67, p. 175.

Higuera-Diaz, J. C. and Fischer, M. P., 2005, Geometry and kinematics of the Nuncios detachment fold complex: implications for lithotectonics in northeastern Mexico, Tectonics, v. 24, TC4010.

Hill, A. C., Arouri, K., Gorjan, P., and Walter, M. R., 2000, Geochemistry of marine and nonmarine environments of a Neoproterozoic cratonic carbonate/evaporite; the Bitter Springs Formation, central Australia: Special Publication - Society for Sedimentary Geology, v. 67, p. 327-344.

Hill, A. C., and Walter, M. R., 2000, Mid-Neoproterozoic (approximately 830-750 Ma) isotope stratigraphy of Australia and global correlation: Precambrian Research, v. 100, p. 181-211.

Hill, A. C., Grey, K., Gostin, V. A. and Webster, L. J., 2004, New records of Late Neoproterozoic Acraman ejecta in the Officer Basin, Australian Journal of Earth Sciences, v.1, p. 47-51.

Hilyard, D., 1990, Willouran basic province, In Jago, J.B. and Moore, P.S. (Eds), The evolution of a late Precambrian - early Palaeozoic rift complex: the Adelaide Geosyncline. Geological Society of Australia, Special Publication v. 16, p. 68-84.

Hoefs, J., 2004, Stable isotope geochemistry: fifth revised and updated edition, Berlin, Springer, 244p.

Hoffman, P. F., Kaufman, A. J., Halverson, G. P. and Schrag, D. P., 1998, A Neoproterozoic snowball Earth, Science, v. 281, p. 1342-1346.

Hoffman, K. H., Condon, D. J., Bowring, S. A. and Crowley, J. L., 2004, U-Pb zircon date from the Neoproterozoic Ghaub Formation, Namibia: Constraints on Marinoan glaciations. Geology, v. 32, p. 817-820.

Hoffman, P. F., 2009, Cottons Breccia of King Island, Tasmania: Glacial or non-glacial, Cryogenian or Ediacaran, Precambrian Research, v. 172, p. 311-322.

Hooper, P. R., 1990, The timing of crustal extension and the eruption of continental flood basalts, Nature, v. 345, p. 246-249.

Hotinski, R. M., Kump, L. R., and Arthur, M. A., 2004, The effectiveness of the Paleoproterozoic biological pump; a δ13C gradient from platform carbonates of the Pethei Group (Great Slave Lake Supergroup, NWT): Geological Society of America Bulletin, v. 116, p. 539-554.

Howchin, W., 1924, The Sturtian Tillite in the Willouran Ranges near Marree (Hergott) and in the northeastern portions of the Flinders Ranges, Report of the Australian Association for the Advancement of Sciences, v. 17, p. 67-76.

Hudec, M. R. and Jackson, M. P. A., 2004, Regional restoration across the Kwanza Basin, Angola: salt tectonics triggered by repeated uplift of a metastable passive margin, AAPG Bulletin, v. 88, p. 971-990.

Hudec, M. R. and Jackson, M, P. A., 2002, Structural segmentation, inversion, and salt tectonics on a passive margin: evolution of the inner Kwanza Basin, Angola, Geological Society of America Bulletin, v. 114, p. 1222-1244.

Ingersoll, R. V., Suczek, C. A., Condie, K. C., and Martell, C., 1984, Early Proterozoic metasediments from north-central Colorado; metamorphism, provenance, and tectonic setting; discussion and reply: Geological Society of America Bulletin, v. 95, p. 985-986.

Ireland, T. R., Floettmann, T., Fanning, C. M., Gibson, G. M., and Preiss, W. V., 1998, Development of the early Paleozoic Pacific margin of Gondwana from detrital-zircon ages across the Delamerian Orogen: Geology, v. 26, p. 243-246.

Jackson, M. A. and Hudec, M. R., 2005, Stratigraphic record of translation down ramps in a passive-margin salt detachment, Journal of Structural Geology, v. 27, p. 889-911.

Jacobsen, S. B., and Kaufman, A. J., 1999, The Sr, C and O isotopic evolution of Neoproterozoic seawater: Chemical Geology, v. 161, p. 37-57.

Janaway, T. M., and Parnell, J., 1989, Carbonate production within the Orcadian Basin, northern Scotland; a petrographic and geochemical study, in Talbot, M. R., and Kelts, K., eds., Palaeogeography, Palaeoclimatology, Palaeoecology, 70, p. 89-105.

Jenkins, R. J. F., 1990, The Adelaide fold belt: tectonic reappraisal, in Jago, J. B. and Moore, P. S., (eds.), The evolution of a late Precambrian-early Palaeozoic rift complex, the Adelaide Geosyncline, Geological Society of Australia Special Publication no. 16, p. 395-420.

Jenkins, R. J. F. and Sandiford, M., 1992, Observations on the tectonic evolution of the southern Adelaide Fold Belt, Tectonophysics, v. 214, p.27-36.

Johns, R K., 1956, The geology of the Farina Military Sheet, Geological Survey of South Australia Report of Investigations, v. 12, p. 15-26.

Karlstrom, K. E., Harlan, S. S., Williams, M. L., McLelland, J., Geissman, J. W., and Ahall, K.-I., 1999, Refining Rodinia; geologic evidence for the Australia-Western U.S. connection in the Proterozoic: GSA Today, v. 9, p. 1-7.

Kaufman, A. J., Hayes, J. M., Knoll A. H. and Germs, G. J. B., 1991, Isotopic composition of carbonates and organic carbon from upper Proterozoic successions in Namibia: stratigraphic variation and effects of diagenesis and metamorphism, Precambrian Research, v. 49, p. 301-327.

Kaufman, A. J., and Knoll, A. H., 1995, Neoproterozoic variations in the C-isotopic composition of seawater; stratigraphic and biogeochemical implications: Precambrian Research, v. 73, p. 27-49.

Kearey, P. and Brooks, M., 1991, An introduction to geophysical exploration, Blackwell Scientific, Oxford, 254p.

Kelly, N. M., Clarke, G. L., and Fanning, C. M., 2002, A two-stage evolution of the Neoproterozoic Rayner structural episode; new U-Pb sensitive high resolution ion microprobe constraints from the Oygarden Group, Kemp Land, East Antarctica: Precambrian Research, v. 116, p. 307-330.

Kelsey, D. E., Powell, R., Wilson, C. J. L. and Steele, D. A., 2003, (Th+U)-Pb monazite ages from Al-Mg-rich metapelites, Rauer Group, east Antarctica, Contributions to Mineral Petrology, v. 146, p. 326-340.

Kendall, A. C., 1992, Evaporites; in Walker, R. G., and James, N. P., (eds) Facies models: response to sea level change, Geological Association of Canada, p. 375-409.

Kendall, B., Creaser, R. A. and Selby, D. 2006, Re-Os geochronology of postglacial black shales in Australia: Constraints on the timing of "Sturtian" glaciations, Geology, v. 34, p. 729-732.

Kendall, B., Creaser, R. A., Calver, C. R., Raub, T. D and Evans, D. A. D., 2009, Correlation of Sturtian diamictite successions in southern Australia and northwestern Tasmania by Re-Os black shale geochronology and the ambiguity of "Sturtian"-type diamictite-cap carbonate pairs as chronostratigraphic marker horizons, Precambrian Research, v. 172, p. 301-310.

Kennedy, M., 1993, The Undoolya Sequence; late Proterozoic salt influenced deposition, Amadeus Basin, central Australia: Australian Journal of Earth Sciences, v. 40, p. 217-228.

Kennedy, M. J., 1996, Stratigraphy, sedimentology, and isotopic geochemistry of Australian Neoproterozoic postglacial cap dolostones; deglaciation, δ13C excursions and carbonate precipitation, Journal of Sedimentary Research, v. 66, p. 1050-1064.

Kennedy, M. J., Runnegar, B., Prave, A. R., Hoffmann, K. H., and Arthur, M. A., 1998, Two or four Neoproterozoic glaciations?: Geology, v. 26, p. 1059-1063.

Kennedy, M. J., Christie-Blick, N., and Sohl, L. E., 2001, Are Proterozoic cap carbonates and isotopic excursions a record of gas hydrate destabilization following Earth's coldest intervals, Geology, v. 29, p. 443-446.

Kilner, B., Macniocaill, C. and Brasier, M., 2005, Low latitude glaciation in the Neoproterozoic of Oman, Geology, v. 33, p. 413 – 416.

Kingsbury, J. A., Miller, C. F., Wooden, J. L., and Harrison, T. M., 1993, Monazite paragenesis and U-Pb systematics in rocks of the eastern Mojave Desert, California, U.S.A.; implications for thermochronometry: Chemical Geology, v. 110, p. 147-167.

Kinsman, D. J. J. and Holland, H.D., 1969, The co-precipitation of cations and CaCO3 IV, the co-precipitation of Sr2+ between 16o and 96o, Geochemica Cosmochima Acta, v. 33, p. 1-7.

Klaassen, N. 1991, The northern Flinders Ranges: mountains, minerals and mines, 1850-1920. Nic Klaassen, Eden Hills, 368p.

Klein, C., Hurlbut, C. S. and Dana, J. D., 1993, Manual of mineralogy: (after James D. Dana), 20th ed., New York, Wiley, 596 p.

Knoll, A. H., 2000, Learning to tell Neoproterozoic time, Precambrian Research, v. 100, p. 3-20.

Knoll, A. H., and Swett, K., 1990, Carbonate deposition during the late Proterozoic era; an example from Spitsbergen: American Journal of Science, v. 290-A, p. 104-132.

Knoll, A.H., Walter, M.R., Narbonne, G.M., Christie-Blick, N., 2006. The Ediacaran Period: a new addition to the geologic time scale. Lethaia 39, 13–30.

Korsch, R. L. and Huston, D. L., 2009, Geodynamics and metallogeny of North Queensland: insights from new deep crustal seismic data, Australian Institute of Geologists Bulletin, v. 49, p. 57-63.

Kositcin, N., and Krapez, B., 2004, Relationship between detrital zircon age-spectra and the tectonic evolution of the late Archaean Witwatersrand Basin, South Africa: Precambrian Research, v. 129, p. 141-168.

Kosler, J., Tubrett, M. N. and Sylvester, P. J., 2000, Appplication of laser ablationICP-MS to U-Th-Pb dating of monazite, Geostandards Newsletter, v. 25, p. 375-386.

Kossow, D. and Krawczyk, C. M., 2002, Structure and quantification of processes controlling the evolution of the inverted NE-German Basin, Marine and Petroleum Geology, v. 19, p. 601-618.

Krieg, G. W., Rogers, P. A., Callen, R. A., Freeman, P. J., Alley, N. F. and Forbes, B. G., 1991, Curdimurka, South Australia, Explanatory notes, 1:250,000 Geological Series, Geological Survey of South Australia, Report SH53-8, 60p.

Krieg, G. W. and Anthony, M., 1992, Curdimurka 1:250,000 Geological Map, Australia 1:250,000 geological series, Sheet SH 53-8, Geological Survey of South Australia.

Kroopnick, P., 1974,13C - CO2 Correlations in the Atmosphere and in Oceanic Surface Water: Eos, Transactions, American Geophysical Union, v. 55, p. 314.

Lambiase, J. J., and Bosworth, W., 1995, Structural controls on sedimentation in continental rifts, in Lambiase, J. J., (ed.) Hydrocarbon habitat in rift basins, Geological Society of London, Special Publications, v. 80, p. 117-144.

Landon, S. M., 1994, Summary, in Landon, S. M., (Ed.) Interior rift basins, American Association of Petroleum Geologists Memoir 59, p. 259-269.

Lanzirotti, A., and Hanson, G. N., 1996, Geochronology and geochemistry of multiple generations of monazite from the Wepawaug Schist, Connecticut, USA; implications for monazite stability in metamorphic rocks: Contributions to Mineralogy and Petrology, v. 125, p. 332-340.

Leeder, M.R., and Gawthorpe, R. L., 1987, Sedimentary models for extensional tilt-block/half-graben basins, in Coward, M. P., Dewey, J. F. and Hancock, P. L., Continental extensional tectonics (Eds.) Geological Society of London Special Publications, v. 28, p. 139-152.

Lemon, N. M., 1985, Physical modeling of sedimentation adjacent to diapirs and comparison with late Precambrian Oratunga breccia body in central Flinders Ranges, South Australia: AAPG Bulletin, v. 69, p. 1327-1338.

Lev, S. M., McLennan, S. M., Meyers, W. J., and Hanson, G. N., 1998, A petrographic approach for evaluating trace-element mobility in a black shale: Journal of Sedimentary Research, v. 68, p. 970-980.

Lev, S. M., McLennan, S. M., and Hanson, G. N., 1999, Mineralogic controls on REE mobility during black-shale diagenesis: Journal of Sedimentary Research, v. 69, p. 1071-1082.

Li, W-X. and Li, X-H., 2003, Adakitic granites within the NE Jiangxi ophiolites, South China: geochemical and Nd isotopic evidence, Precambrian Research, v. 122, p. 29-44.

Li, X. H., Guoging, Z., Zhao, J., Fanning, C. N. and Compston, W.,1994, SHRIMP ion microprobe zircon U-Pb age and Sm-Nd isotopic characteristics of the NE Jiangxi ophiolite and its tectonic implications, Chinese Journal of Geochemistry, v. 13, p. 317-325.

Li, X. H. and McCulloch, M.T., 1996, Secular variations in the Nd isotopic composition of Late Proterozoic sediments from the southern margin of the Yangtze Block: evidence for a Proterozoic continental collision in SE China. Precambrian Research, v.76, p. 67–76.

Li, X. H., Li, Z.X., Ge,W., Zhou, H. W., Li,W. X., Wingate, M. T. D., 2003, Neoproterozoic granitoids in South China: crystal melting above a mantle plume at ca. 825Ma? Precambrian Research, v. 122, p. 45–83.

Li, X. H., Li, W. X., Li, Z. X., Lo, C. H., Wang, J., Ye, M. F. and Yang, Y. H., 2009, Amalgamation between the Yangtze and Cathaysia Blocks in South China: Constraints from SHRIMP U-Pb zircon ages, geochemistry and Nd-Hf isotopes of the Shuangxiwu volcanic rocks, Precambrian Research, v. 174, p. 117-128.

Li, Z. X., Zhang, L., and Powell, C. M., 1995, South China in Rodinia; part of the missing link between Australia-East Antarctica and Laurentia?: Geology, v. 23, p. 407-410.

Li, Z. X., Zhang, L. and Powell, C. M., 1996, Positions of the East Asian cratons in the Neoproterozoic supercontinent Rodinia, Australian Journal of Earth Sciences, v. 43, p. 593-604.

Li, Z. X., Li, X.H., Kinny, P.D. and Wang, J. 1999, The break-up of Rodinia: did it start with a mantle plume beneath South China, Earth and Planetary Science Letters, v. 173, p. 171-181.

Li, Z. X., and Powell, C. M., 2001, An outline of the palaeogeographic evolution of the Australasian region since the beginning of the Neoproterozoic: Earth-Science Reviews, v. 53, p. 237-277.

Li, Z. X., Li, X., Zhou, H., and Kinny, P. D., 2002, Grenvillian continental collision in South China; new SHRIMP U-Pb zircon results and implications for the configuration of Rodinia: Geology, v. 30, p. 163-166.

Li, Z. X., Li, X. H., Kinny, P.D., Wang, J., Zhang, S., Zhou, H.W., 2003, Geochronology of Neoproterozoic syn-rift magmatism in the Yangtze Craton, South China and correlations with other continents: evidence for a mantle superplume that broke up Rodinia. Precambrian Research, v. 122, p. 85–109.

Li, Z. X., Bogdanova, S. V., Collins, A. S., Davidson, A., De Waele, B., Ernst, R. E., Fitzsimmons, I. C. W., Fuck, R. A., Gladkochub, D. P., Jacobs, J., Karlstrom, K. E., Lu, S., Natapov, L. M., Pease, V., Pisarevsky, S. A., Thrane, K. and Vernikovsky, V., 2008, Assembly, configuration and break-up history of Rodinia: A synthesis, Precambrian Research, v. 160, p. 179-210.

Ling, W., Gao, S., Zhang, B., Li, H., Liu, Y. and Cheng, J., 2003, Neoproterozoic tectonic evolution of the northwestern Yangtze craton, South China: implications for amalgamation and break-up of the Rodinia Supercontinent, Precambrian Research, v. 122, p. 111-140.

Lindsay, J. F., 2002, Supersequences, superbasins, supercontinents – evidence from the Neoproterozoic-Early Palaeozoic basins of central Australia, Basin Research, v. 14, p. 207-223.

Lindsay, J. F., Kruse, P. D., Green, O. R., Hawkins, E., Brasier, M. D., Cartlidge, J. and Corfield, R. M., 2005, The Neoproterozoic-Cambrian record in Australia: A stable isotope study, Precambrian Research, v. 145, p. 113-133.

Ling, W., Gao, S., Zhang, B., Li, H., Liu, Y., Cheng, J., Cho, M., and Li, X., 2003, Neoproterozoic tectonic evolution of the northwestern Yangtze Craton, South China; implications for amalgamation and break-up of the Rodinia supercontinent: Precambrian Research, v. 122, p. 111-140.

Ludwig, K. R., 2001, Users manual for Isoplot/Ex, revision 2.49: A geochronological tool kit, p. 55.

Ludwig, K. R., 2003 Users manual for Isoplot 3.00: a geochronological toolkit for Microsoft Excel, Berkeley Geochronology Center Special Publication.

Lund, K., Aleinikoff, J. N., Evans, K. V. and Fanning, C. M., 2003, SHRIMP U-Pb geochronology of Neoproterozoic Windermere Supergroup, central Idaho: Implications for rifting of western Laurentia and synchroneity of Sturtian glacial deposits, Geological Society of America Bulletin, v. 115, p. 349-372.

McBride, B. C., Rowan, M. G. and Weimer, P., 1998, The evolution of allochthonous salt systems, northern Green Canyon and Ewing Bank (offshore Louisiana), norther Gulf of Mexico, American Association of Petroleum Geologists, v. 82, p. 1013-1036.

Mack, G. H. and Stout, D. M., 2005, Unconventional distribution of facies in a continental rift basin: the Pliocene-Pleistocene Mangas Basin, south-western New Mexico, Sedimentolog v.52, p. 1187-1205.

McKenzie, D., 1978, Some remarks on the development of sedimentary basins: Earth and Planetary Science Letters, v. 40, p. 25-32.

McKenzie, J. A., 1981, Holocene dolomitization of calcium carbonate sediments from the coastal sabkhas of Abu Dhabi, U.A.E.; a stable isotope study: Journal of Geology, v. 89, p. 185-198.

McLaren, S., Dunlap, W. J., Sandiford, M. and McDougall, I., 2002 (a), Thermochronology of high heat-producing crust at Mount Painter, South Australia; implications for tectonic reactivation of continental interiors, Tectonics, v. 21, p. no.4, 18.

McLaren, S., Sandiford, M., White, R., and Powell, R., 2002 (b), The thermal evolution of the Mount Painter Province; granite genesis during thermal sag?: Abstracts - Geological Society of Australia, v. 67, p. 182.

McLeod, A. E., Underhill, J. R., Davies, S. J. and Dawers, N. H., 2002, The influence of fault array evolution on synrift sedimentation patterns: controls on deposition in the Strathspey-Brent-Statfjord half graben, northern North Sea. American Association of Petroleum Geologists Bulletin, v. 86, p. 1061-1093.

McRae, T., 1950, The isotopic chemistry of carbonates and a paleotemperature scale. Journal of Chemical Physics, v. 18, p. 859-857.

Mahan, K. H., Wernicke, B. P. and Jercinovic, 2010, Th-U-Pb geochronology of authigenic monazite in the Adelaide rift complex, South Australia, and implications for the age of the type Sturtian and Marinoan glacial deposits, Earth and Planetary Science Letters, v. 289, p. 76 – 86.

Maidment, D. W., Williams, I. S. and Hand, M, 2007, Testing long-term patterns of basin sedimentation by detrital zircon geochronology, Centralian Superbasin, Australia, Basin Research, v. 19, p. 335-360.

Major R. B. and Conor, C. H. H., 1993, The Musgrave Block, in Parker, A. J., (Ed), The geology of South Australia, Volume 1, The Precambrian, Geological Survey of South Australia, Bulletin 54, p. 156-167.

Mandl, G., 2000, Faulting in brittle rocks; an introduction to the mechanics of tectonic faults, Springer, New York, 434p.

Manktelow, N. S., 1990, Structure of the Adelaide Fold Belt, In Jago, J.B. and Moore, P.S. (Eds), The evolution of a late Precambrian - early Palaeozoic rift complex: the Adelaide Geosyncline. Geological Society of Australia, Special Publication v. 16, p. 369-395.

Mapes, R. W., Coleman, D. S., Nogueira, A. C. R. and Housh, T., 2004, How far do zircons travel? Evaluating the significance of detrital zircon provenance using the modern Amazon River fluvial system, Abstracts with Programs - Geological Society of America, v. 36, p. 78.

Marshak, S., 1988 Kinematics of orocline and arc formation in thin-skinned orogens, Tectonics, v. 7, p. 73-86.

Marshak, S., and Floettmann, T., 1996, Structure and origin of the Fleurieu and Nackara arcs in the Adelaide fold-thrust belt, South Australia; salient and recess development in the Delamerian Orogen: Journal of Structural Geology, v. 18, p. 891-908.

Mason, M.G., Thompson, B.P., and Tonkin, D.G., 1978, Regional stratigraphy of the Beda Volcanics, Backy Point Beds and Pandurra Formation on the Stuart Shelf, South Australia, Quarterly Geological Notes, Geological Survey of South Australia, v. 66, p. 2-9.

Mauduit, T., Guerin, G., Brun, J. P. and Lecanu, H., 1997, Raft tectonics: the effects of basal slope angle and sedimentation rate on progressive extension. Journal of Structural Geology, v. 19, p. 1219-1230.

Mawson, D., 1927. Geological notes on an area along the northeastern margin of the north-eastern portion of the Willouran Range, Royal Society of South Australia. Transactions 51, pp 386-390.

Mawson, D., 1940, Tillite and other rocks from Hallet Cove, SA, Transactions of the Royal Society of South Australia, v. 62, p. 362.

Mawson, D., and Sprigg, R. C., 1950, Subdivision of the Adelaide system: Australian Journal of Science, v. 13, p. 69-72.

Mege, D. and Korme, T., 2004, Dyke swarm emplacement in the Ethiopian Large Igneous Province: not only a matter of stress, Journal of volcanology and geothermal research, v. 132, p. 283-310.

Melezhik, V. A., Gorokhov, I. M., Fallick, A. E., and Gjelle, S., 2001, Strontium and carbon isotope geochemistry applied to dating of carbonate sedimentation; an example from high-grade rocks of the Norwegian Caledonides: Precambrian Research, v. 108, p. 267-292.

Melezhik, V. A. and Fallick, A. E., 2003, δ13C and δ18O variations in primary and secondary carbonate phases, several contrasting examples from Palaeoproterozoic δ13C-rich metamorphosed dolostones, Chemical Geology, v. 201, p. 213-228.

Melezhik, V. A., Fallick, A. E. and Pokrovsky, 2005, Enigmatic nature of thick sedimentary carbonates depleted in 13C beyond the canonical mantle value: The challenges to our understanding of the terrestrial carbon cycle, Precambrian Research, v. 137, p. 131-165.

Mendis, P.J. 2002, The origin of the Geological Structures Diapirs, Grabens abd Barite veins in the Flinders Range, South Australia, PhD Thesis (unpublished), University of Adelaide.

Mendelsohn, F., 1961, The Geology of the northern Rhodesian Copperbelt, McDonald, London, 523p.

Menzies, M., Baker, J. and Chazot, G., 2001, Cenozoic plume evolution and flood basalts in Yemen: A key to understanding older examples, In Ernst, R. E., (Ed), Mantle plumes; their identification through time, Geological Society of America, Special Publication, v. 352, p, 23-36.

Miall, A. D., 1977, A review of the braided-river depositional environment: Earth-Science Reviews, v. 13, p. 1-62.

Mildren, S D. and Sandiford, M., 1995, Heat refraction and low pressure metamorphism in the northern Flinders Ranges, South Australia, Australian Journal of Earth Sciences, v. 42, p. 241-247.

Milodowski, A. E., and Zalasiewicz, J. A., 1991, Redistribution of rare earth elements during diagenesis of turbidite/hemipelagite mudrock sequences of Llandovery age from central Wales: Geological Society Special Publications, v. 57, p. 101-124.

Mitchell, M. M., Kohn, B. P and Foster, D. A., 1998, Post-orogenic cooling history of eastern South Australia from apatite FT thermochronology, in van den Haute, P and De Corte, F. (Eds), Advances in fission track geochronology, Kluwer Academic Publishers, Netherlands, p. 207-224.

Mohriak, W. U., Macedo, J. M., Castellani, R. T., Rangel, H. D., Barros, A. Z. N., Latge, M. A. L., Ricci, J. A., Mizusaki, A. M. P., Szatmari, P., Demercian, L. S., Rizzo, J. G., and Aires, J. R., 1995, Salt tectonics and structural styles in the deep-water province of the Cabo Frio region, Rio de Janeiro, Brazil, in Jackson, M. P. A., Roberts, D. G., and Snelson, S., eds., AAPG Memoir, vol.65, p. 273-304.

Montel, J.-M., Foret, S., Veschambre, M., Nicollet, C., and Provost, A., 1996, Electron microprobe dating of monazite: Chemical Geology, v. 131, p. 37-53.

Moores, E. M., 1991, Southwest U.S.-East Antarctic (SWEAT) connection; a hypothesis: Geology, v. 19, p. 425-428.

Morley, C. K., 2007, Development of crestal normal faults associated with deepwater fold growth. Journal of Structural Geology, v. 29, p. 1148-1163.

Morley, C. K. and Guerin, G., 1996, Comparison of gravity-driven deformation styles and behavior associated with mobile shales and salt, Tectonics, v. 15, p. 1154-1170.

Morrison, R. S., and Foden, J. D., 1990, A zoned Middle Cambrian pluton in the Peake and Denison ranges, South Australia: Special Publication - Geological Society of Australia, v. 16, p. 450-464.

Mount, T.J., 1975, Diapirs and diapirism in the Adelaide “Geosyncline’, South Australia, University of Adelaide PhD Thesis (unpublished).

Mourgues, R. and Cobbold, P. R., 2006, Sandbox experiments on gravitational spreading and gliding in the presence of fluid overpressures, Journal of Structural Geology, v. 28, p. 887-901.

Mrazec, L. 1907, Despre cute cu simbure de strapungere: Buletinul Societatii de Stiinte, v. 16, p. 1-12.

Murrell, B., 1977, Stratigraphy and tectonics across the Torrens Hinge Zone between Andamooka and Marree, South Australia, University of Adelaide, PhD Thesis (unpublished).

Miall, A. D., 1977, A review of the braided river depositional environment, Eartch Science Reviews, v. 13, p. 1-62.

Nelson, T. H., and Fairchild, L., 1989, Emplacement and evolution of salt sills in the northern Gulf of Mexico: Bulletin - Houston Geological Society, v. 32, p. 6-7.

Nelson, D. R., 2005a, 178070: amphibolites, Haig Cave; Geochronology dataset 596; in Compilation of geochronology data, June 2006 update: Western Australia Geological Survey.

Nelson, D. R., 2005b, 178071: recrystallized biotite microtonalite, Haig Cave; Geochronology dataset 597; in Compilation of geochronology data, June 2006 update: Western Australia Geological Survey.

Nelson, D. R., 2005c, 178072: tonalitic gneiss, Haig Cave; Geochronology dataset 598; in Compilation of geochronology data, June 2006 update: Western Australia Geological Survey.

Newton, M. S., 1994, Holocene fluctuations of Mono Lake, California: the sedimentary record, in Renaut, R. W. and Last, W. M., (eds), Sedimentology and geochemistry of modern and ancient saline lakes, Special Publication, Society of Sedimentary Geology, v. 50, p. 143-157.

Offler, R. and Fleming, P. D., 1968, A synthesis of folding and metamorphism in the Mt Lofty Ranges, South Australia, Journal of the Geological Society of Australia, v. 15, p. 245-266.

Oliver, N. H. S. and Zakowski, S., 1995, Timing and geometry of deformation, low-pressure metamorphism and anatexis in the eastern Mt Lofty Ranges: the possible role of extension, Australian Journal of Earth Sciences, v. 42, p. 501-507.

Overstreet, W. C., 1967, The geological occurrence of monazite, United States Geological Survey, Professional Paper 530.

Parker, A.J., 1983, Tectonic development of the Adelaide Fold Belt, Geological Society of Australia, Abstracts v. 10. p. 23-28.

Parker, A. J., Cowley, W. M. and Thomson, B. P., 1990, The Torrens Hinge Zone and Spencer Shelf with particular reference to early Adelaidean volcanism, In Jago, J.B. and Moore, P.S. (eds), The evolution of a late Precambrian - early Palaeozoic rift complex: the Adelaide Geosyncline. Geological Society of Australia, Special Publication 16, p. 129-148.

Parrish, R. R., 1990, U-Pb dating of monazite and its application to geological problems: Canadian Journal of Earth Sciences = Journal Canadien des Sciences de la Terre, v. 27, p. 1431-1450.

Paul, E., Flottmann, T., and Sandiford, M., 1999, Structural geometry and controls on basement-involved deformation in the northern Flinders Ranges, Adelaide fold belt, South Australia: Australian Journal of Earth Sciences, v. 46, p. 343-354.

Playfair, 1984

Porter, S. M., Knoll, A. H.and Affaton, P., 2004, Chemostratigraphy of Neoproterozoic cap carbonates from the Volta Basin, West Africa, Precambrian Research, v. 13, p. 99-112.

Powell, C. M., Preiss, W. V., Gatehouse, C. G., Krapez, B., and Li, Z. X., 1994, South Australian record of a Rodinian epicontinental basin and its mid-Neoproterozoic breakup (approximately 700 Ma) to form the palaeo-Pacific Ocean: Tectonophysics, v. 237, p. 113-140.

Pratt, B. R., James, N. P., and Cowan, C. A., 1992, Peritidal carbonates, in Walker, R. G., and James, N. P., eds.: St. Johns, Geological Association of Canada.

Prave, A. R., Fallick, A. E., Thomas, C. W. and Graham, C. M., 2009, A composite C-isotope profile for the Neoproterozoic of Scotland and Ireland, Journal of the Geological Society of London, v. 166, p. 845 – 857.

Preiss, W. V., 1982, Supergroup classification in the Adelaide Geosyncline, Transactions of the Royal Society of South Australia, v. 106, p. 81-83.

Preiss, W. V., 1985, Straitgraphy and tectonics of the Woruma Anticline and associated intrusive breccias, Bulletin - Geological Survey of South Australia, v. 52, p. 85.

Preiss, W.V., 1987, The Adelaide Geosyncline: Late Proterozoic stratigraphy, sedimentation, palaentology and tectonics. The Geological Survey of South Australia, Bulletin 53, 438p.

Preiss, W.V., 1993, Neoproterozoic, in Drexel, J. F., Preiss, W. V. and Parker, A. J., (eds) The geology of South Australia 1, the Precambrian, Bulletin of the Geological Survey of South Australia, v. 54, p. 170-204.

Preiss, W. V., 1997, Revision of lithostratigraphy and structure, and evidence of volcanism in lower Burra Group type sections, Carey Gully-Basket Range area, Mount Lofty Ranges: MESA Journal, v. 7, p. 37-46.

Preiss, W. V., 2000, The Adelaide Geosyncline of South Australia and its significance in Neoproterozoic continental reconstruction: Precambrian Research, v. 100, p. 21-63.

Preiss, W. V. and Forbes, B. G., 1981, Stratigraphy, correlation and sedimentary history of Adelaidean (late Proterozoic) basins in Australia, Precambrian Research, v. 15, p. 255-304.

Preiss, W. V., Dyson, I. A., Reid, P. W. and Cowley, W. M., 1998, Revision of lithostratigraphic classification of the Umberatana Group, MESA Journal, v. 9, p. 36-42.

Preiss, W. V. and Cowley, W. M., 1999, Genetic stratigraphy and revised lithostratigraphic classification of the Burra Group in the Adelaide Geosyncline, MESA Journal, v. 14, p. 30-40.

Prosser, S., Williams, G. D., and Dobb, A., 1993, Rift-related linked depositional systems and their seismic expression: Geological Society Special Publications, v. 71, p. 35-66.

Pyle L. J., Narbonne, G. M., James, N. J., Dalrymple, R. W. and Kaufmann, A. J., 2004, Integrated Ediacaran chronostratigraphy, Wernecke Mountains, northwestern Canada, Precambrian Research, v. 132, p. 1-27.

Raetz, M., Krabbendam, M., and Donaghy, A. G., 2002, Compilation of U-Pb zircon data from the Willyama Supergroup, Broken Hill region, Australia; evidence for three tectonostratigraphic successions and four magmatic events?: Australian Journal of Earth Sciences, v. 49, p. 965-983.

Rainbird, R. H., Heaman, L. M., and Young, G. M., 1992, Sampling Laurentia; detrital zircon geochronology offers evidence for an extensive Neoproterozoic river system originating from the Grenville Orogen: Geology, v. 20, p. 351-354.

Ramsay, J. G., 1967, Folding and fracturing of rocks, McGraw-Hill, New York, 568p.

Rasmussen, B., Fletcher, I. R., and McNaughton, N. J., 2001, Dating low-grade metamorphic events by SHRIMP U-Pb analysis of monazite in shales: Geology, v. 29, p. 963-966.

Rasmussen, B., and Fletcher, I. R., 2002, Indirect dating of mafic intrusions by SHRIMP U-Pb analysis of monazite in contact metamorphosed shale; an example from the Palaeoproterozoic Capricorn Orogen, Western Australia: Earth and Planetary Science Letters, v. 197, p. 287-299.

Ray, J. S., Veizer, J., and Davis, W. J., 2003, C, O, Sr and Pb isotope systematics of carbonate sequences of the Vindhyan Supergroup, India; age, diagenesis, correlations and implications for global events: Precambrian Research, v. 121, p. 103-140.

Rayner, R. A. and Rowlands, N. J., 1980, Stratiform copper in the late Proterozoic Boorloo Delta, South Australia, Mineralium Deposita, v. 15, p. 139-149.

Read, D., Cooper, D. C., and McArthur, J. M., 1987, The composition and distribution of nodular monazite in the lower Palaeozoic rocks of Great Britain: Mineralogical Magazine, v. 51, p. 271-280.

Reid, A. R., 2008, U-Pb zircon dating of the porphyry, Burra Mine, Appendix G in, Drexel., J. F., 2009, Review of the Burra Mine project, 1980 – 2008 – a progress report, South Australia , Department of Primary Industries and Resources, Report Book 2008/16, 8p.

Reid, P. W. and Preiss, W. V., 1999, Parachilna map sheet (second edition), South Australia Geological Survey, Geological Atlas 1:250,000 Series, Sheet SH54-13.

Renaut, R. W. and Tiercelin, J. J., 1994 Lake Bogoria, Kenta Rift valley, a sedimentological overview, in Renaut, R. W and Last, W. M. (eds) Sedimentology and geochemistry of modern and ancient saline lakes, Special Publication – Society for Sedimentary Geology, v. 50, p. 101-123.

Ripperdan, R. L., 1994, Global variations in carbon isotope composition during the latest Neoproterozoic and earliest Cambrian: Annual Review of Earth and Planetary Sciences, v. 22, p. 385-417.

Robertson, R. S., Preiss, W. V., Crooks, A. F., Hill, P. W., and Sheard, M. J., 1998, Review of the Proterozoic geology and mineral potential of the Curnamona Province in South Australia: AGSO Journal of Australian Geology and Geophysics, v. 17, p. 169-182.

Røe, S. L., 1987, Cross-strata and bedforms of probable transitional dune to upper-stage plane-bed origin from a late Precambrian fluvial sandstone, northern Norway: Sedimentology, v. 34, p. 89-101.

Rosen, M. R., and Warren, J., 1990, The origin and significance of groundwater-seepage gypsum from Bristol Dry Lake, California, USA, Sedimentology, v. 37, p. 983-996.

Rosen, M.R., 1994, The importance of groundwater in playas; a review of playa classifications and the sedimentology and hydrology of playas, in Rosen (ed.), Palaeoclimate and basin evolution of Playa systems, Geological Society of America Special Paper, v. 289, p. 1-18.

Rosen, M. R., Turner, J. V., Coshell, L., and Gailitis, V., 1995, The effects of water temperature, stratification, and biological activity on the stable isotopic composition and timing of carbonate precipitation in a hypersaline lake: Geochimica et Cosmochimica Acta, v. 59, p. 979-990.

Ross, G. M., Parrish, R. R., and Winston, D., 1992, Provenance and U-Pb geochronology of the Mesoproterozoic Belt Supergroup (northwestern United States); implications for age of deposition and pre-Panthalassa plate reconstructions: Earth and Planetary Science Letters, v. 113, p. 57-76.

Ross, G. M. and Villeneuve, M. E., 1999, The Belt Basin; provenance insights offer tectonic hindsight, Abstracts with Programs - Geological Society of America, v. 31, p. 300.

Rouby, D., Guillocheau, F., Robin, C, Bouroullec, R., Raillard, S., Castelltort, S. and Nalpas, T., 2003, Rates of deformation of an extensional growth fault/raft system (offshore Congo, West African margin) from combined accommodation measurements and 3-D restoration, 2003, Basin Research, v. 15, p. 183-200.

Rowan, M. G., 1995, Structural styles and evolution of allochthonous salt, central Louisiana outer shelf and uppler slope, American Association of Petroleum Geologists, v. 65, p. 199-228.

Rowan, M. G., Peel, F. J., and Vendeville, B. C., 2004, Gravity-driven fold belts on passive margins: AAPG Memoir, v. 82, p. 157-182.

Rowlands, N. J. and Warin, O. N., Gitological aspects of some Adelaidean stratiform copper deposits, Minerals Science and Engineering, v. 10, p. 258-277.

Rowlands, N.J., Blight, P.G., Jarvis, D.M., and von der Borch, C.C., 1980, Sabhka and playa environments in later Proterozoic grabens, Willouran Ranges, South Australia. Journal of the Geological Society of Australia, 27, 55-68.

Rowlands, N. J., Jarvis, D. M., Benade, D. R., Circosta, G. and Blight, P. G., 1981, South Australia copper project, EL 461 – Willouran Ranges: Fourth annual report on exploration Activities (period 24.12.79 – 3.4.81), Utah Development Company, Open File envelope, 3507 (unpubl), 119p

Rubatto, D., Williams, I. S., and Buick, I. S., 2001, Zircon and monazite response to prograde metamorphism in the Reynolds Range, central Australia: Contributions to Mineralogy and Petrology, v. 140, p. 458-468.

Rutland, R. W. R., Parker, A.J., Pitt, G.M., Preiss, W.V. and Murrell, B., 1981, The Precambrian of South Australia, In Hunter, D.R. (Ed.), Precambrian of the Southern Hemisphere. Developments in Precambrian geology series 2, Elsevier, Amsterdam, p. 309-360.

Sandiford, M., Fraser, G., Arnold, J. Foden, J. and Farrow, T., 1995, Some causes and consequences of high temperature, low pressure metamorphism in the eastern Mt Loft Ranges, South Australia, Australian Journal of Earth Sciences, v.42, p.233-240.

Sandiford, M and McLaren, S., 2002 Tectonic feedback and the ordering of heat producing elements within the continental lithosphere, Earth and Planetary Science Letters, . 204, p. 133-150.

Sandiford, M., Paul, E. and Flottmann, T.,1998, Sedimentary thickness variations and deformation intensity during basin inversion in the Flinders Ranges, South Australia, Journal of Structural Geology, v.20, p.1721-1731.

Sandiford, M., and Wilson, C. J. L., 1984, The structural evolution of the Fyfe Hills-Khmara Bay region, Enderby Land, East Antarctica: Australian Journal of Earth Sciences, v. 31, p. 403-426.

Santos, R. V., de Alvarenga, C. J. S., Dardenne, M. A., Sial, A. N., and Ferreira, V. P., 2000, Carbon and oxygen isotope profiles across Meso-Neoproterozoic limestones from central Brazil; Bambui and Paranoa groups: Precambrian Research, v. 104, p. 107-122.

Saylor, B. Z., Kaufman, A. J., Grotzinger, J. P., and Urban, F., 1998, A composite reference section for terminal Proterozoic strata of southern Namibia: Journal of Sedimentary Research, v. 68, p. 1223-1235.

Scheck, M., Bayer, U., and Lewerenz, B., 2003, Salt movements in the Northeast German Basin and its relation to major post-Permian tectonic phases; results from 3D structural modelling, backstripping and reflection seismic data: Tectonophysics, v. 361, p. 277-299.

Scheck-Wenderoth, M., Krzywiec, P., Zuhlke, R., Maystrenko, Y. and Froitzheim, N., 2008, Permian to Cretaceous tectonics, in McCann, T., (editor), The geology of Central Europe - Volume 2, Mesozoic and Cenozoic, Geological Society, p. 999-1030.

Schidlowski, M., 2001, Carbon isotopes as biogeochemical recorders of life over 3.8 Ga of Earth history; evolution of a concept: Precambrian Research, v. 106, p. 117-134.

Schrag, D. P., Berner, R. A., Hoffman, P. F. and Halverson, G. P., 2002, On the initiation of a snowball Earth, v. 3, 10.1029/2001GC000219.

Schultz, K., 1994, Structure and stratigraphy of the Gulf of Suez, Egypt, in Landon, S. M., (Ed.) Interior rift basins, American Association of Petroleum Geologists Memoir 59, p.57-96

Schultz-Ela, D. D., 2001, Excursus on gravity gliding and gravity spreading, Journal of Structural Geology, v. 23, p. 725-731.

Schultz-Ela, D. D. and Walsh, P., 2002, Modeling of grabens extending above evaporates in Canyonlands National Park, Utah, Journal of Structural Geology, v. 24, p. 247-275.

Scoular, G., 1886, Sketch of the gology of the southern and western part of the Lake Eyre basin, Transactions, Royal Society of South Australia Transactions, v. 9, p. 39-54.

Scrimgeour, I. R., Close, D. F. and Edgoose, C. J., 1999, Petermann Ranges, N.T. 1:250,000 Geological Series Department of Mines and Energy, Northern Territory Geological Survey, Explanatory Notes SG52-7.

Selley, D., 2000, Proterozoic sediment hosted copper deposits. Geological framework and copper mineralization of South Australia, AMIRA/ARC Research Project 544, December 2000 meeting report.

Selley, D. and Bull, S., 2001, Basin architecture during deposition of the lower to middle Umberatana Group, Adelaide Fold Belt, South Australia; implications for Cu mineralization, In P544 Proterozoic sediment-hosted copper deposits. AMIRA/ARC Progress Report, December 2000, p. 1-45.

Selley, D., Broughton, D., Scott, R., Hitzman, M., Bull, S. W., Large, R., R., McGoldrick, P. J., Croaker, M. W., Pollington, N. and Barra, F., 2005, A new look at the geology of the Zambian Copperbelt. In Hedenquist, J. W., Thompson, J. F. H., Goldfarb, R. J. and Richards, J. P., (eds) Economic Geology; one hundredth anniversary volume, 1905 – 2005, p. 965 – 1000.

Sengor, A. M. C., 2001, Elevation as indicator of mantle plume activity, In Ernst, R. E., (Ed), Mantle plumes; their identification through time, Geological Society of America, Special Publication, v. 352, p. 183-225.

Seong-Joo, L., Browne, K. M. and Golubic, S., 2000, On stromatolite lamination, in Riding, R. E. and Awramik, S. M. (eds), Microbial Sediments, Springer-Verlag, Berlin Heidelberg, p. 16-24.

Shaw, R. D., Wellman, P., Gunn, P. J., Whitaker, A. J., Tarlowski, C and Morse, M. P., 1996 Guide to using the Australian crustal elements map, Australian Geological Survey Organisation Record 1996/30.

Shield, G., and Veizer, J., 2002, Precambrian marine carbonate isotope database: version 1.., Geochemistry, geophysics Geosystems, v3(6) 10.1029/2001GC000266.

Shelley, D. C. and Lawton, T. F., 2005, Sequence stratigraphy of tidally influenced deposits in a salt-withdrawal minibasin; upper sandstone member of the Potrerillos Formation (Paleocene), La Popa Basin, Mexico, AAPG Bulletin, v. 89, p. 1157-1179.

Sherkati, S., Molinaro, M., de Lamotte, F. D. and Letouzey, J., 2005, Detachment folding in the Central and Eastern Zagros fold-belt (Iran): salt mobility, multiple detachments and late basement control, Journal of Structural Geology, v. 27, p. 1680-1696.

Shinn, E. A., 1983, The tidal flat environment; in, Scholle, P. A., Bebout, D. G. and Moore, C. H (eds), Carbonate depositional environment, American Association of Petroleum Geologists Memoir 33, p. 171-210.

Shinn, E. A., Steinen, R. P., Lidz, B. H. and Swart, P. K., 1989, Whitings, a sedimentologic dilemma, Journal of Sedimentary Petrology, v. 59, p. 147-161.

Smith, D. B., 1971, Possible displacive halite in the Permian Upper Evaporite Group of northeast Yorkshire: Sedimentology, v. 17, p. 221-232.

Smith, R. D. A., 1995, Reservoir architecture of syn-rift lacustrine turbidite systems, Early Cretaceous, offshore Gabon, in Lambiase, J. J. (ed.), Hydrocarbon habitat in rift basins, Geological Society Special Publications, v. 80, p. 197-210.

Smith, H. A., and Barreiro, B., 1990, Monazite U-Pb dating of staurolite grade metamorphism in pelitic schists: Contributions to Mineralogy and Petrology, v. 105, p. 602-615.

Smith, M. P., Henderson, P., and Zhang, P., 1999, Reaction relationships in the Bayan Obo Fe-REE-Nb deposit Inner Mongolia, China; implications for the relative stability of rare-earth element phosphates and fluorocarbonates: Contributions to Mineralogy and Petrology, v. 134, p. 294-310.

Southgate, P. N., 1991, A sedimentological model for the Loves Creek Member of the Bitter Springs Formation, northern Amadeus Basin, in Korsch, R. and Kennard, J. M., (eds) Geological and geophysical studies in the Amadeus Basin, central Australia, Australian Bureau of Mineral Resources, Bulletin, v. 236, p. 113-126.

Spathopoulos, F., 1996, An insight on salt tectonics in the Angola Basin, South Atlantic: Geological Society Special Publications, v. 100, p. 153-174.

Spiegel, C., Siebel, W., Kuhlemann, J., and Frisch, W., 2004, Toward a comprehensive provenance analysis; a multi-method approach and its implications for the evolution of the Central Alps: Special Paper - Geological Society of America, v. 378, p. 37-50.

Sprigg, R.C., 1947, Early Cambrian (?) jellyfishes from the Flinders Rangers, South Australia, Transcripts of the Royal Society South Australia, v 71, p. 212-224.

Sprigg, R. C., 1949, Thrust structures of the Witchelina area, South Australia, Transactions of the Royal Society of South Australia, v. 73, p. 40-47.

Sprigg, R. C., 1952, Sedimentation in the Adelaide geosyncline and the formation of the continental terrace.

Stewart, J. H., Gehrels, G. E., Barth, A. P., Link, P. K., Christie-Blick, N., and Wrucke, C. T., 2001, Detrital zircon provenance of Mesoproterozoic to Cambrian arenites in the Western United States and northwestern Mexico: Geological Society of America Bulletin, v. 113, p. 1343-1356.

Stewart, S. A., 1996, Influence of detachment layer thickness on style of thin-skinned shortening, Journal of Structural Geology, v. 18, p. 1271-1274.

Stewart, S. A. and Coward, M. P., 1995, Synthesis of salt tectonics in the southern North Sea, UK, Marine and Petroleum Geology, v. 12, p. 457-475.

Stewart, S. A., and Coward, M. P., 1996, Genetic interpretation and mapping of salt structures: First Break, v. 14, p. 135-141.

Stovba, S. M. and Stephenson, R. A., 2002, Style and timing of salt tectonics in the Dniepr-Donets Basin (Ukraine): implications for triggering and driving mechanisms of salt movement in sedimentary basins, Marine and Petroleum Geology, v. 19, p. 1169-1189.

Stuiver, M., 1975, Climate versus changes 13C content of the organic component of lake sediments during the late Quaternary: Quaternary Research, v. 5, p. 251-262.

Sun, S. Q., 1994, A reappraisal of dolomite abundance and occurrence in the Phanerozoic: Journal of Sedimentary Research, Section A: Sedimentary Petrology and Processesj, v. 64, p. 396-404.

Sun, S. S., Sheraton, J. W., Glikson, A. Y., and Stewart, A. J., 1996, A major magmatic event during 1050-1080 Ma in central Australia and an emplacement age for the Giles Complex, in Kennard, J. M., ed., Abstracts - Geological Society of Australia, vol.41, p. 423.

Suppe, J., 1983, Geometry and kinematics of fault bend folding, American Journal of Science, v. 283, p. 684-721.

Suppe J., Chou, G. T. and Hook, S.C., 1992. Rates of folding and faulting determined from growth strata, in McClay, K. R., (Ed), Thrust Tectonics. Chapman and Hall, Suffolk, p. 105-121.

Surge, D. M., Savarese, M., Dodd, J. R., and Lohmann, K. C., 1997, Carbon isotopic evidence for photosynthesis in Early Cambrian oceans: Geology, v. 25, p. 503-506.

Suzuki, K., and Adachi, M., 1991, The chemical Th-U-total Pb isochron ages of zircon and monazite from the gray granite of the Hida Terrane, Japan: Journal of Earth Sciences, Nagoya University, v. 38, p. 11-37.

Swain, G., Woodhouse, A., Hand, M., Barovich, K., Schwarz, M. and Fanning, C. M., 2005, Provenance and tectonic development of the late Archaean Gawler Craton, Australia; U-Pb zircon, geochemical and Sm-Nd isotopic implications, Precambrian Research, v. 141., p. 106-136.

Talbot, J. L., 1967, Subdivision and structure of the Precambrian (Willyama complex and Adelaide system), Weekeroo, South Australia: Transactions of the Royal Society of South Australia, v. 91, p. 45-57.

Talbot, M. R., 1990, A review of the palaeohydrological interpretation of carbon and oxygen isotopic ratios in primary lacustrine carbonates: Chemical Geology; Isotope Geoscience Section, v. 80, p. 261-279.

Talbot, M. R., and Kelts, K., 1990, Paleolimnological signatures from carbon and oxygen isotopic ratios in carbonates from organic carbon-rich lacustrine sediments: AAPG Memoir, v. 50, p. 99-112.

Talbot, C. J., 1993, Spreading of salt structures in the Gulf of Mexico, Tectonophysics, v. 228, p. 151-166.

Tate, R., 1883, List of some plants inhabiting the northeastern part of the Lake Torrens Basin, Transactions, Royal Society of South Australia, v. 6, p. 100-106.

Teasdale, J., 1997, Methods for understanding poorly exposed terranes: the interpretive geolgy and tectono-thermal evolution of the western Gawler Cration, The University of Adelaide, PhD Thesis (unpubl.), 183 pp.

Thomson, B. P., Coats, R. P., Mirams, R. C., Forbes, B. G., Dalgarno, C. R. and Johnson, J. E., 1964, Precambrian rock groups in the Adelaide Geosyncline: a new subdivision, Quarterly Geological Notes, Geological Survey of South Australia, v. 9, p. 1-19.

Thomson, B. P., 1969, Precambrian basement cover – the Adelaide System, in Parkin, L. W., Handbook of South Australian geology, Geological Survey of South Australia, p. 49-83.

Townsend, K. J., Miller, C. F., D'Andrea, J. L., Ayers, J. C., Harrison, T. M. and Coath, C. D., 2000, Low temperature replacement of monazite in the Ireteba granite, Southern Nevada: geochronological implications, Chemical Geology, v. 172, p. 95 – 112.

Tucker, M. E., 1990, Taphonomy; Diagenesis; skeletal carbonates [modified], in Briggs, D. E. G., and Crowther, P. R., (eds), Oxford, Blackwell Sci. Publ., p. 247-250.

Tucker, M. E. and Wright, P. V., 1990, Carbonate sedimentology; Oxford, UK, Blackwell Scientific. 482p.

Turner, E. C., James, N. P., and Narbonne, G. M., 2000, Taphonomic control on microstructure in early Neoproterozoic reefal stromatolites and thrombolites: Palaios, v. 15, p. 87-111.

Ukstins Peate, I., Larsen, M. and Lesher, C. E., 2003, The transition from sedimentation to flood volcanism in the Kangerlussaq Basin, East Greenland: basaltic pyroclastic volcanism during initial Palaeogene continental break-up. Journal of the Geological Society, v. 160, p. 759-772.

Unrug, R., 1988, Mineralization controls and source of metals in the Lufilian fold belt, Shaba (Zaire), Zambia and Angola, Bulletin of the Society of Economic Geologists, v. 83, p. 1247-1258.

Van Schmus, W. R., Bickford, M. E., Condie, K. C., and Anonymous, 1993, Early Proterozoic transcontinental orogenic belts in the United States, Abstracts with Programs - Geological Society of America, 25, p. 44.

Veevers, J. J., 2000 Billion-year earth history of Australia and neighbours in Gondwanaland, GEMOC Press, Sydney.

Veevers, J. J., Powell, C. M. and Roots, S. R., 1991, Review of seafloor spreading around Australia. I. synthesis of seafloor spreading patterns, Australian Journal of Earth Sciences, v. 38, p. 373-389.

Veevers, J. J., Walter, M. R. and Scheibner, E., 1997, Neoproterozoic tectonics of Australia-Antarctica and Laurentia and the 560 Ma birth of the Pacific Ocean reflect the 400 M. Y. Pangean Supercycle, The Journal of Geology, v. 105, 225-242.

Veizer, J., and Hoefs, J., 1976, The nature of O18 O16 and C13 C12 secular trends in sedimentary carbonate rocks: Geochimica et Cosmochimica Acta, v. 40, p. 1387-1395.

Veizer, J., Ala, D., Azmy, K., Bruckschen, P., Buhl, D., Bruhn, F., Carden, G. A. F., Diener, A., Ebneth, S., Godderis, Y., Jasper, T., Korte, C., Pawellek, F. and Strauss, H., 1999, 87Sr/86Sr, δ13C and δ18O evolution of Phanerozoic seawater, Chemical Geology, v. 161, p. 59-88.

Vendeville, B. C., and Jackson, M. P. A., 1992a, The rise of diapirs during thin-skinned extension, Marine and Petroleum Geology, 9, p. 331-353.

Vendeville, B. C., and Jackson, M. P. A., 1992b, The fall of diapirs during thin-skinned extension, Marine and Petroleum Geology, 9, p. 354-371.

Vendeville, B. C., 2005, Salt tectonics driven by sediment progradation; Part I, Mechanics and kinematics: AAPG Bulletin, v. 89, p. 1071-1079.

Verges, J., Marzo, M. and Munoz, J. A., 2002, Growth strata in foreland settings, Sedimentary Geology, v.146, p. 1-9.

von der Borch, C. C., 1980, Evolution of late Proterozoic to early Paleozoic Adelaide Foldbelt, Australia; comparisons with post-Permian rifts and passive margins: Tectonophysics, v. 70, p. 115-134.

Wachniew, P. and Rozanski, K., 1997 Carbon budget of a mid-latitude, groundwater-controlled lake; isotopic evidence for the importance of dissolved inorganic carbon recycling, Geochimica et Cosmochimica Acta, v. 61, p. 2453-2465.

Wade, B. P., Barovich, K. M., Hand, M., Scrimgeour, I. R. and Close, D. F., 2006, Evidence for early Mesoproterozoic arc magmatism in the Musgrave Block; implications for Proterozoic crustal growth and tectonic reconstructions of Australia, Journal of Geology, v. 114, p. 43-63

Wade, B. P., Payne, J. L., Hand, M, and Barovich, K. M., 2007, Petrogenesis of ca. 1.5o Ga granitic gneiss of the Coompana Block; filling the “magmatic gap” of Mesoproterozoic Australia, Australian Journal of Earth Sciences, v. 54, p. 1089-1102.

Walker, R.G., 1992, Turbidites and submarine fans, in Walker, R. G., and James, N. P., (eds) Facies models: response to sea level change, Geological Association of Canada, p. 239-261.

Walter, M. R., Veevers, J. J., Calver, C. R., Gorjan, P., and Hill, A. C., 2000, Dating the 840-544 Ma Neoproterozoic interval by isotopes of strontium, carbon, sulfur in seawater, and some interpretative models: Precambrian Research, v. 100, p. 371-433.

Wang, J., Li, Z.-X., Cho, M., and Li, X., 2003, History of Neoproterozoic rift basins in South China; implications for Rodinia break-up: Precambrian Research, v. 122, p. 141-158.

Warren, J., 1999, Evaporites; their evolution and economics, Oxford, UK, Blackwell Scientific, 438 p.

Warren, J. K., and Kendall, C. G., 1985, Comparison of sequences formed in marine sabkha (subaerial) and salina (subaqueous) settings; modern and ancient: AAPG Bulletin, v. 69, p. 1013-1023.

Webb, B. P., 1963, Diapiric structures in the Flinders Ranges, South Australia, Australian Journal of Science, v. 22, p. 9.

Webb, B. P., 1961, The geological structure of the Blinman dome: Transactions of the Royal Society of South Australia, v. 85, p. 1-6.

Webb et al., 1963

Webb, G., Hand, M., and Preiss, W., 2002, A patchy orogen; allochronous anti-clockwise P-T-t paths across the southern Delamerian fold belt, South Australia, in Preiss, V. P., ed., Abstracts - Geological Society of Australia, vol.67, p. 195.

Weidenbeck, M., Alle, P., Corfu, F., Griffin, W. L., Meier, M., Oberli, F., von Quadt, A., Roddick, J. C. and Spiegel, W., 1995, Three natural zircon standards for U-Th-Pb, Lu-Hf, trace element and REE analyses, Geostandards and Geoanalytical Research, v. 19, p. 1-23.

Weimer, R. J., Howard, J. D. and Lindsay, D. R. 1982, Tidal flats and associated tidal channels, in Scholle, P. A. and Spearing, D. (eds) Sandstone depositional environments. American Association of Petroleum Geologists Memoir 31, p. 191-245.

White, A. H., 1983, Speculations on the Adelaide Rift and the origin of diapirs, In Adelaide Geosyncline sedimentary environments and tectonic settings symposium, Adelaide, 1983, Abstracts of the Geological Society of Australia, v. 10, p. 3-6.

White, R. W., Clarke, G. L., and Nelson, D. R., 1999, SHRIMP U-Pb zircon dating of Grenville-age events in the western part of the Musgrave Block, central Australia: Journal of Metamorphic Geology, v. 17, p. 465-481.

Whitten, D. G. A. and Brook, J. R. V., 1972, The Penguin dictionary of geology, Penguin, Harmondsworth, 495p.

Williams, G.E., 1986, The Acraman impact structure: source of ejecta in late Precambrian shales, South Australia, Science, v. 233, p. 200-203.

Williams, G. E. and Gostin, V. A., 2000, Mantle plume uplift in the sedimentary record: origin of kilometer-deep canyons within late Neoproterozoic successions, South Australia, Journal of the Geological Society, v. 157, p. 759-768.

Williams, M. L., Jercinovic, M. J., and Terry, M. P., 1999, Age mapping and dating of monazite on the electron microprobe; deconvoluting multistage tectonic histories, Geology, v. 27, p. 1023-1026.

Windley, B. F., 1993, Proterozoic anorogenic magmatism and its orogenic connections: Journal of the Geological Society of London, v. 150, p. 39-50.

Wing, B. A., Ferry, J. M., and Harrison, T. M., 2003, Prograde destruction and formation of monazite and allanite during contact and regional metamorphism of pelites; petrology and geochronology, Contributions to Mineralogy and Petrology, v. 145, p. 228-250.

Wingate, M. T. D., Campbell, I. H., Compston, W., and Gibson, G. M., 1998, Ion microprobe U-Pb ages for Neoproterozoic-basaltic magmatism in south-central Australia and implications for the breakup of Rodinia: Precambrian Research, v. 87, p. 135-159.

Wingate, M. T. D., Pisarevsky, S. A. and Evans, D. A. D., 2002, Rodinia connections between Australia and Laurentia: no SWEAT, no AUSWUS? Terra Nova v. 14, p. 121-128.

Wingate, M. T. D., Pirajno, F. and Morris, P. A., 2004, Warakurna large igneous province: a new Mesoproterozoic large igneous province in west-central Australia, Geology, v. 32, p. 105-108.

Wysoczanski, R. J., and Alliborne, A. H., 2004, Age, correlation, and provenance of the Neoproterozoic Skelton Group, Antarctica; Grenville age detritus on the margin of East Antarctica: Journal of Geology, v. 112, p. 401-416.

Xiao, S., Bao, H., Wang, H., Kaufman, A. J., Zhou, C., Li, G., Yuan, X. and Ling, H., 2004, The Neoproterozoic Quruqtagh Group in eastern Chinese Tianshan: evidence for a post-Marinoan glaciations, Precambrian Research, v. 130, p. 1-26.

Ziegler, P. A., 1990, Geological atlas of Western and Central Europe – 2nd edition, Shell International Petroleum Maatschappij B. V., Geological Society, London, Elsevier, 239p.

Zhao, J., McCulloch, M. T., and Korsch, R. J., 1994, Characterisation of a plume-related approximately 800 Ma magmatic event and its implications for basin formation in central-southern Australia: Earth and Planetary Science Letters, v. 121, p. 349-367.

Zhou, C., Tucker, R., Xiao, S., Peng, Z., Yuan, X. and Chen, Z., 2004, New constraints on the ages of Neoproterozoic glaciations in south China, Geology, v. 32, p. 437-440.

Zhang, S., Jiang, Ganqing, Zhang, J., Song, B., Kennedy, M.J. and Christie-Blick, N., 2005, U-Pb sensitive high resolution ion microprobe ages from the Doushantuo Formation in south China: Constraints on late Neoproterozoic glaciations. Geology, v. 33, p. 473-476.

Zhang, S. Jiang, G. and Han, Y., 2008, The age of the Nantuo Formation and Nantuo glaciations in South China, Terra Nova, v. 20, p. 289-294.

APPENDIX 1.
DETRITAL ZIRCON AGE DATA.

Sample PQ1

Analysis	File	Calculated Ages																Hf	+/-1s	Hg	+/-1s	Pb	+/-1s	Th	+/-1s	U	+/-1s
		206Pb/238U	%rsd	age	+/-1s	208Pb/232Th	%rsd	age	+/-1s	207Pb/206P	%rsd	age	+/-1s	207Pb/235U	%rsd	age	+/-1s										
1	C:\HPCHEM\1\DATA\030305\MR05A07.D	0.2178	3.4%	1270	43	0.0708	1.4%	1383	20	0.106	1.9%	1726	32	2.719	4.9%	1334	66	9670	234	0.0	0.2	202	6	586	17	653	24
2	C:\HPCHEM\1\DATA\030305\MR05A08.D	0.2547	3.7%	1463	55	0.0731	2.0%	1426	28	0.099	2.5%	1603	40	3.355	8.3%	1494	124	8602	205	0.5	0.2	107	4	278	11	326	17
3	C:\HPCHEM\1\DATA\030305\MR05A09.D	0.1590	5.3%	951	50	0.0498	3.9%	983	38	0.098	2.7%	1588	42	1.975	8.6%	1107	95	9689	265	0.2	0.2	87	4	357	21	495	29
4	C:\HPCHEM\1\DATA\030305\MR05A10.D	0.1051	4.8%	644	31	0.1002	11.8%	1931	227	0.111	10.5%	1820	192	1.370	14.9%	876	131	9946	665	0.6	0.3	46	3	119	9	396	37
5	C:\HPCHEM\1\DATA\030305\MR05A11.D	0.2115	2.9%	1237	36	0.0858	2.7%	1663	44	0.105	3.4%	1720	58	3.333	8.6%	1489	128	9910	252	-0.1	0.2	62	2	156	8	207	7
6	C:\HPCHEM\1\DATA\030305\MR05A12.D	0.2671	3.2%	1526	48	0.0743	1.8%	1448	26	0.101	2.6%	1644	42	3.949	7.0%	1624	114	9961	221	0.2	0.2	107	3	273	7	293	13
7	C:\HPCHEM\1\DATA\030305\MR05A13.D	0.2513	3.8%	1445	55	0.0679	2.6%	1327	35	0.101	3.5%	1639	57	2.968	7.5%	1399	105	9381	205	0.0	0.2	42	1	99	3	129	4
8	C:\HPCHEM\1\DATA\030305\MR05A14.D	0.2094	3.4%	1226	41	0.0672	2.1%	1315	28	0.102	3.3%	1668	55	2.501	5.9%	1272	75	10911	321	0.4	0.2	90	3	187	6	341	16
9	C:\HPCHEM\1\DATA\030305\MR05A15.D	0.2869	3.5%	1626	58	0.0746	2.1%	1453	30	0.111	2.1%	1809	38	4.092	7.5%	1653	124	9899	226	0.4	0.2	111	3	143	4	315	9
10	C:\HPCHEM\1\DATA\030305\MR05A16.D	0.2058	3.1%	1207	37	0.0635	2.2%	1244	27	0.092	3.0%	1475	44	2.663	7.2%	1318	95	9990	235	0.4	0.2	74	2	141	3	310	17
11	C:\HPCHEM\1\DATA\030305\MR05A17.D	0.2526	4.2%	1452	61	0.0775	2.4%	1508	37	0.104	2.9%	1689	50	3.471	7.7%	1521	116	10931	352	0.1	0.2	69	2	120	3	227	9
12	C:\HPCHEM\1\DATA\030305\MR05A18.D	0.1743	6.1%	1036	63	0.0486	3.9%	958	37	0.097	6.3%	1568	99	1.761	9.0%	1031	92	9406	362	0.2	0.2	24	1	52	2	129	7
1	C:\HPCHEM\1\DATA\030305\MR05A23.D	0.2311	3.6%	1340	49	0.0446	4.0%	882	35	0.107	2.6%	1751	46	3.413	7.3%	1507	110	9534	240	0.6	0.2	114	3	592	46	397	16
2	C:\HPCHEM\1\DATA\030305\MR05A24.D	0.2491	5.0%	1434	72	0.0581	4.5%	1141	51	0.107	2.9%	1747	51	3.215	6.1%	1461	89	9852	251	0.6	0.2	104	3	1005	217	355	15
3	C:\HPCHEM\1\DATA\030305\MR05A25.D	0.1810	3.5%	1072	38	0.0626	2.7%	1227	33	0.106	2.5%	1730	43	2.885	9.6%	1378	132	10004	270	0.0	0.3	119	4	417	33	558	35
4	C:\HPCHEM\1\DATA\030305\MR05A26.D	0.2259	3.6%	1313	47	0.0670	2.2%	1311	29	0.096	3.4%	1556	53	3.218	8.1%	1461	119	9792	275	0.3	0.2	62	2	141	4	225	9
5	C:\HPCHEM\1\DATA\030305\MR05A27.D	0.2627	3.5%	1504	53	0.0713	1.8%	1391	25	0.096	2.9%	1550	45	3.284	6.1%	1477	89	10726	247	0.6	0.2	117	3	269	7	353	9
6	C:\HPCHEM\1\DATA\030305\MR05A28.D	0.3017	3.5%	1700	59	0.0802	2.1%	1559	33	0.110	2.7%	1798	49	4.489	7.3%	1729	127	8917	179	0.3	0.2	56	2	87	2	153	4
7	C:\HPCHEM\1\DATA\030305\MR05A29.D	0.1792	5.3%	1063	56	0.0445	2.8%	880	24	0.099	3.2%	1610	52	2.211	7.4%	1185	88	11348	430	-0.1	0.2	112	5	336	16	602	27
8	C:\HPCHEM\1\DATA\030305\MR05A30.D	0.2685	5.5%	1533	85	0.0680	2.9%	1330	38	0.105	4.2%	1714	73	3.711	8.2%	1574	129	9776	353	0.4	0.2	68	3	146	5	247	12
9	C:\HPCHEM\1\DATA\030305\MR05A31.D	0.3283	5.7%	1830	105	0.0787	2.6%	1531	39	0.108	3.7%	1766	66	4.627	8.8%	1754	155	9833	311	0.6	0.2	105	4	307	15	272	11
10	C:\HPCHEM\1\DATA\030305\MR05A32.D	0.3682	5.4%	2021	109	0.0839	2.5%	1628	41	0.110	3.1%	1805	56	4.818	7.3%	1788	131	9245	313	0.3	0.2	82	3	123	4	214	9
11	C:\HPCHEM\1\DATA\030305\MR05A33.D	0.2026	4.0%	1189	47	0.0664	3.1%	1299	40	0.107	4.9%	1757	86	1.971	8.4%	1106	93	9933	291	0.6	0.2	19	1	54	2	74	3
12	C:\HPCHEM\1\DATA\030305\MR05A34.D	0.1282	3.7%	778	28	0.0477	3.4%	942	32	0.080	3.3%	1206	39	1.232	4.2%	815	34	9833	255	0.4	0.2	241	6	790	18	1553	49
1	C:\HPCHEM\1\DATA\030220\FE20A61.D	0.2314	2.7%	1342	36	0.0413	5.3%	818	43	0.109	4.6%	1776	82	2.487	6.2%	1268	79	7989	179	0.5	0.4	45	1	171	6	152	5
2	C:\HPCHEM\1\DATA\030220\FE20A62.D	0.2883	2.8%	1633	46	0.0519	6.7%	1022	69	0.139	5.9%	2219	131	1.257	11.7%	827	96	7045	161	0.3	0.5	15	1	58	2	37	1
3	C:\HPCHEM\1\DATA\030220\FE20A63.D	0.2745	1.4%	1564	22	0.0503	3.6%	992	36	0.111	2.8%	1815	51	4.740	5.4%	1774	96	9871	222	0.6	0.5	126	3	233	5	368	7
4	C:\HPCHEM\1\DATA\030220\FE20A64.D	0.2239	1.4%	1302	18	0.0167	9.7%	335	32	0.099	3.3%	1615	53	3.642	5.1%	1559	79	11490	231	0.0	#####	116	3	121	5	477	12
5	C:\HPCHEM\1\DATA\030220\FE20A65.D	0.2783	1.8%	1583	29	0.0505	4.0%	996	40	0.110	4.1%	1804	74	3.483	6.0%	1523	91	9196	245	1.0	0.5	68	2	192	5	188	7
6	C:\HPCHEM\1\DATA\030220\FE20A66.D	0.2851	2.1%	1617	34	0.0570	6.9%	1121	78	0.129	4.4%	2080	92	2.401	8.2%	1243	102	8345	155	-0.2	0.5	37	2	53	1	107	3
7	C:\HPCHEM\1\DATA\030220\FE20A67.D	0.2560	2.3%	1469	34	0.0606	13.6%	1190	162	0.133	5.6%	2140	121	1.820	8.1%	1053	85	8716	217	0.0	0.5	28	1	64	2	87	2
8	C:\HPCHEM\1\DATA\030220\FE20A68.D	0.2656	1.5%	1519	23	0.0483	3.5%	953	34	0.102	2.8%	1657	46	4.710	6.0%	1769	107	9645	229	-0.9	0.4	125	3	243	6	382	9
9	C:\HPCHEM\1\DATA\030220\FE20A69.D	0.1978	2.2%	1164	26	0.0348	5.7%	691	40	0.083	5.8%	1266	73	2.524	6.1%	1279	79	11073	301	-0.4	0.4	94	3	149	4	435	14
10	C:\HPCHEM\1\DATA\030220\FE20A70.D	0.1727	2.2%	1027	23	0.0235	3.6%	470	17	0.097	3.2%	1563	51	2.374	5.1%	1235	63	9174	277	-0.5	0.5	146	6	706	30	695	28
11	C:\HPCHEM\1\DATA\030220\FE20A71.D	0.2732	2.3%	1557	36	0.0464	5.5%	917	51	0.107	5.1%	1756	89	2.415	6.2%	1247	77	8400	196	1.0	0.5	51	2	179	11	150	6
12	C:\HPCHEM\1\DATA\030220\FE20A72.D	0.2122	2.3%	1240	28	0.0474	5.1%	936	48	0.111	6.5%	1815	119	1.807	8.9%	1048	93	8229	182	1.1	0.6	36	2	117	5	125	3
1	C:\HPCHEM\1\DATA\030220\FE20A79.D	0.2311	2.1%	1340	28	0.0550	4.1%	1082	44	0.113	4.5%	1841	83	2.661	7.3%	1318	97	9034	221	0.5	0.5	50	2	121	4	167	5
2	C:\HPCHEM\1\DATA\030220\FE20A80.D	0.2682	1.7%	1532	27	0.0587	3.1%	1153	36	0.111	3.4%	1821	61	3.559	6.8%	1540	105	10207	271	-0.3	0.5	105	3	216	6	304	9
3	C:\HPCHEM\1\DATA\030220\FE20A81.D	0.1473	1.7%	886	15	0.0234	4.9%	468	23	0.093	3.7%	1485	54	1.795	5.1%	1044	53	13132	347	0.2	0.5	177	5	323	17	1066	32
4	C:\HPCHEM\1\DATA\030220\FE20A82.D	0.2711	1.7%	1546	27	0.0560	2.1%	1101	24	0.098	3.9%	1583	62	3.238	6.2%	1466	91	8026	162	-1.3	0.5	155	4	658	15	361	9
5	C:\HPCHEM\1\DATA\030220\FE20A83.D	0.2635	1.7%	1508	25	0.0577	2.3%	1135	26	0.109	3.7%	1780	65	3.624	6.2%	1555	96	7942	194	0.6	0.5	135	4	556	13	322	8
6	C:\HPCHEM\1\DATA\030220\FE20A84.D	0.2041	2.3%	1197	28	0.0495	2.5%	977	24	0.105	3.1%	1715	54	3.000	6.5%	1408	92	8859	258	0.4	0.5	186	10	873	54	631	36
7	C:\HPCHEM\1\DATA\030220\FE20A85.D	0.1820	3.4%	1078	36	0.0368	5.4%	730	39	0.100	3.8%	1623	62	2.352	6.8%	1228	84	8029	227	0.1	0.6	174	5	1510	116	727	35
8	C:\HPCHEM\1\DATA\030220\FE20A86.D	0.2038	2.0%	1196	24	0.0217	5.2%	435	23	0.108	3.5%	1763	61	2.904	7.0%	1383	97	8198	250	0.3	0.6	107	4	979	77	395	15
9	C:\HPCHEM\1\DATA\030220\FE20A87.D	0.2804	3.0%	1593	48	0.0577	5.0%	1133	57	0.106	6.1%	1724	105	1.863	8.9%	1068	95	8693	219	0.4	0.5	36	1	98	3	99	3
10	C:\HPCHEM\1\DATA\030220\FE20A88.D	0.2587	2.4%	1483	36	0.0546	3.8%	1075	41	0.121	3.2%	1974	63	3.452	6.8%	1516	103	8391	223	0.2	0.5	91	3	209	7	280	9
11	C:\HPCHEM\1\DATA\030220\FE20A89.D	0.2705	2.5%	1543	38	0.0570	3.0%	1121	34	0.101	2.6%	1644	44	3.783	6.0%	1589	96	12731	267	0.0	0.5	232	7	302	8	722	17
12	C:\HPCHEM\1\DATA\030220\FE20A90.D	0.2516	2.8%	1447	40	0.0621	4.2%	1217	51	0.132	5.1%	2119	109	1.979	9.3%	1108	104	8712	331	-0.8	0.5	43	2	121	6	130	5
1	C:\HPCHEM\1\DATA\030220\FE20A97.D	0.2574	1.5%	1477	21	0.0666	6.8%	1302	88	0.107	1.9%	1751	34	3.804	6.2%	1594	98	11682	235	0.6	0.3	188	4	32	1	680	15
2	C:\HPCHEM\1\DATA\030220\FE20A98.D	0.2477	1.5%	1426	22	0.0507	7.9%	1000	79	0.105	2.0%	1711	34	3.152	4.3%	1446	63	11768	251	0.7	0.4	178	4	46	4	670	15
3	C:\HPCHEM\1\DATA\030220\FE20A99.D	0.2442	2.1%	1409	30	0.0545	2.8%	1072	30	0.104	3.8%	1693	65	2.892	6.6%	1380	91	9050	215	0.7	0.3	69	3	284	15	197	7
4	C:\HPCHEM\1\DATA\030220\FE20A100.D	0.2539	1.9%	1459	27	0.0589	2.8%	1156	33	0.104	3.5%	1699	59	3.100	6.9%	1433	99	8941	271	-0.8	0.4	74	3	271	9	209	8
5	C:\HPCHEM\1\DATA\030220\FE20A101.D	0.2710	2.3%	1546	35	0.0617	4.3%	1209	52	0.108	5.1%	1773	91	1.946	7.2%	1097	79	8917	167	0.9	0.3	26	1	65	1	76	2
6	C:\HPCHEM\1\DATA\030220\FE20A102.D	0.2696	3.0%	1539	46	0.0699	6.0%	1366	82	0.143	4.3%	2260	97	2.276	7.2%	1205	87	9096	264	0.9	0.4	26	1	40	1	84	6
7	C:\HPCHEM\1\DATA\030220\FE20A103.D	0.2680	1.9%	1530	29	0.0578	3.0%	1136	34	0.104	3.5%	1705	60	2.768	6.9%	1347	93	8939	213	-0.2	0.4	65	2	221	7	178	5
8	C:\HPCHEM\1\DATA\030220\FE20A104.D	0.2569	2.2%	1474	32	0.0608	3.3%	1192	40	0.112	4.9%	1833	90	3.095	7.7%	1432	111	8966	281	0.0	0.4	81	4	269	13	235	11
9	C:\HPCHEM\1\DATA\030220\FE20A105.D	0.1244	2.1%	756	16	0.0112	4.6%	225	10	0.136	1.9%	2174	41	2.375	7.1%	1235	87	11496	376	1.0	0.5	171	5	1702	107	1164	39
10	C:\HPCHEM\1\DATA\030220\FE20A106.D	0.2726	2.2%	1554	34	0.0641	3.9%	1255	48	0.114	4.4%	1869	82	3.169	7.2%	1450	104	9028	367	0.3	0.5	103	7	265	22	304	23
11	C:\HPCHEM\1\DATA\030220\FE20A107.D	0.2149	4.5%	1255	57	0.0529	6.9%	1042	72	0.134	10.7%	2145	229	0.757	19.8%	572	114	8041	300	0.1	0.5	12	1	74	3	42	2
12	C:\HPCHEM\1\DATA\030220\FE20A108.D	0.1772	2.5%	1051	26	0.0439	3.9%	868	34	0.084	9.7%	1304	126	1.233	9.9%	816	81	9450	291	-0.5	0.5	44	2	200	7	196	8
1	C:\HPCHEM\1\DATA\030220\FE20A116.D	0.2498	1.5%	1438	22	0.0576	3.1%	1132	35	0.127	3.2%	2058	66	3.549	5.8%	1538	89	9096	170	-0.3	0.3	50	1	172	5	145	3
2	C:\HPCHEM\1\DATA\030220\FE20A117.D	0.0153	3.1%	98	3	0.0414	6.2%	820	51	0.096	10.3%	1544	159	0.966	11.2%	686	77	8470	149	0.0	0.4	13	1	69	2	672	15
3	C:\HPCHEM\1\DATA\030220\FE20A118.D	0.2679	1.5%	1530	22	0.0519	3.1%	1023	32	0.109	4.4%	1787	78	3.120	5.9%	1438	85	9497	163	0.0	0.3	45	1	176	5	123	3
4	C:\HPCHEM\1\DATA\030220\FE20A119.D	0.2600	1.9%	1490	28	0.0560	4.6%	1102	51	0.105	4.6%	1709	78	2.823	6.5%	1362	88	8321	131	-0.1	0.3	38	1	79	2	125	3
5	C:\HPCHEM\1\DATA\030220\FE20A120.D	0.2644	2.2%	1512	33	0.0598	5.6%	1173	65	0.196	27.9%	2796	781	7.564	68.3%	2181	1488	9355	162	-0.3	0.3	35	4	81	2	100	2
6	C:\HPCHEM\1\DATA\030220\FE20A121.D	0.2440	2.1%	1408	29	0.0498	3.9%	983	39	0.106	4.1%	1729	72	3.271	5.8%	1474	86	8161	139	-0.2	0.3	49	1	137	3	178	12
7	C:\HPCHEM\1\DATA\030220\FE20A122.D	0.2184	2.3%	1273	29	0.0683	4.1%	1336	55	0.138	2.7%	2201	60	4.014	6.2%	1637	101	10690	191	0.6	0.4	68	3	149	6	255	11
8	C:\HPCHEM\1\DATA\030220\FE20A123.D	0.2625	2.4%	1503	35	0.0698	31.4%	1364	428	0.128	6.7%	2076	138	2.780	7.5%	1350	101	9191	176	0.2	0.3	40	4	112	4	116	4
9	C:\HPCHEM\1\DATA\030220\FE20A124.D	0.2049	1.9%	1201	23	0.0353	3.8%	702	27	0.144	1.9%	2278	44	4.758	5.3%	1777	94	11281	253	0.4	0.3	114	4	264	12	472	14
10	C:\HPCHEM\1\DATA\030220\FE20A125.D	0.1810	2.0%	1072	22	0.0325	2.7%	646	18	0.105	2.7%	1715	46	2.989	6.0%	1405	84	8907	198	0.0	0.4	135	3	984	31	542	16
11	C:\HPCHEM\1\DATA\030220\FE20A126.D	0.3695	1.3%	2027	27	0.0760	2.9%	1481	43	0.138	1.4%	2203	32	7.855	5.3%	2214	117	8854	191	0.2	0.4	155	4	191	6	359	11
12	C:\HPCHEM\1\DATA\030220\FE20A127.D	0.2568	1.7%	1474	25	0.0579	4.4%	1138	50	0.111	4.3%	1813	77	3.133	7.0%	1441	100	8162	164	0.6	0.4	51	2	114	3	170	7

Shades samples not used.

Sample HSF3	Calculated Ages																Elemental Abundance										Ratio's for concordia															
HSF3	206Pb/238	%rsd	age	+/-1s	208Pb/232T	%rsd	age	+/-1s	207Pb/206P	%rsd	age	+/-1s	207Pb/235	%rsd	age	+/-1s	Hf	+/-1s	Hg	+/-1s	Pb	+/-1s	Th	+/-1s	U	+/-1s	207Pb/235U	+/-1s	206Pb/238U	+/-1s	238U/206Pb	+/-1s	207Pb/206	+/-1s	206Pb/23	+/-1s	232Th/2	206Pb/238U age		Slope
1 C:\DATA\031028\OC28A1.D	0.2731	0.6%	1556	7.9	0.0757	2.3%	1474	33	0.093	1.9%	1497	36	3.500	2.2%	1527	17	11060	283	0.3	0.1	37	1	58	2	108	3	3.50	0.08	0.273	0.002	3.66	0.02	0.093	0.002	1562	8	0.5	1569	8	-1.01
2 C:\DATA\031028\OC28A2.D	0.3359	0.6%	1867	10.2	0.0958	2.3%	1850	41	0.109	1.8%	1779	33	5.005	2.1%	1820	18	9867	252	0.6	0.1	61	2	65	2	145	4	5.01	0.10	0.336	0.002	2.98	0.02	0.109	0.002	1879	10	0.4	1869	10	0.69
3 C:\DATA\031028\OC28A3.D	0.3333	0.8%	1855	12.3	-1.5603	10.9%	#NUM!	#NUM!	0.092	2.1%	1476	40	4.332	2.4%	1700	20	22144	563	375.3	40.4	8382	220	19	1	22671	462	4.33	0.10	0.333	0.003	3.00	0.02	0.092	0.002	1903	12	0.0	1861	12	-3.60
4 C:\DATA\031028\OC28A4.D	0.1989	1.2%	1169	12.5	0.0253	3.5%	504	18	0.167	1.8%	2530	30	4.551	2.1%	1740	18	10552	282	0.5	0.1	559	18	5777	186	1751	49	4.55	0.10	0.199	0.002	5.03	0.06	0.167	0.003	1051	12	3.3	3142	12	-1.34
5 C:\DATA\031028\OC28A5.D	0.2665	0.7%	1523	9.0	0.0729	2.5%	1422	34	0.096	1.9%	1546	35	3.527	2.2%	1533	17	9583	244	0.2	0.1	122	4	184	6	342	10	3.53	0.08	0.266	0.002	3.75	0.02	0.096	0.002	1521	9	0.5	1538	9	-0.87
6 C:\DATA\031028\OC28A6.D	0.2531	0.7%	1454	8.9	0.0765	2.3%	1490	33	0.104	2.2%	1700	40	3.669	2.3%	1565	19	9708	245	0.3	0.1	44	1	125	4	113	4	3.67	0.09	0.253	0.002	3.95	0.03	0.104	0.002	1433	9	1.1	1441	9	-0.23
7 C:\DATA\031028\OC28A7.D	0.2860	0.5%	1622	7.7	0.0796	2.3%	1548	34	0.098	1.8%	1594	33	3.847	2.0%	1603	16	10386	256	0.5	0.1	136	4	156	5	390	9	3.85	0.08	0.286	0.002	3.50	0.02	0.098	0.002	1625	8	0.4	1630	8	-0.93
8 C:\DATA\031028\OC28A8.D	0.2998	0.6%	1690	9.2	0.0827	2.3%	1606	35	0.103	2.0%	1676	38	4.273	2.2%	1688	18	9668	244	-0.1	-0.1	40	1	85	2	97	2	4.27	0.09	0.300	0.002	3.34	0.02	0.103	0.002	1692	9	0.9	1713	9	-0.59
9 C:\DATA\031028\OC28A9.D	0.2545	0.8%	1461	9.8	0.0819	2.5%	1592	38	0.093	2.1%	1484	39	3.275	2.4%	1475	19	7725	192	0.2	0.1	45	1	266	8	89	3	3.27	0.08	0.254	0.002	3.93	0.03	0.093	0.002	1460	10	3.0	1044	10	-1.08
10 C:\DATA\031028\OC28A10.D	0.2761	0.6%	1572	8.3	0.0815	2.2%	1583	34	0.102	1.8%	1664	33	3.883	2.1%	1610	17	9735	242	0.6	0.1	111	4	232	7	289	7	3.88	0.08	0.276	0.002	3.62	0.02	0.102	0.002	1562	8	0.8	1569	8	-1.79
11 C:\DATA\031028\OC28A11.D	0.2798	1.5%	1591	21.5	0.0771	2.7%	1502	38	0.097	4.0%	1560	75	4.091	4.2%	1653	35	6767	162	0.3	0.1	5	0	17	1	10	0	4.09	0.17	0.280	0.004	3.57	0.05	0.097	0.004	1593	21	1.8	1658	21	-4.06
12 C:\DATA\031028\OC28A12.D	0.2282	1.2%	1325	14.7	0.0440	3.0%	871	26	0.097	2.1%	1562	39	2.998	2.6%	1407	20	9643	239	1.1	0.2	149	6	1256	40	456	20	3.00	0.08	0.228	0.003	4.38	0.05	0.097	0.002	1308	15	2.8	2193	15	15.50
1 C:\DATA\031028\OC28B1.D	0.2746	0.6%	1564	9.0	0.0752	2.4%	1465	34	0.093	2.0%	1493	38	3.565	2.2%	1542	18	10865	260	0.3	0.1	34	1	62	2	94	2	3.57	0.08	0.275	0.002	3.64	0.02	0.093	0.002	1571	9	0.7	1584	9	-1.88
2 C:\DATA\031028\OC28B2.D	0.2601	0.7%	1491	10.0	0.0668	2.5%	1307	31	0.099	2.1%	1601	39	3.573	2.3%	1544	19	9978	241	0.5	0.1	65	2	166	5	171	5	3.57	0.08	0.260	0.002	3.84	0.03	0.099	0.002	1481	10	1.0	1548	10	-2.02
3 C:\DATA\031028\OC28B3.D	0.2784	0.7%	1583	9.8	0.0820	2.3%	1593	36	0.090	2.0%	1423	38	3.482	2.2%	1523	18	9893	242	0.2	0.1	51	1	122	3	130	3	3.48	0.08	0.278	0.002	3.59	0.02	0.090	0.002	1598	10	0.9	1580	10	-1.02
4 C:\DATA\031028\OC28B4.D	0.2484	0.7%	1430	8.6	0.0763	2.2%	1486	32	0.104	1.9%	1698	34	3.549	2.1%	1538	17	10377	253	0.1	0.1	67	2	191	6	183	4	3.55	0.07	0.248	0.002	4.03	0.03	0.104	0.002	1407	9	1.0	1411	9	-4.03
5 C:\DATA\031028\OC28B5.D	0.3066	0.6%	1724	8.4	0.0897	2.8%	1737	46	0.107	2.1%	1748	39	4.607	2.4%	1751	20	10591	250	0.2	0.1	75	2	95	3	178	4	4.61	0.11	0.307	0.002	3.26	0.02	0.107	0.002	1721	8	0.5	1722	8	-0.90
6 C:\DATA\031028\OC28B6.D	0.2565	0.7%	1472	9.3	0.0726	2.2%	1416	31	0.090	2.0%	1434	37	3.214	2.2%	1461	17	9940	232	0.3	0.1	39	1	136	4	101	2	3.21	0.07	0.257	0.002	3.90	0.03	0.090	0.002	1475	9	1.3	1500	9	-2.65
7 C:\DATA\031028\OC28B7.D	0.3234	0.8%	1806	12.8	0.0915	2.5%	1769	42	0.102	2.1%	1652	39	4.705	2.4%	1768	20	9215	228	0.3	0.1	33	1	60	2	69	2	4.70	0.11	0.323	0.003	3.09	0.03	0.102	0.002	1826	13	0.9	1816	13	4.43
8 C:\DATA\031028\OC28B8.D	0.2648	0.6%	1514	7.9	0.0633	3.0%	1240	36	0.095	1.9%	1538	35	3.471	2.1%	1521	16	7832	188	-0.1	-0.1	63	2	151	4	188	4	3.47	0.07	0.265	0.002	3.78	0.02	0.095	0.002	1512	8	0.8	1582	8	-1.45
9 C:\DATA\031028\OC28B9.D	0.3482	0.5%	1926	9.1	0.0947	2.3%	1829	39	0.115	1.8%	1884	33	5.658	2.1%	1925	18	9697	228	0.1	0.1	57	2	99	3	118	3	5.66	0.12	0.348	0.002	2.87	0.02	0.115	0.002	1932	9	0.8	1950	9	-0.31
10 C:\DATA\031028\OC28B10.D	0.3050	0.5%	1716	8.0	0.0839	2.3%	1629	36	0.101	1.9%	1641	35	4.653	2.1%	1759	18	9709	234	0.4	0.1	46	1	86	2	111	2	4.65	0.10	0.305	0.002	3.28	0.02	0.101	0.002	1725	8	0.8	1736	8	-1.01
11 C:\DATA\031028\OC28B11.D	0.2535	0.6%	1457	8.2	0.0745	2.3%	1453	32	0.106	1.9%	1737	35	3.944	2.2%	1623	18	9311	224	0.0	0.1	81	2	177	5	260	9	3.94	0.09	0.254	0.002	3.94	0.02	0.106	0.002	1431	8	0.7	1457	8	-3.30
12 C:\DATA\031028\OC28B12.D	0.2469	0.8%	1422	10.4	0.0681	2.3%	1331	30	0.090	2.1%	1430	39	3.353	2.3%	1494	19	7599	176	0.1	0.1	60	2	262	8	176	4	3.35	0.08	0.247	0.002	4.05	0.03	0.090	0.002	1422	10	1.5	1476	10	-5.67
1 C:\DATA\031028\OC28C1.D	0.2608	0.6%	1494	7.4	0.0627	2.3%	1230	28	0.096	2.1%	1548	40	3.348	2.2%	1492	18	9667	229	0.5	0.1	43	1	107	3	150	6	3.35	0.08	0.261	0.001	3.83	0.02	0.096	0.002	1489	7	0.7	1550	7	2.02
2 C:\DATA\031028\OC28C2.D	0.2918	0.5%	1650	7.6	0.0803	2.3%	1560	34	0.098	1.8%	1588	34	3.985	2.1%	1631	17	10122	242	0.2	0.1	70	2	133	4	184	5	3.98	0.08	0.292	0.002	3.43	0.02	0.098	0.002	1657	8	0.7	1670	8	-1.60
3 C:\DATA\031028\OC28C3.D	0.2198	0.7%	1281	7.8	0.0637	2.2%	1249	26	0.103	1.9%	1678	35	3.401	2.0%	1505	16	10113	234	0.3	0.1	111	3	743	19	366	9	3.40	0.07	0.220	0.001	4.55	0.03	0.103	0.002	1252	8	2.0	1314	8	-5.49
4 C:\DATA\031028\OC28C4.D	0.2732	0.5%	1557	6.7	0.0728	2.2%	1421	31	0.094	1.8%	1503	35	4.392	2.1%	1711	18	8531	198	0.2	0.1	66	2	176	6	167	6	4.39	0.09	0.273	0.001	3.66	0.02	0.094	0.002	1562	7	1.1	1604	7	-0.32
5 C:\DATA\031028\OC28C5.D	0.2351	0.4%	1361	4.7	0.0700	2.2%	1367	30	0.098	1.9%	1588	35	3.309	2.0%	1483	16	11488	264	-0.2	-0.1	92	2	315	8	358	12	3.31	0.07	0.235	0.001	4.25	0.02	0.098	0.002	1344	5	0.9	1359	5	0.92
6 C:\DATA\031028\OC28C6.D	0.2621	0.5%	1501	6.3	0.0617	2.7%	1211	32	0.094	1.8%	1508	33	5.366	2.2%	1879	19	9274	214	-0.1	-0.1	83	2	161	4	252	6	5.37	0.12	0.262	0.001	3.81	0.02	0.094	0.002	1500	6	0.6	1554	6	1.51
7 C:\DATA\031028\OC28C7.D	0.2722	0.6%	1552	7.7	0.0742	2.2%	1447	31	0.095	2.0%	1527	37	5.118	2.2%	1839	19	9425	220	0.6	0.1	50	1	182	5	118	3	5.12	0.11	0.272	0.002	3.67	0.02	0.095	0.002	1554	8	1.5	1615	8	-3.19
8 C:\DATA\031028\OC28C8.D	0.2532	0.5%	1455	6.6	0.0684	2.2%	1336	29	0.090	1.9%	1424	36	3.505	2.1%	1528	17	10224	228	0.2	0.1	53	1	135	4	153	4	3.50	0.07	0.253	0.001	3.95	0.02	0.090	0.002	1458	7	0.9	1488	7	-0.63
9 C:\DATA\031028\OC28C9.D	0.2689	0.6%	1535	8.8	0.0740	2.5%	1444	35	0.091	2.1%	1455	39	3.971	2.3%	1628	19	8475	189	0.1	0.1	23	1	29	1	70	1	3.97	0.09	0.269	0.002	3.72	0.02	0.091	0.002	1542	9	0.4	1546	9	0.74
10 C:\DATA\031028\OC28C10.D	0.2635	0.6%	1508	7.5	0.0763	2.4%	1487	34	0.087	2.0%	1351	38	3.253	2.2%	1470	17	8889	208	0.4	0.1	44	1	93	2	127	4	3.25	0.07	0.263	0.001	3.80	0.02	0.087	0.002	1521	8	0.7	1512	8	0.96
11 C:\DATA\031028\OC28C11.D	0.2859	0.6%	1621	8.7	0.0767	2.3%	1493	33	0.093	1.9%	1496	35	3.705	2.1%	1573	17	10065	233	0.2	0.1	51	1	95	3	134	3	3.71	0.08	0.286	0.002	3.50	0.02	0.093	0.002	1633	9	0.7	1648	9	1.21
12 C:\DATA\031028\OC28C12.D	0.3500	0.6%	1935	9.7	0.0952	2.3%	1838	41	0.115	1.9%	1887	34	6.634	2.1%	2064	18	10490	237	0.1	0.1	41	1	54	1	89	2	6.63	0.14	0.350	0.002	2.86	0.02	0.115	0.002	1942	10	0.6	1951	10	0.31
1 C:\DATA\031028\OC28D1.D	0.2039	1.0%	1196	10.6	0.0761	3.5%	1483	50	0.150	3.5%	2351	60	4.242	4.0%	1682	34	9411	196	0.7	0.1	59	2	243	6	188	7	4.24	0.17	0.204	0.002	4.90	0.05	0.150	0.005	1099	11	1.3	1052	11	-5.44
2 C:\DATA\031028\OC28D2.D	0.3124	0.5%	1752	7.9	0.0847	2.3%	1643	36	0.103	1.8%	1681	33	4.773	2.1%	1780	18	9520	209	0.3	0.1	71	2	101	2	179	4	4.77	0.10	0.312	0.002	3.20	0.02	0.103	0.002	1761	8	0.6	1769	8	-0.80
3 C:\DATA\031028\OC28D3.D	0.2724	0.5%	1553	7.0	0.0757	2.3%	1476	33	0.091	1.8%	1445	35	3.997	2.1%	1634	17	11270	245	0.2	0.1	62	2	82	2	182	4	4.00	0.08	0.272	0.001	3.67	0.02	0.091	0.002	1563	7	0.5	1563	7	-0.44
4 C:\DATA\031028\OC28D4.D	0.2593	0.6%	1486	7.8	0.0730	2.3%	1423	32	0.092	2.0%	1468	39	5.631	2.6%	1921	22	9783	210	-0.1	-0.1	30	1	69	2	86	2	5.63	0.14	0.259	0.002	3.86	0.02	0.092	0.002	1488	8	0.8	1502	8	-0.07
5 C:\DATA\031028\OC28D5.D	0.2526	0.7%	1452	8.8	0.0804	2.3%	1563	35	0.098	2.0%	1578	37	3.688	2.2%	1569	18	10315	223	0.3	0.1	71	2	167	4	194	4	3.69	0.08	0.253	0.002	3.96	0.03	0.098	0.002	1441	9	0.9	1421	9	-1.17
6 C:\DATA\031028\OC28D6.D	0.2618	0.5%	1499	6.5	0.0725	2.2%	1414	30	0.089	1.8%	1406	35	3.554	2.1%	1539	17	10557	237	0.2	0.1	80	2	175	5	227	7	3.55	0.07	0.262	0.001	3.82	0.02	0.089	0.002	1507	7	0.8	1519	7	-2.07
7 C:\DATA\031028\OC28D7.D	0.2667	1.0%	1524	13.8	0.0686	2.8%	1342	37	0.087	3.1%	1367	60	3.677	3.7%	1566	30	9418	234	0.2	0.1	45	4	624	38	197	23	3.68	0.14	0.267	0.003	3.75	0.04	0.087	0.003	1538	14	3.2	2084	14	6.63
8 C:\DATA\031028\OC28D8.D	0.2529	0.7%	1454	8.7	0.0748	2.4%	1458	34	0.087	2.1%	1356	41	7.527	3.1%	2176	28	9776	219	0.4	0.1	65	2	171	5	218	7	7.53	0.23	0.253	0.002	3.95	0.03	0.087	0.002	1461	9	0.8	1453	9	-5.24
9 C:\DATA\031028\OC28D9.D	0.1742	0.5%	1035	4.6	0.0308	2.4%	613	15	0.072	1.9%	990	38	1.894	2.1%	1079	14	11117	236	0.0	0.1	82	2	156	4	399	10	1.89	0.04	0.174	0.001	5.74	0.03	0.072	0.001	1037	5	0.4	1082	5	-2.30
10 C:\DATA\031028\OC28D10.D	0.2770	0.6%	1576	8.4	0.0843	2.6%	1635	41	0.095	1.9%	1529	37	9.836	2.8%	2420	27	9015	201	0.2	0.1	48	2	52	1	135	3	9.84	0.28	0.277	0.002	3.61	0.02	0.095	0.002	1581	8	0.4	1570	8	2.09
11 C:\DATA\031028\OC28D11.D	0.3139	0.7%	1760	10.1	0.0853	2.3%	1654	37	0.103	1.9%	1673	35	5.340	2.2%	1875	19	9147	200	0.2	0.1	45	1	65	2	109	3	5.34	0.12	0.314	0.002	3.19	0.02	0.103	0.002	1770	10	0.6	1777	10	-1.80
12 C:\DATA\031028\OC28D12.D	0.2743	0.6%	1563	8.1	0.0739	2.4%	1441	33	0.100	1.9%	1617	34	3.895	2.1%	1613	17	10184	230	0.5	0.1	90	2	189	5	248	5	3.89	0.08	0.274	0.002	3.65	0.02	0.100	0.002	1557	8	0.8	1591	8	-2.14
1 C:\DATA\031028\OC28E1.D	0.2149	0.8%	1255	9.2	0.0731	2.3%	1426	32	0.105	2.2%	1709	40	3.084	2.5%	1429	19	9605	235	0.3	0.1	52	2	124	4	143	6	3.08	0.08	0.215	0.002	4.65	0.04	0.105	0.002	1222	9	0.9	1206	9	-3.77
2 C:\DATA\031028\OC28E2.D	0.3032	0.6%	1707	8.7	0.0872	2.4%	1691	38	0.100	1.9%	1629	35	4.173	2.1%	1669	18	10050	256	0.1	0.1	48	1	53	2	131	4	4.17	0.09	0.303	0.002	3.30	0.02	0.100	0.002	1716	9	0.4	1709	9	1.01
3 C:\DATA\031028\OC28E3.D	0.2939	0.8%	1661	11.1	0.0846	2.6%	1641	41	0.092	2.0%	1464	39	3.737	2.3%	1579	19	8545	215	0.2	0.1	33	1	38	1	96	3	3.74	0.09	0.294	0.002	3.40	0.03	0.092	0.002	1681	11	0.4	1663	11	3.98
4 C:\DATA\031028\OC28E4.D	0.2466	1.0%	1421	12.1	0.0930	3.0%	1798	51	0.099	2.3%	1612	42	3.447	2.5%	1515	20	10155	253	0.2	0.1	29	1	50	1	87	2	3.45	0.09	0.247	0.002	4.06	0.04	0.099	0.002	1405	12	0.6	1356	12	-2.86
5 C:\DATA\031028\OC28E5.D	0.1957	0.9%	1152	9.2	0.0611	2.5%	1199	30	0.096	2.4%	1541	46	2.597	2.6%	1300	19	8718	220	0.1	0.1	30	1	129	4	108	4	2.60	0.07	0.196	0.002	5.11	0.04	0.096	0.002	1129	9	1.2	1131	9	7.54
6 C:\DATA\031028\OC28E6.D	0.3314	0.5%	1845	7.8	0.0918	2.3%	1775	39	0.107	1.8%	1754	32	4.900	2.0%	1802	17	10316	249	0.3	0.1	111	3	133	4	269	6	4.90	0.10	0.331	0.002	3.02	0.01	0.107	0.002	1858	8	0.5	1855	8	3.29
7 C:\DATA\031028\OC28E7.D	0.1718	0.9%	1022	8.7	0.0506	2.4%	998	23	0.074	2.8%	1053	57	1.765	3.0%	1033	20	9796	234	0.4	0.1	23	1	140	5	81	3	1.76	0.05	0.172	0.002	5.82	0.05	0.074	0.002	1021	9	1.7	1042	9	-2.33
8 C:\DATA\031028\OC28E8.D	0.2713	0.6%	1548	7.8	0.0763	2.3%	1486	33	0.090	2.0%	1435	39	3.373	2.3%	1498	18	9175	225	0.2	0.1	31	1	75	2	80	2	3.37	0.08	0.271	0.002	3.69	0.02	0.090	0.002	1558	8	0.9	1566	8	0.82
9 C:\DATA\031028\OC28E9.D	0.2970	0.6%	1677	8.2	0.0824	2.3%	1599	35	0.097	1.9%	1565	36	3.973	2.2%	1629	18	8406	202	0.0	-0.1	43	1	125	4	109	3	3.97	0.09	0.297	0.002	3.37	0.02	0.097	0.002	1689	8	1.2	1707	8	1.81
10 C:\DATA\031028\OC28E10.D	0.2601	0.5%	1490	7.2	0.0560	3.3%	1102	35	0.099	2.2%	1597	41	3.540	2.3%	1536	18	8732	219	0.2	0.1	59	2	464	13	179	5	3.54	0.08	0.260	0.001	3.85	0.02	0.099	0.002	1481	7	2.6	2112	7	-1.96
11 C:\DATA\031028\OC28E11.D	0.3331	0.5%	1854	7.4	0.0940	2.3%	1817	39	0.107	1.8%	1743	33	4.864	2.0%	1796	17	10193	257	0.1	0.1	85	2	84	2	205	5	4.86	0.10	0.333	0.002	3.00	0.01	0.107	0.002	1869	7	0.4	1858	7	0.16
12 C:\DATA\031028\OC28E12.D	0.2221	0.9%	1293	11.1	0.0631	2.7%	1238	32	0.096	2.3%	1544	43	2.946	2.6%	1394	20	8124	208	0.1	0.1	38	1	78	2	113	3	2.95	0.08	0.222	0.002	4.50	0.04	0.096	0.002	1275	11	0.7	1305	11	3.56
1 C:\DATA\031028\OC28F1.D	0.1396	1.0%	842	8.0	0.0439	2.3%	869	19	0.139	1.9%	2209	33	2.644	2.3%	1313	17	8628	213	0.0	0.1	178	5	1000	30	701	21	2.64	0.06	0.140	0.001	7.16	0.07	0.139	0.003	774	8	1.4	826	8	-2.50
2 C:\DATA\031028\OC28F2.D	0.2690	0.5%	1536	7.2	0.0750	2.2%	1462	31	0.091	1.8%	1439	34	3.363	2.1%	1496	16	7527	183	0.0	0.1	94	3	255	7	249	5	3.36	0.07	0.269	0.001	3.72	0.02	0.091	0.002	1544	7	1.0	1561	7	-1.77
3 C:\DATA\031028\OC28F3.D	0.2936	0.6%	1660	9.0	0.0826	2.3%	1604	35	0.101	1.8%	1639	34	4.066	2.1%	1647	17	8886	219	0.3	0.1	115	3	231	7	293	7	4.07	0.08	0.294	0.002	3.41	0.02	0.101	0.002	1662	9	0.8	1673	9	-4.52
4 C:\DATA\031028\OC28F4.D	0.3078	0.5%	1730	7.2	0.0860	2.2%	1668	35	0.100	1.8%	1616	33	4.205	2.0%	1675	17	10170	245	0.4	0.1	120	3	192	5	300	7	4.20	0.09	0.308	0.001	3.25	0.02	0.100	0.002	1743	7	0.6	1741	7	0.10
5 C:\DATA\031028\OC28F5.D	0.2447	0.6%	1411	7.1	0.0647	2.2%	1268	27	0.094	1.8%	1500	34	3.163	2.1%	1448	16	9957	240	0.2	0.1	114	3	345	10	342	10	3.16	0.07	0.245	0.001	4.09	0.02	0.094	0.002	1404	7	1.0	1459	7	4.42
6 C:\DATA\031028\OC28F6.D	0.3158	0.6%	1769	9.6	0.0832	2.3%	1616	36	0.104	1.9%	1691	35	4.515	2.1%	1734	18	8962	210	-0.1	-0.1	60	2	133	4	137	3	4.51	0.10	0.316	0.002	3.17	0.02	0.104	0.002	1779	10	1.0	1816	10	-3.80
7 C:\DATA\031028\OC28F7.D	0.2560	0.5%	1469	6.1	0.0730	2.2%	1424	31	0.092	1.8%	1463	35	3.231	2.0%	1465	16	10457	245	0.2	0.1	72	2	175	5	208	5

Sample DS1		Calculated Ages																Elemental Abundance (ppm)									
Analysis	File	206Pb/238U	%rsd	age	+/-1s	208Pb/232	%rsd	age	+/-1s	207Pb/206P	%rsd	age	+/-1s	207Pb/235U	%rsd	age	+/-1s	Hf	+/-1s	Hg	+/-1s	Pb	+/-1s	Th	+/-1s	U	+/-1s
1	C:\HPCHEM\1\DATA\030219\FE19A07.D	0.2530	2.4%	1454	30.9	0.0749	3.3%	1460	47	0.112	6.1%	1834	111	93.868	113.7%	4623	#NUM!	4575	226	-0.2	-0.1	12	1	46	3	36	2
2	C:\HPCHEM\1\DATA\030219\FE19A08.D	0.2852	3.1%	1617	44.3	0.0945	3.3%	1825	58	0.112	5.6%	1830	102	89.192	138.2%	4571	#NUM!	5322	267	0.1	0.1	35	2	91	5	97	5
3	C:\HPCHEM\1\DATA\030219\FE19A09.D	0.1806	2.4%	1070	23.6	0.0401	2.7%	794	21	0.104	3.9%	1698	72	7.001	79.6%	2112	1212	7447	391	0.0	0.1	119	7	395	23	605	32
4	C:\HPCHEM\1\DATA\030219\FE19A10.D	0.2775	2.3%	1579	32.0	0.0838	2.4%	1627	37	0.108	4.0%	1766	74	39.107	115.0%	3748	#NUM!	5840	333	0.2	0.1	76	5	265	17	221	12
5	C:\HPCHEM\1\DATA\030219\FE19A11.D	0.2718	2.7%	1550	37.8	0.0819	4.0%	1592	61	0.105	6.8%	1710	126	83.378	115.6%	4504	#NUM!	5726	349	0.6	0.2	13	1	38	3	42	3
6	C:\HPCHEM\1\DATA\030219\FE19A12.D	0.2577	2.3%	1478	29.8	0.0816	3.2%	1585	48	0.102	5.0%	1653	93	50.735	112.4%	4007	#NUM!	6161	388	0.0	0.2	30	2	74	5	105	7
7	C:\HPCHEM\1\DATA\030219\FE19A13.D	0.2090	3.9%	1224	43.6	0.0666	6.0%	1304	76	0.093	10.7%	1498	202	5.548	80.2%	1908	1155	4740	275	-0.4	-0.2	20	1	52	3	76	5
8	C:\HPCHEM\1\DATA\030219\FE19A14.D	0.2748	3.2%	1565	45.3	0.0812	4.0%	1578	61	0.104	7.5%	1696	138	8.651	79.8%	2302	1275	5078	331	0.2	0.2	22	1	78	6	65	4
9	C:\HPCHEM\1\DATA\030219\FE19A15.D	0.2539	2.2%	1458	28.7	0.0624	3.1%	1223	36	0.100	4.3%	1630	79	42.335	119.2%	3827	#NUM!	5953	391	0.3	0.2	57	4	151	11	208	15
10	C:\HPCHEM\1\DATA\030219\FE19A16.D	0.2038	2.2%	1196	24.0	0.0555	4.7%	1091	50	0.097	5.7%	1566	107	-0.700	781.5%	-1221	-3000	6454	431	0.0	0.2	22	2	52	4	101	7
11	C:\HPCHEM\1\DATA\030219\FE19A17.D	0.2463	2.3%	1419	29.5	0.0783	3.1%	1524	45	0.105	5.4%	1723	99	38.931	113.1%	3744	#NUM!	5008	304	0.1	0.2	24	2	80	5	81	5
12	C:\HPCHEM\1\DATA\030219\FE19A18.D	0.3176	2.1%	1778	32.8	0.0942	4.4%	1820	76	0.111	5.4%	1809	97	54.062	133.4%	4070	#NUM!	6404	377	-0.2	-0.2	19	1	24	2	57	4
8	C:\HPCHEM\1\DATA\030219\FE19A32.D	0.2645	1.3%	1513	17.4	0.0680	2.5%	1329	32	0.108	3.9%	1763	72	46.091	117.8%	3911	#NUM!	43726	1990	0.6	1.1	472	26	1392	78	1436	59
9	C:\HPCHEM\1\DATA\030219\FE19A33.D	0.2679	1.6%	1530	21.7	0.0797	2.8%	1549	42	0.107	4.5%	1743	82	83.239	122.3%	4502	#NUM!	39231	1908	-2.2	-1.1	337	20	845	51	1037	53
10	C:\HPCHEM\1\DATA\030219\FE19A34.D	0.2032	1.8%	1193	20.1	0.0720	5.6%	1406	76	0.102	5.3%	1669	97	86.665	131.6%	4542	#NUM!	39021	2053	0.1	1.2	233	14	248	16	941	50
11	C:\HPCHEM\1\DATA\030219\FE19A35.D	0.2699	1.3%	1540	17.4	0.0823	2.7%	1599	42	0.116	4.0%	1894	72	84.950	126.4%	4522	#NUM!	37731	1874	-0.5	-1.1	618	36	1528	91	1745	83
12	C:\HPCHEM\1\DATA\030219\FE19A36.D	0.1675	1.7%	999	15.9	0.0322	3.8%	640	24	0.100	4.3%	1619	79	4.519	79.6%	1734	1071	46562	2283	-0.1	-1.0	662	38	2586	154	3114	190
1	C:\HPCHEM\1\DATA\030219\FE19A41.D	0.2466	1.3%	1421	18	0.0544	1.5%	1071	16	0.100	2.6%	1627	42	4.378	4.8%	1708	82	3717	79	0.1	0.2	75	2	363	6	186	4
2	C:\HPCHEM\1\DATA\030219\FE19A42.D	0.2532	1.2%	1455	18	0.0554	2.0%	1090	21	0.095	3.4%	1531	52	4.338	5.2%	1701	88	3694	86	0.0	0.2	59	1	254	5	149	4
3	C:\HPCHEM\1\DATA\030219\FE19A43.D	0.2686	2.1%	1533	31	0.0661	3.6%	1294	47	0.104	4.1%	1690	69	3.703	5.6%	1572	88	4429	116	0.0	0.2	29	1	80	4	78	3
4	C:\HPCHEM\1\DATA\030219\FE19A44.D	0.2849	1.7%	1616	28	0.0649	3.6%	1271	46	0.106	3.0%	1724	51	4.813	4.6%	1787	83	4947	154	0.3	0.2	53	2	62	2	159	6
5	C:\HPCHEM\1\DATA\030219\FE19A45.D	0.2012	2.1%	1182	25	0.0250	3.4%	500	17	0.099	2.7%	1601	44	3.291	4.5%	1479	67	5301	179	0.5	0.2	72	3	259	10	304	12
6	C:\HPCHEM\1\DATA\030219\FE19A46.D	0.1304	2.3%	790	18	0.0241	2.4%	482	11	0.100	3.2%	1624	52	2.173	4.7%	1173	55	5236	141	0.0	0.2	61	2	357	11	362	11
7	C:\HPCHEM\1\DATA\030219\FE19A47.D	0.2685	2.3%	1533	35	0.0606	2.5%	1190	29	0.101	3.7%	1650	61	4.775	5.0%	1780	88	4088	102	-0.1	0.2	46	1	129	3	126	3
8	C:\HPCHEM\1\DATA\030219\FE19A48.D	0.2573	3.0%	1476	44	0.0460	5.1%	909	46	0.104	3.5%	1704	60	4.410	6.4%	1714	109	4246	122	-0.1	0.2	37	1	142	13	116	4
9	C:\HPCHEM\1\DATA\030219\FE19A49.D	0.2522	2.2%	1450	32	0.0575	2.2%	1130	25	0.094	3.6%	1512	54	4.096	5.6%	1653	93	4296	105	0.3	0.2	50	1	150	5	148	4
10	C:\HPCHEM\1\DATA\030219\FE19A50.D	0.2445	3.0%	1410	42	0.0556	2.4%	1094	27	0.106	3.5%	1727	61	4.035	5.5%	1641	90	3467	124	0.1	0.2	47	2	207	10	126	6
11	C:\HPCHEM\1\DATA\030219\FE19A51.D	0.2249	3.8%	1307	49	0.1371	22.4%	2597	582	0.156	7.8%	2410	188	0.730	16.6%	556	92	6463	185	0.3	0.2	3	0	2	0	13	1
12	C:\HPCHEM\1\DATA\030219\FE19A52.D	0.2562	3.2%	1471	47	0.0616	5.6%	1209	67	0.111	6.0%	1823	110	2.102	5.8%	1149	67	3498	102	-0.1	0.2	12	1	25	1	38	1
1	C:\HPCHEM\1\DATA\030219\FE19A59.D	0.2457	1.6%	1416	23	0.0510	3.6%	1006	36	0.102	4.0%	1654	66	4.002	5.6%	1635	91	10106	221	0.8	0.5	80	3	173	6	272	10
2	C:\HPCHEM\1\DATA\030219\FE19A60.D	0.1970	2.0%	1159	23	0.0257	5.1%	514	26	0.102	2.8%	1662	47	3.193	5.4%	1456	79	10212	248	0.0	0.5	152	5	480	26	688	27
3	C:\HPCHEM\1\DATA\030219\FE19A61.D	0.2772	1.5%	1577	24	0.0491	3.6%	968	35	0.112	3.2%	1838	59	4.235	5.0%	1681	85	7470	173	0.4	0.4	78	2	208	6	215	5
4	C:\HPCHEM\1\DATA\030219\FE19A62.D	0.2513	2.4%	1445	34	0.0560	3.7%	1101	41	0.112	4.4%	1832	80	3.540	6.6%	1536	101	7606	241	0.2	0.5	66	2	168	6	213	9
5	C:\HPCHEM\1\DATA\030219\FE19A63.D	0.2378	2.5%	1375	34	0.0303	3.6%	604	22	0.099	3.2%	1608	52	3.530	4.9%	1534	74	9294	396	-0.2	0.4	119	6	252	11	456	20
6	C:\HPCHEM\1\DATA\030219\FE19A64.D	0.3032	2.7%	1707	47	0.0602	3.0%	1181	35	0.111	3.4%	1813	61	4.730	5.7%	1773	101	9242	382	-0.4	0.4	108	5	250	11	293	14
7	C:\HPCHEM\1\DATA\030219\FE19A65.D	0.3037	3.2%	1710	55	0.0599	4.3%	1175	51	0.104	6.3%	1690	106	2.194	8.3%	1179	98	7602	251	-0.5	0.3	28	1	88	3	70	3
8	C:\HPCHEM\1\DATA\030219\FE19A66.D	0.2782	3.1%	1582	49	0.0584	4.5%	1147	52	0.112	5.1%	1833	93	3.316	6.8%	1485	101	9352	344	-0.1	0.4	45	2	74	3	141	5
9	C:\HPCHEM\1\DATA\030219\FE19A67.D	0.1834	2.7%	1085	30	0.0359	3.1%	713	22	0.087	5.0%	1361	68	2.444	6.4%	1256	80	9328	303	-0.3	0.4	89	4	466	23	365	17
10	C:\HPCHEM\1\DATA\030219\FE19A68.D	0.2059	3.4%	1207	41	0.0440	4.9%	871	43	0.092	8.2%	1472	121	1.751	9.3%	1028	96	9522	345	0.3	0.4	29	2	108	5	118	6
11	C:\HPCHEM\1\DATA\030219\FE19A69.D	0.1936	2.1%	1141	24	0.0424	2.9%	838	25	0.079	7.7%	1172	90	2.246	5.9%	1196	70	8436	223	0.2	0.3	46	1	236	6	168	9
12	C:\HPCHEM\1\DATA\030219\FE19A70.D	0.2450	1.9%	1413	27	0.0420	3.0%	832	25	0.109	2.5%	1785	44	4.589	5.4%	1747	94	9009	249	0.5	0.4	129	4	446	13	401	11
1	C:\HPCHEM\1\DATA\030220\FE20A07.D	0.2504	2.0%	1440	29	0.0377	5.3%	749	40	0.105	4.7%	1709	80	3.289	5.8%	1478	85	10480	246	-1.1	0.5	61	2	136	4	202	6
2	C:\HPCHEM\1\DATA\030220\FE20A08.D	0.2280	2.3%	1324	31	0.0312	7.6%	621	47	0.111	4.5%	1820	82	2.697	5.6%	1328	74	10450	222	0.0	0.5	40	1	123	5	158	11
3	C:\HPCHEM\1\DATA\030220\FE20A09.D	0.1622	1.7%	969	17	0.0166	3.8%	332	13	0.104	2.5%	1697	42	3.025	6.3%	1414	89	11020	242	0.1	0.4	163	4	502	13	869	20
4	C:\HPCHEM\1\DATA\030220\FE20A10.D	0.2715	2.1%	1548	33	0.0528	3.5%	1040	36	0.105	4.1%	1711	69	3.466	5.6%	1519	85	9285	217	0.6	0.4	62	2	160	4	169	4
5	C:\HPCHEM\1\DATA\030220\FE20A11.D	0.2622	2.0%	1501	31	0.0389	4.6%	771	35	0.111	1.9%	1808	34	4.561	4.1%	1742	71	11509	306	0.1	0.4	296	9	208	7	1032	30
6	C:\HPCHEM\1\DATA\030220\FE20A12.D	0.2592	2.2%	1486	33	0.0502	3.9%	990	39	0.111	4.2%	1818	76	3.817	5.3%	1596	84	9832	257	0.8	0.5	74	3	198	6	210	6
7	C:\HPCHEM\1\DATA\030220\FE20A13.D	0.2570	2.3%	1475	34	0.0343	4.2%	681	28	0.110	2.8%	1806	50	5.266	5.1%	1863	95	9909	318	-0.7	0.5	150	5	397	15	479	16
8	C:\HPCHEM\1\DATA\030220\FE20A14.D	0.2522	2.0%	1450	29	0.0514	3.7%	1013	37	0.111	6.5%	1812	118	3.408	5.1%	1506	77	8168	192	0.4	0.5	69	2	223	6	187	5
9	C:\HPCHEM\1\DATA\030220\FE20A15.D	0.2481	1.8%	1429	26	0.0381	4.4%	757	33	0.115	2.6%	1875	49	4.821	5.0%	1789	90	10228	261	-0.4	0.4	118	4	165	5	409	11
10	C:\HPCHEM\1\DATA\030220\FE20A16.D	0.1440	2.5%	867	21	0.0162	3.4%	325	11	0.097	3.5%	1573	55	2.367	5.6%	1233	69	9569	219	1.0	0.4	154	5	1413	59	816	30
11	C:\HPCHEM\1\DATA\030220\FE20A17.D	0.2392	2.1%	1383	29	0.0350	8.3%	695	58	0.101	3.9%	1639	63	4.013	5.8%	1637	95	13188	605	0.8	0.6	182	9	123	8	683	30
12	C:\HPCHEM\1\DATA\030220\FE20A18.D	0.1378	1.7%	832	14	0.0187	3.1%	374	12	0.100	2.8%	1621	45	2.438	5.3%	1254	66	10123	293	0.4	0.5	174	6	882	29	1009	32
1	C:\HPCHEM\1\DATA\030220\FE20A25.D	0.2557	1.9%	1468	28	0.0405	6.7%	803	54	0.103	5.4%	1683	91	2.005	6.2%	1117	69	9956	151	-0.5	0.4	28	1	82	2	89	2
2	C:\HPCHEM\1\DATA\030220\FE20A26.D	0.2570	2.1%	1475	31	0.0438	5.5%	866	47	0.112	4.4%	1836	80	2.963	5.5%	1398	77	9498	126	-0.2	0.3	38	1	120	2	112	2
3	C:\HPCHEM\1\DATA\030220\FE20A27.D	0.1905	1.3%	1124	15	0.0093	4.0%	187	7	0.112	2.0%	1832	37	3.707	4.7%	1573	74	10961	157	0.2	0.3	130	3	1156	18	557	7
4	C:\HPCHEM\1\DATA\030220\FE20A28.D	0.2416	2.0%	1395	27	0.0370	4.0%	734	30	0.106	4.1%	1725	71	3.160	5.5%	1448	80	9420	228	0.2	0.3	48	2	209	4	145	3
5	C:\HPCHEM\1\DATA\030220\FE20A29.D	0.2577	1.5%	1478	23	0.0437	3.4%	865	30	0.101	4.0%	1641	66	3.837	5.1%	1601	81	8906	150	0.0	0.3	60	1	227	4	167	3
6	C:\HPCHEM\1\DATA\030220\FE20A30.D	0.2719	1.8%	1550	27	0.0449	3.7%	888	33	0.103	3.6%	1686	61	3.786	5.2%	1590	82	9655	163	0.2	0.3	61	2	194	4	170	3
7	C:\HPCHEM\1\DATA\030220\FE20A31.D	0.2314	1.9%	1342	26	0.0301	3.0%	600	18	0.101	2.6%	1637	43	3.732	5.2%	1578	82	9277	170	0.1	0.3	211	5	782	28	749	21
8	C:\HPCHEM\1\DATA\030220\FE20A32.D	0.2543	1.7%	1461	25	0.0402	4.9%	796	39	0.100	3.7%	1630	60	3.557	5.4%	1540	84	10491	184	0.7	0.4	68	2	157	4	223	7
9	C:\HPCHEM\1\DATA\030220\FE20A33.D	0.2469	2.0%	1422	28	0.0394	5.3%	780	42	0.114	4.4%	1865	81	3.155	5.6%	1446	81	9920	170	0.5	0.4	40	1	127	3	129	3
10	C:\HPCHEM\1\DATA\030220\FE20A34.D	0.2501	1.5%	1439	22	0.0391	3.8%	776	30	0.101	2.4%	1636	39	4.353	5.7%	1703	98	10194	174	-0.2	0.3	173	3	404	8	572	11
11	C:\HPCHEM\1\DATA\030220\FE20A35.D	0.2168	2.1%	1265	27	0.0341	3.9%	678	27	0.099	4.2%	1600	67	2.906	5.7%	1383	78	8996	163	0.1	0.3	59	2	237	6	214	5
12	C:\HPCHEM\1\DATA\030220\FE20A36.D	0.1974	1.4%	1162	16	0.0203	4.4%	406	18	0.098	3.8%	1588	61	3.284	5.8%	1477	85	10653	199	-0.3	0.3	57	1	303	7	234	4
1	C:\HPCHEM\1\DATA\030220\FE20A43.D	0.2564	1.3%	1471	18	0.0430	4.0%	851	34	0.104	3.8%	1691	64	3.459	4.7%	1518	71	10071	143	0.1	0.3	51	1	142	3	155	4
2	C:\HPCHEM\1\DATA\030220\FE20A44.D	0.2009	1.8%	1180	21	0.0331	5.7%	658	38	0.088	6.3%	1375	87	1.981	7.3%	1109	81	10018	224	0.1	0.3	37	1	126	3	151	4
3	C:\HPCHEM\1\DATA\030220\FE20A45.D	0.2027	1.7%	1190	21	0.0333	5.8%	663	39	0.093	6.3%	1484	93	1.938	6.8%	1094	74	9924	202	0.6	0.4	33	1	107	3	134	4
4	C:\HPCHEM\1\DATA\030220\FE20A46.D	0.2278	1.6%	1323	21	0.0389	114.0%	770	878	0.105	2.4%	1723	42	3.558	5.1%	1540	78	13403	454	-0.4	0.5	174	13	330	12	690	27
5	C:\HPCHEM\1\DATA\030220\FE20A47.D	0.2462	2.6%	1419	37	0.0410	7.2%	813	58	0.116	6.9%	1897	132	1.578	7.7%	961	74	9705	235	1.0	0.5	20	1	55	2	65	2
6	C:\HPCHEM\1\DATA\030220\FE20A48.D	0.2909	1.9%	1646	31	0.0777	51.0%	1512	772	0.109	4.6%	1785	82	2.820	6.3%	1361	85	9796	271	-0.7	0.5	64	10	109	4	155	5
7	C:\HPCHEM\1\DATA\030220\FE20A49.D	0.2284	2.7%	1326	36	0.0393	8.1%	779	63	0.114	5.8%	1861	108	2.467	8.7%	1262	109	9946	312	0.4	0.6	53	4	171	12	168	9
8	C:\HPCHEM\1\DATA\030220\FE20A50.D	0.2851	2.5%	1617	41	0.0482	8.8%	951	84	0.129	5.5%	2081	115	1.897	8.7%	1080	94	9271	207	1.0	0.5	32	1	60	2	96	3
9	C:\HPCHEM\1\DATA\030220\FE20A51.D	0.2243	5.3%	1305	69	0.0275	7.3%	548	40	0.108	6.0%	1769	107	2.807	7.2%	1357	98	9615	511	0.2	0.6	80	5	388	24	281	16
10	C:\HPCHEM\1\DATA\030220\FE20A52.D	0.2355	2.0%	1363	28	0.0337	11.7%	670	78	0.121	5.3%	1966	103	3.866	6.6%	1607	106	10052	517	0.5	0.6	154	8	315	19	567	31
11	C:\HPCHEM\1\DATA\030220\FE20A53.D	0.2458	2.1%	1417	29	0.0344	7.3%	684	50	0.109	4.9%	1786	87	2.253	7.1%	1198	85	10508	244	0.2	0.6	43	2	106	4	149	4
12	C:\HPCHEM\1\DATA\030220\FE20A54.D	0.2182	2.5%	1272	32	0.0335	8.1%	666	54	0.168	17.3%	2534	439	4.946	44.1%	1810	798	8212	219	0.1	0.6	42	4	158	11	154	5

Sample DS2		Calculated Ages																Elemental Abundances									
Analysis	File	206Pb/238U	%rsd	age	+/-1s	208Pb/232Th	%rsd	age	+/-1s	207Pb/206Pb	%rsd	age	+/-1s	207Pb/235U	%rsd	age	+/-1s	Hf	+/-1s	Hg	+/-1s	Pb	+/-1s	Th	+/-1s	U	+/-1s
1	C:\DATA\031031\OC31G1.D	0.2821	0.7%	1602	10.0	0.0828	1.1%	1607	17	0.099	1.0%	1611	19	4.737	1.2%	1774	10	11067	273	0.3	0.1	164	4	233	6	468	15
2	C:\DATA\031031\OC31G2.D	0.3871	0.8%	2109	14.5	0.1072	1.5%	2058	29	0.107	1.2%	1756	22	7.273	1.4%	2146	13	10983	277	-0.2	-0.1	65	2	72	2	152	11
3	C:\DATA\031031\OC31G3.D	0.2683	0.7%	1532	9.1	0.0871	1.1%	1688	18	0.093	1.4%	1481	26	4.400	1.5%	1712	12	10722	255	0.1	0.1	49	1	118	3	138	3
4	C:\DATA\031031\OC31G4.D	0.2807	1.0%	1595	13.7	0.0719	1.6%	1402	21	0.101	1.6%	1642	29	4.905	1.8%	1803	16	9572	228	0.3	0.1	84	3	123	4	235	10
5	C:\DATA\031031\OC31G5.D	0.3292	0.6%	1835	10.4	0.1102	1.2%	2113	24	0.111	1.4%	1824	25	6.545	1.6%	2052	14	7801	186	0.2	0.1	40	1	70	2	87	3
6	C:\DATA\031031\OC31G6.D	0.3040	0.9%	1711	13.6	0.0933	1.3%	1803	23	0.035	4.0%	-699	112	1.864	3.8%	1068	25	10226	270	0.0	0.1	87	4	143	7	259	19
7	C:\DATA\031031\OC31G7.D	0.2752	0.8%	1567	10.8	0.1054	2.2%	2025	42	0.099	1.9%	1598	36	4.811	2.0%	1787	17	9358	231	0.5	0.1	47	1	100	3	113	4
8	C:\DATA\031031\OC31G8.D	0.2453	0.5%	1414	6.3	0.0792	1.4%	1540	20	0.103	1.0%	1680	19	4.326	1.2%	1698	10	11241	274	0.5	0.1	207	6	366	10	672	21
9	C:\DATA\031031\OC31G9.D	0.2713	1.0%	1548	14.0	0.1050	1.5%	2019	30	0.095	2.6%	1531	49	4.926	2.5%	1807	21	8342	186	0.2	0.1	34	1	127	3	101	3
10	C:\DATA\031031\OC31G10.D	0.2907	0.5%	1645	7.3	0.0896	0.9%	1735	15	0.096	1.0%	1544	19	4.720	1.2%	1771	10	10756	249	-0.2	-0.1	155	4	324	8	401	8
11	C:\DATA\031031\OC31G11.D	0.1962	1.0%	1155	10.3	0.0517	1.7%	1019	17	0.088	2.5%	1393	47	2.996	2.4%	1407	19	9352	215	0.4	0.1	64	2	340	10	346	18
12	C:\DATA\031031\OC31G12.D	0.0388	1.2%	245	2.9	0.0129	2.6%	259	7	0.050	7.1%	193	164	0.324	7.2%	285	18	9362	221	0.1	0.1	9	1	100	5	132	3
1	C:\DATA\031031\OC31H1.D	0.2367	0.7%	1370	8.5	0.0816	1.4%	1586	21	0.085	1.4%	1316	27	3.449	1.6%	1516	13	9725	241	0.7	0.2	69	2	113	3	218	11
2	C:\DATA\031031\OC31H2.D	0.1622	1.1%	969	10.3	0.0321	1.7%	640	10	0.079	1.9%	1169	38	2.130	2.0%	1158	14	9491	233	0.4	0.1	102	3	1059	30	472	18
3	C:\DATA\031031\OC31H3.D	0.2653	0.7%	1517	9.0	0.0851	1.1%	1650	18	0.094	1.3%	1517	25	4.267	1.4%	1687	12	9268	211	0.1	0.1	74	2	217	6	158	4
4	C:\DATA\031031\OC31H4.D	0.2643	0.5%	1512	7.4	0.0833	1.1%	1617	17	0.097	1.2%	1570	23	4.415	1.3%	1715	11	9128	210	0.4	0.1	63	2	186	5	166	4
5	C:\DATA\031031\OC31H5.D	0.2683	0.8%	1532	10.9	0.0864	1.2%	1675	20	0.094	2.2%	1510	41	4.377	2.3%	1708	19	9165	220	0.8	0.1	16	0	55	1	43	6
6	C:\DATA\031031\OC31H6.D	0.2538	0.4%	1458	5.4	0.0820	1.1%	1592	17	0.090	0.9%	1426	18	3.897	1.1%	1613	9	12527	298	0.2	0.1	165	4	121	3	541	12
7	C:\DATA\031031\OC31H7.D	0.2835	0.6%	1609	7.9	0.0893	0.9%	1730	16	0.097	1.3%	1562	24	4.591	1.4%	1748	12	9189	221	-0.1	-0.1	135	4	414	11	334	7
8	C:\DATA\031031\OC31H8.D	0.2186	0.9%	1275	10.9	0.0413	2.4%	818	19	0.122	1.4%	1988	24	4.526	1.7%	1736	15	11631	409	0.4	0.1	186	6	241	7	499	16
9	C:\DATA\031031\OC31H9.D	0.2483	0.8%	1429	9.6	0.0846	1.2%	1642	19	0.091	1.6%	1445	30	4.025	1.7%	1639	14	11483	280	0.0	-0.1	24	1	46	1	70	2
10	C:\DATA\031031\OC31H10.D	0.2322	0.6%	1346	7.6	0.0781	1.0%	1519	14	0.091	1.0%	1441	20	3.582	1.3%	1546	10	8783	210	0.4	0.1	120	3	403	11	348	8
11	C:\DATA\031031\OC31H11.D	0.1987	0.9%	1168	9.4	0.0942	1.3%	1820	22	0.104	1.5%	1694	28	3.529	1.4%	1534	11	9460	230	0.4	0.1	108	3	288	7	288	9
12	C:\DATA\031031\OC31H12.D	0.2770	0.6%	1576	9.0	0.0947	1.2%	1830	22	0.098	1.2%	1580	22	4.580	1.3%	1746	11	9887	247	0.2	0.1	99	3	170	5	274	8
1	C:\DATA\030403\AP03A61.D	0.2590	0.9%	1485	12.0	0.0761	2.3%	1483	33	0.083	3.0%	1280	58	3.044	2.8%	1419	22	10468	464	0.8	0.2	109	6	288	17	311	12
2	C:\DATA\030403\AP03A62.D	0.2826	1.1%	1604	15.0	0.0799	2.5%	1555	38	0.088	3.2%	1381	62	3.596	3.2%	1549	26	9941	447	0.1	0.2	53	3	133	8	139	5
3	C:\DATA\030403\AP03A63.D	0.2820	1.0%	1601	13.6	0.0867	2.7%	1680	43	0.090	3.0%	1434	56	3.557	2.8%	1540	22	9328	411	0.5	0.2	74	4	111	7	210	8
4	C:\DATA\030403\AP03A64.D	0.2643	1.4%	1512	19.1	0.0833	3.1%	1618	48	0.091	4.2%	1452	81	3.542	3.8%	1537	31	9958	438	0.9	0.2	27	2	81	5	72	3
5	C:\DATA\030403\AP03A65.D	0.2486	1.2%	1431	15.8	0.0768	3.5%	1496	51	0.087	4.2%	1353	80	2.976	3.9%	1401	30	8280	374	0.1	0.2	36	2	100	6	97	4
6	C:\DATA\030403\AP03A66.D	0.2775	1.3%	1579	18.9	0.0819	3.2%	1591	49	0.094	3.9%	1504	73	4.040	3.6%	1642	30	9556	445	-0.1	-0.2	27	2	55	3	73	3
7	C:\DATA\030403\AP03A67.D	0.3054	1.4%	1718	20.7	0.0841	3.3%	1632	52	0.087	3.6%	1363	70	3.843	3.5%	1602	29	11009	521	0.5	0.2	69	4	122	8	187	8
8	C:\DATA\030403\AP03A68.D	0.2530	1.0%	1454	13.1	0.0751	2.6%	1463	37	0.090	3.3%	1421	62	3.108	3.2%	1435	25	10413	477	-0.2	-0.2	84	5	210	13	230	9
9	C:\DATA\030403\AP03A69.D	0.4268	1.1%	2291	21.6	0.1098	3.9%	2105	77	0.119	3.1%	1942	55	7.012	2.9%	2113	26	11033	502	0.1	0.2	86	6	35	2	179	10
10	C:\DATA\030403\AP03A70.D	0.2834	1.1%	1608	15.3	0.0811	2.7%	1576	41	0.089	3.4%	1408	65	3.599	3.2%	1549	26	9374	423	0.0	-0.2	49	3	117	7	131	5
11	C:\DATA\030403\AP03A71.D	0.2427	1.0%	1401	12.9	0.0709	2.5%	1385	34	0.088	3.3%	1374	63	3.269	3.1%	1474	24	8776	389	0.2	0.2	52	3	170	10	157	6
12	C:\DATA\030403\AP03A72.D	0.2805	0.9%	1594	12.1	0.0968	3.3%	1867	59	0.090	3.1%	1417	59	3.585	3.0%	1546	24	12520	552	-0.2	-0.2	64	4	90	5	183	7
1	C:\DATA\030403\AP03A79.D	0.2691	1.5%	1536	20.4	0.0755	3.4%	1470	49	0.072	4.8%	989	97	3.658	4.7%	1562	38	8429	341	0.6	0.2	21	1	42	2	58	2
2	C:\DATA\030403\AP03A80.D	0.2642	1.3%	1511	17.2	0.0832	3.0%	1615	47	0.088	3.9%	1384	75	3.512	3.8%	1530	30	9318	356	0.7	0.2	32	2	51	3	80	3
3	C:\DATA\030403\AP03A81.D	0.2486	1.4%	1431	17.5	0.0769	3.7%	1498	54	0.078	4.0%	1148	79	2.678	3.7%	1323	28	11394	447	0.6	0.2	53	3	77	4	167	7
4	C:\DATA\030403\AP03A82.D	0.0658	1.2%	411	4.7	0.0204	2.1%	409	8	0.045	5.8%	-56	141	0.418	5.7%	355	17	42551	5005	######	#####	#####	####	######	######	#####	######
5	C:\DATA\030403\AP03A83.D	0.2617	0.9%	1498	11.7	0.0834	2.3%	1619	36	0.091	3.2%	1446	61	3.309	3.0%	1483	24	9583	375	0.3	0.2	123	7	285	14	275	9
6	C:\DATA\030403\AP03A84.D	0.2684	1.3%	1533	17.2	0.0802	2.5%	1559	37	0.097	3.7%	1576	70	3.750	3.6%	1582	30	7593	292	0.6	0.2	58	3	180	9	115	4
7	C:\DATA\030403\AP03A85.D	0.3000	1.3%	1691	18.9	0.0886	3.1%	1715	51	0.095	4.0%	1532	74	4.346	3.7%	1702	31	8934	345	-0.2	-0.2	31	2	59	3	73	2
8	C:\DATA\030403\AP03A86.D	0.0891	3.3%	550	17.6	0.0419	29.9%	831	245	0.084	17.0%	1294	331	1.225	19.7%	812	117	9226	473	17.3	80.3	1937	210	2752	201	13013	558
9	C:\DATA\030403\AP03A87.D	0.2352	1.4%	1362	17.3	0.0712	2.6%	1389	34	0.079	3.3%	1161	66	2.625	3.3%	1308	25	8459	358	-0.2	-0.2	88	5	172	9	278	11
10	C:\DATA\030403\AP03A88.D	0.2557	1.4%	1468	18.2	0.0770	2.7%	1499	38	0.084	4.2%	1286	82	2.956	4.2%	1396	32	8736	364	0.2	0.2	30	2	80	4	80	3
11	C:\DATA\030403\AP03A89.D	0.2461	1.1%	1419	13.7	0.0739	2.8%	1442	39	0.075	3.6%	1076	73	2.614	3.6%	1305	27	9421	395	0.0	0.2	44	2	71	4	129	6
12	C:\DATA\030403\AP03A90.D	0.2458	1.4%	1417	17.4	0.0765	2.6%	1490	37	0.089	3.6%	1413	69	2.991	3.6%	1405	28	9386	396	-0.2	-0.2	53	3	135	7	137	5
1	C:\DATA\031028\OC28G1.D	0.2454	0.6%	1415	7.8	0.0642	2.3%	1258	28	0.086	2.0%	1343	38	2.900	2.2%	1382	17	10374	234	0.2	0.1	55	2	140	4	174	4
2	C:\DATA\031028\OC28G2.D	0.2716	0.6%	1549	8.6	0.0730	2.2%	1425	31	0.096	1.9%	1550	36	3.680	2.2%	1567	18	8718	210	0.1	0.1	45	1	144	4	114	3
3	C:\DATA\031028\OC28G3.D	0.2814	0.5%	1598	7.6	0.0766	2.2%	1492	32	0.093	1.8%	1496	34	3.677	2.1%	1566	17	10508	244	0.1	0.1	105	3	235	7	277	5
4	C:\DATA\031028\OC28G4.D	0.2376	0.8%	1374	10.3	0.0583	2.4%	1145	27	0.087	1.9%	1366	36	2.835	2.1%	1365	16	10795	245	0.1	0.1	196	6	797	23	608	13
5	C:\DATA\031028\OC28G5.D	0.3933	0.8%	2138	14.2	0.1015	2.4%	1954	45	0.133	2.3%	2131	39	7.898	2.6%	2219	24	10422	241	0.0	0.1	42	1	87	3	78	2
6	C:\DATA\031028\OC28G6.D	0.2962	0.7%	1673	10.5	0.0833	2.4%	1617	37	0.102	1.9%	1655	34	4.114	2.1%	1657	17	10022	233	0.6	0.1	83	5	129	4	182	4
7	C:\DATA\031028\OC28G7.D	0.3356	0.7%	1866	10.8	0.0932	2.2%	1800	38	0.105	1.8%	1711	32	4.845	2.0%	1793	17	8974	202	0.3	0.1	460	14	943	29	977	26
8	C:\DATA\031028\OC28G8.D	0.2012	1.6%	1182	16.9	0.0617	2.8%	1210	33	0.084	2.8%	1285	54	2.305	2.9%	1214	20	10147	233	0.2	0.1	53	4	144	6	122	3
9	C:\DATA\031028\OC28G9.D	0.2689	0.9%	1535	12.9	0.0802	3.2%	1559	48	0.090	2.5%	1417	48	3.321	2.7%	1486	22	7328	176	0.2	0.1	15	0	21	1	42	1
10	C:\DATA\031028\OC28G10.D	0.3029	0.5%	1705	7.5	0.0851	2.3%	1650	36	0.099	1.8%	1611	34	4.157	2.0%	1666	17	10504	239	0.0	0.1	65	2	107	3	165	3
11	C:\DATA\031028\OC28G11.D	0.2215	0.7%	1290	8.7	0.0321	2.3%	639	15	0.133	1.7%	2144	30	4.061	2.1%	1646	17	11847	269	0.1	0.1	235	7	486	13	812	18
12	C:\DATA\031028\OC28G12.D	0.3307	0.9%	1842	15.0	0.0930	2.7%	1797	46	0.100	2.2%	1623	41	4.642	2.4%	1757	20	9155	211	0.4	0.1	65	3	144	6	156	8
1	C:\DATA\031030\OC30C1.D	0.1940	0.9%	1143	9.1	0.0741	1.4%	1446	20	0.075	1.6%	1075	33	2.629	1.9%	1309	14	10536	283	0.2	0.1	46	2	211	6	145	3
2	C:\DATA\031030\OC30C2.D	0.2889	0.7%	1636	10.0	0.1102	1.6%	2114	31	0.097	1.3%	1562	23	4.996	1.6%	1819	14	11111	278	0.7	0.1	90	2	82	2	251	5
3	C:\DATA\031030\OC30C3.D	0.3659	0.7%	2010	12.0	0.1388	1.5%	2627	37	0.118	1.2%	1929	22	7.814	1.6%	2210	15	9919	246	1.3	0.2	112	3	141	4	226	5
4	C:\DATA\031030\OC30C4.D	0.4555	0.7%	2420	14.9	0.1564	1.4%	2937	37	0.165	1.1%	2507	18	13.320	1.5%	2703	15	9745	253	1.5	0.1	147	5	262	8	210	7
5	C:\DATA\031030\OC30C5.D	0.1926	0.7%	1136	7.1	0.0725	1.3%	1416	18	0.078	1.4%	1147	28	2.689	1.8%	1325	13	8826	227	0.4	0.1	122	4	911	27	326	8
6	C:\DATA\031030\OC30C6.D	0.2793	0.8%	1588	11.0	0.1071	1.5%	2056	29	0.096	1.4%	1543	27	4.815	1.8%	1788	15	9918	250	0.7	0.1	95	3	188	6	228	8
7	C:\DATA\031030\OC30C7.D	0.2846	1.0%	1614	14.7	0.1005	1.7%	1936	31	0.091	1.8%	1439	34	4.698	2.1%	1767	18	11126	296	0.2	0.1	36	1	85	3	96	4
8	C:\DATA\031030\OC30C8.D	0.2669	0.7%	1525	10.1	0.0982	1.4%	1894	25	0.089	1.4%	1407	26	4.253	1.7%	1684	14	9673	245	-0.1	-0.1	73	2	267	8	179	5
9	C:\DATA\031030\OC30C9.D	0.2675	1.0%	1528	13.2	0.1049	1.5%	2016	28	0.094	1.6%	1508	30	4.510	2.0%	1733	17	9451	259	0.8	0.1	44	1	120	4	118	5
10	C:\DATA\031030\OC30C10.D	0.2692	1.0%	1537	14.3	0.0973	1.8%	1877	31	0.091	2.1%	1445	40	4.393	2.3%	1711	19	8682	221	0.5	0.1	36	1	100	3	94	3
11	C:\DATA\031030\OC30C11.D	0.2417	0.8%	1396	10.1	0.0717	1.4%	1400	19	0.096	1.2%	1551	23	4.159	1.7%	1666	14	11224	287	0.5	0.1	150	4	230	7	493	12
12	C:\DATA\031030\OC30C12.D	0.2418	0.7%	1396	9.3	0.0955	1.5%	1843	26	0.088	1.5%	1372	28	3.889	1.8%	1611	15	9284	237	0.1	0.1	68	2	205	6	209	7

Shaded analyses not used

DS3

File	Calculated Ages																Elemental abundances									
	206Pb/238U	%rsd	age	+/-1s	208Pb/232Th	%rsd	age	+/-1s	207Pb/206Pb	%rsd	age	+/-1s	207Pb/235U	%rsd	age	+/-1s	Hf	+/-1s	Hg	+/-1s	Pb	+/-1s	Th	+/-1s	U	+/-1s
C:\DATA\031030\OC30A1.D	0.2707	0.9%	1544	11.7	0.1051	1.7%	2019	32	0.092	1.9%	1477	35	4.274	2.2%	1688	18	9794	242	0.4	0.1	41	1	110	3	114	3
C:\DATA\031030\OC30A2.D	0.2004	1.0%	1178	10.8	0.0875	1.8%	1695	29	0.091	1.8%	1440	34	3.120	2.3%	1438	18	9828	228	0.7	0.1	47	1	109	3	193	4
C:\DATA\031030\OC30A3.D	0.2821	0.7%	1602	9.9	0.1121	1.5%	2148	30	0.097	1.3%	1571	25	4.664	1.7%	1761	14	10585	254	0.5	0.1	66	2	133	4	166	4
C:\DATA\031030\OC30A4.D	0.2835	0.9%	1609	12.8	0.1311	2.0%	2489	47	0.101	1.9%	1650	36	4.988	2.2%	1817	19	10306	248	0.2	0.1	33	1	69	2	81	2
C:\DATA\031030\OC30A5.D	0.2473	1.7%	1425	21.4	0.0926	1.8%	1790	31	0.236	1.3%	3094	20	10.069	2.6%	2441	24	13314	321	0.6	0.1	302	9	362	10	1056	36
C:\DATA\031030\OC30A6.D	0.2652	0.9%	1516	11.7	0.1056	1.6%	2028	30	0.096	1.9%	1542	36	4.538	2.2%	1738	18	8860	213	0.6	0.1	21	1	66	2	52	1
C:\DATA\031030\OC30A7.D	0.2810	0.9%	1597	13.0	0.1042	1.5%	2004	29	0.097	1.3%	1573	25	4.638	1.8%	1756	15	9984	234	0.5	0.1	142	4	292	8	420	11
C:\DATA\031030\OC30A8.D	0.2527	0.7%	1452	8.8	0.1019	1.5%	1961	29	0.089	1.4%	1412	27	3.946	1.8%	1623	15	7899	186	0.1	0.1	49	1	103	3	141	4
C:\DATA\031030\OC30A9.D	0.2563	0.7%	1471	8.7	0.1016	1.5%	1957	27	0.093	1.2%	1496	23	4.070	1.6%	1648	13	9041	217	0.5	0.1	80	3	222	9	207	10
C:\DATA\031030\OC30A10.D	0.1707	0.8%	1016	7.5	0.0628	2.1%	1232	25	0.075	1.6%	1056	32	2.131	2.0%	1159	14	10097	231	0.2	0.1	59	2	177	5	285	7
C:\DATA\031030\OC30A11.D	0.2642	0.8%	1511	10.7	0.1071	1.6%	2057	31	0.093	1.6%	1482	31	4.331	2.0%	1699	16	9290	211	0.0	0.1	34	1	66	2	98	4
C:\DATA\031030\OC30A12.D	0.2030	1.0%	1192	11.0	0.0959	1.8%	1851	32	0.098	2.0%	1583	38	3.347	2.3%	1492	18	10252	248	0.4	0.1	35	1	98	3	117	5
C:\DATA\031030\OC30B1.D	0.1958	0.9%	1153	9.3	0.0783	1.6%	1524	23	0.078	2.7%	1143	53	2.654	2.9%	1316	22	8674	231	0.6	0.1	19	1	143	4	53	2
C:\DATA\031030\OC30B2.D	0.2505	0.7%	1441	9.6	0.1040	1.7%	2000	33	0.091	1.4%	1450	27	4.132	1.8%	1661	15	10690	277	0.5	0.1	79	3	155	5	225	8
C:\DATA\031030\OC30B3.D	0.2779	0.7%	1581	10.3	0.1117	1.6%	2141	32	0.095	1.6%	1527	30	4.553	1.9%	1741	16	7831	205	0.4	0.1	32	1	83	3	80	3
C:\DATA\031030\OC30B4.D	0.2476	1.0%	1426	12.6	0.0978	1.6%	1887	28	0.090	1.8%	1430	35	3.850	2.2%	1603	18	8781	235	0.5	0.1	22	1	75	2	61	2
C:\DATA\031030\OC30B5.D	0.2611	0.8%	1495	11.2	0.1050	1.5%	2019	29	0.090	1.3%	1429	24	3.969	1.7%	1628	14	10578	285	0.3	0.1	94	3	132	4	289	7
C:\DATA\031030\OC30B6.D	0.3085	0.8%	1733	11.6	0.1221	1.5%	2329	33	0.100	1.5%	1620	28	5.361	1.9%	1879	16	8675	232	0.5	0.1	38	1	89	3	86	2
C:\DATA\031030\OC30B7.D	0.1951	0.7%	1149	7.7	0.0809	1.5%	1572	23	0.078	1.6%	1146	33	2.616	2.0%	1305	15	9667	257	0.3	0.1	56	2	241	7	188	4
C:\DATA\031030\OC30B8.D	0.2629	0.9%	1505	12.1	0.1091	1.6%	2093	31	0.094	1.7%	1505	33	4.460	2.1%	1723	17	9423	252	0.2	0.1	34	1	108	3	116	5
C:\DATA\031030\OC30B9.D	0.2096	0.6%	1227	6.9	0.0868	1.6%	1682	25	0.081	1.4%	1226	27	2.933	1.8%	1390	14	9533	241	0.3	0.1	63	2	147	4	230	5
C:\DATA\031030\OC30B10.D	0.2555	0.7%	1467	9.7	0.1109	1.7%	2127	34	0.096	1.7%	1553	32	4.302	1.8%	1694	15	11055	288	1.2	0.1	73	2	136	4	387	22
C:\DATA\031030\OC30B11.D	0.3003	0.8%	1693	12.1	0.1170	1.6%	2237	34	0.104	1.7%	1699	30	5.456	2.0%	1894	17	9195	239	0.3	0.1	25	1	68	2	58	2
C:\DATA\031030\OC30B12.D	0.3178	0.8%	1779	11.9	0.1325	1.6%	2515	39	0.110	1.4%	1791	25	5.989	1.8%	1974	16	8842	231	1.1	0.2	82	2	183	6	176	5
C:\DATA\031030\OC30C1.D	0.1940	0.9%	1143	9.1	0.0741	1.4%	1446	20	0.077	1.6%	1120	32	2.629	1.9%	1309	14	10536	283	0.2	0.1	46	2	211	6	145	3
C:\DATA\031030\OC30C2.D	0.2889	0.7%	1636	10.0	0.1102	1.6%	2114	31	0.099	1.2%	1604	23	4.996	1.6%	1819	14	11111	278	0.7	0.1	90	2	82	2	251	5
C:\DATA\031030\OC30C3.D	0.3659	0.7%	2010	12.0	0.1388	1.5%	2627	37	0.121	1.2%	1969	22	7.814	1.6%	2210	15	9919	246	1.3	0.2	112	3	141	4	226	5
C:\DATA\031030\OC30C4.D	0.4480	0.7%	2386	13.8	0.1581	1.3%	2967	37	0.168	1.1%	2542	18	13.181	1.5%	2693	14	9745	253	1.5	0.1	147	5	262	8	210	7
C:\DATA\031030\OC30C5.D	0.1926	0.7%	1136	7.1	0.0725	1.3%	1416	18	0.080	1.4%	1192	28	2.689	1.8%	1325	13	8826	227	0.4	0.1	122	4	911	27	326	8
C:\DATA\031030\OC30C6.D	0.2793	0.8%	1588	11.0	0.1071	1.5%	2056	29	0.098	1.4%	1590	26	4.815	1.8%	1788	15	9918	250	0.7	0.1	95	3	188	6	228	8
C:\DATA\031030\OC30C7.D	0.2590	1.0%	1485	13.8	0.0974	1.7%	1879	31	0.091	2.1%	1452	40	4.302	2.3%	1694	19	11126	296	0.2	0.1	36	1	85	3	96	4
C:\DATA\031030\OC30C8.D	0.2669	0.7%	1525	10.1	0.0982	1.4%	1894	25	0.091	1.4%	1451	26	4.253	1.7%	1684	14	9673	245	-0.1	-0.1	73	2	267	8	179	5
C:\DATA\031030\OC30C9.D	0.2675	1.0%	1528	13.2	0.1049	1.5%	2016	28	0.096	1.6%	1551	30	4.510	2.0%	1733	17	9451	259	0.8	0.1	44	1	120	4	118	5
C:\DATA\031030\OC30C10.D	0.2473	1.0%	1425	13.0	0.0965	1.6%	1863	28	0.092	1.7%	1465	32	4.332	2.1%	1699	18	8682	221	0.5	0.1	36	1	100	3	94	3
C:\DATA\031030\OC30C11.D	0.2333	0.9%	1352	11.2	0.0687	1.4%	1343	18	0.099	1.3%	1597	24	4.149	1.7%	1664	14	11224	287	0.5	0.1	150	4	230	7	493	12
C:\DATA\031030\OC30C12.D	0.2427	0.7%	1401	9.3	0.0986	1.4%	1901	26	0.090	1.5%	1424	29	4.012	1.8%	1637	15	9284	237	0.1	0.1	68	2	205	6	209	7
C:\DATA\031030\OC30D1.D	0.1513	0.6%	908	5.3	0.0393	1.6%	778	12	0.118	1.1%	1926	19	3.253	1.5%	1470	11	9508	232	0.3	0.1	158	5	616	18	496	10
C:\DATA\031030\OC30D2.D	0.2130	1.0%	1245	10.9	0.0610	2.0%	1197	23	0.081	1.5%	1210	30	2.991	2.0%	1405	15	12119	299	0.1	0.1	73	3	80	2	278	8
C:\DATA\031030\OC30D3.D	0.2863	0.7%	1623	10.1	0.1053	1.4%	2024	27	0.094	1.3%	1509	24	4.730	1.7%	1773	14	9727	253	0.3	0.1	111	3	316	9	260	8
C:\DATA\031030\OC30D4.D	0.2664	0.9%	1522	12.3	0.0966	1.6%	1863	28	0.087	1.6%	1364	32	4.160	2.0%	1666	16	9420	225	0.3	0.1	28	1	67	2	78	2
C:\DATA\031030\OC30D5.D	0.2161	1.1%	1261	12.4	0.0928	1.9%	1793	33	0.078	1.5%	1144	29	2.930	1.9%	1390	14	10273	250	0.6	0.4	136	4	181	5	508	12
C:\DATA\031030\OC30D6.D	0.2617	1.4%	1499	18.4	0.1128	3.5%	2160	71	0.101	4.3%	1638	81	5.092	5.9%	1835	51	7617	181	0.7	0.1	21	1	61	2	44	1
C:\DATA\031030\OC30D7.D	0.2900	1.2%	1641	16.7	0.1380	2.6%	2613	65	0.131	3.5%	2108	61	6.946	3.6%	2105	32	9255	219	0.3	0.1	30	1	66	2	50	1
C:\DATA\031030\OC30D8.D	0.2516	1.0%	1447	12.8	0.0944	1.5%	1824	27	0.092	2.0%	1459	39	4.256	2.3%	1685	19	6849	175	0.1	0.1	27	1	106	4	63	2
C:\DATA\031030\OC30D9.D	0.2478	1.0%	1427	12.3	0.1056	1.5%	2029	30	0.098	1.4%	1587	26	4.483	1.8%	1728	15	9797	253	0.4	0.1	80	2	190	6	200	5
C:\DATA\031030\OC30D10.D	0.3037	0.8%	1710	11.9	0.1037	1.5%	1995	28	0.101	1.2%	1645	23	5.499	1.7%	1900	15	9613	229	0.4	0.1	89	2	191	5	222	8
C:\DATA\031030\OC30D11.D	0.1964	0.8%	1156	8.4	0.0762	1.4%	1484	20	0.074	1.3%	1046	26	2.558	1.7%	1289	13	10296	248	0.0	0.1	101	3	381	10	363	7
C:\DATA\031030\OC30D12.D	0.2695	0.8%	1538	10.5	0.1026	1.5%	1975	28	0.089	1.5%	1407	29	4.233	1.8%	1681	15	9557	231	-0.1	-0.1	43	1	109	3	114	2
C:\DATA\031030\OC30E1.D	0.2172	1.1%	1267	12.3	0.0781	1.8%	1519	26	0.101	1.7%	1636	32	3.747	2.0%	1581	16	9024	213	0.2	0.1	103	3	345	9	310	7
C:\DATA\031030\OC30E2.D	0.1924	1.1%	1134	11.2	0.0816	1.6%	1585	25	0.095	2.2%	1525	41	3.244	2.4%	1468	19	9153	212	0.2	0.1	18	1	93	3	60	2
C:\DATA\031030\OC30E3.D	0.2661	1.1%	1521	15.2	0.1006	1.9%	1937	35	0.092	2.7%	1469	52	4.529	3.0%	1736	25	8137	188	0.1	0.1	14	0	45	1	36	1
C:\DATA\031030\OC30E4.D	0.1961	0.9%	1154	9.0	0.0701	1.6%	1369	22	0.082	1.4%	1248	26	2.940	1.8%	1392	13	10023	242	0.0	0.1	141	4	481	13	487	10
C:\DATA\031030\OC30E5.D	0.3197	1.2%	1788	19.0	0.1164	2.1%	2225	45	0.102	2.2%	1669	41	6.381	2.7%	2030	24	9113	217	0.7	0.1	15	1	29	1	36	2
C:\DATA\031030\OC30E6.D	0.1878	0.9%	1109	9.1	0.0701	1.5%	1370	19	0.075	1.9%	1060	39	2.476	2.2%	1265	16	10881	251	-0.1	-0.1	27	1	186	5	87	2
C:\DATA\031030\OC30E7.D	0.2925	0.8%	1654	11.2	0.1046	1.4%	2011	26	0.097	1.3%	1567	25	4.913	1.7%	1804	14	6993	167	0.2	0.1	80	2	183	5	199	5
C:\DATA\031030\OC30E8.D	0.2350	1.0%	1360	11.9	0.0879	1.6%	1702	26	0.083	1.7%	1263	33	3.407	2.0%	1506	16	8774	201	0.4	0.1	42	1	144	4	126	3
C:\DATA\031030\OC30E9.D	0.2564	0.9%	1472	11.8	0.0749	1.9%	1460	27	0.095	1.6%	1531	30	4.583	1.9%	1746	16	11724	271	0.0	0.1	74	3	113	4	206	9
C:\DATA\031030\OC30E10.D	0.2644	1.0%	1512	13.2	0.0935	2.2%	1806	38	0.091	2.1%	1446	40	4.410	2.3%	1714	19	9021	201	-0.3	-0.1	18	0	37	1	55	1
C:\DATA\031030\OC30E11.D	0.3046	0.8%	1714	11.4	0.1099	1.5%	2108	29	0.097	1.5%	1573	28	5.251	1.8%	1861	16	11089	254	0.0	0.1	47	1	105	3	112	2
C:\DATA\031030\OC30E12.D	0.2254	0.7%	1311	8.1	0.0957	1.6%	1848	28	0.084	2.0%	1283	39	3.381	2.2%	1500	17	8381	186	0.4	0.1	64	2	201	7	337	19
C:\DATA\031030\OC30F1.D	0.3775	1.0%	2064	17.0	0.1410	1.8%	2666	46	0.126	1.5%	2046	27	8.594	2.0%	2296	18	7783	191	0.6	0.1	32	1	64	2	66	2
C:\DATA\031030\OC30F2.D	0.2665	1.0%	1523	13.2	0.1063	1.5%	2042	29	0.096	1.4%	1548	26	4.527	1.8%	1736	15	9976	250	0.2	0.1	71	2	173	5	206	6
C:\DATA\031030\OC30F3.D	0.3247	0.9%	1813	14.0	0.1200	1.6%	2291	35	0.104	1.5%	1701	27	6.010	1.8%	1977	16	10674	259	0.1	0.1	40	1	57	2	95	3
C:\DATA\031030\OC30F4.D	0.2453	1.3%	1414	16.0	0.1033	1.9%	1986	36	0.102	2.9%	1658	54	4.693	3.1%	1766	27	8454	201	0.5	0.1	10	0	31	1	26	1
C:\DATA\031030\OC30F5.D	0.2810	0.7%	1597	10.2	0.1078	1.4%	2069	28	0.091	1.1%	1439	22	4.425	1.6%	1717	13	10759	253	0.0	0.1	138	4	315	9	374	12
C:\DATA\031030\OC30F6.D	0.2931	0.7%	1657	10.8	0.1290	1.8%	2453	42	0.098	1.3%	1592	23	4.969	1.6%	1814	14	8842	207	0.1	0.1	82	2	73	2	230	5
C:\DATA\031030\OC30F7.D	0.1872	0.8%	1106	7.6	0.0720	1.5%	1405	20	0.075	1.5%	1074	31	2.445	1.9%	1256	13	8743	201	-0.1	-0.1	46	1	135	4	188	5
C:\DATA\031030\OC30F8.D	0.2511	0.7%	1444	9.6	0.0677	1.5%	1323	20	0.096	1.3%	1546	24	4.206	1.7%	1675	14	9758	225	0.5	0.1	60	2	207	6	185	6
C:\DATA\031030\OC30F9.D	0.3062	0.7%	1722	10.1	0.1096	1.4%	2103	28	0.102	1.2%	1657	22	5.349	1.6%	1877	14	8835	201	-0.4	-0.1	118	4	182	5	298	8
C:\DATA\031030\OC30F10.D	0.2825	1.5%	1604	21.9	0.1050	1.8%	2018	34	0.094	2.8%	1515	53	4.960	3.0%	1813	26	6467	145	0.0	0.1	12	0	39	1	28	1
C:\DATA\031030\OC30F11.D	0.2629	1.1%	1505	15.2	0.0959	2.2%	1851	38	0.090	3.1%	1421	60	4.115	3.1%	1657	26	7614	174	0.2	0.1	21	1	86	3	59	3
C:\DATA\031030\OC30F12.D	0.2437	0.9%	1406	10.8	0.0887	1.5%	1718	24	0.085	1.7%	1318	34	3.629	2.1%	1556	17	8928	210	0.5	0.1	34	1	110	3	100	3

lyses not used

Sample DS4		Calculated Age																Elemental Abundances (ppm)									
Analysis	File	206Pb/238U	%rsd	age	+/-1s	208Pb/232Th	%rsd	age	+/-1s	207Pb/206Pb	%rsd	age	+/-1s	207Pb/235U	%rsd	age	+/-1s	Hf	+/-1s	Hg	+/-1s	Pb	+/-1s	Th	+/-1s	U	+/-1s
1	C:\HPCHEM\1\DATA\030311\MR11A28.D	0.3023	4.4%	1703	65.7	0.0704	2.3%	1375	31	0.101	3.3%	1651	62	4.732	4.8%	1773	41	10163	464	0.2	0.1	175	9	236	12	417	19
2	C:\HPCHEM\1\DATA\030311\MR11A29.D	0.2699	2.3%	1540	31.6	0.0661	2.6%	1294	33	0.095	2.9%	1519	54	3.913	3.4%	1616	28	8943	394	0.4	0.1	60	3	76	4	171	9
3	C:\HPCHEM\1\DATA\030311\MR11A30.D	0.2341	2.0%	1356	24.8	0.0557	2.7%	1095	29	0.083	4.8%	1260	93	4.151	5.0%	1664	41	8740	393	0.2	0.2	32	2	105	5	93	4
4	C:\HPCHEM\1\DATA\030311\MR11A31.D	0.2304	1.6%	1337	19.5	0.0518	2.5%	1021	25	0.083	3.3%	1277	65	3.431	3.6%	1512	29	11382	581	0.0	-0.2	62	3	113	6	202	10
5	C:\HPCHEM\1\DATA\030311\MR11A32.D	0.1756	2.2%	1043	20.8	0.0426	3.0%	843	25	0.068	4.3%	863	89	2.739	4.8%	1339	36	9211	414	-0.6	-0.2	40	2	106	5	165	7
6	C:\HPCHEM\1\DATA\030311\MR11A33.D	0.3344	1.8%	1860	28.8	0.0384	2.0%	762	15	0.137	2.1%	2190	37	7.030	2.6%	2115	24	10285	479	0.1	0.2	283	14	711	35	608	27
7	C:\HPCHEM\1\DATA\030311\MR11A34.D	0.3020	4.3%	1701	65.1	0.0668	2.8%	1308	36	0.100	3.9%	1625	72	4.379	5.0%	1708	42	8559	434	-0.1	-0.1	50	3	85	4	143	7
8	C:\HPCHEM\1\DATA\030311\MR11A35.D	0.2982	3.4%	1682	49.8	0.0727	3.0%	1418	41	0.099	4.1%	1605	77	4.571	4.8%	1744	41	8201	392	0.2	0.2	25	1	57	3	63	4
9	C:\HPCHEM\1\DATA\030311\MR11A36.D	0.1707	8.2%	1016	77.9	0.0053	4.0%	108	4	0.227	5.6%	3028	90	5.129	8.4%	1841	74	12665	801	0.4	0.1	435	28	5891	397	1607	108
10	C:\HPCHEM\1\DATA\030311\MR11A37.D	0.2780	4.4%	1581	62.3	0.0655	3.1%	1282	39	0.095	3.6%	1529	67	4.097	4.9%	1654	41	11203	537	0.0	-0.2	41	2	59	3	121	6
11	C:\HPCHEM\1\DATA\030311\MR11A38.D	0.3116	5.0%	1748	76.7	0.0652	2.5%	1278	31	0.102	3.7%	1664	69	4.902	5.4%	1803	46	8134	432	0.2	0.1	60	3	143	8	156	8
12	C:\HPCHEM\1\DATA\030311\MR11A39.D	0.2548	3.3%	1463	43.1	0.0606	4.8%	1190	56	0.104	7.1%	1693	131	3.923	7.1%	1618	59	6191	275	0.0	0.1	9	0	16	1	28	1
1	C:\HPCHEM\1\DATA\030311\MR11A46.D	0.5042	7.4%	2632	163.0	0.1092	3.2%	2096	65	0.140	4.1%	2231	70	8.916	7.3%	2329	69	10148	606	0.2	0.1	183	12	173	11	377	28
2	C:\HPCHEM\1\DATA\030311\MR11A47.D	0.5190	7.3%	2695	162.9	0.1069	3.2%	2052	62	0.132	3.7%	2129	66	9.284	6.9%	2366	66	8744	538	0.2	0.1	185	12	307	22	357	32
3	C:\HPCHEM\1\DATA\030311\MR11A48.D	0.4943	6.7%	2589	143.6	0.1153	3.3%	2205	69	0.146	3.5%	2302	61	10.075	6.5%	2442	62	9254	560	0.2	0.2	83	5	107	7	150	10
4	C:\HPCHEM\1\DATA\030311\MR11A50.D	0.2851	4.3%	1617	62.3	0.0708	2.7%	1382	36	0.091	3.6%	1453	68	3.952	5.2%	1624	43	7445	355	0.3	0.1	52	3	117	6	139	7
5	C:\HPCHEM\1\DATA\030311\MR11A51.D	0.3443	6.4%	1907	107.1	0.0800	3.1%	1555	46	0.098	3.8%	1596	70	4.839	6.4%	1792	56	7165	374	0.2	0.1	100	6	140	8	280	16
6	C:\HPCHEM\1\DATA\030311\MR11A52.D	0.6099	5.1%	3070	126.0	0.1448	3.3%	2734	84	0.213	3.1%	2928	50	19.268	5.2%	3055	51	9837	494	0.2	0.1	155	8	34	2	206	11
7	C:\HPCHEM\1\DATA\030311\MR11A53.D	0.2741	5.0%	1562	69.3	0.0751	3.0%	1463	42	0.088	4.1%	1375	79	3.688	5.9%	1569	48	8422	379	0.2	0.1	47	2	141	7	114	6
8	C:\HPCHEM\1\DATA\030311\MR11A54.D	0.2973	4.7%	1678	69.9	0.0818	3.1%	1589	47	0.094	4.0%	1510	76	4.474	5.7%	1726	49	9000	422	-0.1	-0.1	29	1	59	3	76	4
9	C:\HPCHEM\1\DATA\030311\MR11A55.D	0.4768	6.1%	2513	128.7	0.1119	2.9%	2144	59	0.141	3.9%	2240	68	9.858	5.9%	2422	56	8806	480	0.0	-0.1	78	4	142	8	129	7
10	C:\HPCHEM\1\DATA\030311\MR11A56.D	0.2737	2.2%	1560	30.5	0.0893	2.5%	1729	42	0.110	3.3%	1804	59	4.439	3.8%	1720	32	8424	340	0.3	0.1	81	4	248	11	189	8
11	C:\HPCHEM\1\DATA\030311\MR11A57.D	0.2884	4.4%	1633	64.5	0.0758	2.7%	1476	39	0.092	3.3%	1475	62	3.970	4.9%	1628	41	7171	329	0.1	0.1	60	3	94	5	161	7
12	C:\HPCHEM\1\DATA\030311\MR11A49.D	0.3065	6.2%	1723	94.5	0.0775	3.4%	1510	49	0.085	3.9%	1313	76	3.811	6.2%	1595	51	9613	496	0.0	0.2	56	3	60	3	178	10
1	C:\HPCHEM\1\DATA\030311\MR11A64.D	0.2911	4.4%	1647	63.7	0.0586	2.4%	1150	27	0.091	3.6%	1447	68	4.112	4.9%	1657	41	7460	350	-0.2	-0.1	48	2	154	8	114	5
2	C:\HPCHEM\1\DATA\030311\MR11A65.D	0.3408	6.3%	1891	104.4	0.0628	2.6%	1232	31	0.094	3.2%	1515	61	4.802	5.8%	1785	50	9543	489	-0.6	-0.1	119	6	189	10	321	17
3	C:\HPCHEM\1\DATA\030311\MR11A66.D	0.3168	5.6%	1774	86.9	0.0626	2.5%	1227	30	0.098	3.4%	1589	63	4.602	5.5%	1750	47	9559	465	0.4	0.1	105	5	159	8	285	14
4	C:\HPCHEM\1\DATA\030311\MR11A67.D	0.4956	2.8%	2595	60.1	0.1018	2.2%	1959	41	0.206	2.4%	2877	38	16.090	3.4%	2882	33	7816	339	0.2	0.2	114	5	90	4	151	6
5	C:\HPCHEM\1\DATA\030311\MR11A68.D	0.1729	2.5%	1028	23.5	0.0417	3.6%	825	29	0.077	5.6%	1121	113	2.132	5.6%	1159	39	9934	553	-0.5	-0.4	50	3	208	13	185	11
6	C:\HPCHEM\1\DATA\030311\MR11A69.D	0.2588	4.2%	1484	56.5	0.0570	2.8%	1120	31	0.088	3.5%	1382	68	3.645	4.7%	1559	38	10728	499	0.1	0.1	59	3	81	4	181	8
7	C:\HPCHEM\1\DATA\030311\MR11A70.D	0.2942	3.7%	1663	54.2	0.0602	2.7%	1182	31	0.104	3.4%	1690	63	4.631	4.7%	1755	40	9759	444	0.2	0.2	49	2	86	4	122	5
8	C:\HPCHEM\1\DATA\030311\MR11A71.D	0.1439	1.6%	867	12.6	0.0366	3.0%	727	21	0.127	2.8%	2055	49	2.899	3.0%	1382	23	10171	400	0.0	0.2	131	6	539	24	556	20
9	C:\HPCHEM\1\DATA\030311\MR11A72.D	0.2994	4.9%	1688	73.4	0.0566	2.3%	1114	25	0.097	2.8%	1561	52	4.427	5.4%	1717	46	9283	490	0.2	0.2	178	12	451	25	438	25
10	C:\HPCHEM\1\DATA\030311\MR11A73.D	0.3863	2.7%	2106	48.9	0.0833	2.2%	1618	34	0.141	2.2%	2241	38	8.479	3.2%	2284	30	10658	486	0.1	0.2	206	10	135	7	393	18
11	C:\HPCHEM\1\DATA\030311\MR11A74.D	0.1405	4.3%	847	34.0	0.0248	3.2%	496	16	0.096	3.1%	1546	58	2.063	5.5%	1137	39	9119	453	0.3	0.2	246	13	795	44	1014	66
12	C:\HPCHEM\1\DATA\030311\MR11A75.D	0.2965	5.4%	1674	80.5	0.0629	3.2%	1232	38	0.106	4.8%	1731	88	4.444	5.5%	1721	47	9723	541	0.4	0.3	57	3	101	6	150	9
1	C:\HPCHEM\1\DATA\030311\MR11A82.D	0.2454	1.7%	1415	21.4	0.0789	2.5%	1535	37	0.095	2.9%	1533	55	3.624	3.6%	1555	29	8635	372	-0.1	-0.2	67	9	100	5	161	6
2	C:\HPCHEM\1\DATA\030311\MR11A83.D	0.2755	4.7%	1569	65.6	0.0490	2.9%	967	28	0.118	2.8%	1929	50	4.627	5.1%	1754	43	8333	411	-0.2	-0.1	149	8	615	33	364	22
3	C:\HPCHEM\1\DATA\030311\MR11A84.D	0.3103	5.7%	1742	87.5	0.0850	2.8%	1648	45	0.094	3.9%	1505	75	4.093	6.2%	1653	52	7997	415	0.1	0.2	56	3	97	5	140	7
4	C:\HPCHEM\1\DATA\030311\MR11A85.D	0.4428	6.5%	2363	130.8	0.1168	2.8%	2233	60	0.151	3.7%	2352	63	9.770	6.7%	2413	63	9095	479	-0.4	-0.2	88	5	255	14	108	6
5	C:\HPCHEM\1\DATA\030311\MR11A86.D	0.4259	5.3%	2287	103.8	0.1182	2.5%	2258	53	0.145	3.3%	2290	57	9.605	5.5%	2398	52	9001	475	-0.2	-0.2	91	5	261	15	114	6
6	C:\HPCHEM\1\DATA\030311\MR11A87.D	0.4478	4.9%	2386	99.2	0.1276	3.4%	2428	78	0.149	3.8%	2338	64	11.070	5.8%	2529	56	6955	359	0.4	0.2	57	4	58	3	85	6
7	C:\HPCHEM\1\DATA\030311\MR11A88.D	0.2659	3.5%	1520	47.8	0.0896	3.0%	1734	49	0.100	3.5%	1618	66	4.191	5.1%	1672	43	8696	407	0.6	0.2	63	3	101	5	162	11
8	C:\HPCHEM\1\DATA\030311\MR11A89.D	0.2526	2.7%	1452	34.5	0.0798	2.3%	1552	35	0.089	2.9%	1404	56	3.453	3.9%	1517	31	8159	401	0.4	0.2	71	4	132	7	191	11
9	C:\HPCHEM\1\DATA\030311\MR11A90.D	0.3762	1.7%	2058	30.9	0.1072	2.0%	2058	38	0.151	2.4%	2354	41	8.708	3.1%	2308	29	8248	383	0.0	-0.2	175	9	239	12	287	14
10	C:\HPCHEM\1\DATA\030311\MR11A91.D	0.2669	2.2%	1525	29.5	0.0921	2.8%	1780	48	0.104	3.5%	1704	64	4.382	4.0%	1709	33	8523	399	-0.2	-0.2	47	2	62	3	119	6
11	C:\HPCHEM\1\DATA\030311\MR11A92.D	0.3092	7.9%	1737	121.7	0.0764	4.0%	1488	58	0.101	6.5%	1650	121	3.704	8.3%	1572	69	8326	459	0.2	0.1	23	1	42	2	65	4
12	C:\HPCHEM\1\DATA\030311\MR11A93.D	0.2553	5.3%	1466	69.7	0.0648	3.9%	1269	48	0.099	4.4%	1613	82	4.011	6.6%	1636	55	9186	484	0.2	0.2	80	4	325	18	270	16
1	C:\HPCHEM\1\DATA\030311\MR11A98.D	0.3034	6.1%	1708	91.6	0.0810	2.5%	1574	38	0.095	3.6%	1526	67	4.406	5.8%	1713	49	8800	466	-0.2	-0.2	120	6	292	16	295	16
2	C:\HPCHEM\1\DATA\030311\MR11A99.D	0.2543	6.6%	1461	87.3	0.0696	3.6%	1360	47	0.089	6.2%	1413	120	3.209	7.7%	1459	61	9027	494	0.3	0.1	35	2	122	7	96	6
3	C:\HPCHEM\1\DATA\030311\MR11A100.D	0.2558	3.5%	1468	45.6	0.0414	3.1%	820	25	0.094	2.8%	1505	54	3.625	4.3%	1555	34	10636	529	-0.1	-0.1	175	9	159	8	542	32
4	C:\HPCHEM\1\DATA\030311\MR11A101.D	0.2497	3.5%	1437	45.5	0.0758	3.6%	1477	52	0.096	2.8%	1543	53	3.729	4.7%	1578	38	10365	532	0.3	0.1	178	9	70	4	519	27
5	C:\HPCHEM\1\DATA\030311\MR11A102.D	0.1802	7.6%	1068	75.3	0.0545	4.8%	1073	50	0.069	9.9%	901	204	1.959	11.0%	1102	77	8483	462	0.0	-0.2	12	1	48	3	46	3
6	C:\HPCHEM\1\DATA\030311\MR11A103.D	0.2678	7.2%	1529	99.2	0.0836	5.3%	1622	83	0.093	5.8%	1496	109	3.942	8.2%	1622	69	6953	344	0.0	-0.2	33	2	57	3	88	5
7	C:\HPCHEM\1\DATA\030311\MR11A104.D	0.2189	4.6%	1276	53.0	0.0365	4.1%	725	29	0.095	5.2%	1522	97	3.247	6.3%	1468	50	7355	369	0.4	0.1	17	1	68	4	54	3
8	C:\HPCHEM\1\DATA\030311\MR11A105.D	0.2551	4.3%	1465	56.6	0.0853	2.9%	1654	46	0.094	3.5%	1502	66	3.605	5.0%	1551	41	8430	438	-0.2	-0.1	116	6	221	12	299	17
9	C:\HPCHEM\1\DATA\030311\MR11A106.D	0.4012	5.8%	2174	108.6	0.1216	3.3%	2320	72	0.139	4.2%	2214	73	8.997	6.4%	2338	60	9005	492	0.5	0.1	50	3	56	3	102	6
10	C:\HPCHEM\1\DATA\030311\MR11A107.D	0.2595	7.0%	1487	93.3	0.0650	3.1%	1272	38	0.094	3.8%	1508	71	3.801	6.8%	1593	56	9049	539	0.4	0.2	98	6	265	16	286	18
11	C:\HPCHEM\1\DATA\030311\MR11A108.D	0.3019	6.6%	1701	99.6	0.0806	2.7%	1566	41	0.094	4.3%	1500	81	4.243	6.4%	1682	54	6537	375	0.0	#####	65	4	234	14	154	10
12	C:\HPCHEM\1\DATA\030311\MR11A109.D	0.2747	5.1%	1565	71.6	0.0833	3.0%	1616	46	0.088	3.6%	1374	70	3.876	5.8%	1609	48	9238	486	-0.4	-0.2	74	4	133	7	213	16
1	C:\HPCHEM\1\DATA\030311\MR11A116.D	0.2860	3.8%	1621	54.9	0.0988	4.0%	1905	72	0.101	4.0%	1634	75	4.461	5.6%	1724	47	7859	408	0.7	0.2	105	12	88	10	124	12
2	C:\HPCHEM\1\DATA\030311\MR11A117.D	0.3864	3.3%	2106	60.2	0.0753	2.8%	1467	40	0.146	2.7%	2304	46	8.898	4.3%	2328	40	9246	465	0.3	0.2	178	10	212	12	285	16
3	C:\HPCHEM\1\DATA\030311\MR11A118.D	0.2576	3.1%	1478	40.5	0.0347	4.8%	689	32	0.096	2.8%	1554	53	3.942	4.1%	1622	34	10395	486	0.0	0.1	120	6	269	14	368	19
4	C:\HPCHEM\1\DATA\030311\MR11A119.D	0.3707	7.8%	2033	137.3	0.0266	4.3%	531	23	0.154	3.3%	2389	56	8.562	7.2%	2293	68	10747	569	0.4	0.2	397	22	1073	62	941	51
5	C:\HPCHEM\1\DATA\030311\MR11A120.D	0.2736	6.3%	1559	88.4	0.0778	3.2%	1515	47	0.090	4.7%	1425	89	3.506	6.2%	1529	50	8116	444	0.2	0.1	33	2	91	5	89	5
6	C:\HPCHEM\1\DATA\030311\MR11A121.D	0.3198	6.5%	1789	101.7	0.0838	4.0%	1627	62	0.087	5.1%	1360	99	4.467	7.2%	1725	62	8887	499	0.2	0.2	23	1	37	2	62	4
7	C:\HPCHEM\1\DATA\030311\MR11A122.D	0.1590	5.9%	951	52.0	0.0465	2.7%	920	25	0.061	4.2%	639	90	1.446	5.9%	908	36	9155	499	0.3	0.1	49	3	156	9	236	13
8	C:\HPCHEM\1\DATA\030311\MR11A123.D	0.2521	6.2%	1449	80.5	0.0521	3.2%	1027	32	0.093	3.7%	1491	70	3.603	6.1%	1550	49	9796	500	-0.1	-0.1	59	3	142	8	182	10
9	C:\HPCHEM\1\DATA\030311\MR11A124.D	0.3260	5.7%	1819	91.5	0.0829	2.6%	1609	41	0.098	3.0%	1577	55	5.044	5.8%	1827	51	8378	456	0.0	0.2	177	10	259	15	423	25
10	C:\HPCHEM\1\DATA\030311\MR11A125.D	0.2185	3.8%	1274	44.3	0.0739	3.3%	1442	46	0.087	4.4%	1365	85	3.117	5.4%	1437	42	9498	529	-0.4	-0.2	52	3	95	5	154	9
11	C:\HPCHEM\1\DATA\030311\MR11A126.D	0.1430	4.5%	861	36.1	0.0293	2.6%	584	15	0.134	3.1%	2156	54	3.034	5.0%	1416	39	7319	417	-0.2	-0.2	242	14	1704	105	1086	73
12	C:\HPCHEM\1\DATA\030311\MR11A127.D	0.1666	3.4%	993	31.0	0.0573	3.8%	1126	42	0.065	7.9%	771	165	1.647	7.8%	988	51	9280	517	0.5	0.3	17	1	59	4	63	3

Shaded samples not used

Sample DS5		Calcuated Age																Elemental Abundance									
Analysis		206Pb/238U	%rsd	age	+/-1s	208Pb/232Th	%rsd	age	+/-1s	207Pb/206Pb	%rsd	age	+/-1s	207Pb/235U	%rsd	age	+/-1s	Hf	+/-1s	Hg	+/-1s	Pb	+/-1s	Th	+/-1s	U	+/-1s
1	C:\DATA\030402\AP02A62.D	0.2471	0.8%	1424	11	0.0295	2.5%	587	15	0.095	1.4%	1535	22	1.386	9.1%	883	80	10062	119	0.7	0.2	203	4	316	6	650	14
2	C:\DATA\030402\AP02A63.D	0.2974	0.6%	1678	11	0.0338	3.2%	672	22	0.100	1.5%	1621	24	1.693	7.6%	1006	76	10943	124	-0.4	0.2	135	2	183	3	359	7
3	C:\DATA\030402\AP02A64.D	0.3284	1.2%	1831	22	0.0471	7.7%	931	72	0.125	2.6%	2033	54	1.858	11.9%	1066	127	8845	111	0.3	0.2	19	1	30	1	44	1
4	C:\DATA\030402\AP02A65.D	0.5937	1.0%	3004	30	0.0710	6.5%	1387	90	0.208	1.0%	2891	30	6.909	10.9%	2100	228	9019	99	0.3	0.3	58	1	44	1	71	1
5	C:\DATA\030402\AP02A66.D	0.3513	1.1%	1941	21	0.0436	5.4%	863	46	0.120	2.6%	1961	51	2.439	13.5%	1254	170	9118	113	0.6	0.2	35	1	67	3	75	2
6	C:\DATA\030402\AP02A67.D	0.3573	0.9%	1969	18	0.0418	4.3%	827	36	0.118	1.4%	1923	26	2.586	11.6%	1297	151	9873	126	0.7	0.3	90	2	121	3	196	6
7	C:\DATA\030402\AP02A68.D	0.2998	1.2%	1690	20	0.0596	7.7%	1170	90	0.159	2.1%	2447	51	2.385	13.6%	1238	169	8623	134	0.2	0.3	32	1	47	1	79	2
8	C:\DATA\030402\AP02A69.D	2.1545	11.8%	7406	871	2.0533	35.1%	22561	7908	1.028	3.7%	5276	194	104.282	40.5%	4728	1913	8247	92	-0.3	0.3	900	149	80	2	89	2
9	C:\DATA\030402\AP02A70.D	0.2573	1.7%	1476	26	0.0366	6.1%	726	44	0.141	3.3%	2236	73	1.370	14.6%	876	128	8331	163	0.4	0.2	14	0	46	1	41	1
10	C:\DATA\030402\AP02A71.D	0.5536	1.0%	2840	28	0.0674	5.1%	1318	67	0.240	0.9%	3120	27	6.976	10.4%	2108	220	7042	100	-0.2	0.3	70	1	55	1	88	1
11	C:\DATA\030402\AP02A72.D	0.2753	0.8%	1568	12	0.0344	4.5%	684	31	0.110	1.6%	1793	28	1.763	8.1%	1032	84	9025	117	0.2	0.3	116	2	142	2	334	6
12	C:\DATA\030402\AP02A73.D	0.2383	1.2%	1378	17	0.0338	5.4%	672	36	0.120	2.6%	1950	51	1.680	13.9%	1001	139	8457	135	-0.1	0.3	28	1	68	1	87	2
1	C:\DATA\030402\AP02A80.D	0.2769	1.1%	1576	18	0.0259	6.4%	516	33	0.120	2.1%	1949	42	1.802	13.8%	1046	144	8627	131	0.4	0.2	37	1	94	3	93	2
2	C:\DATA\030402\AP02A81.D	0.1969	1.0%	1158	12	0.0087	6.3%	174	11	0.113	1.1%	1854	21	1.138	8.4%	771	65	12275	135	0.5	0.2	154	4	378	16	635	20
3	C:\DATA\030402\AP02A82.D	0.2483	0.8%	1430	11	0.0186	6.0%	373	23	0.115	1.4%	1882	26	1.544	13.9%	948	131	8971	146	-0.5	0.3	114	2	251	5	339	5
4	C:\DATA\030402\AP02A83.D	0.2559	0.8%	1469	11	0.0264	7.6%	527	40	0.112	1.3%	1829	24	1.519	8.3%	938	78	10908	128	0.3	0.2	122	2	61	1	392	8
5	C:\DATA\030402\AP02A84.D	0.2741	0.8%	1561	12	0.0302	11.4%	601	68	0.113	1.5%	1845	27	1.656	10.8%	992	107	10937	96	0.4	0.2	74	2	39	1	218	4
6	C:\DATA\030402\AP02A85.D	0.3241	0.9%	1810	15	0.0277	4.4%	553	24	0.130	1.5%	2104	31	2.650	15.2%	1315	200	8372	90	0.4	0.2	66	1	180	4	131	2
7	C:\DATA\030402\AP02A86.D	0.2622	0.7%	1501	11	0.0239	6.0%	477	28	0.109	1.5%	1775	26	1.509	10.0%	934	94	8029	64	0.4	0.3	137	2	103	2	418	4
8	C:\DATA\030402\AP02A87.D	0.1913	2.3%	1129	26	0.0124	19.1%	249	47	0.115	1.7%	1878	32	1.159	9.1%	781	71	7849	111	0.4	0.3	192	7	600	21	752	15
9	C:\DATA\030402\AP02A88.D	0.2935	2.4%	1659	39	0.0313	16.7%	622	104	0.135	3.1%	2167	67	1.667	16.7%	996	167	8160	331	0.0	0.3	37	2	121	5	86	3
10	C:\DATA\030402\AP02A89.D	0.2040	1.0%	1197	12	0.0152	6.4%	304	19	0.105	1.4%	1714	24	1.196	12.8%	799	102	10696	134	0.2	0.3	136	2	354	11	511	13
11	C:\DATA\030402\AP02A90.D	0.1952	0.8%	1149	9	0.0176	9.7%	352	34	0.125	1.0%	2025	20	1.206	5.5%	804	44	10854	85	0.4	0.2	165	2	147	3	673	9
12	C:\DATA\030402\AP02A91.D	0.2095	0.9%	1226	11	0.0187	5.3%	374	20	0.102	2.6%	1667	43	1.316	17.0%	853	145	9826	81	0.6	0.2	49	1	149	2	166	2
1	C:\DATA\030402\AP02A98.D	0.2945	1.7%	1664	29	0.0247	3.9%	494	19	0.144	3.5%	2270	79	1.237	15.7%	818	129	9054	91	0.3	0.3	34	1	341	9	28	1
2	C:\DATA\030402\AP02A99.D	0.2536	0.9%	1457	13	0.0242	4.6%	484	22	0.106	1.9%	1735	33	1.586	14.2%	965	137	9583	111	0.4	0.3	68	1	140	2	203	3
3	C:\DATA\030402\AP02A100.D	0.1861	1.4%	1100	15	0.0193	7.0%	387	27	0.095	4.3%	1532	65	0.875	12.9%	638	82	9340	165	0.2	0.2	45	2	166	9	186	11
4	C:\DATA\030402\AP02A101.D	0.2119	0.7%	1239	9	0.0201	4.3%	401	17	0.096	2.0%	1553	31	1.117	11.0%	761	84	7806	87	-0.1	0.2	112	2	234	3	402	7
5	C:\DATA\030402\AP02A102.D	0.2278	0.9%	1323	12	0.0216	7.0%	432	30	0.105	2.2%	1714	37	1.331	12.5%	859	107	7942	86	0.4	0.2	65	2	146	4	219	5
6	C:\DATA\030402\AP02A103.D	0.2035	1.4%	1194	17	0.0224	6.9%	448	31	0.103	3.7%	1676	63	1.082	16.4%	745	122	8234	131	0.3	0.3	31	1	101	2	112	2
7	C:\DATA\030402\AP02A104.D	0.2715	1.5%	1548	23	0.0275	6.1%	549	34	0.125	2.9%	2035	59	1.498	14.5%	929	135	7288	118	0.3	0.3	30	1	123	3	67	1
8	C:\DATA\030402\AP02A105.D	0.2891	0.7%	1637	12	0.0262	4.5%	523	24	0.117	1.5%	1916	30	2.013	10.7%	1120	120	9624	119	0.0	0.2	88	1	147	2	228	2
9	C:\DATA\030402\AP02A106.D	0.1851	1.3%	1095	14	0.0177	6.6%	355	23	0.108	3.4%	1765	60	0.974	14.6%	690	101	8571	94	-0.2	0.2	19	0	100	1	71	1
10	C:\DATA\030402\AP02A107.D	0.2812	1.2%	1597	19	0.0327	8.7%	650	57	0.125	2.8%	2034	56	1.955	13.9%	1100	153	8702	124	0.9	0.3	30	1	48	1	82	1
11	C:\DATA\030402\AP02A108.D	0.2019	1.3%	1185	15	0.0110	11.5%	221	25	0.114	1.2%	1867	22	1.145	6.4%	775	49	10179	144	0.4	0.3	201	4	650	29	778	10
12	C:\DATA\030402\AP02A109.D	0.2706	0.8%	1544	13	0.0264	5.2%	526	27	0.115	1.5%	1884	27	1.844	12.1%	1061	128	8705	123	0.3	0.3	116	2	168	4	330	7
1	C:\DATA\031028\OC28H1.D	0.2982	0.6%	1682	8.9	0.0849	2.4%	1647	39	0.100	1.9%	1623	36	4.136	2.2%	1661	18	8985	223	0.3	0.1	41	1	43	1	107	2
2	C:\DATA\031028\OC28H2.D	0.5825	0.5%	2959	11.2	0.1433	2.3%	2706	58	0.222	1.7%	2995	27	17.736	2.0%	2976	19	6008	151	0.2	0.1	468	13	336	9	632	17
3	C:\DATA\031028\OC28H3.D	0.3405	0.6%	1889	10.5	0.0935	2.3%	1807	39	0.109	1.9%	1788	35	5.158	2.2%	1846	19	7256	183	0.2	0.1	51	1	83	2	114	3
4	C:\DATA\031028\OC28H4.D	0.4664	0.7%	2468	14.5	0.1320	2.8%	2506	66	0.149	1.8%	2337	31	9.614	2.2%	2399	20	9495	238	0.3	0.1	197	6	233	7	310	8
5	C:\DATA\031028\OC28H5.D	0.2990	0.6%	1686	8.3	0.0876	2.4%	1697	39	0.098	1.8%	1587	34	4.049	2.1%	1644	18	9816	247	0.4	0.1	81	2	53	1	221	5
6	C:\DATA\031028\OC28H6.D	0.3047	0.6%	1715	8.4	0.0858	2.3%	1664	37	0.096	1.9%	1548	36	4.089	2.2%	1652	18	9190	233	-0.1	-0.1	47	1	87	2	115	3
7	C:\DATA\031028\OC28H7.D	0.3434	0.6%	1903	9.5	0.0931	2.2%	1800	39	0.106	1.8%	1734	33	5.034	2.1%	1825	18	10233	256	0.1	0.1	196	7	299	10	485	20
8	C:\DATA\031028\OC28H8.D	0.3249	0.6%	1813	9.5	0.0933	2.3%	1802	39	0.099	1.8%	1612	33	4.414	2.1%	1715	17	10167	254	0.2	0.1	134	4	242	7	330	12
9	C:\DATA\031028\OC28H9.D	0.6438	0.6%	3204	16.3	0.1719	2.3%	3207	67	0.232	1.8%	3066	28	20.775	2.0%	3128	20	9775	243	0.0	-0.1	77	2	98	3	74	2
10	C:\DATA\031028\OC28H10.D	0.3303	0.7%	1840	10.7	0.0931	2.3%	1799	40	0.108	1.8%	1772	33	4.973	2.1%	1815	18	9956	254	-0.3	-0.1	92	3	134	4	225	7
11	C:\DATA\031028\OC28H11.D	0.2891	0.7%	1637	9.9	0.0818	2.3%	1589	35	0.100	2.0%	1617	38	4.045	2.3%	1643	19	9679	238	0.2	0.1	32	1	99	3	71	2
12	C:\DATA\031028\OC28H12.D	0.3168	0.6%	1774	9.3	0.0916	2.3%	1772	40	0.107	1.9%	1749	35	4.648	2.2%	1758	19	10039	258	1.1	0.2	58	2	87	3	131	4
1	C:\DATA\031028\OC28I1.D	0.2657	0.6%	1519	8.3	0.0736	2.3%	1436	32	0.088	2.0%	1388	38	3.239	2.2%	1466	17	9062	205	0.5	0.1	41	3	73	7	110	2
2	C:\DATA\031028\OC28I2.D	0.2817	0.6%	1600	8.0	0.0797	2.3%	1549	35	0.099	1.9%	1609	35	3.943	2.1%	1622	17	10194	216	0.2	0.1	85	2	179	5	220	7
3	C:\DATA\031028\OC28I3.D	0.2588	0.6%	1484	8.3	0.0729	2.3%	1423	32	0.040	3.2%	-377	83	1.426	3.4%	900	20	9404	227	0.2	0.1	35	1	71	2	108	4
4	C:\DATA\031028\OC28I4.D	0.3078	0.6%	1730	8.9	0.0838	2.3%	1627	35	0.103	1.9%	1680	35	4.399	2.2%	1712	18	11153	250	0.3	0.1	48	1	73	2	121	3
5	C:\DATA\031028\OC28I5.D	0.2960	0.5%	1672	7.8	0.0835	2.2%	1621	35	0.097	1.9%	1575	35	4.024	2.1%	1639	17	9259	204	0.1	0.1	59	1	124	3	145	3
6	C:\DATA\031028\OC28I6.D	0.2739	0.6%	1560	8.3	0.0794	2.3%	1545	34	0.099	1.9%	1606	35	3.707	2.1%	1573	17	10378	227	0.1	0.1	82	2	132	4	254	12
7	C:\DATA\031028\OC28I7.D	0.2721	0.6%	1551	8.6	0.0809	2.3%	1573	35	0.093	1.8%	1487	35	3.458	2.1%	1518	17	8856	189	0.1	0.1	94	2	155	4	274	6
8	C:\DATA\031028\OC28I8.D	0.2086	0.6%	1222	6.5	0.0607	2.3%	1191	27	0.077	1.8%	1118	36	2.195	2.1%	1179	15	11121	254	0.2	0.1	100	3	153	4	389	10
9	C:\DATA\031028\OC28I9.D	0.2903	0.5%	1643	7.2	0.0738	2.2%	1439	31	0.106	1.8%	1739	33	4.249	2.0%	1684	17	10211	232	0.8	0.1	156	4	260	6	456	10
10	C:\DATA\031028\OC28I10.D	0.2954	0.8%	1668	11.4	0.0839	2.3%	1629	37	0.098	2.2%	1587	41	4.072	2.5%	1649	20	8939	197	-0.1	-0.1	29	1	117	3	58	1
11	C:\DATA\031028\OC28I11.D	0.3141	0.7%	1761	10.1	0.0886	2.3%	1715	37	0.108	1.9%	1769	34	4.742	2.2%	1775	18	10055	225	0.0	-0.1	58	3	147	12	116	3
12	C:\DATA\031028\OC28I12.D	0.2034	0.5%	1194	6.0	0.0592	2.3%	1162	26	0.075	1.9%	1055	38	2.083	2.1%	1143	15	11485	258	0.5	0.1	64	2	168	4	242	5
1	C:\DATA\031030\OC30G1.D	0.2718	0.9%	1550	11.9	0.0987	1.4%	1902	26	0.091	1.5%	1446	28	4.538	1.9%	1738	16	8251	207	0.0	-0.1	37	1	124	4	95	3
2	C:\DATA\031030\OC30G2.D	0.3487	0.7%	1928	12.0	0.1240	1.5%	2362	33	0.105	1.2%	1717	22	6.664	1.6%	2068	14	9480	237	0.2	0.1	90	3	123	4	211	7
3	C:\DATA\031030\OC30G3.D	0.2706	1.2%	1544	16.5	0.0853	2.0%	1655	32	0.095	1.7%	1530	32	4.590	2.2%	1747	19	8027	225	0.0	0.1	62	2	200	6	191	6
4	C:\DATA\031030\OC30G4.D	0.5475	1.1%	2815	24.4	0.1806	1.6%	3355	50	0.138	1.3%	2203	22	13.836	1.7%	2739	16	9683	262	0.4	0.1	159	6	129	5	282	14
5	C:\DATA\031030\OC30G5.D	0.3566	1.0%	1966	16.3	0.1431	1.7%	2704	43	0.116	1.5%	1888	27	7.523	2.0%	2176	18	8660	232	0.0	0.1	106	5	137	7	279	21
6	C:\DATA\031030\OC30G6.D	0.3075	0.7%	1729	10.5	0.1118	1.4%	2143	28	0.099	1.2%	1608	22	5.477	1.6%	1897	14	9492	239	0.1	0.1	97	3	154	4	249	5
7	C:\DATA\031030\OC30G7.D	0.3217	0.9%	1798	14.3	0.1181	1.6%	2256	34	0.099	1.5%	1608	27	5.773	1.8%	1942	16	8855	233	-0.2	-0.1	69	2	152	5	163	7
8	C:\DATA\031030\OC30G8.D	0.2760	0.9%	1571	12.9	0.1050	1.5%	2019	28	0.093	1.9%	1484	35	4.751	2.2%	1776	18	9066	230	0.5	0.1	28	1	114	3	67	4

9	C:\DATA\031030\OC30G9.D	0.2878	0.7%	1631	10.3	0.1043	1.4%	2005	26	0.090	1.2%	1418	24	4.641	1.6%	1757	14	9086	231	0.2	0.1	89	3	205	6	233	5
10	C:\DATA\031030\OC30G10.D	0.2893	0.8%	1638	11.2	0.1097	1.7%	2105	33	0.093	1.4%	1485	27	4.965	1.9%	1813	16	9497	249	0.4	0.1	86	3	214	6	218	6
11	C:\DATA\031030\OC30G11.D	0.3447	1.0%	1909	16.5	0.1532	2.0%	2880	53	0.117	1.6%	1915	29	7.576	1.9%	2182	17	7503	191	0.1	0.1	52	2	63	2	84	2
12	C:\DATA\031030\OC30G12.D	0.2945	0.7%	1664	10.1	0.1060	1.4%	2037	27	0.098	1.2%	1577	22	5.161	1.6%	1846	14	9973	254	-0.3	-0.1	115	3	207	6	303	7
1	C:\DATA\031030\OC30H1.D	0.2987	0.8%	1685	12.2	0.1095	1.6%	2101	32	0.092	1.6%	1459	30	4.913	2.0%	1804	17	9419	207	0.2	0.1	34	1	79	2	88	3
2	C:\DATA\031030\OC30H2.D	0.4037	0.7%	2186	12.7	0.1107	1.8%	2122	37	0.141	1.1%	2240	20	10.523	1.6%	2482	15	11484	247	0.1	0.1	205	5	150	4	437	11
3	C:\DATA\031030\OC30H3.D	0.1912	1.0%	1128	10.3	0.0666	1.5%	1304	18	0.078	2.3%	1138	47	2.653	2.7%	1315	20	9147	194	0.3	0.1	18	0	161	4	49	1
4	C:\DATA\031030\OC30H4.D	0.3054	0.7%	1718	10.0	0.1067	1.4%	2048	27	0.097	1.2%	1563	22	5.284	1.6%	1866	13	11695	251	0.4	0.1	109	3	191	5	280	6
5	C:\DATA\031030\OC30H5.D	0.3117	0.7%	1749	11.5	0.1129	1.5%	2163	31	0.097	1.3%	1570	24	5.447	1.7%	1892	15	9616	206	-0.2	-0.1	65	2	100	2	165	3
6	C:\DATA\031030\OC30H6.D	0.3223	0.7%	1801	11.0	0.1168	1.4%	2232	30	0.097	1.2%	1571	22	5.645	1.6%	1923	14	11059	239	0.3	0.1	103	3	141	4	255	7
7	C:\DATA\031030\OC30H7.D	0.2827	0.8%	1605	11.0	0.0971	1.4%	1873	25	0.088	1.5%	1390	28	4.533	1.8%	1737	15	9085	194	0.1	0.1	43	1	148	4	106	2
8	C:\DATA\031030\OC30H8.D	0.2572	0.9%	1475	12.0	0.1019	1.5%	1962	29	0.093	1.8%	1478	35	4.357	2.0%	1704	17	8460	185	0.0	-0.1	24	1	83	2	61	1
9	C:\DATA\031030\OC30H9.D	0.2672	0.9%	1527	11.7	0.0969	1.6%	1869	28	0.089	1.5%	1402	28	4.304	1.8%	1694	15	9981	217	0.5	0.1	43	1	74	2	132	4
10	C:\DATA\031030\OC30H10.D	0.2939	0.8%	1661	12.0	0.1077	1.5%	2067	29	0.098	1.6%	1596	31	5.407	1.9%	1886	17	9106	192	0.0	0.1	29	1	78	2	70	1
11	C:\DATA\031030\OC30H11.D	0.4107	0.7%	2218	13.4	0.1509	1.5%	2840	39	0.136	1.1%	2183	20	10.364	1.6%	2468	15	11580	249	0.1	0.1	201	5	232	6	425	10
12	C:\DATA\031030\OC30H12.D	0.3195	0.7%	1787	10.9	0.1162	1.4%	2221	30	0.102	1.2%	1660	22	5.871	1.6%	1957	14	10489	216	0.1	0.1	105	3	130	3	258	5

Shaded analyses not used.

Sample REC1		Calculated Ages																Elemental Abundances (ppm)											
Analysis		206Pb/238U	%rsd	age	+/-1s	208Pb/232Th	%rsd	age	+/-1s	207Pb/206Pb	%rsd	age	+/-1s	207Pb/235U	%rsd	age	+/-1s	Hf	+/-1s	Hg	+/-1s	Pb	+/-1s	Th	+/-1s	U	+/-1s
1	C:\DATA\030402\AP02A23.D	0.2699	3.2%	1540	50	0.1500	11.7%	2824	330	0.221	4.2%	2991	126	2.199	9.9%	1181	117	8744	770	0.1	0.7	160	14	165	17	569	55
2	C:\DATA\030402\AP02A24.D	0.1460	1.7%	879	15	0.0299	3.8%	596	23	0.091	3.0%	1456	44	1.018	11.4%	713	82	9335	96	0.2	0.3	77	2	203	9	454	25
3	C:\DATA\030402\AP02A25.D	0.1999	1.7%	1175	20	0.0375	4.3%	745	32	0.103	2.6%	1688	44	1.440	7.7%	906	70	9958	234	0.8	0.3	131	4	236	13	521	15
4	C:\DATA\030402\AP02A26.D	0.1206	2.1%	734	15	0.0143	9.3%	288	27	0.092	1.6%	1461	23	0.733	6.2%	558	34	10526	70	0.7	0.3	354	14	6657	568	1869	97
5	C:\DATA\030402\AP02A27.D	0.2135	1.8%	1247	23	0.0324	4.1%	644	26	0.098	2.0%	1589	32	1.460	8.5%	914	78	8464	142	0.0	0.3	148	3	404	10	559	23
6	C:\DATA\030402\AP02A28.D	0.1938	1.0%	1142	11	0.0280	3.5%	558	20	0.095	3.8%	1532	59	1.546	11.6%	949	110	9057	80	0.5	0.3	41	1	187	6	147	3
7	C:\DATA\030402\AP02A29.D	0.1782	1.1%	1057	12	0.0209	7.4%	419	31	0.132	1.2%	2121	25	1.572	5.7%	959	54	9508	83	0.1	0.3	141	2	890	76	563	12
8	C:\DATA\030402\AP02A30.D	0.1965	1.3%	1156	14	0.0349	5.5%	693	38	1.705	21.3%	5977	1276	45.199	187.3%	3892	7289	9119	83	-0.3	0.3	39	28	60	1	65	1
9	C:\DATA\030402\AP02A31.D	13.3601	2.0%	17176	346	373.7075	11.1%	119781	13323	0.751	0.2%	4832	8	237.886	8.5%	5560	475	821	451	8801.4	2299.9	7573730	231888	5196	534	159991	7457
10	C:\DATA\030402\AP02A32.D	0.2514	0.9%	1446	13	0.0346	2.6%	688	18	0.108	2.3%	1768	40	2.084	10.5%	1144	120	8178	126	0.3	0.3	61	1	259	4	151	1
11	C:\DATA\030402\AP02A33.D	0.1940	1.4%	1143	16	0.0313	4.9%	623	31	0.112	4.0%	1834	74	1.272	10.8%	833	90	8759	91	0.1	0.3	17	0	77	1	61	1
12	C:\DATA\030402\AP02A34.D	0.3562	0.6%	1964	13	0.0553	5.2%	1089	56	0.157	0.9%	2421	22	4.140	9.5%	1662	158	10020	137	0.6	0.3	123	2	61	1	274	6
1	C:\DATA\030402\AP02A41.D	0.1542	2.8%	924	26	0.0350	9.7%	696	67	0.182	5.8%	2668	155	1.303	14.4%	847	122	9843	581	0.3	0.4	21	1	139	10	113	10
2	C:\DATA\030402\AP02A42.D	0.1910	1.3%	1127	14	0.0345	4.3%	686	30	0.114	4.1%	1866	76	1.337	10.4%	862	89	9739	99	0.6	0.3	15	0	81	1	58	1
3	C:\DATA\030402\AP02A43.D	0.1907	1.2%	1125	14	0.0305	3.1%	608	19	0.097	4.2%	1562	66	1.559	14.1%	954	135	8818	91	-0.2	0.3	29	1	163	2	109	1
4	C:\DATA\030402\AP02A44.D	0.1966	1.6%	1157	19	0.0342	4.3%	680	29	0.144	4.0%	2275	90	1.135	13.6%	770	105	7924	85	0.6	0.3	10	0	71	1	37	1
5	C:\DATA\030402\AP02A45.D	0.2723	7.8%	1553	121	0.1681	53.1%	3140	1667	0.284	8.8%	3386	298	8.275	52.0%	2262	1177	11147	100	0.4	0.3	248	62	328	5	375	4
6	C:\DATA\030402\AP02A46.D	0.1269	1.4%	770	11	0.0344	5.2%	683	35	0.111	3.2%	1809	58	1.079	14.2%	743	106	8656	113	0.6	0.2	26	1	81	4	172	5
7	C:\DATA\030402\AP02A47.D	0.2063	2.3%	1209	27	0.0382	5.8%	758	44	0.149	6.1%	2331	142	2.067	14.0%	1138	159	8305	318	-0.1	0.3	40	2	173	6	156	12
8	C:\DATA\030402\AP02A48.D	0.1917	1.2%	1130	13	0.0326	4.1%	648	27	0.112	3.2%	1833	59	1.564	10.0%	956	95	8554	134	-0.1	0.3	28	1	166	5	100	2
9	C:\DATA\030402\AP02A49.D	0.2567	1.3%	1473	19	0.0457	4.1%	903	37	0.130	3.1%	2102	66	1.827	10.6%	1055	112	7876	78	0.7	0.2	15	0	47	1	44	1
10	C:\DATA\030402\AP02A50.D	0.1771	1.1%	1051	12	0.0306	3.1%	610	19	0.097	3.3%	1566	52	1.479	11.9%	922	109	9175	171	0.0	0.2	40	1	234	8	159	3
11	C:\DATA\030402\AP02A51.D	0.2755	1.0%	1569	15	0.0470	3.8%	929	35	0.107	2.8%	1754	50	2.338	10.3%	1224	126	9300	150	0.3	0.3	38	1	70	1	114	3
12	C:\DATA\030402\AP02A53.D	0.1923	1.5%	1134	17	0.0347	5.2%	689	36	0.137	3.3%	2195	72	1.238	12.3%	818	101	9470	118	0.2	0.3	11	0	66	1	42	1
1	C:\DATA\030403\AP03A07.D	0.2012	1.3%	1182	15	0.0287	5.6%	571	32	0.095	3.0%	1520	46	1.238	14.4%	818	118	10153	162	0.7	0.3	50	1	85	1	191	3
2	C:\DATA\030403\AP03A08.D	0.3551	1.1%	1959	22	0.0392	7.5%	777	58	0.169	0.7%	2550	17	4.105	13.0%	1655	215	9549	125	1.5	0.3	191	3	300	10	365	6
3	C:\DATA\030403\AP03A09.D	0.2929	1.4%	1656	24	0.0391	6.0%	775	46	0.118	2.2%	1930	42	2.235	16.2%	1192	194	9700	95	0.4	0.3	57	2	97	4	141	5
4	C:\DATA\030403\AP03A10.D	0.1679	1.0%	1001	10	0.0254	2.9%	507	15	0.129	1.0%	2087	21	1.262	6.9%	829	57	11670	138	-0.2	0.3	240	3	866	10	892	10
5	C:\DATA\030403\AP03A11.D	0.1894	1.2%	1118	13	0.0269	4.0%	536	22	0.095	2.3%	1534	35	1.194	13.3%	798	106	9093	115	0.8	0.3	102	2	302	4	365	6
7	C:\DATA\030403\AP03A13.D	0.0963	7.3%	593	43	0.0115	10.3%	231	24	0.124	7.0%	2018	142	0.406	24.1%	346	83	78444	14429	184304.0	61893.8	201851451	14626270	8950878640	######	#######	######
8	C:\DATA\030403\AP03A14.D	0.4335	0.9%	2321	21	0.0513	3.7%	1011	37	0.198	0.6%	2812	17	5.274	8.9%	1865	167	10329	144	0.2	0.3	305	4	157	5	498	5
9	C:\DATA\030403\AP03A15.D	0.2558	1.5%	1468	22	0.0354	5.2%	703	37	0.112	2.7%	1837	49	1.745	13.4%	1025	138	8832	128	0.9	0.3	46	1	124	3	119	2
10	C:\DATA\030403\AP03A16.D	0.2174	3.1%	1268	39	0.0455	19.4%	899	174	0.138	6.7%	2205	148	1.630	19.7%	982	194	9020	523	0.5	0.5	80	4	224	13	253	13
11	C:\DATA\030403\AP03A17.D	0.2698	1.3%	1540	20	0.0377	4.1%	748	30	0.122	1.9%	1989	38	2.160	16.4%	1168	192	8419	79	0.3	0.3	59	1	167	3	136	2
12	C:\DATA\030403\AP03A18.D	0.3570	1.0%	1968	20	0.0418	3.7%	828	30	0.158	0.7%	2434	16	3.795	12.8%	1592	203	9522	123	0.7	0.3	256	4	410	11	479	9
1	C:\DATA\030403\AP03A25.D	0.2788	1.9%	1585	30	0.0342	7.5%	680	51	0.128	2.5%	2065	52	1.551	14.6%	951	139	9267	132	0.6	0.3	27	1	61	1	68	1
2	C:\DATA\030403\AP03A26.D	0.2664	1.9%	1522	29	0.0304	7.5%	606	45	0.134	3.5%	2155	75	1.152	20.5%	778	159	6710	104	-0.2	0.3	18	1	65	2	43	1
3	C:\DATA\030403\AP03A27.D	0.2687	2.3%	1534	36	0.0362	9.9%	719	72	0.151	2.9%	2356	69	1.017	21.7%	712	155	6800	121	0.5	0.3	12	0	38	1	32	1
4	C:\DATA\030403\AP03A28.D	0.0953	1.1%	587	6	0.0195	8.6%	391	34	0.113	1.4%	1849	25	0.577	7.2%	462	33	11826	174	0.3	0.3	251	4	464	8	1950	28
5	C:\DATA\030403\AP03A29.D	0.1675	1.8%	998	18	0.0242	8.0%	483	39	0.091	2.8%	1445	41	0.910	15.9%	657	104	10393	317	-0.6	0.4	92	3	196	7	413	12
6	C:\DATA\030403\AP03A30.D	0.1804	1.3%	1069	14	0.0205	5.6%	410	23	0.087	3.9%	1350	53	1.031	19.4%	719	139	10090	111	0.3	0.3	51	1	189	2	194	2
7	C:\DATA\030403\AP03A31.D	0.2393	1.2%	1383	17	0.0257	5.0%	513	26	0.102	1.4%	1669	24	1.451	14.7%	910	134	11655	186	0.2	0.3	154	3	195	4	496	11
8	C:\DATA\030403\AP03A32.D	0.4915	0.9%	2577	24	0.0601	11.3%	1180	134	0.245	0.4%	3150	13	6.797	11.1%	2085	232	11432	162	0.6	0.3	300	5	135	5	415	5
9	C:\DATA\030403\AP03A33.D	0.1884	1.0%	1113	12	0.4902	26.5%	8063	2138	0.093	2.9%	1483	44	1.131	19.9%	768	153	15190	175	0.1	0.3	56	1	1	0	250	2
10	C:\DATA\030403\AP03A34.D	0.1822	1.2%	1079	13	0.0206	6.1%	413	25	0.090	3.1%	1436	45	1.205	20.6%	803	165	10698	113	0.3	0.3	46	1	146	2	179	2
11	C:\DATA\030403\AP03A35.D	0.2528	1.5%	1453	22	0.0310	7.7%	618	48	0.118	2.6%	1930	50	1.599	16.3%	970	158	7520	57	-0.3	0.3	35	1	72	1	100	2
12	C:\DATA\030403\AP03A36.D	0.3032	1.2%	1707	21	0.0398	9.5%	788	75	0.130	1.8%	2100	38	2.340	16.8%	1225	206	6644	63	-0.2	0.3	46	1	43	1	116	2
1	C:\DATA\030403\AP03A43.D	0.2015	11.4%	1183	134	0.0847	56.9%	1644	936	0.138	10.7%	2204	235	0.739	8.1%	562	45	11822	632	1.0	0.3	182	10	105	7	988	50
2	C:\DATA\030403\AP03A44.D	0.1158	1.5%	706	10	0.0148	4.5%	298	13	0.105	1.6%	1720	28	0.733	9.5%	558	53	10427	130	-0.1	0.3	180	2	999	25	1103	17
3	C:\DATA\030403\AP03A45.D	0.1858	1.0%	1099	11	0.0246	2.8%	491	14	0.084	3.1%	1299	40	1.087	18.5%	747	138	10447	120	-0.3	0.3	99	1	451	7	353	4
4	C:\DATA\030403\AP03A46.D	0.2708	1.2%	1545	19	0.0386	5.3%	766	40	0.111	1.4%	1822	25	1.823	11.3%	1054	119	11226	154	-0.3	0.4	140	3	123	3	418	12
5	C:\DATA\030403\AP03A47.D	0.1734	1.0%	1031	11	0.0260	7.2%	519	37	0.092	2.1%	1460	30	0.919	9.7%	662	64	10600	119	-1.2	0.3	155	2	215	17	724	9
6	C:\DATA\030403\AP03A48.D	0.2649	1.3%	1515	20	0.0382	5.2%	758	39	0.112	2.8%	1831	51	1.647	14.3%	988	141	9771	134	-0.1	0.4	51	2	128	4	136	4
7	C:\DATA\030403\AP03A49.D	0.1959	1.5%	1153	18	0.0297	4.9%	591	29	0.099	3.4%	1597	54	1.185	16.3%	794	130	8347	75	0.0	0.4	51	2	201	7	173	3
8	C:\DATA\030403\AP03A50.D	0.1600	2.5%	957	24	0.0325	5.2%	646	34	0.099	2.7%	1604	43	1.015	17.6%	712	125	10357	203	0.8	0.5	158	9	265	13	864	51
9	C:\DATA\030403\AP03A51.D	0.2690	1.1%	1536	17	0.0385	3.7%	764	29	0.114	1.8%	1870	33	2.130	16.0%	1159	185	7794	140	0.6	0.5	133	4	305	13	346	10
10	C:\DATA\030403\AP03A52.D	0.2504	1.2%	1441	17	0.0308	4.1%	614	25	0.103	2.2%	1688	37	1.634	14.4%	983	142	9300	251	-0.1	0.5	125	3	396	12	347	10
11	C:\DATA\030403\AP03A53.D	0.2675	1.2%	1528	19	0.0358	5.0%	711	35	0.117	2.4%	1904	46	1.786	17.9%	1040	186	9445	92	0.5	0.3	40	1	103	2	104	2
12	C:\DATA\030403\AP03A54.D	0.1818	0.8%	1077	9	0.0255	3.5%	510	18	0.081	2.7%	1229	33	0.949	10.3%	677	70	11888	93	0.9	0.3	104	1	241	3	435	4
1	C:\DATA\031030\OC30I1.D	0.2900	0.8%	1641	12.3	0.1094	1.6%	2098	31	0.086	1.6%	1344	31	4.593	1.9%	1748	16	10087	241	0.2	0.1	63	2	120	4	190	9
2	C:\DATA\031030\OC30I2.D	0.2804	0.8%	1593	10.9	0.0492	1.9%	970	18	0.094	1.3%	1518	25	4.781	1.7%	1782	15	9656	230	0.3	0.1	48	1	145	4	140	3
3	C:\DATA\031030\OC30I3.D	0.3250	0.9%	1814	13.6	0.1154	1.6%	2207	33	0.101	1.5%	1645	28	5.935	1.8%	1966	16	9358	220	0.0	0.1	43	1	64	2	102	2
4	C:\DATA\031030\OC30I4.D	0.0829	0.9%	514	4.6	0.0175	1.9%	351	7	0.078	1.4%	1155	28	1.148	1.8%	776	10	11472	274	0.4	0.1	120	3	846	22	1314	30
5	C:\DATA\031030\OC30I5.D	0.2935	0.9%	1659	12.6	0.1075	1.5%	2065	29	0.091	1.9%	1441	35	4.965	2.1%	1813	18	7978	192	-0.1	-0.1	28	1	106	3	60	1
6	C:\DATA\031030\OC30I6.D	0.1955	0.8%	1151	8.6	0.0690	1.5%	1349	20	0.073	1.9%	1006	39	2.585	2.1%	1296	16	9571	226	0.1	0.1	28	1	123	3	104	3
7	C:\DATA\031030\OC30I7.D	0.2034	0.9%	1194	9.9	0.0748	1.4%	1459	20	0.075	1.4%	1067	28	2.760	1.8%	1345	14	9967	243	0.3	0.1	51	2	178	5	186	6
8	C:\DATA\031030\OC30I8.D	0.2275	1.2%	1321	14.2	0.0790	1.6%	1538	23	0.076	2.6%	1099	53	3.281	3.0%	1477	24	9865	232	-0.1	-0.1	21	1	148	5	62	3
9	C:\DATA\031030\OC30I9.D	0.2019	1.2%	1185	12.6	0.0811	1.7%	1576	26	0.068	2.5%	879	52	2.661	2.7%	1318	20	9690	233	0.4	0.1	30	1	135	4	102	3
10	C:\DATA\031030\OC30I10.D	0.2206	0.8%	1285	9.2	0.0828	1.4%	1608	22	0.076	1.5%	1083	31	3.010	1.8%	1410	14	9572	257	0.4	0.1	77	3	344	13	244	12
11	C:\DATA\031030\OC30I11.D	0.3356	1.2%	1866	20.0	0.1305	2.4%	2480	56	0.111	2.7%	1815	48	8.039	2.9%	2235	26	7308	176	0.1	0.1	21	1	20	1	30	1
12	C:\DATA\031030\OC30I12.D	0.3668	0.8%	2014	13.8	0.1000	4.9%	1927	91	0.130	1.2%	2103	21	8.969	1.6%	2335	15	11560	273	0.3	0.1	221	7	396	11	565	17

Shaded analyses not used

Sample B2		Calculated Ages															Elemental Abundance									
Analysis	File	206Pb/238U	%rsd	age	+/-1s	208Pb/232T	%rsd	age	+/-1s	207Pb/206P	%rsd	age	+/-1s	207Pb/235U	%rsd	age	+/-1s	Hf	+/-1s	Hg	+/-1s	Pb	+/-1s	Th	+/-1s	U	+/-1s
1	C:\DATA\031031\OC31A1.D	0.1681	0.4%	1001	3.9	0.0605	1.1%	1187	13	0.126	1.2%	2039	22	3.832	1.1%	1600	9	10919	269	0.3	0.1	272	8	605	19	884	24
2	C:\DATA\031031\OC31A2.D	0.2791	1.1%	1587	15.2	0.0865	1.6%	1676	25	0.092	2.7%	1468	52	5.241	3.1%	1859	27	8010	200	0.7	0.1	11	0	43	1	24	1
3	C:\DATA\031031\OC31A3.D	0.2884	0.7%	1634	10.5	0.0913	1.3%	1765	21	0.099	1.6%	1606	29	4.991	1.7%	1818	15	9295	224	0.4	0.1	23	1	47	1	57	1
	C:\DATA\031031\OC31A4.D	0.2117	0.6%	1238	6.6	0.0694	1.2%	1357	15	0.089	1.3%	1410	25	3.274	1.5%	1475	12	9825	236	0.1	0.1	57	2	148	4	212	5
5	C:\DATA\031031\OC31A5.D	0.3789	0.5%	2071	8.3	0.1100	1.0%	2109	20	0.138	0.9%	2201	15	8.996	1.1%	2338	10	11230	275	0.0	-0.1	138	4	99	3	281	6
6	C:\DATA\031031\OC31A6.D	0.2466	0.6%	1421	8.0	0.0802	1.1%	1559	16	0.092	1.3%	1457	25	3.910	1.5%	1616	12	8916	223	0.4	0.1	41	1	139	4	110	2
7	C:\DATA\031031\OC31A7.D	0.2838	0.5%	1611	6.8	0.0893	1.2%	1730	19	0.100	1.1%	1626	21	4.879	1.3%	1799	11	8961	231	0.1	0.1	60	2	99	3	158	4
8	C:\DATA\031031\OC31A8.D	0.1934	0.6%	1140	6.7	0.0568	1.3%	1116	14	0.081	1.1%	1233	22	2.744	1.3%	1340	10	11116	285	-0.2	-0.1	110	3	221	7	483	15
9	C:\DATA\031031\OC31A9.D	0.2646	0.6%	1513	7.5	0.0898	1.3%	1738	21	0.101	1.2%	1642	22	4.742	1.3%	1775	11	9991	240	0.8	0.1	70	2	111	4	191	7
10	C:\DATA\031031\OC31A10.D	0.2896	0.6%	1640	9.2	0.0870	1.1%	1686	17	0.106	1.2%	1735	23	5.214	1.4%	1855	12	9989	248	0.1	0.1	82	2	183	5	211	5
11	C:\DATA\031031\OC31A11.D	0.2544	0.7%	1461	8.6	0.0743	1.2%	1449	17	0.079	1.3%	1178	25	3.527	1.4%	1533	11	10293	264	0.3	0.1	80	2	129	4	295	11
12	C:\DATA\031031\OC31A12.D	0.1633	0.4%	975	4.0	0.0521	1.0%	1027	10	0.070	1.1%	918	24	1.939	1.3%	1095	9	10914	265	0.4	0.1	75	2	208	6	361	8
1	C:\DATA\031031\OC31B1.D	0.2248	0.8%	1307	9.5	0.0724	1.4%	1412	20	0.084	1.9%	1295	37	3.414	2.0%	1508	16	0	#DIV/0!	0.0	#DIV/0!	0	#DIV/0!	0	#DIV/0!	0	#DIV/0!
2	C:\DATA\031031\OC31B2.D	0.1958	0.5%	1152	5.1	0.0716	1.4%	1397	20	0.077	1.1%	1110	22	2.569	1.2%	1292	9	0	#DIV/0!	0.0	#DIV/0!	0	#DIV/0!	0	#DIV/0!	0	#DIV/0!
3	C:\DATA\031031\OC31B3.D	0.2930	0.5%	1657	8.0	0.0923	1.0%	1784	17	0.101	1.2%	1650	23	5.146	1.3%	1844	12	0	#DIV/0!	0.0	#DIV/0!	0	#DIV/0!	0	#DIV/0!	0	#DIV/0!
	C:\DATA\031031\OC31B4.D	0.2111	0.5%	1235	5.3	0.0686	1.0%	1341	14	0.082	1.3%	1255	25	2.996	1.5%	1407	11	0	#DIV/0!	0.0	#DIV/0!	0	#DIV/0!	0	#DIV/0!	0	#DIV/0!
5	C:\DATA\031031\OC31B5.D	0.2841	0.8%	1612	11.4	0.0885	1.4%	1715	22	0.091	1.7%	1446	32	4.739	1.7%	1774	15	0	#DIV/0!	0.0	#DIV/0!	0	#DIV/0!	0	#DIV/0!	0	#DIV/0!
6	C:\DATA\031031\OC31B6.D	0.4426	0.5%	2362	9.3	0.1347	0.9%	2555	22	0.153	0.9%	2381	16	11.599	1.1%	2573	10	0	#DIV/0!	0.0	#DIV/0!	0	#DIV/0!	0	#DIV/0!	0	#DIV/0!
7	C:\DATA\031031\OC31B7.D	0.2026	0.7%	1189	7.2	0.0706	1.6%	1379	21	0.087	1.6%	1352	31	2.999	1.8%	1407	14	0	#DIV/0!	0.0	#DIV/0!	0	#DIV/0!	0	#DIV/0!	0	#DIV/0!
8	C:\DATA\031031\OC31B8.D	0.1832	0.7%	1085	6.6	0.0589	1.0%	1156	11	0.078	1.7%	1139	35	2.490	1.8%	1269	13	0	#DIV/0!	0.0	#DIV/0!	0	#DIV/0!	0	#DIV/0!	0	#DIV/0!
9	C:\DATA\031031\OC31B9.D	0.1923	0.6%	1134	5.8	0.0635	1.1%	1245	13	0.076	1.5%	1093	30	2.545	1.6%	1285	11	0	#DIV/0!	0.0	#DIV/0!	0	#DIV/0!	0	#DIV/0!	0	#DIV/0!
10	C:\DATA\031031\OC31B10.D	0.1964	0.5%	1156	4.8	0.0631	1.4%	1236	17	0.093	1.3%	1490	25	3.089	1.5%	1430	12	0	#DIV/0!	0.0	#DIV/0!	0	#DIV/0!	0	#DIV/0!	0	#DIV/0!
11	C:\DATA\031031\OC31B11.D	0.1055	0.7%	646	4.5	0.0404	1.2%	801	10	0.092	1.2%	1472	24	1.660	1.5%	993	9	0	#DIV/0!	0.0	#DIV/0!	0	#DIV/0!	0	#DIV/0!	0	#DIV/0!
12	C:\DATA\031031\OC31B12.D	0.2799	0.6%	1591	8.4	0.0897	1.0%	1737	17	0.099	1.2%	1610	23	4.773	1.4%	1780	12	0	#DIV/0!	0.0	#DIV/0!	0	#DIV/0!	0	#DIV/0!	0	#DIV/0!
1	C:\DATA\031031\OC31C1.D	0.2718	0.5%	1550	6.8	0.0852	1.1%	1652	17	0.091	1.0%	1449	18	4.246	1.2%	1683	10	9741	249	0.2	0.1	147	4	202	6	422	10
2	C:\DATA\031031\OC31C2.D	0.2796	0.8%	1589	11.7	0.0864	1.5%	1676	24	0.099	1.9%	1603	36	5.057	2.0%	1829	17	9453	230	0.4	0.1	16	0	35	1	40	1
3	C:\DATA\031031\OC31C3.D	0.1796	0.8%	1065	7.6	0.0608	1.1%	1194	12	0.082	2.2%	1249	44	2.654	2.2%	1316	16	9527	247	0.5	0.1	21	1	124	4	72	2
	C:\DATA\031031\OC31C4.D	0.2902	0.7%	1642	9.6	0.0940	1.1%	1816	19	0.106	1.5%	1732	27	5.404	1.6%	1885	14	10347	264	0.3	0.1	36	1	141	4	71	2
5	C:\DATA\031031\OC31C5.D	0.2905	0.5%	1644	8.0	0.0910	1.0%	1760	17	0.102	1.2%	1667	22	5.075	1.3%	1832	11	10092	254	0.6	0.1	67	2	160	5	156	4
6	C:\DATA\031031\OC31C6.D	0.2891	0.5%	1637	7.3	0.0847	1.1%	1644	17	0.102	0.9%	1652	17	5.036	1.1%	1825	10	10201	254	0.3	0.1	158	4	106	3	446	9
7	C:\DATA\031031\OC31C7.D	0.3152	0.7%	1766	10.8	0.1826	1.8%	3390	56	0.146	1.0%	2303	17	7.970	1.3%	2228	12	11456	299	0.1	0.1	158	5	34	1	378	10
8	C:\DATA\031031\OC31C8.D	0.2634	0.7%	1507	9.9	0.0829	1.4%	1610	21	0.091	1.7%	1436	32	4.190	1.8%	1672	15	7851	190	0.3	0.1	21	1	41	1	60	1
9	C:\DATA\031031\OC31C9.D	0.2030	0.6%	1192	7.1	0.0559	1.2%	1100	13	0.097	1.0%	1575	20	3.352	1.3%	1493	10	9445	251	0.1	0.1	120	4	454	16	392	15
10	C:\DATA\031031\OC31C10.D	0.2913	0.7%	1648	9.5	0.0922	1.3%	1782	22	0.093	1.3%	1481	25	4.800	1.5%	1785	13	12172	313	-0.2	-0.1	47	1	65	2	131	5
11	C:\DATA\031031\OC31C11.D	0.4610	0.5%	2444	9.9	0.1433	1.1%	2707	28	0.155	0.9%	2405	16	12.307	1.1%	2628	11	10359	257	0.1	0.1	116	3	112	3	184	5
12	C:\DATA\031031\OC31C12.D	0.3617	0.6%	1990	10.2	0.1095	0.9%	2100	19	0.127	1.2%	2061	22	8.123	1.4%	2245	12	8630	209	0.6	0.1	84	2	316	9	122	3
1	C:\DATA\031031\OC31D1.D	0.1906	0.7%	1125	6.8	0.0566	1.3%	1113	15	0.074	1.2%	1037	25	2.422	1.4%	1249	10	10809	249	0.5	0.1	80	2	125	4	387	17
2	C:\DATA\031031\OC31D2.D	0.1678	0.6%	1000	5.3	0.0545	1.2%	1073	13	0.073	1.6%	1027	31	2.102	1.7%	1149	12	9734	211	-0.1	-0.1	55	1	146	4	271	7
3	C:\DATA\031031\OC31D3.D	0.2037	0.6%	1195	6.1	0.0660	1.0%	1292	12	0.077	1.4%	1125	27	2.712	1.6%	1332	12	9271	214	0.1	0.1	51	1	217	5	162	3
	C:\DATA\031031\OC31D4.D	0.3256	0.7%	1817	11.1	0.1017	1.3%	1957	24	0.105	1.3%	1711	24	6.037	1.5%	1981	13	9628	214	0.4	0.1	39	1	59	1	93	2
5	C:\DATA\031031\OC31D5.D	0.1911	0.8%	1128	7.8	0.0618	1.2%	1212	14	0.077	2.2%	1112	45	2.570	2.3%	1292	17	9564	228	0.5	0.1	21	1	113	4	70	3
6	C:\DATA\031031\OC31D6.D	0.2213	0.7%	1289	8.0	0.0657	1.0%	1286	13	0.085	1.4%	1305	27	3.162	1.6%	1448	12	9074	212	0.4	0.1	84	2	231	7	284	9
7	C:\DATA\031031\OC31D7.D	0.1718	0.5%	1022	4.4	0.0602	1.2%	1182	14	0.077	1.1%	1114	22	2.341	1.2%	1225	9	9755	224	0.1	0.1	101	3	306	8	413	9
8	C:\DATA\031031\OC31D8.D	0.1599	0.6%	956	4.9	0.0526	1.1%	1036	12	0.069	1.6%	901	33	1.896	1.6%	1080	11	9364	209	0.3	0.1	35	1	127	3	158	3
9	C:\DATA\031031\OC31D9.D	0.1852	0.4%	1096	4.5	0.0583	1.0%	1146	11	0.074	1.1%	1029	22	2.326	1.2%	1220	9	10764	246	0.1	0.1	107	3	294	7	433	9
10	C:\DATA\031031\OC31D10.D	0.3186	0.6%	1783	8.9	0.1038	1.2%	1996	22	0.103	1.2%	1687	22	5.718	1.3%	1934	12	10185	236	0.2	0.1	59	2	89	2	137	3
11	C:\DATA\031031\OC31D11.D	0.1835	0.8%	1086	7.5	0.0622	1.5%	1220	18	0.073	2.4%	1005	48	2.354	2.4%	1229	17	9307	213	0.3	0.1	19	0	59	1	78	2
12	C:\DATA\031031\OC31D12.D	0.1752	0.5%	1041	4.6	0.0537	1.2%	1057	12	0.078	1.1%	1142	22	2.386	1.3%	1238	9	7992	182	0.0	-0.1	206	5	534	13	914	21
1	C:\DATA\031031\OC31E1.D	0.2982	0.5%	1682	7.5	0.0947	1.1%	1828	19	0.099	1.1%	1596	21	5.014	1.3%	1822	11	11212	888	0.4	0.1	72	6	125	10	178	14
2	C:\DATA\031031\OC31E2.D	0.4541	0.5%	2414	9.9	0.1354	0.9%	2567	22	0.155	0.9%	2397	16	11.899	1.1%	2597	10	10074	230	0.4	0.1	160	4	178	4	257	5
3	C:\DATA\031031\OC31E3.D	0.4652	0.6%	2462	12.9	0.1408	1.1%	2663	27	0.164	1.0%	2498	16	13.164	1.2%	2691	11	9592	235	0.4	0.1	129	4	158	4	199	6
	C:\DATA\031031\OC31E4.D	0.2118	0.5%	1238	5.7	0.0692	1.0%	1353	14	0.078	1.2%	1136	24	2.799	1.3%	1355	10	9523	230	0.2	0.1	90	2	302	8	304	7
5	C:\DATA\031031\OC31E5.D	0.1645	0.4%	982	4.0	0.0535	1.0%	1053	10	0.067	1.2%	846	25	1.881	1.3%	1074	8	10635	252	0.2	0.1	93	2	228	6	447	9
6	C:\DATA\031031\OC31E6.D	0.2848	1.0%	1615	14.8	0.0943	2.7%	1822	47	0.099	2.5%	1611	47	5.386	2.9%	1883	25	10779	268	0.0	0.1	27	1	34	1	73	4
7	C:\DATA\031031\OC31E7.D	0.2610	0.5%	1495	6.4	0.0835	1.1%	1620	17	0.091	1.1%	1450	22	4.104	1.3%	1655	11	9443	223	0.3	0.1	80	2	200	5	221	5
8	C:\DATA\031031\OC31E8.D	0.3195	0.5%	1787	8.1	0.0986	1.1%	1901	20	0.101	1.2%	1647	23	5.550	1.4%	1908	12	9445	223	0.5	0.1	67	2	119	3	152	4
9	C:\DATA\031031\OC31E9.D	0.1569	0.7%	939	6.4	0.0500	1.5%	986	14	0.073	1.5%	1017	31	1.917	1.6%	1087	11	10209	231	0.4	0.1	97	3	368	12	525	21
10	C:\DATA\031031\OC31E10.D	0.2428	0.9%	1401	11.1	0.0766	1.8%	1492	25	0.089	1.9%	1412	36	3.746	2.2%	1581	18	9102	205	0.0	0.1	36	1	82	2	107	3
11	C:\DATA\031031\OC31E11.D	0.2804	0.8%	1593	12.0	0.0900	1.3%	1742	22	0.097	1.9%	1573	36	4.798	2.0%	1785	17	8262	186	0.1	0.1	19	1	53	1	47	1
12	C:\DATA\031031\OC31E12.D	0.1897	0.7%	1120	6.7	0.0426	1.5%	844	12	0.084	1.6%	1292	31	2.750	1.7%	1342	13	12205	272	0.2	0.1	103	3	246	6	471	11

Shaded samples not used in final results

Sample B4		Calculated Age																Elemental Abundance									
Analysis	File	206Pb/238U	%rsd	age	+/-1s	208Pb/232T	%rsd	age	+/-1s	207Pb/206P	%rsd	age	+/-1s	207Pb/235U	%rsd	age	+/-1s	Hf	+/-1s	Hg	+/-1s	Pb	+/-1s	Th	+/-1s	U	+/-1s
1	C:\HPCHEM\1\DATA\030305\MR05A41.D	0.2744	4.6%	1563	72	0.0736	3.2%	1436	46	0.121	2.3%	1972	46	4.375	8.3%	1708	141	11684	319	-0.1	0.2	63	2	218	13	192	11
2	C:\HPCHEM\1\DATA\030305\MR05A42.D	0.3124	4.5%	1753	79	0.0857	1.8%	1662	31	0.120	2.0%	1961	39	4.858	7.9%	1795	143	8352	201	0.1	0.2	139	4	247	8	363	12
3	C:\HPCHEM\1\DATA\030305\MR05A43.D	0.1747	3.9%	1038	41	0.0471	2.0%	930	19	0.079	4.1%	1162	48	1.780	8.1%	1038	85	9558	236	0.2	0.2	97	3	348	10	452	13
4	C:\HPCHEM\1\DATA\030305\MR05A44.D	0.1110	4.1%	679	28	0.0439	2.9%	869	25	0.168	1.9%	2536	49	1.934	4.7%	1093	51	11829	322	0.4	0.2	182	7	822	48	1218	48
5	C:\HPCHEM\1\DATA\030305\MR05A45.D	0.1754	3.9%	1042	41	0.0438	3.2%	867	27	0.134	2.2%	2153	48	2.922	7.6%	1388	105	11170	280	-0.5	0.2	86	3	318	18	414	27
6	C:\HPCHEM\1\DATA\030305\MR05A46.D	0.0723	3.4%	450	15	0.0316	2.1%	629	13	0.174	1.5%	2595	39	1.411	5.3%	894	47	6829	266	0.5	0.2	114	5	1250	65	920	45
7	C:\HPCHEM\1\DATA\030305\MR05A47.D	0.1599	4.0%	956	38	0.0445	1.9%	880	17	0.073	4.1%	1005	41	1.359	7.1%	871	62	10620	274	0.3	0.2	134	4	370	11	730	23
8	C:\HPCHEM\1\DATA\030305\MR05A48.D	0.0985	4.0%	605	24	0.0609	1.8%	1194	22	0.158	1.4%	2436	34	1.681	4.9%	1002	49	12975	396	0.2	0.2	231	7	624	21	1818	70
9	C:\HPCHEM\1\DATA\030305\MR05A49.D	0.1239	3.3%	753	25	0.0410	3.9%	811	32	0.134	2.3%	2150	51	1.850	5.0%	1064	54	11013	345	0.3	0.2	109	5	399	16	657	25
10	C:\HPCHEM\1\DATA\030305\MR05A50.D	0.2625	4.2%	1503	63	0.1019	5.1%	1962	100	0.137	2.0%	2190	43	4.329	7.1%	1699	121	10265	377	0.3	0.2	206	10	356	14	605	22
11	C:\HPCHEM\1\DATA\030305\MR05A51.D	0.1804	4.5%	1069	48	0.0503	2.6%	992	26	0.080	4.0%	1191	48	1.759	7.5%	1030	77	10548	281	0.0	0.2	84	3	137	4	441	20
12	C:\HPCHEM\1\DATA\030305\MR05A52.D	0.2892	4.2%	1637	69	0.0806	2.5%	1567	40	0.109	4.1%	1788	73	2.997	6.9%	1407	98	9200	245	0.3	0.2	28	1	75	2	76	3
1	C:\HPCHEM\1\DATA\030305\MR05A57.D	0.2473	2.2%	1424	32	0.0682	2.4%	1334	32	0.111	1.9%	1815	34	3.433	5.6%	1512	85	11419	243	0.6	0.2	115	3	136	4	355	10
2	C:\HPCHEM\1\DATA\030305\MR05A58.D	0.1805	3.9%	1070	42	0.0628	10.6%	1231	130	0.081	5.0%	1228	61	1.728	8.1%	1019	82	12188	487	0.3	0.2	94	4	89	4	492	28
3	C:\HPCHEM\1\DATA\030305\MR05A60.D	0.1593	4.2%	953	40	0.0571	3.2%	1122	35	0.092	4.4%	1471	65	2.066	9.8%	1138	112	9171	221	0.4	0.2	61	2	192	5	283	8
4	C:\HPCHEM\1\DATA\030305\MR05A61.D	0.2185	8.7%	1274	110	0.0477	4.4%	942	41	0.191	2.5%	2750	69	3.506	8.0%	1529	122	8487	421	0.7	0.2	334	17	1565	100	1661	98
5	C:\HPCHEM\1\DATA\030305\MR05A62.D	0.2951	8.1%	1667	135	0.0582	4.1%	1144	46	0.114	5.6%	1871	104	2.709	10.6%	1331	142	9642	500	0.5	0.2	58	3	186	19	262	19
6	C:\HPCHEM\1\DATA\030305\MR05A64.D	0.2205	7.0%	1284	90	0.0510	2.7%	1005	27	0.101	5.8%	1651	95	2.218	9.2%	1187	109	9452	516	0.5	0.2	141	7	619	29	579	29
7	C:\HPCHEM\1\DATA\030305\MR05A65.D	0.2523	5.6%	1450	81	0.0602	2.6%	1182	30	0.088	4.0%	1377	55	2.773	9.7%	1348	131	9266	353	0.7	0.2	112	4	283	10	390	15
8	C:\HPCHEM\1\DATA\030305\MR05A66.D	0.1311	5.2%	794	41	0.0464	2.8%	917	26	0.124	2.3%	2016	46	2.119	9.4%	1155	108	11753	468	0.1	0.2	145	5	389	14	933	51
9	C:\HPCHEM\1\DATA\030305\MR05A67.D	0.2291	7.6%	1330	101	0.0678	5.6%	1325	75	0.105	5.1%	1713	88	2.297	10.0%	1211	121	11203	696	0.2	0.2	116	8	207	20	624	43
10	C:\HPCHEM\1\DATA\030305\MR05A68.D	0.3082	7.3%	1732	126	0.0593	3.3%	1165	38	0.098	6.3%	1578	99	2.746	9.8%	1341	131	10814	547	0.3	0.2	109	6	165	8	455	28
11	C:\HPCHEM\1\DATA\030305\MR05A63.D	0.1167	5.9%	712	42	0.0367	4.0%	728	29	0.133	6.4%	2138	137	0.979	11.1%	693	77	7648	270	0.5	0.2	9	0	68	3	51	2
1	C:\HPCHEM\1\DATA\030305\MR05A75.D	0.2403	4.1%	1388	56	0.0678	2.5%	1326	34	0.096	3.4%	1548	52	3.186	9.2%	1454	134	8823	243	0.7	0.2	77	3	143	5	244	9
2	C:\HPCHEM\1\DATA\030305\MR05A76.D	0.1304	3.4%	790	27	0.0448	7.5%	885	66	0.115	2.5%	1881	47	1.900	6.4%	1081	69	11073	312	0.2	0.2	211	6	795	30	1138	36
3	C:\HPCHEM\1\DATA\030305\MR05A77.D	0.1596	4.1%	954	40	0.0436	2.6%	862	22	0.081	6.8%	1212	83	1.861	8.7%	1067	93	8884	236	0.0	0.2	44	1	217	7	190	6
4	C:\HPCHEM\1\DATA\030305\MR05A78.D	0.1625	4.0%	971	38	0.0799	2.0%	1555	32	0.298	1.1%	3460	40	6.275	7.4%	2015	149	9093	243	0.2	0.2	178	5	864	23	466	14
5	C:\HPCHEM\1\DATA\030305\MR05A79.D	0.2895	4.7%	1639	78	0.0799	2.8%	1554	44	0.108	2.8%	1774	50	4.403	7.8%	1713	134	10570	305	-0.2	0.2	82	3	64	2	259	17
6	C:\HPCHEM\1\DATA\030305\MR05A80.D	0.2137	6.1%	1249	76	0.0547	3.0%	1077	32	0.101	3.8%	1637	62	2.534	9.8%	1282	125	9273	376	0.2	0.2	116	5	220	9	516	25
7	C:\HPCHEM\1\DATA\030305\MR05A81.D	0.1669	3.9%	995	39	0.0503	3.1%	992	31	0.079	7.4%	1176	86	1.644	8.8%	987	87	8598	197	0.4	0.2	33	1	81	2	153	6
8	C:\HPCHEM\1\DATA\030305\MR05A82.D	0.1624	3.9%	970	38	0.0603	2.8%	1183	33	0.084	3.0%	1301	39	1.680	5.1%	1001	51	11667	346	-0.3	0.2	176	5	204	8	894	35
9	C:\HPCHEM\1\DATA\030305\MR05A83.D	0.3871	4.0%	2109	85	0.1243	2.4%	2369	57	0.186	1.6%	2707	44	9.505	7.7%	2388	184	7596	209	-0.1	0.2	87	3	82	2	162	6
10	C:\HPCHEM\1\DATA\030305\MR05A84.D	0.1517	4.1%	911	37	0.0482	2.9%	952	27	0.093	5.3%	1490	79	1.936	9.7%	1094	106	9803	238	0.5	0.2	57	2	122	5	309	16
11	C:\HPCHEM\1\DATA\030305\MR05A85.D	0.3053	3.8%	1717	65	0.0831	2.7%	1614	44	0.116	1.9%	1898	36	4.114	5.3%	1657	87	10657	314	0.1	0.2	194	6	132	11	519	20
12	C:\HPCHEM\1\DATA\030305\MR05A86.D	0.1300	6.8%	788	54	0.0673	3.5%	1316	46	0.199	2.7%	2819	75	3.122	9.5%	1438	136	12336	455	0.4	0.2	69	3	264	15	409	23
1	C:\HPCHEM\1\DATA\030305\MR05A91.D	0.1357	3.3%	820	27	0.0582	8.0%	1143	92	0.092	4.7%	1464	69	1.709	11.7%	1012	119	11455	417	0.1	0.2	100	4	118	3	583	26
2	C:\HPCHEM\1\DATA\030305\MR05A92.D	0.1565	4.6%	937	43	0.0488	3.9%	962	38	0.075	4.8%	1069	51	1.469	7.3%	918	67	11716	327	0.2	0.2	96	3	86	5	555	22
3	C:\HPCHEM\1\DATA\030305\MR05A93.D	0.1365	4.7%	825	39	0.0386	3.2%	766	24	0.329	29.4%	3611	1061	4.823	83.7%	1789	1497	11688	366	0.3	0.2	104	20	195	12	558	19
4	C:\HPCHEM\1\DATA\030305\MR05A94.D	0.2196	4.4%	1280	56	0.0572	2.1%	1124	24	0.087	3.6%	1361	49	2.498	7.6%	1271	96	8409	264	0.6	0.2	126	4	412	13	430	15
5	C:\HPCHEM\1\DATA\030305\MR05A95.D	0.2341	5.0%	1356	67	0.0910	6.3%	1760	111	0.134	3.9%	2153	83	4.130	10.8%	1660	180	10190	308	-0.1	0.2	165	10	442	14	440	16
6	C:\HPCHEM\1\DATA\030305\MR05A96.D	0.2770	4.7%	1576	73	0.0806	2.4%	1566	38	0.111	2.5%	1820	46	4.018	7.3%	1638	119	12021	323	0.1	0.2	70	2	141	4	190	7
7	C:\HPCHEM\1\DATA\030305\MR05A97.D	0.1424	5.2%	858	44	0.0427	7.0%	846	59	0.100	9.1%	1616	147	0.814	12.9%	605	78	7227	209	-0.3	0.2	7	0	22	1	42	2
8	C:\HPCHEM\1\DATA\030305\MR05A98.D	0.1548	4.0%	928	37	0.1012	2.3%	1949	44	0.176	1.0%	2613	27	3.247	4.7%	1469	69	10820	315	0.0	0.2	283	9	462	20	1207	35
9	C:\HPCHEM\1\DATA\030305\MR05A99.D	0.1313	4.2%	795	33	0.0401	2.6%	794	20	0.090	3.3%	1420	47	1.505	6.2%	932	58	11811	322	0.3	0.2	122	4	262	11	771	34
10	C:\HPCHEM\1\DATA\030305\MR05A100.D	0.2601	4.8%	1490	71	0.0747	2.8%	1456	41	0.103	4.3%	1672	71	2.942	7.2%	1393	101	9316	296	0.1	0.2	35	1	119	4	89	3
11	C:\HPCHEM\1\DATA\030305\MR05A101.D	0.1067	4.2%	653	28	0.0290	2.7%	578	15	0.103	2.7%	1681	46	1.457	8.7%	913	79	9707	346	0.4	0.2	122	5	1036	46	784	36
12	C:\HPCHEM\1\DATA\030305\MR05A102.D	0.3699	4.2%	2029	86	0.1086	2.8%	2084	59	0.199	1.4%	2815	39	8.501	5.5%	2286	127	7831	210	0.1	0.2	375	12	829	30	634	25
1	C:\HPCHEM\1\DATA\030305\MR05A109.D	0.1609	4.1%	962	39	0.0538	2.3%	1058	24	0.109	2.5%	1775	44	2.147	5.4%	1164	63	9935	283	0.1	0.2	135	5	499	26	611	33
2	C:\HPCHEM\1\DATA\030305\MR05A110.D	0.2748	4.0%	1565	63	0.0670	4.5%	1310	58	0.133	1.3%	2135	28	4.661	6.4%	1760	113	11179	291	0.2	0.2	184	5	174	15	525	16
3	C:\HPCHEM\1\DATA\030305\MR05A111.D	0.1622	3.5%	969	34	0.0499	2.2%	984	21	0.075	4.4%	1081	48	1.604	7.6%	972	74	9023	230	0.0	0.2	109	3	284	8	477	14
4	C:\HPCHEM\1\DATA\030305\MR05A112.D	0.2775	3.8%	1579	60	0.0992	2.3%	1911	43	0.135	1.6%	2167	35	5.001	6.1%	1819	111	11782	328	0.0	0.2	160	5	92	3	450	25
5	C:\HPCHEM\1\DATA\030305\MR05A113.D	0.1653	6.6%	986	65	0.0432	6.0%	855	51	0.090	6.7%	1417	94	1.633	8.5%	983	84	11141	360	0.6	0.2	29	2	45	1	163	19
6	C:\HPCHEM\1\DATA\030305\MR05A114.D	0.1945	4.2%	1146	48	0.0640	1.9%	1254	24	0.106	2.5%	1726	44	2.696	6.6%	1327	87	8920	235	0.4	0.2	150	4	421	12	531	18
7	C:\HPCHEM\1\DATA\030305\MR05A115.D	0.1724	2.6%	1025	27	0.0491	2.1%	970	20	0.123	1.9%	1995	38	2.904	5.1%	1383	70	10672	178	0.2	0.2	117	3	645	23	390	15
8	C:\HPCHEM\1\DATA\030305\MR05A116.D	0.1655	4.7%	987	46	0.0559	2.5%	1099	27	0.096	4.1%	1547	64	2.105	7.2%	1150	83	10467	204	-0.3	0.2	54	2	195	5	209	8
9	C:\HPCHEM\1\DATA\030305\MR05A117.D	0.3987	3.4%	2163	73	0.1082	1.5%	2076	32	0.180	1.1%	2648	28	10.233	6.4%	2456	158	8969	222	0.2	0.2	213	6	298	7	341	12
10	C:\HPCHEM\1\DATA\030305\MR05A118.D	0.2150	5.0%	1256	63	0.0556	2.3%	1093	25	0.091	3.6%	1445	52	2.386	7.9%	1238	98	10677	338	0.4	0.2	150	5	404	13	533	18
11	C:\HPCHEM\1\DATA\030305\MR05A119.D	0.1652	5.3%	985	53	0.0429	2.5%	849	22	0.080	6.0%	1188	72	1.484	8.1%	924	75	7636	258	0.3	0.2	76	3	376	12	337	11
12	C:\HPCHEM\1\DATA\030305\MR05A120.D	0.1934	5.0%	1140	57	0.0294	4.3%	586	25	0.102	3.7%	1652	62	2.478	10.6%	1266	134	10633	331	0.0	0.2	58	2	301	22	248	12
1	C:\HPCHEM\1\DATA\030305\MR05A125.D	0.4454	4.9%	2375	116	0.0994	2.5%	1915	47	0.177	1.3%	2623	34	11.102	7.8%	2532	198	10049	267	0.6	0.2	245	7	192	9	429	16
2	C:\HPCHEM\1\DATA\030305\MR05A126.D	0.4840	4.3%	2545	109	0.1199	2.2%	2288	51	0.171	1.5%	2569	39	11.716	7.2%	2582	187	11176	286	0.2	0.2	107	3	111	3	155	5
3	C:\HPCHEM\1\DATA\030305\MR05A127.D	0.1785	6.3%	1059	66	0.0655	11.1%	1283	142	0.101	7.2%	1649	118	2.336	14.7%	1223	180	10890	444	0.1	0.2	74	3	171	7	365	16
4	C:\HPCHEM\1\DATA\030305\MR05A128.D	0.1820	5.1%	1078	55	0.0566	3.1%	1112	34	0.081	4.3%	1233	53	1.790	6.7%	1042	70	12515	382	0.0	0.2	143	5	135	9	674	20
5	C:\HPCHEM\1\DATA\030305\MR05A129.D	0.1786	5.5%	1059	58	0.1924	3.4%	3557	121	0.148	2.8%	2320	66	2.882	5.4%	1377	75	11794	363	0.4	0.2	221	10	119	9	1011	51
6	C:\HPCHEM\1\DATA\030305\MR05A130.D	0.1335	4.4%	808	36	0.0444	2.1%	878	18	0.135	2.1%	2158	46	2.456	8.5%	1259	107	10245	311	0.2	0.2	102	3	535	20	479	16
7	C:\HPCHEM\1\DATA\030305\MR05A131.D	0.4177	7.0%	2250	159	0.0918	3.7%	1774	66	0.125	3.5%	2024	70	6.188	9.5%	2003	190	11623	529	0.3	0.2	102	5	69	4	252	12
8	C:\HPCHEM\1\DATA\030305\MR05A132.D	0.3456	6.0%	1913	114	0.0838	2.4%	1627	39	0.116	4.8%	1895	92	3.766	10.7%	1586	169	9145	317	0.7	0.2	49	3	130	7	99	8
9	C:\HPCHEM\1\DATA\030305\MR05A133.D	0.4891	6.1%	2567	156	0.1185	2.7%	2264	62	0.166	2.3%	2513	59	10.033	7.7%	2438	188	10316	381	0.2	0.2	95	4	107	4	148	5
10	C:\HPCHEM\1\DATA\030305\MR05A134.D	0.2211	5.7%	1288	73	0.0588	2.2%	1156	25	0.089	3.9%	1398	55	2.404	7.6%	1244	94	8175	277	0.1	0.2	102	4	493	24	312	15
11	C:\HPCHEM\1\DATA\030305\MR05A135.D	0.3312	7.0%	1844	129	0.0785	3.1%	1528	48	0.115	3.6%	1880	67	4.425	9.1%	1717	157	9461	393	0.3	0.2	72	3	125	6	195	8
12	C:\HPCHEM\1\DATA\030305\MR05A136.D	0.3311	4.2%	1844	78	0.0971	2.2%	1872	42	0.129	2.3%	2082	48	6.103	8.1%	1991	162	9365	242	0.4	0.2	88	3	117	3	187	5
1	C:\HPCHEM\1\DATA\030311\MR11A12.D	0.1422	2.9%	857	23.3	0.0357	2.6%	709	18	0.064	4.8%	736	101	1.421	5.4%	898	33	8933	421	-0.1	-0.1	52	3	177	9	285	16
2	C:\HPCHEM\1\DATA\030311\MR11A13.D	0.1691	1.6%	1007	14.8	0.0502	2.6%	990	25	0.084	2.3%	1293	46	2.135	2.7%	1160	19	10704	486	-0.1	-0.1	135	6	92	4	689	35
3	C:\HPCHEM\1\DATA\030311\MR11A14.D	0.1668	2.4%	994	21.7	0.0458	3.1%	905	27	0.077	4.1%	1126	82	1.854	4.4%	1065	30	9246	404	-0.1	-0.2	53	3	189	9	282	17
4	C:\HPCHEM\1\DATA\030311\MR11A15.D	0.1562	4.7%	935	40.9	0.0581	5.1%	1142	57	0.165	3.7%	2512	63	4.012	6.9%	1637	57	9613	478	-0.3	-0.2	233	13	988	53	869	44
5	C:\HPCHEM\1\DATA\030311\MR11A16.D	0.1830	4.4%	1083	43.8	0.0414	1.9%	819	16	0.076	3.5%	1106	71	2.103	4.6%	1150	32	7322	374	0.2	0.1	97	5	373	20	431	26
6	C:\HPCHEM\1\DATA\030311\MR11A17.D	0.1585	4.8%	949	42.8	0.0360	2.4%	715	17	0.065	4.7%	782	98	1.562	5.9%	955	37	9626	490	0.2	0.1	35	2	152	8	180	11
7	C:\HPCHEM\1\DATA\030311\MR11A18.D	0.1195	3.7%	728	25.3	0.0158	2.4%	317	7	0.096	2.6%	1545	49	1.713	3.9%	1014	25	11929	600	-0.1	-0.1	145	8	686	36	991	50
8	C:\HPCHEM\1\DATA\030311\MR11A19.D	0.2044	6.9%	1199	75.5	0.0360	2.8%	715	20	0.088	4.1%	1390	79	2.561	6.5%	1290	49	8330	510	0.1	0.1	157	10	636	41	832	56
9	C:\HPCHEM\1\DATA\030311\MR11A20.D	0.1843	6.3%	1090	63.7	0.0442	7.2%	875	62	0.073	11.2%	1011	227	1.946	10.8%	1097	75	8732	426	-0.1	-0.1	10	1	37	2	47	3
10	C:\HPCHEM\1\DATA\030311\MR11A21.D	0.2336	3.7%	1354	45.9	0.0301	2.3%	599	14	0.177	2.6%	2627	43	6.268	4.0%	2014	35	12694	617	0.4	0.1	386	20	1189	61	1202	68
11	C:\HPCHEM\1\DATA\030311\MR11A22.D	0.1064	4.4%	652	27.6	0.0512	2.9%	1009	28	0.125	4.1%	2031	73	1.760	4.1%	1031	27	11005	539	0.3	0.1	99	6	363	20	798	71
12	C:\HPCHEM\1\DATA\030311\MR11A23.D	0.4551	4.0%	2418	81.2	0.1016	2.3%	1956	43	0.148	2.8%	2318	47	10.589	4.7%	2488	44	7878	403	0.2	0.1	92	5	87	5	172	15

Shaded samples not used.

APPENDIX 2.
STABLE ISOTOPE DATA

Sample No	Hole No	From	To	Strat	Type	Lithology	Condition	mineralogy	del13C	del18O	del18Opdb
630568a	WD19	66.8	66.9	Breccia	vein	na	fresh	calcite	-0.3	24.8	-5.9
630568b	WD19	66.8	66.9	10-Breccia	matrix	mg	weather	calcite	-1.1	25.0	-5.7
630568c	WD19	66.8	66.9	10-Breccia	clasts	fg	altered	calcite	-1.0	23.1	-7.5
630574a	WD19	160.3	160.4	10-Breccia	clasts	fg	altered	dolomite	2.2	14.5	-15.9
630574b	WD19	160.3	160.4	10-Breccia	matrix	na	weather	dolomite	2.4	7.8	-22.4
630574c	WD19	160.3	160.4	10-Breccia	matrix	na	fresh	dolomite	1.6	13.8	-16.5
1062				10-Breccia	matrix	na	fresh	calcite	-5.0	22.9	-7.8
OGD1				10-Breccia	clasts	fg	fresh	dolomite	5.3	20.7	-9.8
OGD2				10-Breccia	clasts	fg	fresh	dolomite	6.5	21.7	-8.9
485b				1-Bungarider	Strat	sst	fresh	dolomite	3.5	20.5	-10.0
630566	WD19	51	51.2	2-Burra Gp	matrix	mg	weather	calcite	-0.9	20.9	-9.7
630576	WD19	176	176.1	2-Burra Gp	matrix	cg	fresh	dolomite and calc	1.4	-0.4	-30.3
630581a	WD19	196.3	196.4	2-Burra Gp	Strat	cg	fresh	dolomite	2.1	17.9	-12.6
630581b	WD19	196.3	196.4	2-Burra Gp	Strat	fg	fresh	dolomite	0.3	20.8	-9.8
630582	WD19	206.8	206.9	2-Burra Gp	matrix	na	fresh	dolomite	1.2	-0.7	-30.7
630585a	WD19	228.7	228.8	2-Burra Gp	nodule	na	fresh	dolomite	0.0	14.2	-16.2
630585b	WD19	228.7	228.8	2-Burra Gp	Strat	sst	altered	dolomite	-1.4	18.8	-11.7
630586a	WD19	260.7	260.8	2-Burra Gp	Strat	fg	fresh	dolomite	-0.6	16.7	-13.7
630586b	WD19	260.7	260.8	2-Burra Gp	diagenetic	na	altered	dolomite	-3.8	24.0	-6.6
630508	WD31	47.5	47.6	3-Boorloo Siltstone	vein	na	fresh	dolomite	-9.0	11.3	-19.0
630525	WD31	131.1	131.2	3-Boorloo Siltstone	vein	na	fresh	dolomite	-10.7	16.3	-14.1
630527	WD23	19.2	19.3	3-Boorloo Siltstone	Strat	fg	fresh	dolomite	-0.5	18.0	-12.5
630528	WD23	26.8	26.9	3-Boorloo Siltstone	Strat	fg	fresh	dolomite	-0.9	18.4	-12.1
630529	WD23	28.7	28.8	3-Boorloo Siltstone	Strat	mg	fresh	dolomite	-1.6	19.4	-11.2
630530	WD23	36.45	36.6	3-Boorloo Siltstone	Strat	mg	fresh	dolomite	-1.6	18.0	-12.4
630532	WD23	45.7	45.9	3-Boorloo Siltstone	Strat	sst	fresh	dolomite	-4.6	17.0	-13.4
630535	WD23	72.1	72.3	3-Boorloo Siltstone	Strat	fg	fresh	dolomite	-4.2	17.5	-13.0
630536	WD23	73.1	73.3	3-Boorloo Siltstone	Strat	fg	fresh	dolomite	-4.7	17.4	-13.1
630551	WD23	144.8	144.9	3-Boorloo Siltstone	Strat	sst	fresh	calcitic siltstone	-12.0	17.2	-13.3
630556	WD23	212.1	212.2	3-Boorloo Siltstone	vein	na	fresh	dolomite	-7.3	16.6	-13.9
630557	WD23	216.7	216.8	3-Boorloo Siltstone	vein	na	fresh	dolomite and calc	-8.3	17.9	-12.6
630559	WD23	236.6	236.7	3-Boorloo Siltstone	vein	na	fresh	dolomite	-11.5	17.5	-13.0
630518g	WD31	132.2	132.3	3-Boorloo Siltstone	Strat	sst	fresh	dolomite	-12.4	16.3	-14.1
630518n	WD31	132.2	132.3	3-Boorloo Siltstone	diagenetic	na	fresh	dolomite	-12.1	15.2	-15.2
630531g	WD23	37.4	37.6	3-Boorloo Siltstone	Strat	fg	fresh	dolomite	-2.1	17.9	-12.6

Sample No	Hole No	From	To	Strat	Type	Lithology	Condition	mineralogy	del13C	del18O	del18Opdb
630531v	WD23	37.4	37.6	3-Boorloo Siltstone	vein	na	fresh	dolomite	-2.3	17.9	-12.6
630534g	WD23	58.2	58.4	3-Boorloo Siltstone	Strat	sst	fresh	dolomite	-7.4	16.9	-13.5
630534v	WD23	58.2	58.4	3-Boorloo Siltstone	vein	na	fresh	dolomite			-29.9
733n				3-Boorloo Siltstone	diagenetic	na	fresh	calcite	-6.0	4.6	-25.4
BSD1				3-Boorloo Siltstone	Strat	sst	fresh	calcite	-8.0	19.7	-10.9
BSD10b				3-Boorloo Siltstone	Strat	mg	fresh	dolomite	0.3	19.6	-10.9
BSD10m				3-Boorloo Siltstone	Strat	fg	fresh	dolomite	0.1	19.0	-11.5
BSD10t				3-Boorloo Siltstone	Strat	mg	fresh	calcite	0.3	19.8	-10.7
BSD12m				3-Boorloo Siltstone	Strat	mg	fresh	calcite	1.1	20.4	-10.1
BSD12t				3-Boorloo Siltstone	Strat	fg	fresh	dolomite	1.5	18.6	-11.9
BSD2				3-Boorloo Siltstone	Strat	fg	fresh	calcite	-6.5	19.4	-11.2
BSD3				3-Boorloo Siltstone	Strat	fg	fresh	calcite	-6.0	20.8	-9.8
BSD4				3-Boorloo Siltstone	Strat	fg	fresh	dolomite	-4.8	18.4	-12.1
BSD5m				3-Boorloo Siltstone	Strat	sst	fresh	dolomite	-4.4	18.2	-12.3
BSD5t				3-Boorloo Siltstone	Strat	fg	fresh	dolomite	-4.3	18.0	-12.5
BSD6m				3-Boorloo Siltstone	Strat	fg	fresh	dolomite and calc	-3.9	18.9	-11.6
BSD6t				3-Boorloo Siltstone	Strat	sst	fresh	calcite	-3.8	19.0	-11.5
BSD7m				3-Boorloo Siltstone	Strat	fg	fresh	dolomite	-1.5	18.6	-11.9
BSD7t				3-Boorloo Siltstone	Strat	fg	fresh	dolomite	-1.7	19.4	-11.1
BSD8b				3-Boorloo Siltstone	Strat	fg	fresh	dolomite	-1.9	19.0	-11.5
BSD8t				3-Boorloo Siltstone	Strat	fg	fresh	dolomite	-0.9	18.8	-11.7
BSD9b				3-Boorloo Siltstone	Strat	fg	weather	calcite	-2.6	26.6	-4.1
CFL1				4-Cooranna Formation	weathering	na	weather	calcite	-4.4	26.3	-4.4
1332				4-Cooranna Formation	Strat	sst	weather	calcite	-4.7	22.8	-7.8
1525				4-Cooranna Formation	Strat	sst	fresh	calcite	-8.5	18.3	-12.2
819				4-Cooranna Formation	Strat	sst	fresh	dolomite	-7.7	18.8	-11.7
824				4-Cooranna Formation	Strat	fg	fresh	dolomite	-11.1	17.0	-13.5
1509a				5-Hogan Dolomite	Strat	fg	fresh	calcite	-6.2	20.3	-10.2
570b				5-Hogan Dolomite	diagenetic	na	fresh	dolomite	-9.2	18.8	-11.7
REG6				5-Hogan Dolomite	Strat	sst	fresh	dolomite and calc	-4.0	20.9	-9.6
REG7				5-Hogan Dolomite	Strat	sst	fresh	dolomite	-2.1	20.3	-10.2
RFM1				6-Recovery Formation	clasts	fg	fresh	dolomite	-2.0	15.6	-14.8
RFM2				6-Recovery Formation	clasts	fg	fresh	dolomite	-2.1	15.6	-14.8
REG1				6-Recovery Formation	vein	na	fresh	calcite	-4.8	19.7	-10.8
REG2				6-Recovery Formation	vein	na	fresh	dolomite	-3.9	16.3	-14.2

Sample No	Hole No	From	To	Strat	Type	Lithology	Condition	mineralogy	del13C	del18O	del18Opdb
REG4g				6-Recovery Formation	Strat	fg	fresh	calcite	-4.7	22.8	-7.8
REG4v				6-Recovery Formation	diagenetic	na	fresh	calcite	-3.0	18.5	-12.0
REG5				6-Recovery Formation	Strat	cg	fresh	calcite	-4.5	25.2	-5.5
630699	WD34	17.6	17.8	7-Dunns Mine Limestone	Strat	cg	fresh	calcite	-2.0	20.4	-10.2
630702	WD34	79.1	79.2	7-Dunns Mine Limestone	Strat	fg	fresh	calcite	-3.9	15.0	-15.4
630718	WD5	69.5	69.7	7-Dunns Mine Limestone	Strat	mg	fresh	calcite	-3.1	16.9	-13.5
630720	WD5	71.2	71.4	7-Dunns Mine Limestone	Strat	cg	fresh	calcite	-2.7	16.9	-13.5
630721	WD5	73.4	73.6	7-Dunns Mine Limestone	Strat	mg	fresh	calcite	-2.7	19.7	-10.8
630724	WD5	86.8	87	7-Dunns Mine Limestone	Strat	cg	fresh	calcite	-3.2	17.4	-13.1
630726	WD5	99.5	99.6	7-Dunns Mine Limestone	Strat	mg	fresh	calcite	-2.7	16.5	-13.9
630728	WD5	103.8	104	7-Dunns Mine Limestone	Strat	cg	altered	calcite	-2.5	14.1	-16.3
630730	WD5	119.5	119.6	7-Dunns Mine Limestone	Strat	cg	altered	calcite	-1.4	17.8	-12.7
630732	WD6	157.2	157.3	7-Dunns Mine Limestone	vein	na	fresh	calcite	-3.4	7.6	-22.6
630738	WD16	23.1	23.2	7-Dunns Mine Limestone	Strat	cg	fresh	calcite	-3.1	17.3	-13.2
630741	WD16	68.4	68.6	7-Dunns Mine Limestone	Strat	mg	fresh	calcite	-3.0	14.7	-15.7
630743	WD16	116.2	116.3	7-Dunns Mine Limestone	Strat	fg	fresh	calcite	-2.3	14.1	-16.3
631129	WD16	163.7	163.8	7-Dunns Mine Limestone	Strat	fg	altered	dolomite	-3.1	16.9	-13.5
631131a	WD16	169.7	169.8	7-Dunns Mine Limestone	Strat	sst	fresh	dolomitic siltstone	-2.5	18.9	-11.6
631132	WD16	174.1	174.2	7-Dunns Mine Limestone	vein	na	fresh	calcite	-0.2	16.2	-14.2
631136	WD21	119.8	119.9	7-Dunns Mine Limestone	vein	na	fresh	dolomite	-2.6	21.1	-9.5
630722a	WD5	80.6	80.7	7-Dunns Mine Limestone	Strat	cg	fresh	calcite	-3.2	16.5	-13.9
630722b	WD5	80.6	80.7	7-Dunns Mine Limestone	Strat	sst	fresh	calcitic siltstone	-6.2	17.8	-12.7
630729a	WD5	117.4	117.6	7-Dunns Mine Limestone	clasts	fg	altered	dolomite and calc	-2.6	14.3	-16.1
630729b	WD5	117.4	117.6	7-Dunns Mine Limestone	matrix	na	fresh	calcite	-5.1	21.2	-9.3
630731a	WD5	138	138.2	7-Dunns Mine Limestone	clasts	fg	altered	dolomite	-1.7	15.0	-15.4
630731b	WD5	138	138.2	7-Dunns Mine Limestone	matrix	na	altered	dolomite	-1.7	13.4	-16.9
630740a	WD16	51.2	51.3	7-Dunns Mine Limestone	Strat	mg	fresh	calcite	-3.2	16.0	-14.4
630740b	WD16	51.2	51.3	7-Dunns Mine Limestone	Strat	sst	fresh	calcite	-2.7	16.1	-14.3
630746a	WD16	159	159.2	7-Dunns Mine Limestone	Strat	fg	fresh	dolomite	-3.8	18.3	-12.2
630746b	WD16	159	159.2	7-Dunns Mine Limestone	nodule	na	fresh	dolomite	-3.1	16.2	-14.2
630700a	WD34	29.1	29.25	7-Dunns Mine Limestone	nodule	na	fresh	calcite	-2.3	18.4	-12.1
630700b	WD34	29.1	29.25	7-Dunns Mine Limestone	Strat	cg	fresh	calcite	-2.4	18.2	-12.2
630723a	WD5	82.3	82.7	7-Dunns Mine Limestone	Strat	cg	fresh	calcite	-3.1	20.4	-10.1
630723b	WD5	82.3	82.7	7-Dunns Mine Limestone	Strat	sst	fresh	calcitic siltstone	-2.9	18.9	-11.6
630723c	WD5	82.3	82.7	7-Dunns Mine Limestone	Strat	cg	fresh	calcite	-3.2	21.0	-9.6

Sample No	Hole No	From	To	Strat	Type	Lithology	Condition	mineralogy	del13C	del18O	del18Opdb
630723d	WD5	82.3	82.7	7-Dunns Mine Limestone	Strat	sst	fresh	calcitic siltstone	-2.8	19.3	-11.2
631131b	WD16	169.7	169.8	7-Dunns Mine Limestone	diagenetic	na	fresh	dolomite and calc	-3.6	18.7	-11.8
1353a				7-Dunns Mine Limestone	Alteration	fg	altered	dolomite and calc	-1.4	19.7	-10.8
1353b				7-Dunns Mine Limestone	Alteration	mg	weather	calcite	-2.6	28.0	-2.8
1353c				7-Dunns Mine Limestone	Alteration	sst	weather	dolomite	-4.4	28.1	-2.6
1353d				7-Dunns Mine Limestone	Alteration	mg	altered	dolomite	-1.3	17.1	-13.4
1353e				7-Dunns Mine Limestone	Alteration	sst	weather	calcite	-2.0	27.0	-3.8
DM3				7-Dunns Mine Limestone	vein	na	fresh	calcite	-1.6	12.1	-18.2
DM4				7-Dunns Mine Limestone	vein	na	fresh	dolomite	-0.4	16.4	-14.0
DM6f				7-Dunns Mine Limestone	vein	na	fresh	dolomite	-2.4	16.6	-13.8
DM6w				7-Dunns Mine Limestone	vein	na	weather	calcite	-2.1	28.7	-2.1
630704b	WD34	141.1	141.3	8-Dome Sandstone	matrix	na	fresh	dolomite	-0.2	14.3	-16.1
630704c	WD34	141.1	141.3	8-Dome Sandstone	clasts	na	weather	calcite	-2.3	19.4	-11.1
1675				8-Dome Sandstone	Strat	sst	altered	dolomite	2.3	22.5	-8.1
DomeC1				8-Dome Sandstone	Strat	fg	fresh	calcitic siltstone	1.4	17.1	-13.3
MY902				8-Dome Sandstone	diagenetic	na	fresh	dolomite	0.2	17.7	-12.8
1612				9-Black Knob Marble	Strat	fg	fresh	calcite	1.8	8.6	-21.6
BKC1				9-Black Knob Marble	Strat	fg	fresh	calcite	2.2	21.7	-8.9
BKC2g				9-Black Knob Marble	Strat	fg	fresh	calcite	-8.7	21.9	-8.7
BKC2v				9-Black Knob Marble	Strat	na	fresh	calcite	-12.6	17.8	-12.6

APPENDIX 3.
MONAZITE GEOCHRONOLOGY DATA

Sample DS2	Calculated Age							
Sample Name	Pb ppm	Th ppm	U ppm	Th 1σ	U 1σ	Pb 1σ	**age Ma**	**1σ**
DS2_monA-1	0.050	1.783	0.047	259	59	95	**576**	**107**
DS2_monA-2	0.045	1.564	0.046	246	61	94	**588**	**120**
DS2_monB-1	0.071	3.608	0.035	340	43	97	**425**	**57**
DS2_monB-3	0.082	3.459	0.039	332	45	97	**506**	**59**
DS2_monB-4	0.014	0.499	0.030	186	69	93	**529**	**340**
DS2_monB-2	0.016	0.097	0.033	154	75	92	**1624**	**835**
DS2_monC-2	0.088	5.135	0.042	393	40	97	**372**	**41**
DS2_monC-1	0.141	7.696	0.061	467	40	99	**399**	**28**
DS2_monC-5	0.021	0.696	0.058	199	71	93	**521**	**231**
DS2_monC-7	0.027	0.715	0.046	199	70	94	**677**	**236**
DS2_monC-4	0.020	0.509	0.027	184	67	93	**725**	**337**
DS2_monC-3	0.042	0.957	0.031	212	62	94	**866**	**191**
DS2_monC-6	0.018	0.193	0.028	161	73	92	**1329**	**658**
DS2_monD-3	0.002	0.079	0.023	153	75	86	**291**	**1230**
DS2_monD-1	0.021	0.483	0.037	182	70	93	**756**	**333**
DS2_monD-2	0.018	0.363	0.047	173	73	92	**757**	**381**
DS2_monE-3	0.011	0.648	0.004	195	34	95	**371**	**317**
DS2_monE-5	0.037	1.244	0.039	230	62	95	**595**	**152**
DS2_monE-2	0.037	1.027	0.052	214	67	94	**689**	**171**
DS2_monE-4	0.026	0.661	0.038	194	67	93	**721**	**256**
DS2_monE-1	0.029	0.531	0.034	185	69	94	**970**	**310**
DS2_monF-4	0.055	1.782	0.050	257	61	95	**624**	**107**
DS2_monF-3	0.036	0.867	0.043	208	66	94	**794**	**201**
DS2_monF-2	0.026	0.411	0.022	176	67	94	**1164**	**409**
DS2_monF-1	0.021	0.306	0.026	169	71	95	**1178**	**503**
DS2_monF-5	0.024	0.117	0.047	152	76	94	**1805**	**619**
DS2_monG-3	0.007	0.639	0.041	192	69	92	**216**	**266**
DS2_monG-1	0.023	0.395	0.041	176	72	94	**932**	**375**
DS2_monG-2	0.041	0.443	0.048	178	72	95	**1466**	**320**
DS2_monG-4	0.027	0.193	0.049	159	75	92	**1558**	**500**
DS2_monH-1	0.015	0.953	0.041	215	65	93	**309**	**189**
DS2_monH-2	0.019	0.869	0.046	209	68	93	**420**	**202**
DS2_monH-3	0.016	0.540	0.049	185	71	93	**497**	**292**
DS2_monH-4	0.011	0.424	0.024	178	67	93	**502**	**406**
DS2_monI-1	0.006	0.199	0.034	155	74	91	**455**	**643**
DS2_monI-2	0.023	0.501	0.036	185	70	94	**817**	**324**
DS2_monI-3	0.011	0.085	0.014	151	73	93	**1665**	**1360**
DS2_monJ-1	0.023	0.575	0.040	187	70	94	**709**	**288**
DS2_monJ-2	0.026	0.601	0.030	187	67	93	**821**	**287**
DS2_monJ-3	0.030	0.301	0.022	167	69	94	**1720**	**508**
DS2_monK-5	0.089	4.680	0.048	376	44	97	**413**	**44**
DS2_monK-6	0.113	5.880	0.050	416	40	99	**415**	**36**
DS2_monK-4	0.050	2.210	0.037	280	52	97	**480**	**91**
DS2_monK-2	0.064	2.604	0.030	297	46	95	**528**	**78**
DS2_monK-1	0.051	2.055	0.023	272	44	96	**533**	**99**
DS2_monK-3	0.061	2.363	0.036	286	50	95	**548**	**84**
DS2_monK-7	0.024	0.659	0.016	194	57	94	**737**	**287**
DS2_monL-2	0.011	0.213	0.019	160	70	93	**840**	**714**
DS2_monL-1	0.019	0.395	0.016	174	63	94	**944**	**450**
DS2_monM-2	0.015	0.232	0.057	164	75	92	**763**	**467**
DS2_monM-1	0.045	0.833	0.034	205	65	95	**1052**	**214**
DS2_monN-3	0.004	0.689	0.028	195	65	91	**101**	**262**
DS2_monN-1	0.026	1.647	0.038	252	57	95	**327**	**119**
DS2_monN-4	0.015	0.495	0.023	184	65	93	**589**	**358**
DS2_monN-2	0.034	0.874	0.039	210	66	94	**754**	**203**
DS2_monO-1	0.019	0.668	0.051	195	71	94	**518**	**246**
DS2_monO-4	0.018	0.674	0.017	195	58	94	**536**	**283**
DS2_monO-2	0.026	0.513	0.034	182	69	94	**914**	**320**
DS2_monO-3	0.018	0.192	0.064	158	76	93	**973**	**472**
DS2_monP-1	0.056	1.702	0.040	256	58	95	**672**	**114**
DS2_monP-2	0.022	0.510	0.015	183	61	93	**857**	**360**

	Monazite Analyses																			
Sample Name	**Si**	**Al**	**Fe**	**Ca**	**Pb SP5/1**	**Y**	**Th**	**U**	**La**	**Ce**	**Pr**	**Nd**	**Sm**	**Gd**	**Dy**	**Er**	**P**	**O**	**Total**
DS2_monA-1	0.060	0.000	0.003	0.349	0.050	0.598	1.783	0.047	14.015	26.352	2.725	9.923	1.465	0.754	0.258	0.073	12.428	26.121	97.002
DS2_monA-2	0.063	0.006	0.025	0.285	0.045	0.553	1.564	0.046	14.020	26.485	2.794	9.995	1.529	0.755	0.215	0.029	12.532	26.247	97.186
DS2_monB-1	0.151	0.000	0.010	0.382	0.071	0.484	3.608	0.035	13.283	26.251	2.716	10.000	1.698	0.945	0.235	0.049	12.518	26.504	98.938
DS2_monB-3	0.077	0.001	0.013	0.493	0.082	0.303	3.459	0.039	13.863	25.869	2.613	9.614	1.686	0.914	0.146	0.038	12.575	26.403	98.186
DS2_monB-4	0.008	0.006	0.014	0.138	0.014	0.566	0.499	0.030	14.239	27.590	2.924	10.530	1.610	0.785	0.261	0.068	12.781	26.666	98.728
DS2_monB-2	0.006	0.000	0.006	0.089	0.016	0.425	0.097	0.033	14.835	28.231	2.865	9.985	1.465	0.666	0.165	0.076	12.729	26.533	98.220
DS2_monC-2	0.187	0.000	0.012	0.595	0.088	0.279	5.135	0.042	12.885	24.939	2.584	9.878	1.718	0.998	0.177	0.060	12.532	26.475	98.583
DS2_monC-1	0.238	0.000	0.020	1.009	0.141	0.371	7.696	0.061	12.135	23.371	2.521	9.218	1.711	1.001	0.199	0.102	12.393	26.396	98.581
DS2_monC-5	0.016	0.000	0.014	0.219	0.021	0.621	0.696	0.058	14.058	27.205	2.916	10.200	1.600	0.803	0.262	0.091	12.670	26.454	97.900
DS2_monC-7	0.020	0.000	0.007	0.240	0.027	0.653	0.715	0.046	13.981	27.211	2.803	10.319	1.599	0.867	0.292	0.059	12.980	26.874	98.690
DS2_monC-4	0.008	0.000	0.010	0.105	0.020	0.442	0.509	0.027	14.432	27.926	2.844	10.362	1.423	0.656	0.188	0.018	12.706	26.498	98.174
DS2_monC-3	0.025	0.000	0.015	0.177	0.042	0.550	0.957	0.031	13.885	27.175	2.879	10.493	1.585	0.786	0.269	0.025	12.614	26.386	97.892
DS2_monC-6	0.006	0.000	0.022	0.163	0.018	0.526	0.193	0.028	15.394	27.787	2.763	9.622	1.371	0.638	0.193	0.074	12.758	26.571	98.125
DS2_monD-3	0.000	0.001	0.011	0.154	0.002	0.311	0.079	0.023	16.572	28.430	2.685	8.762	1.132	0.530	0.173	0.077	12.864	26.720	98.524
DS2_monD-1	0.015	0.005	0.022	0.152	0.021	0.554	0.483	0.037	14.256	27.732	2.845	10.450	1.562	0.816	0.257	0.066	12.820	26.723	98.816
DS2_monD-2	0.004	0.000	0.028	0.195	0.018	0.466	0.363	0.047	14.704	27.875	2.806	10.003	1.347	0.722	0.127	0.060	12.740	26.534	98.039
DS2_monE-3	0.030	0.000	0.000	0.271	0.011	0.291	0.648	0.004	15.964	28.130	2.642	9.080	1.115	0.472	0.120	0.016	12.838	26.697	98.330
DS2_monE-5	0.032	0.002	0.009	0.294	0.037	0.626	1.244	0.039	13.749	27.017	2.838	10.344	1.555	0.867	0.279	0.075	12.782	26.652	98.440
DS2_monE-2	0.027	0.000	0.012	0.290	0.037	0.671	1.027	0.052	13.950	27.165	2.803	10.190	1.602	0.861	0.310	0.057	12.779	26.661	98.496
DS2_monE-4	0.045	0.003	0.023	0.240	0.026	0.284	0.661	0.038	16.563	28.070	2.653	8.669	1.074	0.466	0.119	0.053	12.718	26.586	98.291
DS2_monE-1	0.021	0.004	0.018	0.107	0.029	0.378	0.531	0.034	14.180	27.922	2.908	10.393	1.423	0.756	0.222	0.003	12.759	26.565	98.252
DS2_monF-4	0.054	0.003	0.011	0.367	0.055	0.742	1.782	0.050	12.567	25.734	2.869	10.530	1.668	0.953	0.315	0.164	12.666	26.328	96.857
DS2_monF-3	0.054	0.000	0.005	0.266	0.036	0.303	0.867	0.043	15.313	27.525	2.691	8.961	1.084	0.570	0.167	0.087	12.672	26.349	96.993
DS2_monF-2	0.025	0.000	0.012	0.237	0.026	0.289	0.411	0.022	15.562	27.667	2.597	9.194	1.139	0.587	0.162	0.063	12.549	26.176	96.718
DS2_monF-1	0.007	0.001	0.017	0.121	0.021	0.494	0.306	0.026	14.011	27.272	2.899	10.618	1.582	0.829	0.296	0.059	12.757	26.499	97.815
DS2_monF-5	0.000	0.003	0.082	0.174	0.024	0.665	0.117	0.047	13.885	26.787	2.859	10.530	1.625	0.892	0.317	0.071	12.721	26.405	97.204
DS2_monG-3	0.020	0.000	0.027	0.195	0.007	0.637	0.639	0.041	13.874	27.028	2.817	10.352	1.579	0.831	0.273	0.087	12.716	26.454	97.576
DS2_monG-1	0.007	0.010	0.016	0.218	0.023	0.538	0.395	0.041	14.470	27.315	2.796	10.123	1.536	0.828	0.222	0.079	12.744	26.527	97.888
DS2_monG-2	0.015	0.000	0.020	0.253	0.041	0.579	0.443	0.048	14.449	27.358	2.830	10.173	1.540	0.871	0.265	0.089	12.683	26.515	98.171
DS2_monG-4	0.008	0.000	0.014	0.160	0.027	0.601	0.193	0.049	14.180	27.476	2.854	10.619	1.638	0.846	0.293	0.120	12.603	26.409	98.089
DS2_monH-1	0.038	0.004	0.012	0.274	0.015	0.573	0.953	0.041	14.197	27.228	2.760	10.075	1.526	0.830	0.254	0.053	12.783	26.637	98.254
DS2_monH-2	0.030	0.000	0.003	0.228	0.019	0.650	0.869	0.046	13.798	27.260	2.828	10.378	1.664	0.856	0.258	0.027	12.671	26.491	98.077
DS2_monH-3	0.004	0.000	0.004	0.260	0.016	0.652	0.540	0.049	14.384	27.157	2.756	10.257	1.507	0.885	0.247	0.124	12.653	26.450	97.944
DS2_monH-4	0.014	0.000	0.011	0.162	0.011	0.475	0.424	0.024	14.539	27.773	2.819	10.028	1.541	0.680	0.221	0.047	12.849	26.673	98.291
DS2_monI-1	0.010	0.004	0.027	0.085	0.006	0.505	0.199	0.034	14.048	27.844	2.813	10.446	1.554	0.730	0.253	0.087	12.726	26.480	97.850
DS2_monI-2	0.021	0.002	0.024	0.173	0.023	0.628	0.501	0.036	14.024	27.442	2.884	10.467	1.603	0.858	0.279	0.067	12.686	26.522	98.240
DS2_monI-3	0.002	0.000	0.027	0.060	0.011	0.387	0.085	0.014	14.892	28.436	2.847	9.921	1.393	0.664	0.196	0.100	12.745	26.556	98.336
DS2_monJ-1	0.025	0.000	0.010	0.170	0.023	0.487	0.575	0.040	14.384	27.486	2.878	10.034	1.405	0.705	0.216	0.109	12.650	26.383	97.579
DS2_monJ-2	0.013	0.001	0.010	0.152	0.026	0.528	0.601	0.030	14.305	27.729	2.860	10.186	1.557	0.689	0.168	0.000	12.634	26.405	97.892
DS2_monJ-3	0.010	0.000	0.014	0.111	0.030	0.352	0.301	0.022	15.530	28.366	2.782	9.499	1.262	0.590	0.139	0.000	12.748	26.570	98.324
DS2_monK-5	0.106	0.000	0.019	0.657	0.089	0.330	4.680	0.048	12.964	25.125	2.584	9.616	1.638	0.950	0.210	0.054	12.579	26.409	98.058
DS2_monK-6	0.133	0.007	0.022	0.833	0.113	0.306	5.880	0.050	13.070	24.165	2.505	9.120	1.667	0.909	0.210	0.074	12.671	26.554	98.285
DS2_monK-4	0.118	0.000	0.015	0.249	0.050	0.386	2.210	0.037	13.659	26.804	2.777	9.926	1.504	0.796	0.197	0.069	12.560	26.350	97.706
DS2_monK-2	0.051	0.002	0.021	0.392	0.064	0.240	2.604	0.030	14.438	26.490	2.607	9.629	1.574	0.925	0.170	0.040	12.771	26.646	98.692
DS2_monK-1	0.039	0.000	0.025	0.292	0.051	0.274	2.055	0.023	14.482	27.070	2.692	9.766	1.584	0.887	0.177	0.052	12.623	26.477	98.568
DS2_monK-3	0.080	0.000	0.006	0.290	0.061	0.289	2.363	0.036	13.131	26.374	2.770	10.518	1.824	1.027	0.196	0.057	12.613	26.401	98.035
DS2_monK-7	0.022	0.000	0.015	0.221	0.024	0.348	0.659	0.016	16.176	28.056	2.633	8.895	1.104	0.521	0.157	0.076	12.698	26.522	98.142
DS2_monL-2	0.011	0.000	0.002	0.164	0.011	0.281	0.213	0.019	16.449	28.066	2.620	8.629	1.055	0.519	0.137	0.044	12.495	26.128	96.845
DS2_monL-1	0.027	0.000	0.008	0.211	0.019	0.296	0.395	0.016	16.215	27.739	2.593	8.776	0.994	0.548	0.125	0.062	12.461	26.070	96.557
DS2_monM-2	0.000	0.000	0.018	0.216	0.015	0.666	0.232	0.057	13.892	27.464	2.855	10.281	1.647	0.880	0.291	0.085	12.703	26.469	97.770
DS2_monM-1	0.017	0.000	0.013	0.265	0.045	0.682	0.833	0.034	13.852	27.266	2.812	10.320	1.706	0.829	0.274	0.107	12.725	26.581	98.363
DS2_monN-3	0.017	0.000	0.025	0.187	0.004	0.551	0.689	0.028	14.261	27.390	2.834	10.313	1.548	0.801	0.266	0.035	12.734	26.560	98.242
DS2_monN-1	0.050	0.000	0.020	0.316	0.026	0.667	1.647	0.038	13.508	26.657	2.808	10.146	1.592	0.903	0.309	0.078	12.581	26.364	97.709
DS2_monN-4	0.015	0.000	0.024	0.130	0.015	0.414	0.495	0.023	14.859	27.983	2.787	9.928	1.369	0.692	0.217	0.050	12.787	26.622	98.409
DS2_monN-2	0.024	0.000	0.022	0.217	0.034	0.635	0.874	0.039	13.809	26.978	2.835	10.238	1.598	0.866	0.242	0.119	12.832	26.623	97.985
DS2_monO-1	0.021	0.000	0.016	0.276	0.019	0.666	0.668	0.051	13.772	27.091	2.755	10.195	1.615	0.880	0.271	0.076	12.643	26.373	97.387
DS2_monO-4	0.020	0.007	0.007	0.315	0.018	0.672	0.674	0.017	14.118	26.841	2.768	10.086	1.571	0.819	0.210	0.050	12.694	26.427	97.314
DS2_monO-2	0.022	0.000	0.019	0.312	0.026	0.564	0.513	0.034	14.241	27.502	2.793	10.154	1.579	0.770	0.253	0.084	12.614	26.429	97.911
DS2_monO-3	0.005	0.000	0.010	0.211	0.018	0.747	0.192	0.064	13.862	27.018	2.803	10.505	1.659	0.882	0.257	0.076	12.653	26.367	97.329
DS2_monP-1	0.049	0.000	0.013	0.355	0.056	0.660	1.702	0.040	13.578	26.635	2.732	10.216	1.644	0.888	0.313	0.120	12.726	26.591	98.316
DS2_monP-2	0.021	0.006	0.021	0.102	0.022	0.395	0.510	0.015	14.775	27.933	2.782	10.084	1.435	0.675	0.184	0.046	12.761	26.588	98.352

Sample Rook Tuff	Calculated Age							
Sample Name	Pb ppm	Th ppm	U ppm	Th 1σ	U 1σ	Pb 1σ	**age Ma**	**1σ**
RTa_monA-1	95	7024	190	197	60	95	**279**	**276**
RTa_monB-1	739	35087	416	336	46	98	**452**	**59**
RTa_monB-2	2898	52607	2257	399	72	106	**1055**	**38**
RTa_monB-3	124	4993	120	182	58	95	**512**	**386**
RTa_monB-4	61	3507	137	174	64	94	**345**	**525**
RTa_monB-5	3850	73070	1087	461	53	110	**1100**	**31**
RTa_monB-6	1041	36294	316	341	41	99	**619**	**58**
RTa_monB-7	1019	41206	403	359	43	99	**533**	**51**
RTa_monC-1	715	38866	505	352	49	99	**394**	**54**
RTa_monC-2	435	10915	201	221	54	97	**829**	**181**
RTa_monD-1	527	12559	114	233	41	97	**898**	**162**
RTa_monE-1	1104	17528	777	258	67	97	**1195**	**103**
RTa_monE-2	2780	29430	1859	312	73	105	**1662**	**61**
RTa_monE-3	2946	33448	1672	328	71	106	**1616**	**57**
RTa_monF-1	4524	64915	7993	437	95	111	**1076**	**26**
RTa_monF-2	4063	69336	3805	451	79	111	**1082**	**29**
RTa_monF-3	4081	59266	6418	422	91	111	**1101**	**29**
RTa_monF-4	3336	56024	4149	411	82	108	**1044**	**33**
RTb_monA-1	885	36040	442	341	48	97	**525**	**57**
RTb_monA-2	749	29873	331	314	45	97	**538**	**69**
RTb_monA-3	559	26883	270	302	43	97	**449**	**77**
RTb_monA-4	468	14522	301	243	55	96	**669**	**135**
RTb_monA-5	734	14404	73	242	29	96	**1099**	**141**
RTb_monB-1	630	24246	356	290	50	95	**551**	**82**
RTb_monB-2	718	24452	834	290	64	96	**587**	**77**
RTb_monB-3	250	6631	403	197	69	94	**695**	**257**
RTb_monB-4	410	10121	206	218	56	95	**837**	**191**
RTb_monB-5	543	16842	212	256	47	95	**686**	**118**
RTb_monC-1	1077	45422	368	375	39	98	**514**	**46**
RTb_monC-2	1004	39410	364	353	42	98	**550**	**53**
RTb_monC-3	1261	44063	585	368	49	97	**609**	**46**
RTb_monC-4	268	4679	266	182	68	93	**1053**	**356**
RTb_monC-5	335	7532	236	201	61	95	**887**	**245**
RTb_monC-6	123	3811	206	174	67	93	**608**	**450**
RTb_monC-7	782	34432	418	333	47	96	**487**	**59**
RTb_monD-1	1122	56655	600	411	45	99	**427**	**37**
RTb_monD-2	1242	56099	595	409	45	99	**477**	**37**
RTb_monD-3	393	14569	166	243	45	95	**578**	**137**
RTb_monD-4	377	9761	157	216	51	95	**810**	**200**
RTb_monD-5	437	7334	61	200	38	94	**1265**	**266**
RTb_monE-1	693	26995	321	300	46	97	**549**	**76**
RTb_monE-2	844	27180	388	303	50	96	**658**	**74**
RTb_monE-3	259	8646	244	209	60	94	**609**	**217**
RTb_monE-4	678	14675	826	241	70	95	**857**	**118**
RTb_monE-5	569	13300	355	236	59	95	**866**	**142**
RTb_monE-6	613	13171	245	234	54	96	**963**	**148**
RTb_monE-7	680	23655	275	288	46	95	**615**	**85**
RTb_monE-8	718	34008	589	331	53	96	**446**	**59**

Sample Name	Monazite Analyses																		
	Si	Al	Fe	Ca	Pb SP5/1	Y	Th	U	La	Ce	Pr	Nd	Sm	Gd	Dy	Er	P	O	Total
RTa_monA-1	0.017	0.006	0.033	0.136	0.010	0.173	0.702	0.019	13.243	26.661	3.016	11.264	2.042	1.222	0.153	0.062	12.586	26.273	97.616
RTa_monB-1	0.193	0.000	0.050	0.554	0.074	0.440	3.509	0.042	11.721	24.721	2.818	10.626	2.033	1.225	0.259	0.063	12.666	26.491	97.485
RTa_monB-2	0.273	0.001	0.020	0.710	0.290	0.343	5.261	0.226	11.969	23.971	2.787	10.043	1.911	1.237	0.205	0.058	12.190	26.065	97.559
RTa_monB-3	0.006	0.003	0.016	0.220	0.012	0.151	0.499	0.012	13.720	26.637	2.797	10.996	2.030	1.190	0.136	0.000	12.806	26.515	97.747
RTa_monB-4	0.008	0.004	0.009	0.220	0.006	0.167	0.351	0.014	14.125	26.873	2.858	10.864	1.941	1.201	0.180	0.039	12.715	26.480	98.053
RTa_monB-5	0.527	0.000	0.015	0.625	0.385	0.161	7.307	0.109	11.980	24.257	2.604	9.897	1.430	0.645	0.066	0.051	11.838	25.894	97.792
RTa_monB-6	0.081	0.007	0.028	0.554	0.104	0.357	3.629	0.032	11.551	24.556	2.822	11.309	2.227	1.493	0.297	0.042	12.650	26.469	98.206
RTa_monB-7	0.076	0.004	0.036	0.617	0.102	0.473	4.121	0.040	11.712	24.429	2.722	10.714	2.137	1.244	0.248	0.059	12.528	26.263	97.525
RTa_monC-1	0.074	0.000	0.018	0.587	0.072	0.489	3.887	0.051	12.000	24.961	2.751	10.739	2.033	1.253	0.338	0.051	12.855	26.781	98.938
RTa_monC-2	0.564	0.339	0.079	0.142	0.044	0.193	1.092	0.020	13.324	26.424	2.969	10.865	1.914	1.069	0.103	0.038	12.677	27.233	99.090
RTa_monD-1	0.075	0.002	0.056	0.148	0.053	0.188	1.256	0.011	12.816	26.585	2.945	11.468	2.158	1.144	0.141	0.017	12.832	26.680	98.574
RTa_monE-1	0.021	0.003	0.022	0.394	0.110	0.208	1.753	0.078	12.297	25.926	2.926	11.122	2.058	1.135	0.145	0.000	12.584	26.195	96.977
RTa_monE-2	0.081	0.000	0.033	0.503	0.278	0.063	2.943	0.186	11.559	25.556	3.002	11.625	1.881	0.808	0.082	0.011	12.435	26.087	97.133
RTa_monE-3	0.087	0.001	0.031	0.541	0.295	0.115	3.345	0.167	12.227	25.550	2.888	10.915	1.674	0.756	0.125	0.053	12.641	26.390	97.798
RTa_monF-1	0.138	0.000	0.017	1.094	0.452	1.956	6.492	0.799	10.726	22.326	2.397	8.944	1.467	1.232	0.566	0.203	12.575	26.511	97.896
RTa_monF-2	0.260	0.002	0.015	0.950	0.406	2.134	6.934	0.381	10.323	22.362	2.395	9.086	1.848	1.503	0.626	0.163	12.408	26.493	98.289
RTa_monF-3	0.117	0.000	0.016	1.032	0.408	1.787	5.927	0.642	11.209	22.970	2.406	9.021	1.486	1.190	0.587	0.225	12.766	26.771	98.559
RTa_monF-4	0.216	0.000	0.008	0.834	0.334	2.150	5.602	0.415	10.953	22.946	2.507	9.236	1.577	1.315	0.664	0.155	12.508	26.526	97.947
RTb_monA-1	0.116	0.000	0.063	0.553	0.089	0.450	3.604	0.044	11.991	25.179	2.797	10.805	2.019	1.316	0.279	0.029	12.679	26.602	98.615
RTb_monA-2	0.058	0.000	0.045	0.527	0.075	0.360	2.987	0.033	13.481	25.820	2.716	9.853	1.698	1.038	0.221	0.000	12.635	26.440	97.989
RTb_monA-3	0.034	0.000	0.042	0.414	0.056	0.349	2.688	0.027	11.996	25.747	2.855	11.306	2.180	1.246	0.220	0.004	12.662	26.460	98.284
RTb_monA-4	0.068	0.000	0.056	0.203	0.047	0.168	1.452	0.030	12.568	26.249	2.949	11.332	2.156	1.193	0.170	0.034	12.555	26.251	97.481
RTb_monA-5	0.063	0.000	0.094	0.251	0.073	0.220	1.440	0.007	12.410	25.993	2.944	11.472	2.225	1.311	0.238	0.068	12.668	26.428	97.906
RTb_monB-1	0.125	0.062	0.033	0.384	0.063	0.313	2.425	0.036	12.001	25.507	2.987	11.216	2.169	1.318	0.228	0.011	12.708	26.599	98.185
RTb_monB-2	0.530	0.425	0.099	0.391	0.072	0.419	2.445	0.083	11.884	24.866	2.774	10.582	1.993	1.221	0.289	0.061	12.489	26.861	97.484
RTb_monB-3	0.021	0.005	0.021	0.172	0.025	0.161	0.663	0.040	13.698	26.661	2.844	10.978	2.026	1.193	0.133	0.031	12.802	26.550	98.024
RTb_monB-4	0.029	0.002	0.027	0.152	0.041	0.276	1.012	0.021	12.821	26.062	2.947	11.309	2.461	1.583	0.263	0.002	12.789	26.575	98.373
RTb_monB-5	0.121	0.018	0.042	0.204	0.054	0.241	1.684	0.021	12.217	25.662	2.915	11.482	2.423	1.433	0.274	0.095	12.533	26.308	97.727
RTb_monC-1	0.097	0.000	0.017	0.660	0.108	0.497	4.542	0.037	11.805	24.769	2.718	10.659	2.005	1.348	0.270	0.030	12.598	26.509	98.668
RTb_monC-2	0.259	0.002	0.021	0.662	0.100	0.587	3.941	0.036	11.390	24.039	2.698	10.540	1.987	1.271	0.336	0.047	12.494	26.281	96.691
RTb_monC-3	0.118	0.000	0.020	0.620	0.126	0.493	4.406	0.059	11.677	24.561	2.757	10.845	2.007	1.302	0.320	0.080	12.596	26.487	98.474
RTb_monC-4	0.249	0.009	0.518	0.104	0.027	0.182	0.468	0.027	13.440	26.605	2.933	11.055	1.771	0.920	0.152	0.047	12.435	26.328	97.268
RTb_monC-5	0.013	0.000	0.014	0.137	0.034	0.194	0.753	0.024	13.397	26.999	2.928	11.206	2.035	1.164	0.110	0.021	12.676	26.428	98.131
RTb_monC-6	0.004	0.000	0.013	0.070	0.012	0.109	0.381	0.021	13.558	27.221	2.996	11.179	1.959	1.066	0.107	0.038	12.749	26.456	97.939
RTb_monC-7	0.071	0.001	0.099	0.536	0.078	0.516	3.443	0.042	11.945	24.913	2.776	10.922	2.021	1.322	0.310	0.073	12.519	26.316	97.903
RTb_monD-1	0.131	0.009	0.015	0.846	0.112	0.543	5.666	0.060	11.435	23.843	2.657	10.398	2.015	1.328	0.333	0.052	12.509	26.418	98.366
RTb_monD-2	0.136	0.001	0.022	0.840	0.124	0.508	5.610	0.060	11.369	23.907	2.649	10.272	1.929	1.299	0.279	0.060	12.606	26.479	98.148
RTb_monD-3	0.049	0.004	0.061	0.241	0.039	0.227	1.457	0.017	13.274	26.108	2.864	11.081	2.183	1.299	0.238	0.059	12.779	26.628	98.607
RTb_monD-4	0.013	0.000	0.023	0.268	0.038	0.216	0.976	0.016	12.726	26.262	2.959	11.370	2.182	1.452	0.182	0.056	12.722	26.452	97.911
RTb_monD-5	0.013	0.000	0.031	0.175	0.044	0.151	0.733	0.006	13.814	26.594	2.878	10.919	2.008	1.126	0.159	0.043	12.644	26.338	97.676
RTb_monE-1	0.027	0.000	0.025	0.508	0.069	0.345	2.700	0.032	13.608	26.001	2.765	10.072	1.683	1.096	0.259	0.037	12.655	26.488	98.371
RTb_monE-2	0.033	0.004	0.037	0.441	0.084	0.376	2.718	0.039	11.905	25.377	2.821	11.140	2.152	1.411	0.279	0.027	12.665	26.410	97.916
RTb_monE-3	0.048	0.008	0.044	0.184	0.026	0.137	0.865	0.024	13.688	26.662	2.909	10.989	2.111	1.211	0.152	0.064	12.726	26.551	98.399
RTb_monE-4	0.024	0.000	0.017	0.254	0.068	0.312	1.468	0.083	12.756	26.245	2.801	11.029	2.098	1.276	0.215	0.033	12.645	26.343	97.666
RTb_monE-5	0.023	0.001	0.022	0.238	0.057	0.204	1.330	0.036	12.726	26.164	2.930	11.394	2.249	1.301	0.137	0.023	12.635	26.348	97.818
RTb_monE-6	0.050	0.005	0.029	0.291	0.061	0.219	1.317	0.025	12.233	25.759	3.030	11.738	2.401	1.459	0.238	0.037	12.744	26.530	98.164
RTb_monE-7	0.053	0.000	0.026	0.406	0.068	0.327	2.366	0.028	12.543	25.749	2.845	10.834	2.137	1.239	0.247	0.080	12.731	26.535	98.212
RTb_monE-8	0.035	0.000	0.025	0.528	0.072	0.407	3.401	0.059	11.710	24.963	2.790	11.311	2.197	1.365	0.278	0.061	12.614	26.403	98.219

Sample 630706	Calculated Age							
Monazite No.	Pb ppm	Th ppm	U ppm	age Ma	± 1σ (Myrs	Th 1sig	U 1sig	Pb 1sig
22 / 1: 630706_mnzA1	1034	45595	522	487	21	231	66	44
23 / 1: 630706_mnzA2	692	24081	142	626	39	178	45	44
24 / 1: 630706_mnzA3	2422	39926	3752	1010	20	219	123	46
25 / 1: 630706_mnzB1	306	9715	529	594	82	132	109	42
26 / 1 : 630706_mnzB2	355	12324	353	585	71	142	94	43
29 / 1 : 630706_mnzD1	1489	34636	662	890	28	207	83	46
30 / 1: 630706_mnzD2	708	31441	359	483	30	198	66	44
31 / 1: 630706_mnzD3	824	24910	452	691	42	286	81	49
32 / 1 : 630706_mnzD4	1308	67700	761	416	16	436	66	50
33 / 1: 630706_mnzD5	639	25542	309	536	41	289	68	49
34 / 1 : 630706_mnzD6	1985	30826	1586	1196	34	310	111	52
37 / 1 : 630706_mnzE2	6032	85173	4535	1303	14	483	121	59
39 / 1 : 630706_mnzF1	654	15328	243	892	68	239	75	49
40 / 1 : 630706_mnzF2	2121	27147	1919	1363	37	296	119	52
41 / 1: 630706_mnzF3	953	19544	914	928	50	261	107	50
42 / 1: 630706_mnzF4	374	10745	655	643	85	216	111	49

Sample 630706	Analyses (%)																								
Monazite No.	Si	Al	K	Fe	Ca	Sr	Pb SP5/1	Y	Th	U	La	Ce	Pr	Nd	Sm	Eu	Gd	Dy	Yb	Er	P	S	As	O	Total
22 / 1: 630706_mnzA1	0	0.060	0.061	0.110	0.654	-0.01	0.11	0.37	4.560	0.052	12.403	24.514	2.684	9.772	1.665	0.382	0.965	0.226	0.017	0.025	12.452	0.026	0.025	26.526	97.982
23 / 1: 630706_mnzA2	0	0.006	0.022	0.114	0.323	0.00	0.07	0.26	2.408	0.014	13.625	26.611	2.830	10.373	1.856	0.426	0.990	0.161	0.070	0.054	12.421	0.010	0.030	26.492	99.331
24 / 1: 630706_mnzA3	0	0.007	-0.012	0.232	1.007	0.04	0.25	1.50	3.993	0.375	11.473	23.911	2.629	9.074	1.359	0.166	1.014	0.475	0.029	0.115	12.382	0.142	0.002	26.303	96.546
25 / 1: 630706_mnzB1	0	0.112	0.173	0.160	0.206	0.01	0.03	0.10	0.972	0.053	14.377	27.256	2.854	9.895	1.505	0.381	0.619	0.131	0.034	0.052	12.336	0.029	0.026	26.351	97.870
26 / 1 : 630706_mnzB2	0	0.019	0.080	0.248	0.613	0.10	0.04	0.21	1.232	0.035	17.337	27.278	2.382	7.716	0.967	0.312	0.413	0.111	0.003	-0.052	12.641	0.235	0.006	27.003	99.073
29 / 1 : 630706_mnzD1	0	0.005	-0.012	0.130	0.500	0.02	0.15	0.48	3.464	0.066	12.309	25.445	2.847	10.469	2.165	0.474	1.149	0.224	-0.016	0.003	12.438	0.011	0.033	26.431	98.948
30 / 1: 630706_mnzD2	0	0.007	0.017	0.128	0.366	0.00	0.07	0.31	3.144	0.036	13.356	26.227	2.788	10.455	1.744	0.459	1.014	0.220	0.020	0.020	12.247	0.026	0.025	26.368	99.268
31 / 1: 630706_mnzD3	0	0.004	-0.012	0.133	0.382	0.02	0.09	0.33	2.491	0.045	13.017	26.149	2.851	10.726	2.109	0.486	1.022	0.230	-0.017	0.008	12.410	0.025	0.018	26.397	99.028
32 / 1 : 630706_mnzD4	0	0.067	0.085	0.172	0.948	0.02	0.13	0.41	6.770	0.076	12.264	23.925	2.500	9.369	1.714	0.413	1.014	0.227	0.017	0.066	12.046	0.020	0.034	26.396	99.121
33 / 1: 630706_mnzD5	0	0.034	0.061	0.154	0.345	0.00	0.07	0.35	2.554	0.031	13.282	26.414	2.764	10.525	1.759	0.461	1.010	0.223	0.038	0.006	12.463	0.022	0.032	26.641	99.462
34 / 1 : 630706_mnzD6	0	0.005	0.014	0.133	0.561	0.05	0.20	0.96	3.083	0.159	11.775	25.605	2.905	10.642	1.873	0.320	1.083	0.353	0.062	0.050	12.426	0.098	0.011	26.599	99.093
37 / 1 : 630706_mnzE2	1	0.004	0.043	0.151	0.341	0.01	0.61	0.70	8.517	0.454	13.069	24.444	2.528	8.179	1.074	0.197	0.677	0.189	0.026	0.040	10.915	0.065	0.015	25.669	99.002
39 / 1 : 630706_mnzF1	0	0.012	0.058	0.486	0.795	0.17	0.07	0.26	1.533	0.024	15.192	28.301	2.629	8.579	0.842	0.261	0.399	0.134	0.027	0.045	12.399	0.370	0.012	27.026	99.662
40 / 1 : 630706_mnzF2	0	0.007	0.040	0.168	0.669	0.09	0.22	0.97	2.715	0.192	11.365	25.657	3.067	11.217	1.666	0.268	0.851	0.306	0.018	0.078	12.444	0.149	0.016	26.691	98.979
41 / 1: 630706_mnzF3	0	0.002	0.016	0.167	0.744	0.13	0.10	0.22	1.954	0.091	10.972	27.783	3.268	11.500	1.630	0.355	0.677	0.177	0.054	0.018	12.330	0.240	0.012	26.672	99.201
42 / 1: 630706_mnzF4	0	0.139	0.174	0.364	0.456	0.06	0.04	0.20	1.075	0.066	15.221	26.783	2.624	8.725	1.336	0.367	0.673	0.131	0.021	0.021	12.155	0.121	0.018	26.419	97.515

Sample 630694	Calculated Age							
Sample Name	Pb ppm	Th ppm	U ppm	Th 1σ	U 1σ	Pb 1σ	**age Ma**	**1σ**
1 / 1 : 630694_mnzA1	2951	65086	876	426	72	54	**943**	**18**
11 / 1 : 630694_mnzE2	209	2877	309	104	120	42	**939**	**244**
12 / 1: 630694_mnzE3	357	14656	393	151	93	43	**444**	**60**
13 / 1: 630694_mnzE4	233	3373	463	107	123	43	**864**	**196**
14 / 1 : 630694_mnzF1	86	1302	327	96	127	41	**424**	**384**
15 / 1: 630694_mnzF2	896	35520	333	208	59	44	**521**	**27**
16 / 1: 630694_mnzF3	562	19851	278	168	73	43	**560**	**46**
17 / 1 : 630694_mnzF4	2358	48794	3019	239	119	47	**869**	**18**
18 / 1 : 630694_mnzG1	709	25662	227	183	58	44	**564**	**37**
19 / 1 : 630694_mnzH1	204	4300	261	112	112	41	**701**	**181**
2 / 1: 630694_mnzA2	952	36312	322	333	57	50	**545**	**30**
20 / 1 : 630694_mnzH2	204	3701	159	107	105	45	**851**	**240**
21 / 1 : 630694_mnzI1	215	3972	289	110	114	47	**778**	**215**
3 / 1 : 630694_mnzB1	457	9896	123	211	67	59	**891**	**126**
4 / 1 : 630694_mnzB2	706	27107	259	298	59	49	**531**	**39**
5 / 1 : 630694_mnzB3	289	9931	166	211	78	48	**527**	**101**
6 / 1 : 630694_mnzC1	1084	10119	3411	212	135	49	**1055**	**51**
7 / 1 : 630694_mnzD1	596	15582	477	243	95	49	**718**	**63**
8 / 1: 630694_mnzD2	553	20590	393	169	83	43	**523**	**44**
9 / 1 : 630694_mnzE1	175	1993	240	101	122	43	**1044**	**352**
11 / 1 : 630694_Mon8_a1	269	4261	316	111	114	41	**967**	**178**
12 / 1: 630694_Mon8_a2	4294	53642	1445	248	95	49	**1600**	**20**
13 / 1 : 630694_Mon8_a3	385	9655	334	132	94	41	**734**	**84**
15 / 1 : 630694_Mon9_a2	155	1186	234	96	123	44	**1276**	**517**
16 / 1 : 630694_Mon10_a1	156	1248	250	91	111	39	**1278**	**430**
17 / 1 : 630694_Mon11_a1	110	4856	310	114	111	38	**271**	**144**
18 / 1 : 630694_Mon12_a1	117	1309	389	97	126	39	**662**	**334**
19 / 1 : 630694_Mon13_a1	123	3377	274	104	110	39	**447**	**203**
8 / 1 : 630694_Mon6_a2	103	305	535	91	134	54	**688**	**556**

	Monazite Analyses																										
Sample Name	Si	Al	K	Fe	Ca	Sr	Pb SP5/1	Y	Th	U	La	Ce	Pr	Nd	Sm	Eu	Gd	Dy	Yb	Er	P	S	As	O	Total
1 / 1 : 630694_mnzA1	0.354	0.006	0.027	0.086	0.752	-0.002	0.295	0.584	6.509	0.088	12.248	24.087	2.600	9.418	1.227	0.073	0.709	0.251	0.009	0.061	11.915	0.004	0.016	25.842	97.159
11 / 1 : 630694_mnzE2	0.175	0.023	0.043	0.070	0.077	0.038	0.021	0.207	0.288	0.031	12.784	27.827	3.026	11.454	2.025	0.344	1.058	0.189	-0.007	-0.015	12.397	0.001	0.000	26.341	98.398
12 / 1: 630694_mnzE3	0.368	0.099	0.094	0.079	0.177	0.036	0.036	0.254	1.466	0.039	12.445	26.491	3.036	11.359	2.273	0.451	1.182	0.219	0.039	0.052	12.269	0.004	0.006	26.489	98.962
13 / 1: 630694_mnzE4	0.326	0.034	0.051	0.072	0.046	0.040	0.023	0.274	0.337	0.046	16.123	26.578	2.694	9.892	1.756	0.353	1.071	0.203	0.042	0.031	12.433	-0.001	0.017	26.614	99.055
14 / 1 : 630694_mnzF1	0.098	0.062	0.036	0.151	0.055	0.016	0.009	0.301	0.130	0.033	12.517	27.377	3.109	11.782	2.184	0.413	1.256	0.236	0.027	0.037	12.566	0.003	0.011	26.554	98.963
15 / 1: 630694_mnzF2	0.160	0.007	0.022	0.085	0.418	0.003	0.090	0.333	3.552	0.033	12.510	25.448	2.944	10.940	2.106	0.243	1.258	0.275	0.031	0.017	12.521	0.003	0.013	26.598	99.606
16 / 1: 630694_mnzF3	0.112	0.006	0.031	0.153	0.232	0.019	0.056	0.370	1.985	0.028	12.779	25.890	2.923	11.253	2.213	0.380	1.371	0.234	0.017	0.049	12.538	0.002	-0.006	26.513	99.149
17 / 1 : 630694_mnzF4	0.671	0.054	0.051	0.084	0.689	0.109	0.236	1.066	4.879	0.302	12.946	23.920	2.480	9.219	1.659	0.275	1.298	0.455	0.046	0.078	12.302	0.062	0.011	27.013	99.905
18 / 1 : 630694_mnzG1	0.176	0.015	0.008	0.102	0.268	0.023	0.071	0.304	2.566	0.023	12.759	25.990	2.928	10.929	2.167	0.430	1.196	0.199	0.019	0.054	12.534	0.003	0.011	26.584	99.358
19 / 1 : 630694_mnzH1	0.071	0.010	-0.001	0.104	0.052	0.015	0.020	0.256	0.430	0.026	11.900	26.977	3.060	12.179	2.335	0.479	1.485	0.284	-0.011	-0.024	12.690	0.006	0.001	26.584	98.927
2 / 1: 630694_mnzA2	1.131	0.749	0.055	0.142	0.393	0.036	0.095	0.300	3.631	0.032	12.292	24.535	2.758	10.422	2.041	0.260	1.166	0.236	0.016	0.013	12.018	0.000	-0.005	27.381	99.695
20 / 1 : 630694_mnzH2	0.386	0.058	0.034	0.180	0.059	0.026	0.020	0.247	0.370	0.016	12.381	27.176	3.186	11.705	2.108	0.504	1.230	0.214	0.029	0.009	12.555	-0.001	-0.001	26.810	99.301
21 / 1 : 630694_mnzI1	0.194	0.088	0.026	0.110	0.063	0.034	0.022	0.216	0.397	0.029	12.723	27.578	3.111	11.481	1.978	0.401	1.013	0.153	0.010	0.065	12.285	0.000	0.015	26.267	98.259
3 / 1 : 630694_mnzB1	0.261	0.006	0.006	0.090	0.980	0.091	0.046	0.283	0.990	0.012	16.461	26.919	2.531	9.032	0.997	0.214	0.479	0.112	0.016	0.000	11.715	0.850	0.009	27.024	99.122
4 / 1 : 630694_mnzB2	0.178	0.014	0.017	0.108	0.329	0.011	0.071	0.321	2.711	0.026	13.124	25.863	2.822	10.526	2.086	0.247	1.170	0.216	0.023	0.054	12.288	0.002	0.004	26.236	98.445
5 / 1 : 630694_mnzB3	0.326	0.008	0.033	0.127	0.665	0.014	0.029	0.301	0.993	0.017	15.943	27.315	2.692	9.619	0.986	0.163	0.445	0.129	0.037	0.030	11.845	0.649	0.003	26.945	99.313
6 / 1 : 630694_mnzC1	0.242	0.222	0.036	0.185	0.245	-0.005	0.108	1.045	1.012	0.341	12.361	24.880	2.845	11.015	2.240	0.319	1.490	0.456	0.056	0.108	12.385	-0.001	-0.003	26.522	98.106
7 / 1 : 630694_mnzD1	0.872	0.331	0.105	0.154	0.225	0.151	0.060	0.191	1.558	0.048	14.939	26.043	2.404	9.575	1.595	0.316	0.857	0.155	0.031	0.018	12.438	0.046	0.017	27.381	99.507
8 / 1: 630694_mnzD2	0.249	0.035	0.084	0.145	0.207	0.023	0.055	0.282	2.059	0.039	12.703	26.070	2.923	11.035	1.952	0.295	1.177	0.194	0.021	0.022	12.432	0.004	0.017	26.451	98.474
9 / 1 : 630694_mnzE1	0.372	0.058	0.049	0.066	0.056	0.019	0.018	0.247	0.199	0.024	12.419	27.505	3.171	11.863	2.121	0.383	1.173	0.185	0.048	0.023	12.350	0.001	0.028	26.560	98.938
11 / 1 : 630694_Mon8_a1	1.561	0.018	0.009	0.111	0.069	0.049	0.027	0.281	0.426	0.032	14.521	26.242	2.735	10.373	1.815	0.425	1.186	0.287	0.024	-0.018	12.483	0.002	0.006	27.886	100.549
12 / 1: 630694_Mon8_a2	0.253	0.017	0.000	0.095	0.782	0.016	0.429	0.257	5.364	0.145	12.498	25.324	2.708	9.878	1.569	0.212	0.653	0.116	0.006	0.037	12.355	0.015	0.011	26.489	99.229
13 / 1 : 630694_Mon8_a3	7.861	0.101	0.008	0.220	0.134	0.072	0.039	0.228	0.966	0.033	14.048	23.534	2.406	8.934	1.571	0.359	0.874	0.197	0.009	-0.015	11.025	0.001	0.014	32.432	105.052
15 / 1 : 630694_Mon9_a2	0.406	0.075	0.025	0.101	0.035	0.019	0.016	0.289	0.119	0.023	12.129	26.983	3.065	11.829	2.193	0.467	1.252	0.215	0.031	0.020	12.798	0.002	0.016	27.055	99.162
16 / 1 : 630694_Mon10_a1	2.553	1.280	0.008	0.606	0.345	0.016	0.016	0.249	0.125	0.025	10.373	22.981	2.778	10.307	1.916	0.452	1.020	0.160	0.043	0.034	11.918	0.009	-0.018	28.307	95.503
17 / 1 : 630694_Mon11_a1	0.273	0.097	0.058	0.150	0.117	0.027	0.011	0.228	0.486	0.031	12.477	27.060	3.031	11.514	2.123	0.475	1.169	0.177	0.003	0.010	12.681	0.003	0.008	26.840	99.048
18 / 1 : 630694_Mon12_a1	0.482	0.204	0.039	0.114	0.046	0.018	0.012	0.265	0.131	0.039	12.315	27.387	3.106	11.632	2.145	0.472	1.223	0.232	0.008	-0.021	12.548	0.003	0.015	27.000	99.415
19 / 1 : 630694_Mon13_a1	0.802	0.861	0.063	0.184	0.099	0.006	0.012	0.154	0.338	0.027	13.578	26.129	2.905	10.532	1.881	0.420	0.994	0.152	0.041	-0.010	12.062	0.005	0.009	27.058	98.299
8 / 1 : 630694_Mon6_a2	0.062	0.012	-0.010	0.113	0.056	0.104	0.010	0.503	0.031	0.054	15.587	26.590	2.674	9.883	1.844	0.514	1.390	0.382	0.048	0.019	12.745	0.009	0.014	26.753	99.386

Sample 630713	Calculated Age							
Sample Name	Pb ppm	Th ppm	U ppm	Th 1σ	U 1σ	Pb 1σ	**age Ma**	**1σ**
43 / 1: 630713_mnzC1	3601	42815	1518	225	103	49	**1599**	**25**
44 / 1: 630713_mnzD1	636	20239	160	265	53	49	**639**	**52**
45 / 1: 630713_mnzD2	4099	45988	1131	368	92	55	**1750**	**28**
46 / 1 : 630713_mnzb1	2052	84937	460	479	43	52	**520**	**14**
47 / : 630713_mnzb2	1434	17692	767	251	105	51	**1485**	**60**
48 / 1: 630713_mnzb3	1276	19060	651	269	103	52	**1268**	**57**
49 / 1: 630713_mnzb4	4074	44626	3163	364	120	56	**1564**	**25**
50 / 1: 630713_mnzb5	3999	48753	1682	380	103	57	**1569**	**26**
51 / 1: 630713_mnza1	1472	59612	236	406	33	51	**529**	**19**
52 / 1 : 630713_mnza2	1204	51659	186	383	31	51	**497**	**22**
53 / 1: 630713_mnza3	1154	33930	128	320	32	50	**719**	**32**
54 / 1 : 630713_mnza4	937	25204	333	287	70	49	**754**	**42**
55 / 1 : 630713_mnza5	644	28735	298	303	62	49	**454**	**37**
56 / 1 : 630713_mnza6	1625	68431	528	433	54	51	**504**	**16**
57 / 1 : 630713_mnza7	754	31767	240	314	52	49	**489**	**33**
58 / 1: 630713_mnza8	378	12771	234	227	80	47	**553**	**78**
60 / 1 : 630713_mnza10	210	4244	128	176	94	46	**796**	**218**
61 / 1 : 630713_mnza11	723	22035	130	272	44	50	**674**	**50**
62 / 1 : 630713_mnza12	1499	73192	503	447	50	50	**436**	**15**
63 / 1 : 630713_mnza13	1024	33176	217	322	48	48	**645**	**32**
65 / 1 : 630713_mnzb6	4314	45076	3794	366	125	56	**1579**	**24**
66 / 1: 630713_mnzb7	3928	45818	3742	365	122	53	**1434**	**22**
70 / 1: 630713_mnzb11	1604	32584	765	313	84	49	**987**	**32**
33 / 1: 630715_Mon7_a1	822	34332	340	206	56	42	**506**	**26**
41 / 1 : 630715_Mon9_a1	1319	53469	359	248	48	45	**533**	**18**
43 / 1 : 630715_Mon7_a3	1255	54600	270	250	39	45	**499**	**18**

Sample 630713	Monazite Analyses																								
Sample Name	Si	Al	K	Fe	Ca	Sr	Pb SP5/1	Y	Th	U	La	Ce	Pr	Nd	Sm	Eu	Gd	Dy	Yb	Er	P	S	As	O	Total
43 / 1: 630713_mnzC1	0.206	-0.002	0.021	0.071	0.861	0.035	0.360	0.535	4.282	0.152	9.456	23.897	3.136	12.922	2.486	0.232	1.117	0.290	0.017	0.026	12.114	0.231	0.015	26.440	98.898
44 / 1: 630713_mnzD1	0.077	0.000	-0.006	0.100	0.533	0.040	0.064	0.354	2.024	0.016	11.214	25.189	3.186	13.020	2.274	0.509	0.895	0.210	0.054	0.032	12.211	0.183	0.040	26.338	98.556
45 / 1: 630713_mnzD2	0.152	-0.006	-0.005	0.060	0.791	-0.027	0.410	2.923	4.599	0.113	11.466	23.063	2.563	9.294	1.439	0.020	1.397	0.752	0.068	0.210	12.484	0.009	0.000	26.610	98.385
46 / 1 : 630713_mnzb1	0.331	0.001	-0.018	0.065	1.188	0.019	0.205	0.266	8.494	0.046	11.099	22.409	2.507	9.578	1.937	0.524	0.973	0.150	0.047	0.040	11.984	0.014	0.008	25.962	97.830
47 / : 630713_mnzb2	0.059	-0.002	0.005	0.086	0.970	0.039	0.143	0.891	1.769	0.077	10.236	25.240	3.256	12.859	1.970	0.418	0.865	0.274	0.047	0.042	12.390	0.376	0.053	26.912	98.975
48 / 1: 630713_mnzb3	0.076	-143.152	-0.011	0.069	0.958	0.048	0.128	1.022	1.906	0.065	9.637	24.966	3.783	16.192	2.770	0.508	1.098	0.315	0.053	0.071	12.707	0.388	0.012	-99.276	-165.668
49 / 1: 630713_mnzb4	0.091	-0.014	0.006	0.010	1.217	-0.034	0.407	3.044	4.463	0.316	10.572	22.946	2.578	9.365	1.502	-0.035	1.390	0.773	0.129	0.232	12.445	0.323	-0.009	27.004	98.722
50 / 1: 630713_mnzb5	0.149	-0.006	-0.015	0.050	1.302	-0.030	0.400	3.063	4.875	0.168	10.986	22.602	2.505	8.877	1.533	-0.003	1.327	0.769	0.111	0.273	12.371	0.350	0.002	27.029	98.685
51 / 1: 630713_mnza1	0.149	0.002	-0.025	0.077	1.114	0.044	0.147	0.255	5.961	0.024	12.558	24.134	2.528	9.804	1.679	0.428	0.763	0.133	0.011	0.026	12.313	0.155	0.028	26.514	98.822
52 / 1 : 630713_mnza2	0.167	0.002	0.001	0.076	0.762	0.043	0.120	0.279	5.166	0.019	12.855	24.555	2.639	9.893	1.897	0.517	1.004	0.179	0.044	0.021	12.370	0.030	0.043	26.436	99.115
53 / 1: 630713_mnza3	0.091	0.004	0.021	0.068	0.524	0.028	0.115	0.157	3.393	0.013	13.480	25.995	2.716	10.220	1.799	0.446	0.801	0.093	0.051	-0.036	12.355	0.022	0.041	26.292	98.688
54 / 1 : 630713_mnza4	0.074	0.004	-0.017	0.075	0.438	0.008	0.094	0.220	2.520	0.033	14.204	26.643	2.788	10.057	1.688	0.452	0.777	0.087	0.036	0.026	12.391	0.025	0.025	26.376	99.022
55 / 1 : 630713_mnza5	0.173	0.005	0.005	0.083	0.318	-0.004	0.064	0.258	2.874	0.030	13.228	26.147	2.838	10.565	1.955	0.446	1.012	0.172	-0.004	0.095	12.345	0.006	0.055	26.365	99.031
56 / 1 : 630713_mnza6	0.296	0.001	0.012	0.045	0.886	-0.003	0.163	0.525	6.843	0.053	12.235	23.406	2.523	9.612	2.076	0.388	1.191	0.293	0.060	0.011	12.263	0.032	0.044	26.478	99.432
57 / 1 : 630713_mnza7	0.164	0.003	-0.029	0.060	0.465	-0.006	0.075	0.383	3.177	0.024	15.128	26.160	2.543	9.037	1.511	0.317	0.824	0.205	0.008	0.069	12.296	0.037	0.063	26.376	98.885
58 / 1: 630713_mnza8	0.031	-0.001	-0.013	0.051	0.228	-0.003	0.038	0.169	1.277	0.023	14.561	27.450	2.863	10.271	1.678	0.386	0.730	0.178	-0.032	0.040	12.579	0.014	0.020	26.502	99.040
60 / 1 : 630713_mnza10	0.015	0.005	-0.009	0.093	0.159	0.016	0.021	0.169	0.424	0.013	14.879	27.761	2.801	10.101	1.799	0.366	0.836	0.162	0.032	0.056	12.594	0.039	0.005	26.519	98.857
61 / 1 : 630713_mnza11	0.051	0.005	-0.008	0.048	0.325	0.032	0.072	0.180	2.204	0.013	14.082	26.867	2.774	10.235	1.779	0.417	0.776	0.129	0.012	0.017	12.625	0.018	0.031	26.595	99.275
62 / 1 : 630713_mnza12	0.306	0.008	-0.009	0.046	1.033	0.014	0.150	0.424	7.319	0.050	12.015	22.974	2.453	9.300	2.020	0.407	1.157	0.253	0.035	-0.003	11.958	0.034	0.030	25.993	97.967
63 / 1 : 630713_mnza13	0.139	0.035	0.000	0.056	0.520	0.022	0.102	0.153	3.318	0.022	11.894	25.634	2.820	11.014	2.316	0.478	0.954	0.141	-0.002	0.014	11.404	0.018	0.026	25.043	96.121
65 / 1 : 630713_mnzb6	0.064	-0.007	0.026	0.006	1.186	-0.024	0.431	2.481	4.508	0.379	11.232	23.136	2.527	9.200	1.490	0.008	1.412	0.733	0.089	0.212	12.615	0.224	-0.001	27.014	98.940
66 / 1: 630713_mnzb7	0.135	0.029	-0.012	0.019	1.183	-0.019	0.393	2.514	4.582	0.374	10.627	22.687	2.425	9.179	1.538	-0.008	1.364	0.768	0.099	0.210	11.456	0.258	0.016	25.503	95.318
70 / 1: 630713_mnzb11	0.146	0.014	0.009	18.641	0.558	0.013	0.160	0.751	3.258	0.077	8.040	17.048	1.989	7.149	1.201	0.119	0.820	0.291	0.009	0.043	8.644	0.064	0.019	23.908	92.970
33 / 1: 630715_Mon7_a1	8.784	0.242	-0.004	0.409	0.592	0.048	0.082	0.261	3.433	0.034	11.391	21.670	2.443	8.788	1.303	0.385	0.706	0.162	0.033	-0.023	10.018	0.038	0.050	32.100	102.944
41 / 1 : 630715_Mon9_a1	0.198	0.010	-0.008	0.181	0.885	0.003	0.132	0.364	5.347	0.036	11.651	23.585	2.664	10.293	1.995	0.481	1.014	0.240	0.026	0.002	12.777	0.024	0.034	26.825	98.760
43 / 1 : 630715_Mon7_a3	0.377	0.004	0.016	0.342	0.567	0.029	0.126	0.437	5.460	0.027	12.179	24.879	2.505	10.121	1.680	0.423	0.937	0.267	0.037	0.014	12.407	0.026	0.044	26.713	99.616

Sample 630726	Calculated Age							
Sample Name	Pb ppm	Th ppm	U ppm	Th 1σ	U 1σ	Pb 1σ	**age Ma**	**1σ**
1 / 1 : 630726_mnz4_a1	263	13415	463	146	99	41	337	62
10 / 1 : 630726_mnz8_a2	295	13255	331	147	91	41	400	64
11 / 1 : 630726_mnz8_a3	339	13608	199	147	74	42	471	65
2 / 1: 630726_mnz4_a2	330	14409	282	151	83	42	426	60
3 / 1: 630726_mnz5_a1	394	14535	494	150	97	41	497	57
4 / 1 : 630726_mnz6_a1	440	16867	490	158	95	42	488	51
5 / 1 : 630726_mnz6_a2	329	13802	260	148	82	42	444	63
6 / 1 : 630726_mnz7_a1	294	12111	433	141	99	41	425	67
7 / 1 : 630726_mnz7_a2	332	11619	361	141	97	41	511	71
8 / 1 : 630726_mnz7_a3	442	15850	312	156	84	42	538	56
9 / 1 : 630726_mnz8_a1	221	9034	343	129	100	40	405	89
1 / 1 : 630726_Mon1-a1	301	8305	249	130	96	44	644	107
10 / 1 : 630726_Mon3-a1	150	7470	149	125	83	40	315	113
2 / 1 : 630726_Mon1-a2	336	15326	314	153	85	42	409	57
3 / 1 : 630726_Mon1-a3	328	12810	1683	146	124	41	358	50
4 / 1 : 630726_Mon1-a4	334	13647	259	147	83	42	456	64
5 / 1 : 630726_Mon1-a5	244	9521	414	134	105	41	424	84
6 / 1 : 630726_Mon2-a1	287	10872	276	137	89	41	479	78
7 / 1 : 630726_Mon2-a2	272	10027	366	136	101	41	469	81
8 / 1 : 630726_Mon2-a3	375	11077	305	139	92	43	622	79
9 / 1 : 630726_Mon2-a4	162	6998	377	122	105	39	348	107

	Monazite Analyses																								
Sample Name	Si	Al	K	Fe	Ca	Sr	Pb SP5/1	Y	Th	U	La	Ce	Pr	Nd	Sm	Eu	Gd	Dy	Yb	Er	P	S	As	O	Total
1 / 1 : 630726_mnz4_a1	0.166	0.042	0.001	0.091	0.206	-0.001	0.026	0.144	1.342	0.046	15.241	28.377	2.853	9.539	1.159	0.198	0.450	0.121	0.029	0.058	12.458	0.009	0.019	26.550	99.123
10 / 1 : 630726_mnz8_a2	0.125	0.006	0.001	0.171	0.328	-0.004	0.030	0.102	1.326	0.033	13.126	28.818	3.276	11.121	1.177	0.183	0.411	0.058	-0.004	0.014	12.637	0.005	0.030	26.780	99.749
11 / 1 : 630726_mnz8_a3	0.120	0.005	0.002	0.202	0.390	-0.013	0.034	0.114	1.361	0.020	13.893	28.904	3.123	10.518	1.104	0.226	0.402	0.072	0.076	-0.011	12.646	0.003	0.023	26.837	100.048
2 / 1: 630726_mnz4_a2	0.115	0.001	-0.034	0.066	0.111	-0.015	0.033	0.112	1.441	0.028	12.331	28.784	3.324	11.933	1.317	0.132	0.401	0.057	0.031	0.023	12.518	0.002	0.021	26.514	99.244
3 / 1: 630726_mnz5_a1	1.166	0.065	0.111	0.120	0.155	0.009	0.039	0.141	1.454	0.049	14.220	27.191	2.822	9.273	1.105	0.200	0.405	0.036	0.009	0.019	11.971	-0.001	0.033	26.636	97.227
4 / 1 : 630726_mnz6_a1	0.158	0.007	0.009	0.068	0.137	-0.007	0.044	0.122	1.687	0.049	13.061	28.713	3.193	11.122	1.226	0.177	0.387	0.057	0.008	-0.018	12.473	0.002	0.023	26.508	99.205
5 / 1 : 630726_mnz6_a2	0.193	0.006	0.004	0.088	0.148	-0.002	0.033	0.133	1.380	0.026	11.929	28.904	3.352	11.761	1.222	0.208	0.423	0.035	-0.016	0.042	12.664	-0.003	0.014	26.730	99.274
6 / 1 : 630726_mnz7_a1	1.031	0.067	0.029	0.149	0.171	0.011	0.029	0.140	1.211	0.043	14.471	27.739	2.844	9.157	1.071	0.192	0.364	0.077	0.034	0.031	12.064	0.004	0.019	26.689	97.638
7 / 1 : 630726_mnz7_a2	0.126	0.028	0.017	0.142	0.156	-0.017	0.033	0.116	1.162	0.036	12.121	29.414	3.382	11.510	1.175	0.199	0.379	0.068	0.004	0.010	12.352	0.004	0.031	26.345	98.790
8 / 1 : 630726_mnz7_a3	0.125	0.009	0.026	0.207	0.398	-0.017	0.044	0.116	1.585	0.031	12.850	27.929	3.205	11.469	1.313	0.205	0.444	0.089	-0.001	-0.024	12.557	0.001	0.027	26.626	99.212
9 / 1 : 630726_mnz8_a1	0.411	0.024	0.000	0.211	2.867	-0.044	0.022	0.118	0.903	0.034	14.517	26.987	2.809	7.954	1.050	0.231	0.368	0.062	0.049	0.030	12.283	0.009	0.015	26.933	97.843
1 / 1 : 630726_Mon1-a1	0.104	0.005	0.012	0.083	0.125	-0.002	0.030	0.209	0.831	0.025	11.792	27.541	3.366	13.151	1.847	0.186	0.710	0.101	0.010	-0.069	12.439	-0.001	0.022	26.396	98.912
10 / 1 : 630726_Mon3-a1	0.118	0.023	0.023	0.090	0.178	0.000	0.015	0.254	0.747	0.015	10.954	26.911	3.411	13.632	2.035	0.221	0.779	0.104	0.043	0.036	12.951	0.002	0.029	27.020	99.591
2 / 1 : 630726_Mon1-a2	0.126	0.004	-0.001	0.084	0.152	-0.005	0.034	0.107	1.533	0.031	13.018	28.336	3.091	11.490	1.295	0.184	0.450	0.094	0.018	0.038	12.558	0.003	0.031	26.573	99.241
3 / 1 : 630726_Mon1-a3	0.489	0.038	-0.026	0.094	0.250	0.015	0.033	0.193	1.281	0.168	12.700	27.663	3.170	11.464	1.267	0.145	0.471	0.116	0.028	0.040	12.171	0.007	0.015	26.399	98.188
4 / 1 : 630726_Mon1-a4	0.121	0.005	0.009	0.095	0.154	-0.003	0.033	0.102	1.365	0.026	13.316	28.877	3.206	11.273	1.234	0.181	0.362	0.093	0.002	-0.004	12.674	0.004	0.032	26.798	99.955
5 / 1 : 630726_Mon1-a5	0.136	0.010	0.029	0.091	0.106	-0.005	0.024	0.196	0.952	0.041	11.921	27.630	3.348	12.899	1.734	0.232	0.649	0.100	0.019	0.003	12.645	0.000	0.023	26.697	99.479
6 / 1 : 630726_Mon2-a1	0.125	0.009	-0.046	0.072	0.247	-0.005	0.029	0.151	1.087	0.028	11.509	25.898	3.035	10.901	1.388	0.192	0.483	0.105	0.018	0.046	11.854	0.001	0.031	24.877	92.033
7 / 1 : 630726_Mon2-a2	0.114	0.015	-0.018	0.078	0.165	-0.009	0.027	0.142	1.003	0.037	11.901	27.040	3.162	11.948	1.515	0.199	0.568	0.105	-0.021	0.032	12.199	0.003	0.026	25.763	95.994
8 / 1 : 630726_Mon2-a3	0.336	0.161	0.073	0.096	0.231	0.009	0.038	0.137	1.108	0.031	11.960	28.643	3.337	11.803	1.268	0.138	0.405	0.077	0.050	-0.005	12.784	0.002	0.023	27.184	99.885
9 / 1 : 630726_Mon2-a4	3.435	1.529	0.092	0.119	1.037	0.008	0.016	0.197	0.700	0.038	9.774	24.339	3.247	12.849	2.008	0.172	0.770	0.137	0.032	-0.044	11.330	0.000	0.027	29.566	101.376

APPENDIX 4.
GRAVITY MODEL DETAILS

Cross-sections

Model 1: moderate density basement, salt at depth

Model 2: low density basement, no salt at depth

Model 3: steep normal fault adjacent the Muloorina Gravity ridge

Long sections

Model 1: high density basement high beneath the South Hill Domain, no basalt.

Model 2: basement rises to the southeast but no isolated high density block below the South Hill Domain, thickened basalt

Model 3: High density basement below the South Hill Domain but no basement high

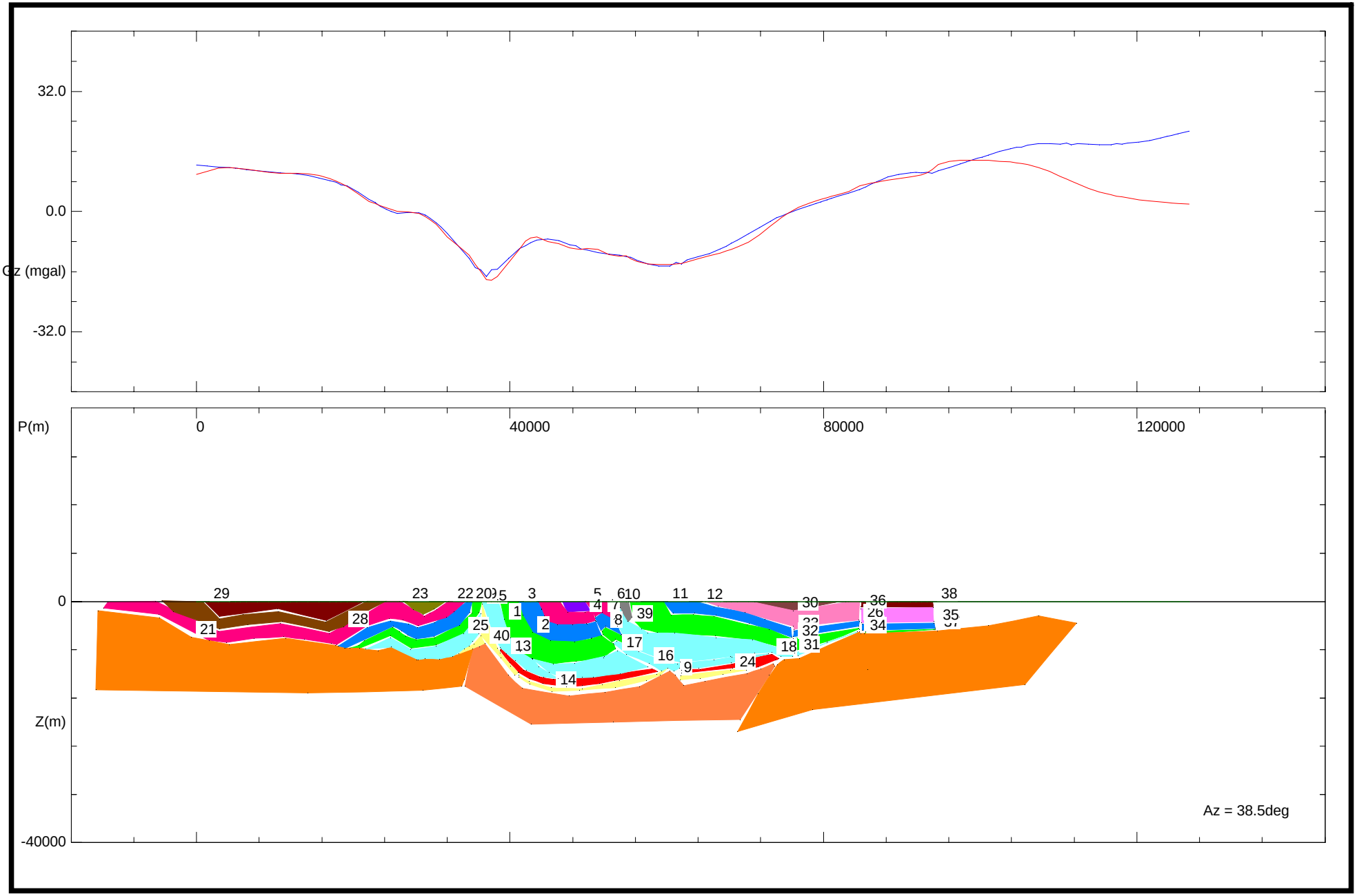
32.0
0.0
Gz (mgal)
-32.0
P(m)
0
40000
80000
120000
0
Z(m)
-40000
Az = 38.5deg

Model Summary

Body	Type	Description	X	Y	Z	Strike	Dip	Plunge	Density	A	B	C
9	PolyPrism	basement - 2.64	212208.7	6689637.6	-12258.3	-51.5	0.0	0.0	2.640		0.0	
14	PolyPrism	Evaporites - 2.3	202381.5	6677286.0	-14257.5	-51.5	0.0	0.0	2.400		0.0	
13	PolyPrism	basalt 3.0	198791.2	6672773.5	-8648.1	-51.5	0.0	0.0	3.000		0.0	
1	PolyPrism	Curdimurka 2.58	198664.3	6672613.6	-3012.2	-51.5	0.0	0.0	2.580		0.0	
12	PolyPrism	Skillogalee - 2.70	214055.4	6691958.7	-82.7	-51.5	0.0	0.0	2.700		0.0	
11	PolyPrism	Emeroo - 2.65	211318.9	6688519.3	-55.1	-51.5	0.0	0.0	2.650		0.0	
15	PolyPrism	Evaporites - 2.3	196902.8	6670400.1	-421.5	-51.5	0.0	0.0	2.300		0.0	
10	PolyPrism	Curdimurka - 2.58	207493.1	6683710.7	-84.7	-51.5	0.0	0.0	2.580		0.0	
8	PolyPrism	Emeroo - 2.65	206707.2	6682723.0	-4348.5	-51.5	0.0	0.0	2.650		0.0	
7	PolyPrism	Skillogalee Dolomite - 2.72	206466.1	6682419.9	-1804.0	-51.5	0.0	0.0	2.720		0.0	
6	PolyPrism	Myrtle Springs - 2.65	206897.3	6682961.9	-63.2	-51.5	0.0	0.0	2.650		0.0	
5	PolyPrism	Tapley Hill - 2.62	205037.6	6680624.5	-24.6	-51.5	0.0	0.0	2.620		0.0	
4	PolyPrism	Myrtle Springs - 2.65	205050.8	6680641.1	-1804.4	-51.5	0.0	0.0	2.650		0.0	
3	PolyPrism	Skillogalee Dolomite - 2.72	199839.2	6674090.7	-46.7	-51.5	0.0	0.0	2.710		0.0	
2	PolyPrism	Emeroo sg - 2.65	200888.6	6675409.7	-5097.7	-51.5	0.0	0.0	2.650		0.0	
18	PolyPrism	basalt 3.0	219896.5	6699300.2	-8748.6	-51.5	0.0	0.0	3.000		0.0	
31	PolyPrism	Curdimurka 2.58	221747.3	6701626.4	-8509.3	-51.5	0.0	0.0	2.580		0.0	
30	PolyPrism	Lower Wilpena - 2.65	221620.7	6701467.3	-1471.2	-51.5	0.0	0.0	2.650		0.0	
27	PolyPrism	Basement - 2.71	226887.6	6708087.2	-5055.0	-51.5	0.0	0.0	2.710		0.0	
26	PolyPrism	Tapley Hill 2.62	226799.0	6707975.8	-3018.6	-51.5	0.0	0.0	2.620		0.0	
24	PolyPrism	Evaporites - 2.3	216652.7	6695223.2	-11344.8	-51.5	0.0	0.0	2.400		0.0	
16	PolyPrism	Curdimurka 2.58	210136.1	6687032.7	-10243.8	-51.5	0.0	0.0	2.580		0.0	
17	PolyPrism	Curdimurka 2.58	207640.1	6683895.5	-8189.2	-51.5	0.0	0.0	2.580		0.0	
29	PolyPrism	Upper Wilpena - 2.7	174844.5	6642675.5	-42.2	-51.5	0.0	0.0	2.700		0.0	
19	PolyPrism	Emeroo - 2.65	196092.2	6669381.1	-46.7	-51.5	0.0	0.0	2.650		0.0	
20	PolyPrism	Skillogalee - 2.68	195665.5	6668845.0	-9.7	-51.5	0.0	0.0	2.680		0.0	
22	PolyPrism	Umberatana - 2.65	194215.2	6667022.0	69.8	-51.5	0.0	0.0	2.650		0.0	
23	PolyPrism	Lower Wilpena - 2.70	190643.2	6662532.5	41.5	-51.5	0.0	0.0	2.700		0.0	
28	PolyPrism	Lower Wilpena - 2.65	185877.9	6656543.1	-4146.9	-51.5	0.0	0.0	2.650		0.0	
21	PolyPrism	basement - 2.72	173777.7	6641334.7	-5948.0	-51.5	0.0	0.0	2.720		0.0	
25	PolyPrism	Curdimurka 2.58	195421.4	6668538.0	-5344.6	-51.5	0.0	0.0	2.580		0.0	
40	PolyPrism	evaporites -	197102.1	6670650.5	-6968.9	-51.5	0.0	0.0	2.300		0.0	
39	PolyPrism	Hogan Dolomite 2.7	208485.4	6684957.9	-3311.5	-51.5	0.0	0.0	2.700		0.0	
38	PolyPrism	Lower Wilpena - 2.62	232689.7	6715379.7	-43.6	-51.5	0.0	0.0	2.620		0.0	
37	PolyPrism	Emeroo 2.65	232877.5	6715615.7	-4610.9	-51.5	0.0	0.0	2.650		0.0	
36	PolyPrism	Tapley Hill 2.62	227017.1	6708250.0	-1141.6	-51.5	0.0	0.0	2.620		0.0	
35	PolyPrism	Skillogalee 2.72	232798.4	6715516.3	-3566.0	-51.5	0.0	0.0	2.720		0.0	
34	PolyPrism	basement 2.72	227014.8	6708247.0	-5321.4	-51.5	0.0	0.0	2.720		0.0	
33	PolyPrism	Skillogalee 2.72	221668.5	6701527.4	-4841.9	-51.5	0.0	0.0	2.720		0.0	
32	PolyPrism	Emeroo - 2.65	221628.1	6701476.6	-6192.2	-51.5	0.0	0.0	2.650		0.0	

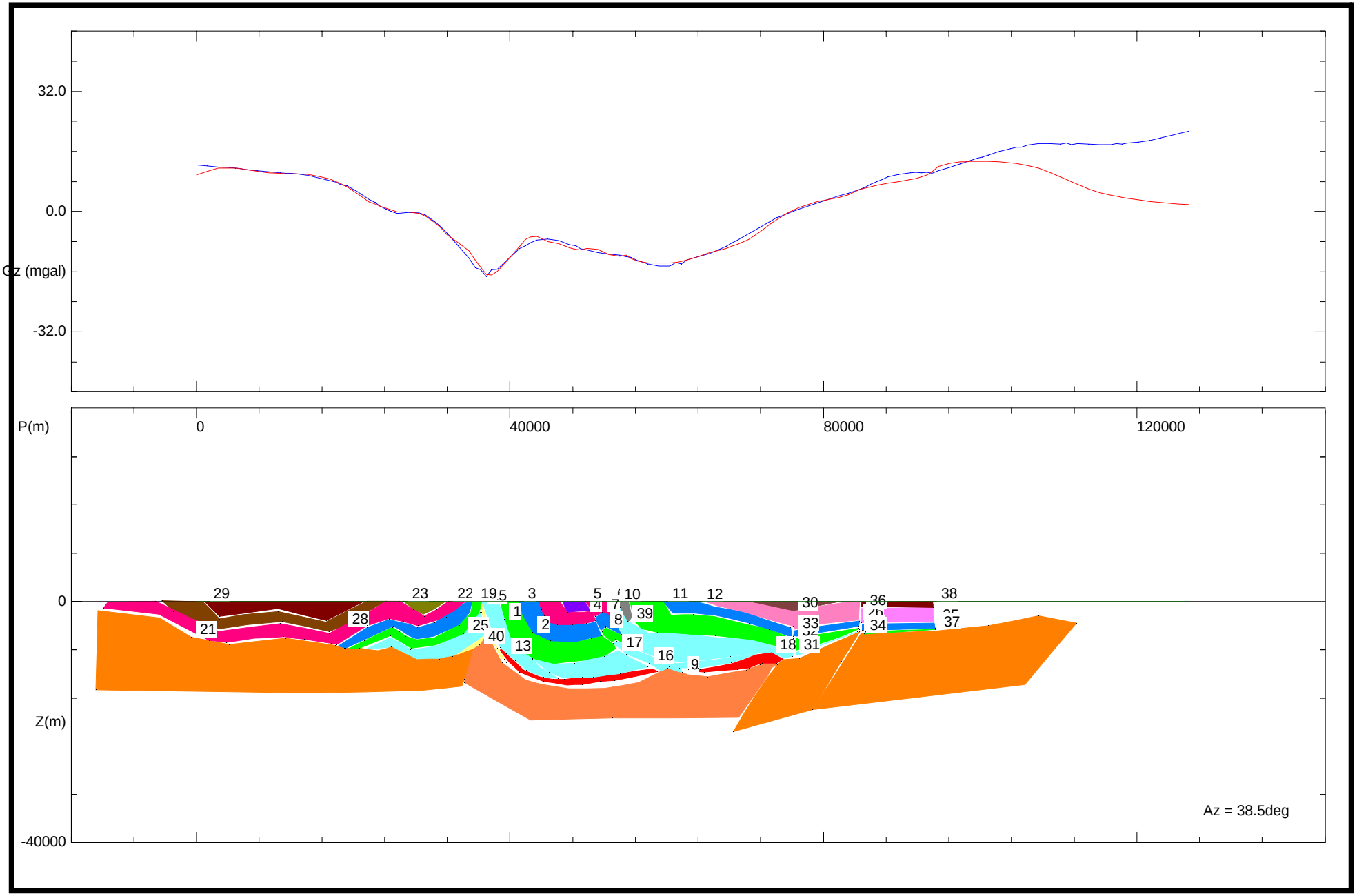
32.0
0.0
-32.0
Gz (mgal)
P(m)
0
40000
80000
120000
0
Z(m)
-40000
Az = 38.5deg

Model Summary

Body	Type	Description	X	Y	Z	Strike	Dip	Plunge	Density	A	B	C
2	PolyPrism	Emeroo sg - 2.65	200888.6	6675409.7	-5097.7	-51.5	0.0	0.0	2.650		0.0	
3	PolyPrism	Skillogalee Dolomite - 2.72	199839.2	6674090.7	-46.7	-51.5	0.0	0.0	2.710		0.0	
4	PolyPrism	Myrtle Springs - 2.65	205050.8	6680641.1	-1804.4	-51.5	0.0	0.0	2.650		0.0	
5	PolyPrism	Tapley Hill - 2.62	205037.6	6680624.5	-24.6	-51.5	0.0	0.0	2.620		0.0	
6	PolyPrism	Myrtle Springs - 2.65	206897.3	6682961.9	-63.2	-51.5	0.0	0.0	2.650		0.0	
7	PolyPrism	Skillogalee Dolomite - 2.72	206466.1	6682419.9	-1804.0	-51.5	0.0	0.0	2.720		0.0	
8	PolyPrism	Emeroo - 2.65	206707.2	6682723.0	-4348.5	-51.5	0.0	0.0	2.650		0.0	
10	PolyPrism	Curdimurka - 2.58	207493.1	6683710.7	-84.7	-51.5	0.0	0.0	2.580		0.0	
15	PolyPrism	Evaporites - 2.3	196902.8	6670400.1	-421.5	-51.5	0.0	0.0	2.300		0.0	
11	PolyPrism	Emeroo - 2.65	211318.9	6688519.3	-55.1	-51.5	0.0	0.0	2.650		0.0	
12	PolyPrism	Skillogalee - 2.70	214055.4	6691958.7	-82.7	-51.5	0.0	0.0	2.700		0.0	
1	PolyPrism	Curdimurka 2.58	198664.3	6672613.6	-3012.2	-51.5	0.0	0.0	2.580		0.0	
13	PolyPrism	basalt 3.0	198791.2	6672773.5	-8648.1	-51.5	0.0	0.0	3.000		0.0	
9	PolyPrism	basement - 2.58	212801.4	6690382.6	-11795.1	-51.5	0.0	0.0	2.620		0.0	
25	PolyPrism	Curdimurka 2.58	195421.4	6668538.0	-5344.6	-51.5	0.0	0.0	2.580		0.0	
21	PolyPrism	basement - 2.72	173777.7	6641334.7	-5948.0	-51.5	0.0	0.0	2.720		0.0	
28	PolyPrism	Lower Wilpena - 2.65	185877.9	6656543.1	-4146.9	-51.5	0.0	0.0	2.650		0.0	
23	PolyPrism	Lower Wilpena - 2.70	190643.2	6662532.5	41.5	-51.5	0.0	0.0	2.700		0.0	
22	PolyPrism	Umberatana - 2.65	194215.2	6667022.0	69.8	-51.5	0.0	0.0	2.650		0.0	
20	PolyPrism	Skillogalee - 2.68	195665.5	6668845.0	-9.7	-51.5	0.0	0.0	2.680		0.0	
19	PolyPrism	Emeroo - 2.65	196092.2	6669381.1	-46.7	-51.5	0.0	0.0	2.650		0.0	
29	PolyPrism	Upper Wilpena - 2.7	174844.5	6642675.5	-42.2	-51.5	0.0	0.0	2.700		0.0	
17	PolyPrism	Curdimurka 2.58	207640.1	6683895.5	-8189.2	-51.5	0.0	0.0	2.580		0.0	
16	PolyPrism	Curdimurka 2.58	210136.1	6687032.7	-10243.8	-51.5	0.0	0.0	2.580		0.0	
26	PolyPrism	Tapley Hill 2.62	226799.0	6707975.8	-3018.6	-51.5	0.0	0.0	2.620		0.0	
27	PolyPrism	Basement - 2.71	226887.6	6708087.2	-5055.0	-51.5	0.0	0.0	2.710		0.0	
30	PolyPrism	Lower Wilpena - 2.65	221620.7	6701467.3	-1471.2	-51.5	0.0	0.0	2.650		0.0	
31	PolyPrism	Curdimurka 2.58	221747.3	6701626.4	-8509.3	-51.5	0.0	0.0	2.580		0.0	
18	PolyPrism	basalt 3.0	219870.3	6699267.3	-8484.0	-51.5	0.0	0.0	3.000		0.0	
32	PolyPrism	Emeroo - 2.65	221628.1	6701476.6	-6192.2	-51.5	0.0	0.0	2.650		0.0	
33	PolyPrism	Skillogalee 2.72	221668.5	6701527.4	-4841.9	-51.5	0.0	0.0	2.720		0.0	
34	PolyPrism	basement 2.72	227014.8	6708247.0	-5321.4	-51.5	0.0	0.0	2.720		0.0	
35	PolyPrism	Skillogalee 2.72	232798.4	6715516.3	-3566.0	-51.5	0.0	0.0	2.720		0.0	
36	PolyPrism	Tapley Hill 2.62	227017.1	6708250.0	-1141.6	-51.5	0.0	0.0	2.620		0.0	
37	PolyPrism	Emeroo 2.65	232877.5	6715615.7	-4610.9	-51.5	0.0	0.0	2.650		0.0	
38	PolyPrism	Lower Wilpena - 2.62	232689.7	6715379.7	-43.6	-51.5	0.0	0.0	2.620		0.0	
39	PolyPrism	Hogan Dolomite 2.7	208485.4	6684957.9	-3311.5	-51.5	0.0	0.0	2.700		0.0	
40	PolyPrism	evaporites -	196686.3	6670128.0	-7128.7	-51.5	0.0	0.0	2.300		0.0	

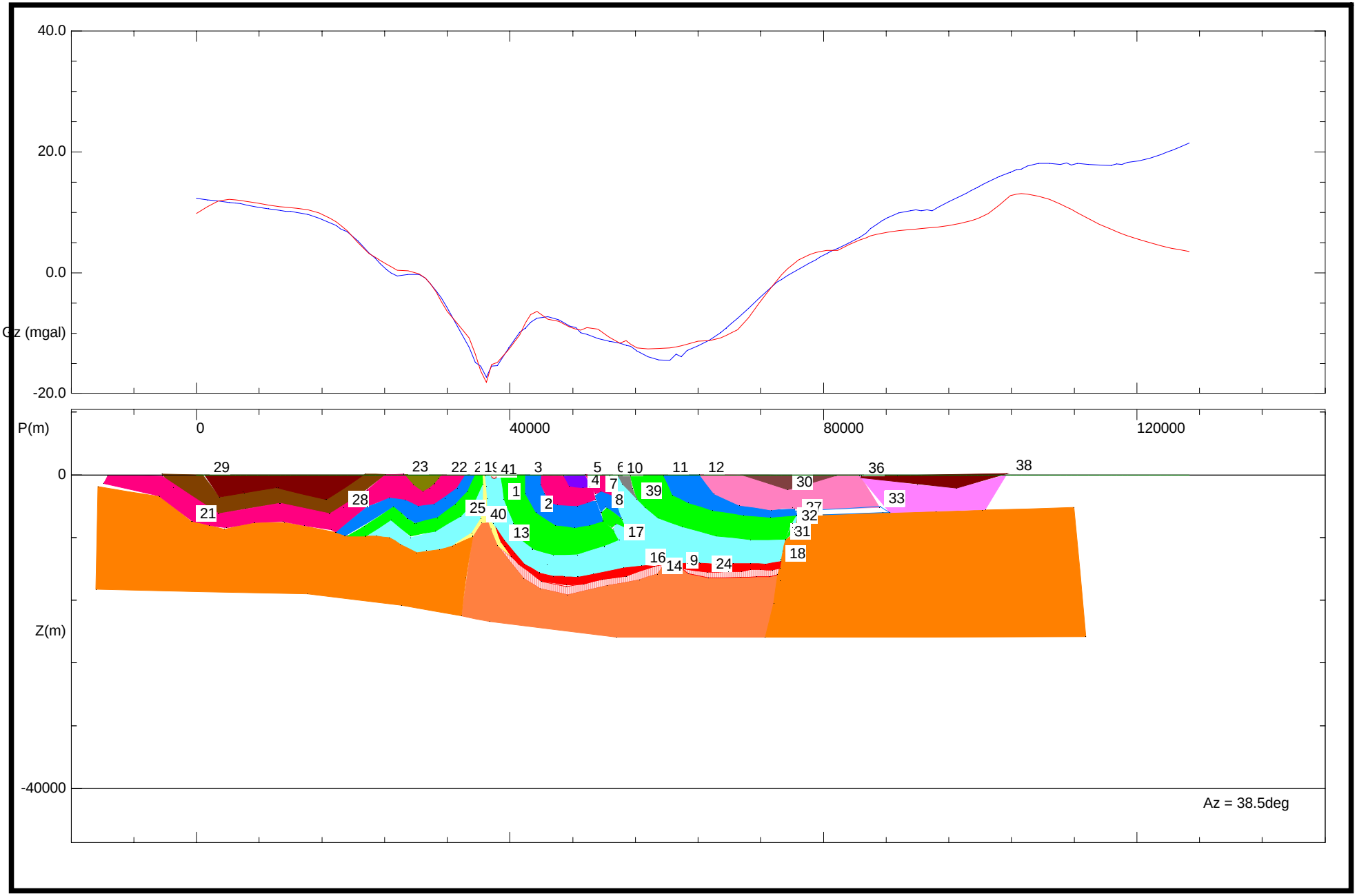
40.0
20.0
0.0
Gz (mgal)
-20.0
P(m)
0
40000
80000
120000
0
Z(m)
-40000
29
23
22
41
3
5
10
11
12
36
38
30
7
39
1
2
8
28
21
25
40
13
17
32
31
33
18
16
14
9
24
Az = 38.5deg

Model Summary

Body	Type	Description	X	Y	Z	Strike	Dip	Plunge	Density	A	B	C
14	PolyPrism	Paralana quartzite	210801.4	6687868.8	-12653.8	-51.5	0.0	0.0	2.680		0.0	
2	PolyPrism	Emeroo sg - 2.65	201156.7	6675746.6	-4748.6	-51.5	0.0	0.0	2.650		0.0	
3	PolyPrism	Skillogalee Dolomite - 2.72	200324.6	6674700.7	-31.6	-51.5	0.0	0.0	2.710		0.0	
4	PolyPrism	Myrtle Springs - 2.65	204863.6	6680405.7	-1626.3	-51.5	0.0	0.0	2.650		0.0	
5	PolyPrism	Tapley Hill - 2.62	205037.6	6680624.5	-24.6	-51.5	0.0	0.0	2.620		0.0	
6	PolyPrism	Myrtle Springs - 2.65	206897.3	6682961.9	-63.2	-51.5	0.0	0.0	2.650		0.0	
7	PolyPrism	Skillogalee Dolomite - 2.72	206329.7	6682248.5	-2136.2	-51.5	0.0	0.0	2.720		0.0	
8	PolyPrism	Emeroo - 2.65	206789.3	6682826.2	-4239.7	-51.5	0.0	0.0	2.650		0.0	
10	PolyPrism	Curdimurka - 2.60	207680.9	6683946.8	-128.3	-51.5	0.0	0.0	2.600		0.0	
15	PolyPrism	Evaporites - 2.3	197126.8	6670681.6	-119.9	-51.5	0.0	0.0	2.300		0.0	
11	PolyPrism	Emeroo - 2.65	211318.9	6688519.3	-55.1	-51.5	0.0	0.0	2.650		0.0	
12	PolyPrism	Skillogalee - 2.70	214153.6	6692082.1	-31.6	-51.5	0.0	0.0	2.700		0.0	
1	PolyPrism	Curdimurka 2.58	198583.3	6672511.7	-3124.2	-51.5	0.0	0.0	2.600		0.0	
13	PolyPrism	basalt 3.0	198659.3	6672607.8	-8430.5	-51.5	0.0	0.0	3.000		0.0	
9	PolyPrism	basement - 2.58	212716.3	6690275.6	-11932.8	-51.5	0.0	0.0	2.620		0.0	
24	PolyPrism	Paralana quartzite	214767.2	6692853.4	-12403.4	-51.5	0.0	0.0	2.680		0.0	
25	PolyPrism	Curdimurka 2.58	195185.2	6668241.2	-5251.2	-51.5	0.0	0.0	2.600		0.0	
21	PolyPrism	basement - 2.72	173777.7	6641334.7	-5948.0	-51.5	0.0	0.0	2.720		0.0	
28	PolyPrism	Lower Wilpena - 2.65	185877.9	6656543.1	-4146.9	-51.5	0.0	0.0	2.650		0.0	
23	PolyPrism	Lower Wilpena - 2.70	190643.2	6662532.5	41.5	-51.5	0.0	0.0	2.700		0.0	
22	PolyPrism	Umberatana - 2.65	193719.1	6666398.5	7.6	-51.5	0.0	0.0	2.650		0.0	
20	PolyPrism	Skillogalee - 2.68	195581.5	6668739.3	7.6	-51.5	0.0	0.0	2.680		0.0	
19	PolyPrism	Emeroo - 2.65	196344.2	6669698.0	7.6	-51.5	0.0	0.0	2.650		0.0	
29	PolyPrism	Upper Wilpena - 2.7	174844.5	6642675.5	-42.2	-51.5	0.0	0.0	2.700		0.0	
17	PolyPrism	Curdimurka 2.60	207780.0	6684071.3	-8351.1	-51.5	0.0	0.0	2.600		0.0	
16	PolyPrism	Curdimurka 2.58	209503.6	6686237.7	-11538.3	-51.5	0.0	0.0	2.600		0.0	
26	PolyPrism	Tapley Hill 2.62	228433.1	6710029.7	-4168.1	-51.5	0.0	0.0	2.620		0.0	
27	PolyPrism	Basement - 2.71	221903.6	6701822.9	-5126.1	-51.5	0.0	0.0	2.710		0.0	
30	PolyPrism	Lower Wilpena - 2.65	221167.2	6700897.4	-1880.1	-51.5	0.0	0.0	2.650		0.0	
31	PolyPrism	Curdimurka 2.58	221003.7	6700691.9	-8201.7	-51.5	0.0	0.0	2.600		0.0	
18	PolyPrism	basalt 3.0	220627.0	6700218.4	-11058.8	-51.5	0.0	0.0	3.000		0.0	
41	PolyPrism	basalt block	197688.5	6671387.6	-350.9	-51.5	0.0	0.0	2.400		0.0	
32	PolyPrism	Emeroo - 2.65	221589.7	6701428.4	-6218.5	-51.5	0.0	0.0	2.650		0.0	
36	PolyPrism	Tapley Hill 2.62	226863.5	6708056.9	-168.1	-51.5	0.0	0.0	2.620		0.0	
38	PolyPrism	Lower Wilpena - 2.62	238602.1	6722810.9	159.6	-51.5	0.0	0.0	2.620		0.0	
39	PolyPrism	Hogan Dolomite 2.7	209179.5	6685830.3	-3109.2	-51.5	0.0	0.0	2.700		0.0	
40	PolyPrism	evaporites -	196859.4	6670345.4	-6104.1	-51.5	0.0	0.0	2.300		0.0	
33	PolyPrism	Skillogalee Dolomite	228475.0	6710082.0	-4000.0	-51.5	0.0	0.0	2.720		0.0	

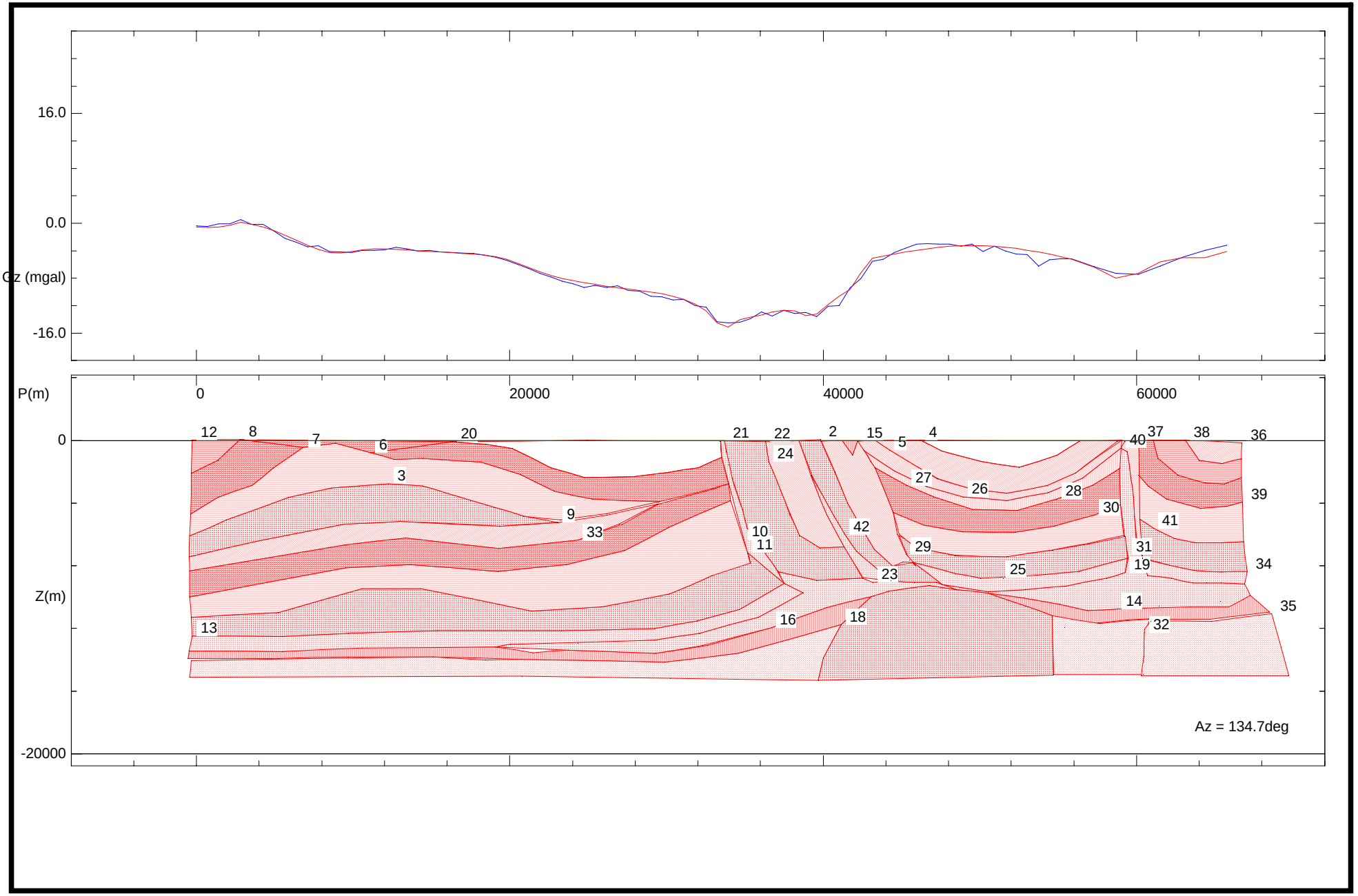
16.0
0.0
Gz (mgal)
-16.0
P(m)
0
20000
40000
60000
Z(m)
-20000
12
8
7
6
20
21
22
2
15
5
4
40
37
38
36
24
3
27
26
28
39
9
30
41
33
10
42
11
29
31
34
23
25
19
14
35
13
16
18
32
Az = 134.7deg

Model Summary

longsection5

Regional polynomial coefficients

Channel	Degree	a0	a1	a2	a3	a4	a5
Gz	0	-20.629275					

Body	Type	Description	X	Y	Z	Strike	Dip	Plunge	Density	A	B	C
9	PolyPrism	Myrtle Springs	201558.4	6685906.3	-5238.8	44.7	0.0	0.0	2.650		0.0	
15	PolyPrism	Tapley Hill	215148.0	6672458.7	-14.4	44.7	0.0	0.0	2.620		0.0	
5	PolyPrism	Tapley Hill	216590.8	6671031.0	-608.4	44.7	0.0	0.0	2.620		0.0	
14	PolyPrism	Paralana Quartzite	226920.9	6660808.8	-10756.1	44.7	0.0	0.0	2.680		0.0	
12	PolyPrism	Myrtle Springs	184955.8	6702335.4	21.1	44.7	0.0	0.0	2.650		0.0	
11	PolyPrism	Curdimurka	210165.2	6677389.4	-7162.3	44.7	0.0	0.0	2.580		0.0	
10	PolyPrism	Emeroo	209937.4	6677614.9	-6316.1	44.7	0.0	0.0	2.650		0.0	
8	PolyPrism	Skillogalee	187121.3	6700192.5	74.4	44.7	0.0	0.0	2.700		0.0	
7	PolyPrism	Emeroo	189984.9	6697358.9	-443.6	44.7	0.0	0.0	2.650		0.0	
6	PolyPrism	Skillogalee	193041.9	6694333.8	-764.4	44.7	0.0	0.0	2.680		0.0	
4	PolyPrism	Amberoona	217982.0	6669654.4	25.1	44.7	0.0	0.0	2.620		0.0	
1	PolyPrism		208921.7	6678620.2	-18.8	44.7	0.0	0.0	2.600		0.0	
3	PolyPrism	Curdimurka	193874.0	6693510.6	-2779.1	44.7	0.0	0.0	2.600		0.0	
13	PolyPrism	Noranda Volcs	184955.8	6702335.4	-12470.5	44.7	0.0	0.0	3.000		0.0	
2	PolyPrism	CSg sds	213456.1	6674132.9	49.6	44.7	0.0	0.0	2.600		0.0	
19	PolyPrism	Wywyana	227288.5	6660445.1	-8433.7	44.7	0.0	0.0	2.300		0.0	
31	PolyPrism	Curdimurka	227385.3	6660349.3	-7298.5	44.7	0.0	0.0	2.630		0.0	
29	PolyPrism	Cudrimurka	217355.1	6670274.7	-7274.3	44.7	0.0	0.0	2.650		0.0	
27	PolyPrism	Myrtle Shale	217362.8	6670267.1	-2871.2	44.7	0.0	0.0	2.650		0.0	
26	PolyPrism	Tillite	219938.1	6667718.7	-3589.5	44.7	0.0	0.0	2.620		0.0	
25	PolyPrism	Noranda Volcs	221658.2	6666016.6	-8741.4	44.7	0.0	0.0	3.000		0.0	
24	PolyPrism	Curdimurka Siltstone	211115.0	6676449.5	-1352.4	44.7	0.0	0.0	2.650		0.0	
22	PolyPrism	Dome Sds	210970.1	6676593.0	-77.5	44.7	0.0	0.0	2.630		0.0	
16	PolyPrism	Paralana Quartzite	211229.4	6676336.4	-11951.1	44.7	0.0	0.0	2.680		0.0	
17	PolyPrism	basement granite	214402.5	6673196.4	-11763.4	44.7	0.0	0.0	2.660		0.0	
18	PolyPrism	Basement granodiorite	214402.5	6673196.4	-11763.4	44.7	0.0	0.0	2.800		0.0	
20	PolyPrism	Skillogalee	196747.3	6690667.2	-88.9	44.7	0.0	0.0	2.720		0.0	
21	PolyPrism	Wywyana	209095.7	6678447.7	-18.8	44.7	0.0	0.0	2.300		0.0	
23	PolyPrism	Wywyana	215845.9	6671768.1	-9071.2	44.7	0.0	0.0	2.300		0.0	
28	PolyPrism	Skillogalee	224173.4	6663527.6	-3743.8	44.7	0.0	0.0	2.700		0.0	
30	PolyPrism	Emeroo Subgroup	225895.4	6661823.6	-4752.6	44.7	0.0	0.0	2.650		0.0	
33	PolyPrism	Skillogalee Dolomite	202463.1	6685011.0	-6353.8	44.7	0.0	0.0	2.720		0.0	
32	PolyPrism	Basement 3	228159.2	6659583.5	-12253.5	44.7	0.0	0.0	2.720		0.0	
34	PolyPrism	Noranda Volcanics	232802.8	6654988.4	-8351.9	44.7	0.0	0.0	3.000		0.0	
35	PolyPrism	Basement	233925.0	6653877.9	-11055.5	44.7	0.0	0.0	2.780		0.0	
36	PolyPrism	Umb	232569.4	6655219.4	-141.5	44.7	0.0	0.0	2.620		0.0	
37	PolyPrism	Skillogalee	227886.4	6659853.4	60.8	44.7	0.0	0.0	2.700		0.0	
38	PolyPrism	Myrtle	229997.3	6657764.6	25.1	44.7	0.0	0.0	2.650		0.0	
39	PolyPrism	Emeroo	232590.0	6655199.0	-3944.4	44.7	0.0	0.0	2.650		0.0	
40	PolyPrism	Curdi Breccia	227093.1	6660638.4	-483.7	44.7	0.0	0.0	2.650		0.0	
41	PolyPrism	Dome Sandstone	228565.8	6659181.1	-5589.2	44.7	0.0	0.0	2.630		0.0	
42	PolyPrism	Wywyana	214568.9	6673031.8	-5994.7	44.7	0.0	0.0	2.300		0.0	

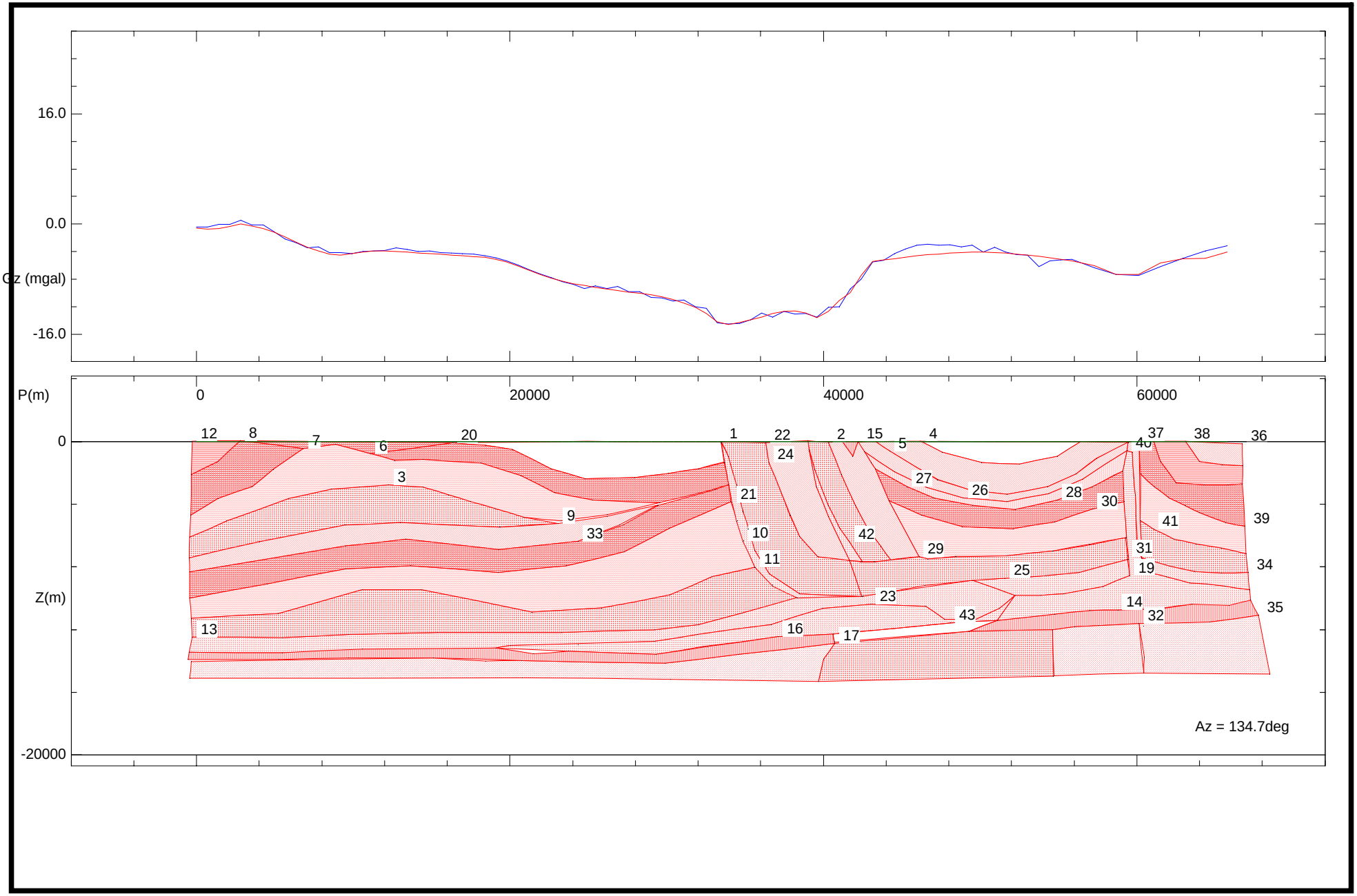
16.0
0.0
Gz (mgal)
-16.0
P(m)
0
20000
40000
60000
Z(m)
-20000
12
8
7
6
20
1
22
2
15
5
4
37
38
36
24
3
21
27
26
28
30
9
33
10
42
41
39
11
29
31
19
34
25
23
14
35
43
32
13
16
17
Az = 134.7deg

Model Summary

longsection5

Regional polynomial coefficients

Channel	Degree	a0	a1	a2	a3	a4	a5
Gz	0	-20.629275					

Body	Type	Description	X	Y	Z	Strike	Dip	Plunge	Density	A	B	C
2	PolyPrism	CSg sds	213802.7	6673790.0	-32.6	44.7	0.0	0.0	2.600		0.0	
13	PolyPrism	Noranda Volcs	184955.8	6702335.4	-12470.5	44.7	0.0	0.0	3.000		0.0	
3	PolyPrism	Curdimurka	193874.0	6693510.6	-2779.1	44.7	0.0	0.0	2.600		0.0	
1	PolyPrism		208921.7	6678620.2	-18.8	44.7	0.0	0.0	2.600		0.0	
4	PolyPrism	Amberoona	217982.0	6669654.4	25.1	44.7	0.0	0.0	2.620		0.0	
6	PolyPrism	Skillogalee	193041.9	6694333.8	-764.4	44.7	0.0	0.0	2.680		0.0	
7	PolyPrism	Emeroo	189984.9	6697358.9	-443.6	44.7	0.0	0.0	2.650		0.0	
8	PolyPrism	Skillogalee	187121.3	6700192.5	74.4	44.7	0.0	0.0	2.700		0.0	
10	PolyPrism	Emeroo	209937.4	6677614.9	-6316.1	44.7	0.0	0.0	2.650		0.0	
11	PolyPrism	Curdimurka	210488.3	6677069.7	-8008.3	44.7	0.0	0.0	2.580		0.0	
12	PolyPrism	Myrtle Springs	184955.8	6702335.4	21.1	44.7	0.0	0.0	2.650		0.0	
14	PolyPrism	Paralana Quartzite	226920.9	6660808.8	-10756.1	44.7	0.0	0.0	2.680		0.0	
5	PolyPrism	Tapley Hill	216590.8	6671031.0	-608.4	44.7	0.0	0.0	2.620		0.0	
15	PolyPrism	Tapley Hill	215148.0	6672458.7	-14.4	44.7	0.0	0.0	2.620		0.0	
9	PolyPrism	Myrtle Springs	201558.4	6685906.3	-5238.8	44.7	0.0	0.0	2.650		0.0	
30	PolyPrism	Emeroo Subgroup	225798.7	6661919.3	-4283.2	44.7	0.0	0.0	2.650		0.0	
28	PolyPrism	Skillogalee	224173.4	6663527.6	-3743.8	44.7	0.0	0.0	2.700		0.0	
23	PolyPrism	Wywyana	215737.5	6671875.3	-10386.6	44.7	0.0	0.0	2.300		0.0	
20	PolyPrism	Skillogalee	196747.3	6690667.2	-88.9	44.7	0.0	0.0	2.720		0.0	
18	PolyPrism	Basement granodiorite	214092.9	6673502.8	-12893.3	44.7	0.0	0.0	2.800		0.0	
17	PolyPrism	basement granite	214092.9	6673502.8	-12893.3	44.7	0.0	0.0	2.660		0.0	
16	PolyPrism	Paralana Quartzite	211538.9	6676030.1	-12457.3	44.7	0.0	0.0	2.680		0.0	
22	PolyPrism	Dome Sds	210970.1	6676593.0	-77.5	44.7	0.0	0.0	2.630		0.0	
24	PolyPrism	Curdimurka Siltstone	211115.0	6676449.5	-1352.4	44.7	0.0	0.0	2.650		0.0	
25	PolyPrism	Noranda Volcs	221812.9	6665863.4	-8724.5	44.7	0.0	0.0	3.000		0.0	
26	PolyPrism	Tillite	219938.1	6667718.7	-3589.5	44.7	0.0	0.0	2.620		0.0	
27	PolyPrism	Myrtle Shale	217362.8	6670267.1	-2871.2	44.7	0.0	0.0	2.650		0.0	
29	PolyPrism	Cudrimurka	217923.9	6669711.8	-7362.1	44.7	0.0	0.0	2.650		0.0	
31	PolyPrism	Curdimurka	227385.3	6660349.3	-7298.5	44.7	0.0	0.0	2.630		0.0	
19	PolyPrism	Wywyana	227464.1	6660271.3	-8561.5	44.7	0.0	0.0	2.300		0.0	
21	PolyPrism	Wywyana	209424.2	6678122.7	-3880.3	44.7	0.0	0.0	2.300		0.0	
42	PolyPrism	Wywyana	214770.1	6672832.6	-6435.7	44.7	0.0	0.0	2.300		0.0	
41	PolyPrism	Dome Sandstone	228565.8	6659181.1	-5589.2	44.7	0.0	0.0	2.630		0.0	
40	PolyPrism	Curdi Breccia	227344.6	6660389.5	-569.8	44.7	0.0	0.0	2.650		0.0	
39	PolyPrism	Emeroo	232684.8	6655105.2	-5392.5	44.7	0.0	0.0	2.650		0.0	
38	PolyPrism	Myrtle	229997.3	6657764.6	25.1	44.7	0.0	0.0	2.650		0.0	
37	PolyPrism	Skillogalee	227886.4	6659853.4	60.8	44.7	0.0	0.0	2.700		0.0	
36	PolyPrism	Umb	232569.4	6655219.4	-141.5	44.7	0.0	0.0	2.620		0.0	
35	PolyPrism	Basement	233303.9	6654492.5	-11100.8	44.7	0.0	0.0	2.780		0.0	
34	PolyPrism	Noranda Volcanics	232841.5	6654950.1	-8370.3	44.7	0.0	0.0	3.000		0.0	
32	PolyPrism	Basement 3	227888.3	6659851.5	-11612.7	44.7	0.0	0.0	2.720		0.0	
33	PolyPrism	Skillogalee Dolomite	202463.1	6685011.0	-6353.8	44.7	0.0	0.0	2.720		0.0	
43	PolyPrism	Paralana Quartzite	219346.5	6668304.1	-11588.6	44.7	0.0	0.0	2.680		0.0	

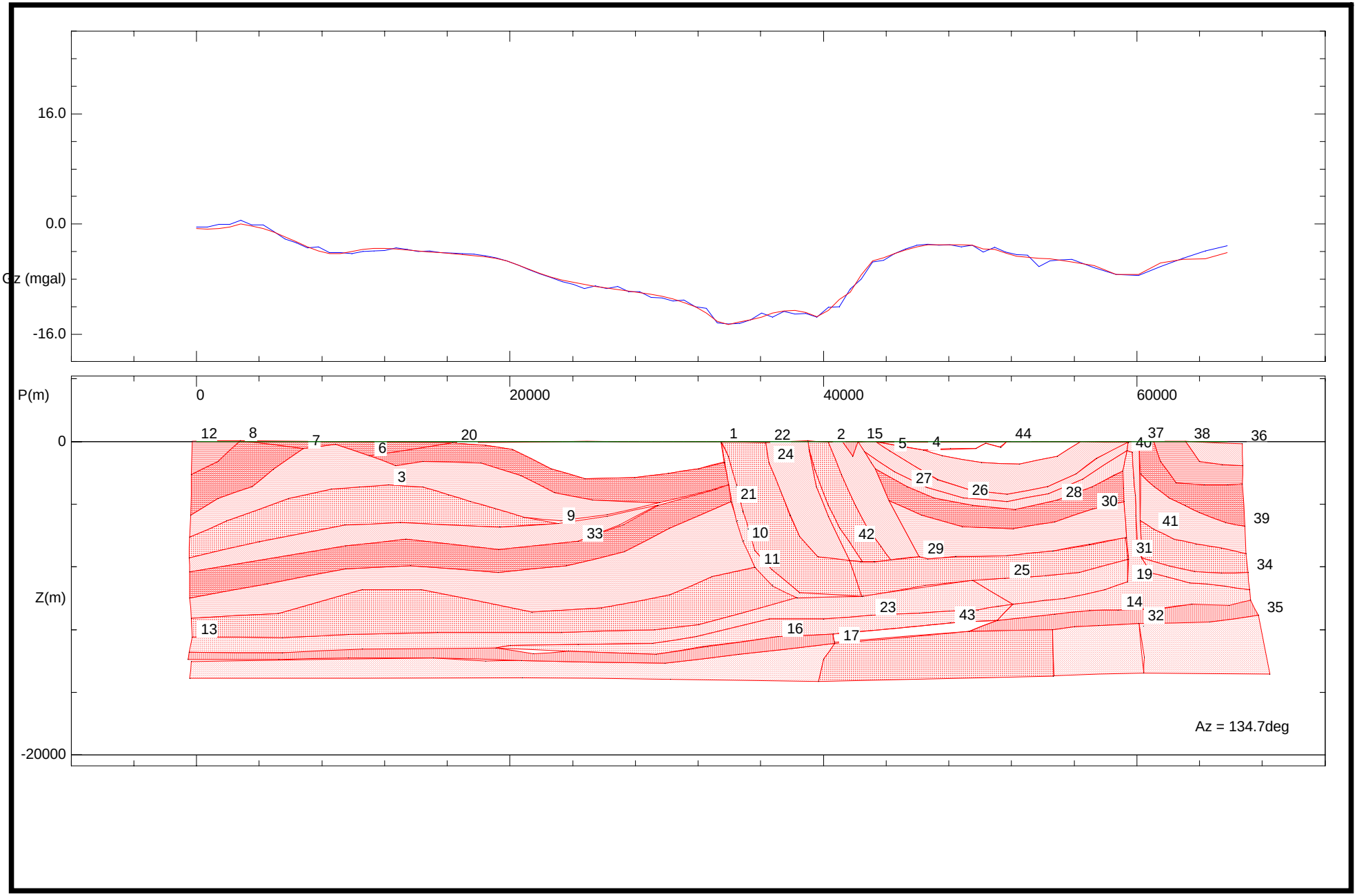
16.0
0.0
Gz (mgal)
-16.0
P(m)
0
20000
40000
60000
Z(m)
-20000
12
8
7
6
20
1
22
2
15
5
4
44
40
37
38
36
24
3
21
27
26
28
30
41
39
9
33
10
42
29
31
34
11
25
19
23
14
35
43
32
13
16
17
Az = 134.7deg

Model Summary

longsection5

Regional polynomial coefficients

Channel	Degree	a0	a1	a2	a3	a4	a5
Gz	0	-20.629275					

Body	Type	Description	X	Y	Z	Strike	Dip	Plunge	Density	A	B	C
2	PolyPrism	CSg sds	213802.7	6673790.0	-32.6	44.7	0.0	0.0	2.600		0.0	
13	PolyPrism	Noranda Volcs	184955.8	6702335.4	-12470.5	44.7	0.0	0.0	3.000		0.0	
3	PolyPrism	Curdimurka	193874.0	6693510.6	-2779.1	44.7	0.0	0.0	2.600		0.0	
1	PolyPrism		208921.7	6678620.2	-18.8	44.7	0.0	0.0	2.600		0.0	
4	PolyPrism	Amberoona	218138.2	6669499.8	-545.2	44.7	0.0	0.0	2.620		0.0	
6	PolyPrism	Skillogalee	193003.2	6694372.1	-904.5	44.7	0.0	0.0	2.680		0.0	
7	PolyPrism	Emeroo	189984.9	6697358.9	-443.6	44.7	0.0	0.0	2.650		0.0	
8	PolyPrism	Skillogalee	187121.3	6700192.5	74.4	44.7	0.0	0.0	2.700		0.0	
10	PolyPrism	Emeroo	209937.4	6677614.9	-6316.1	44.7	0.0	0.0	2.650		0.0	
11	PolyPrism	Curdimurka	210488.3	6677069.7	-8008.3	44.7	0.0	0.0	2.580		0.0	
12	PolyPrism	Myrtle Springs	184955.8	6702335.4	21.1	44.7	0.0	0.0	2.650		0.0	
14	PolyPrism	Paralana Quartzite	226920.9	6660808.8	-10756.1	44.7	0.0	0.0	2.680		0.0	
5	PolyPrism	Tapley Hill	216590.8	6671031.0	-608.4	44.7	0.0	0.0	2.620		0.0	
15	PolyPrism	Tapley Hill	215148.0	6672458.7	-14.4	44.7	0.0	0.0	2.620		0.0	
9	PolyPrism	Myrtle Springs	201558.4	6685906.3	-5238.8	44.7	0.0	0.0	2.650		0.0	
30	PolyPrism	Emeroo Subgroup	225798.7	6661919.3	-4283.2	44.7	0.0	0.0	2.650		0.0	
28	PolyPrism	Skillogalee	224173.4	6663527.6	-3743.8	44.7	0.0	0.0	2.700		0.0	
23	PolyPrism	Wywyana	215737.5	6671875.3	-11095.0	44.7	0.0	0.0	2.300		0.0	
20	PolyPrism	Skillogalee	196747.3	6690667.2	-88.9	44.7	0.0	0.0	2.720		0.0	
18	PolyPrism	Basement granodiorite	214092.9	6673502.8	-12893.3	44.7	0.0	0.0	2.700		0.0	
17	PolyPrism	basement granite	214092.9	6673502.8	-12893.3	44.7	0.0	0.0	2.660		0.0	
16	PolyPrism	Paralana Quartzite	211538.9	6676030.1	-12457.3	44.7	0.0	0.0	2.680		0.0	
22	PolyPrism	Dome Sds	210970.1	6676593.0	-77.5	44.7	0.0	0.0	2.630		0.0	
24	PolyPrism	Curdimurka Siltstone	211115.0	6676449.5	-1352.4	44.7	0.0	0.0	2.650		0.0	
25	PolyPrism	Noranda Volcs	221812.9	6665863.4	-8724.5	44.7	0.0	0.0	3.000		0.0	
26	PolyPrism	Tillite	219938.1	6667718.7	-3589.5	44.7	0.0	0.0	2.620		0.0	
27	PolyPrism	Myrtle Shale	217362.8	6670267.1	-2871.2	44.7	0.0	0.0	2.650		0.0	
29	PolyPrism	Cudrimurka	217923.9	6669711.8	-7362.1	44.7	0.0	0.0	2.650		0.0	
31	PolyPrism	Curdimurka	227385.3	6660349.3	-7298.5	44.7	0.0	0.0	2.630		0.0	
19	PolyPrism	Wywyana	227385.3	6660349.3	-8942.5	44.7	0.0	0.0	2.300		0.0	
21	PolyPrism	Wywyana	209424.2	6678122.7	-3880.3	44.7	0.0	0.0	2.300		0.0	
42	PolyPrism	Wywyana	214770.1	6672832.6	-6435.7	44.7	0.0	0.0	2.300		0.0	
41	PolyPrism	Dome Sandstone	228565.8	6659181.1	-5589.2	44.7	0.0	0.0	2.630		0.0	
40	PolyPrism	Curdi Breccia	227344.6	6660389.5	-569.8	44.7	0.0	0.0	2.650		0.0	
39	PolyPrism	Emeroo	232684.8	6655105.2	-5392.5	44.7	0.0	0.0	2.650		0.0	
38	PolyPrism	Myrtle	229997.3	6657764.6	25.1	44.7	0.0	0.0	2.650		0.0	
37	PolyPrism	Skillogalee	227886.4	6659853.4	60.8	44.7	0.0	0.0	2.700		0.0	
36	PolyPrism	Umb	232569.4	6655219.4	-141.5	44.7	0.0	0.0	2.620		0.0	
35	PolyPrism	Basement	233303.9	6654492.5	-11100.8	44.7	0.0	0.0	2.780		0.0	
34	PolyPrism	Noranda Volcanics	232841.5	6654950.1	-8370.3	44.7	0.0	0.0	3.000		0.0	
32	PolyPrism	Basement 3	227888.3	6659851.5	-11612.7	44.7	0.0	0.0	2.720		0.0	
33	PolyPrism	Skillogalee Dolomite	202463.1	6685011.0	-6353.8	44.7	0.0	0.0	2.720		0.0	
43	PolyPrism	Paralana Quartzite	219346.5	6668304.1	-11588.6	44.7	0.0	0.0	2.680		0.0	
44	PolyPrism	surface laterite	221891.8	6665785.4	-13.9	44.7	0.0	0.0	2.720		0.0	